



Designing New Silyl Lewis Acids for Synthesis and Catalysis

An der Fakultät für Mathematik und Naturwissenschaften
der Carl von Ossietzky Universität Oldenburg
zur Erlangung des Grades und Titels eines

Doktors der Naturwissenschaften (Dr. rer. nat.)

angenommene Dissertation

von

M.Sc. Sandra Künzler

geboren am 6. Januar 1991 in Rotenburg (Wümme)

The research for this work was performed in the Institute of Chemistry at the Carl von Ossietzky Universität Oldenburg under supervision of Prof. Dr. Thomas Müller from March 2016 until May 2019.

This work was supported by the Deutsche Forschungsgemeinschaft (DFG-Mu1440-12/1), by the Deutscher Akademischer Austauschdienst (DAAD, Project 57316614, Weak Interactions in Stabilized Silylium Ions (WISSI), funding program “Programm Projektbezogener Personenaustausch Frankreich 2017”) and by the Carl von Ossietzky University Oldenburg (CvO). Calculations were performed at the HPC clusters HERO and CARL, located at the CvO and funded by the DFG (INST 184/108-1 FUGG and INST 184/157-1 FUGG) and the Ministry of Science and Culture of the Lower Saxony State.

Referee: Prof. Dr. Thomas Müller

Second referee: Prof. Dr. Yannick Landais

Day of Disputation: 05.12.2019

– El saber no ocupa lugar y nunca sabe nadie lo que le traerá el día de mañana –

Antonio Muñoz Molina



Acknowledgements

First of all, I would like to thank my supervisor, Prof. Thomas Müller, for the opportunity to prepare this thesis in his research group and providing the interesting topic as well as for the support and constant discussion during this time. I would further like to thank Prof. Yannick Landais for agreeing to be the second referee of this thesis and in particular for giving me the chance to join his research group; I appreciate the great time I had in Bordeaux. I thank Prof. Rüdiger Beckhaus for being the third referee.

I would like to thank Dr. Annemarie Schäfer and Dr. Lena Albers for their scientific and professional support. Furthermore, I thank Maria as well as Uwe for taking care of the laboratories as well as I would like to thank Petra for dealing with all the bureaucratic obstacles during this time.

Many thanks go to the analytical department. Especially, to Andrea who spent a lot of time recording the numerous non-routine NMR experiments and for the inspiring discussions as well as for teaching me how to deal with the NMR spectrometer. Moreover, I appreciate the work of Dieter for acquiring the NMR spectra, Marc for X-ray analyses, Rainer for measuring GC/MS spectra, Francesco for measuring mass spectra, and Burghard for performing elemental analyses. Dr. Stefan Harfst is thanked for support with computational issues.

I want to express my special thanks to my group members and colleagues of the department of chemistry. I appreciate working with Saskia and Anastasia and I am grateful not only for the fruitful cooperation but also for the friendship. Furthermore, I would like to thank Wiebke, Jelte, Gül, Alex P. and all other former members especially Thorben, Dong, Crispin, Dennis, Henning, Xiao and the members of the Beckhaus group for good collegueship. I would like to express my gratefulness to the members of the Hilt's and the Christoffer's groups, especially Lars, Sebastian, Corinna, Felicia, Julian and Daniel for support regarding the measurements of GC and chiral GC as well as for advice in organic synthesis issues. I appreciate the work of Marie, Marcel, Julian and Sarah and their contributions to this work. Moreover, I thank Claire, Anthony and Suman as well as the other members of the Landais group for affiliating me as a group member during my stay in Bordeaux.

I would like to thank Prof. Kim Baines for the support and advice during the writing process.

Finally, I would like to thank my family and friends for their support and their trust. Most importantly, I would like to thank Jonas Biehl; Agradeço seu apoio, paciência e amor. Tudo isso não seria possível sem você!

Thank you very much!



I hereby certify that I wrote this doctoral dissertation independently and that I used only the indicated sources. I did not submit this dissertation as a whole or in parts to any other university for evaluation for a conferral of a doctorate. I declare that all the data disclosed in this thesis are true and correct.

I affirm that I followed the guidelines for good scientific practice at the Carl von Ossietzky Universität Oldenburg. In connection with this dissertation project, I did not claim any commercial mentoring services.



Publications and Conference Contributions

1. Paper: N. Kordts, S. Künzler, S. Rathjen, T. Sieling, H. Großekappenberg, M. Schmidtman, T. Müller, **Silyl Chalconium Ions: Synthesis, Structure and Application in Hydrodefluorination Reactions**, *Chem. Eur. J.* **2017**, *23*, 10068-10079.
2. Paper: S. Künzler, S. Rathjen, A. Merk, M. Schmidtman, T. Müller, **An Experimental Acidity Scale for Intramolecularly Stabilized Silyl Lewis Acids**, *Chem. Eur. J.* **2019**, *25*, 15123-15130.
3. Poster: **Aryloxy Stabilized Silyl Cations**, Sandra Künzler, Thomas Müller, 8th European Silicon Days, Poznan, Poland, August **2016**.
4. Poster: **Silyl Oxonium and Silyl Sulfonium Ions as Surrogates for Transition Metal Catalysts**, Sandra Künzler, Marie S. Würdemann, Marcel Wernke, Thomas Müller, 22th European Conference on Organometallic Chemistry, Amsterdam, Netherlands, July **2017**.
5. Poster: **Synthesis and Properties of Thionyl Stabilized Hydridosilyl Cations**, Sandra Künzler, Thomas Müller, 10th Anglo-German Inorganic Chemistry Meeting, Göttingen, Germany, August **2017**.
6. Poster: **Chalcogenyl Stabilized Silyl Cations as Catalysts in Hydrosilylation Reactions of Nitriles**, Sandra Künzler, Thomas Müller, 15th International Symposium on Inorganic Ring Systems, Kyoto, Japan, June **2018**.
7. Short Talk: **Oxygen vs Sulfur Stabilized Silyl Cations – Which is the Better Lewis Acidic Catalyst**, 9th European Silicon Days, Saarbrücken, Germany, September **2018**.
8. Poster: **Peri-Interactions in Silylchalcogenyl-Substituted Acenaphthenes**, Sandra Künzler, Thomas Müller, 22. Norddeutsches Doktorandenkolloquium, Oldenburg, Germany, October **2019**.



Abstract

The development of Lewis acidic catalysts is of current interest in organic synthesis. Silyl cations possess high Lewis acidities and therefore they show a remarkable capability to act as catalysts in e.g. Diels-Alder and hydrosilylation reactions. The present studies focused on the synthesis and characterization of intramolecularly phenoxy- and thiophenyl-stabilized silyl borates with the naphthyl or acenaphthyl scaffold as backbone. The naphthyl/acenaphthyl backbone enforces the intramolecular interaction between the silicon atom and the donor moiety. This feature supports the reactive silicon center to react with substrates in a reversible manner. Moreover, asymmetrical substitution at the silicon center in addition to the intramolecular stabilization enables the possibility to generate chiral silyl cations whereby this system is also suitable for asymmetric catalysis.

Silyl borates were synthesized via hydride transfer reaction of the corresponding silanes with trityl borate $[\text{Ph}_3\text{C}][\text{B}(\text{C}_6\text{F}_5)_4]$. NMR and X-ray analysis as well as quantum mechanical calculations revealed remarkable structural differences between phenoxy- and thiophenyl-stabilized silyl cations. While the oxygen atom in silyloxonium ions shows a trigonal planar coordination sphere, the sulfur atom in silylsulfonium ions exhibits a trigonal pyramidal coordination sphere. Non-symmetrical substitution at the silicon atom leads to chirality at the silicon center and in addition to the trigonal pyramidal coordination sphere of the sulfur derivatives to the formation of *cis/trans* isomers.

To investigate the Lewis acidity of intramolecularly stabilized silyl cations, an NMR-based method for the assessment of the Lewis acidity using 4-fluorobenzonitrile as a probe was developed. This method is a useful tool in the design and fine-tuning of silyl Lewis acidic catalysts, since it allows the distinction between silyl cations stabilized by donor moieties of very similar donor capacities.

The catalytic activity of silyl borates was demonstrated in Diels-Alder cyclizations and hydrosilylation reactions of nitriles. While silyloxonium borates show a higher activity in Diels-Alder reactions as silylsulfonium ions, silylsulfonium ions are more active in hydrosilylation reactions of nitriles. The reason is their distinct Lewis acidity. Silyloxonium ions exhibit a higher Lewis acidity as silylsulfonium ions, which is important for a good performance in Diels-Alder reactions. However, in hydrosilylation reactions, this higher Lewis acidity is counterproductive, since the bond to the hydrosilylation product is strong and therefore the release of the product exhibits a higher barrier.

In summary, this work demonstrates how the design and fine tuning of Lewis acidic catalysts can be pursued and investigated.

Kurzzusammenfassung

Die Entwicklung Lewis-acider Katalysatoren ist in der organischen Synthese von aktuellem Interesse. Silylkationen besitzen eine hohe Lewis-Acidität und haben daher ein großes Potential als Katalysatoren in z. B. Diels-Alder-, Mukaiyama-Aldol- und Hydrosilylierungsreaktionen zum Einsatz zu kommen. In der vorliegenden Arbeit geht es um die Synthese und Charakterisierung von intramolekular phenoxy- und thiophenylstabilisierten Silylkationen. Als organisches Grundgerüst dient das Naphthyl- und das Acenaphthylgrundgerüst. Dieses fördert die Wechselwirkung zwischen dem Lewis-aciden Siliciumzentrum und dem Donorsubstituenten und unterstützt somit eine reversible Wechselwirkung des Siliciumzentrums mit Substraten, wodurch die katalytische Wirkung der Silylkationen maßgeblich geprägt wird. Ferner bietet asymmetrische Substitution der Silylgruppe die Möglichkeit chirale Silylkationen zu erzeugen, womit diese Spezies als Katalysator in der asymmetrischen Synthese geeignet ist.

Die Silylborate wurden durch Hydridtransferreaktion der entsprechenden Silane mit Tritylborat $[\text{Ph}_3\text{C}][\text{B}(\text{C}_6\text{F}_5)_4]$ synthetisiert. NMR- und Röntgenstrukturanalyse, sowie quantenmechanische Berechnungen ergaben bemerkenswerte strukturelle Unterschiede zwischen den phenoxy- und den thiophenylstabilisierten Silylkationen. Während das Sauerstoffatom in Silyloxoniumionen eine trigonal planare Koordinationssphäre aufweist, ist das Schwefelatom in Silylsulfoniumionen trigonal pyramidal koordiniert. Asymmetrische Substitution am Siliciumatom führt zusätzlich zur trigonal pyramidalen Koordination der Schwefelderivate zur Bildung von *cis/trans*-Isomeren.

Zur Untersuchung der Lewis-Acidität der intramolekular stabilisierten Silylkationen wurde eine NMR-basierte Methode zur Bestimmung der Lewis-Acidität unter Verwendung von 4-Fluorbenzonnitril als Sonde entwickelt. Diese Methode ermöglicht die Unterscheidung zwischen Silylkationen, die durch Donoreinheiten mit sehr ähnlichen Donorkapazitäten stabilisiert werden und ist somit ein nützliches Werkzeug für das Design von Lewis-aciden Katalysatoren.

Die katalytische Aktivität der Silylborate wurde anhand von Diels-Alder- und Hydrosilylierungsreaktionen von Nitrilen gezeigt. Während die Silyloxoniumionen bei Diels-Alder-Reaktionen eine höhere Aktivität als die Silylsulfoniumionen zeigen, sind die Silylsulfoniumionen bei Hydrosilylierungsreaktionen von Nitrilen aktiver. Der Grund ist, dass die Silyloxoniumionen eine höhere Lewis-Acidität als die Silylsulfoniumionen aufweisen, was sich positiv auf ihre Aktivität bei Diels-Alder-Reaktionen auswirkt. Bei Hydrosilylierungsreaktionen ist diese höhere Lewis-Acidität jedoch kontraproduktiv, da die Bindung an das Hydrosilylierungsprodukt zu stark ist und daher die Freisetzung des Produkts erschwert wird. Zusammenfassend zeigt diese Arbeit, wie die Feinabstimmung des Designs von Lewis-aciden Katalysatoren verfolgt und untersucht werden kann.

Table of Contents

1 Introduction	1
1.1 Silylium Ions	1
1.1.1 Stabilization Strategies for Silicon-Based Cations.....	2
1.1.2 Syntheses of Silyl Cations.....	6
1.2 Applications of Silyl Cations	7
1.2.1 Assessment of the Lewis Acidity	10
1.3 Chiral Silicon Compounds	12
1.3.1 Chiral Silyl Cations.....	14
2 Motivation and Objective	19
3 Results and Discussion	23
3.1 Acenaphthyl and Naphthyl Silanes	23
3.1.1 Syntheses	23
3.1.2 Comparison of Silanes.....	24
3.1.3 Chiral Resolution	25
3.1.3.1 Derivatization with an Auxiliary	26
3.1.3.2 Kinetic Resolution	33
a) Oxidation of the Thiophenyl Group	34
b) Dehydrogenative Si – O Coupling	37
3.1.3.3 Summary of the Chiral Resolution of Silanes.....	43
3.1.4 Crystal Structures of Acenaphthyl Silanes and Phenylmethylsilanol.....	46
3.2 Phenoxy- and Thiophenyl-Stabilized Silyl Cations – A Comparison of the Dimethylsilyl-Substituted Derivatives	55
3.2.1 Coordination Environment of the Oxygen Atom in Silyloxonium Ions	59
3.3 Asymmetrically Substituted Silyl Cations.....	67
3.3.1 Phenoxy-Stabilized Chiral Silyl Cations	67
3.3.2 Thiophenyl-Stabilized Chiral Silyl Cations	74
3.3.3 Chiral Memory	80
3.4 Chalcogenyl-Stabilized Hydridosilyl Cations	85
3.5 Dynamic Process of Sulfonium ions	93
3.6 Summary of Naphthyl- and Acenaphthyl-Substituted Silyloxonium and -sulfonium Borates....	103
3.7 Silylnitrilium Ions.....	108

3.8 Applications and Reactivity	120
3.8.1 Assessment of the Lewis Acidity	120
3.8.2 Reaction of Nitrilium Ions with a Si – H Source.....	128
3.8.3 Catalytic Activity of Silylchalconium Borates	135
3.8.3.1 Hydrosilylation Reaction of Nitriles.....	135
3.8.3.2 DFT Studies on the Mechanism of the Hydrosilylation Reaction of Nitriles	146
3.8.3.3 Diels Alder Reaction	161
4 Summary and Future Perspectives	166
5 Experimental Part.....	176
5.1 General Remarks	176
5.2 Syntheses of Starting Materials	178
5.2.1 Diaryl ethers	178
5.2.2 Bromo-Substituted Silyl Naphthalenes and Acenaphthenes	179
5.3 Syntheses of Naphthyl and Acenaphthyl Silanes	182
5.4 Chiral Resolution of Acenaphthyl Silanes.....	190
5.4.1 Pd-NP Catalyzed Dehydrogenative Si-O Coupling.....	190
5.4.2 Kinetic Resolution – Oxidation of Thiophenyl Group.....	194
5.4.3 Kinetic Resolution - Dehydrogenative Si-O Coupling	195
5.4.4 Reduction of Siloxanes	202
5.5 Synthesis of Silyl Borates.....	203
5.5.1 Chiral Memory Experiments	210
5.6 Syntheses of Silylnitrilium Borates.....	212
5.6.1 Assessment of the Lewis Acidity	222
5.7 Synthesis of Silyliminium Borates	223
5.8 Catalytic Reactions with Silyl Borates as Catalysts.....	228
5.8.1 Hydrosilylation Reaction	228
5.8.2 Diels-Alder Reaction (DAR).....	232
5.9 Calculation of the Free Gibbs Energy Barrier from VT NMR Data.....	235
6 Computational Details.....	236
7 Literature.....	238

1 Introduction

As one of the most abundant elements in the earth crust, silicon has a major impact on the modern world economy. Silicon dioxide and silicates are used in technical applications for example in steel refinement or as component of cement, mortar and stucco and for the production of glass.^[1] Furthermore, silicon's semiconductor properties are extremely important in the modern world. Semiconductor electronics are installed in computers, cell phones etc., whereby silicon became an essential part of modern technology. Not to forget its significant role as semiconductor in the development of photovoltaic solar panels, which is currently one of the key technologies in the combat against climate change.^[2]

Nevertheless, the chemical properties of silicon are not less important than its physical properties.^[3] Organosilicon compounds exhibit an exceptional potential to act as Lewis acidic catalyst and for the production of fine chemicals. Especially, cationic silicon compounds attracted a lot of attention in the last decades.^[4] However, the synthesis and rather the isolation of these very reactive silicon species is a major challenge in synthetic chemistry.^[5] The focus of this work is the development of positively charged silicon species in which their reactivity can be controlled and fine-tuned.^[6] Strategies for the generation and isolation of these reactive organosilicon compounds and especially approaches for the fine tuning of their reactivity as well as their applications will be discussed in this introduction.

1.1 Silylium Ions

In classical silylium ions, the silicon atom bears a positive charge, is tricoordinated and exhibits a trigonal planar coordination sphere. As such, they are isolobal to boranes and known as the heavier homologues of carbocations.^[7] Despite their close relation to carbocations, silylium ions were detected and recognized as reactive intermediates nearly 100 years later as their lighter congeners.^[8] The reason is their high reactivity. In contrast to carbon, silicon exhibits a lower electronegativity, whereby the positive charge in silylium ions is more localized at the silicon atom as in the corresponding carbocations. Furthermore, the atomic radius of the silicon atom is bigger than that of the carbon atom. As a consequence, the overlap of the orbitals of the silicon atom with those of the organic moieties is lower, and the positive charge is little delocalized by π -conjugation or hyperconjugation. Thus, silylium ions exhibit a very high Lewis acidity and react as strong electrophiles with any kind of nucleophiles. Their high Lewis acidity demands strategies of

stabilization to isolate silylium ions but it also shapes their reactivity and their potential to act as Lewis acidic catalyst in organic synthesis.^[7, 9]

1.1.1 Stabilization Strategies for Silicon-Based Cations

In the past 30 years, a comprehensive tool box of stabilization strategies for silylium ions and silyl cations has been explored and developed. In this section, a collection of important strategies is discussed on the basis of some selected examples.

An important step for a successful isolation of silyl cations is the choice of the right counter anion. Suitable examples are low coordinating anions, such as tetrakis(pentafluorophenyl)borate $[\text{B}(\text{C}_6\text{F}_5)_4]^-$ (TPFPB) (Figure 1), perhalogenated *closo*-dodecaborates $[\text{B}_{12}\text{X}_{12}]^{2-}$ ($\text{X} = \text{Cl}, \text{Br}$) (Figure 1), halogenated monocarba-*closo*-dodecaborates $[\text{RCB}_{11}\text{H}_{11-n}\text{X}_n]^-$ ($\text{R} = \text{H}, \text{alkyl}; \text{X} = \text{F}, \text{Cl}, \text{Br}, \text{I}; n = 6, 11$) or amine substituted *closo*-dodecaborates such as $[\text{Me}_3\text{NB}_{12}\text{Cl}_{11}]^-$ as well as halogenated alkoxy aluminates, e.g. $[\text{Al}(\text{OC}(\text{CF}_3)_3)_4]^-$ (Figure 1).^[9-10] These anions are characterized by their low nucleophilicity, whereby they do not interact with the majority of silyl cations. In routine procedures, TFPFB is generally the counter anion of choice.^[9]

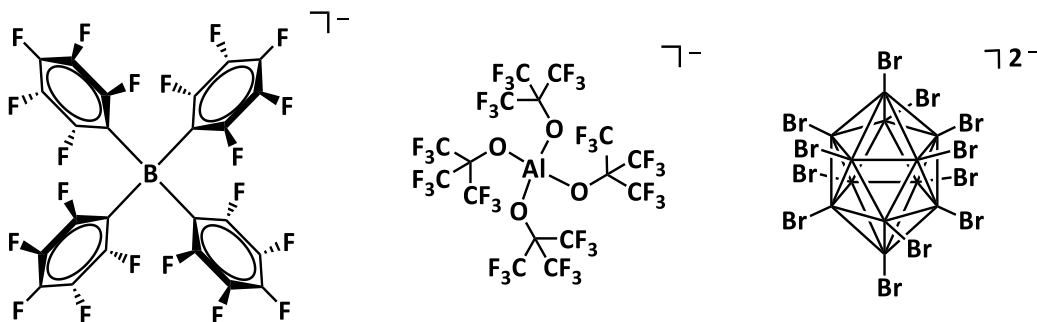


Figure 1 – Examples for low coordinating counter anions ($[\text{B}(\text{C}_6\text{F}_5)_4]^-$, $[\text{Al}(\text{OC}(\text{CF}_3)_3)_4]^-$ and $[\text{B}_{12}\text{X}_{12}]^{2-}$)

The stabilization of the positive charged silicon atom via aromatic solvents such as benzene and toluene or chlorobenzene is a common way to synthesize silyl cations. The silicon atom interacts with the solvent molecule by formation of arenium ions, or in case of chlorobenzene, under formation of chloronium ions (Figure 2).^[11] This stabilization strategy is convenient, since the synthesis can be directly carried out in these solvents. Using TFPFB as counter anion, a two-layer system is formed in toluene and benzene. The lower layer contains the obtained silyl borate in a high concentration, whereby its characterization via NMR spectroscopy is simple. At this point, it is important to have in mind that the coordination sphere of the silicon center in silyl arenium ions increases from the ideal

three in *silylium ions* to four and therefore the general term *silyl cation* is better suited for these kind of stabilized cationic silicon compounds.

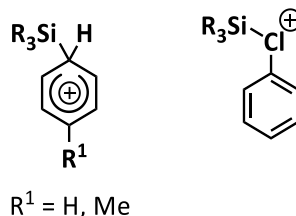
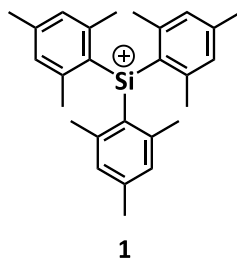


Figure 2 – Examples for solvent stabilized silyl cations (left: arenium ion, right: chloronium ion).

A major breakthrough in the research of silylium ions has been the synthesis and isolation of trimesitylsilylium carborate **1** [$HCB_{11}Me_5Br_6$], the first free, tricoordinated silylium ion which was characterized using X-ray diffraction analysis.^[8b, 12] In 2002, Reed and Lambert achieved this breakthrough using the effect of very bulky mesityl moieties to stabilize the highly reactive silicon center by steric shielding, whereby the positive charged silicon atom is protected sterically against the attack of nucleophiles. Trimesitylsilylium ion **1** is characterized by its trigonal planar coordination sphere and a ^{29}Si NMR chemical shift of $\delta^{29}Si = 225$.^[12] In contrast, solvent-stabilized silyl cations (Figure 2) exhibit a rather trigonal pyramidal coordination sphere and their ^{29}Si NMR chemical shifts are in the range of $\delta^{29}Si = 88-98$.^[9]



Another very effective way to stabilize silyl cations is the intramolecular stabilization. A nice example was reported in 2001 by Müller in his pioneering work about silyl borate **2** [$B(C_6F_5)_4$]. The silicon center is stabilized by a three-center two-electron Si – H – Si bridge (Figure 3). This structural motif was later adopted by R. Panisch, who synthesized naphthyl-substituted silyl borate **3** [$B(C_6F_5)_4$]. Despite their identical stabilization, the reactivity of these silyl cations **2** and **3** against nitriles differ from each other. While Müller's silyl cation **2** forms nitrilium ion **4**, Panisch's naphthyl silyl cation **3** forms iminium ion **5** (Figure 3). In addition, naphthyl derivative **3** is more stable and survives heating in toluene for several days whereas silyl cation **2** tends to decompose at room temperature.^[13] These distinctive properties emphasize the importance of the backbones used in terms of the reactivity and stability of such compounds.

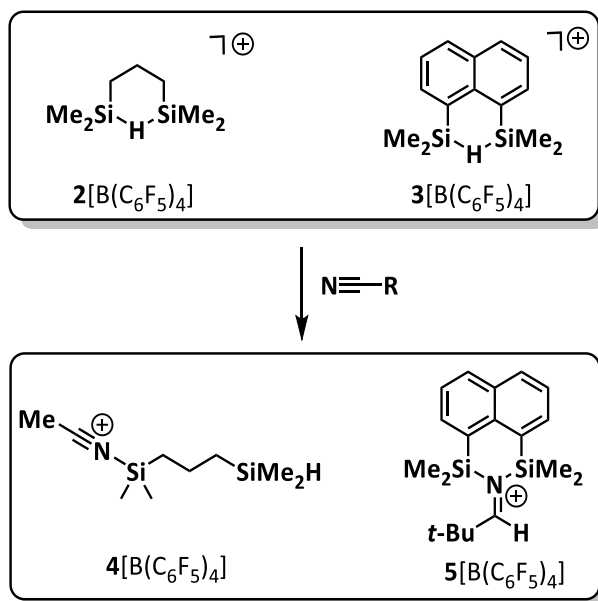


Figure 3 – Examples for Si – H – Si stabilized silyl borates and their reaction with nitriles.

Inspired by the results of R. Panisch, N. Kordts used the naphthyl scaffold as backbone and introduced a donor moiety in *peri*-position to the silyl group. This spacial proximity of a donor and an acceptor moiety in naphthyl compounds has precedents in the literature.^[14] As donor she decided to use chalcogenyl groups because chalcogen atoms are known to be weak electron donors. Doing so, a molecule is created which provides an available vacant acceptor orbital at the silyl group and a filled donor orbital (electron lone pair) at the chalcogenyl substituent.^[6a] The spatially close relation of acceptor and donor is a feature known from transition metals, which possess a vacant acceptor and a filled donor orbital within one atom (Figure 4). Due to this, transition metals are efficient catalysts in bond activation reactions of small molecules such as H₂ and CO₂. Even though this field has been dominated by transition metal species, many main group compounds such as frustrated Lewis pairs (FLPs) emerged in the past decades and showed, that they are able to activate small molecules as well.^[15] Using a remote donor substituent for the stabilization of a silylium ion enables the possibility to mimic the reactivity of transition metals compounds and FLPs, whereby these silyl cations are promising candidates to act in bond activation reactions.^[15e, 16]

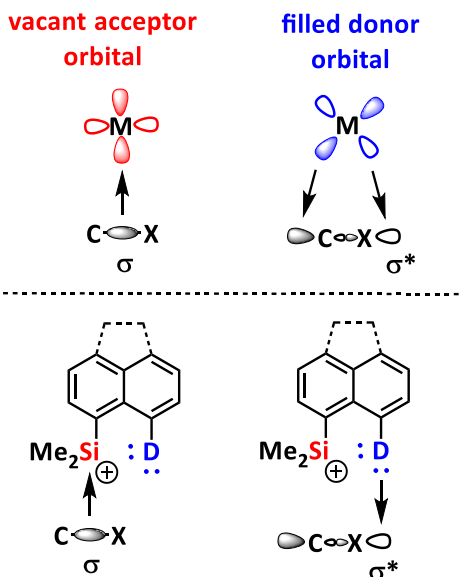


Figure 4 – Schematic illustration of the interaction of a vacant acceptor and a filled donor orbital of transition metals (M) with the σ and σ^* orbital of a C–X bond (X = C, H, N, O) and comparison to chalcogenyl stabilized silyl cations **6** (D = OPh, SPh, SePh, TcPh).

A further advantage using chalcogenyl substituents is manifested in the discrete donor ability of chalcogen atoms. Depending on the chalcogen used, the Lewis acidity of the silicon center is influenced differently and, in consequence, it can be fine-tuned by the chosen donor.^[6] The possibility of influencing and, thereby, controlling the Lewis acidity of the silicon center by the usage of different donors was shown by Siegel and co-workers. In their silyl cations **7**, they used the 2,6-diarylphenyl scaffold, whereby the stabilization takes place by lateral ring interactions. They found, that using an electron rich lateral arene substituent as in silyl cation **7a**, single $\eta^1 \pi$ coordination dominates, while in case of silyl cation **7b**, the fluorine silicon interaction dominates. The different substitution pattern leads to distinct Lewis acidities of these compounds, apparent by their ^{29}Si NMR resonances (Figure 5).^[17]

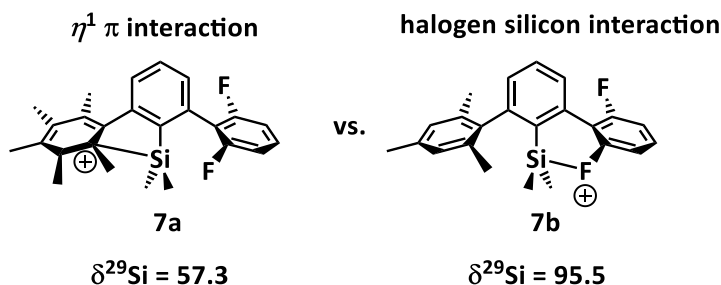
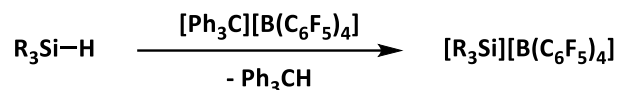


Figure 5 – Comparison of the ^{29}Si NMR chemical resonances of silyl cation **7a** stabilized via $\eta^1 \pi$ coordination and silyl cation **7b** stabilized via a fluoro substituent.

1.1.2 Syntheses of Silyl Cations

Since the quest for the generation and isolation of silylium ions started, various strategies for their synthesis have been developed. Here, a selection of the most common and convenient approaches will be discussed.

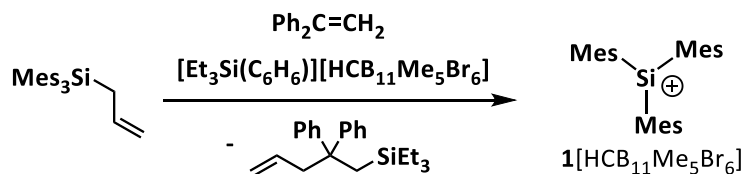
The most common way for generating silyl cations in condensed phase is the hydride transfer reaction by Corey.^[18] The corresponding hydrosilanes react with strong Lewis acids to give silyl cations and the corresponding hydrogenated Lewis acid. Mostly triphenylcarbenium (trityl) borate $[\text{Ph}_3\text{C}][\text{B}(\text{C}_6\text{F}_5)_4]$ is used as hydride acceptor (Scheme 1).



Scheme 1 – Synthesis of silyl borates via hydride transfer reaction of a hydrosilane with trityl borate.

The driving force of the hydride transfer reaction is defined by formation of a C – H bond which is stronger than the Si – H bond. Typical solvents for the Corey reaction are aromatic solvents such as benzene and toluene. In these solvents, purification of silyl borates with TFPFB as counter anion is straight forward due to the formation of a biphasic system with an ionic and a non-ionic layer. The non-ionic by-product triphenylmethane can be easily removed by washing the non-ionic layer with benzene or hexanes.^[9]

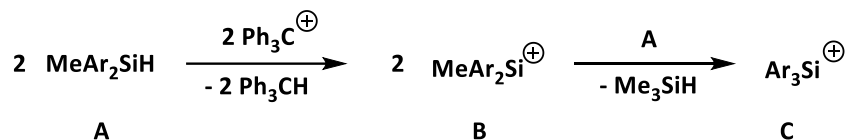
However, the Corey reaction is not suitable for the preparation of triarylsilylium ions due to the bulky substituents of the reactants. Trimesitylsilylium ion **1** was synthesised by the heterolytic cleavage of a Si – C bond (Scheme 2).^[12] This method requires very strong electrophiles such as carbocations or silyl arenium ions and a good leaving group at the silicon center. As leaving group usually an allyl substituent is used. As shown in Scheme 2, the leaving group is activated by the Lewis acid and reacts with 1,1-diphenylethylene to the by-product 1-allyl-1,1-diphenyl-2-(triethylsilyl)ethane and the product silylium carborate **1** $[\text{HCB}_{11}\text{Me}_5\text{Br}_6]$ is formed.^[8a, 9, 19]



Scheme 2 – Synthesis of trimesitylsilylium carborate **1** $[\text{HCB}_{11}\text{Me}_5\text{Br}_6]$ via heterolytic cleavage of a Si – C bond.

Another way to synthesize triarylsilylium ions was established by Müller and co-workers in 2011 (Scheme 3). In this reaction diaryl methylsilane **A** is treated with trityl cation wherein diarylmethylsilyl

cation **B** is formed as intermediate. Silyl cation **B** reacts directly with silane **A** in a substituent exchange reaction to form triarylsilyl cation **C** and by-product trimethylsilane (Scheme 3).^[9, 20]



Scheme 3 – Synthesis of triarylsilylium ions via substituent exchange reaction.

Recently, Oestreich and co-workers developed a new method for the synthesis of silyl cations via cleavage of Si – C(sp³) bonds using Reeds carborate acid [C₆H₇][HCB₁₁H₅Br₆]. This method allows the formation of anion-stabilized silyl cations directly from unfunctionalized precursors such as SiR₄ (R = Me, Et, *n*-Bu). Moreover, other substituents such as allyl, vinyl, benzyl and phenyl are also suitable leaving groups (Table 1). Due to this method, Oestreich and co-workers were able to obtain previously unavailable trimethylsilyl-substituted dimethylsilyl cation [Me₃Si-SiMe₂]⁺ (Table 1) and carborate-stabilized hydrogen-substituted silyl cations (see Chapter 3.4).^[21]

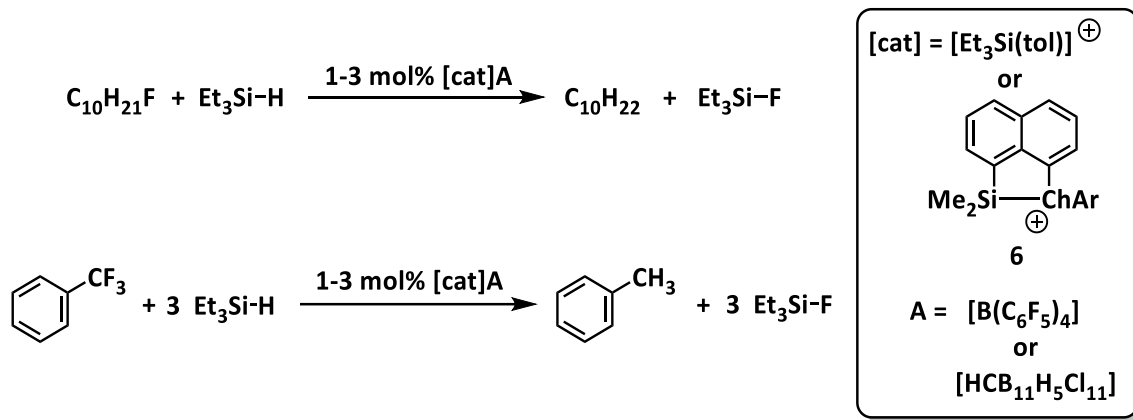
Table 1 – Synthesis of anion stabilized silyl cations via protonation with Reeds carborate acid.^[21]

$\text{SiR}_4 \xrightarrow[\text{- RH}]{[\text{C}_6\text{H}_6 \cdot \text{H}][\text{HCB}_{11}\text{H}_5\text{Br}_6]} [\text{SiR}_3][\text{HCB}_{11}\text{H}_5\text{Br}_6]$		
Silane	RH	Silyl Cation
R ₄ Si (R = Me, Et, <i>n</i> -Bu)	R-H (R = Me, Et, <i>n</i> -Bu)	R ₃ Si ⁺ (R = Me, Et, <i>n</i> -Bu)
<i>i</i> -Pr ₂ Me ₂ Si	Me-H	<i>i</i> -Pr ₂ MeSi ⁺
<i>t</i> -BuMe ₃ Si	Me-H	<i>t</i> -BuMe ₂ Si ⁺
(allyl)R ₃ Si (R = <i>i</i> -Pr, Me)	allyl-H	R ₃ Si ⁺ (R = <i>i</i> -Pr, Me)
(vinyl)Me ₃ Si	vinyl-H	Me ₃ Si ⁺
PhMe ₃ Si	Ph-H	Me ₃ Si ⁺
(PhCH ₂)Me ₃ Si	PhCH ₂ -H	Me ₃ Si ⁺
Me ₃ Si-SiMe ₃	Me-H	[Me ₃ Si-SiMe ₂] ⁺

1.2 Applications of Silyl Cations

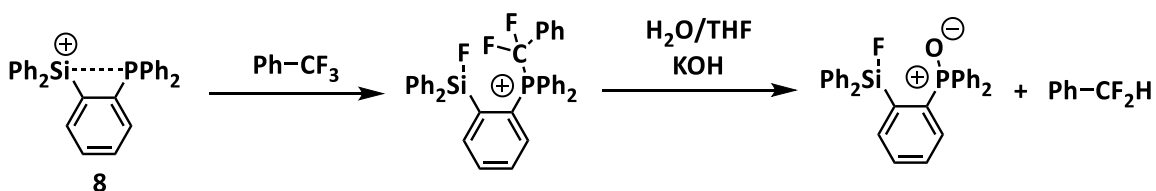
Due to their remarkable high Lewis acidity, silyl cations are potent reagents and catalysts in organic synthesis and catalytic processes.^[4] One of these processes is the hydrodefluorination (HDF) reaction. The transformation of a C – F bond in fluoroalkanes into a C – H bond is performed via the exchange of a fluoride by a hydride (Scheme 4). For this transformation a strong Lewis acid (LA) is required, since the activation barrier for the heterolytic cleavage of a C – F bond is high (bond dissociation energy BDE(C – F) = 500-545 kJmol⁻¹).^[22] Driving force for this reaction is the formation of a very strong

LA – F bond. Silyl Lewis acids exhibit this exceptional Lewis acidity required and have a very high fluorine ion affinity.^[23] First examples were reported by the groups of Ozerov^[24] and Müller^[6a, 13b, 25]. While Ozerov and co-workers used triethylsilyl cation as a catalyst, Müller and co-workers used initially their naphthyl-substituted Si – H – Si bridged cation^[13b] and showed later that chalcogenyl-stabilized silyl cations **6**^[6a] are also active in HDF reactions.



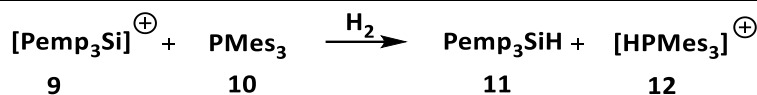
Scheme 4 – Hydrodefluorination reaction of decyl fluoride and trifluorotoluene catalyzed by silyl Lewis acids.

In 2017, Stephan and co-workers reported the stepwise hydrodefluorination reaction of trifluorotoluene using a stoichiometric amount of the frustrated Lewis pair **8** containing a silylium substituent and a phosphino moiety. In this reaction, selectively one C – F bond is activated, as shown in Scheme 5. The remaining two fluorine atoms can be substituted successively through two further mono-hydrodefluorination steps via the reaction of PhCF_2H and PhCFH_2 with FLP **8**. To date, other silyl cation-based hydrodefluorination reagents are not able to transfer selectively only one C – F bond of trifluorotoluene.^[22]

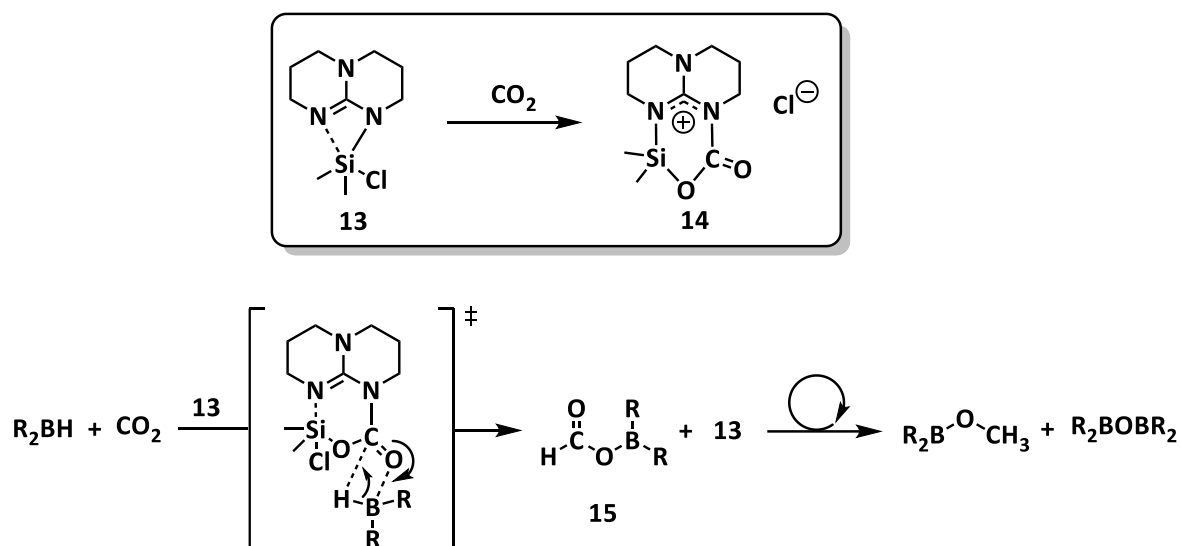


Scheme 5 – Activation of a C – F bond in trifluorotoluene by FLP **8**.^[22]

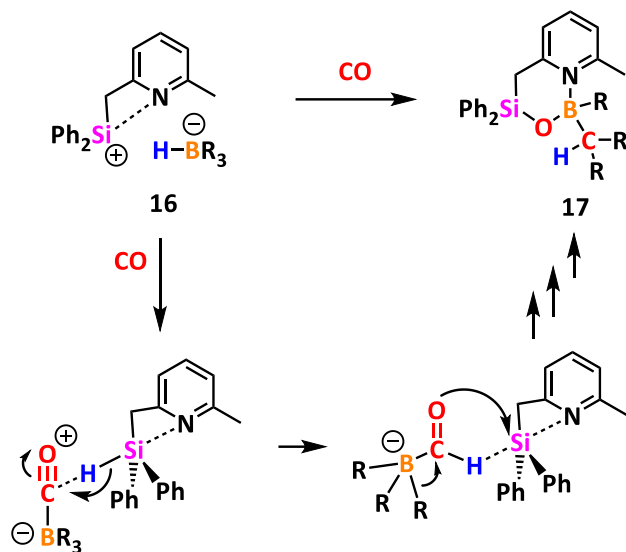
Silylium ion based FLPs are not only able to activate C – F bonds but also small molecules such as H_2 and CO_2 . For example, Müller and co-workers formed a FLP of tris(pentamethylphenyl)silylium borate **9** $[\text{B}(\text{C}_6\text{F}_5)_4]$ and trimesityl phosphane **10** and treated it with H_2 . In this reaction, silane **11** and phosphonium borate **12** $[\text{B}(\text{C}_6\text{F}_5)_4]$ were generated (Scheme 6).^[16] In following studies, A. Merk et al. found that the reaction proceeds via a single-electron transfer mechanism.^[26]

Scheme 6 – Activation of H₂ with a silylium ion based FLP.^[16]

The group of Cantat showed in 2016 that their nitrogen/silicon FLP **13** act as catalyst in the hydroboration reaction of CO₂. Their investigations revealed that the mechanism of this reaction proceeds via the FLP/CO₂ adduct **14** which was formed selectively by the insertion of CO₂ into the Si – N bond. Adduct **14** reacts with a hydroborane under formation of product **15** and reformation of catalyst **13** (Scheme 7).^[27]

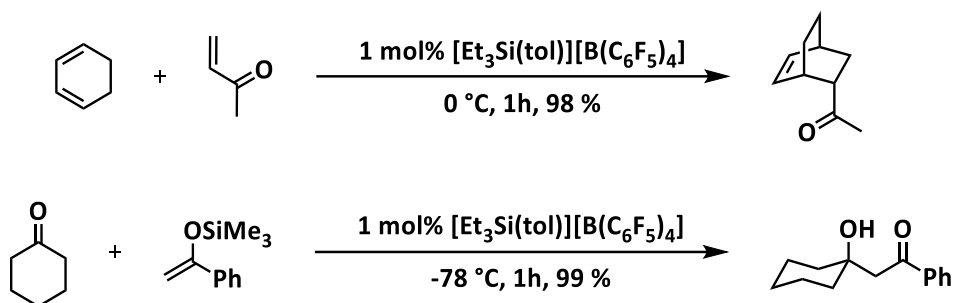
Scheme 7 – Activation of CO₂ by Si/N FLP **13** (above) and catalytic hydroboration of CO₂ with FLP **13** as catalyst.^[27]

In a similar vein, van der Vlugt and co-workers are able to activate CO with their pyridylsilyl hydroborate **16** [HB(C₆F₅)₃]. The reaction results in a complete cleavage of the CO triple bond and the formation of a C – H and two C – C bonds along with the formation of a Si – O – B unit (Scheme 8). The authors discussed the detailed mechanism of the formation of compound **17** on the basis of DFT calculations.^[4]



Scheme 8 – Proposed mechanism of the activation of CO via pyridyl substituted silyl hydro borate **16**[HB(C₆F₅)₃] (R = C₆F₅).^[4]

Other reactions in which silyl Lewis acids act as catalysts are the Diels-Alder cyclization and the Mukayama aldol condensation as shown for the first time in studies of toluene stabilized silyl borate [Et₃Si(tol)][B(C₆F₅)₄] (Scheme 9).^[28]



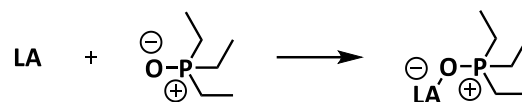
Scheme 9 – Toluene stabilized triethylsilyl cation as catalyst in a Diels Alder reaction (above) and a Mukayama aldol condensation (below).^[28]

Recent progress using silyl cations as catalysts in Diels-Alder reactions was achieved in particular by the group of Oestreich. They used ferrocenyl-stabilized silyl cations, as well as silylsulfonium ions (see Chapter 1.3.1).^[29]

1.2.1 Assessment of the Lewis Acidity

The reactivity and efficiency as a catalyst of silyl cations correlates with their Lewis acidity which depends on the substitution pattern of the silicon center and, more importantly, on the stabilizing environment. Therefore, a special interest on the development of tools for the comparison and quantification of their Lewis acidity has evolved. In the last decades, different methods and scales for

the assessment of the Lewis acidity of Lewis acids have been developed and established.^[30] These methods are based on the Lewis acid/base adduct formation with a Lewis base that serves as a probe. The most common example is the Gutmann-Beckett method. The Lewis acid (LA) of interest is treated with triethylphosphine oxide (Et₃PO) to form the corresponding LA/LB adduct (Scheme 10).^[31]



Scheme 10 – Formation of a Lewis acid/Et₃PO adduct to measure the Lewis acidity according to Gutmann Beckett.

The difference of the ³¹P NMR resonance of free Et₃PO and the Et₃PO/LA adduct serves as measure for the Lewis acidity. Figure 6 shows the $\Delta\delta^{31}\text{P}$ values of tris(pentafluorophenyl)borane (BCF), trimesitylsilylium ion **1** and borenium ion **18**.^[31]

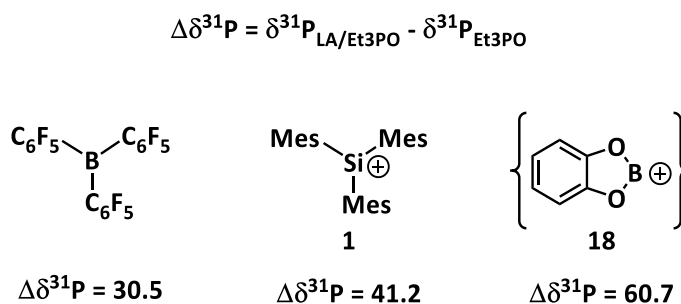


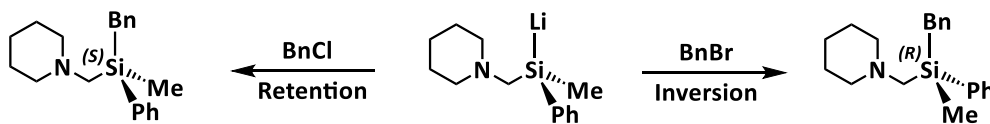
Figure 6 – Determination of the $\Delta\delta^{31}\text{P}$ value as measure for the Lewis acidity according to Gutmann-Beckett and the $\Delta\delta^{31}\text{P}$ values of three Lewis acids.^[31-32]

Another example is Childs method which relies on the ¹H NMR chemical shift change of the γ -H atom of crotonaldehyde upon coordination to a Lewis acid.^[33] This method is not suitable for silyl Lewis acids, since the silyl cation/croton aldehyde adduct tends to undergo follow-up reactions.^[32] A further method was developed by Hilt and co-workers. They use the ²H NMR chemical shift of the γ -deuterium atom of perdeuterated pyridine upon coordination to the Lewis acid to quantify the Lewis acidity.^[34] Both, the Hilt and the Gutmann-Beckett methods revealed the high Lewis acidity of silylium ions. However, they are not suitable for donor-stabilized silyl Lewis acid, since the interaction between the Lewis acidic silicon center and the probe is strong and, as a consequence, the silicon-donor interaction is cancelled.^[32, 34c, 35] The development of a new assessment method for intramolecularly stabilized silyl cations will be disclosed in Chapter 3.8.1.

1.3 Chiral Silicon Compounds

Asymmetric synthesis and catalysis are important for the production of natural products or medically relevant substances and form a part of every day's challenge in organic synthesis. Carbon-based chiral compounds are well-known and widely exploited. However, compounds with a silicon stereogenic center are not that well explored. Although, chiral silicon compounds have a high potential in various fields in chemistry. For example, they can be used as molecular model systems for studies on processes at solid-surfaces.^[36] Here, the introduction of chirality in mesoporous organosilicates seems to be a promising approach.^[37] Another field is the use of siloxide ligands in transition metal complexes, where they show a high potential due to their positive influence on the reactivity and the tolerance of functional groups of transition metal complexes which can be used as catalysts. An example is a molybdenum-based complex of the group of Fürstner, which can be used in metathesis reactions.^[38] Insertion of chiral siloxide ligands might open the possibility to use those catalysts in asymmetric reactions.^[39]

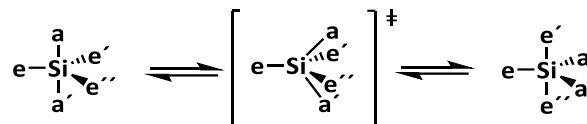
Another aspect is the use of compounds with a stereogenic silicon atom as chiral probes in the elucidation of reaction mechanisms as shown by the groups of Oestreich^[40] and Strohmann^[41]. For example, Strohmann and co-workers showed, that the reaction pathway of the reaction between silyl lithium compounds with benzyl halides proceeds either through a S_N2 mechanism with the silicon atom acting as nucleophile or through a halogen-lithium exchange reaction with subsequent nucleophilic attack of the carbanion to the silicon center. Which of the two mechanisms takes place depends on the benzyl halide used (Scheme 11). Using benzyl bromide, inversion of the configuration at the silicon atom indicates that the reaction proceeds via halogen-lithium exchange with subsequent nucleophilic attack of the formed carbanion, while retention of configuration at the silicon atom occurs using benzyl chloride, indicating the S_N2 pathway in which the silicon compound acts as nucleophile.^[41]



Scheme 11 – Reaction of a silyl lithium compound with benzyl halides: inversion of configuration at the silicon atom with benzyl bromide and retention of configuration at the silicon atom with benzyl chloride.^[41]

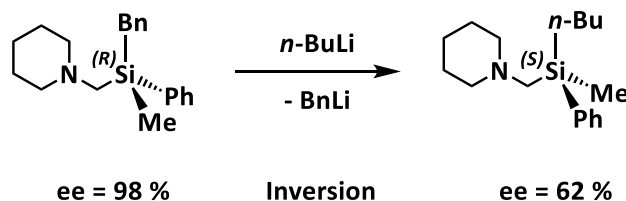
Nevertheless, the full potential of chiral silicon compounds is not exploited yet because of one vast challenge which is caused by the capacity of the silicon atom to form stable pentavalent intermediates. These pentavalent intermediates tend to undergo dynamic processes like the Berry

pseudo rotation (BPR, Scheme 12), which leads in case of stereogenic silicon centers to the loss of the stereo information.^[42]



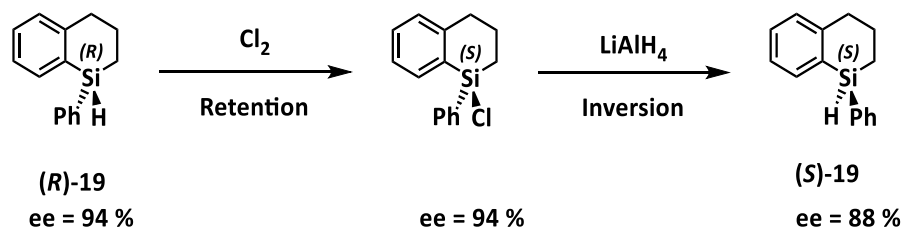
Scheme 12 – Berry pseudo rotation at a pentacoordinated silicon center.

But how can BPR and the accompanying loss of chiral information be avoided? Basically, two strategies can be pursued on the basis of a kinetically controlled reaction. The use of substituents with rather low electronegativities, such as alkyl or aryl moieties, suppresses the formation of stable pentavalent intermediates. In consequence, the transformations are determined by the nature of the nucleophile and its way to interact with the stereogenic silicon center. An example is provided by Strohmann and co-workers, who investigated the selective Si – C(sp³) bond cleavage using carbanionic nucleophiles (Scheme 13).^[43]



Scheme 13 – Nucleophilic substitution at chiral silicon compound via Si – C(sp³) bond cleavage.^[43]

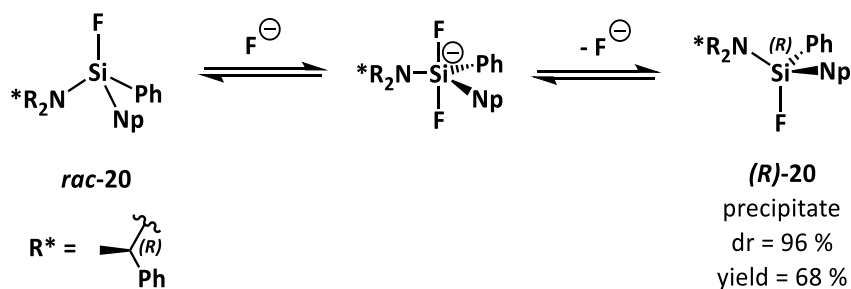
Furthermore, embedding of the chiral silicon center into a ring system can provide a certain stereogenic stability. Hereby, chiral integrity is based on the formation of extreme unfavorable conformers during BPR, since interchange of the substituents leads to high ring strain. Oestreich and co-workers showed via chlorination and subsequent reduction of silane **19** that the ring system leads to a good stereo control of this reaction (Scheme 14).^[44]



Scheme 14 – Chlorination and subsequent reduction of silane **19**.^[44]

In contrast, if BPR is evoked purposely, it can be used for enantiomeric enrichment of the chiral compound in a thermodynamical manner. Hereby, substituents with a high electronegativity are

required which leads to stable pentavalent intermediates. In these intermediates, BPR leads, often in combination with a chiral backbone, to the formation of the thermodynamically favored diastereomer. As a result, enrichment of one diastereomer via epimerization is possible.^[45] An example was provided in 1999 by Tamao and co-workers, who showed that fluorosilane **20** undergoes epimerization by treatment with a catalytic amount of AgF in acetonitrile, whereby (*R*)-fluorosilane (*R*)-**20** precipitates (Scheme 15).^[45a]

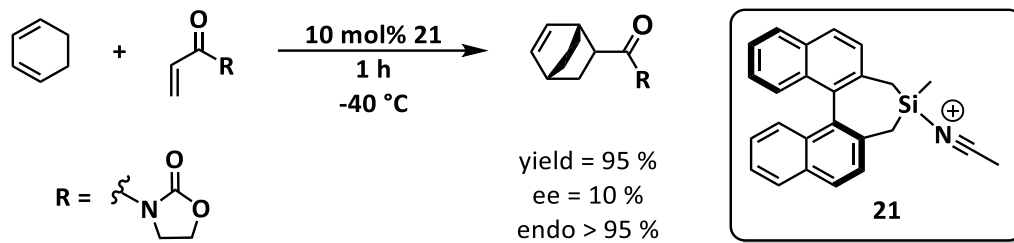


Scheme 15 – Optical resolution of racemic fluorosilane **20** via epimerization (reaction conditions: 5 mol% AgF, CH₃CN, r.t., 24 h).^[45a]

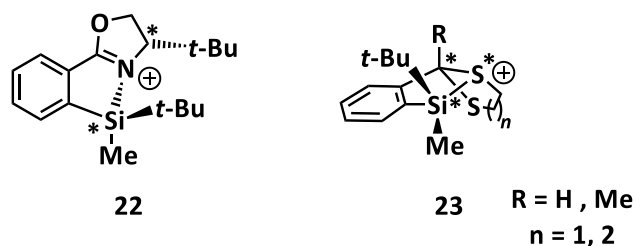
1.3.1 Chiral Silyl Cations

In general, there are two possibilities to introduce chirality in silyl cations. The first possibility is via a chiral backbone such as the binaphthyl substituent which exhibits axial chirality. The other possibility is to generate chirality directly at the silicon atom. This is only feasible if the silicon center is inter- or intramolecularly stabilized. The coordination number of the silicon center is expanded from the ideal tri- to tetracoordination. If the silicon center bears four different substituents, it becomes a chiral center. In this chapter, different representatives of chiral silyl cations are presented.

In 1998, researchers around Jørgensen and Helmchen were the first who reported on chiral silicon cations. They performed the synthesis of silyl nitrilium ion **21** with the binaphthyl backbone.^[46] Here, chirality is exclusively introduced via the axial chirality of the backbone, whereby the silicon center remains achiral. They used silylnitrilium ion **21** in the Diels-Alder reaction shown in Scheme 16 and achieved a certain asymmetric induction with ee = 10 % of the Diels-Alder product.^[46a]

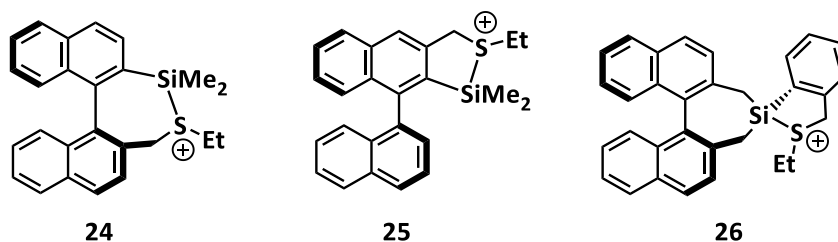
Scheme 16 – Asymmetric Diels-Alder reaction catalyzed by silylnitrilium ion **21**.^[46a]

Oestreich and co-workers reported their first chiral silyl cations in 2014 with oxazoline-stabilized silyl cation **22** and thionyl-stabilized silyl cation **23**, which are synthesized through the standard Corey protocol from the corresponding hydrosilanes. These compounds exhibit two to three chiral centers and the positively charged silicon atom is one of these centers.



Regarding oxazoline-stabilized silyl cation **22**, Oestreich and co-workers unambiguously showed, that the stabilization occurs exclusively via the nitrogen atom, even though the oxygen atom is a potential donor for the stabilization as well. Hereby, a small preference for the formation of one diastereomer was observed after ionization. Addition of one equivalent acetonitrile led to diastereomeric enrichment via epimerization. Oxazoline-stabilized derivative **22** showed no activity as catalyst in Diels-Alder reactions. In contrast, formation of thionyl-stabilized silyl cation **23** occurred directly in a stereoselective manner and it showed a good catalytic activity in Diels-Alder test reactions.^[29b]

Inspired by their results of chiral silylsulfonium ions **23**, Oestreich and co-workers merged their findings with the idea of Jørgensen and Helmchen, who used the binaphthyl backbone. The result is the synthesis of species **24**, **25** and **26**. In asymmetric Diels-Alder reactions, all derivatives **24**, **25** and **26** showed a good catalytic activity, but using species **24** and **25** as catalysts, no enantiomeric enrichment of the Diels-Alder product was obtained. Only using species **26** as an catalyst, the Diels Alder product was obtained with an ee of 11 %.^[29c]



Thereupon, P. Shaykhutdinova pursued this strategy and introduced the binaphthyl backbone as bridge between the silicon and the sulfur atom, what led to better results for the stereinduction of silylsulfonium ion **27a** in asymmetric Diels-Alder reactions (Figure 7).

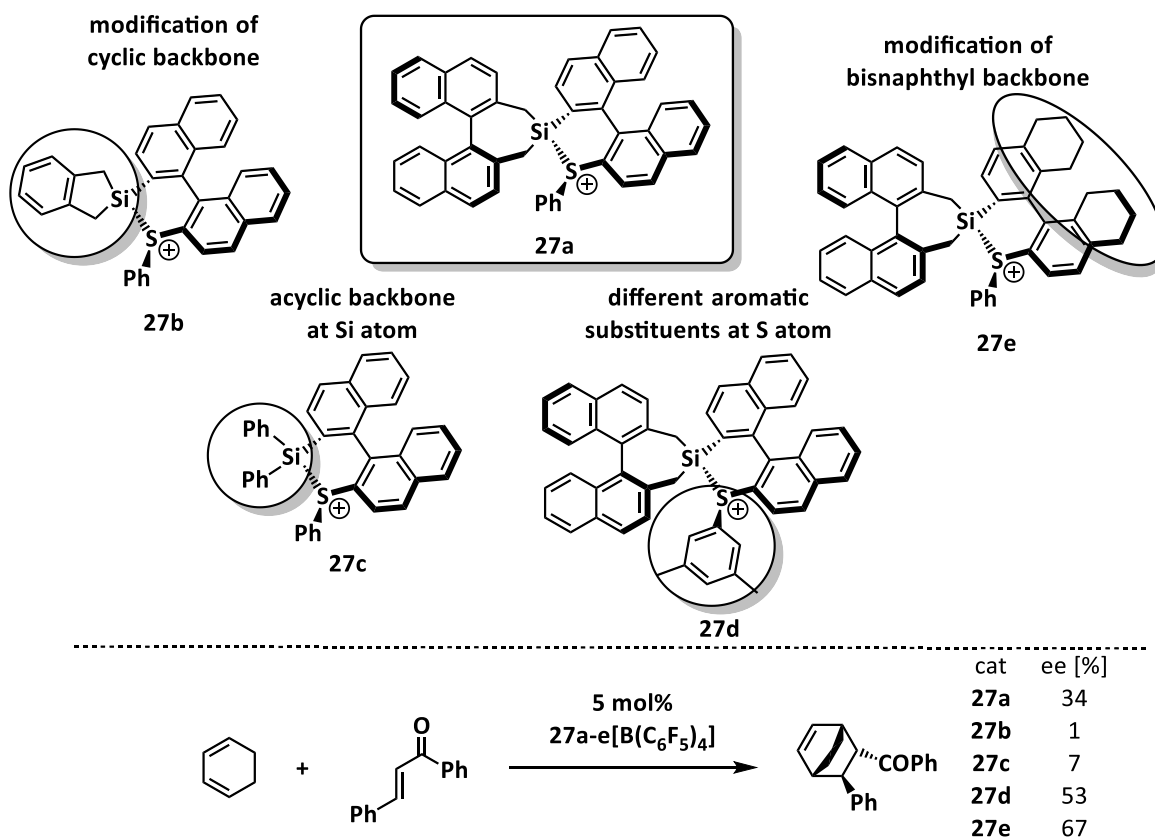
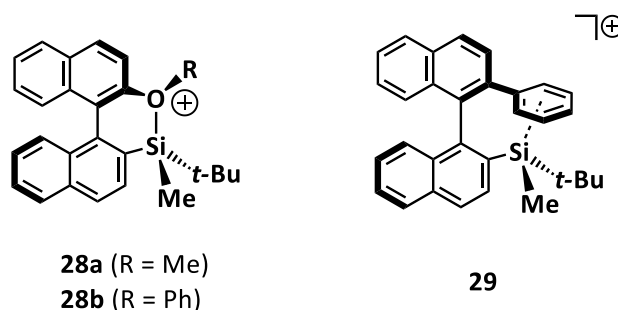


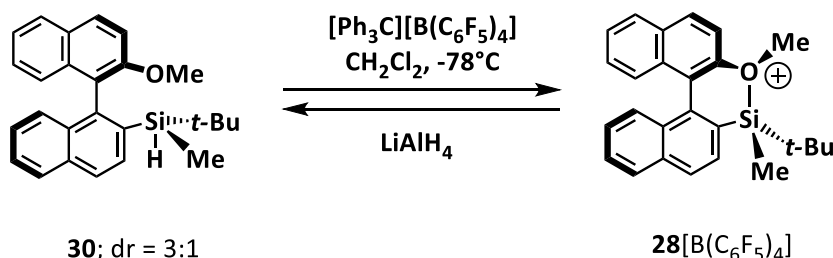
Figure 7 – Some representatives of chiral silylsulfonium ions **27** and their stereoinductive performance as a chiral catalyst in an example for a asymmetric Diels-Alder reaction.^[29e]

In her studies, she successively modified the substitution pattern at the silicon atom (as in **27b,c**), the aryl substituent at the sulfur atom (as in **27d**) and even modified the silicon sulfur bridging binaphthyl backbone (as in **27e**) to investigate the influence of these modification on the stereoinductive performance of chiral silyl Lewis acids in Diels-Alder cyclizations. Hereby, silylsulfonium ion **27e** showed the best results in the stereinduction with an enantiomeric excess of the Diels-Alder product of ee = 67 %.^[29d-g]

In all these examples, chiral induction is induced by the chiral backbone and the chiral sulfur atom but the silicon atom does not bear chirality. Chiral silyl Lewis acids with a chirality center at the silicon atom and a chiral backbone were reported by Landais and co-workers. They studied the chiral integrity of silyl cations **28** and **29** which are also based on the binaphthyl backbone and stabilized via a remote oxygen-based substituent or phenyl group.^[45d]



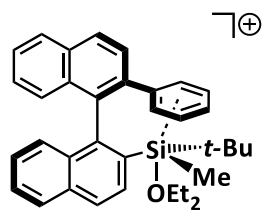
Their studies showed, that silyloxonium ions **28** can be generated from the corresponding hydrosilanes **30** using the standard Corey protocol. After addition of lithium aluminiumhydride, they were able to regenerate the corresponding silane **30** (Scheme 17). When the procedure is carried out at low temperature (-78 °C), the diastereomeric ratio of the corresponding silanes **30** does not change after the process, indicating that the overall reaction takes place under retention of the configuration at the silicon atom.^[45d]



Scheme 17 – Hydride transfer reaction of silane **30** to form silyl borate **28**[B(C₆F₅)₄] and its subsequent reduction, revealing chiral integrity at the silicon atom during the process.^[45d]

Interestingly, in contrast to the work of Müller and co-workers,^[6a] silyloxonium ion **28** exhibits an oxygen atom with a trigonal pyramidal coordination environment. This point will be further discussed in Chapter 3.2.1.

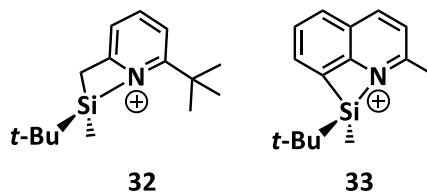
Aryl-stabilized silyl cation **29** is less stable than silyloxonium ion **28** and was stabilized via addition of one equivalent diethylether and characterized as silyloxonium ion **31**.



31

The addition of an external donor leads in both species **28** and **29** to epimerization, whereby a diastereomeric enrichment of silyloxonium ion **28** and a diminishment of the diastereomeric ratio of aryl-stabilized species **29** was observed. These observations led to the conclusion, that the interaction between the silicon center and a donor with an electron lone pair is much stronger than the Si – π -interaction. This conclusion is an important fact for the design of donor-stabilized chiral silyl cations.^[45d]

Landais and co-workers are currently pursuing their investigations regarding the chiral memory of intramolecularly stabilized silyl cations using pyridyl- and quinoline-stabilized silyl cations **32** and **33**. Here, they intentionally pose the question, which impact the chiral backbone, namely the binaphthyl scaffold, has on the chiral memory by using achiral backbones.^[47] The results of these studies will be further discussed in Chapter 3.3.3.

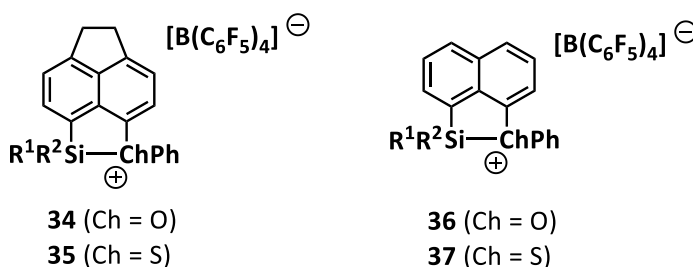


32

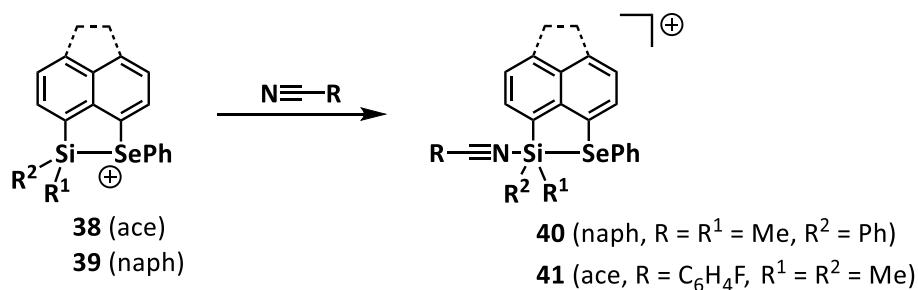
33

2 Motivation and Objective

The development of Lewis acidic catalysts is of current interest in organic synthesis.^[48] Due to their high Lewis acidity, silyl cations show a conspicuous capability to act as catalysts in e.g. hydrodefluorination, Diels-Alder and Mukaiyama aldol reactions.^[4] The present studies focus on the synthesis and characterization of intramolecularly phenoxy- and thiophenyl-stabilized silyl borates **34-37**[B(C₆F₅)₄] with the acenaphthyl or naphthyl scaffold as backbone. The Lewis acidity of the silicon center is defined by the intramolecular interaction with the donor substituent (OPh or SPh). The discrete donor abilities of the chalcogenyl substituents control the reactivity of the resulting silyl cations **34-37** and enable the fine-tuning of their reactivity.

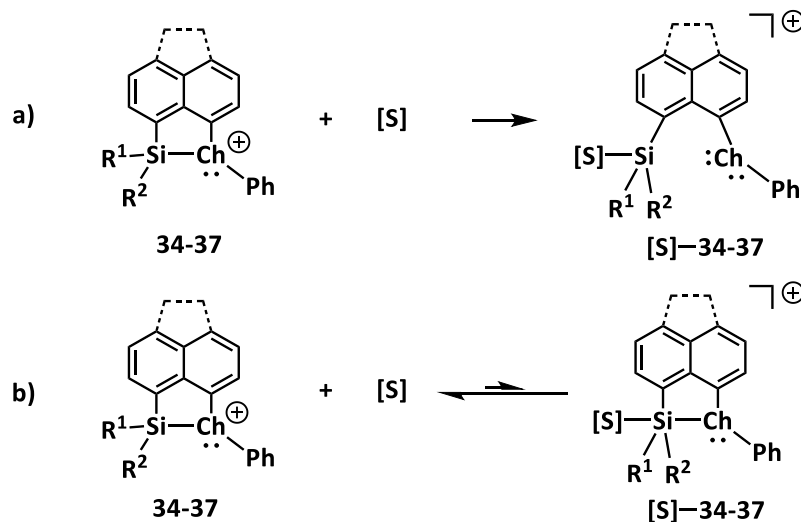


The characterization of silyl borates **34-37**[B(C₆F₅)₄] will include the assessment of their Lewis acidity. As described in the introduction, there is a lack of suitable probes especially for intramolecularly stabilized Lewis acids. Therefore, to investigate the Lewis acidity of silyl cations **34-37**, an NMR-based method shall be developed and evaluated. 4-Fluorobenzonitrile (FBN) seems to be a promising probe because of two facts. Firstly, nitriles are weak electron donors and known to form stable adducts with silyl cations. Previous studies showed, that intramolecularly selenyl-stabilized silyl cations **38** and **39** react with nitriles to form pentacoordinated silicon species **40** and **41** and that the interaction with the donor moiety, here the selenyl substituent, is retained upon coordination of a nitrile (Scheme 18). Secondly, the fluoro substituent at FBN allows the monitoring using ¹⁹F NMR spectroscopy. In addition, quantum mechanical calculations will be performed to investigate the properties of silyl cations **34-37**.



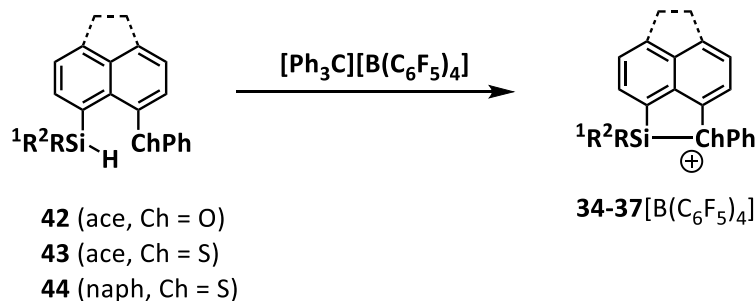
Scheme 18 – Formation of nitrilium ions **40** and **41** from the corresponding silyl cations **38** and **39** (anion $[\text{B}(\text{C}_6\text{F}_5)_4]$ omitted for clarity).

The cyclic arrangement of silyl cations **34-37** is an important feature for their catalytic activity. On the one hand, the naphthyl/acenaphthyl backbone supports the interaction of the silicon center with the chalcogen atom. This is important for the reversibility of the reactions of silyl cations **34-37** with substrates **[S]**. If the interaction between the silicon center and the substrate/product is too strong, a stable intermediate **[S]-34-37** is formed and silyl cations **34-37** will not be regenerated as the catalyst of the reaction (Scheme 19, a)). On the other hand, the integrity of the backbone pulls the silicon and the chalcogen atoms to a certain extent apart and, thereby, prevents an interaction between the two atoms which is too strong. If the silicon/chalcogen interaction would be too strong, an interaction of silyl cations **34-37** with a substrate **[S]** might not be possible and the intermediate **[S]-34-37** will not be formed (Scheme 19, b)). A good balance between a too weak and a too strong Si/Ch interaction makes silyl cations **34-37** to promising Lewis acidic catalysts.



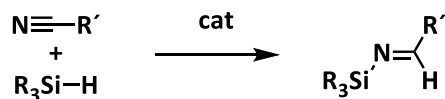
Scheme 19 – a) Irreversible reaction of silyl cations **34-37** with a substrate **[S]** to form intermediate **[S]-34-37** as a result of a too weak Si/Ch interaction; b) nearly no interaction between silyl cations **34-37** and the substrate **[S]** as a result of a too strong Si/Ch interaction and the reaction equilibrium shifted in favor of the educts **34-37** and **[S]**.

To achieve the synthesis of silyl borates **34-37**[B(C₆F₅)₄] (Scheme 20), the synthesis of a variety of precursor silanes **42-44** with different substitution patterns (R¹ = R² = Me (**a**); R¹ = Me, R² = Ph (**b**); R¹ = Me, R² = *t*-Bu (**c**); R¹ = H, R² = Ph (**d**)) will be accomplished. In the context of catalysis in organic chemistry, a pronounced interest in the development of enantioselective catalysts has evolved.^[48-49] Therefore, the synthesis of asymmetrically substituted silanes **42b,c**; **43b,c**, **44b** and their chiral resolution are of special interest to generate chiral silyl borates **34-37**[B(C₆F₅)₄] which are promising candidates to act as catalysts in asymmetrical Diels-Alder cyclizations.



Scheme 20 – Synthesis of silylchalconium borates **34-37**[B(C₆F₅)₄] via the Corey protocol (R¹ = R² = Me (**a**); R¹ = Me, R² = Ph (**b**); R¹ = Me, R² = *t*-Bu (**c**); R¹ = H, R² = Ph (**d**)).

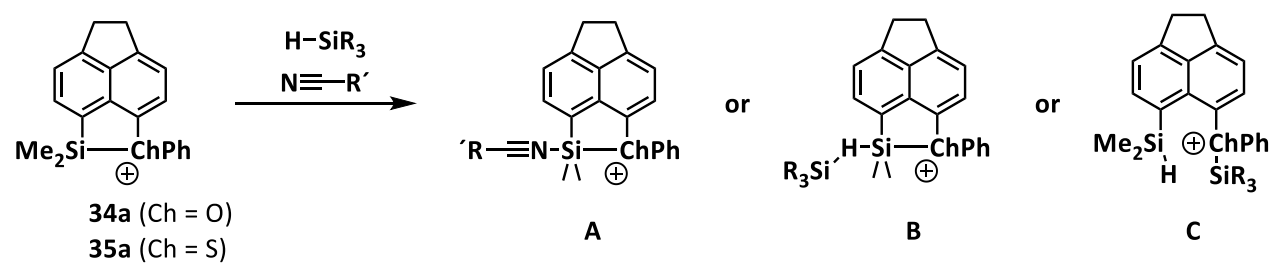
Another field of interest for industry and medicinal chemistry is the synthesis of silicon-containing compounds and materials. A convenient way to synthesize silicon-containing compounds is by the hydrosilylation reaction of unsaturated substrates such as ketones, alkenes, imines and nitriles.^[50] Especially silylated imines, products of the hydrosilylation reaction of nitriles, are important compounds and intermediates in pharmaceutical industry.^[50b, 51] Therefore, another catalytic reaction which will be focused on, is the hydrosilylation reaction of nitriles (Scheme 21).



Scheme 21 – Hydrosilylation reaction of a nitrile.

The investigation of the reaction mechanism will provide further insight on the reactivity of silylchalconium ions **34** and **35**. In general, there are two possible ways of how silyl cations **34** and **35** interact with the substrates, namely the nitrile and the hydrosilane (Scheme 22). Firstly, as a classical Lewis acid to form a LA/LB adduct **A** with the nitrile or to form a Si – H – Si bridge **B** with the hydrosilane. Secondly, due to their amphiphilic character, chalcogenyl-stabilized silyl cations **34a** and

35a are able to activate the Si – H bond of the hydrosilane in a transition metal-like manner as shown in intermediate **C**.



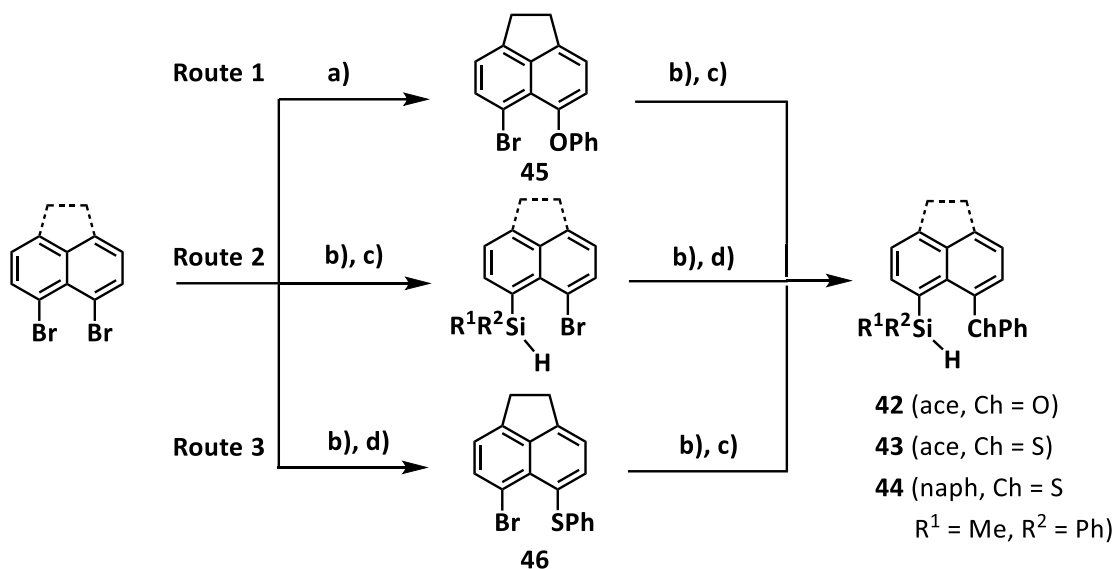
Scheme 22 – Possible intermediates **A**, **B** or **C** in the hydrosilylation reaction of nitriles using silyl cations **34a** or **35a** as catalysts.

3 Results and Discussion

3.1 Acenaphthyl and Naphthyl Silanes

3.1.1 Syntheses

Phenoxy-substituted derivatives **42** were synthesized starting from 5,6-dibromoacenaphthene and sodium phenolate to generate phenyl acenaphthyl ether **45** by an Ullmann-type reaction in a good isolated yield of 75 %. Diaryl ether **45** was converted to silanes **42** by a metalation/salt metathesis sequence using the corresponding chlorosilane as electrophile (Scheme 23, Route 1). The isolated yields for dimethyl-, phenylmethyl- and phenyl-substituted derivatives **42a,b,d** are good (65-78%), whereby *tert*-butyl-substituted derivative **42c** was obtained in a rather moderate yield of 39 %. A reason for the lower yield might be the higher steric demand of the *tert*-butyl substituent in comparison to the methyl or phenyl moieties.



Scheme 23 – Syntheses of silanes **42**, **43** and **44** ($R^1 = R^2 = \text{Me}$ (a); $R^1 = \text{Me}, R^2 = \text{Ph}$ (b); $R^1 = \text{Me}, R^2 = t\text{-Bu}$ (c); $R^1 = \text{H}, R^2 = \text{Ph}$ (d)): a) 1 equiv. PhONa, 0.5 equiv. Cu_2O , diglyme, 160 °C; b) 1 equiv. *n*-BuLi, THF, -80 °C; c) 1 equiv. RMeSiHCl or PhSiH_2Cl , THF, -80 °C, $R = \text{Me}, \text{Ph}, t\text{-Bu}$; d) 1 equiv. PhSSPh, THF, -80 °C.

The synthesis of thiophenyl-substituted derivatives **43** and **44** is realized by two subsequent metalation/salt metathesis sequences starting from 5,6-dibromoacenaphthene or 1,8-dibromonaphthalene. Hereby, it is possible that first the silyl group and second the thiophenyl substituent is installed (Scheme 23, Route 2)^[6a] or vice versa (Scheme 23, Route 3). For this work, the latter route turned out to be more convenient, since the substituents at the silicon center should be altered. Herein, the diaryl thioether **46** was obtained in a yield of 80 %. The yields of silanes **43a,b,c**

and **44** are in general good, too (65-96%). However, as observed with the phenoxy-substituted derivative **42c**, the corresponding thiophenyl-substituted *tert*-butylmethylsilane **43c** was obtained in a yield of 30 %.

3.1.2 Comparison of Silanes

All synthesized silanes **42-44** are unknown to literature and were fully characterized by multinuclear NMR and IR spectroscopy as well as using high-resolution mass spectrometry and elemental analysis. The NMR and IR data are summarized in Table 2. Silanes **42-44** show the expected ^1H NMR chemical shift for the hydrogen atoms which are attached to the silicon atom in the range from $\delta^1\text{H} = 4.95$ to 5.89 and the corresponding ^{29}Si NMR chemical shifts are between $\delta^{29}\text{Si} = 1.3$ and -31.3 . Here, it is noticeable that the ^{29}Si NMR chemical shifts of dimethyl- and methylphenyl-substituted derivatives **42a,b**, **43a,b** and **44** with $\delta^{29}\text{Si} = -13.5$ to -17.7 are distinct high field shifted in comparison to the *tert*-butyl-substituted derivatives **42c** and **43c** ($\delta^{29}\text{Si} = 1.3$ to -3.2).

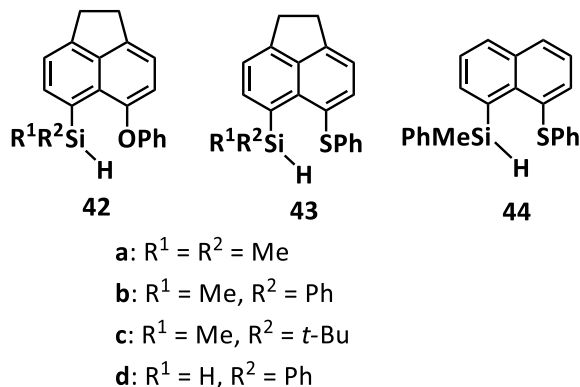


Table 2 – Selected NMR and IR spectroscopic parameters of the silanes **42-44** (for NMR C_6D_6 , r.t., and IR ATR).

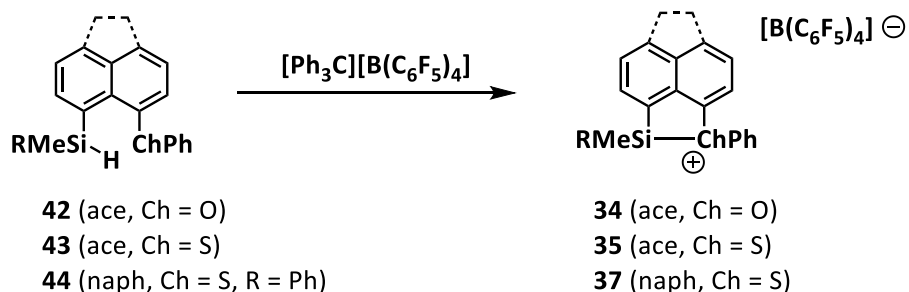
Silane	$\delta^1\text{H}$	$\delta^1\text{H Me}$	$\delta^{29}\text{Si}$	$^1J_{\text{H,Si}}$	$^3J_{\text{H,Si}}$	$\delta^{13}\text{C}$	$\tilde{\nu} (\text{Si-H}) [\text{cm}^{-1}]$
42a	5.20	0.70	-13.5	191.1	3.7	-1.5	2097, 2142
42b	5.63	0.84	-14.7	196.2	3.7	-2.9	2096, 2136
42c	4.95	0.56	1.3	192.9	3.8	-4.8	2090, 2151
42d	5.61	-	-30.7	201.8	-	-	2117
43a	5.39	0.63	-17.7	189.4	3.5	0.2	2106
43b	5.89	0.88	-17.2	202.8	3.6	-1.0	2091
44	5.83	0.85	-16.9	203.0	3.5	-0.5	2144
43c	5.41	0.54	-3.2	200.2	3.7	-3.3	2175
43d	5.80	-	-31.3	203.8	-	-	2088, 2151

This effect of the *tert*-butyl moiety to the ^{29}Si NMR resonance was found in the literature. One example is the ferrocenyl-substituted *tert*-butylmethylsilane of Oestreich and co-workers, which exhibits a ^{29}Si NMR chemical shift of $\delta^{29}\text{Si} = -2.8$.^[29a] Another example is *tert*-butylmethylphenylsilane,

described by Larson and Torres, which has a ^{29}Si NMR chemical shift of $\delta^{29}\text{Si} = -1.3$, whereas cyclohexylmethylphenylsilane exhibits a ^{29}Si NMR resonance of $\delta^{29}\text{Si} = -9.0$.^[52] Furthermore, the ^{29}Si NMR chemical shifts of the dihydrosilanes **42d** and **43d** with $\delta^{29}\text{Si} = -30.7$ to -31.3 are even more high-field shifted than the dimethyl- and methylphenyl-substituted derivatives **42a,b**, **43a,b** and **44** what is in the expected range of secondary silanes.^[53] The Si-H coupling constants are in the expected range of $^1J_{\text{H,Si}} = 189$ to 203 Hz. And the IR absorption bands for the Si-H stretching vibration of all silanes **42-44** are in the expected range of 2088 - 2151 cm^{-1} . Hereby it is noteworthy, that silanes **42a,b,c** and **43d** show two IR bands due to Fermi-resonance.^[54] So far, it could not be determined which of the two bands is the underlying fundamental vibration.

3.1.3 Chiral Resolution

Due to the asymmetric substitution of silanes **42b,c**, **43b,c** and **44**, the silicon atom is a stereogenic center. Hydrosilanes are precursors of silyl borates. The chirality of silanes **42b,c**, **43b,c** and **44** enables the possibility to generate the corresponding chiral silyl borates **34b,c**[$\text{B}(\text{C}_6\text{F}_5)_4$], **35b,c**[$\text{B}(\text{C}_6\text{F}_5)_4$] and **37b**[$\text{B}(\text{C}_6\text{F}_5)_4$] (Scheme 24). However, silanes **42b,c**, **43b,c** and **44** are obtained as racemic mixtures and their chiral resolution has to be realized in order to generate enantiomerically enriched silyl borates.



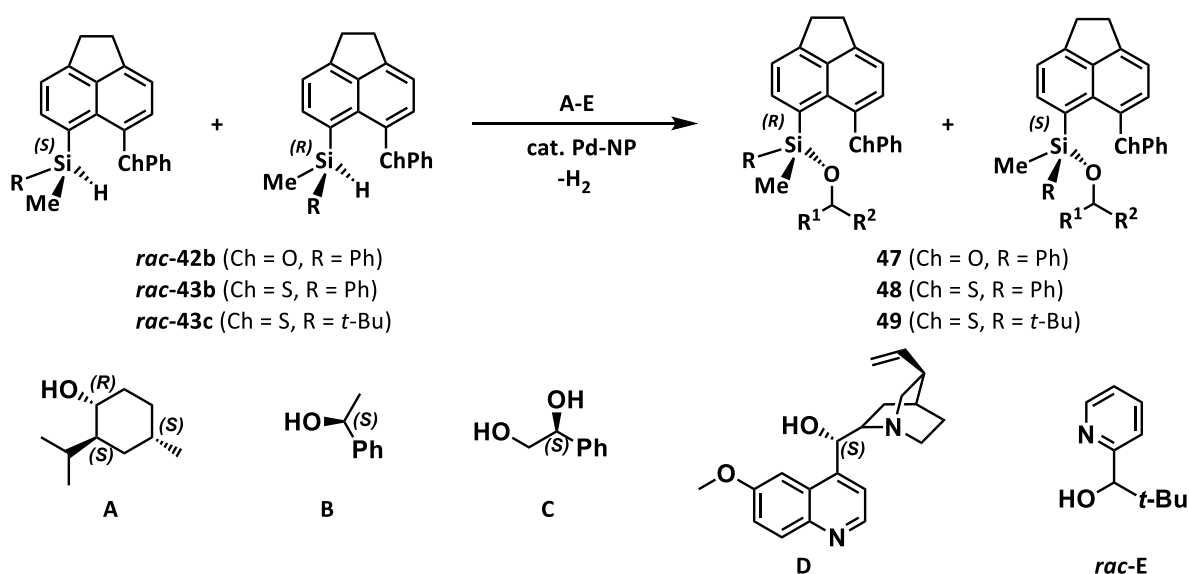
Scheme 24 – Generation of silyl borates **34**[$\text{B}(\text{C}_6\text{F}_5)_4$], **35**[$\text{B}(\text{C}_6\text{F}_5)_4$] and **37**[$\text{B}(\text{C}_6\text{F}_5)_4$] from silanes **42**, **43** and **44** (R = Ph (b), *t*-Bu (c)).

Generally, two approaches to achieve the separation of the enantiomers of racemic mixtures can be pursued.^[55] The first approach is the resolution of the enantiomers through the reaction with an enantiomerically pure reagent in order to generate the corresponding diastereomeric derivatives. These diastereomers can usually be separated by column chromatography or by crystallization.^[56] The second approach is the kinetic resolution and is based on an enantiomerically selective derivatization. For this purpose, either an enantioselective catalyst or an enantioselective reagent is necessary. To achieve the consumption of only one enantiomer either 0.5 equiv. of the reagent/auxiliary is used or

the reaction is stopped after half of the starting compound is consumed. As a consequence, only one enantiomer reacts and the other one remains unaffected. In general, the separation of the derivatized enantiomer and the not reacted enantiomer is easy. One general disadvantage to be mentioned on kinetic resolution results if the enantiomeric selectivity is poor which can compromise the resulting enantiomeric ratio.^[57] In this section, the tested approaches to realize the resolution of racemic silanes **42b**, **43b,c** and **44** are discussed. (A short remark on the Schemes and Figures in this chapter: the distinction between (*R*)- and (*S*)-silane is only illustrative and not proven experimentally.)

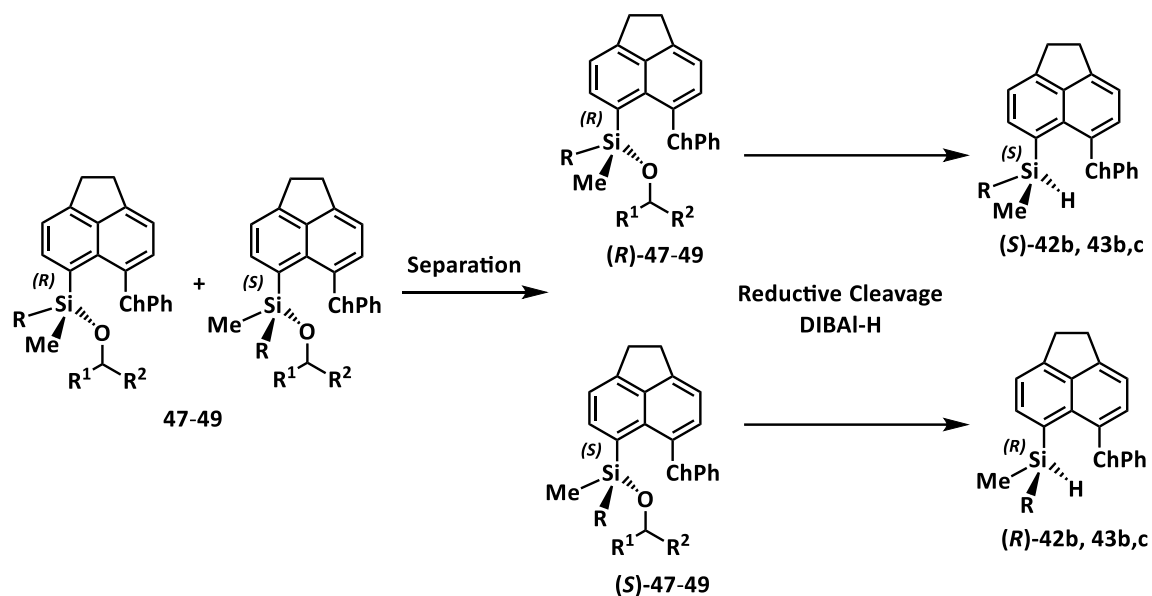
3.1.3.1 Derivatization with an Auxiliary

The first approach to achieve the chiral resolution of racemic silanes **42b** and **43b,c** was the chemical derivatization by dehydrogenative coupling with enantiomerically pure alcohols **A-D** to give diastereotopic siloxanes **47**, **48** and **49** (Scheme 25). Pyridyl alcohol **E** was used as racemic mixture in these experiments for evaluation purposes. The reaction is catalyzed by palladium nanoparticles (Pd-NP).^[58]



Scheme 25 – Derivatization of racemic silanes **42b** and **43b,c** with an alcohol **A-E** via Pd-NP catalysis.

The resulting siloxanes **47**, **48** and **49** should be separated by column chromatography and afterwards retransformed to enantioenriched silanes **42b** and **43b,c** via reductive cleavage. Convenient reducing agents are aluminium hydrides, for example di-*iso*-butylaluminium hydride (DIBAL-H), since the reaction proceeds under retention of configuration at the silicon center (Scheme 26).^[59]



Scheme 26 – Separation of diastereotopic siloxanes **47**, **48** and **49** and their subsequent reduction to corresponding silanes **42b** and **43b,c**.

Initially, thiophenyl-substituted methylphenyl silane **rac-43b** was chosen to test the dehydrogenative coupling with different auxiliaries **A-E**. To generate the corresponding siloxanes **48A-E**, a reaction tube was charged with the silane **rac-43b**, the alcohol (**A**, **C-E**) and a catalytic amount of Pd-NP. The solids were dissolved/suspended in di-*n*-butyl ether and the reaction mixture was heated to the temperature and for the time indicated in Table 3. In case of the liquid alcohol **B**, it was added to the mixture after addition of the solvent. Siloxanes **48A,B,E** were obtained in bad to moderate yields (Table 3, Entries 1-7). It is noticeable, that elevated temperatures (70-100°C) are needed to complete the reactions (see Entry 2-3, 6-7, Table 3).

Table 3 - Dehydrogenative Si – O Coupling of silanes **42b** and **43b,c** and different alcohols **A-D**. *Impure yield of siloxanes **47** and **48**, the impurity is the by-product silanol **50** or **51**.

$(rac)\text{-42b (Ch = O)}$
 $(rac)\text{-43b (Ch = S)}$

A-E

47 (Ch = O)
48 (Ch = S)

51 (Ch = O)
50 (Ch = S)

A **B** **C** **D** **E**

Entry	Silane	Alcohol	Equiv. Alcohol	Reac. Cond.	Consumption of silane	Yield Siloxanes	Separation
1	43b	A	2.5	70 °C, 18 h	not complete	12 %	not possible
2	43b	B	2.5	70 °C, 6 h	no reaction	-	-
3				100 °C, 16h	complete	12 %	not possible
4	43b	C	1.0	100 °C, 16 h	complete	45 %*	not possible
5	43b	D	1.0	100 °C, 96 h	no reaction	-	-
6	43b	E	1.0	70 °C, 16 h	no reaction	-	-
7				100 °C, 72 h	complete	28 %*	not possible
8	42b	C	1.0	70 °C, 16 h	complete	54 %*	not possible

The ^{29}Si INEPT NMR spectra of the menthyl, the 1-phenylethyl and the pyridylsilyl ethers **48A,B,E** are shown in Figure 8. The ^{29}Si NMR chemical shifts of the silyl ethers **48A,B,E** are in the range of $\delta^{29}\text{Si} = -6.5$ and -8.1 which is in the same region compared to the silyl ethers of Landais and co-workers ($\delta^{29}\text{Si} = -8.6$ - 4.1).^[58] In the ^{29}Si NMR spectrum of pyridyl-substituted silyl ethers **48E** a further silicon species with a ^{29}Si NMR chemical shift of $\delta^{29}\text{Si} = -4.6$ was detected. This silicon species was assigned to the by-product silanol **50**.

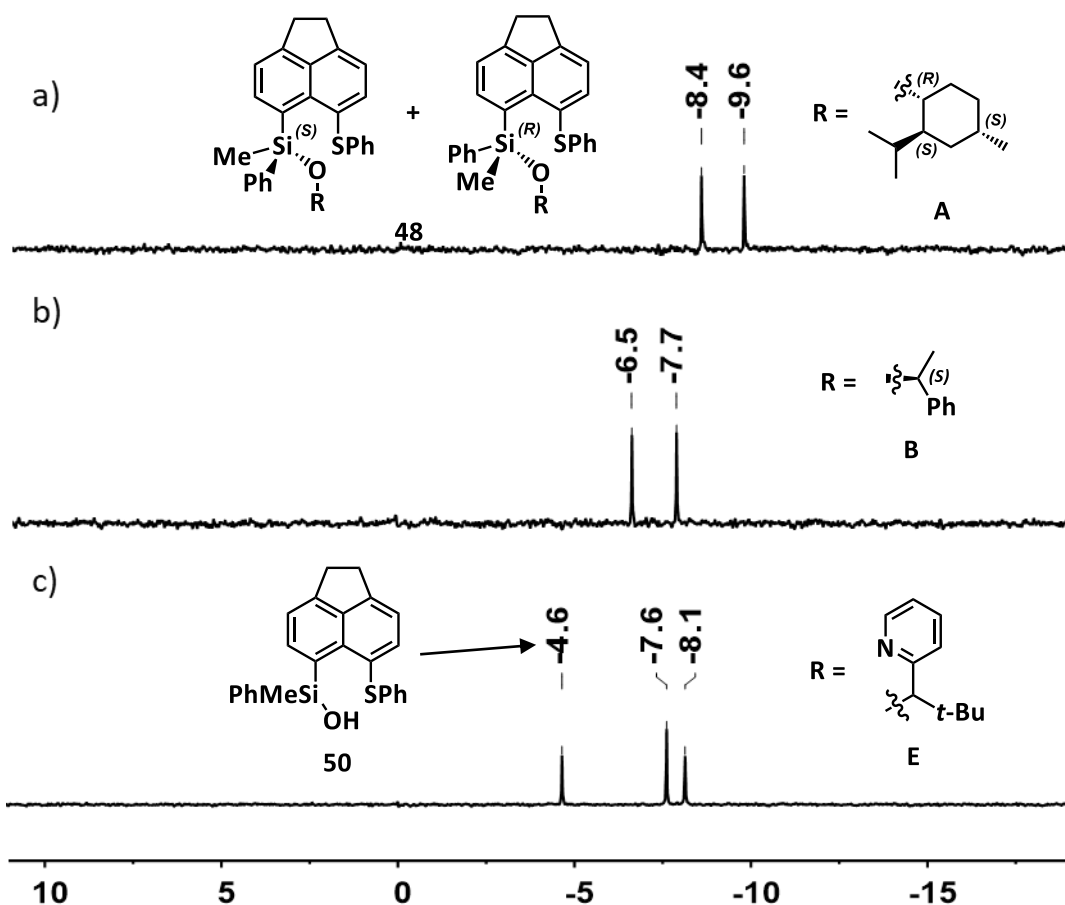
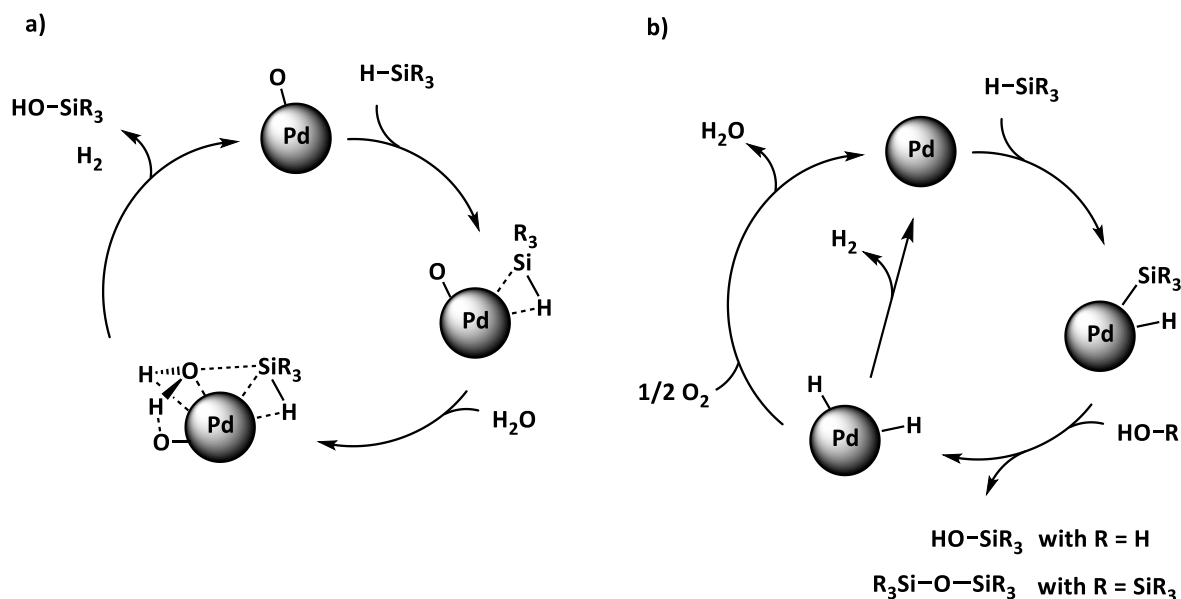


Figure 8 – $^{29}\text{Si}\{^{60}\text{I}\}$ INEPT NMR spectra (60 MHz, 298 K, CDCl_3) of the synthesized silyl ethers **48A** (spectrum a)), **48B** (spectrum b)) and **48E** (spectrum c)) after purification.

The formation of silanol **50** was observed in all attempts and is not unusual since the conversion from hydrosilanes to silanols catalyzed by Pd-NP is well-known.^[61] There are two possible explanations for the formation of silanol **50**. The first possibility is residual moisture present in the reaction mixture. The mechanism of the reaction of a hydrosilane with water catalyzed by Pd-Nps is shown in Scheme 27a).^[61a] The first two steps are the complexation of the substrates hydrosilane and water by the nanoparticles and in the subsequent step dihydrogen and the product silanol are released. At this point, it is important to mention that in the proposed mechanism of Shimizu et al. there is an oxygen atom attached to the nanoparticle surface which plays an important role in the reaction.^[61a] The Pd-NPs used in this work were provided by the group of Landais and were prepared by the reduction of palladium(II) chloride in the presence of a carbon-based solid support material under anaerobic conditions. The X-ray photoelectron spectroscopy (XPS) analysis shows that the Pd-NPs consist of Pd^0 (70 %) and PdO (30 %); whereby, Landais and co-workers describe that the PdO might be the result

of the oxidation of Pd⁰ during the XPS analysis.^[58] However, the positive effect of attached oxygen atoms at the Pd surface on the reactivity of Pd-NPs is well-known, the H₂O cleavage works as well with a clean Pd surface.^[61a, 62] Consequently, residual moisture in the reaction mixture can be the reason for the formation of silanol **50**.



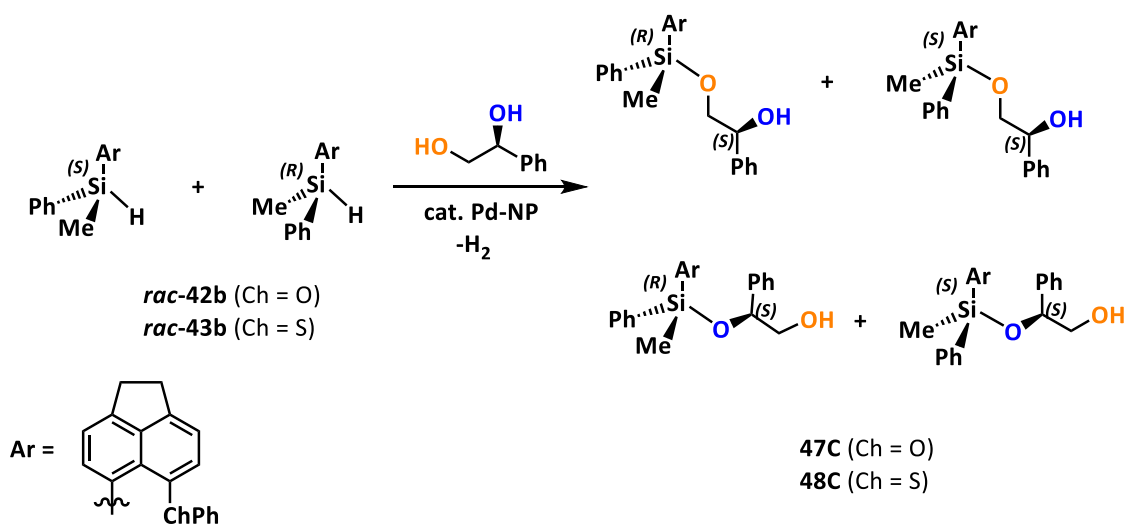
Scheme 27 – Proposed mechanisms for the Si – O coupling using Pd-NP as catalyst.^[61]

The second possibility is oxygen present in the reaction mixture. In that case the proposed mechanism in Scheme 27b) holds.^[61b] The reaction starts with the activation of the Si – H bond by the Pd-NPs. After the formation of the product, there are two hydrogen atoms left at the nanoparticle surface which react either to dihydrogen (as shown in mechanism a)) or with oxygen to water. The production of water again opens the possibility to generate silanol **50** as described in the first mechanism a). The mechanism for the dehydrogenative coupling of hydrosilanes with an alcohol is probably in close analogy to the proposed mechanisms in Scheme 27.

The separation of the diastereomeric siloxanes **48A,B,E** should be performed by column chromatography; but, none of the mixtures of derivatives **48A,B,E** was successfully separated. Furthermore, in Entry 4 and 7 (Table 3) siloxanes **48E** were not separated from the by-product silanol **50**.

Diol **C** can react either with the primary alcohol or with the secondary alcohol. The possible reaction products are shown in Scheme 28. Investigations of the Landais group showed that the reaction of

primary alcohols are kinetically favored compared to the reaction of secondary alcohols; whereby, the stereoselectivity of the reaction of a silane with diol **C** is generally good.^[58]



Scheme 28 – Dehydrogenative coupling of silanes **42b** and **43b** with diol **C**.

Interestingly, the reaction of diol **C** with phenoxy derivative **42b** was more selective compared to the reaction of diol **C** with thiophenyl derivative **43b**. The ^{29}Si INEPT NMR spectra of the siloxanes **47C** and **48C** are shown in Figure 9. The species with a ^{29}Si NMR chemical shift of $\delta^{29}\text{Si} = -2.0$ in the lower spectrum of phenoxy-substituted derivative **47C** was tentatively assigned to the corresponding silanol **51**. The ^{29}Si INEPT NMR spectrum of siloxanes **47C** show only two ^{29}Si NMR chemical shifts ($\delta^{29}\text{Si} = -1.7$ and -1.4), indicating that two diastereomers were obtained. The reaction of thiophenyl derivative **43b** yielded in a mixture of four species ($\delta^{29}\text{Si} = -6.2, -4.9, -4.7$ and -4.4) and silanol **50** ($\delta^{29}\text{Si} = -4.6$) (Figure 9, above). The complexity of the mixture obtained with thiophenyl derivative **43b** makes a clear identification of the reaction products difficult and a further purification was not possible. Also the separation of siloxanes **47C** was not successful.

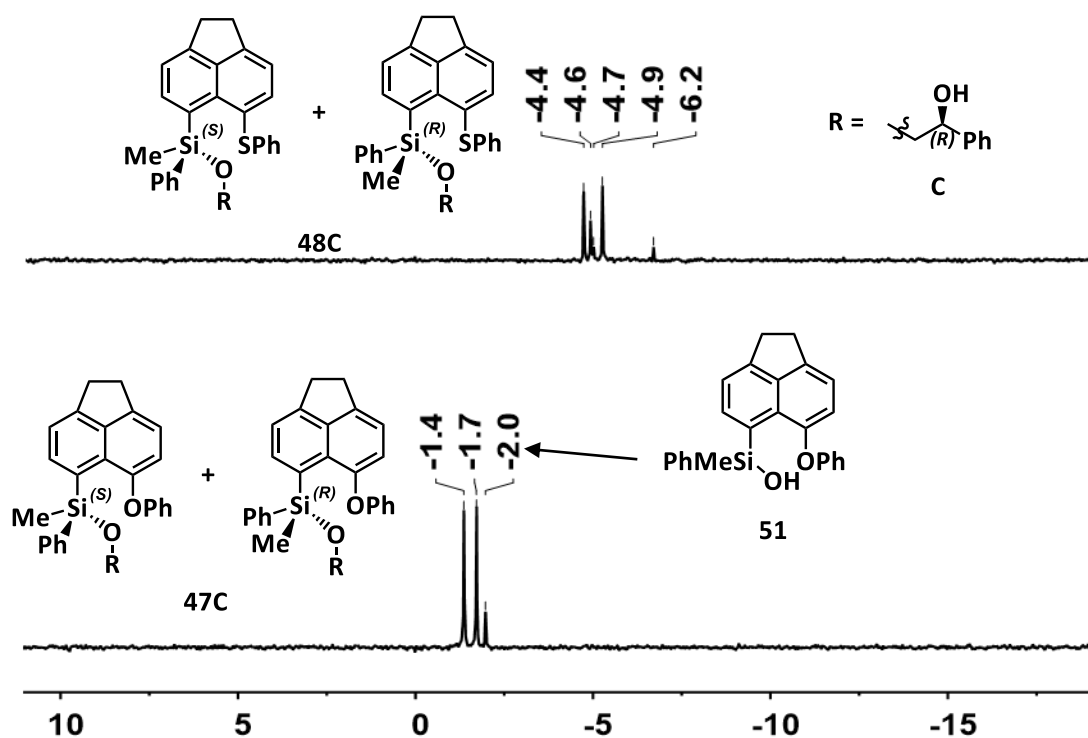


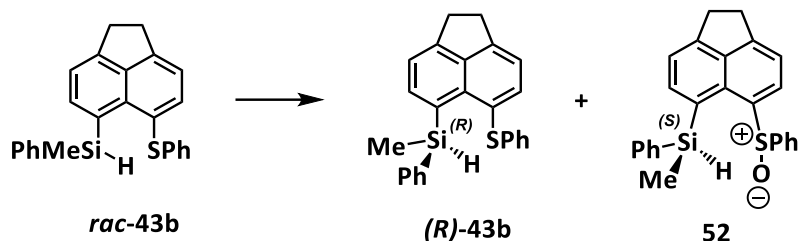
Figure 9 – $^{29}\text{Si}\{^1\text{H}\}$ INEPT NMR spectra (60 MHz, 298 K, CDCl_3) of the synthesized silyl ethers **47C** and **48C** after purification.

Using quinidine **D** as an auxiliary (Entry 5, Table 3) no reaction was observed. The reason is probably the steric demand of quinidine **D**. Since the separation of the racemic methylphenyl-substituted silanes **42b** and **43b** was not successful, *tert*-butylmethyl silane **43c** was treated with phenyl ethanol **B** and pyridyl ethanol **E**; however, no reaction was observed under the described conditions (*n*- Bu_2O , 100 °C, several days; for details see Experimental Part).

The separation of none of the diastereomeric mixtures of the synthesized siloxanes **47** and **48** was successful. Therefore, the second chiral resolution strategy was tested which will be discussed in the following chapter.

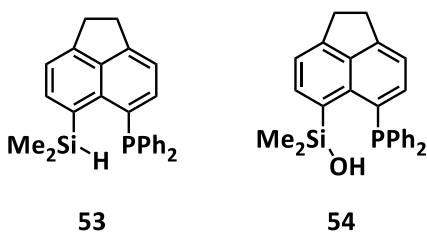
3.1.3.2 Kinetic Resolution

Two strategies for the kinetic resolution of racemic silanes **42b**, **43b,c** and **44** were tested. The first strategy is the enantiomerically selective oxidation of the thionyl group (Scheme 29).

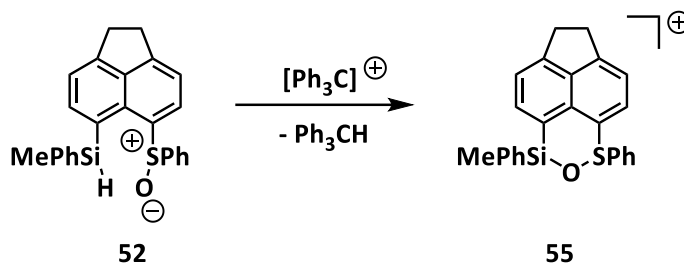


Scheme 29 – Enantioselective oxidation of the thiophenyl moiety in silane **43b** (the distinction between (*R*)- and (*S*)-silane is illustrative and not proven experimentally).

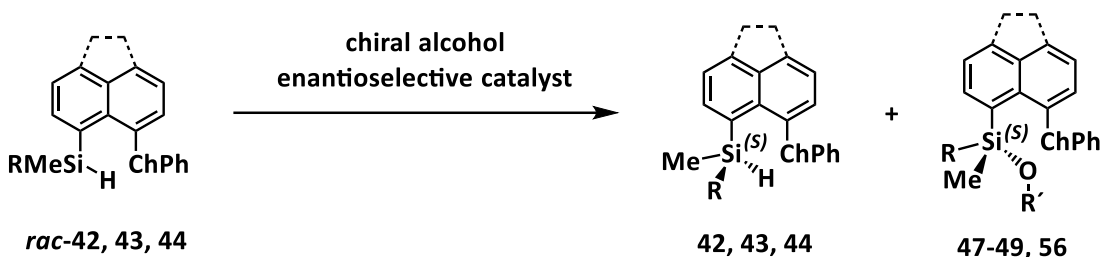
This strategy is only suitable for the thiophenyl-substituted derivatives **43b,c** and **44**, whereby, silane **43b** was chosen as a model system for this experiments. The disadvantage that only silanes with a thiophenyl substituent can be separated through this strategy is compensated by the believed straight forward separation of the remaining thiophenyl ether **43b** from the resulting oxidized species **52** via column chromatography. Furthermore, oxidized derivative **52** is by itself an interesting species in terms of the studies of the interactions in *peri*-substituted acenaphthyl compounds. E. Hupf et al. studied the interaction of the Si – H...P, Si – H...E⁻ – P⁺ (E = S, Se) and Si – OH...E⁻ – P⁺ (E = O, S, Se) of 5-diphenylphosphinoacenaphth-6-yl-silane **53** and -silanol **54**.^[63]



In their studies, they show that the intramolecular hydrogen bridges in organo-H-silane **53** are weaker than of organosilanol **54**. 6-Phenylmethylsilyl-5-phenylsulfonylacenaphthene **52** is the precursor for the corresponding silyl cation **55** (Scheme 30). The interaction between the Lewis acidic silicon center of cation **55** and the sulfoxide group would be of interest.

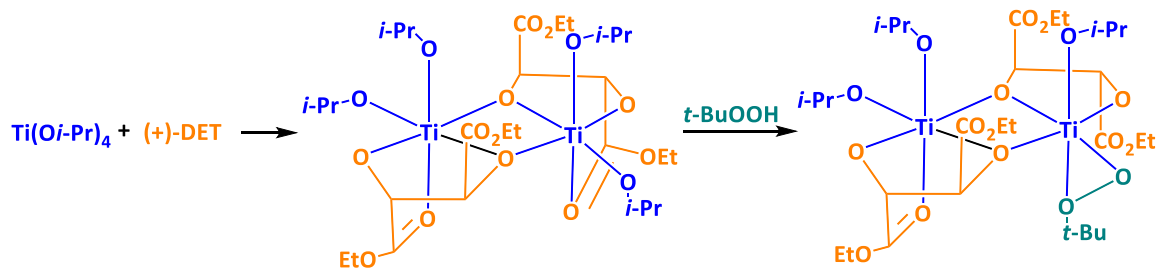
Scheme 30 – Formation of sulfonyl stabilized silyl cation **55** from silane **52**.

The second strategy tested, is the enantiomerically selective dehydrogenative Si – O coupling (Scheme 31).^[64] This strategy is promising since the dehydrogenative coupling of silanes **42b**, **43b** and **44** with an alcohol was already shown to be successful with the Pd-NP catalysis as described in the previous section (Chapter 3.1.3.1). Moreover, the separation of silanes **42b**, **43b,c** and **44** from siloxanes **47-49** and **56** is thought to be straightforward.

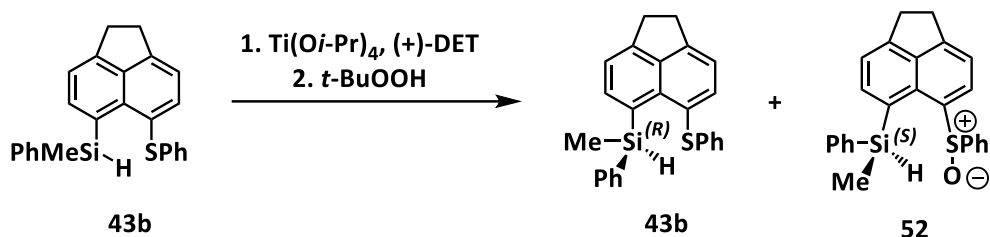
Scheme 31 – Kinetic resolution of silanes **42b** (ace, Ch = O, R = Ph), **43b,c** (ace, Ch = S, R = Ph (**b**), *t*-Bu (**c**)) and **44** (naph, Ch = S, R = Ph) via enantioselective dehydrogenative Si – O coupling (the distinction between (*R*)- and (*S*)-silane is illustrative and not proven experimentally).

a) Oxidation of the Thiophenyl Group

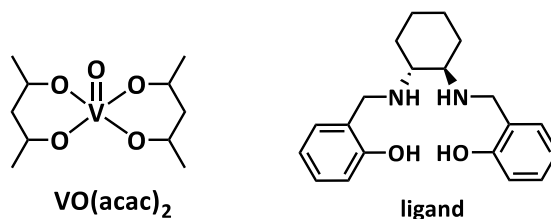
Oxidation of a sulfide with two different substituents results in the formation of a sulfoxide in which the sulfur atom is a stereogenic center. This oxidation can be performed in an enantioselective manner using an approach which is based on the asymmetric epoxidation using titanium tetrakis-*iso*-propoxide ($\text{Ti}(\text{O}i\text{-Pr})_4$) with the diethyl tartrate ligand as an asymmetrical reagent (Scheme 32). Hereby, it is crucial for the enantioselectivity of this reaction that the tartrate is enantiomerically pure (e.g. (+)-diethyl L-tartrate ((+)-DET)). As oxidant *tert*-butyl hydroperoxide is used. Treating a prochiral sulfide with the chiral Sharpless reagent leads to the attack of only one of the two enantiotopic lone pairs at the sulfur atom.^[65]

Scheme 32 – Formation of the chiral Sharpless reagent.^[66]

To perform the enantiomerically selective oxidation of the thiophenyl ether **43b**, the starting material was dissolved in dichloromethane. The Sharpless reagent was used in an equimolar amount (Scheme 33). Therefore 4.0 equiv. (+)-DET and 2.0 equiv. $\text{Ti}(\text{O}i\text{-Pr})_4$ were added to the reaction mixture. The oxidant $t\text{-BuOOH}$ was added at low temperature ($-40\text{ }^\circ\text{C}$). The reaction was monitored via TLC. After 16 h no conversion of the silane **43b** was observed. For that reason, the mixture was warmed to $-20\text{ }^\circ\text{C}$ for one day and later even to r.t. for further two days, but no reaction was observed. After 4 days, the reaction was stopped and 84 % of the starting thioether **43b** was recovered.

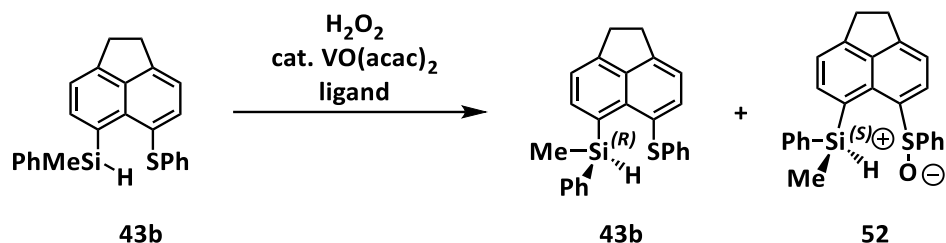
Scheme 33 - Approach for the enantioselective oxidation of thiophenyl silyl acenaphthene **43b** (the distinction between (*R*)- and (*S*)-silane is illustrative and not proven experimentally).

The second approach to achieve the asymmetrical oxidation of thiophenyl acenaphthene **43b** was using a vanadium-salan catalyst (Scheme 34). The catalyst consists of vanadyl acetylacetonate ($\text{VO}(\text{acac})_2$) and (*R,R*)-*N,N'*-bissalicyl-*N,N'*-dimethyl-1,1-diaminocyclohexane as the ligand.^[67]



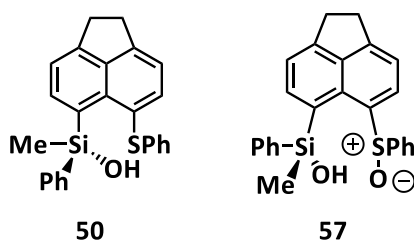
The reaction was performed in chloroform at $0\text{ }^\circ\text{C}$ to room temperature. The catalyst was formed by the reaction of 0.04 equiv. of $\text{VO}(\text{acac})_2$ with 0.06 equiv. of the ligand. One equiv. of the silane **43b**

was added at r.t. to the catalyst mixture. The oxidant H_2O_2 was added at $0\text{ }^\circ\text{C}$. The reaction mixture was then allowed to warm to r.t. and the reaction progress was monitored via TLC.



Scheme 34 – Enantioselective oxidation of the thiophenyl group in silane **43b** catalyzed by a vanadium-salan catalyst (the distinction between (*R*)- and (*S*)-silane is illustrative and not proven experimentally).

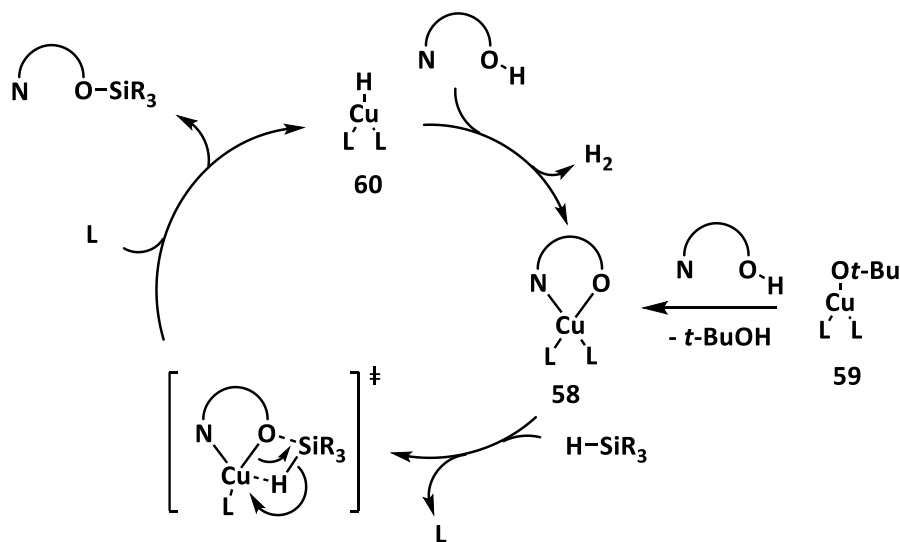
After two days the reaction was stopped and subsequently purified via column chromatography resulting in recovery of 75% of the starting silane **43b**. The ^1H NMR spectrum of the second fraction collected showed two different Si-H signals, whereby, one signal was assigned to the starting silane **43b**. The aliphatic as well as the aromatic region of the ^1H NMR spectrum are too crowded to allow a further assignment of the second Si-H species. The ^{29}Si INEPT NMR spectrum of this fraction reveals the complexity of the obtained mixture and shows six different silicon species ($\delta^{29}\text{Si} = -17.1$ (**43b**), -12.0 , -11.2 , -6.2 , -5.3 and -4.0 in CDCl_3). The signal at $\delta^{29}\text{Si} = -17.1$ was assigned to the starting material **43b**. The silanol **50**, which was already observed in the experiments regarding the dehydrogenative Si – O coupling discussed in Chapter 3.1.3.1, has a ^{29}Si NMR chemical shift of $\delta^{29}\text{Si} = -4.6$. This exact chemical shift was not observed, but the formation of the silanol **50** is likely in this reaction. Even the sulfoxide substituted silanol **57** could be formed as a by-product in this reaction. Both would give a similar ^{29}Si NMR chemical shift in this region.^[63]



However, the complexity of this mixture did not allow a clear identification of the reaction products and further purification was unsuccessful. Furthermore, no explicit hint for the formation of the desired product **52** was obtained. Therefore, this resolution route was abandoned.

b) Dehydrogenative Si – O Coupling

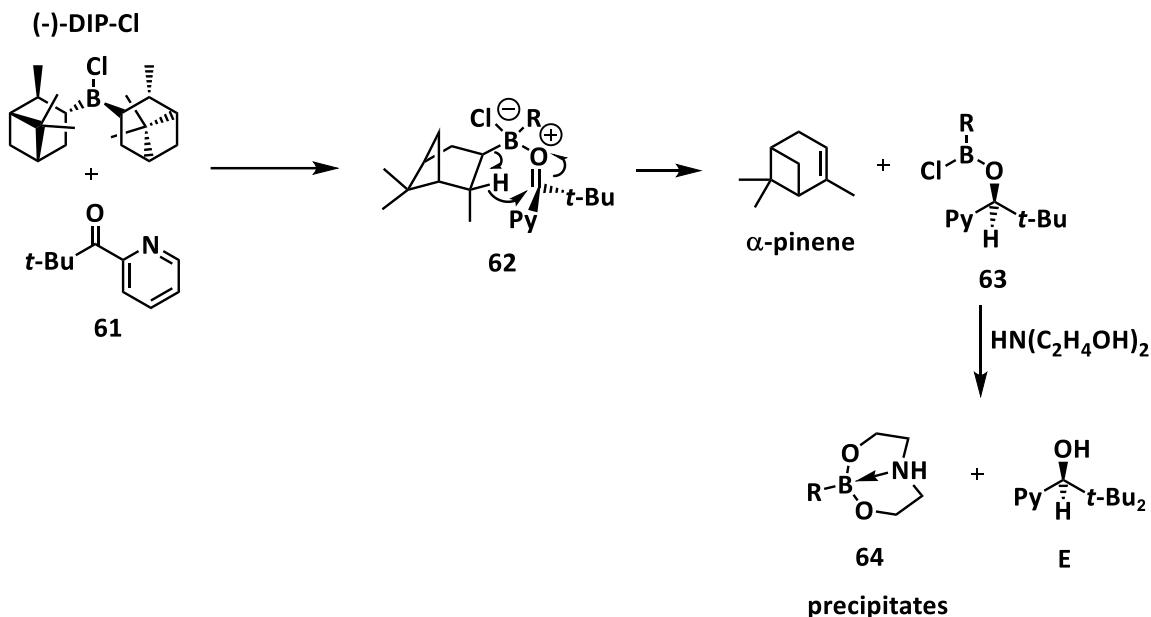
The third method to obtain enantiomerically enriched silanes **42b**, **43b,c** and **44** is the enantiomerically selective dehydrogenative coupling of silanes **42b**, **43b,c** and **44** with an alcohol. Therefore, an undemanding copper(I) catalyst was used. To achieve the selectivity required, the chiral alcohol must possess a remote donor which allows a bidentate binding to the Cu(I)-catalyst. An illustration of the mechanism, which was proposed by Oestreich and co-workers, is shown in Scheme 35. The chelate complex, copper(I) alkoxide **58**, with the bidentate alcohol as ligand is formed by an alkoxide exchange from *tert*-butoxide species **59**. Copper(I) alkoxide **58** reacts with a hydrosilane to give the corresponding silyl ether and the catalytically active species, copper(I) hydride **60**. A new catalytic cycle starts with the reaction of copper(I) hydride **60** and the bidentate alcohol with release of dihydrogen and regeneration of the chelate complex, copper(I) species **58**.^[64]



Scheme 35 – Schematic illustration of the reaction mechanism of the dehydrogenative Si – O coupling catalyzed via a copper(I) catalyst.^[64]

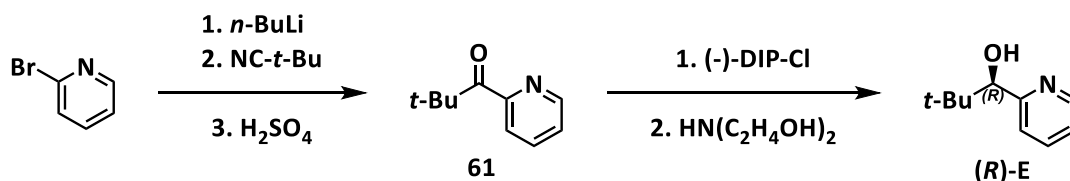
A reasonable candidate for the bidentate alcohol is *tert*-butyl-substituted pyridylmethanol **E**.^[64] This alcohol is not commercial available and the synthesis, in particular the chiral resolution is challenging. The most convenient way to generate enantiomerically enriched pyridyl alcohol **E** turned out to be by the enantiomerically selective reduction of the corresponding ketone **61** with (-)-B-chlorodiisopinocampheylborane ((-)-DIP-Cl).^[68] The mechanism of the reduction of ketone **61** with DIP-Cl is shown in Scheme 36. Initially, the nucleophilic attack of the ketone to the borane occurs to form adduct **62**. The steric obstruction between the methyl group of the isopinocampheyl substituent and the sterically demanding *tert*-butyl group leads to the *Re*-attack of the hydride which

is released from the isopinocampheyl group to the carbonyl carbon atom. The hydride is transferred with release of α -pinene and intermediate **63**. Addition of diethanol amine leads to the formation of by-product **64**, which precipitates, and the product, alcohol **E**, in enantiomerically enriched form.^[69]



Scheme 36 – Mechanism of the reduction of ketone **61** with (-)-DIP-Cl.

Ketone **61** was synthesized according to the literature^[70] by lithiation of 1-bromopyridine with *n*-butyl lithium and subsequent reaction with pivalonitrile (Scheme 37). After hydrolysis ketone **61** was obtained in a good yield (94 %). Then ketone **61** was reduced using (-)-DIP-Cl to give alcohol (**R**)-**E** in a moderate yield (55 %), but with a good enantiomeric excess of ee = 96% (determined via chiral GC).



Scheme 37 – Synthesis of enantiomerically enriched pyridyl-*tert*-butyl-substituted methanol (**R**)-**E**.

With pyridyl alcohol (**R**)-**E** in hand, the dehydrogenative coupling with chiral silanes **42b**, **43b,c** and **44** was performed. A Schlenk tube was charged with copper(I) chloride and triphenylphosphane and the solids were dissolved/suspended in toluene. Subsequently, sodium *tert*-butoxide was added to give a yellow solution. The starting silane **42b**, **43b,c** or **44** and 0.5 equiv. of alcohol (**R**)-**E** were

dissolved in toluene, respectively. First, the solution of the alcohol (**R**)-**E** was added to the catalyst mixture and, second, the solution of the silane **42b**, **43b,c** or **44**. The reaction mixture was stirred for 16 h at r.t. and afterwards filtrated through a thin layer of silica gel to remove the Cu(I) species. After removal of the solvent, the crude product was purified in two steps. First, a short column chromatography using petroleum ether/ethyl acetate (100:0 → 70:30) which resulted in two fractions. The first fraction obtained was a mixture of the remaining silane **42b**, **43b,c** or **44** and residue of triphenylphosphane. The second fraction consists of a mixture of the corresponding silyl ethers **47E**, **48E**, **49E** or **56**. Both fractions needed a second purification via column chromatography or preparative TLC. The ^{29}Si NMR spectrum of thiophenyl-substituted silyl ether **48E** is shown as one example in Figure 10 in comparison to the product mixture obtained in the Pd-catalyzed reaction (Chapter 3.1.3.1). The ^{29}Si NMR spectrum shows that one diastereomer of **48E** is obtained in excess. Moreover, the amount of the by-product silanol **50** is for the Cu-catalyzed reaction less than for the Pd-catalyzed reaction.

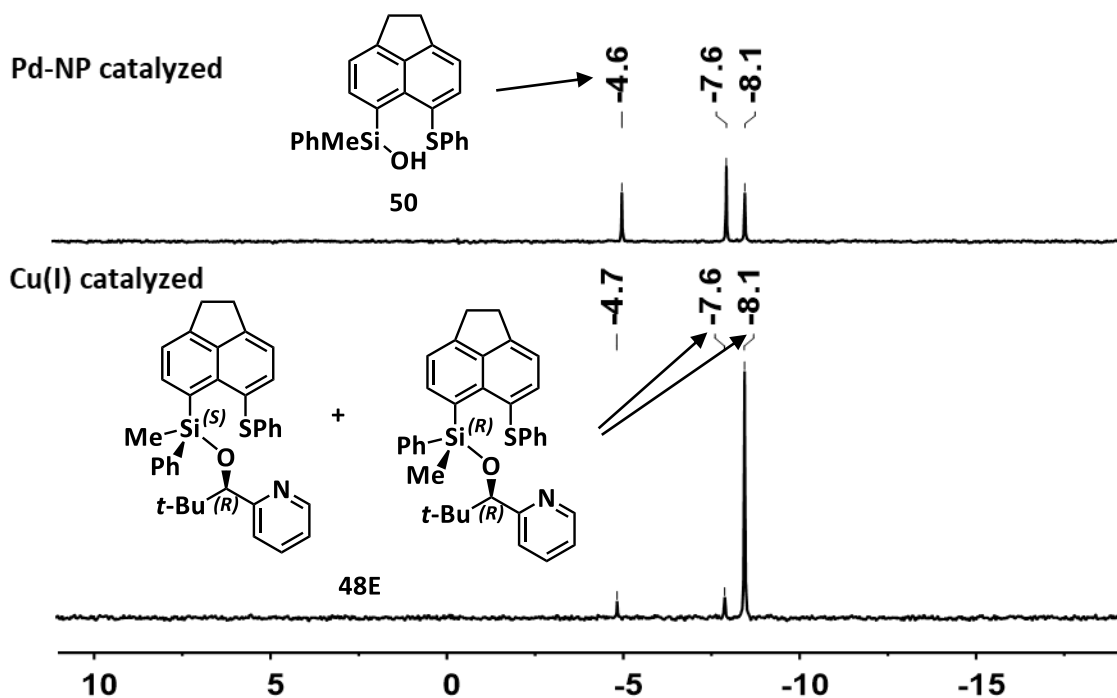


Figure 10 – Comparison of the $^{29}\text{Si}\{^1\text{H}\}$ INEPT NMR spectra (300 MHz, 298 K, CDCl_3) of the silyl ethers **48E** synthesized via Pd- and Cu-catalysis after purification.

The results for the dehydrogenative Si – O coupling are summarized in Table 4. The remaining silane is always the (+)-enantiomer and the silane which is obtained from the reduction of the corresponding siloxane is the (-)-enantiomer. As already observed with the Pd-NP-catalyzed dehydrogenative Si – O coupling, the Cu(I)-catalyzed alternative for this reaction was also not

applicable for *tert*-butyl-substituted silane **43c**. No formation of the corresponding silyl ethers **49E** was observed; hence, the chiral resolution of derivative **43c** was not achieved. The kinetic resolution of derivatives **42b**, **43b** and **44** was successful (Table 4). The separation of (+)-silane **42b** from triphenylphosphane was challenging and was not achieved by column chromatography or recrystallization. Therefore, the oxidation of triphenylphosphane was tested. The (+)-silane **42b**/Ph₃P mixture was dissolved in petroleum ether and an aqueous hydrogen peroxide solution was added. After stirring for 1 h at room temperature a white solid precipitated. However, the Ph₃P was not completely consumed after this time. The complete removal was achieved by stirring the mixture for 16 h. The long reaction time led to decomposition of (+)-silane **42b** (ca. 30 %). Nevertheless, after filtration and column chromatography, (+)-silane **42b** was obtained purely (Table 4, Entry 1). The optical rotation of (+)-silane **42b** is $[\alpha]_D = +12^\circ$ ($c = 0.01 \text{ molL}^{-1}$, Et₂O) and the enantiomeric excess is $ee = 54 \%$ (chiral HPLC).

Table 4 – Results of the kinetic resolution of silanes **42b**, **43b,c** and **44** via copper catalyzed dehydrogenative Si – O coupling.

<p> 42b (ace, Ch = O, R = Ph) 43b (ace, Ch = S, R = Ph) 44 (naph, Ch = S, R = Ph) </p> <p> (R)-E </p> <p> (+)-42b, 43b, 44 </p> <p> 47E (ace, Ch = O) 48E (ace, Ch = S) 56 (naph, Ch = S) </p>						
Entry	Silane	Yield (+)-silane	$[\alpha]_D$ (+)-silane	ee (+)-silane	Yield Siloxane	dr Siloxane
1	42b	97 % ^{a)}	+12° (0.01 molL ⁻¹ , Et ₂ O)	54 %	123 % ^{b)}	85:15
2	43b	80 %	+11° (0.06 molL ⁻¹ , Et ₂ O)	66 %	69 %	91:9
3	44	59 %	+17° (0.04 molL ⁻¹ , Et ₂ O)	84 %	75 %	93:7

(a) Mixture with ca. 15 % Ph₃P, b) yield is too high since 0.6 equiv. pyridyl alcohol **E** was used and remaining impurities.)

The moderate enantiomeric excess of (+)-silane **42b** is reflected by the diastereomeric ratio of the corresponding siloxane **47E** with $dr = 85:15$. To determine the dr the integrals of the ¹H NMR signals of the hydrogen atom, marked in blue, are used (¹H NMR see Figure 11).

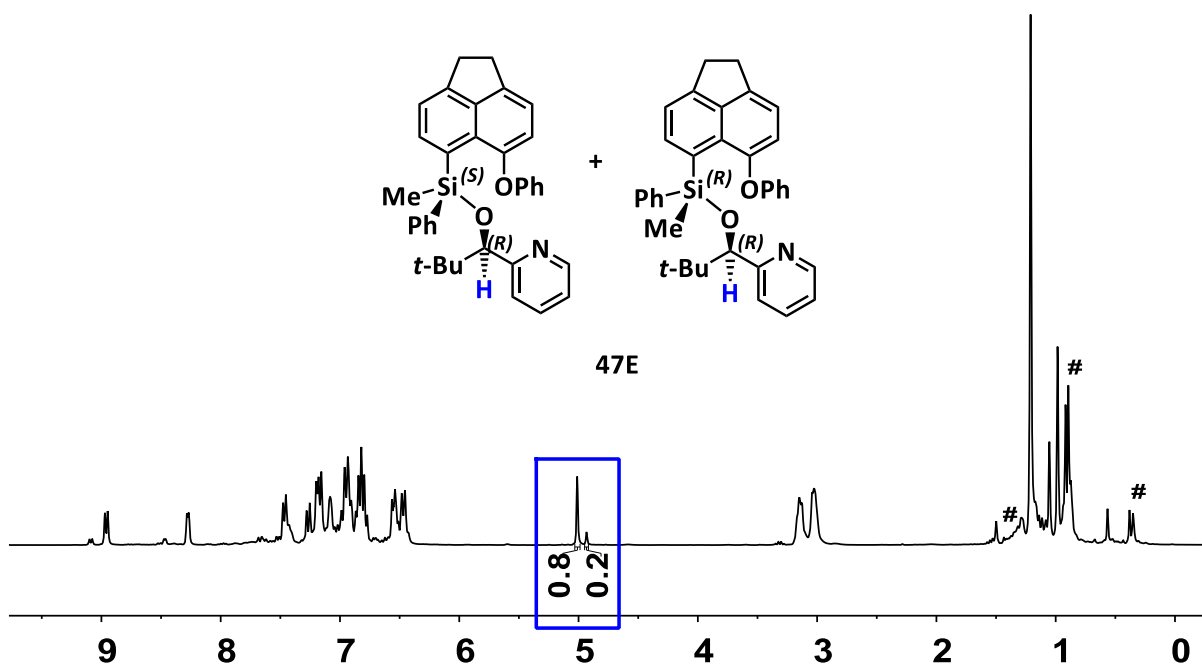


Figure 11 – ^1H NMR spectrum (300 MHz, 297 K, C_6D_6) of diastereomeric phenoxy substituted silyl ethers **47E** (# impurities).

Improved results were obtained for the chiral resolution of the thiophenyl-substituted derivatives **43b** and **44**. Remaining (+)-silanes **43b** and **44** as well as silyl ethers **48E** and **56** were obtained in good yields (Table 4, Entry 2, 3). The (+)-enantiomers **43b** and **44** were successfully purified via column chromatography. The measured enantiomeric excess is $ee = 66\%$ for acenaphthene derivative **43b** and is $ee = 84\%$ for naphthyl derivative **44**. The diastereomeric ratio of the corresponding siloxanes **48E** and **56** is $dr = 91:9$ and $93:7$, respectively, and is enhanced compared to the diastereomeric ratio of phenoxy-substituted derivative **47E** ($dr = 85:15$, Table 4, Entry 1).

The reduction of silyl ethers **47E**, **48E** and **56** was performed at r.t. in Et_2O using two equiv. DIBAL-H. After stirring the mixture for 18 h, the reaction was quenched with 1 M HCl solution. Subsequent aqueous work up and purification by column chromatography or preparative TLC gave (-)-silanes **42b**, **43b** and **44** in good yields (69-82 %, Table 5). The enantiomeric excesses are moderate with $ee = 64\%$ for thiophenyl derivatives **43b** and **44**, respectively, and $ee = 54\%$ for phenoxy derivative **42b**.

Table 5 – Results of the reduction of siloxanes **47E**, **48E** and **56** with DIBAL-H.

<p> 47E (ace, Ch = O) 48E (ace, Ch = S) 56 (naph, Ch = S) </p> <p> (-)-42b (ace, Ch = O) (-)-43b (ace, Ch = S) (-)-44 (naph, Ch = S) </p>						
Entry	Siloxane	dr Siloxane	Silane	Yield (-)-silane	ee (-)-silane	$[\alpha]_D$ (-)-silane
1	47E	85:15	42b	80 %	54 %	-11° (0.05 molL ⁻¹ , Et ₂ O)
2	48E	91:9	43b	82 %	64 %	-11° (0.02 molL ⁻¹ , Et ₂ O)
3	56	94:6	44	69 %	64 %	-15° (0.04 molL ⁻¹ , Et ₂ O)

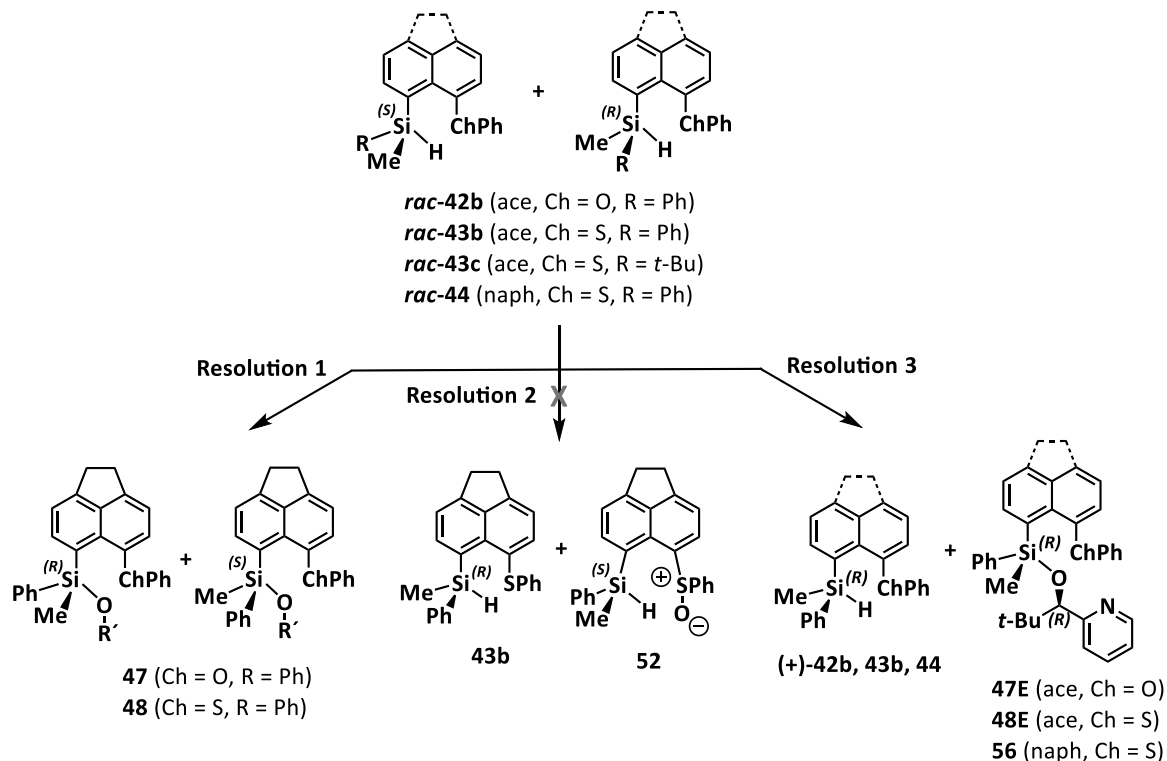
In conclusion, the chiral resolution by enantiomerically selective Cu(I)-catalyzed dehydrogenative coupling of silanes **42b**, **43b** and **44** was achieved. The resolution of racemic *tert*-butyl-substituted derivative **43c** was not achieved. The results of derivatives **42b**, **43b** and **44** are summarized in Table 6. The optical rotations of the enantiomers measured for both acenaphthyl-substituted derivatives **42b** and **43b** show nearly identical values with opposite signs for enantiomers A and B indicating similar ee values for both enantiomers, which was confirmed by the chiral HPLC measurements (Table 5, Entries 1, 2). The values of naphthyl derivative **44** show a slight discrepancy. While the dr of the corresponding siloxane **56**, which is determined from the ¹H NMR spectrum, shows the best value of these studies, the measured ee of the corresponding (-)-silane **44** is with ee = 64 % similar to the values obtained for silane **43b** (Table 5, Entry 3). However, the (+)-enantiomer **44** was obtained with an enantiomeric excess of ee = 84 %, which is the best result in these studies.

Table 6 – Summary of the kinetic resolution of silanes.

Entry	Silane	$[\alpha]_D$ (+)-silane	ee (+)-silane	$[\alpha]_D$ (-)-silane	ee (-)-silane
1	42b	+12° (0.01 molL ⁻¹ , Et ₂ O)	56 %	-11° (0.02 molL ⁻¹ , Et ₂ O)	54 %
2	43b	+11° (0.06 molL ⁻¹ , Et ₂ O)	66 %	-11° (0.05 molL ⁻¹ , Et ₂ O)	64 %
3	44	+17° (0.04 molL ⁻¹ , Et ₂ O)	84 %	-15° (0.04 molL ⁻¹ , Et ₂ O)	64 %

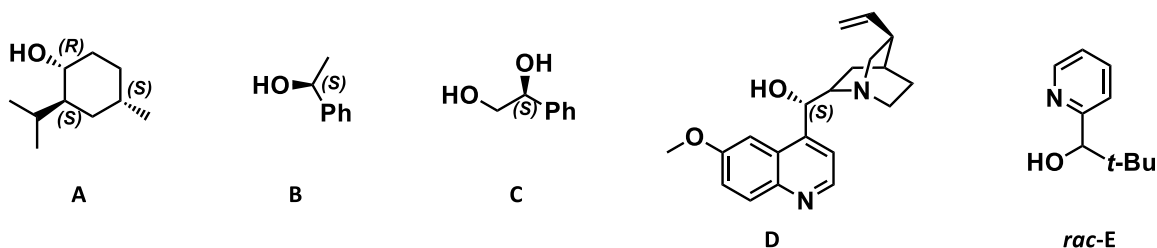
3.1.3.3 Summary of the Chiral Resolution of Silanes

In summary, three approaches for the chiral resolution of silanes **42b**, **43b,c** and **44** were tested (Scheme 38).



Scheme 38 – Overview of the tested approaches for the chiral resolution of silanes **42b**, **43b,c** and **44** (Resolution 1: derivatization with an enantiomerically pure alcohol, Resolution 2: kinetic resolution via oxidation of the thiophenyl group, Resolution 3: kinetic resolution via enantiomerically selective dehydrogenative coupling with an alcohol).

The first approach was the Resolution 1 (Scheme 38) via the dehydrogenative coupling of silanes **rac-42b** and **rac-43b** with an enantiomerically enriched alcohol **A-D** and pyridyl alcohol **rac-E** to give siloxanes **47C**, **48A,B,C,E**. The pyridyl alcohol **E** is not commercial available and was, initially, used as racemic mixture for evaluation purposes. The reaction was catalyzed by palladium nanoparticles.^[58]



These studies revealed, that the dehydrogenative coupling reaction of acenaphthyl silanes **rac-42b** and **rac-43b,c** proceeds only with the phenylmethyl-substituted silanes **rac-42b**, **rac-43b**. The *tert*-

butylmethyl-substituted silane **rac-43b** did not undergo the reaction with the tested alcohols **C** and **E**. The reason is most likely the steric demand of the *tert*-butyl substituent. The assumption, that the reaction is limited regarding sterically demanding reagents was also observed by the reaction of the sterically demanding quinidine **D** and silane **rac-43b** which was not successful as well.

Siloxanes **47C**, **48A,B,C,E** were obtained in bad to moderate yields (12-54 %). The obtained siloxanes **47C**, **48A,B,C** should be separated via column chromatography and then reduced to generate enantiomerically enriched silanes **42b** and **43b**. However, the separation of none of the siloxane mixtures was successful. Furthermore, the formation of the by-product silanol **50/51** was observed in all attempts. Therefore, this resolution route was abandoned and the kinetic resolution of silanes **rac-42b**, **rac-43b,c** and **rac-44** was tested.

The first kinetic approach was the Resolution 2 (Scheme 38) via enantiomerically selective oxidation of the thiophenyl group of silane **rac-43b** to give species **52**. Two reagents were tested, namely the Sharpless reagent and the vanadium-salan catalyst (Figure 12). The silane **43b** was inert against the tested reagents, and thus, the product **52** was not obtained (Scheme 38). Therefore, this resolution route was not further pursued.

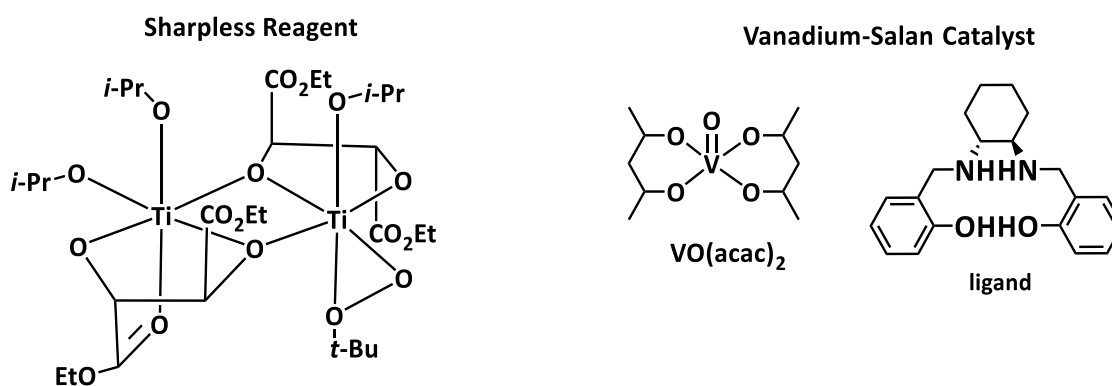
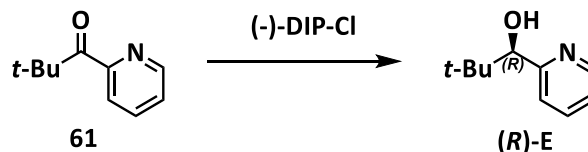


Figure 12 – Tested chiral reagents for the enantiomerically selective oxidation of the thiophenyl group of silane **43b**.

The second kinetic approach was the Resolution 3 (Scheme 38) via the enantiomerically selective Cu(I)-catalyzed dehydrogenative coupling of silanes **rac-42b**, **rac-43b,c** and **rac-44** with pyridyl alcohol (**R**)-**E**. As mentioned before, the pyridyl alcohol (**R**)-**E** is not commercially available and was synthesized by the enantiomerically selective reduction of the corresponding ketone **61** with (-)-*B*-chlorodiisopinocampheylborane ((-)-DIP-Cl) (Scheme 39).



Scheme 39 - Enantiomerically selective reduction of the ketone **61** with (-)-B-chlorodiisopinocampheylborane ((-)-DIP-Cl) to give pyridyl alcohol **(R)-E**.

The results of the enantiomerically selective dehydrogenative Si – O coupling reaction are summarized in Table 7. Again, the sterically demanding *tert*-butylmethyl-substituted silane **rac-43c** did not undergo the reaction. The reactions of phenylmethyl-substituted silanes **rac-42b**, **rac-43b** and **rac-44** to give the corresponding siloxanes **47E**, **48E** and **56** were successful. The remaining enantiomer was for all silanes the (+)-enantiomer and the enantiomer resulting from the reduction of the siloxane the (-)-enantiomer.

Table 7 – Summary of the results (yield and enantiomeric excess) of the kinetic resolution of silanes **42b**, **43b,c** and **44** via the dehydrogenative coupling with pyridyl alcohol **(R)-E**.

$$\text{PhMeSi-H-ChPh} \xrightarrow{0.5 \text{ (R)-E, [Cu]}} \text{PhMeSi-O-t-Bu-ChPh} \xrightarrow{\text{DIBAL-H}} \text{PhMeSi-H-ChPh}$$

rac-42b (ace, Ch = O, R = Ph)
rac-43b (ace, Ch = S, R = Ph)
rac-44 (naph, Ch = S, R = Ph)

(+)-42b, 43b, 44

47E (ace, Ch = O)
48E (ace, Ch = S)
56 (naph, Ch = S)

(-)-42b, 43b, 44

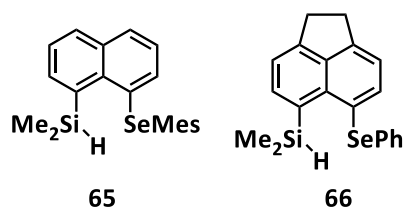
Entry	Silane	Yield (+)-silane	ee (+)-silane	Yield Siloxane	dr Siloxane	Yield (-)-silane	ee (-)-silane
1	42b	97 % ^{a)}	54 %	123 % ^{b)}	85:15	80 %	54 %
2	43b	80 %	66 %	69 %	91:9	82 %	64 %
3	44	59 %	84 %	75 %	93:7	69 %	64 %

(a) Mixture with ca. 15 % Ph₃P, b) yield is too high since 0.6 equiv. pyridyl alcohol **E** was used and remaining impurities.)

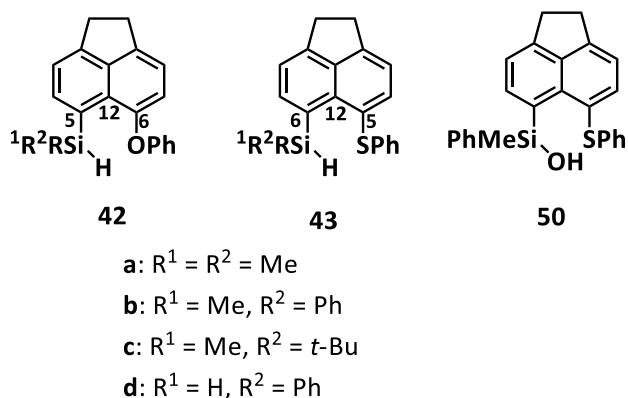
The yields of the reactions, dehydrogenative coupling as well as reduction of siloxanes, were good to moderate (59-82 %). The enantiomeric excesses of the silanes **(+)/(–)-42b**, **(+)/(–)-43b** and **(–)-44** are moderate (ee = 54-66 %). The best result was obtained with silane **(+)-44** with an ee of 84 %.

3.1.4 Crystal Structures of Acenaphthyl Silanes and Phenylmethylsilanol

Previous studies showed that selenyl- and telluryl-substituted acenaphthyl silanes exhibit in the NMR experiments a characteristic chalcogen hydrogen through space coupling.^[6a] The X-ray structures of selenyl-substituted derivatives **65** and **66** show that the hydrogen atom of the silyl substituent is *syn* relative to the selenium atom with Se/H distances of $d(\text{Se}/\text{H}) = 276$ pm (for **65**) and $d(\text{Se}/\text{H}) = 289$ pm (for **66**) which are significant smaller than the sum of the van der Waals radii ($\Sigma \text{vdW}(\text{Se}/\text{H}) = 300$ pm).^[71] Due to these observations a certain interaction between the hydrogen and the chalcogen atom is assumed.^[6a]



In this chapter, the interactions of the two substituents in *peri*-position of acenaphthyl silanes **42** and **43** and silanol **50** are discussed by means of the molecular structures and DFT calculations at the M06-2X/Def2-TZVP level of theory. Single crystals suitable for X-ray analysis have been obtained of silanes **42a,b,d**, **43a-d** and silanol **50** (Figure 14 - Figure 16).



To investigate the interaction between the chalcogen atom and the hydrogen or even the silicon atom, the molecular structures were examined by different parameters. This structural classification of naphthyl and acenaphthyl species was introduced and established by Woollins and co-workers and further expanded by Hupf et al. (Figure 13).^[72] The first parameter is the distance between the *peri*-atoms which is in unstrained acenaphthene $d(\text{H}/\text{H}) = 270$ pm. The second parameter is the sum of the bay angles ($\Sigma\beta$) which is the sum of the angles E-C5-C12, C5-C12-C6 and C12-C6-E' ($\Sigma\beta = 368^\circ$ for unstrained acenaphthene).^[73] And the third parameter is the out-of-plane distance of the *peri*-

substituents from the mean central plane spanned by the ten carbon atoms of the acenaphthene backbone. The larger is the distance of the *peri*-substituents to the acenaphthene plane, the higher are the repulsive interactions between the *peri*-atoms. Further parameters which can be taken to account are the torsion angles of which one is illustrated in Figure 13. The ideal value is 180°, whereas torsion angles near this value indicate either attractive or no *peri*-interactions.

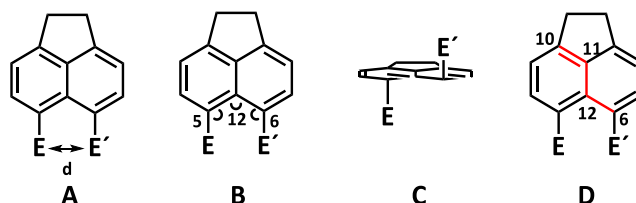


Figure 13 – Structural parameter in *peri*-substituted acenaphthenes (A: peri-distance, B: $\Delta\beta$, C: out-of-plane distance, D: torsion angle).

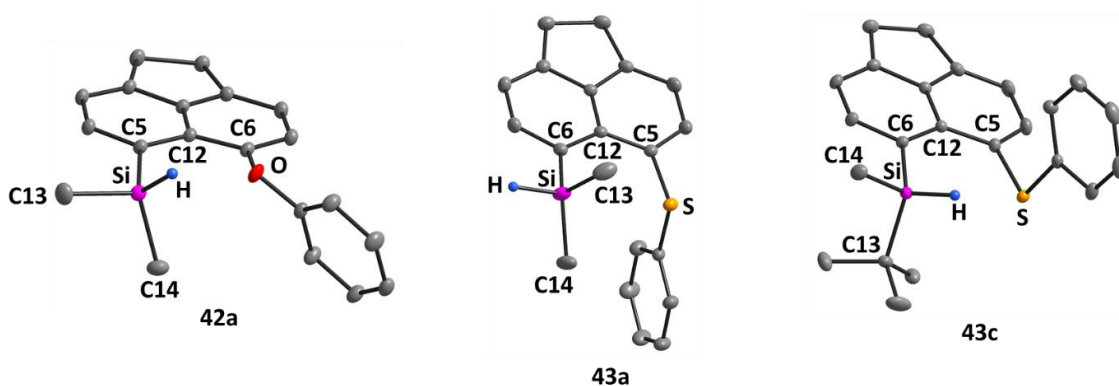


Figure 14 – Molecular structures of dimethyl silane **42a** (left), dimethyl silane **43a** (middle) and *tert*-butylmethyl silane **43c** (right) (thermal ellipsoids at 50% probability, H atoms omitted for clarity except the Si – H). Pertinent bond lengths [pm] and bond angles [°]; dimethyl silane **42a** (left, triclinic space group P-1): Si/O 291.27(8), Si – C5 188.87(9), O – C6 138.29(10), O/H 268, Si-C5-C12 125.47(6), C5-C12-C6 127.32(8), C12-C6-O 115.31(7), C5-Si-C13 108.778(4), C5-Si-C14 109.41(4), C13-Si-C14 107.87(5). Dimethyl silane **43a** (middle, triclinic space group P-1): Si/S 329.37(4), Si – C6 188.97(10), S – C5 177.05(10), Si – H 141.4(16), S-C5-C12 121.636(7), Si-C6-C12 130.086(7), C5-C12-C6 128.61(8), C6-Si-C13 111.965(54), C6-Si-C14 120.036(51), C13-Si-C14 112.468(67). *tert*-Butylmethyl silane **43c** (right, triclinic space group P-1): Si/S 333.49(3), Si – C6 190.15(5), S – C5 177.16(5), Si – H 138, S/H 281, S-C5-C12 123.20(4), Si-C6-C12 130.63(3), C5-C12-C6 128.99(4), C6-Si-C13 110.063(23), C6-Si-C14 108.420(25), C13-Si-C14 108.718(24).

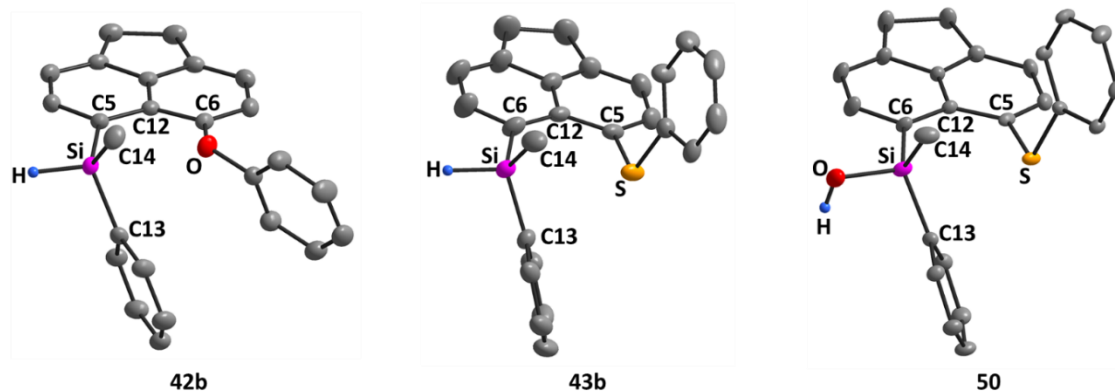


Figure 15 – Molecular structures of phenylmethyl silane **42b** (left), phenylmethyl silane **43b** (middle) and silanol **49** (right) (thermal ellipsoids at 50 % probability, H atoms omitted for clarity except the Si – H and O – H). Pertinent bond lengths [pm] and bond angles [°]; phenylmethyl silane **42b** (left, triclinic space group P-1): Si/O 292.227(1), Si – C5 187.58(1), O – C6 138.81(1), Si – H 141.(2), O-C5-C12 114.68(1), Si-C6-C12 126.79(8), C5-C12-C6 127.36(1), C5-Si-C13 109.411(62), C5-Si-C14 116.93(6), C13-Si-C14 112.56(7). Phenylmethyl silane **43b** (middle, monoclinic space group Cc): Si/S 330.55(2), Si – C6 189.6(5), S – C5 178.4(4), Si – H 147.(5), S-C5-C12 121.8(4), Si-C6-C12 132.1(3), C5-C12-C6 128.2(4), C6-Si-C13 113.5(3), C6-Si-C14 115.7(3), C13-Si-C14 (111.2(3). Silanol **50** (right, monoclinic space group Cc): Si/S 325.74(11), Si – C6 189.6(3), S – C5 177.9(3), Si – O 168.0(2), S-C5-C12 121.2(2), Si-C6-C12 130.6(2), C5-C12-C6 128.8(2), C6-Si-C13 114.66(13), C6-Si-C14 115.10(15), C13-Si-C14 113.48(14).

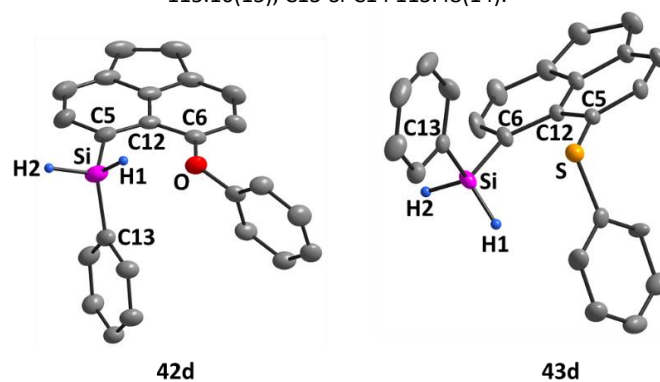


Figure 16 – Molecular structures of phenyl silane **42d** (left) and phenyl silane **43d** (right) (thermal ellipsoids at 50 % probability, H atoms omitted for clarity except the Si – H). Pertinent bond lengths [pm] and bond angles [°]; phenyl silane **42d** (left, monoclinic space group P2₁/c): Si/O 286.8(1), Si – C5 187.50(16), O – C6 138.56(15), Si – H1 139(1), O/H1 262.(5), O-C5-C12 115.01(12), Si-C6-C12 126.10(11), C5-C12-C6 126.97(12), i-C-O-C5 118.44(11). Phenyl silane **43d** (right, monoclinic space group P2₁/c): Si/S 314.86(7), Si – C6 185.9(3), S – C5 177.16(5), Si – H 133.(5), S/H 284.(06), S-C5-C12 121.56(18), Si-C6-C12 127.80(18), C5-C12 C6 128.5(2), i-C-S-C5 104.90(19).

To classify whether repulsive or attractive interactions between the *peri*-substituents in silanes **42**, **43** and silanol **50** are present, the presented parameters are summarized in Table 8. In general, the angles in the bay region are for the thiophenyl-substituted derivatives **43** with $\Sigma\beta = 378\text{--}384^\circ$ larger compared to those of the phenoxy-substituted derivatives **42** ($\Sigma\beta = 368\text{--}369^\circ$). Notably, the phenoxy derivatives **42** exhibit a similar value for the sum of the bay angles as unstrained acenaphthene ($\Sigma\beta = 368^\circ$). The bay angle of the *tert*-butylmethylsilyl-substituted thiophenyl compound **43c** is largest compared to compounds **42**, **43** and **50** and is by 16° higher than in unstrained acenaphthene. The out-of-plane distances of both *peri*-substituents of silanes **42** and **43** are rather small ($d = 0.5\text{--}41.2$

pm). Dimethyl-substituted thiophenyl derivative **43a** shows the highest out-of-plane distance for the silicon atom with $d(\text{Si}) = 41.2$. In compounds **42**, **43** and **50**, the distance between the substituents in the *peri*-positions is higher than the distance in unstrained acenaphthene ($d(\text{Si}/\text{D}) = 287\text{-}333\text{pm}$ vs $d(\text{H}/\text{H}) = 270\text{ pm}$) but distinct smaller than the corresponding sum of the van der Waals radii of the silicon and the chalcogen atom ($\Sigma\text{vdW}(\text{Si}/\text{O}) = 362\text{ pm}$, $\Sigma\text{vdW}(\text{Si}/\text{S}) = 390\text{ pm}$).^[71] This can indicate a slightly attractive interaction between the silicon center and the chalcogen atom. The torsion angle of all compounds is close to 180° suggesting either attractive or no interactions between the substituents in the *peri*-positions.

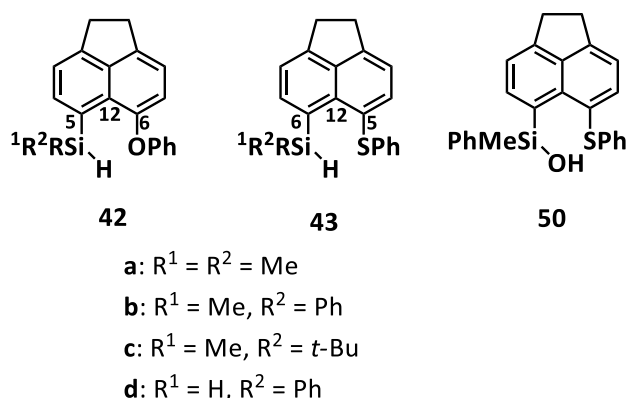


Table 8 – Selected structural parameters of silanes **42**, **43** and silanol **50**. (Dihedral angle C12-C5-Si-H or C12-C6-Si-H, $\Sigma\text{vdW}(\text{Si}/\text{O}) = 362\text{ pm}$, $\Sigma\text{vdW}(\text{Si}/\text{S}) = 390\text{ pm}$), $\Sigma\beta = 368^\circ$ and *peri*-distance 270 pm in unstrained acenaphthene.

Compound	D	D – Si [pm]	$\Sigma\beta$ [°]	d(Si) [pm]	d(D) [pm]	$\Sigma\alpha(\text{SiC}_3)$ [°]	$\Sigma\alpha(\text{D})$ [°]	Torsion angle [°]	Dihedral angle [°]
42a	OPh	291.3	368.1	27.8	-13.7	326.1	345.8	178.3	61.6
42b	OPh	292.2	368.9	21.3	-11.7	338.9	351.5	179.8	171.4
42d	OPh	286.8	368.1	0.5	5.2	336.5	353.7	176.2	52.5
43a	SPh	329.4	380.3	41.2	-13.2	352.5	289.6	177.7	168.3
43b	SPh	330.6	382.1	6.9	-3.2	340.5	295.2	179.4	170.4
43c	SPh	333.5	383.8	5.6	13.2	327.2	281.9	177.1	38.5
43d	SPh	314.9	377.9	3.2	6.4	339.3	282.8	177.6	60.9
50	SPh	325.7	380.6	3.5	-9.4	343.3	294.2	178.9	174.1

As described in the beginning, the direction of the hydrogen atom attached to the silicon atom is even more remarkable for acenaphthyl silanes **42**, **43** and is indicated by the dihedral angle (Figure 17, Table 8, for OPh derivatives **42**: C12-C5-Si-H, for SPh derivatives **43**: C12-C6-Si-H).

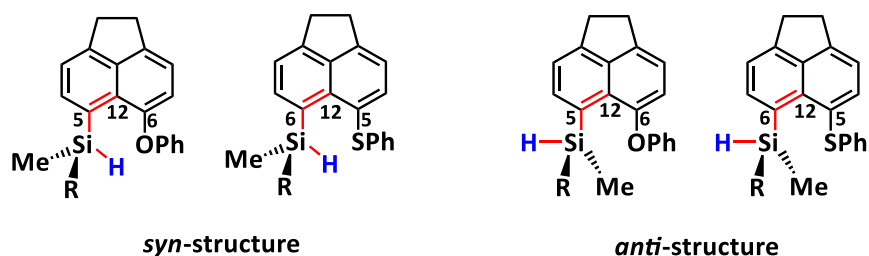


Figure 17 – Illustration of the *syn*- and *anti*-structures of silanes **42** and **43**, whereby *syn* and *anti* refer to the position of the hydrogen atom relative to the chalcogen atom and the dihedral angle marked in red (R = Me, Ph, *t*-Bu).

The hydrogen atom of *tert*-butylmethyl thiophenyl-substituted derivative **43c** is *syn* relative to the sulfur atom ($\text{C12-C6-Si-H} = 38.5^\circ$), whereby, the S/H distance is by 9 pm smaller than the sum of the van der Waals radii ($d\text{S/H} = 281 \text{ pm}$, $\Sigma\text{vdW (S/H)} = 290 \text{ pm}$).^[71] A similar value is observed in dihydrogen derivative **43d** ($d\text{S/H} = 284 \text{ pm}$). The corresponding phenoxy derivative **42d** exhibits a O/H distance which is by 21 pm shorter compared to that of thiophenyl derivative **43d** and match the sum of the H/O van der Waals radii ($d\text{H/O} = \Sigma\text{vdW (O/H)} = 262 \text{ pm}$).^[71] Dimethylsilyl phenoxy acenaphthene **42a** also crystallizes with the hydrogen atom *syn* relative to the oxygen atom ($\text{C12-C5-Si-H} = 61.6^\circ$, $d\text{(O/H)} = 268.4 \text{ pm}$). The O/H distance is by 6 pm larger compared to the sum of the van der Waals radii. These observations are similar to those of selenyl-substituted derivatives **65**, **66** (see above). In contrast, the hydrogen/oxygen atom of both phenylmethyl-substituted silanes **42b** and **43b**, of dimethyl thiophenyl acenaphthene **43a** and of silanol **50** is positioned *anti* relative to the chalcogen atom (*anti*-structures, dihedral angle = $168\text{--}174^\circ$). Interestingly, the sum of the bond angles of the silicon atom to the carbon substituents show for these derivatives **42b**, **43a,b** and **50** a trigonal flattening ($\Sigma\alpha(\text{Si}) = 339\text{--}352^\circ$). In return, derivatives **42a** and **43c** with the hydrogen atom *syn* relative to the chalcogen atom (*syn*-structures) exhibit a sum of the bond angles around the silicon atom of $\Sigma\alpha(\text{Si}) = 326\text{--}327^\circ$ confirming their tetrahedral coordination sphere.

The trigonal flattening of the silicon center in the *anti*-structures indicates an interaction between the silicon and the sulfur atoms. If the sulfur atom donates electron density to the silicon atom, it is assumed that the silicon-hydrogen interaction is weakened compared to the Si – H bond in the *syn*-structures. The relative strength of the Si – H bond in *syn*- and *anti*-structures can be compared by the IR resonance.^[74] The value for the experimental determined IR resonance (ATR, solid state) of *tert*-butylmethyl derivative **43c** (*syn*-structure) is by $69\text{--}84 \text{ cm}^{-1}$ larger compared to the wave numbers of the derivatives **43a** and **43b** (*anti*-structures) (Table 9).

Table 9 – Calculated energy difference ΔE for the two conformers of silanes **43a**, **43b** and **43c** and comparison of the corresponding calculated Si – H IR bands (M062X/Def2-TZVP) with the experimental determined values. (Scaling factor for calculated $\tilde{\nu}(\text{Si} - \text{H})$ values is 0.9619, details see Computational Details.)

Compound	$\Delta E (E(\text{syn}) - E(\text{anti}))$ [kJmol ⁻¹]	$\tilde{\nu}(\text{Si} - \text{H})^{\text{calc}}$ [cm ⁻¹] <i>syn</i>	$\tilde{\nu}(\text{Si} - \text{H})^{\text{calc}}$ [cm ⁻¹] <i>anti</i>	$\tilde{\nu}(\text{Si} - \text{H})^{\text{exp}}$ [cm ⁻¹]	Solid state
43a	-3.3	2162	2090	2106	<i>anti</i>
43b	-1.2	2153	2103	2091	<i>anti</i>
43c	-0.6	2169	2102	2175	<i>syn</i>

The bathochromic shift of the wave number of the *anti*-structures (**43a**, **43b**) compared to the *syn*-structure (**43c**) indicates a weakened Si – H bond in the *anti*-structures (**43a**, **43b**). The calculated IR resonances for both conformers (*syn* and *anti*) show the same trend for all three species **43a-c** (Table 9). Consequently, the shift of the Si – H IR resonance might reflect whether the hydrogen atom is *syn* or *anti* relative to the chalcogen atom.

The calculated energy difference (ΔE) between the conformers of compounds **43a,b,c** is small ($\Delta E = 0.6\text{-}3.3$ kJmol⁻¹, Table 9) indicating that there is energetically no favored conformation. The analysis of the electron density in the framework of Bader's theory of atoms in molecules (QTAIM) of the two conformers shows a bond path with a bond critical point (bcp) between the hydrogen and the sulfur atom in the *syn*-structures and between the silicon and the sulfur atom in the *anti*-structures. The 2D Laplacian contour plots of the dimethylsilyl and the *tert*-butylmethylsilyl derivatives **43a** and **43c** are shown in Figure 18.^[75] The bond path in the QTAIM analysis between the silicon and the sulfur atom of the *anti*-structures might indicate a beginning S_N2 reaction at the silicon center with the sulfur atom as the nucleophile and the hydride as the leaving group. This could explain the weakened Si – H bond in the *anti*-structures indicated by the position of the Si – H IR bands.

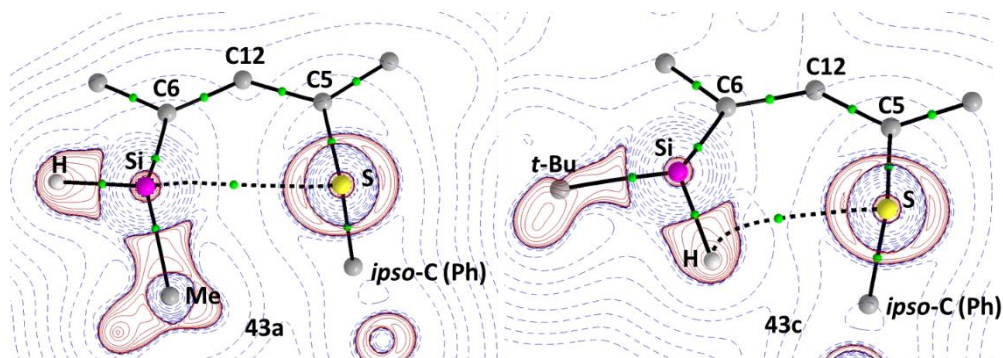


Figure 18 – 2D contour plots of the calculated Laplacian of the electron density, $\nabla^2\rho(r)$, in the Si-C12-Ch plane of dimethylsilane **43a** as example for an *anti*-structure (left) and methyl-*tert*-butylsilane **43c** as example for a *syn*-structure (right). Relevant parts of the molecular graphs of the silanes are projected onto the respective contour plot. Green spheres are the bond critical points (bcp). Black lines show the bond paths, which follow the line of maximum electron density: solid lines show bond paths with bcp of electron density $> 0.05 \text{ e} \cdot \text{\AA}^{-3}$, dashed lines show bond paths with bcp in which the electron density is between $0.05\text{-}0.008 \text{ e} \cdot \text{\AA}^{-3}$. Red contours indicate regions of local charge accumulation ($\nabla^2\rho(r) < 0$); blue contours indicate regions of local charge depletion ($\nabla^2\rho(r) > 0$).^[75]

Characteristic for a S_N2 reaction is the pentacoordinated intermediate. If in the *anti*-silanes a beginning S_N2 reaction is visible, the silicon center should adopt a coordination sphere which indicates the transition from a tetrahedral coordination sphere to a trigonal bipyramid. This can be determined via the geometrical goodness ($\Delta\Sigma(\Theta)$) which is defined as the difference of the sum of the equatorial and axial angles; thus, a tetrahedral structure exhibits a geometrical goodness of $\Delta\Sigma(\Theta) = 0^\circ$ and a perfect trigonal bipyramid exhibits a value of $\Delta\Sigma(\Theta) = 90^\circ$.^[76] To apply this for silanes **43**, the difference between the sum of the bond angles around the silicon atom ($\Sigma\alpha(\text{Si})$, equatorial angles) and the sum of the bond angles of the Si – H bond to the Si – C bonds ($\Sigma(\text{H-Si-C})$, axial angles) are used (Figure 19).

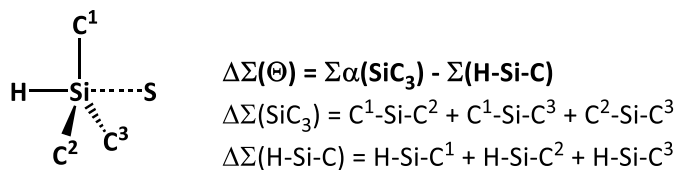


Figure 19 – Determination of the geometrical goodness ($\Delta\Sigma(\Theta)$) of silanes **43** with the sum of the bond angles around the silicon atom ($\Sigma\alpha(\text{SiC}_3)$, equatorial angles) and the sum of the bond angles of the Si – H bond to the Si – C bonds ($\Sigma(\text{H-Si-C})$, axial angles).

A scheme of a bimolecular S_N2 reaction at a silicon atom is shown in Figure 20.^[77] In the educt (Me_3SiY) the silicon atom exhibits a perfect tetrahedral coordination environment indicated by $\Delta\Sigma(\Theta) = 0^\circ$. When the nucleophile (X) approaches, the sum of the bond angles around the silicon center

increases, whereby the value for $\Delta\Sigma(\Theta)$ approximates 45° . In the intermediate, the silicon atom exhibits a trigonal bipyramidal coordination environment in which $\Delta\Sigma(\Theta)$ is 90° .

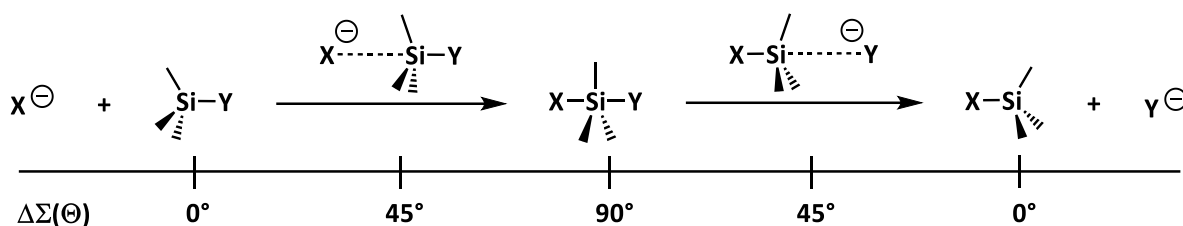


Figure 20 – Schematic illustration of a bimolecular S_N2 reaction at a silicon atom with the corresponding value for the geometrical goodness ($\Delta\Sigma(\Theta)$) of the stages of the reaction.

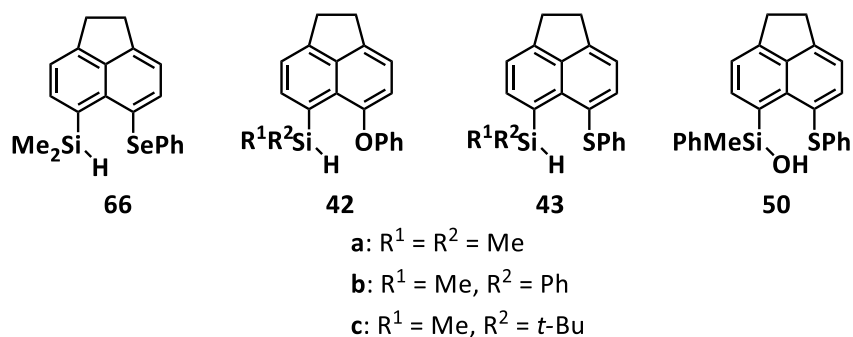
The geometrical goodness ($\Delta\Sigma(\Theta)$) of silanes **42b**, **43a,b** and silanol **50** were calculated from the X-ray diffraction data and are listed in Table 10. The values are in the range of 22 – 42° and are significantly higher than in a perfect tetrahedral coordination environment. Consequently, a starting S_N2 reaction in silanes is indicated. The closer the value is to 45° , the more pronounced is the degree of the starting S_N2 reaction. The most pronounced degree is present in dimethylsilyl thiophenyl acenaphthene **43a** ($\Delta\Sigma(\Theta) = 42^\circ$), followed by the thiophenyl-substituted silanol **50** ($\Delta\Sigma(\Theta) = 32^\circ$).

Table 10 – Comparison of the geometrical goodness ($\Delta\Sigma(\Theta)$) of silanes **42b**, **43a,b** and silanol **50** determined from X-ray structure.

Compound	$\Delta\Sigma(\Theta)$ [$^\circ$]
42b	22
43a	42
43b	25
50	32

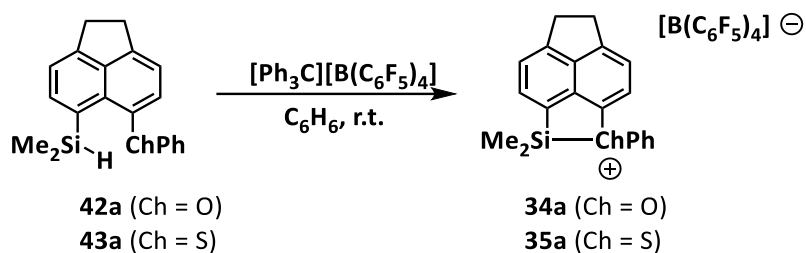
In conclusion, the interactions of the *peri*-atoms in acenaphthyl silanes **42**, **43** and silanol **50** appear to be rather attractive than repulsive. This is manifested in the relative small *peri*-distances, sum of the bay angles and out-of-plane distances of the silicon and the chalcogen atom in the crystal structures. Furthermore, indications of an interaction either between the hydrogen and the chalcogen atoms (*syn*-conformers) or between the silicon and the chalcogen atoms (*anti*-conformers) were recognized using DFT calculations and QTAIM analysis. These indications are supported by the analysis of the solid state structures. For example, in the *syn*-structure, *tert*-butylmethyl thiophenyl-substituted derivative **43c**, the S/H distance is by 9 pm smaller than the sum of the van der Waals radii. In the *anti*-structures, the value of the geometrical goodness ($\Delta\Sigma(\Theta)$) indicates a beginning

S_N2 reaction at the silicon center with the chalcogen atom as the nucleophile and the hydride as the leaving group. Further experimental support is given by the Si – H IR absorption band, which reflects the relative strength of the Si – H bond. The *syn*-structures show a hypsochromic shift of $\tilde{\nu}(\text{Si} - \text{H})$ compared to the *anti*-structures (*syn*-conformers **66** and **43c** $\tilde{\nu}(\text{Si} - \text{H}) = 2138^{[6a]}$ and 2175 cm^{-1} vs *anti*-conformers **43a** and **43b** $\tilde{\nu}(\text{Si} - \text{H}) = 2106$ and 2091 cm^{-1}), indicating that in *anti*-structures the Si – H bonds are weakened. This supports the theory of a beginning S_N2 reaction with the chalcogen atom as the nucleophile and the hydride as the leaving group. In return, this demonstrates the attractive interaction between the silicon and the chalcogen atom.



3.2 Phenoxy- and Thiophenyl-Stabilized Silyl Cations – A Comparison of the Dimethylsilyl-Substituted Derivatives

Silyl borates **34a**[B(C₆F₅)₄] and **35a**[B(C₆F₅)₄] were synthesized using the Corey reaction of the corresponding silanes **42a** and **43a** with trityl borate [Ph₃C][B(C₆F₅)₄] (Scheme 40) and fully characterized by multinuclear NMR spectroscopy.^[6a]



Scheme 40 - Synthesis of silyl borates **34a**[B(C₆F₅)₄] and **35a**[B(C₆F₅)₄].

The ²⁹Si NMR chemical shifts of silyl borates **34a**[B(C₆F₅)₄] and **35a**[B(C₆F₅)₄] are distinct low-field shifted ($\delta^{29}\text{Si} = 77$ (**34a**), 66 (**35a**)) compared to their corresponding precursors ($\delta^{29}\text{Si} = -14$ (**42a**), -18 (**43a**)) which is induced by the ionization. The observed deshielding of oxonium ion **34a** ($\Delta\delta^{29}\text{Si}_{\text{silane,cation}} = 91$) is higher than that of sulfonium ion **35a** ($\Delta\delta^{29}\text{Si}_{\text{silane,cation}} = 84$). In general, literature-known triarylsilylium ions exhibit a ²⁹Si NMR resonance of $\delta^{29}\text{Si} = 210$ -230 whereas known solvent-stabilized silyl cations have a ²⁹Si NMR chemical shift of $\delta^{29}\text{Si} = 88$ -97.^[9] The presented species **34a** and **35a** show with $\delta^{29}\text{Si} = 77$ and 66 a ²⁹Si NMR chemical shift which is comparable to the solvent-stabilized silyl cations. The ²⁹Si NMR chemical shifts of silyl cations **34a** and **35a** are independent of the solvent (**34a**: $\delta^{29}\text{Si} = 77.5$ (C₇D₈), 77.4 (C₆D₆), 78.1 (CD₂Cl₂); **35a**: $\delta^{29}\text{Si} = 66.0$ (C₇D₈), 65.8 (C₆D₆), 66.4 (CD₂Cl₂)) whereby an interaction of the positively charged silicon center with the solvent is ruled out. As a consequence, the stabilization of the electron deficient silicon center occurs exclusively intramolecularly by the remote donor substituent, namely OPh or SPh. Hence, silyl cations **34a** and **35a** are characterized by a direct linkage between the silicon and the chalcogen atom. In the ¹H NMR as well as in the ¹³C NMR spectrum one signal for the two methyl groups attached to the silicon center of phenoxy-stabilized silyl cation **34a** is observed (Figure 21, above). In contrast to these findings, sulfonium ion **35a** shows two signals for the methyl groups at the silicon atom in the ¹H NMR (Figure 21, below) as well as in the ¹³C NMR spectrum.

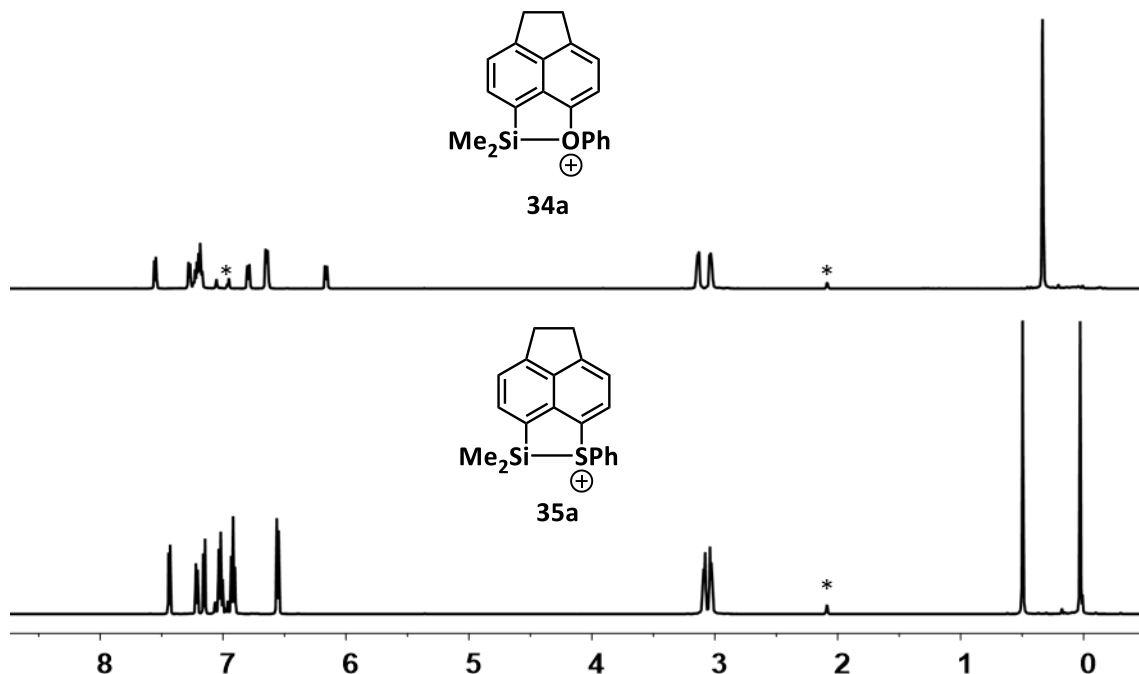


Figure 21 – ^1H NMR spectra (500 MHz, 305 K, C_7D_8) of phenoxy-stabilized silyl borate **34a** $[\text{B}(\text{C}_6\text{F}_5)_4]$ (above) and thiophenyl stabilized silyl borate **35a** $[\text{B}(\text{C}_6\text{F}_5)_4]$ (below) ($^*\text{C}_6\text{D}_5\text{CD}_2\text{H}$).

The non-equivalence of the methyl groups in sulfonium ion **35a** is not unexpected due to the predicted pyramidal coordination sphere of the sulfur atom. This pyramidalization implies a *syn/anti* relation of the phenyl substituent at the sulfur atom to the methyl groups at the silicon atom. The non-equivalence of the methyl groups at the silicon atom is also observed in the corresponding selenium and tellurium derivatives.^[6a] In fact, this substantiates the statement that a direct linkage between the silicon and the sulfur atom is apparent.

S. Rathjen was able to obtain single crystals suitable for X-ray diffraction spectroscopy of acenaphthyl-substituted sulfonium ion **35a** in the crystal of **35a** $_2[\text{B}_{12}\text{Br}_{12}]$ from a dichloromethane/*n*-hexane solution (Figure 22).^[78] Thiophenyl-stabilized silyl *closo*-borate **35a** $_2[\text{B}_{12}\text{Br}_{12}]$ crystallizes in the orthorhombic space group *Pnma* and shows well separated cations and anions. The closest distance between the bromine of the *closo*-borate and the silicon atom is $d(\text{Br}/\text{Si}) = 506$ pm and the closest distance to the sulfur atom is $d(\text{Br}/\text{S}) = 547$ pm which is distinct larger than the sum of the van der Waals radii, respectively ($\Sigma\text{vdW}(\text{Si}/\text{Br}) = 393$ pm, $\Sigma\text{vdW}(\text{S}/\text{Br}) = 363$ pm).^[71] The Si – S bond length is $d(\text{Si} - \text{S}) = 232.1$ pm and by 5 pm longer than the sum of the covalent radii for a Si/S single bond.^[79] The sum of the bay angles is $\Sigma\beta = 353.3^\circ$ and by 15° smaller compared to unstrained acenaphthene,^[73] demonstrating the attractive interaction between the *peri*-atoms. The sum of the bond angles around the silicon atom shows a trigonal flattening of the silicon atom ($\Sigma\alpha(\text{Si}) = 348.2^\circ$ compared to the ideal

value of a tetrahedral coordination environment $\Sigma\alpha = 328.2^\circ$). The sulfur atom exhibits a trigonal pyramidal coordination sphere with $\Sigma\alpha(S) = 307.7^\circ$.

At this point the question arises, whether the oxygen derivative **34a** is actually different in structure or a dynamic process in the molecule induces the equivalence of the methyl groups. The low temperature NMR experiment at -90°C of the naphthyl-substituted oxonium ion **36a** does not show a significant line broadening of the singlet signal of the methyl groups.^[6a] In the first instance, this shows that either the dynamic process is fast at the NMR time scale even at -90°C or oxonium ion **36a** exhibits a ground state structure with a higher symmetry as its heavier homologues.

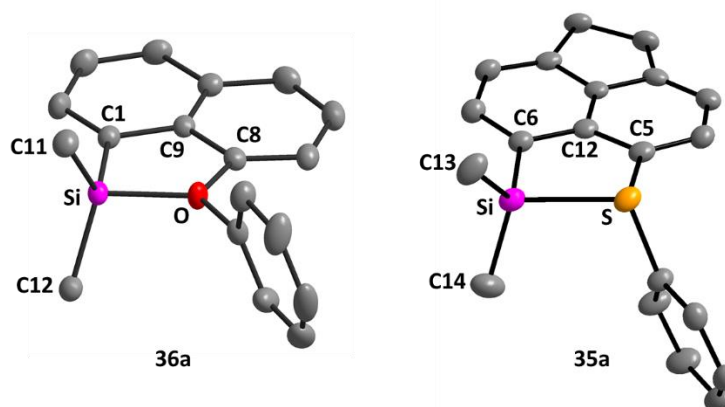


Figure 22 – Molecular structures of oxonium ion **36a** in the crystal of **36a**[HCB₁₁H₅Br₆] (left) and sulfonium ion **35a** in the crystal of **35a**₂[B₁₂Br₁₂] (thermal ellipsoids at 50 % probability, H atoms and counter ion omitted for clarity). Pertinent bond lengths [pm] and bond angles [°]; oxonium ion **36a**: Si – O 183.75(14), Si – C1 185.04(25), O – C8 144.01(28), Si-C1-C9 109.25(17), C1-C9-C8 118.76(21), C9-C8-O 109.89(19), C1-Si-C11 115.31(10), C1-Si-C12 118.32(11), C11-Si-C12 117.87(10), C8-O-Si 113.43(12), C8-O-C13 121.30(16), Si-O-C13 125.25(13). Sulfonium ion **35a**: Si – S 232.08(11), Si – C6 185.17(3), S – C5 177.91(3), Si-C6-C12 113.73(2), C6-C12-C5 125.14(3), C12-C5-S 114.55(2), C6-Si-C13 118.32(14), C6-Si-C14 116.79(15), C13-Si-C14 113.06(18), C5-O-Si 94.34(11), C5-O-C15 103.72(13), Si-O-C15 109.65(11).

Single crystals suitable for X-ray diffraction spectroscopy of the naphthyl-substituted oxonium ion **36a** were obtained in the crystal of **36a**[HCB₁₁H₅Br₆] from a dichloromethane/*n*-hexane solution (Figure 22). Phenoxy-stabilized silyl carborate **36a**[HCB₁₁H₅Br₆] crystallizes in the monoclinic space group *P*2₁/*c* and shows well separated cations and anions. While the closest distance for the bromine substituent at the carborate and the silicon atom is $d(\text{Br}/\text{Si}) = 404$ pm, the closest distance to the oxygen atom is $d(\text{Br}/\text{O}) = 395$ pm. Both values are larger than the sum of the van der Waals radii, respectively ($\Sigma\text{vdW}(\text{Br}/\text{Si}) = 393$ pm, $\Sigma\text{vdW}(\text{Br}/\text{O}) = 335$ pm).^[71] The Si – O bond length in naphthyl-substituted cation **36a** is $d(\text{Si} - \text{O}) = 183.8$ pm and is by 20 pm longer than an average Si – O bond in compounds with a tetra coordinated silicon atom and a dicoordinated oxygen atom ($d(\text{Si} - \text{O}) = 163$ pm).^[80] Furthermore, this bond length is by 5-6 pm longer than the Si – O bond length of silylated oxonium ions ($d(\text{Si} - \text{O}) = 177.7$ - 178.5 pm).^[81] The attractive interaction of the silicon and the oxygen

atom leads to a pronounced distortion of the five membered ring which is formed by the naphthyl backbone and the two connected *peri*-substituents. The sum of the bay angles in silyloxonium ion **36a** is $\Sigma\beta = 337.9^\circ$ and distinctively smaller than in unstrained naphthalene ($\Sigma\beta = 360^\circ$).^[72b] The sum of the bond angles around the silicon atom ($\Sigma\alpha(\text{Si}) = 351.3^\circ$) reveals its pronounced trigonal flattening (ideal value $\Sigma\alpha(\text{Si}) = 328.2^\circ$). The oxygen atom exhibits a perfect trigonal planar coordination sphere with $\Sigma\alpha(\text{O}) = 360.0^\circ$ upon which a dynamic process, which induces the equivalence of the methyl groups attached to the silicon atom, is ruled out.

The crystal structures do not only provide evidence for the structure of cations **36a** and **35a**, it also gives the possibility to check the reliability of the quantum mechanical calculations at the DFT M06-2X/Def2-TZVP level of theory of the structures of the presented cationic systems. Comparison of the parameter from the X-ray structures and the calculated structures of cations **36a** and **35a** are in good agreement (Table 11). The deviation of the listed parameters is in the range of 0.03 – 0.3 %. Only the deviation of the sum of the bond angles around the sulfur atom of sulfonium ion **35a** is ca. 3 %. In both structures, the prediction of the out-of-plane distances does not fit that nicely. However, the out-of-plane distortion of the *peri*-substituents is only related to small forces and is likely to be strongly influenced by intermolecular interactions in the solid state. Consequently, for all other parameters, the used M06-2X/Def2-TZVP level of theory is suitable for the DFT calculations of the presented cationic system. Backed up by the good agreement of X-ray and calculated structures, it is possible to compare the calculated structural parameters of the corresponding acenaphthyl analogs. The naphthyl-substituted oxonium ion **36a** and the acenaphthyl-substituted oxonium ion **34a** exhibit nearly identical values (Table 11), indicating, that there is no significant difference between the naphthyl and the acenaphthyl substitution.

Table 11 – Selected calculated parameters (M062X/def2-TZVP) and structural parameters in parentheses for dimethylsilyl cations **36a**, **34a** and **35a**.

Compound	D	D – Si [pm]	$\Sigma\beta$ [°]	d(Si) [pm]	d(D) [pm]	$\Sigma\alpha(\text{SiC}_3)$ [°]	$\Sigma\alpha(\text{D})$ [°]
36a	OPh	183.2 (183.8)	337.7 (337.9)	0.6 (3.2)	0.9 (9.5)	351.7 (351.5)	359.4 (360.0)
34a	OPh	185.4	337.3	0.002	-0.001	352.2	360.0
35a	SPh	232.1 (232.1)	353.4 (353.3)	18.1 (9.8)	-8.0 (-18.0)	349.0 (348.2)	299.4 (307.7)

3.2.1 Coordination Environment of the Oxygen Atom in Silyloxonium Ions

As shown in Chapter 3.2 via NMR spectroscopy and X-ray diffraction analysis, phenoxy-stabilized dimethylsilyl cation **36a** exhibits an oxygen atom with a perfect trigonal planar coordination environment.^[6a] The trigonal planar coordination sphere of the oxygen atom of silyloxonium ions has been preceded in literature. An example is silyloxonium ion **67**, which was described by M. Kira and H. Sakurai in 1992 and nine years later characterized via X-ray spectroscopy by Driess and co-workers.^[81c, 82] The sum of the bond angles around the oxygen atom is $\Sigma\alpha(O) = 359^\circ$, proving the perfect trigonal planar coordination sphere of the oxygen atom. Another example is species **68**, reported by A. Schäfer et al. in 2014, in which the bond angles around the oxygen atom is $\Sigma\alpha(O) = 360^\circ$.^[81a]

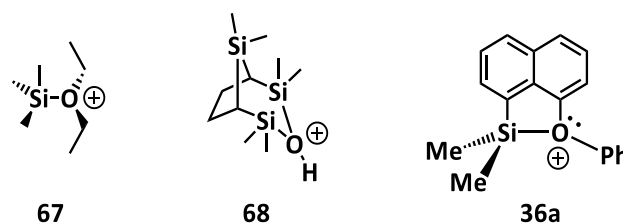
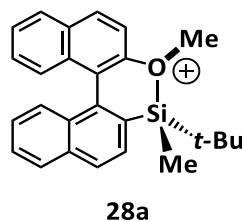


Figure 23 – Examples of silyloxonium ions with an oxygen atom exhibiting a perfect trigonal planar coordination environment.

In contrast to these findings, Ducos et al. demonstrated based on NMR experiments and DFT calculations that the oxygen atom in binaphthyl-substituted silyloxonium ion **28a** exhibits a trigonal pyramidal coordination sphere.^[45d]



The nature of the silicon oxygen bond and bond angles was widely discussed in terms of the differences between organic ethers and disiloxanes.^[80, 83] While the bond angle C-O-C of ethers is about $110\text{--}114^\circ$, the Si-O-Si angle of disiloxanes is in the range of $145\text{--}150^\circ$.^[80] As reasons for the widened Si-O-Si angle compared to the C-O-C angle, hyperconjugation between the lone pair at the oxygen atom (n_O) and the π^* (SiR_3) as well as the strong polarization of the Si – O bond and the thereof resulting repulsive interactions between the silicon moieties were discussed.^[80, 83a] In accordance with the valence shell electron pairs repulsion (VSEPR) concept of Gillespie and Nyholm, the oxygen

atom in silyloxonium ions is of the type AX₃E and should form a trigonal pyramidal structure as the NH₃ molecule (Figure 24). In oxonium ions with three carbon-based moieties, such as species **69** and **70**, the analogy to NH₃ is given; whereby, it is important to notice that triethyloxonium ion **69** shows a significant trigonal flattening.^[84]

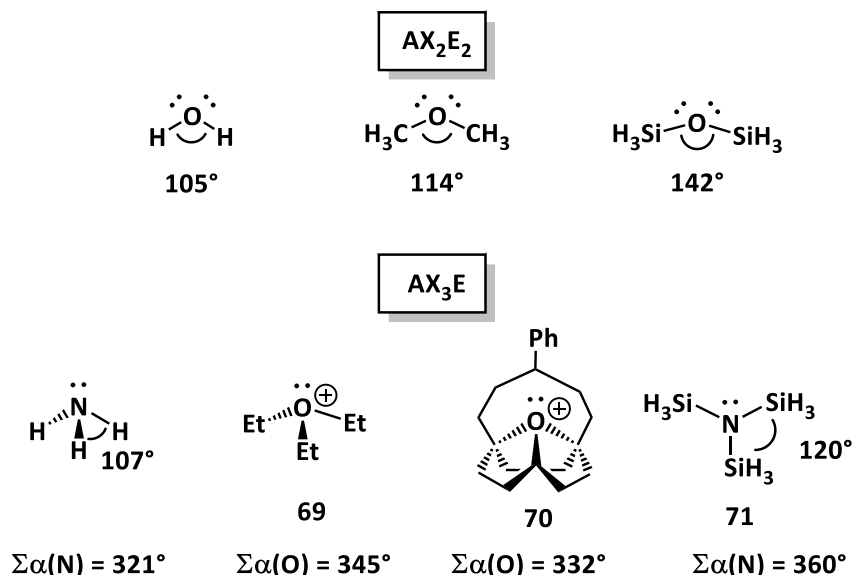
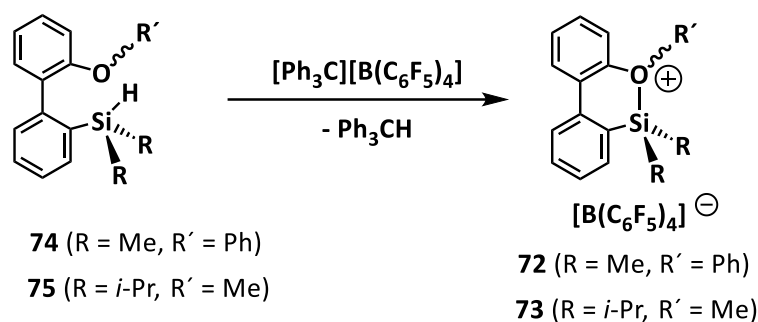


Figure 24 – Comparison of the bond angles in structures which follow the VSEPR concept with the corresponding silylated structures.

The effect of silyl groups to the coordination environment of the central atom was also observed for trisilylamine **71** in which the sum of the bond angles around the nitrogen atom is 360° (Figure 24). Y. Mo et al. describe that, besides the $n_{\text{N}} \rightarrow \sigma_{\text{SiH}}^*$ negative hyperconjugation stereoelectronic effects due to the high polarized N – Si bond are the reason for the trigonal planar coordination sphere of the nitrogen atom.^[85]

In order to investigate the coordination environment of the oxygen atom in silyloxonium ions biphenyl derivatives **72** and **73** were prepared (Scheme 41). These investigations are in cooperation with the group of Prof. Landais in Bordeaux and the precursor silanes **74** and **75** were provided by his co-worker A. Fernandes. Two considerations regarding the design of the model compounds in comparison to Ducos' silyloxonium ion **28a** were made. On the one hand, the backbone should be simplified by going from the binaphthyl system to the biphenyl substituent to verify the impact of the backbone to the coordination environment of the oxygen atom. On the other hand, the influence of steric stress due to different substituents with different steric demand at the silicon atom should be avoided. Therefore, the silicon atom bears either *iso*-propyl or methyl groups. The preparation

was carried out in dichloromethane- d_2 at $-80\text{ }^\circ\text{C}$ for dimethylsilyl borate **72** $[\text{B}(\text{C}_6\text{F}_5)_4]$ and at $-80\text{ }^\circ\text{C}$ - r.t. for di-*iso*-propylsilyl borate **73** $[\text{B}(\text{C}_6\text{F}_5)_4]$ (Scheme 41, for details see Experimental Part).



Scheme 41 – Corey reaction of biphenylsilanes **74** and **75** with trityl borate to give silyl borates **72** $[\text{B}(\text{C}_6\text{F}_5)_4]$ and **73** $[\text{B}(\text{C}_6\text{F}_5)_4]$.

The subsequent NMR measurements were done at $-90\text{ }^\circ\text{C}$. The NMR spectra of di-*iso*-propyl derivative **73** are shown as an example in Figure 25-26. In the ^{29}Si NMR spectrum (Figure 25), one resonance at $\delta^{29}\text{Si} = 49.3$ was observed which is within the expected range of intramolecularly stabilized silyloxonium ions (vide infra). The second ^{29}Si chemical shift at $\delta^{29}\text{Si} = 8.3$ was assigned to the corresponding cyclic biphenyl-di-*iso*-propylsiloxane which is the results of the follow up reaction of silyl cation **73** with remaining silane **75** under release of methane. This side reaction has been preceded in the literature.^[6a, 45d]

If the oxygen atom in species **73** exhibits a trigonal pyramidal coordination sphere, it is expected that two sets of signals are detected for the *i*-Pr groups at the silicon atom in the ^1H NMR spectrum. However, the ^1H NMR spectrum reveals only one set of signals which are assigned to the *i*-Pr groups ($\delta^1\text{H} = 1.04$ (6 H), 1.22 (6 H), 1.62 (2 H), Figure 26).

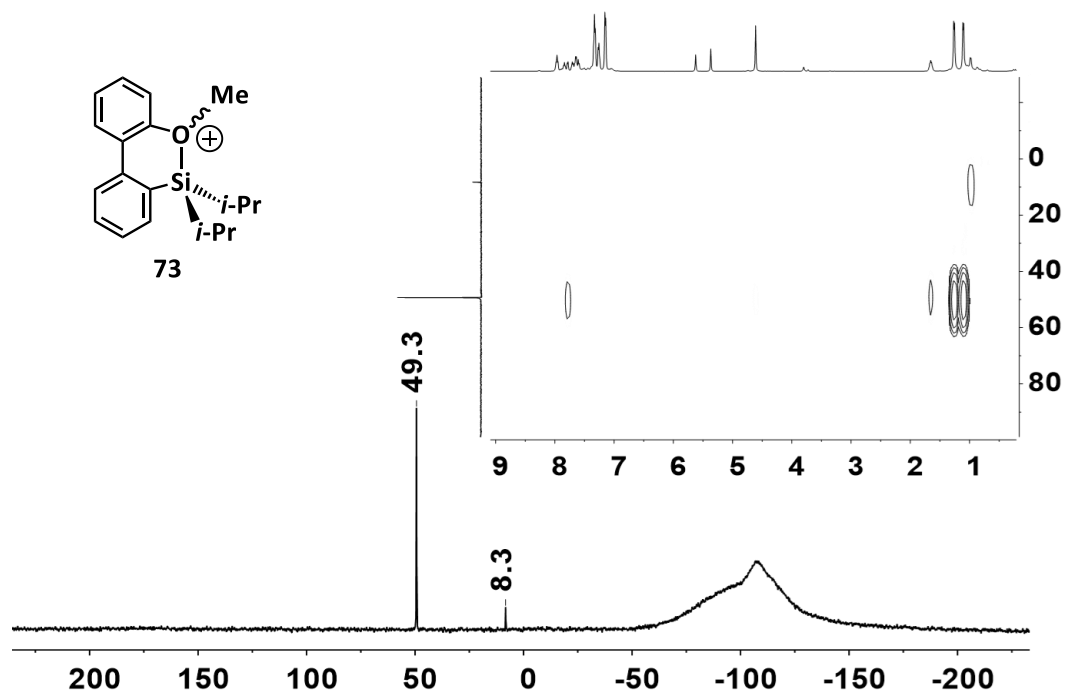


Figure 25 – $^{29}\text{Si}\{^1\text{H}\}$ NMR spectrum (99 MHz, 183 K, CD_2Cl_2) and $^1\text{H}/^{29}\text{Si}$ HMBC spectrum (500 MHz, 183 K, CD_2Cl_2) of di-*iso*-propylsilyl borate **73**[$\text{B}(\text{C}_6\text{F}_5)_4$].

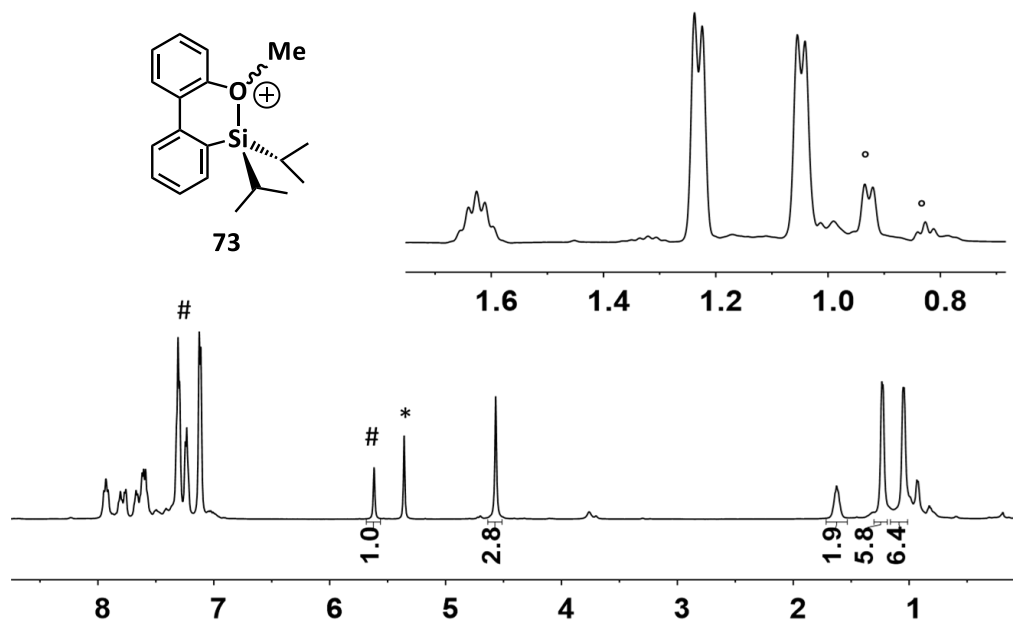
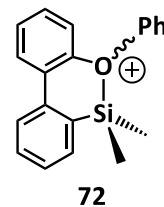


Figure 26 – ^1H NMR spectrum (500 MHz, 183 K, CD_2Cl_2) of di-*iso*-propylsilyl borate **73**[$\text{B}(\text{C}_6\text{F}_5)_4$] (extract lb = -8 Hz, gb = 5 Hz; * CDHCl_2 , # Ph_3CH , ° impurities).

The same results were obtained for dimethylsilyl cation **72**. The ^{29}Si NMR chemical shift of silyloxonium ion **72** is at $\delta^{29}\text{Si} = 59.5$ and only one singlet signal for the two methyl groups attached to the silicon atom at $\delta^1\text{H} = 0.80$ is detected. In conclusion, a symmetric ground state structure of silyloxonium ions **72** and **73** is indicated; however, a dynamic process within the molecule which leads to equality of the substituents at the silicon atom which is fast at the NMR time scale at $-90\text{ }^\circ\text{C}$ is still a possibility to consider.



To further investigate the coordination environment of the oxygen atom of silyloxonium ions **72** and **73**, their structures were optimized using DFT calculations (M06-2X/Def2-TZVP). For comparison, the structure of the corresponding biphenyl(dimethylsilyl) thiophenyl derivative **76** was calculated, too. The resulting optimized structures are shown in Figure 27.

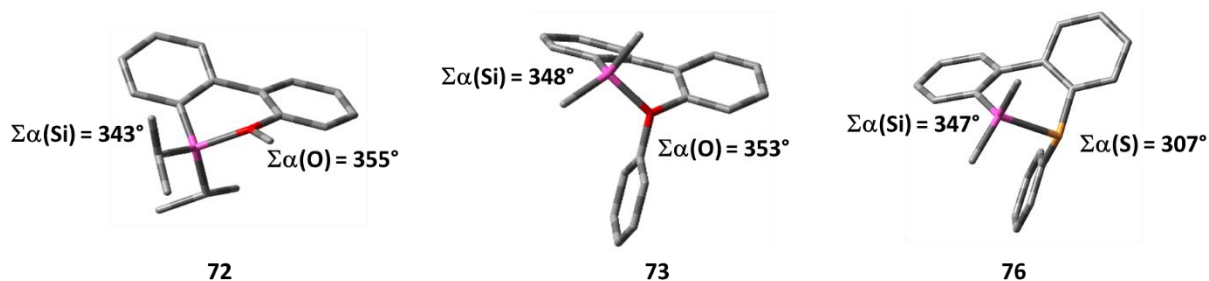


Figure 27 – Optimized structures of dimethyl and di-iso-propylsilyl cations **72**, **73** and thiophenyl derivative **76** (M06-2X/Def2-TZVP; hydrogen atoms omitted for clarity).

The two phenyl groups of the biphenyl substituent are twisted against each other, respectively, whereby the whole molecule shows a certain distortion compared to naphthyl- and acenaphthyl-substituted dimethylsilyloxonium ions **34a** and **36a**. The sum of the bond angles around the silicon atom of the calculated structure of biphenyl-substituted silyloxonium ions **72**, **73** and sulfonium ion **76** reveals their trigonal flattening which is fairly less pronounced than in the acenaphthyl congeners **34a** and **36a** ($\Sigma\alpha(\text{Si}) = 343\text{-}348^\circ$ in species **72**, **73** and **76** vs. $\Sigma\alpha(\text{Si}) = 352^\circ$ in species **34a** and **36a**). The deviation of the perfect trigonal planar coordination sphere of the oxygen atoms of species **72** and **73** is $5\text{-}7^\circ$, suggesting a rather trigonal planar coordination environment. In contrast, the sum of the bond angles around the sulfur atom is $\Sigma\alpha(\text{S}) = 307^\circ$ and reveals the trigonal pyramidal coordination environment.

Despite the trigonal coordination sphere of the oxygen atom in species **72** and **73**, the distortion resulting from the twist in the biphenyl system suggests an inequality of the substituents at the silicon atom. However, in the ^1H NMR spectrum at $-90\text{ }^\circ\text{C}$ only one signal set was observed for both species **72** and **73**. Therefore, a transition state (TS) optimization of silyl cations **72** and **73** was performed on

the basis of a perfect planar conformer of species **72** and **73** (Figure 28). The resulting structure of the TS calculation shows an imaginary frequency which includes the twisting of the C – C bond connecting the two phenyl groups of the biphenyl substituent. The twisting of the phenyl groups against each other leads to the swinging of the substituent at the oxygen atom from one side to the other (indicated by displacement vectors, Figure 28 a), b)). In consequence, this motion provides the NMR spectroscopic equality of the substituents attached to the silicon atom. The calculated energy barrier of this motion is $\Delta G = 15 \text{ kJmol}^{-1}$ for di-*iso*-propyl derivative **73** and is $\Delta G = 25 \text{ kJmol}^{-1}$ for dimethyl derivative **72** (M06-2X/Def2-TZVP). Due to this small barrier, it is not unexpected, that the dynamic process was not detectable using VT NMR spectroscopy.

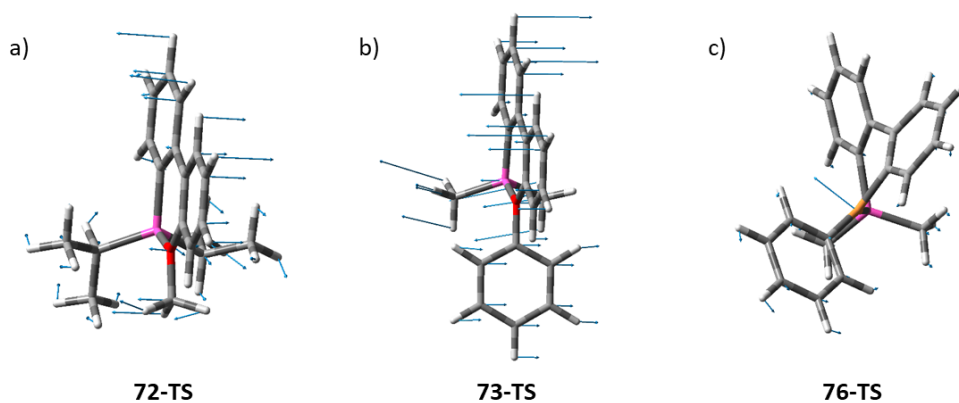


Figure 28 – Optimized transition state structures of a) dimethylsilyloxonium ion **72** b) di-*iso*-propylsilyloxonium ion **73** and c) di-*iso*-propylsilylsulfonium ion **76** (M06-2X/Def2-TZVP).

The TS calculation of thiophenyl derivative **76** results in a free Gibbs energy of the inversion of the configuration of 73 kJmol^{-1} (M06-2X/Def2-TZVP). The calculated negative frequency of the structure of the transition state shows unambiguously the motion of the sulfur atom and not the motion derived from the twisting of the biphenyl system as observed in oxonium ions **72** and **73** (see displacement vectors, Figure 28 c)). These results manifest the difference in behavior of the phenoxy substituent in comparison to the thiophenyl substituent. This difference is further emphasized by the comparison of the corresponding acyclic derivatives **77** and **78** (Figure 29). The sum of the bond angles around the silicon atom shows the typical trigonal flattening, respectively, ($\Sigma\alpha(\text{Si}) = 346^\circ$ in **77**, 345° in **78**).

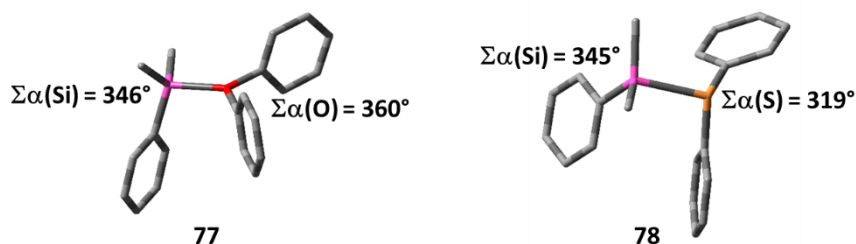


Figure 29 – Optimized structures of acyclic derivatives **77** and **78** (M062X/def2-TZVP; hydrogen atoms omitted for clarity).

The sum of the bond angles around the oxygen atom in silyloxonium ion **77** is $\Sigma\alpha(\text{O}) = 360^\circ$, demonstrating the perfect trigonal planar coordination environment of the oxygen atom; whereas the value of the sulfur atom in silylsulfonium ion **78** is $\Sigma\alpha(\text{S}) = 319^\circ$, demonstrating the trigonal pyramidal coordination environment of the sulfur atom.

The results of the DFT optimizations of all considered structures are summarized in Table 12. In general, the oxygen atom in silyloxonium ions exhibit a trigonal planar coordination environment ($\Sigma\alpha(\text{O}) = 353\text{-}360^\circ$). The exception is *tert*-butylmethyl binaphthyl derivative **28a** of Landais and co-workers, in which the oxygen atom exhibits a certain trigonal pyramidalization ($\Sigma\alpha(\text{O}) = 344^\circ$). In contrast to the acyclic silyloxonium ion **77**, in the cyclic silyloxonium ions **72** and **73** the coordination environment of the oxygen atom in the cyclic derivatives **72** and **73** diverge from perfect planarity (ideal value $\Sigma\alpha(\text{O}) = 360^\circ$) by 5-7°.

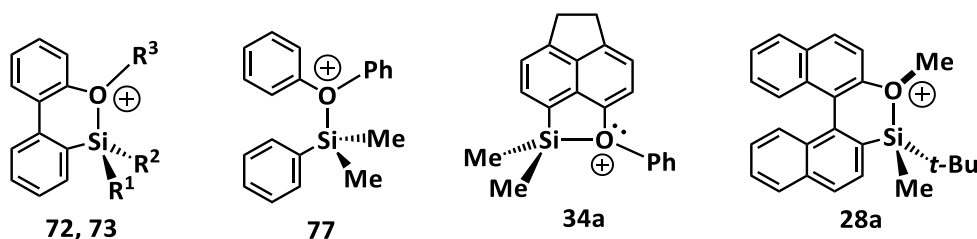


Table 12 – Calculated structural parameters of biphenylsilyl cations **72**, **73**, **76** and acyclic silyl cations **77** and **78** in comparison to acenaphthyl and binaphthyl derivatives **34a**, **35a**, **28a** (M06-2X/Def2-TZVP).

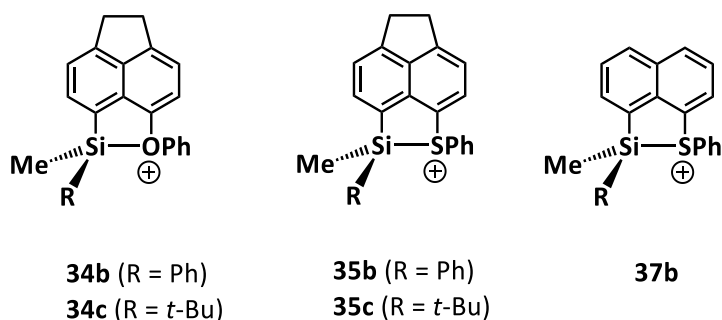
Compound	D	$\Sigma\alpha(\text{SiC}_3)$ [°]	$\Sigma\alpha(\text{D})$ [°]	Si – D [pm]
72	OPh	348	353	182
73	OPh	343	355	183
77	OPh	346	360	183
34a	OPh	352	360	185
28a	OMe	347	344	184

Even though the deviation from a perfect trigonal planar coordination environment in silyloxonium ion **72** and **73** is marginal, this indicates that the backbone might be the crucial factor for the trigonal

pyramidal coordination sphere of the oxygen atom in Ducos' silyloxonium ion **28a**. Another aspect which might have an impact on the coordination environment of the oxygen atom in silyloxonium ions is the substitution pattern at the silicon atom. The results of the investigations regarding asymmetrical phenoxy-stabilized silyl cations will be discussed in Chapter 3.3.1.

3.3 Asymmetrically Substituted Silyl Cations

Silyl cations exhibit a high Lewis acidity; and therefore, are effective catalysts in e.g. hydrodefluorination, Diels-Alder and Mukaiyama aldol reactions.^[9, 29a, 29c, 29d, 48, 86] In this context, a pronounced interest in the development of enantioselective catalysts has evolved. Unsymmetrical substitution at the silicon atom, as in naphthyl- and acenaphthyl-based silyloxonium and silylsulfonium ions **34**, **35** and **37**, results in a Lewis acidic catalyst system, in which on the one hand, the Lewis acidity can be tuned via the remote donor substituent; and, on the other hand, the absolute stereo configuration can be controlled via the substitution pattern at the silicon atom and the chalcogen atom. In this chapter, the synthesis and characterization of asymmetrically substituted silylchalconium borates **34b,c** [$B(C_6F_5)_4$], **35b,c** [$B(C_6F_5)_4$] and **37b** [$B(C_6F_5)_4$] is described.



3.3.1 Phenoxy-Stabilized Chiral Silyl Cations

As discussed in Chapter 3.2.1, the oxygen atom in symmetrically substituted silyloxonium ions **34a** and **36a** exhibit a trigonal planar coordination environment. The *tert*-butylmethyl silyloxonium ion **28a** of Ducos et al. contrasts these findings.^[45d] In this context, the question which arises is if unsymmetrical substitution at the silicon center would trigger a trigonal pyramidalized coordination environment of the oxygen atom in the acenaphthyl-based system, too (Figure 30).

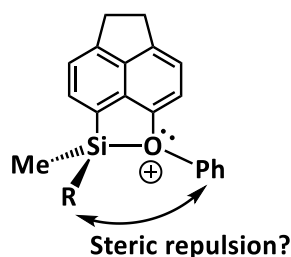
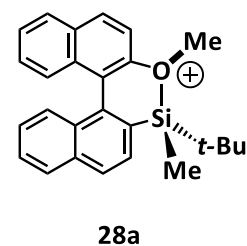
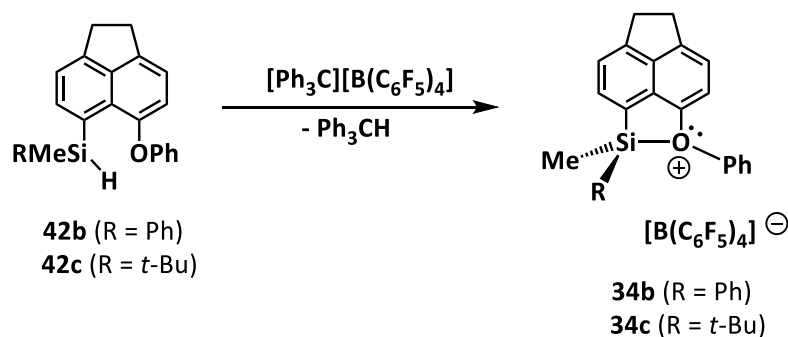


Figure 30 – Concept of asymmetrical substitution in acenaphthyl based silyloxonium ions **34**.

Hereby, the interaction (repulsive, or even attractive) of the phenyl moiety at the oxygen atom and the substituents at the silicon atom would be the important factor. To investigate the effect of an asymmetrical substitution pattern at the silicon center, the phenyl and the *tert*-butyl moieties were chosen as second substituent at the silicon center because of their distinct steric demand. Furthermore, the acenaphthyl substituent was chosen as backbone, due to its easier synthetic access compared to the naphthyl backbone. If the change in the substitution pattern at the silicon atom leads to a trigonal pyramidal coordination environment of the oxygen atom, it would become a chiral center. In addition to the chiral center at the silicon atom, the formation of diastereomers for silyloxonium ions **34b,c** is expected. The diastereomers can be differentiated via their ^{29}Si NMR chemical shifts. Otherwise, if the oxygen atom exhibits a trigonal planar coordination environment there is no formation of diastereomers and, hence, only one signal in the ^{29}Si NMR spectrum is expected.

Silyloxonium borates **34b,c**[$\text{B}(\text{C}_6\text{F}_5)_4$] were obtained via the Corey reaction of the corresponding silanes **42b,c** with trityl borate in quantitative yield without significant formation of side-products. (Scheme 42).



Scheme 42 – Synthesis of asymmetrical substituted silyloxonium borates **34b,c**[$\text{B}(\text{C}_6\text{F}_5)_4$].

In the ^{29}Si NMR spectrum of phenylmethylsilyl cation **34b** one signal at $\delta^{29}\text{Si} = 60.8$ is observed, which is in the expected region for intramolecularly stabilized silyloxonium ions (**34a**, **36a**: $\delta^{29}\text{Si} = 71.4$, $77.4^{[6a]}$; **28a**: $\delta^{29}\text{Si} = 52.2$, $52.9^{[45d]}$). In the high-field region of the ^1H NMR spectrum of phenylmethylsilyl cation **34b** one signal at $\delta^1\text{H} = 0.63$ is detected which is assigned to the methyl substituent at the silyl group (Figure 31). In the low-field region of the ^1H NMR spectrum six signals are detected with a total integral of 10 H; however, a total integral of 14 H was expected (4 H for the acenaphthyl moiety and 10 H for the two phenyl groups). The signals at $\delta^1\text{H} = 6.15$ (1 H), 6.83 (1 H), 7.37 (1 H) and 7.61 (1 H) were assigned to the acenaphthyl hydrogen atoms (Figure 31). For the phenyl group attached to the silicon atom two multiplets at $\delta^1\text{H} = 7.00$ (2 H) and 7.10 (3 H) are

observed. The multiplet at $\delta^1\text{H} = 7.31$ (1H) was assigned to the *p*-H atom of the phenoxy substituent. The resonances for the *o*- and *m*-H atoms of the phenoxy moiety have not been detected.

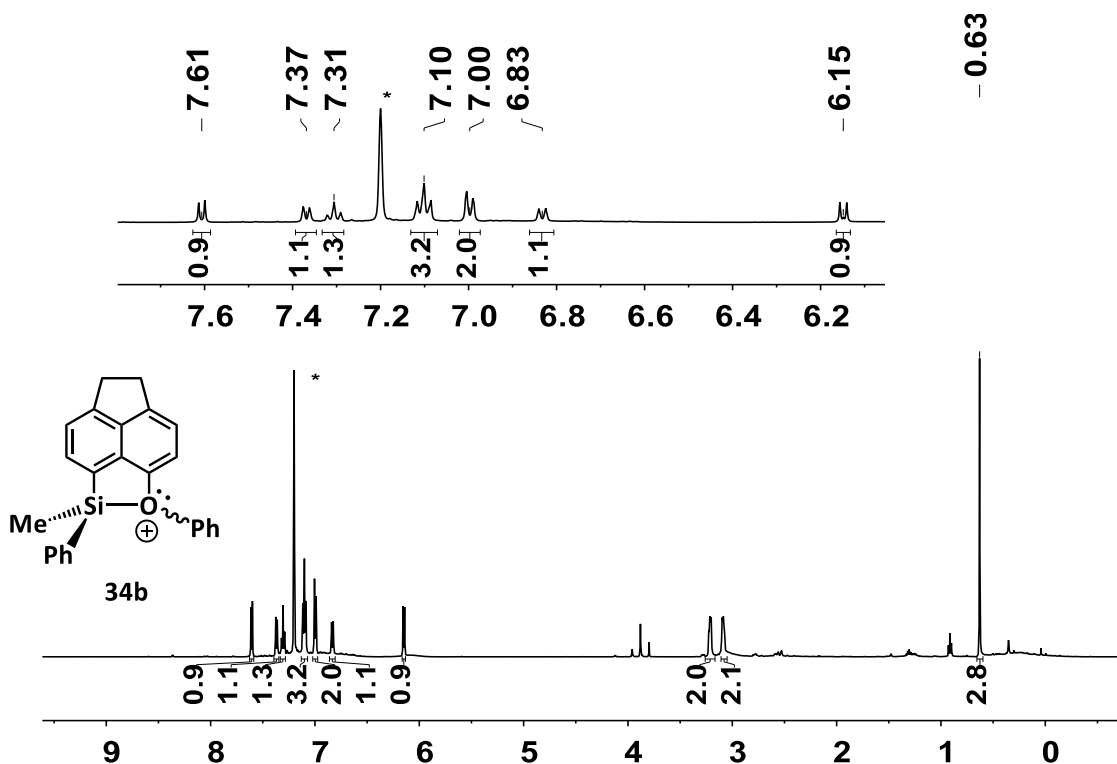


Figure 31 – ^1H NMR spectrum (500 MHz, 305 K, C_6D_6) of phenylmethyl silyl borate **34b** $[\text{B}(\text{C}_6\text{F}_5)_4]$ ($^*\text{C}_6\text{D}_5\text{H}$).

Similar to the results of silyl cation **34b**, in the ^{29}Si NMR spectrum of *tert*-butylmethylsilyl cation **34c** only one signal at $\delta^{29}\text{Si} = 72.2$ was detected. The ^1H NMR spectrum of silyl cation **34c** shows only one signal for the methyl ($\delta^1\text{H} = 0.37$ (3 H)) and one signal for the *t*-Bu group ($\delta^1\text{H} = 0.69$ (9 H)), respectively (Figure 32). For the acenaphthyl substituent the expected four signals ($\delta^1\text{H} = 6.18, 6.80, 7.29, 7.50$ with 1 H, respectively) were detected. In the low-field region, a multiplet at $\delta^1\text{H} = 7.13$ - 7.23 with an integral of 4 H was detected and was assigned to the phenoxy group. However, for the phenoxy substituent 5 H have to be observed. Moreover, this multiplet signal overlaps with the benzene- d_5H signal. Due to this overlap the integral is even higher than it would be without the overlap with the benzene- d_5H signal. The detailed examination of the low-field region reveals that this multiplet at $\delta^1\text{H} = 7.13$ - 7.23 is broadened compared to the other signals and that there are two additional signals at approximately $\delta^1\text{H} = 6.53$ and 6.94 which are broadened, too. The question is, if there is a certain pyramidalization of the oxygen atom that leads to the broadened signals due to coalescence, or, is there some kind of hindered rotation of the phenoxy moiety.

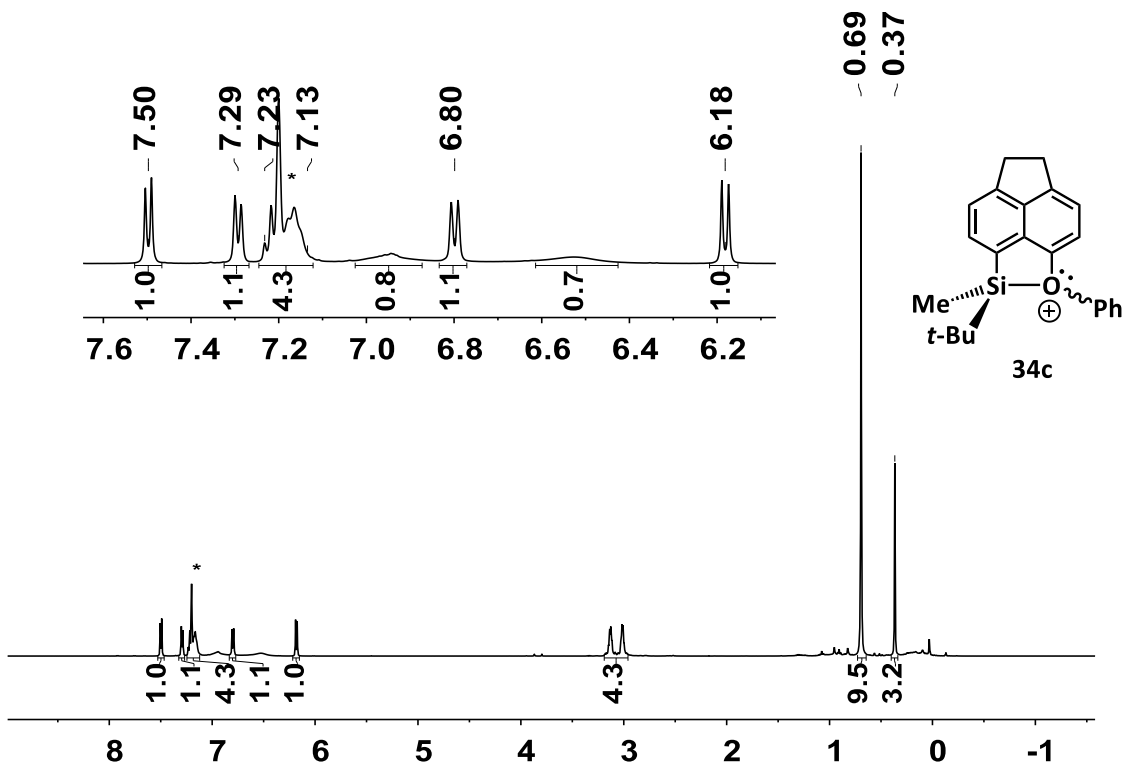


Figure 32 – ^1H NMR spectrum (500 MHz, 305 K, C_6D_6) of *tert*-butylmethyl silyl borate **34c**[$\text{B}(\text{C}_6\text{F}_5)_4$] (* $\text{C}_6\text{D}_5\text{H}$).

To investigate the anomaly of the ^1H NMR spectrum of *tert*-butylmethylsilyl cation **34c**, a low temperature NMR experiment was performed. Silyl borate **34c**[$\text{B}(\text{C}_6\text{F}_5)_4$] was dried under high-vacuum and dissolved in dichloromethane- d_2 . The signals in the ^1H NMR spectrum show no significant line broadening; however unidentified impurities are observable which are probably the result of decomposition (Figure 33). Due to the impurities the overall integral in the aromatic region is by 1.5 H higher than expected. The ^{29}Si INEPT NMR spectra at 193 K and 263 K are shown in Figure 34. The ^{29}Si NMR chemical shift does not change upon solvent or temperature change ($\delta^{29}\text{Si} = 72.3$ in DCM-d_2 at 193 K and 263 K, $\delta^{29}\text{Si} = 72.2$ in benzene- d_6 at 305 K). Consequently, under the described conditions, the formation of diastereomers cannot be observed.

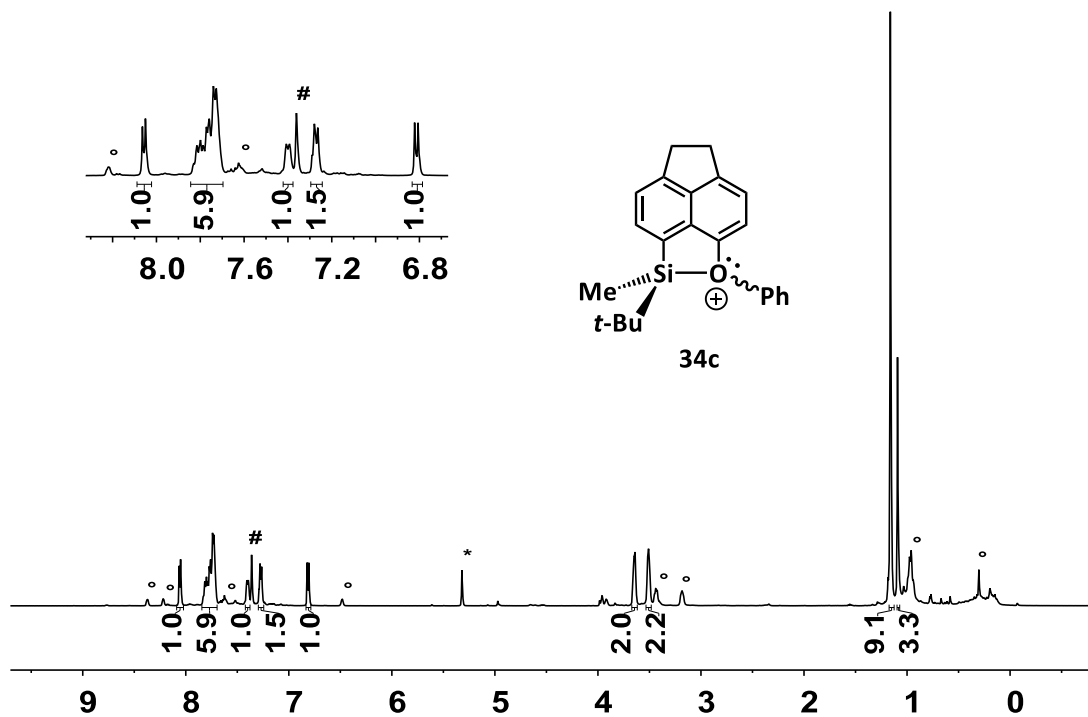


Figure 33 – ^1H NMR spectrum (500 MHz, 263 K, CD_2Cl_2) of *tert*-butylmethyl silyl borate **34c**[$\text{B}(\text{C}_6\text{F}_5)_4$] (* CDHCl_2 , # residual $\text{C}_6\text{D}_5\text{H}$, ° impurities possibly due to decomposition).

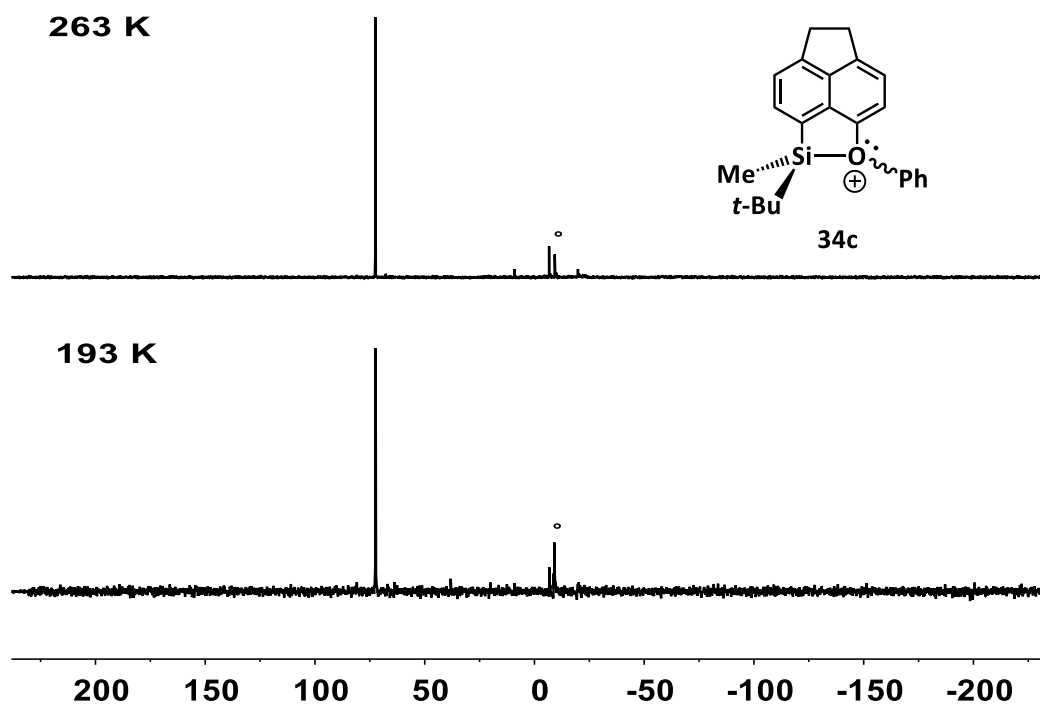


Figure 34 – $^{29}\text{Si}\{^1\text{H}\}$ INEPT NMR spectra (99 MHz, CD_2Cl_2 , 263 K, 193 K, D3 = 0.0122, D4 = 0.0313) of *tert*-butylmethyl silyl borate **34c**[$\text{B}(\text{C}_6\text{F}_5)_4$] (° impurities probably due to decomposition).

Unfortunately, with phenylmethyl derivative **34b** a low temperature NMR experiment was not possible due to its fast degradation in dichloromethane- d_2 .

To further investigate the coordination environment of the oxygen atom in silyloxonium ions **34b** and **34c**, DFT calculations with the standard method/basis set (M06-2X/Def2-TZVP) were performed. Starting from a structure with a trigonal pyramidal coordination environment of the oxygen atom ($\Sigma\alpha(O) = 345^\circ$) resulted after optimization in a structure with an oxygen atom that exhibits a trigonal planar coordination sphere ($\Sigma\alpha(O) = 359^\circ$, Figure 35).

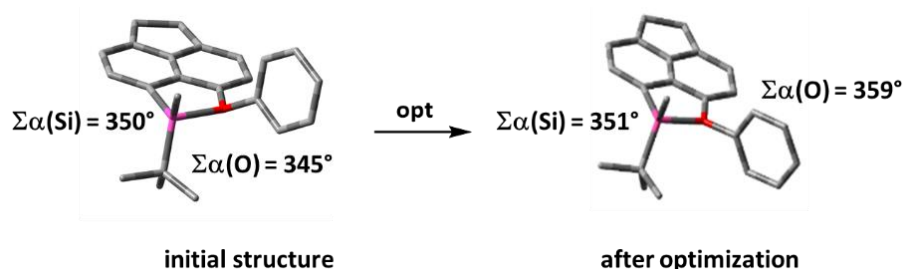
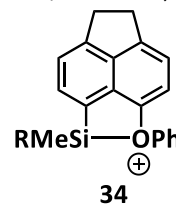


Figure 35 – Structure optimization of *tert*-butylmethyl silyloxonium ion **34c** (M062X/Def2-TZVP, hydrogen atoms omitted for clarity).

The comparison of the calculated structural parameter of the investigated silyloxonium ions **34** is summarized in Table 13. The sum of the bond angles around the silicon atom shows in all three species its pronounced trigonal flattening ($\Sigma\alpha(\text{Si}) = 351\text{-}353^\circ$), whereas the value of the oxygen atom is in all silyloxonium ions **34** close to 360° ($\Sigma\alpha(\text{Si}) = 357\text{-}360^\circ$). This results suggest that, in accordance to the experimental results, the coordination environment of the oxygen atom is trigonal planar.

Table 13 – Calculated structural parameter of acenaphthyl substituted silyloxonium ions **34** (M06-2X/Def2-TZVP).

Silyl cation	$\Sigma\alpha(\text{SiC}_3)$ [°]	$\Sigma\alpha(\text{O})$ [°]	Si – O [pm]
34a (R = Me)	352	360	185
34b (R = Ph)	353	357	187
34c (R = <i>t</i> -Bu)	351	359	187



In conclusion, in silyloxonium ions **34**, the substitution pattern at the silicon atom does not influence the coordination environment of the oxygen atom. This conclusion is reflected by the observations of A. Fernandes. In his thesis, he describes the formation of *tert*-butylmethyl-substituted silyl cation **79** with the biphenyl backbone (Figure 36). In the ^{29}Si NMR spectrum only one signal at $\delta^{29}\text{Si} = 55.7$ (at 253 K) is detected.^[47b] Furthermore, A. Fernandes was able to obtain single crystals suitable for X-ray diffraction analysis of silyloxonium borate **79**[$\text{B}(\text{C}_6\text{F}_5)_4$]. The sum of the bond angles around the silicon atom is $\Sigma\alpha(\text{Si}) = 344.8^\circ$ and around the oxygen atom is $\Sigma\alpha(\text{O}) = 354.7^\circ$ ^[47b]. These values do

not differ much from the calculated values obtained for the symmetrically substituted derivatives **72** and **73** which were discussed in Chapter 3.2.1 ($\Sigma\alpha(\text{Si}) = 343\text{-}348^\circ$, $\Sigma\alpha(\text{O}) = 353\text{-}355^\circ$, M06-2X/Def2-TZVP). In general, that shows that the substitution pattern at the silicon atom does not influence the coordination sphere of the oxygen atom in silyloxonium ions. The trigonal pyramidalization of the oxygen atom in Ducos' silyloxonium ion **28a** is consequently caused by the binaphthyl backbone and not by the unsymmetrical substitution pattern at the silicon atom (Figure 36).

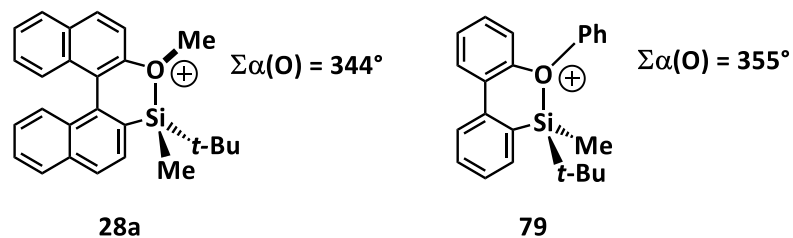
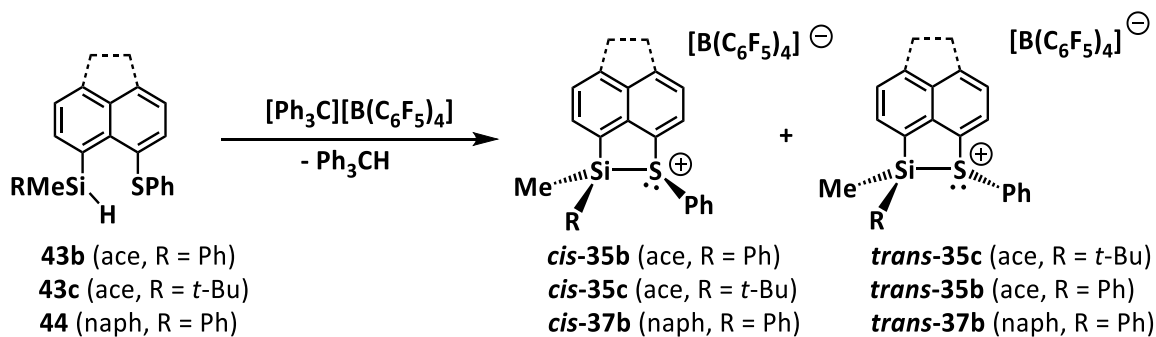


Figure 36 – Intramolecular stabilized silyloxonium ions **28a** and **79** and their sum of the bond angles around the oxygen atom (for biphenyl derivative **28a** $\Sigma\alpha(\text{O})$ is calculated (M06-2X/Def2-TZVP) and the value of $\Sigma\alpha(\text{O})$ of biphenyl derivative **79** was extracted from the X-ray structure^[47b]).

3.3.2 Thiophenyl-Stabilized Chiral Silyl Cations

In contrast to silyloxonium ions **34**, silylsulfonium ions **35** and **37** exhibit a sulfur atom which has a trigonal pyramidal coordination sphere.^[6a] This trigonal pyramidal coordination sphere of the sulfur atom in addition to the asymmetric substitution at the silicon atom leads to the formation of *cis/trans*-isomers of silylsulfonium ions **35b,c** and **37b**. This means, that the second substituent at the silicon atom (R = Ph or *t*-Bu) is either *syn* to the phenyl substituent at the sulfur atom (*cis*-isomer) or *anti* (*trans*-isomer) (Scheme 43).



Scheme 43 – Synthesis of asymmetrical substituted silylsulfonium borates **35b**[B(C₆F₅)₄], **35c**[B(C₆F₅)₄] and **37b**[B(C₆F₅)₄].

In this context, it is of interest to investigate how the substitution pattern at the silicon atom does influence the *cis/trans* ratio and how the backbone effects this ratio. To examine these aspects, three different chiral silyl borates **35b**[B(C₆F₅)₄], **35c**[B(C₆F₅)₄] and **37b**[B(C₆F₅)₄] were synthesized according to the Corey reaction in Scheme 43. All obtained silyl borates **35b**[B(C₆F₅)₄], **35c**[B(C₆F₅)₄] and **37b**[B(C₆F₅)₄] are compounds unknown to literature and were characterized by multinuclear NMR spectroscopy. First, the phenylmethylsilyl-substituted derivatives **35b** and **37b** are discussed. As an example the ¹H NMR spectrum of naphthyl silyl borate **37b**[B(C₆F₅)₄] is shown in Figure 37. The expected two signal sets of the two diastereomers *cis-37b* and *trans-37b* are detected. The two resonances of the methyl groups at δ¹H = 0.33 and 0.73 are in a ratio of 40:60 (for **35b**: δ¹H = 0.34, 0.80 in toluene-d₈).

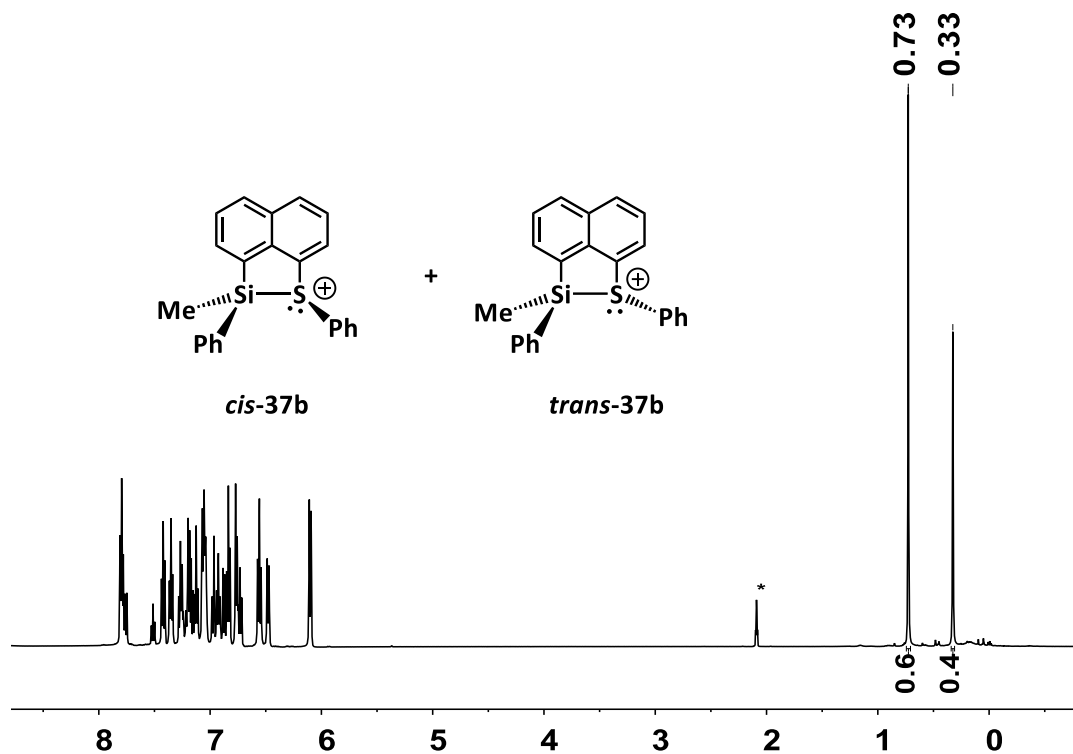


Figure 37 – ^1H NMR spectrum (500 MHz, 305 K, C_7D_8) of naphthyl-substituted phenylmethylsilyl sulfonium borate **37b** $[\text{B}(\text{C}_6\text{F}_5)_4]$ ($^*\text{C}_6\text{D}_5\text{CD}_2\text{H}$).

The same is reflected in the ^{29}Si NMR spectrum with two signals at $\delta^{29}\text{Si} = 42.9$ and 45.5 (Figure 38) (for **35b**: $\delta^{29}\text{Si} = 51.2, 53.9$ in toluene- d_8). The ^{29}Si NMR chemical shifts are in the same region as those of intramolecularly thionyl-stabilized silyl cations **27** with the binaphthyl backbone of Oestreich and co-workers ($^{29}\text{Si} = 32.0\text{-}57.6$).^[29c, 29d]

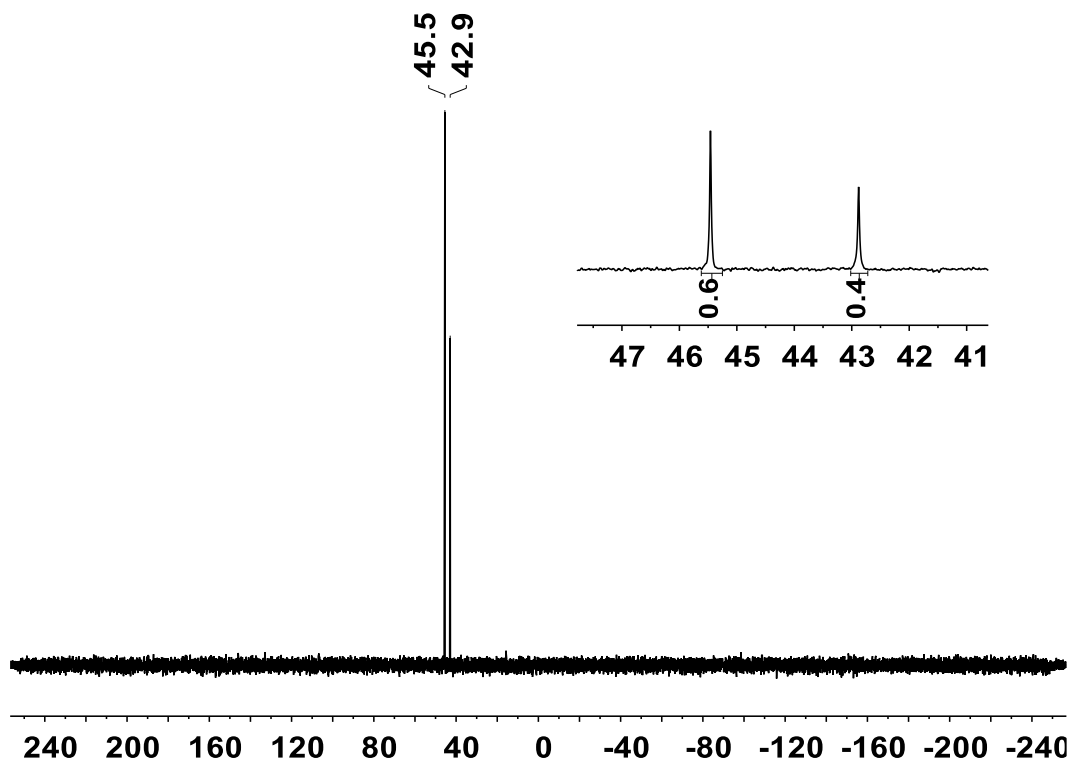


Figure 38 – $^{29}\text{Si}\{^1\text{H}\}$ NMR spectrum (99 MHz, 305 K, C_7D_8) of naphthyl substituted phenylmethylsilyl sulfonium borate **37b** $[\text{B}(\text{C}_6\text{F}_5)_4]$.

To assign the signals the *cis*- and to the *trans*-isomer, the nuclear Overhauser effect (NOE) was used. By irradiation of the first methyl ^1H NMR resonance ($\delta^1\text{H} = 0.33$) an increase of the second resonance ($\delta^1\text{H} = 6.48$) in the aromatic region, which was assigned to the *o*-H atoms, was observed (Figure 39, c). By irradiation of the second methyl resonance ($\delta^1\text{H} = 0.73$) the other *o*-Ph-H signal at $\delta^1\text{H} = 6.10$ disappears (Figure 39, b). Consequently, the first methyl group resonance ($\delta^1\text{H} = 0.33$) represents the *trans*-isomer and the second ($\delta^1\text{H} = 0.73$) the *cis*-isomer.

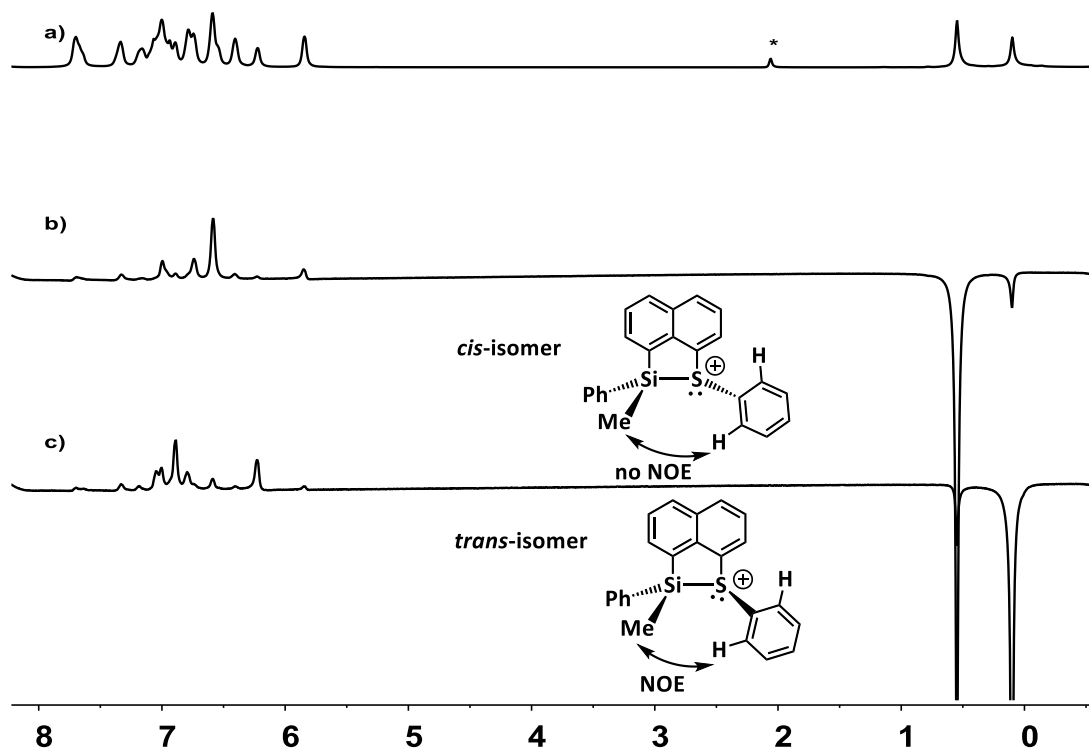


Figure 39 – ^1H and ^1H NOE NMR spectra (500 MHz, 305 K, C_7D_8) of naphthyl substituted phenylmethylsilyl sulfonium borate **37b** $[\text{B}(\text{C}_6\text{F}_5)_4]$ (* $\text{C}_6\text{D}_5\text{CD}_2\text{H}$; a) ^1H spectrum, b) ^1H NOE spectrum irradiation at $\delta^1\text{H} = 0.73$, c) ^1H NOE spectrum irradiation at $\delta^1\text{H} = 0.33$).

The observation, that the ^1H NMR signal of the *syn*-methyl group is at higher field compared to the ^1H NMR resonance of the *anti*-methyl group is consistent with the results of N. Kordts and K. Ruger and can be considered as general rule for this type of cations.^[87]

Interestingly, the *cis*-isomer of the phenylmethylsilyl-substituted silyl cations **35b** and **37b** is the main product, indicating that not a repulsive interaction between the two phenyl groups takes place but rather an attractive interaction. K. Ruger and P. Tholen made the same observations for the corresponding naphthyl- and acenaphthyl-substituted selenyl-stabilized phenylmethylsilyl cations.^[87b, 88] The DFT calculations of the *cis/trans*-isomers of phenylmethylsilyl cations **35b** and **37b** also show that the *cis*-isomer is more stable compared to the *trans*-isomer. The energy difference between the isomers is $\Delta G = 1.4 \text{ kJmol}^{-1}$ for the naphthyl derivative **37b** and is $\Delta G = 1.8 \text{ kJmol}^{-1}$ for the acenaphthyl species **35b** (M06-2X/Def2-TZVP, SCRF(solvent = toluene)). With these values the equilibrium constant for the two isomers was calculated. The equilibrium constant is $K = 1.4$ for the naphthyl-substituted cation **37b** whereof a *cis/trans* ratio of 64:36 is calculated. The calculated

equilibrium constant is $K = 2.1$ for acenaphthyl derivative **35b** whereof a *cis/trans* ratio of 67:33 results. These values are in relatively good agreement to the experimental determined value of 60:40.

In contrast to these findings, the change of the substitution pattern to *tert*-butylmethylsilyl as in species **35c** results in the formation of only one isomer indicated by only one set of signals in the ^1H NMR (Figure 40) and ^{29}Si NMR spectrum even at $-90\text{ }^\circ\text{C}$ ($^{29}\text{Si} = 70.0$ in benzene- d_6 and $^{29}\text{Si} = 70.3$ in dichloromethane- d_2).

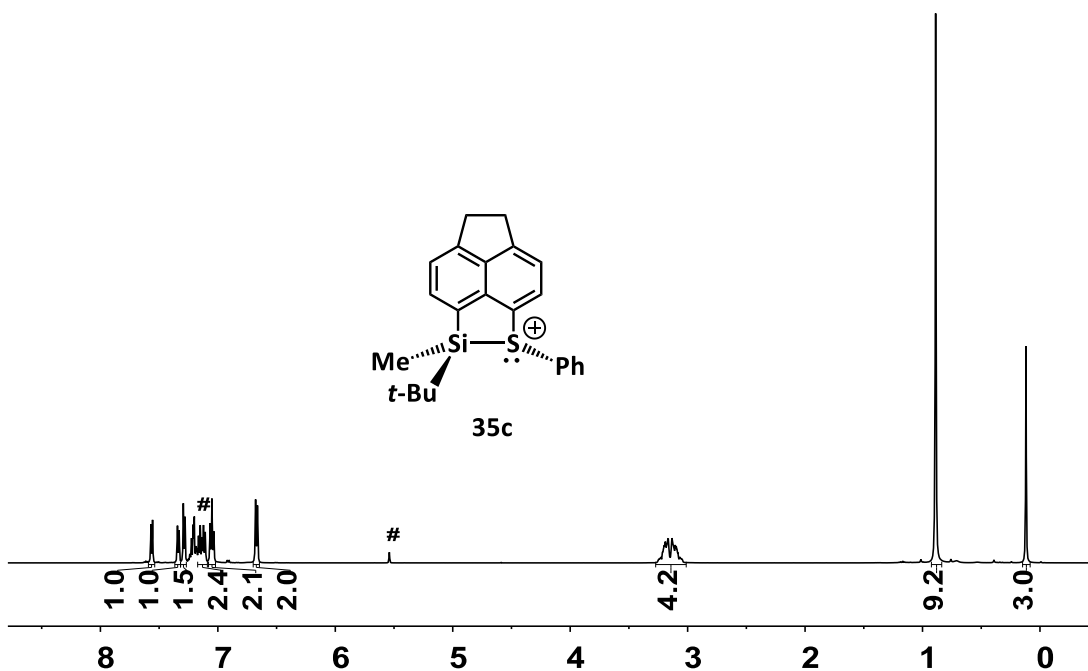
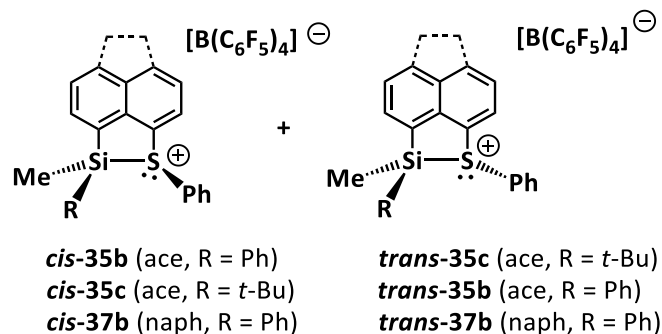


Figure 40 – ^1H NMR spectra (500 MHz, 305 K, C_6D_6) of acenaphthyl substituted *tert*-butylmethylsilyl sulfonium borate **35c** $[\text{B}(\text{C}_6\text{F}_5)_4]$ (# residual Ph_3CH).

The calculated energy difference of the isomers of cation **35c** is with $\Delta G = 13.1\text{ kJmol}^{-1}$ distinct higher than that of the phenylmethylsilyl-substituted derivatives **35b** and **37b**. The calculated equilibrium constant is $K = 0.005$ which gives a ratio of $>99:1$. In this case the *trans*-isomer is more stable than the *cis*-isomer indicating the strong repulsive interaction between the *tert*-butyl group at the silicon atom and the thiophenyl group. This observation is in accordance to the results of K. Ruger. In the NOE NMR experiment for the corresponding naphthylselenyl derivative, the NOE effect between the methyl substituent at the silicon atom and the phenyl group at the sulfur atom was observed; hence, the *trans*-isomer is the formed species.^[87b]

In summary, the synthesis and characterization via NMR spectroscopy of naphthyl- and acenaphthyl-substituted silylsulfonium borates **35b** $[\text{B}(\text{C}_6\text{F}_5)_4]$, **35c** $[\text{B}(\text{C}_6\text{F}_5)_4]$ and **37b** $[\text{B}(\text{C}_6\text{F}_5)_4]$ was performed. The

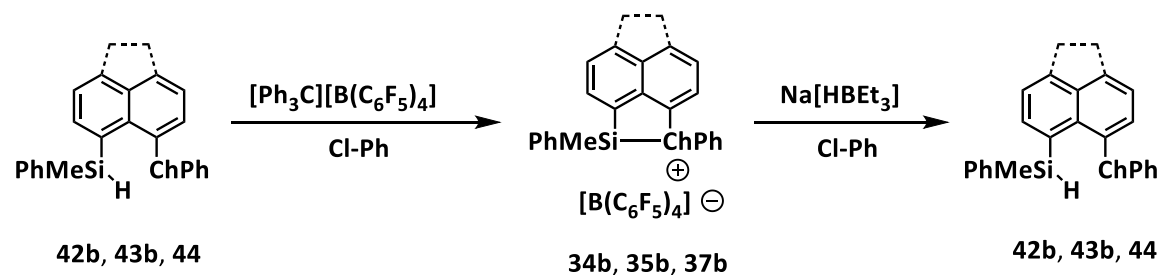
phenylmethylsilyl-substituted derivatives **35b** and **37b** form the expected two isomers (*cis* and *trans*) in a ratio of 60:40. The *cis*-isomer is the main compound in this mixture which was shown by the NOE NMR experiment. The DFT calculations are in accordance with the experimental results.



In contrast to phenylmethylsilyl cations **35b** and **37b**, *tert*-butylmethylsilyl cation forms only the *trans*-isomer. In general, these studies show that the substitution pattern of silylsulfonium ions influences the *cis/trans*-ratio. Hereby, the steric obstruction is higher between the *tert*-butyl group at the silicon atom and the phenyl group at the sulfur atom as in silyl cation **35c** compared to the steric repulsion between the two phenyl substituents as in silyl cations **35b** and **37b**. Furthermore, the comparison of naphthyl- and acenaphthyl-substituted derivatives **35b** and **37b** shows no significant difference between the two backbones, naphthyl and acenaphthyl. The results of silylsulfonium ions **35a,c** and **37b** are in agreement with previous studies of the corresponding selenyl-substituted derivatives.^[87b, 88] The difference between the *cis/trans*-ratios of phenylmethylsilyl-substituted derivatives **35b**, **37b** and *tert*-butylmethyl-substituted derivative **35c** demonstrate that the choice of the substitution pattern at the silicon atom influences and consequently controls the configuration of the sulfur atom.

3.3.3 Chiral Memory

For the use of chiral silyl borates **34b**[B(C₆F₅)₄], **35b**[B(C₆F₅)₄] and **37b**[B(C₆F₅)₄] in asymmetric catalysis, it is essential that there is no loss of the stereochemical information during the ionization and later on during the catalytic process. In this chapter, the chiral integrity of silyl cations **34b**, **35b** and **37b** is discussed. A direct measurement of the enantiomeric ratio of moisture sensitive silyl borates **34b**[B(C₆F₅)₄], **35b**[B(C₆F₅)₄] and **37b**[B(C₆F₅)₄] is difficult. Therefore, the chiral information was accessed indirectly by so called test for chiral memory.^[45d] For this experiment silyl borates **34b**[B(C₆F₅)₄], **35b**[B(C₆F₅)₄] and **37b**[B(C₆F₅)₄] were synthesized as usual and then retransformed to the corresponding silanes **42b**, **43b** and **44** by a subsequent reduction (Scheme 44). Hereby, the formation of the chiral silyl cations **34b**, **35b** and **37b** and the subsequent reduction occurs under inversion of the configuration at the silicon center, respectively.^[89] That means, that the overall reaction occurs under retention of the configuration. After the experiment, silanes **42b**, **43b** and **44** were analysed via optical rotation and chiral HPLC. The enantiomeric excess of silanes **42b**, **43b** and **44** before and after the chiral memory experiment were compared to see if racemization takes place during the reaction sequence. As hydride source a 1 M solution of sodium triethyl borohydride in toluene was used. The results are summarized in Table 14.



Scheme 44 – Formation of chiral silyl borates **34b**[B(C₆F₅)₄] (ace, Ch = O), **35b**[B(C₆F₅)₄] (**43b** (ace, Ch = S) and **37b**[B(C₆F₅)₄] (naph, Ch = S) and its subsequent reduction to regenerate the corresponding silanes **42b** (ace, Ch = O), **43b** (ace, Ch = S) and **44** (naph, Ch = S).

In the first attempt naphthyl-substituted phenylmethyl thiophenyl-stabilized silyl borate **37b**[B(C₆F₅)₄] was used because it shows the best $[\alpha]_D$ and ee values. The reaction was carried out in chlorobenzene at room temperature. The silane (+)-**44** was treated with trityl borate and the mixture was stirred for 20 min. Subsequently, the borohydride was added and the mixture was stirred overnight. After purification an optical rotation of $[\alpha]_D = 0^\circ$ ($c = 0.004 \text{ molL}^{-1}$, Et₂O) was measured, indicating complete racemization (Table 14, Entry 1). In the second reaction phenoxy-stabilized silyl borate **34b**[B(C₆F₅)₄] was used (Table 14, Entry 2). This time the reaction was carried out at -40 °C.

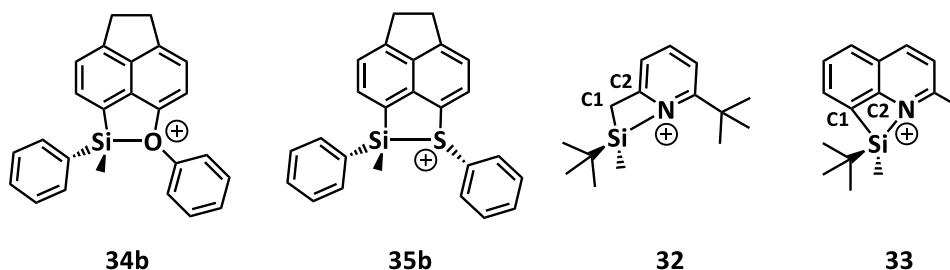
The borohydride was added after 30 min stirring at $-40\text{ }^{\circ}\text{C}$. The mixture was slowly warmed to r.t. over night. After work up and purification an optical rotation of $[\alpha]_{\text{D}} = -4^{\circ}$ ($c = 0.005\text{ molL}^{-1}$, Et_2O) was obtained which corresponds to an ee of 32 %. Compared to the values of silane **(-)-42b** before the experiment reveals that racemization of about 41 % has occurred. To obtain a better result, the experiment was repeated at $-80\text{ }^{\circ}\text{C}$ but here only the decomposition of the silyl borate **34b** $[\text{B}(\text{C}_6\text{F}_5)_4]$ was observed. A reason for the decomposition is most likely the solvent dichloromethane. The best result was obtained with thiophenyl-substituted silyl borate **35b** $[\text{B}(\text{C}_6\text{F}_5)_4]$ (Table 14, Entry 4). At $-40\text{ }^{\circ}\text{C}$, the complete conservation of the chiral information was observed.

Table 14 – Results for the chiral memory of silyl borates **34b** $[\text{B}(\text{C}_6\text{F}_5)_4]$, **35b** $[\text{B}(\text{C}_6\text{F}_5)_4]$ and **37b** $[\text{B}(\text{C}_6\text{F}_5)_4]$ ($[\alpha]_{\text{D}}$ measured in Et_2O , for the concentration see Experimental Part, ee determined via chiral HPLC).

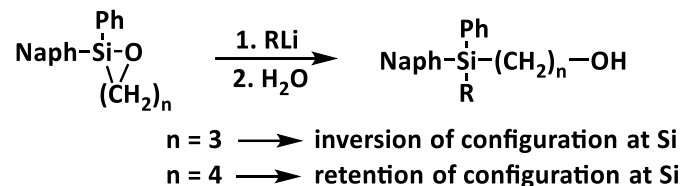
Entry	Silane	Conditions	$[\alpha]_{\text{D}}$, ee start	$[\alpha]_{\text{D}}$, ee end
1	(+)-44	Cl-Ph, r.t., 30 min	$+17^{\circ}$, 84 %	0°
2	(-)-42b	Cl-Ph, $-40\text{ }^{\circ}\text{C}$, 30 min	-11° , 54 %	-4° , 32 %
3	(-)-42b	DCM, $-80\text{ }^{\circ}\text{C}$, 20 min	-11° , ee = 54 %	decomposition
4	(-)-43b	Cl-Ph, $-40\text{ }^{\circ}\text{C}$, 15 min	-10° , 64 %	-9° , 64 %

These results show, that at r.t. racemization occurs, which was prevented by a lower reaction temperature. A complete conservation of the chiral information was only observed with thiophenyl derivative **35b**. A reason for the better performance of the thiophenyl-stabilized silyl cation **35b** compared to the phenoxy derivative **34b** might be the trigonal pyramidal coordination sphere of the sulfur atom which enables the stereocontrol of silylsulfonium ions **35** and **37**.

A. Fernandes observed similar behavior in the investigations to pyridyl-stabilized chiral silyl cation **32**. In the chiral memory experiment, he observed at r.t. a loss of the chiral information of about 84 % (from initially ee $> 90\%$ to ee = 14 %). At $0\text{ }^{\circ}\text{C}$ he achieved with his system complete conservation of the chiral information.^[47a, 47b] C. Laye observes with her quinoline system **33** a loss of the chiral information of about 59 % (from ee = 98 % to ee = 40 %) even at $-80\text{ }^{\circ}\text{C}$.^[47a, 47c]



The difference in the chiral memory of silyl cations **32** and **33** seems to be related to their ring strain. Corriu demonstrated that ring strain in organosilanes can influence the stereochemistry of the nucleophilic substitution reaction at the silicon center as shown in Scheme 45.^[89]



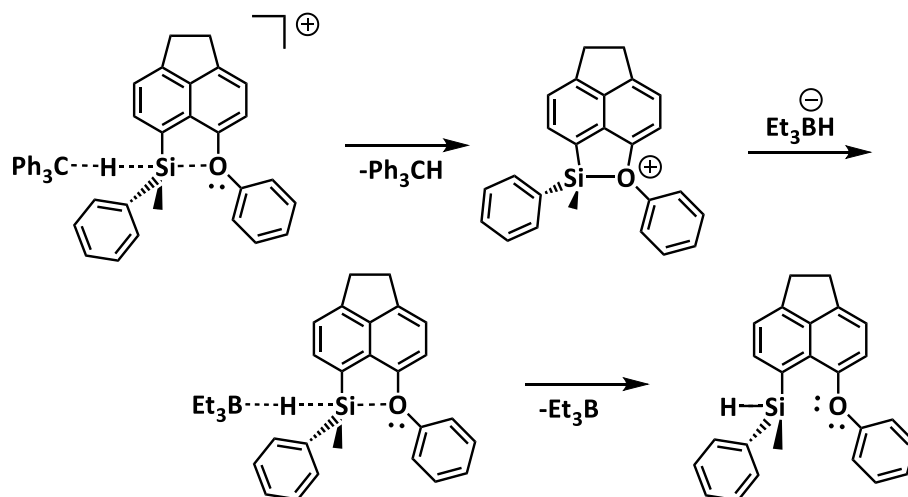
Scheme 45 – Nucleophilic substitution reaction at the silicon atom in cyclic organo-silicon compounds.

The ring strain of acenaphthyl derivatives **34b** and **35b** is manifested by the sum of the angles in the bay region. The sum of the bay angles of **34b** and **35b** is $\Sigma\beta = 338^\circ$ for silyloxonium ion **34b** and is $\Sigma\beta = 354^\circ$ for silylsulfonium ion **35b** (M06-2X/Def2-TZVP), whereby both values are lower than in unstrained acenaphthene ($\Sigma\beta = 368^\circ$).^[73] Nonetheless, in oxonium ion **34b** the ring strain is more pronounced as in sulfonium ion **35b**. The quinoline- and the pyridine-based silyl cations **32** and **33** form a four membered ring with the silicon, the nitrogen and two carbon atoms, respectively.^[47a] The main difference is, that in quinoline derivative **33** both carbon atoms exhibit a sp^2 hybridization and in pyridine derivative **32** one sp^2 and one sp^3 carbon atom are present. Even if the ring angles are nearly identical (Table 15), the difference in the hybridization of the carbon atoms leads to a more pronounced ring strain in quinoline derivative **33** as in pyridine derivative **32**.

Table 15 – Comparison of the calculated bond angles in pyridine and quinoline based silyl cations **32** and **33** (M06-2X/def2-TZVP, * sp^3 carbon atom in pyridinium ion).^[47a]

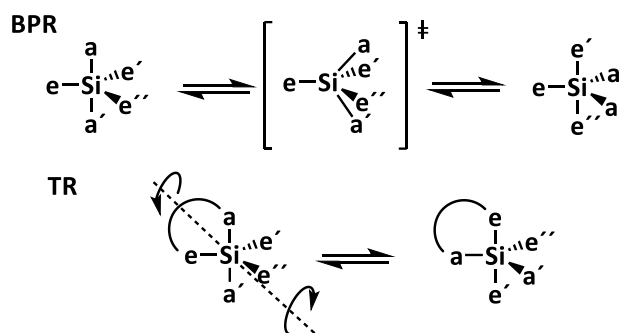
	Silyl cation 32	Silyl cation 33
Si-C1*-C2	87.0°	88.8°
C1*-C2-N	106.5°	108.5°
C2-N-Si	91.1°	89.2°
N-Si-C1*	75.0°	73.3°

However, the ring strain alone does not explain the loss of stereochemical information. During ionization and subsequent reduction in the chiral memory experiment, the silicon center passes twice through a pentavalent intermediate in which the silicon atom exhibits a trigonal bipyramidal coordination environment (Scheme 46).



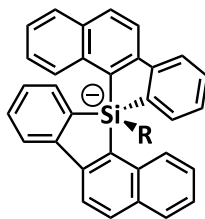
Scheme 46 – Reaction pathway of the ionization of silane **42b** and the reduction of silyl cation **34b**.

Pentacoordinated compounds are known to undergo dynamic processes, namely the Berry pseudorotation (BPR)^[42c, 90] or the turnstile rotation (TR).^[91] The BPR leads to the exchange of both axial substituents of a trigonal bipyramid with two equatorial substituents, whereby the molecule goes through a square pyramidal transition state (Scheme 47, BPR). In the TR, a group consisting of two equatorial and one axial substituent (e' , e'' and a') turns against the remaining group consisting of one equatorial and one axial substituent (e and a) with the central atom forming the pivot (Scheme 47, TR). These processes lead to racemization.



Scheme 47 – Schematic illustration of the Berry pseudorotation (BPR) and the turnstile rotation (TR).

Lammertsma and co-workers described this non-dissociative racemization process for chiral silicates **80**, even though this compounds exhibit two bidentate substituents. They observe fast racemization at r.t. (within 30 min) of methyl-substituted compound **80a** and relative slow racemization of about 50 % within 1 h at r.t. of phenyl-substituted compound **80b**.^[90]



80a (R = Me)

80b (R = Ph)

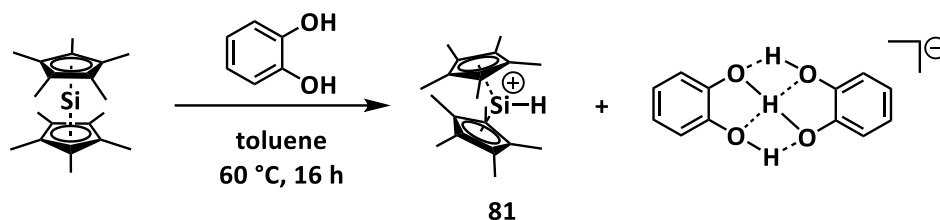
80c (R = F)

Interestingly, silicate **80c**, with the fluoro substituent, does not undergo racemization and displays a perfect chiral integrity at r.t. over days. This is quite remarkable due to the fact, that the fluorine atom is in an equatorial instead of an axial position.^[90]

In conclusion, chiral silylchalconium ions **34b**, **35b** and **37b** undergo racemization during the chiral memory experiment. This racemization was slower and even prevented by a low reaction temperature. For the use of chiral silyl chalconium borates **34b**[B(C₆F₅)₄], **35b**[B(C₆F₅)₄] and **37b**[B(C₆F₅)₄] as asymmetric catalysts that means, that the catalytic reactions have to be carried out at low reaction temperatures.

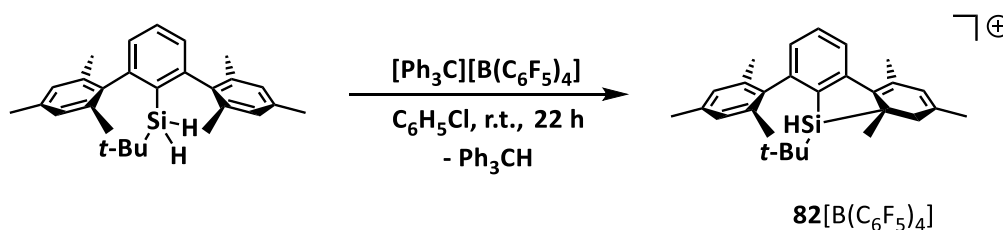
3.4 Chalcogenyl-Stabilized Hydridosilyl Cations

In the last sections the synthesis and characterization of a series of phenoxy- and thiophenyl-stabilized silyl borates **34**[B(C₆F₅)₄] and **35**[B(C₆F₅)₄] was described. Silyl borates **34**[B(C₆F₅)₄] and **35**[B(C₆F₅)₄] exhibit three carbon-based substituents at the silicon atom and a remote donor group which stabilizes and controls the reactivity of the highly electrophilic silicon center. Due to this substitution pattern, silyl borates **34**[B(C₆F₅)₄] and **35**[B(C₆F₅)₄] are stable even at elevated temperatures (90 °C) and relatively simple to access and handle when maintained under inert conditions. Other representatives of the silyl cation family are secondary silyl cations. In this species one carbon-based moiety is substituted by a hydrogen atom. These hydridosilyl cations show a very high reactivity and undergo reactions with the solvent benzene under release of protons or dihydrogen.^[92] In general, secondary silyl cations are promising candidates for hydrosilylation reagents or for the use as precursors of silylenes.^[92-93] However, due to their high reactivity they have rarely been observed in condensed phase. One example is species **81** of Jutzi and Bunte which was synthesized by the protonation of decamethylsilicocene (Scheme 48).^[94]



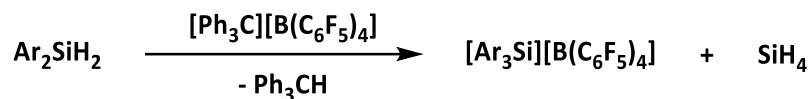
Scheme 48 – Synthesis of secondary silylium ion **81** via protonation of decamethylsilicocenium.^[94]

Another example is the hydrogen-substituted silyl cation **82** which was reported by H. Großekappenberg and synthesized using the standard Corey procedure (Scheme 49). Secondary silyl cation **82** is stabilized by formation of an intramolecularly stabilized arenium ion complex which was established via DFT calculations and AIM analysis.^[53a]



Scheme 49 – Synthesis of silyl borate **82**[B(C₆F₅)₄] via the standard Corey procedure.^[53a]

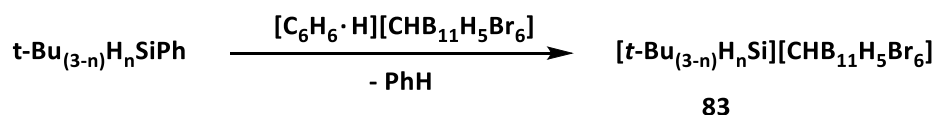
However, the Corey procedure leads for diaryl-substituted derivatives always to the formation of triarylsilylium ions due to substituent exchange reactions (Scheme 50).^[53a]



Ar = Pemp, Tipp

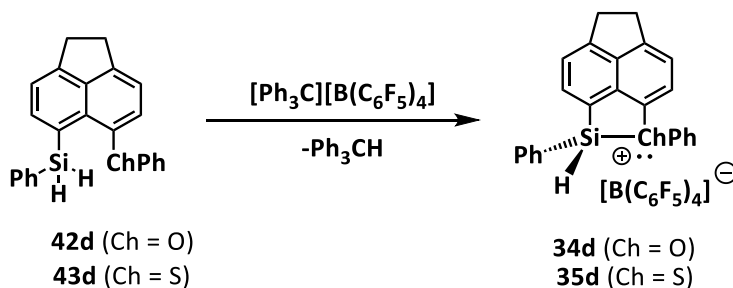
Scheme 50 – Reaction of diarylsilanes with trityl borate.^[53a]

Recently, Oestreich and co-workers described the synthesis and characterization via NMR spectroscopy and XRD analysis of secondary and primary silylium ions **83a** and **83b** as well as the formation of SiH_3^+ **83c**. The synthesis of secondary silylium ions **83** was realized either using the classical Corey procedure or using the cleavage of a Si – C bond by protonation with Reed's carborate acid $[\text{C}_6\text{H}_6 \cdot \text{H}][\text{CHB}_{11}\text{H}_5\text{Br}_6]$ (Scheme 51). Silylium ions **83** are stabilized via the bromine atom of the carborate. The Si – Br bond length are in the range of 238-247 pm which is elongated compared to a neutral Si – Br bond (Me_3SiBr $d(\text{Si} - \text{Br}) = 224$ pm).^[95]



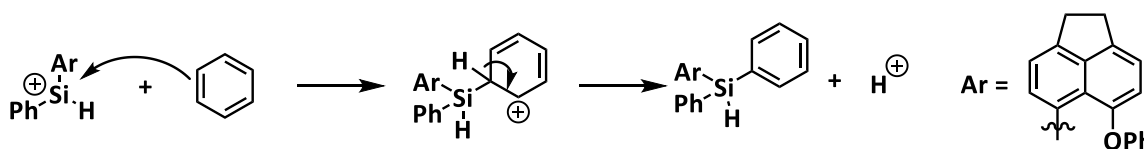
Scheme 51 – Synthesis of silylium carborates **83** $[\text{CHB}_{11}\text{H}_5\text{Br}_6]$ ($n = 1$ (**a**), $n = 2$ (**b**), $n = 3$ (**c**)).^[95]

Based on the experiences with phenoxy- and thiophenyl-stabilized silyl cations **34a-c** and **35a-c**, the synthesis of silyl borates **34d** $[\text{B}(\text{C}_6\text{F}_5)_4]$ and **35d** $[\text{B}(\text{C}_6\text{F}_5)_4]$ should be accomplished. Therefore, the corresponding silanes **42d** and **43d** were treated with trityl borate to perform the standard hydride transfer reaction (Scheme 52).



Scheme 52 – Synthesis of hydridosilyl borates **34d** $[\text{B}(\text{C}_6\text{F}_5)_4]$ and **35d** $[\text{B}(\text{C}_6\text{F}_5)_4]$.

The results of the synthesis attempts to generate the phenoxy-stabilized silyl borate **34d**[B(C₆F₅)₄] are summarized in Table 16. In general, the ¹H NMR as well as the ¹³C NMR spectra reveal the complete consumption of trityl cation in all experiments. In the ¹⁹F NMR spectra of the first and the second attempt (Table 16, Entry 1, 2), the decomposition of the anion and the formation of tris(pentafluorophenyl)borane (BCF) was observed. The formation of BCF from borate [B(C₆F₅)₄]⁻ is described as a proton-induced process.^[96] The presence of protons is not surprising, since secondary silylium ions react with aromatic solvents under release of dihydrogen or protons (Scheme 53).^[53a, 92]



Scheme 53 – Supposed reaction of hydridosilyl cation **34d** with benzene under release of a proton.

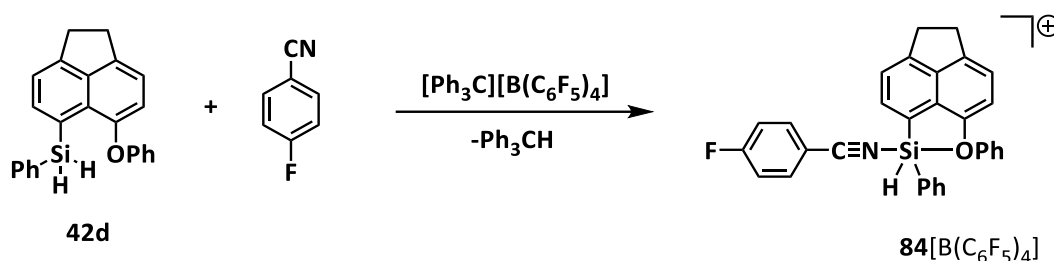
The formation of BCF was prevented by adding the proton sponge 2,6-di-*tert*-butyl-4-methylpyridine (DTBMP) to the mixture (Table 16, Entry 4, 5). However, this did not prevent side-reactions. In the ²⁹Si NMR spectra of the reaction mixtures, hints for the formation of triphenylsilane (Entry 3, 4; $\delta^{29}\text{Si} = -17.8$ (C₇D₈), -18.3 (CD₂Cl₂)), diphenylsilane (Entry 3; $\delta^{29}\text{Si} = -34.2$ (C₇D₈)) and phenylsilane (Entry 4; $\delta^{29}\text{Si} = -58.4$ (CD₂Cl₂)) were found. Due to the significant low-field shift of $\Delta\delta^{29}\text{Si} = 60\text{--}70$ of silyl cations compared to their precursor silanes, for hydridosilyloxonium ion **34d** a ²⁹Si NMR resonance of about $\delta^{29}\text{Si} = 30\text{--}40$ is expected. The ²⁹Si NMR resonances which are in the expected region ($\delta^{29}\text{Si} = 27.7\text{--}42.6$) do not show correlations to a hydrogen atom in the ¹H/²⁹Si HMQC NMR spectrum as it is expected for hydridosilyloxonium ion **34d**.

Table 16 – Summary of the synthesis attempts of phenoxy-stabilized silyloxonium borate **34d**[B(C₆F₅)₄] (DTBMP = 2,6-di-*tert*-butyl-4-methylpyridine).

Entry	Reaction conditions	additives	BCF:[B(C ₆ F ₅) ₄] ⁻	$\delta^{29}\text{Si}$
1	C ₆ D ₆ , r.t.	-	1:1	78.3, 60.8, 42.3, 30.4, -3.2 ^a , -30.4 ^a , -51.1 ^a
2	C ₆ D ₅ Cl, r.t.	NC(C ₆ H ₄ F)	1:9	64.0, 42.5, 30.4, -3.1 ^a , -50.7 ^a , -79.8 ^a
3	C ₇ D ₈ , -40 °C – r.t.	DTBMP	0:1	77.6, 60.0, 42.6, 30.3, -3.2 ^a , -17.8 ^a , -34.2 ^a
4	CD ₂ Cl ₂ , -80 °C	DTBMP	0:1	27.7, -18.3 ^a , -30.3 ^a , -58.4 ^a

a) Si – H species.

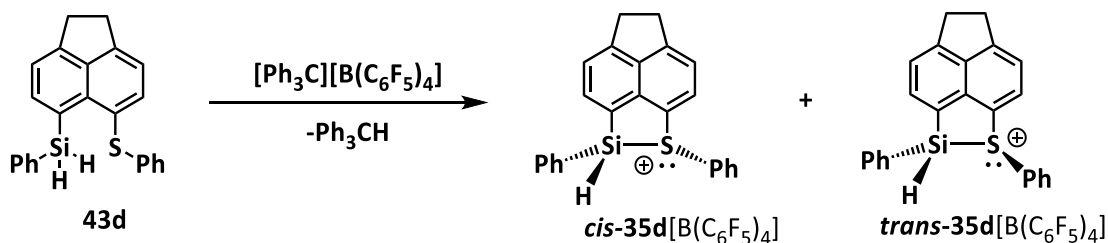
A typically successful approach to stabilize highly reactive silyl cations is the formation of the corresponding nitrilium ion (*vide infra*). Therefore, 4-fluorobenzonitrile (FBN) was added to the reaction mixture (Table 16, Entry 2). However, the formation of the corresponding nitrilium ion **84** was not observed (Scheme 54). Instead the decomposition of the nitrile was observed (evidenced by the ^{19}F NMR spectrum).



Scheme 54 – Suggested formation of nitrilium borate **84** $[\text{B}(\text{C}_6\text{F}_5)_4]$ by the reaction of silane **42d** with trityl borate in the presence of 4-fluorobenzonitrile.

The complexity of the obtained reaction mixtures did not allow a clear identification of the products of the reaction of phenylsilyl phenoxy acenaphthene **42d** and trityl borate.

Given that silylsulfonium ions **35** are in general more stable than silyloxonium ions **34**, the synthesis of thiophenyl-stabilized hydridosilyl borate **35d** $[\text{B}(\text{C}_6\text{F}_5)_4]$ was more promising. The reaction of the corresponding silane **43d** with trityl borate was carried out in benzene- d_6 at room temperature. As already shown in Chapter 3.3.2, asymmetrically substituted silylsulfonium ions **35b** and **37b** form *cis/trans*-isomers due to the trigonal pyramidal coordination environment of the sulfur atom. Therefore the formation of diastereomers is also expected for secondary silylsulfonium ion **35d** (Scheme 55).



Scheme 55 – Synthesis of thiophenyl-stabilized hydridosilyl borate **35d** $[\text{B}(\text{C}_6\text{F}_5)_4]$.

The ^{29}Si NMR spectrum shows two signals at $\delta^{29}\text{Si} = 27.2$ and 37.0 which are somewhat high-field shifted compared to their chiral analogues **35b** and **37b** ($\delta^{29}\text{Si} = 42.9$ - 53.9) and within the region of

binaphthyl-based intramolecularly stabilized silylsulfonium ions **27** of Oestreich and co-workers (^{29}Si = 32.0-57.6). The $^1\text{H}/^{29}\text{Si}$ HMQC spectrum reveals the connection between these two ^{29}Si NMR resonances to a ^1H NMR resonance in the region of $\delta^1\text{H} = 5-6$, respectively (Figure 41). This indicates the direct linkage of the formed silicon species to a hydrogen atom as expected for hydridosilyl cations.

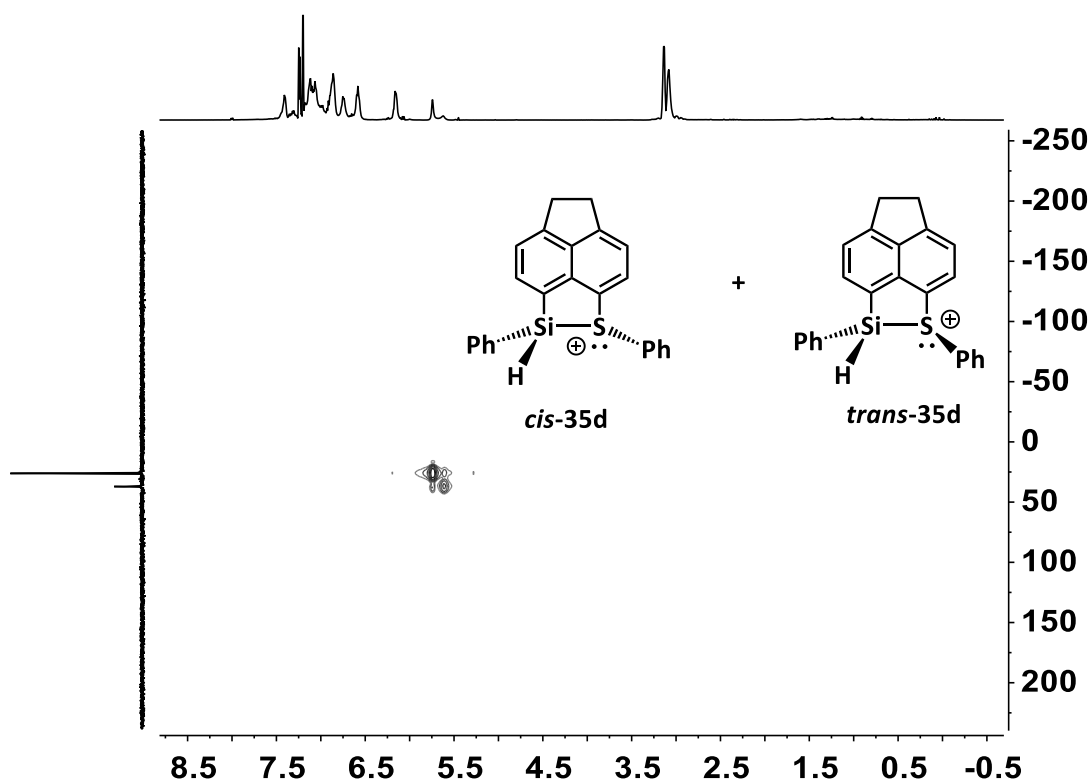
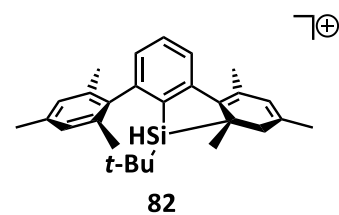


Figure 41 – $^1\text{H}/^{29}\text{Si}$ HMQC NMR spectrum (500 MHz, 305 K, C_6D_6) of the reaction mixture of the hydridosilyl borate **35d** $[\text{B}(\text{C}_6\text{F}_5)_4]$.

The ^{29}Si - ^1H coupled INEPT NMR spectrum is shown in Figure 42. The $^1J_{\text{Si,H}}$ coupling constant is $^1J_{\text{Si,H}} = 260$ Hz for the main isomer and is $^1J_{\text{Si,H}} = 263$ Hz for the second isomer, which is significantly higher compared to the starting silane **43d** ($^1J_{\text{Si,H}} = 204$ Hz). This increase indicates an enhanced s-orbital contribution of the Si – H bond. The magnitude of the coupling constant of silylsulfonium ion **35d** is also higher in comparison to that of the di-*tert*-butylsilylium ion **83a** which is $^1J_{\text{Si,H}} = 233$ Hz^[95] as well as to that of the silyl cation **82** which is $^1J_{\text{Si,H}} = 240$ Hz.^[53a] This indicates that the s-orbital contribution of the Si – H bond is more pronounced in silylsulfonium ion **35d** compared to the other derivatives **83a** and **82**. Therefore, silylsulfonium ion **35d** is assumed to be closer to the, for silylium ions expected, sp^2 hybridization than **83a** and **82**. The ^1H NMR resonance of the Si – H of



thiophenyl-stabilized silyl cation **35d** which is with $\delta^1\text{H} = 5.62, 5.74$ (C_6D_6) low-field shifted compared to H. Großekappenbergs and Oestreichs secondary silyl cations **82** ($\delta^1\text{H} = 4.25$ in $\text{C}_6\text{D}_5\text{Cl}$)^[53a] and **83a** ($\delta^1\text{H} = 5.09$ in $\text{C}_6\text{D}_4\text{Cl}_2$).^[95]

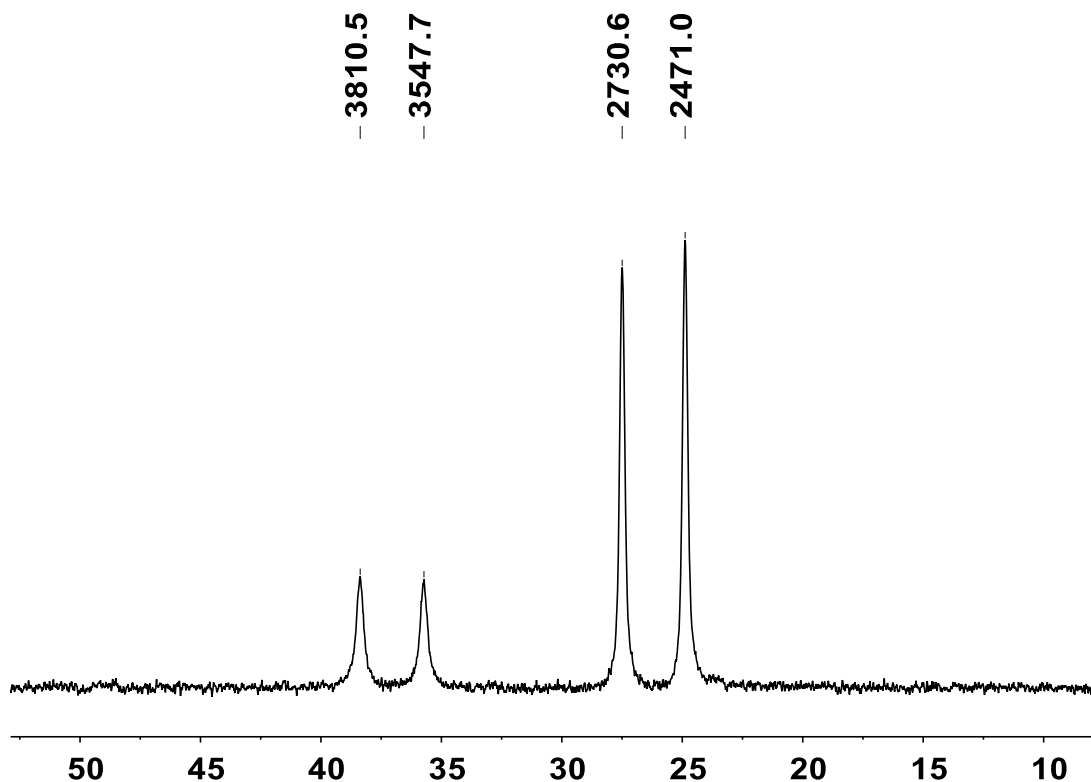


Figure 42 – ^{29}Si INEPT spectrum (99 MHz, 305 K, C_6D_6 , $D_3 = D_4 = 0.001$ s) of hydridosilylsulfonium borate **35d**[$\text{B}(\text{C}_6\text{F}_5)_4$].

At room temperature the ^1H NMR spectrum of species **35d** shows broad signals. Therefore, the sample was dried under high-vacuum and dissolved in toluene- d_8 to allow the NMR analysis at low temperatures. At room temperature, the two signals of the hydrogen atoms attached to the silicon atom appear in the ^1H NMR spectrum as one broad signal. Cooling the sample to 243 K leads to the separation into the two previously observed signals (Figure 43). Unfortunately, due to the proximity of the Si – H signals to the signals in the aromatic region, it was not possible to determine via NOE experiments which of the two isomers, *cis-35d* or *trans-35d*, is the excess compound.

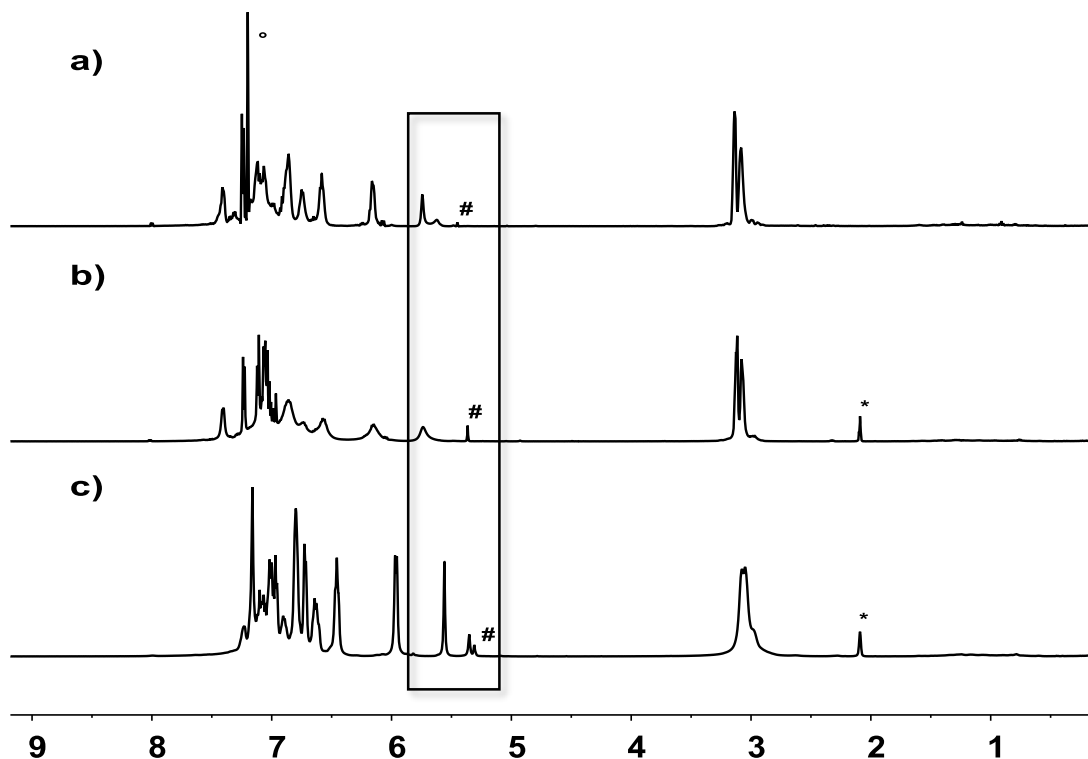


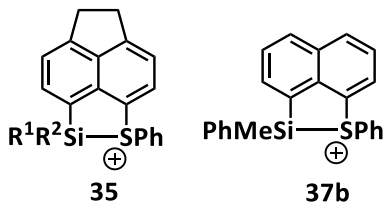
Figure 43 – Comparison of the ^1H NMR spectra (500 MHz) of hydridosilyl borate **35d**[$\text{B}(\text{C}_6\text{F}_5)_4$]: a) 305 K, C_6D_6 ; b) 305 K, C_7D_8 , c) 243 K, C_7D_8 . (* $\text{C}_6\text{D}_5\text{CD}_2\text{H}$, ° $\text{C}_6\text{D}_5\text{H}$, # Residual Ph_3CH).

From the studies of phenylmethylsilyl derivatives **35b** and **37b** it is known, that the *cis*-isomer is the main compound. In this cases the result of the NOE NMR experiments and the DFT calculations are in a good agreement. For this reason, DFT calculations of hydridosilyl cation **35d** were performed as well. The calculated energy difference between both isomers is very low ($\Delta E = 6 \text{ kJmol}^{-1}$, $\Delta G = 0.8 \text{ kJmol}^{-1}$, M06-2X/Def2-TZVP) and predict that the *trans*-isomer is more stable. The thereof predicted *trans/cis* ratio is 58:42, whereby in the experiment (^1H NMR spectrum) a ratio of 79:21 was determined. Including the solvent toluene into the calculations leads to very similar values ($\Delta E = 7 \text{ kJmol}^{-1}$, $\Delta G = 0.7 \text{ kJmol}^{-1}$, M06-2X/Def2-TZVP, SCRF(solvent = toluene)). Consequently, the calculations do not reflect the experiment that good compared to the calculations of phenylmethylsilyl derivatives **35b** and **37b**. The poor fit of calculated and experimental results is rationalized considering an estimated error of about $\pm 1 \text{ kJmol}^{-1}$ for the calculations. Thus, an energy difference of about $\Delta G \approx 0\text{-}2 \text{ kJmol}^{-1}$ has to be considered, whereby the ratio increases to 69:31. Nevertheless, the result is not clear enough to make a closing statement about the predominant isomer.

In conclusion, the synthesis of phenoxy-stabilized secondary silyl borate **34d**[B(C₆F₅)₄] failed due to its high reactivity. However, changing the remote donor substituent to thiophenyl resulted in the successful synthesis of the target compound **35d**[B(C₆F₅)₄]. Here, two isomers, *cis*-**35d** and *trans*-**35d**, were obtained, which is in close analogy to phenylmethyl-substituted silylsulfonium borates **35b**[B(C₆F₅)₄] and **37b**[B(C₆F₅)₄]. Hydridosilylsulfonium borate **35d**[B(C₆F₅)₄] is stable for several days in benzene and does not decompose even under heating to 80 °C in toluene. This is quite remarkable regarding the high lability of secondary silyl cations described in the literature.^[53a, 92]

3.5 Dynamic Process of Sulfonium ions

In variable temperature NMR experiments of silylsulfonium borates **35a,b,d**[B(C₆F₅)₄] and **37b**[B(C₆F₅)₄] a dynamic process including the substituents at the silicon atom was observed.



a: R¹ = R² = Me

b: R¹ = Me, R² = Ph

d: R¹ = H, R² = Ph

As one example, the ¹H VT NMR spectra of silylsulfonium borate **35a**[B(C₆F₅)₄] are shown in Figure 44. The dynamic process influences the chemical shifts of the methyl groups attached to the silicon center (see high-field region in Figure 44). Coalescence of the signals assigned to the dimethylsilyl substituent is reached at 378 K. For silylsulfonium ion **35a** the estimated free Gibbs energy of the process is $\Delta G(378 \text{ K}) = 74 \text{ kJmol}^{-1}$.

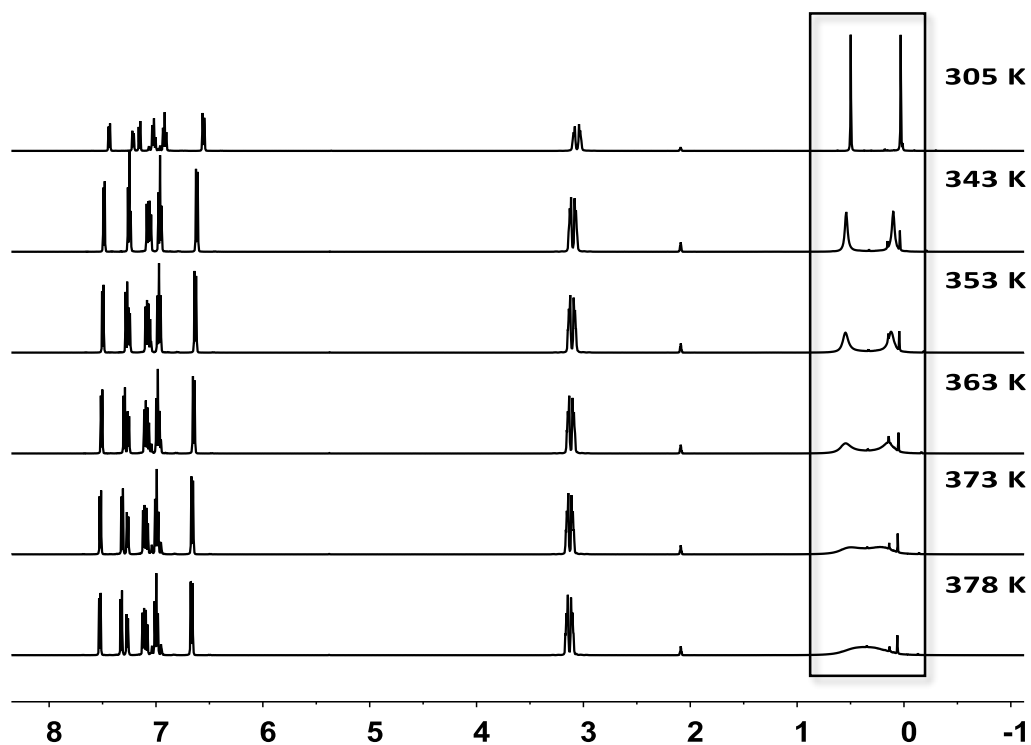
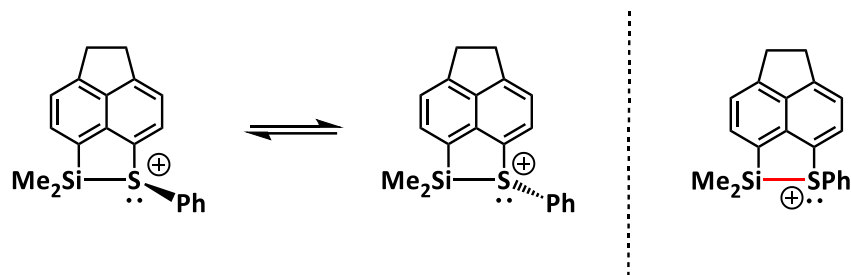


Figure 44 – VT ¹H NMR spectra (500 MHz, C₇D₈) of sulfonium borate **35a**[B(C₆F₅)₄].

Possible underlying processes which lead to the exchange of the substituents at the silicon atom of sulfonium ions **35a,b,d** and **37b** are either the inversion of configuration at the sulfur atom, or, the heterolytic cleavage of the Si – S bond (Scheme 56).



Scheme 56 – Inversion process of the sulfur atom (left) and heterolytic cleavage of Si – S bond (right) of silyl cation **35a**.

The inversion process is realized via a transition state (TS) in which the sulfur atom exhibits a trigonal planar coordination sphere (Figure 45). For this process a free Gibbs energy of $\Delta G = 73 \text{ kJmol}^{-1}$ was calculated (M06-2X/Def2-TZVP) for silyl cation **35a**.

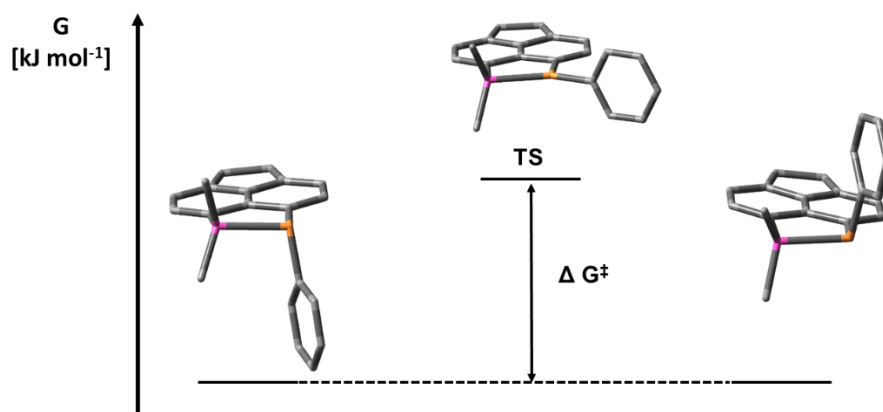
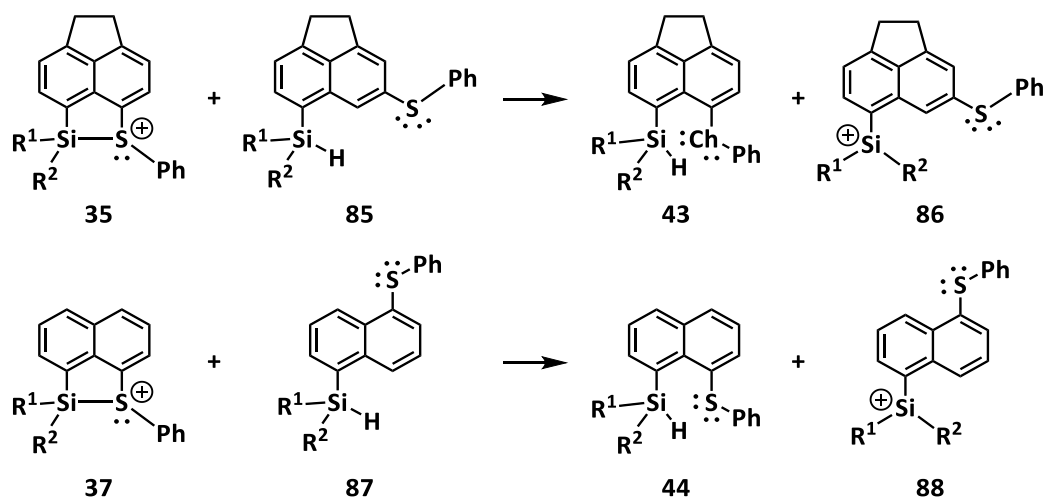


Figure 45 – Diagram of the calculated relative free Gibbs energy of the transition state and the ground state structures of the inversion process of the sulfur atom of silyl cation **35a** (M06-2X/Def2-TZVP).

The second process includes the heterolytic cleavage of the silicon sulfur bond which leads to free rotation of the thiophenyl as well as the dimethylsilyl group. To calculate the bond dissociation energy of the Si – Ch bond in silyl cations **35** and **37**, isodesmic equations were used (Scheme 57). This theoretic consideration is not perfect in two terms: first, the *peri*-substituted silanes **43/44** are destabilized due to steric repulsion between the *peri*-substituents compared to the corresponding isomers **85/87**. This leads to a prediction of a too strong Si – Ch bond. Second, the conjugation of the 3p orbital of the silicon atom with the π -system of the aryl substituent in cationic isomers **86/88** exhibits a stabilizing effect on the positively charged silicon atom which is less pronounced in the

corresponding stabilized cations **35/37**. This leads to a prediction of a too weak Si – Ch bond. However, these two contemplations are reversing each other, whereby, isodesmic equation is considered a reliable approach to estimate the bond dissociation energy (BDE) between the silicon and the sulfur atom in these systems.



Scheme 57 – Isodesmic equations for the calculation of the bond dissociation energy of the Si – Ch bond in silyl cations **35** and **37**.

The calculated bond dissociation energy for dimethylsilyl derivative **35a** is with BDE = 144 kJmol⁻¹ (M06-2X/Def2-TZVP) distinctively higher than the free Gibbs energy calculated for the inversion of the configuration of the sulfur atom ($\Delta G = 73$ kJmol⁻¹, (M06-2X/Def2-TZVP)). Comparison of the two calculated values with the experimental determined free Gibbs energy ($\Delta G = 74$ kJmol⁻¹) suggests that the inversion of the sulfur atom is more likely the underlying process for the dynamic behavior of thiophenyl-stabilized silyl cation **35a**.

The results of the VT NMR experiments and the calculations of sulfonium ions **35b,d** and **37b** are summarized in Table 17. The naphthyl derivative **37b** has in comparison to the acenaphthyl derivative **35b** a higher bond dissociation energy (BDE = 168 kJmol⁻¹ vs 141 kJmol⁻¹). The distance of the *peri*-positions at the acenaphthene backbone is compared to the naphthyl substituent by 20 pm widened, hence, a stronger interaction between the silicon and the sulfur atom in naphthyl derivative **37b** is expected. The free Gibbs energies calculated for the inversion process of phenylmethylsilyl-substituted derivatives **35b** and **37b** are in the range of $\Delta G^{\text{calc}} = (71-74)$ kJmol⁻¹. The free Gibbs energies determined via VT NMR experiment of the chiral derivatives **35b** and **37b** for the dynamic process are $\Delta G^{\text{exp}} = (72-74)$ kJmol⁻¹ and are similar to the free Gibbs energies calculated for the

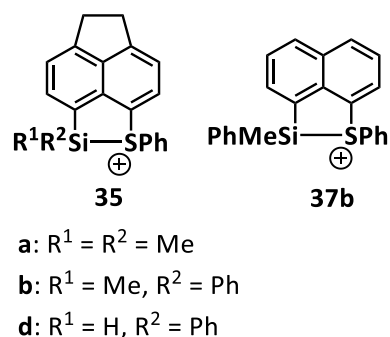
inversion process. Hence, the inversion of the configuration of the sulfur atom is likely to be the underlying process. This result is consistent to that of silylsulfonium ion **35a**. Interestingly, there is no significant difference in the free Gibbs energy of the inversion process between the phenylmethyl-substituted derivatives **35b** and **37b** compared to the dimethyl-substituted derivative **35a** despite their different substitution pattern.

Table 17 – Comparison of the free Gibbs energy determined via VT NMR experiments (details see Chapter 5.9) and the calculated energies for the inversion of the configuration of the sulfur atom and the BDE of the Si – S bond (M062X/def2-TZVP).

Compound	ΔG^{exp} [kJmol ⁻¹]	ΔG^{calc} [kJmol ⁻¹]	BDE [kJmol ⁻¹]
35a	74 ± 1	73	144
37b	72 ± 1	71	168
35b	74 ± 1	74	141
35d	65 ± 1	74	143

The experimental determined values of the free Gibbs energy for the inversion process at the sulfur atom are, in general, consistent with those calculated. One exception is hydridosilyl derivative **35d**. The experimental value is $\Delta G^{\text{exp}} = 65 \text{ kJmol}^{-1}$ whereby the calculated value is $\Delta G^{\text{calc}} = 74 \text{ kJmol}^{-1}$. One consideration not made yet is the effect of the solvent which was not included in the calculation. Therefore, the inversion process was calculated again including the solvent toluene, resulting in a free Gibbs energy barrier of $\Delta G^{\text{calc}} = 75 \text{ kJmol}^{-1}$. This inversion barrier is similar to that calculated without the solvent ($\Delta G^{\text{calc}} = 74 \text{ kJmol}^{-1}$ without solvent, $\Delta G^{\text{calc}} = 75 \text{ kJmol}^{-1}$ with solvent). In consequence, the inversion barriers calculated for the other derivatives **35a**, **37b** and **35b** are expected to be suitable, even though the solvent was not included into the calculations. However, the calculated free Gibbs energy of the inversion process of silyl cation **35d** is still by 10 kJmol⁻¹ higher than the experimental value. The possible reason will be discussed below.

In conclusion, the dynamic process observed with silylsulfonium borates **35a,b,d**[B(C₆F₅)₄] and **37b**[B(C₆F₅)₄] results from an inversion of the configuration of the sulfur atom.



At this point, another phenomenon observed with sulfonium ions **35a,b,d** and **37b** shall be discussed. Dimethylsilyl borate **35a**[B(C₆F₅)₄] was prepared in benzene-d₆ to allow an NMR measurement directly after the preparation. The cationic phase was washed twice with ca. 0.3 mL benzene-d₆ and then transferred to the NMR tube for analysis. The ¹H NMR spectrum obtained is shown in Figure 46

(after reaction). A broad singlet signal in the high-field region which was assigned to the dimethylsilyl substituent was observed ($w(1/2) = 76$ Hz). The sample was then measured every one to four days. In the first days the broad signal got sharper (see spectrum after 9 days) ($w(1/2) = 12$ Hz) and then after 13 days it splits up into two signals ($w(1/2) = 35$ Hz). After 20 days the two singlet signals ($w(1/2) = 6$ Hz), which were expected for dimethylsilyl cation **35a**, were detected. Later no further change was observed.

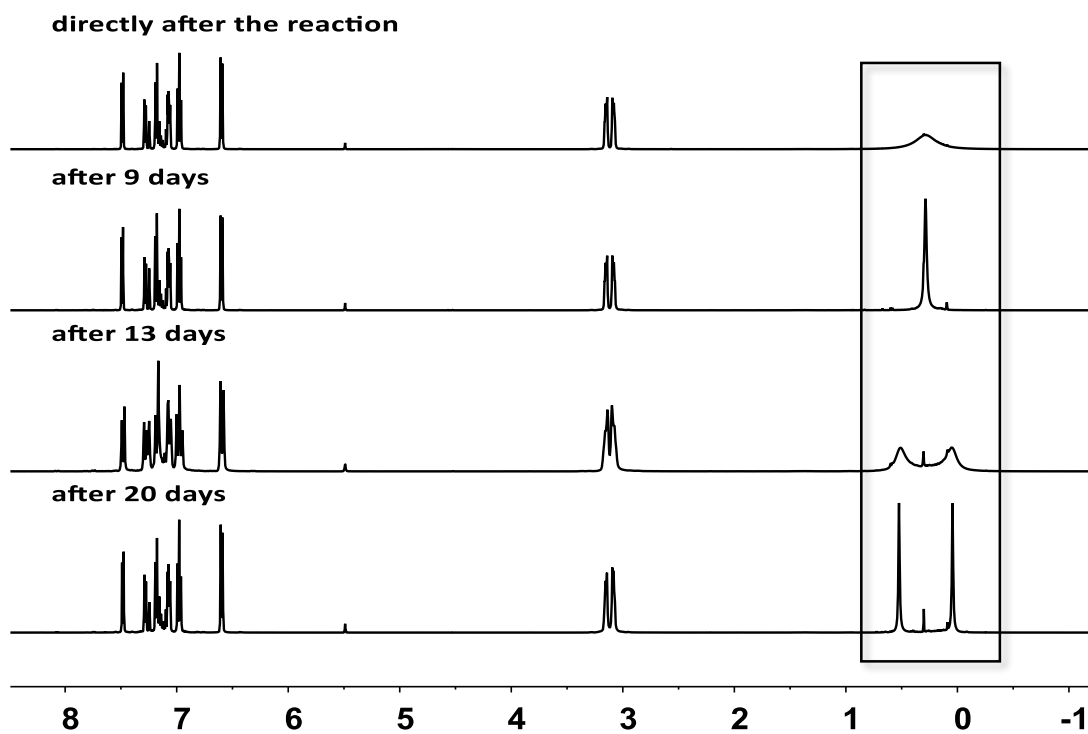
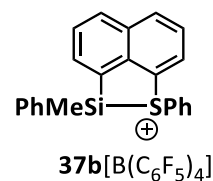


Figure 46 – Comparison of the ^1H NMR spectra (300 MHz, 298 K, C_6D_6) of silyl borate **35a** $[\text{B}(\text{C}_6\text{F}_5)_4]$ measured over a period of time.

The naphthyl-substituted phenylmethylsilyl derivative **37b** shows a similar behavior.

This compound was prepared directly in toluene- d_8 and washed twice with ca. 0.3 mL toluene- d_8 prior to the NMR measurement. Broadened signals which were assigned to the methyl group at the silicon atom were observed in the high-field of the ^1H NMR



spectrum ($w(1/2) = 60$ Hz). Two weeks after the preparation of the sample, it was purified by washing the polar phase and subsequently analysed by a VT NMR experiment (Figure 47, left). The line broadening was unchanged. Coalescence was observed at 328 K which results in a free Gibbs energy barrier of $\Delta G^{\text{exp}} = 63$ kJmol^{-1} . This value is by 6 kJmol^{-1} lower compared to the calculated value (Table

17). The exact same sample was stored and analyzed six months later (Figure 47, right). At room temperature no line broadening was observed ($w(1/2) = 3$ Hz) and coalescence was observed at 368 K which results in a free Gibbs energy barrier of $\Delta G^{\text{exp}} = 72$ kJmol⁻¹. This value is now similar to that calculated ($\Delta G^{\text{calc}} = 71$ kJmol⁻¹). The difference of the free Gibbs energy barrier between the two VT NMR experiments is 9 kJmol⁻¹.

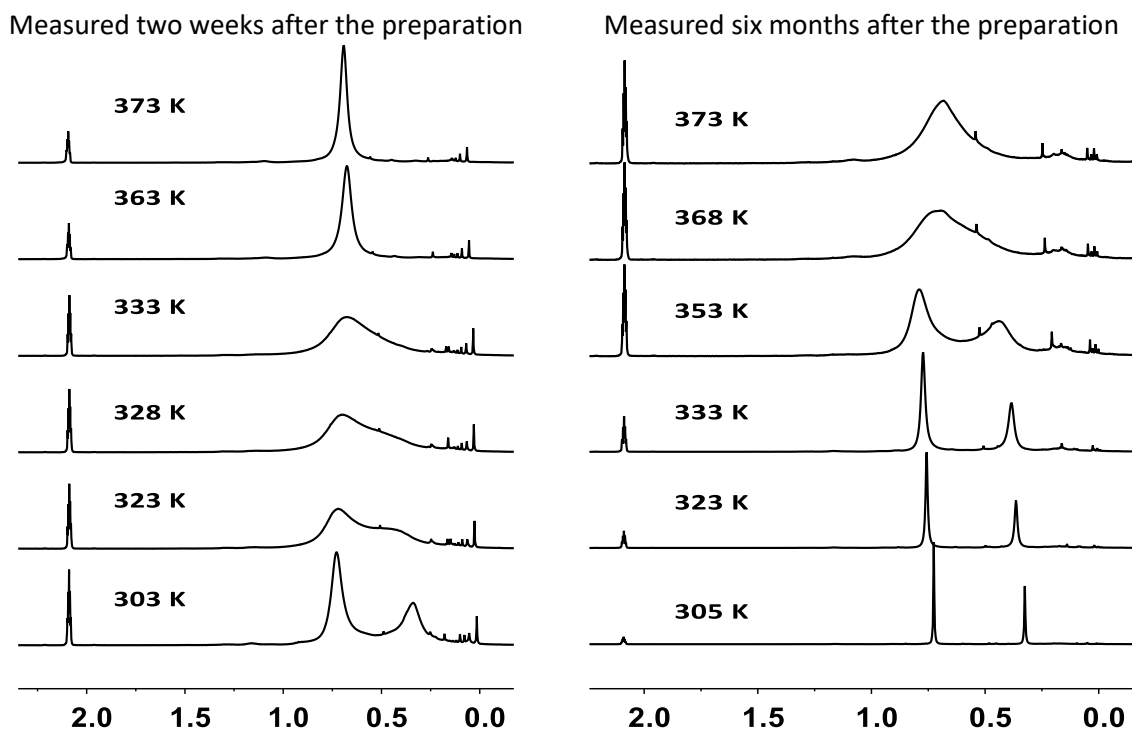
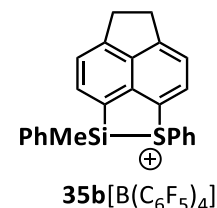


Figure 47 – Comparison of the VT ¹H NMR spectra (500 MHz, C₇D₈) of silyl borate **37b**[B(C₆F₅)₄] two weeks (left) and six months (right) after preparation.

For the acenaphthyl-substituted phenylmethylsilyl derivative **35b**, this phenomenon was even more pronounced. Silyl borate **35b**[B(C₆F₅)₄] was prepared in benzene, the polar phase was washed once with *n*-pentane and dried in high-vacuum. The NMR spectrum was measured in toluene-*d*₈ (Figure



48, above). For the SiMe₂ groups of the isomers *cis*-**35b** and *trans*-**35b** only one broad signal was observed. Furthermore, not all signals in the aromatic region are affected by the line broadening. Due to the relative high amount of triphenyl methane and benzene, the sample was purified a second time (polar phase washed twice with *n*-pentane). The ¹H NMR spectrum measured after the second purification is shown also in Figure 48 (lower spectrum). The signals do not show any line broadening ($w(1/2) = 3$ Hz) and the subsequent VT NMR experiment gave the expected value for the free Gibbs energy barrier of the inversion process ($\Delta G^{\text{exp}} = 74$ kJmol⁻¹ vs $\Delta G^{\text{calc}} = 74$ kJmol⁻¹).

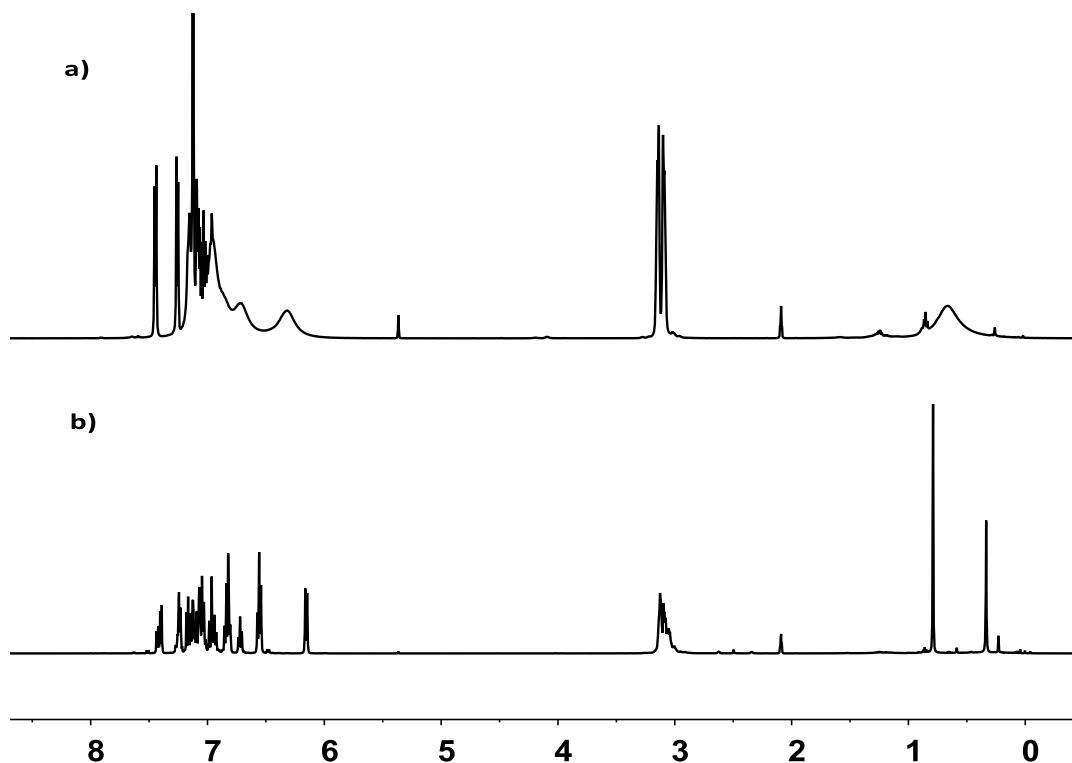
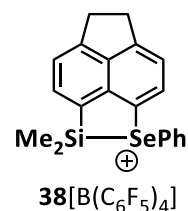


Figure 48 – ^1H NMR spectra (500 MHz, 305 K, C_7D_8) of silyl borate **35b** $[\text{B}(\text{C}_6\text{F}_5)_4]$ a) before and b) after second purification.

Another important aspect is that the ^{29}Si NMR spectrum is not affected. The line broadening appears only in the ^1H and ^{13}C NMR spectra. Similar observations were made by S. Rathjen with the acenaphthyl-substituted dimethylsilyl cation **38** which is stabilized by a selenyl group.^[78]



The examples discussed so far were all measured in toluene- d_8 or benzene- d_6 . Therefore, a possible explanation could be that the two phases are not completely separated and diffusion of the two phases is taking place. Therefore, acenaphthyl-substituted thiophenyl-stabilized dimethylsilyl cation **35a** was measured in dichloromethane- d_2 and chlorobenzene- d_5 , respectively (Figure 49, lower spectrum in DCM- d_2 and above in chlorobenzene- d_5). Both reactions were not perfectly clean. For the sample in DCM- d_2 , the silyl borate **35a** $[\text{B}(\text{C}_6\text{F}_5)_4]$ was prepared in benzene, purified, dried under high-vacuum and dissolved in DCM- d_2 . The other sample was prepared in chlorobenzene- d_5 and analysed via NMR spectroscopy, without any purification, directly after the preparation. Both spectra show no significant line broadening (Figure 49). This could confirm the hypothesis, that the biphasic system in benzene and toluene causes the line broadening. But then one would assume that all signals in the ^1H NMR spectrum would be affected; however, this is not the case (Figure 48 and vide infra).

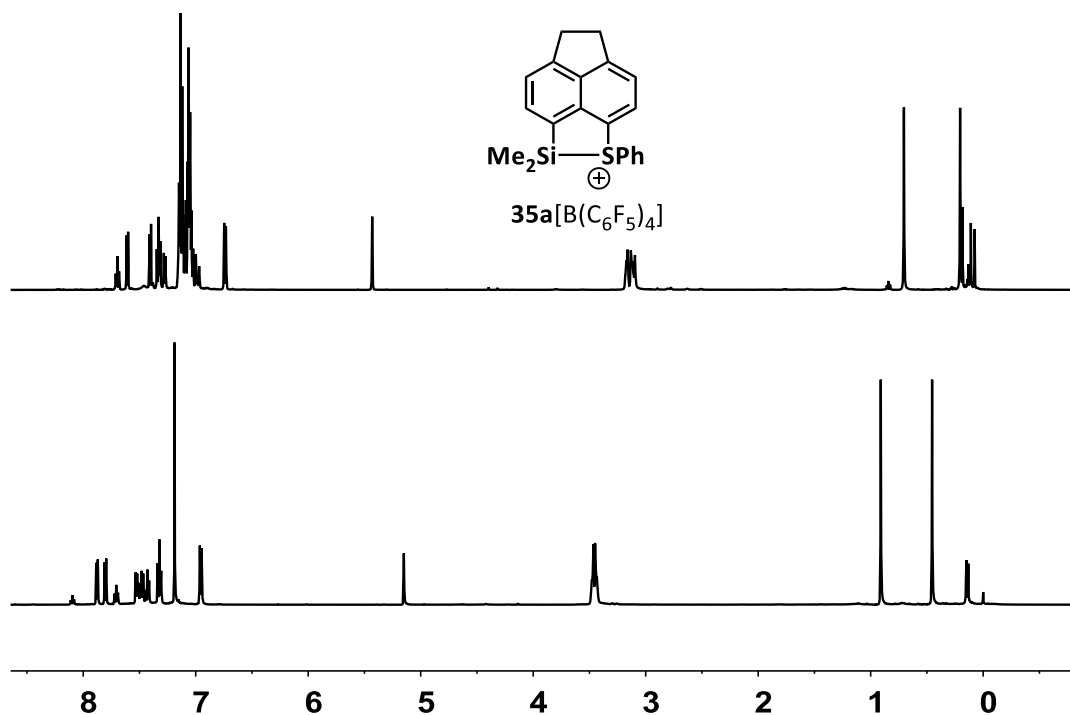
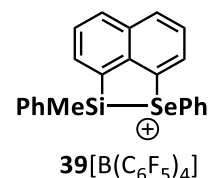


Figure 49 – ^1H NMR spectrum (500 MHz, 305 K, CD_2Cl_2) and ^1H NMR spectrum (500 MHz, 305 K, $\text{C}_6\text{D}_5\text{Cl}$) of silyl borate $\mathbf{35a}[\text{B}(\text{C}_6\text{F}_5)_4]$.

K. Rürger observed a similar behavior with the phenylmethyl-substituted selenyl-stabilized silyl cation $\mathbf{39}$. A comparison of the ^1H NMR spectra of selenyl-stabilized silyl borate $\mathbf{39}[\text{B}(\text{C}_6\text{F}_5)_4]$ in different solvents is shown in Figure 50. The first spectrum (a) shows silyl borate $\mathbf{39}[\text{B}(\text{C}_6\text{F}_5)_4]$ in toluene- d_8 . The borate $\mathbf{39}[\text{B}(\text{C}_6\text{F}_5)_4]$ was



prepared and purified in toluene, dried under high-vacuum and dissolved in toluene- d_8 . Here, a significant line broadening of the methyl groups of both isomers, *cis*- $\mathbf{39}$ and *trans*- $\mathbf{39}$, was observed. In the aromatic region, the line broadening affects not all signals. The signals, which are not affected, are those of the naphthyl substituent. After one week, the solution of silyl borate $\mathbf{39}[\text{B}(\text{C}_6\text{F}_5)_4]$ in toluene- d_8 was divided into several fractions, dried under high-vacuum and dissolved in different solvents, namely in dichloromethane- d_2 and chlorobenzene- d_5 (Figure 50, b), c). In these two solvents sharp signals without any line broadening were observed.^[87b]

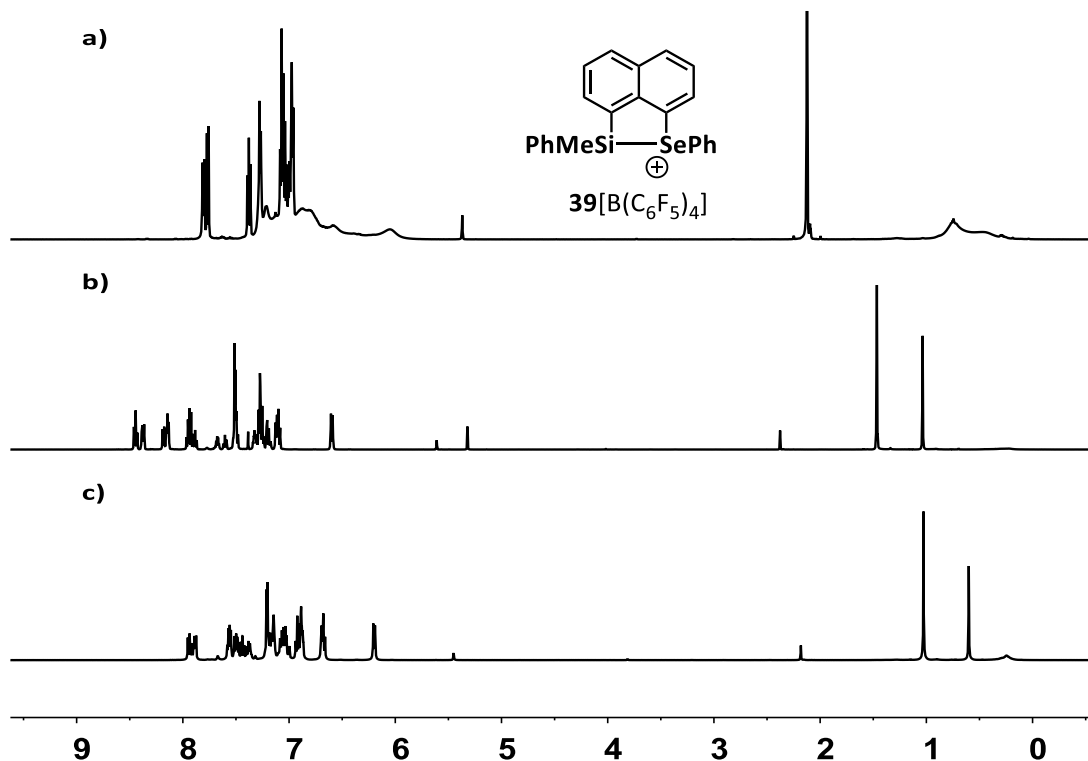
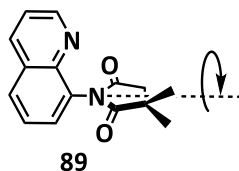


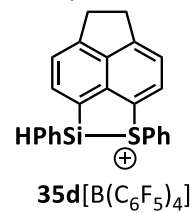
Figure 50 – ^1H NMR spectra (500 MHz, 305 K) of silylselenium borate **39** $[\text{B}(\text{C}_6\text{F}_5)_4]$ in a) C_7D_8 , b) CD_2Cl_2 and c) $\text{C}_6\text{D}_5\text{Cl}$.

An effect which seems similar was reported by Shimizu and co-workers in quinoline imides **89**. Here, the rotation of the imide moiety accelerates by addition of acid, whereby coalescence of the methyl groups is obtained by addition of 2 equiv. H^+ .^[97] However, to date, it is not clear, which chemical is additionally present or formed with time in the reaction mixtures of silylchalconium borates **35** $[\text{B}(\text{C}_6\text{F}_5)_4]$, **37** $[\text{B}(\text{C}_6\text{F}_5)_4]$, **38** $[\text{B}(\text{C}_6\text{F}_5)_4]$ and **39** $[\text{B}(\text{C}_6\text{F}_5)_4]$ that could be the origin for this phenomenon. Currently, S. Rathjen is investigating the phenomenon further.^[78]



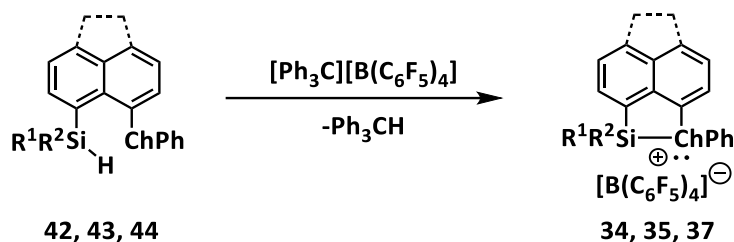
In conclusion, even if the origin of the broadened signals in the ^1H NMR spectra is not completely understood to date, it is important to consider that this broadened signals can lead to a falsified result in the determination of the coalescence temperature in the VT NMR experiment for silylchalconium borates **35** $[\text{B}(\text{C}_6\text{F}_5)_4]$, **37** $[\text{B}(\text{C}_6\text{F}_5)_4]$, **38** $[\text{B}(\text{C}_6\text{F}_5)_4]$ and **39** $[\text{B}(\text{C}_6\text{F}_5)_4]$. As described above, the difference between the calculated and the experimental determined free Gibbs energy of the

inversion process of hydridosilyl cation **35d** was 10 kJmol^{-1} (Table 17). The VT NMR experiment was carried out just one day after the preparation and could not be repeated, since, after three months storage, the hydridosilyl cation **35d** was decomposed. However, it is assumed that the poor fit of the calculated and the experimental determined values of the free Gibbs energy of the hydridosilyl cation **35d** is caused by the phenomenon of the broadened signals in the ^1H NMR spectrum.



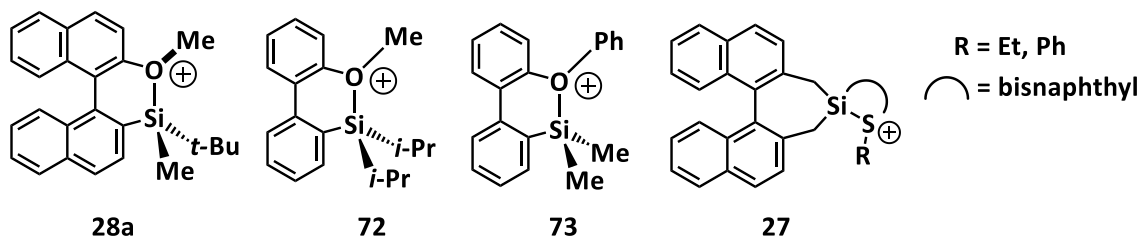
3.6 Summary of Naphthyl- and Acenaphthyl-Substituted Silyloxonium and -sulfonium Borates

Literature unknown silyloxonium and -sulfonium borates **34**[B(C₆F₅)₄], **35**[B(C₆F₅)₄] and **37**[B(C₆F₅)₄] were synthesized via the standard Corey reaction (Scheme 58) and fully characterized by multinuclear NMR spectroscopy. Selected NMR data are summarized in Table 18.



Scheme 58 – Synthesis of silyloxonium and -sulfonium borates **34**[B(C₆F₅)₄] (ace, Ch = O), **35**[B(C₆F₅)₄] (ace, Ch = S) and **37**[B(C₆F₅)₄] (naph, Ch = S) via the Corey reaction (R¹ = R² = Me (a), R¹ = Me, R² = Ph (b), R¹ = Me, R² = *t*-Bu (c), R¹ = H, R² = Ph (d)).

Due to the trigonal pyramidal coordination environment of the sulfur atom in silylsulfonium ions **35** and **37**, the methyl groups at the silicon atom are *syn* or *anti* relative to the SPh group. Hereby, the ¹H NMR and ¹³C NMR chemical shifts of the *syn*-methyl group is always at higher field compared to the *anti*-methyl group (Table 18). Silyloxonium ions **34** instead exhibit a trigonal planar coordinated oxygen atom, whereby, the methyl groups are equivalent and no formation of *cis/trans* isomers was observed. The ²⁹Si NMR chemical shifts of silyloxonium borates **34**[B(C₆F₅)₄] is between δ²⁹Si = 60.8-77.4 and are somewhat low-field shifted compared to the ²⁹Si NMR resonance of silyloxonium borate **28a**[B(C₆F₅)₄] of Ducos et al. (δ²⁹Si = 52.2, 52.9). The ²⁹Si NMR chemical shifts of biphenyl derivatives **72** and **73** are in the same range (δ²⁹Si = 49.3 and 59.5). In comparison, the ²⁹Si NMR chemical shifts of silylsulfonium borates **35**[B(C₆F₅)₄] and **37**[B(C₆F₅)₄] are in the range of δ²⁹Si = 26.0-70.0 and comparable to those of binaphthyl-substituted silylsulfonium borates **27**[B(C₆F₅)₄] of Oestreich and co-workers (δ²⁹Si = 32.0-57.6).^[29c, 29d]



The deviation of the calculated and experimental determined ^{29}Si NMR resonances is 2-10 % for silyloxonium ions **34** and is 8-28 % for silylsulfonium ions **35** and **37**. The largest difference shows acenaphthylphenylmethyl derivative **35b** with $\Delta\delta^{29}\text{Si} = 16.5$.

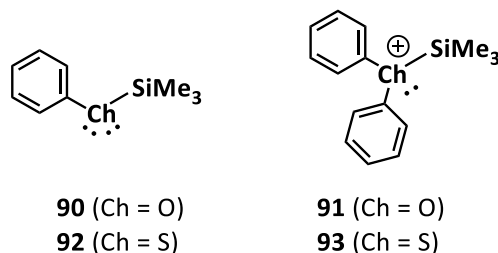
The ^{29}Si NMR chemical shift of the *trans*-isomer of the phenylmethyl-substituted derivatives **35b** and **37b** is high-field shifted compared to the corresponding *cis*-isomer. This is also reflected by the corresponding calculated ^{29}Si NMR resonances. In contrast, the calculated ^{29}Si NMR chemical shifts of hydridosilyl cation **35d** of the *cis*-isomer is high-field shifted compared to the *trans*-isomer. For the experimental values of hydridosilyl cation **35d**, it was not possible to distinguish *cis* and *trans* via the NOE NMR experiment and also the calculation of the equilibrium constant and the thereof resulting *cis/trans* ratio was not clear. Comparison of the calculated ^{29}Si NMR resonance indicates, that the main isomer is the *cis*-isomer. This is in analogy to the results of the phenylmethyl-substituted derivatives **35b** and **37b**. Here, also the *cis*-isomer is the main compound, which was clearly proven via the NOE NMR experiment. In contrast to these findings, the *tert*-butylmethyl derivative **35c** is stereoselectively formed as the *trans*-isomer.

Table 18 – Selected NMR data (in C_6D_6) of silyloxonium and –sulfonium borates **34**[$\text{B}(\text{C}_6\text{F}_5)_4$] (ace, Ch = O), **35**[$\text{B}(\text{C}_6\text{F}_5)_4$] (ace, Ch = S) and **37**[$\text{B}(\text{C}_6\text{F}_5)_4$] (naph, Ch = S; $\text{R}^1 = \text{R}^2 = \text{Me}$ (**a**), $\text{R}^1 = \text{Me}$, $\text{R}^2 = \text{Ph}$ (**b**), $\text{R}^1 = \text{Me}$, $\text{R}^2 = t\text{-Bu}$ (**c**), $\text{R}^1 = \text{H}$, $\text{R}^2 = \text{Ph}$ (**d**)). (* main isomer) and comparison of the calculated ^{29}Si NMR chemical shift (M06-2X/Def2-TZVP//M06L/Def2-TZVP).

Silyl cation	Donor	$\delta^1\text{H SiMe}_n$	$\delta^{13}\text{C SiMe}_n$	$\delta^{29}\text{Si exp}$	$\delta^{29}\text{Si calc}$
34a	OPh	0.41	0.6	77.4	69.5
34b	OPh	0.63	-3.9	60.8	59.5
34c	OPh	0.37	-4.9	72.2	67.2
35a	SPh	-0.01 (<i>syn</i>) 0.47 (<i>anti</i>)	-3.0 (<i>syn</i>) -0.3 (<i>anti</i>)	65.8	71.4
35b	SPh	0.34 (<i>trans</i>) 0.80 (<i>cis</i>)	-5.4 (<i>trans</i>) -2.8 (<i>cis</i>)	42.7 (<i>trans</i>) 45.2* (<i>cis</i>)	59.3 (<i>trans</i>) 59.8 (<i>cis</i>)
37b	SPh	0.33 (<i>trans</i>) 0.73 (<i>cis</i>)	-6.1 (<i>trans</i>) -3.4 (<i>cis</i>)	42.9 (<i>trans</i>) 45.5* (<i>cis</i>)	48.2 (<i>trans</i>) 50.9 (<i>cis</i>)
35c	SPh	0.12 (<i>trans</i>)	-7.2 (<i>trans</i>)	70.0 (<i>trans</i>)	76.2 (<i>trans</i>)
35d	SPh	-	-	26.0* 37.0	34.0 (<i>cis</i>) 43.0 (<i>trans</i>)

The interaction between the silicon and the oxygen or sulfur atom was investigated using DFT methods (M06-2X/Def2-TZVP). Selected calculated structural parameters of silyloxonium and –sulfonium ions are given in Table 19. The deviation between the calculated structural parameters and the experimental determined values is between 0.03-3 % (Table 19). The Si – O distance in derivatives **34** is with $d(\text{Si} - \text{O}) = 185\text{-}187$ pm by 3-4 % larger than the sum of the covalent radii ($\Sigma cr(\text{Si} - \text{O}) = 179$ pm)^[79] and by 10-11 % larger than the calculated bond length of silylated ether **90** ($d(\text{Si} -$

O) = 167 pm).^[6a] The calculated bond length of acyclic silyloxonium ion **91** is with $d(\text{Si} - \text{O}) = 182 \text{ pm}$ ^[6a] by only 3-5 pm (2-3 %) shorter than in silyloxonium ions **34**. The same trend is reflected in silylsulfonium ions **35** and **37**. The deviation of the Si – S bond length in silylsulfonium ions **35** and **37** to the sum of the covalent radii is 6 %, whereas the deviation to silyl thioether **92** is 7-8% ($d(\text{Si} - \text{S}) = 216 \text{ pm}$)^[6a] and to acyclic silylsulfonium ion **93** is 4-5 % ($d(\text{Si} - \text{S}) = 223 \text{ pm}$).^[6a]



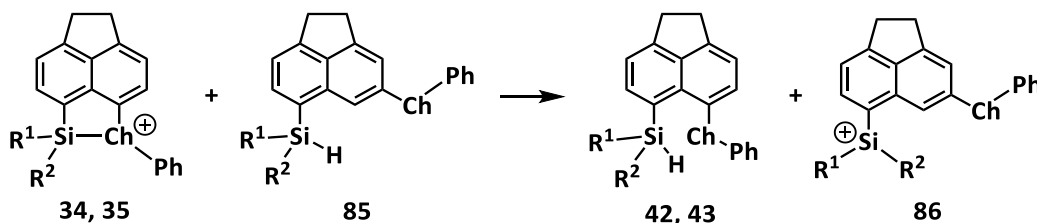
The five membered ring formed by the naphthyl/acenaphthyl backbone, the silicon and the chalcogen atom shows for both silyloxonium and silylsulfonium ions **34**, **35** and **37** a certain ring strain which is manifested in the sum of the bay angles. For silyloxonium ions **34** the sum of the bay angles is by 8 % and for silylsulfonium ions **35** and **37** by 4 % smaller than in unstrained acenaphthene ($\Sigma\beta = 368^\circ$).^[73]

Table 19 – Selected calculated structural parameters (structural data from XRD is given in parentheses for comparison) and bond dissociation energies of silyl cations **34** (ace, Ch = O), **35** (ace, Ch = S) and **37** (naph, Ch = S; R¹ = R² = Me (**a**), R¹ = Me, R² = Ph (**b**), R¹ = Me, R² = *t*-Bu (**c**), R¹ = H, R² = Ph (**d**)). (M06-2X/Def2-TZVP).

Silyl cation	Donor	Si – D [pm]	$\Sigma\alpha(\text{Si})$ [°]	$\Sigma\alpha(\text{D})$ [°]	$\Sigma\beta$ [°]	BDE [kJmol ⁻¹]
34a	OPh	185	352	360	337	104
34b	OPh	187	351	359	338	101
34c	OPh	187	353	357	338	120
35a	SPh	232 (232)	349 (348)	299 (308)	353 (353)	144
35b	SPh	234	351 (<i>cis</i>) 350 (<i>trans</i>)	298	354	141 (<i>cis</i>) 136 (<i>trans</i>)
37b	SPh	232	350 (<i>cis</i>) 349 (<i>trans</i>)	297 (<i>cis</i>) 299 (<i>trans</i>)	354	169 (<i>cis</i>) 164 (<i>trans</i>)
35c	SPh	232	349	299	353	164 (<i>trans</i>)
35d	SPh	233 (<i>cis</i>) 232 (<i>trans</i>)	351 (<i>cis</i>) 350 (<i>trans</i>)	297 (<i>cis</i>) 299 (<i>trans</i>)	354	143 (<i>cis</i>) 137 (<i>trans</i>)

The BDE of the acyclic silylchalconium ions **91** and **93** is for the oxygen derivative **91** BDE(Si – O) = 214 kJmol⁻¹ and for the sulfur derivative **93** BDE(Si – S) = 215 kJmol⁻¹. Acenaphthyl silyloxonium ions **34** exhibit a BDE of 101-120 kJmol⁻¹ and for silylsulfonium ions **35** and **37** BDE(Si – S) = 136-169 kJmol⁻¹

¹ is obtained, which is in both cases distinct smaller than in the acyclic derivatives. This comparatively weaker Si – O/S bond is the result of the ring strain in naphthyl/acenaphthyl silyl cations **34**, **35** and **37**. Herein, the change from the naphthyl to the acenaphthyl backbone weakens the Si – S bond in phenylmethylsilyl derivative **37** by 28 kJmol⁻¹. Notably, the change of the substitution pattern at the silicon atom from dimethyl to *tert*-butylmethyl results in a stronger Si – Ch linkage (for **34c** by 16 kJmol⁻¹ and for **35c** by 20 kJmol⁻¹). A possible reason might be justified by the calculation of the BDE. As described in Chapter 3.5, the BDE was calculated using the isodesmic equation shown for acenaphthyl derivatives **34** and **35** in Scheme 59. The isodesmic equation is not perfect for two reasons; on the one hand, the *peri*-substituted silane **43** is destabilized due to steric repulsion between the *peri*-substituents compared to the corresponding isomer **85** what leads to a prediction of a too strong Si – Ch bond. On the other hand, the stabilizing effect of the conjugation of the 3p orbital of the silicon atom with the aryl substituent is higher in isomer **86** compared to silyl cations **34/35** which leads to a prediction of a too weak Si – Ch bond. Since these effects are reversing it was assumed that they cancel out each other and, therefore, the isodesmic equation was presumed to be suitable for the prediction of the BDE in silyl cations **34** and **35**.



Scheme 59 – Isodesmic equations for the calculation of the bond dissociation energy of the Si – Ch bond in silyl cations **35** and **37**.

However, for the *tert*-butylmethyl-substituted derivatives **34c/35c**, the sterically demanding *tert*-butyl substituent leads to distortion in isomer **86-t-Bu** compared to isomer **86-Me**, as demonstrated by the torsion angles of the phenoxy-substituted derivatives in Figure 51. As a consequence, the conjugation of the 3p orbital at the silicon atom with the π -system of the acenaphthyl substituent is less pronounced in the *tert*-butylmethylsilyl-substituted derivative of isomer **86** than in the dimethylsilyl-substituted derivative of **86**. Therefore, it is assumed that the prediction of the BDE of *tert*-butylmethylsilyl cations **34c** and **35c** gives a higher BDE compared to the dimethylsilyl cations **34a** and **35a**.

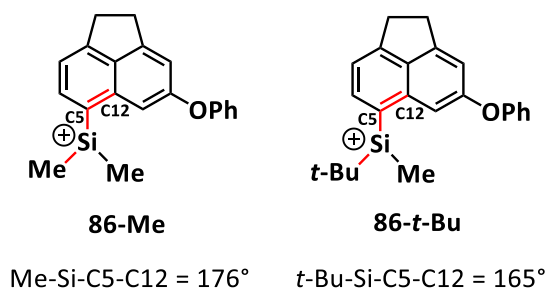
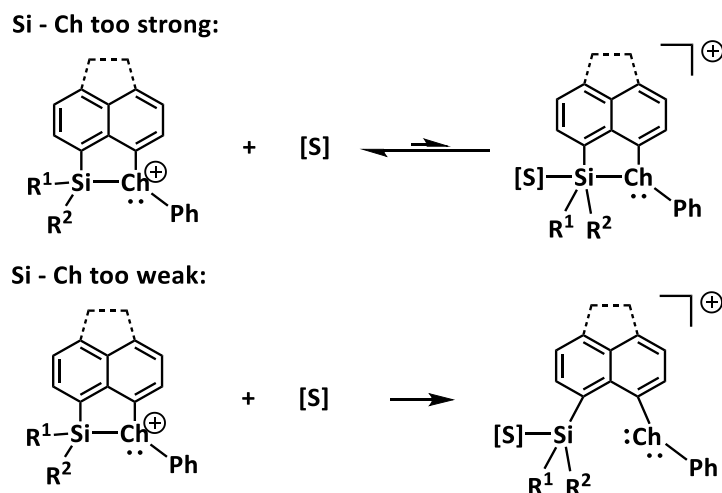


Figure 51 – Illustration of the torsion angles in the dimethyl- and *tert*-butylmethyl-substituted isomers **86**.

Regarding the use of silylchalconium ions **34**, **35** and **37** as catalysts, two important considerations about the Si – Ch linkage must be made. On the one hand, the Si – Ch linkage should not be too strong, since this would quench the reactive Lewis acidic silicon center completely. As a result, no interaction between the silicon center and the substrate would be possible. On the other hand, a too weak Si – Ch interaction can result in the cleavage of the Si – Ch bond. As a consequence, the bond between the substrate and the silyl cation will be strong and the reaction stops at this point (Scheme 60).

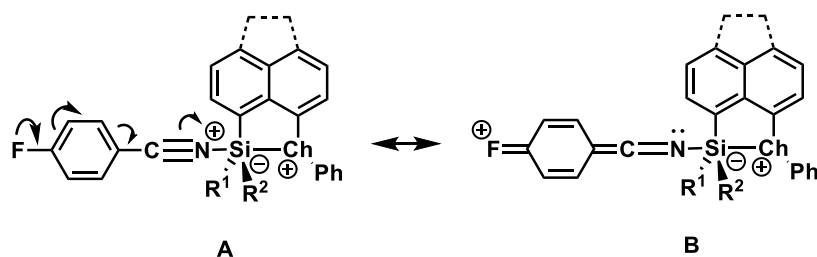


Scheme 60 – Concept of a too strong or too weak Si – Ch linkage in silyloxonium and –sulfonium ions **34**, **35** and **37** ([S] is some kind of substrate).

The nature of the Si–Ch bond in the presence of a possible substrate will be discussed in the following chapter. As a model system serves the complex formed of silyl cations **34**, **35**, **36** and **37** with a nitrile.

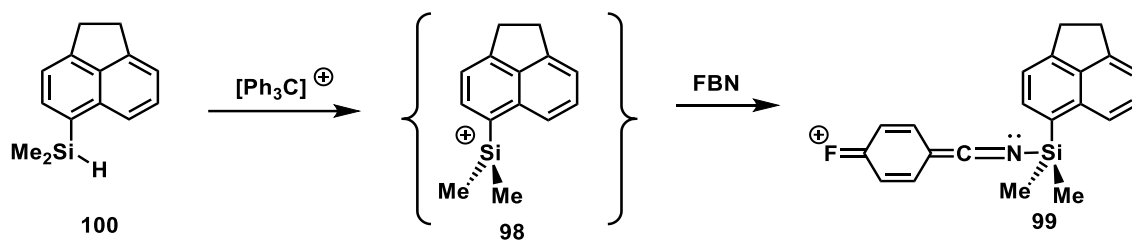
3.7 Silylnitrilium Ions

Silyl cations react with nitriles to give nitrilium ions. The nitrile acts as an external electron donor whereby the covalent silicon-nitrogen interaction leads to an increase in the coordination number at the silicon center.^[98] This increase in the coordination number implies an increase in the electron density at the silicon atom whereby the ²⁹Si NMR chemical resonance experiences a high-field shift compared to the corresponding cation. Hereby, the bonding situation in silylnitrilium ions **94-97** will be investigated, especially regarding the intramolecular stabilization via the remote donor substituent, OPh and SPh. In this terms, the effects of the different backbones, naphthalene and acenaphthene, and different substitution patterns at the silicon atom (Me₂, PhMe, *t*-BuMe and PhH) shall be discussed. 4-Fluorobenzonitrile (FBN) was chosen as the nitrile because of the fluoro substituent which can be easily detected via NMR spectroscopy. The formulation of resonance structures of nitrilium ions **94-97** shows, that the interaction between the nitrile and the silicon center affects the fluorine atom (Scheme 61) what should be visible via the ¹⁹F NMR resonance. The Si – N linkage is also influenced by the Si – Ch linkage. FBN is therefore a promising probe to get an insight of the silicon chalcogen linkage.

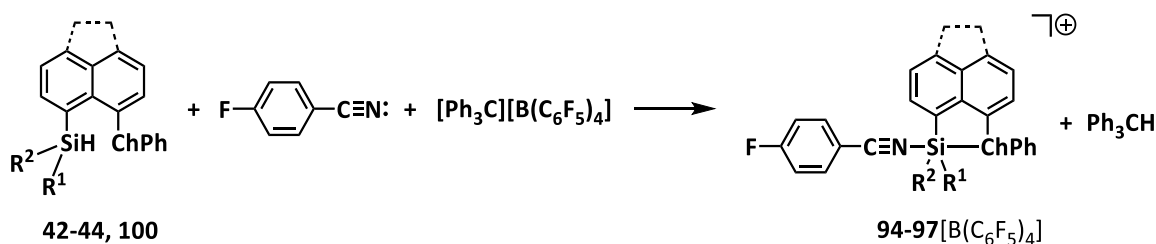


Scheme 61 – Resonance structures of nitrilium ions **94-97** (**94**: Ch = O, R¹ = R² = Me (ace), **95a**: Ch = S, R¹ = R² = Me (ace), **96**: Ch = O, R¹ = R² = Me (naph), **97**: Ch = S, R¹ = R² = Me (naph), **95b**: Ch = S, R¹ = Me, R² = Ph (ace), **95c**: Ch = S, R¹ = Me, R² = *t*-Bu (ace), **95d**: Ch = S, R¹ = Ph, R² = H (ace)).

The reactivity of chalcogenyl-stabilized silyl cations **34-37**, which were synthesized in this work, with FBN was examined. Furthermore, the naphthyl-substituted dimethylsilylsulfonium ion **37a** of N. Kordts was included in this study to have a further naphthyl derivative for comparison. Another compound included is the 5-dimethylsilylacenaphthyl derivative **98** without a remote donor substituent. Even though the dimethylsilyl cation **98** is highly reactive and cannot be prepared as the free cation **98**, its corresponding nitrilium ion **99** is accessible and provides a model compound in which no remote donor substituent influences the silicon nitrile interaction (Scheme 62).

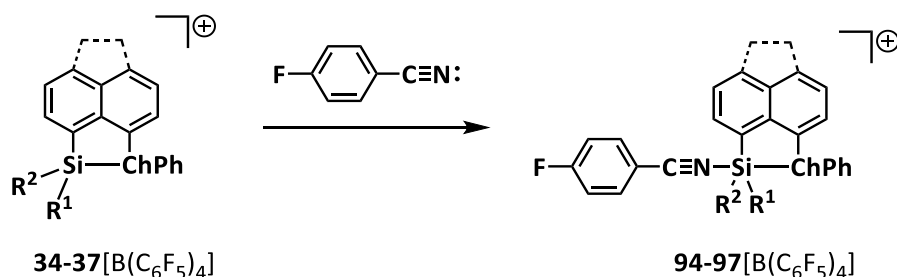
Scheme 62 - Formation of nitrilium ion **99** without remote donor substituent.

To synthesize silylnitrilium borates **94-97**[B(C₆F₅)₄] (Scheme 63), a Schlenk tube was charged with the corresponding silane, trityl borate and FBN. The solids were dissolved in dichloromethane-d₂ and the mixture was stirred for 5-10 min. If the silane was oily, two separated Schlenk tubes were used; one charged with the silane (in 0.2 mL CD₂Cl₂) and the other with trityl borate and FBN (in 0.3-0.4 mL CD₂Cl₂). The trityl borate/FBN mixture was then added to the silane and the mixture was stirred for 5-10 min and subsequently analysed using NMR spectroscopy.



Scheme 63 – Preparation of nitrilium borates **94-97**[B(C₆F₅)₄] in dichloromethane-d₂. (**94**: Ch = O, R¹ = R² = Me (ace), **95a**: Ch = S, R¹ = R² = Me (ace), **96**: Ch = O, R¹ = R² = Me (naph), **97**: Ch = S, R¹ = R² = Me (naph), **95b**: Ch = S, R¹ = Me, R² = Ph (ace), **95c**: Ch = S, R¹ = Me, R² = t-Bu (ace), **95d**: Ch = S, R¹ = Ph, R² = H (ace)).

Nitrilium borates **94-97**[B(C₆F₅)₄] were obtained in quantitative yield. However, once prepared, it was usually not possible to separate nitrilium borates **94-97**[B(C₆F₅)₄] from the side product triphenyl methane. To obtain pure compounds **94-97**[B(C₆F₅)₄], the corresponding silyl borate **34-37**[B(C₆F₅)₄] was prepared in benzene, what allows its purification due to the formation of two phases, a polar and a nonpolar phase. The nonpolar by-product triphenyl methane was removed from the polar phase by washing with benzene or *n*-pentane. After removal of the solvent under high-vacuum, a solution of 4-fluorobenzene in 0.7 mL dichloromethane-d₂ was added to the silyl borate **34-37**[B(C₆F₅)₄] at room temperature (Scheme 64). The mixture was stirred for 5 min and then transferred to an NMR tube for analysis.



Scheme 64 – Preparation of nitrilium borates **94-97** $[\text{B}(\text{C}_6\text{F}_5)_4]$ from purified silyl borates **34-37** $[\text{B}(\text{C}_6\text{F}_5)_4]$ (**34a**, **94**: Ch = O, $\text{R}^1 = \text{R}^2 = \text{Me}$ (ace); **36**, **96**: Ch = O, $\text{R}^1 = \text{R}^2 = \text{Me}$ (naph); **35a**, **95a**: Ch = S, $\text{R}^1 = \text{R}^2 = \text{Me}$ (ace); **37a**, **97**: Ch = S, $\text{R}^1 = \text{R}^2 = \text{Me}$ (naph); **35b**, **95b**: Ch = S, $\text{R}^1 = \text{Me}$, $\text{R}^2 = \text{Ph}$ (ace); **35d**, **95d**: Ch = S, $\text{R}^1 = \text{Ph}$, $\text{R}^2 = \text{H}$ (ace); **35c**, **95c**: Ch = S, $\text{R}^1 = \text{Me}$, $\text{R}^2 = t\text{-Bu}$ (ace)).

Pertinent NMR data of silylnitrilium borates **94-97** $[\text{B}(\text{C}_6\text{F}_5)_4]$ are listed in Table 20. The ^{29}Si NMR chemical shift of nitrilium ions **94-97** are high-field shifted compared to the corresponding cations indicating the coordination of the nitrile to the silicon center. The most pronounced difference is observed in hydridosilyl cation **95d** ($\Delta\delta^{29}\text{Si} = 83$, Entry 3) followed by the two phenoxy-substituted dimethylsilyl cations **94** and **96** ($\Delta\delta^{29}\text{Si} = 61$, 70; Entry 1, 2). The thiophenyl-stabilized silylnitrilium ions **95a,b** and **97** exhibit a difference in the chemical shift compared to the corresponding silyl cation **35a,b** and **37a** between $\Delta\delta^{29}\text{Si} = 31$ and 45. An exception is the thiophenyl-stabilized *tert*-butylmethyl-substituted derivative **95c** (Entry 7). In contrast to every other nitrilium ion, it exhibits no difference in the ^{29}Si NMR resonance compared to its silyl cation analog **35c**. This suggests that there is no interaction between the silicon center and the nitrile, which may be explained by the huge steric demand of the *tert*-butyl moiety.

Table 20 – Pertinent NMR data of nitrilium borates **94-97** $[\text{B}(\text{C}_6\text{F}_5)_4]$ (**94**: Ch = O, $\text{R}^1 = \text{R}^2 = \text{Me}$ (ace), **95a**: Ch = S, $\text{R}^1 = \text{R}^2 = \text{Me}$ (ace), **96**: Ch = O, $\text{R}^1 = \text{R}^2 = \text{Me}$ (naph), **97**: Ch = S, $\text{R}^1 = \text{R}^2 = \text{Me}$ (naph), **95b**: Ch = S, $\text{R}^1 = \text{Me}$, $\text{R}^2 = \text{Ph}$ (ace), **95c**: Ch = S, $\text{R}^1 = \text{Me}$, $\text{R}^2 = t\text{-Bu}$ (ace), **95d**: Ch = S, $\text{R}^1 = \text{Ph}$, $\text{R}^2 = \text{H}$ (ace); in CD_2Cl_2 , $\Delta\delta^{29}\text{Si}$ is the difference of the ^{29}Si NMR chemical shift to the corresponding silyl borates).

Entry	Silylnitrilium ion	Donor	$\delta^{19}\text{F}$	$^1J_{\text{C,F}}$ [Hz]	$\delta^{29}\text{Si}$ nitrilium	$\Delta\delta^{29}\text{Si}$
1	99	-	-86.6	273	23.0	-
2	94	OPh	-87.8	269	16.3	61
3	96	OPh	-93.9 (305 K) -90.2 (233 K)	264 (305 K) 268 (233 K)	1.6	70
4	95d	SPh	-91.5	264	-46.0	72, 83
5	95a	SPh	-94.3	264	29.5	36
6	95b	SPh	-95.5	263	6.4	36, 45
7	97	SPh	-99.6	259	26.2	31
8	95c	SPh	-101.3	258	70.2	0.2
9	FBN	-	-103.4	256	-	-

Notably, not only do the oxygen derivatives **94** and **96** show only one signal for the methyl groups connected to the silicon atom in the ^1H NMR and ^{13}C NMR spectra, but the sulfur derivatives **95** and **97** do as well. For example, the ^1H NMR spectrum of dimethylsilylnitrilium borate **95a** $[\text{B}(\text{C}_6\text{F}_5)_4]$ is shown in Figure 52. Furthermore, the chiral thiophenyl-stabilized nitrilium ion **95b** forms only one isomer instead of the expected two (*cis* and *trans*) indicating that the silicon-sulfur interaction has been weakened, or even broken due to the coordination of the nitrile to the silicon center.

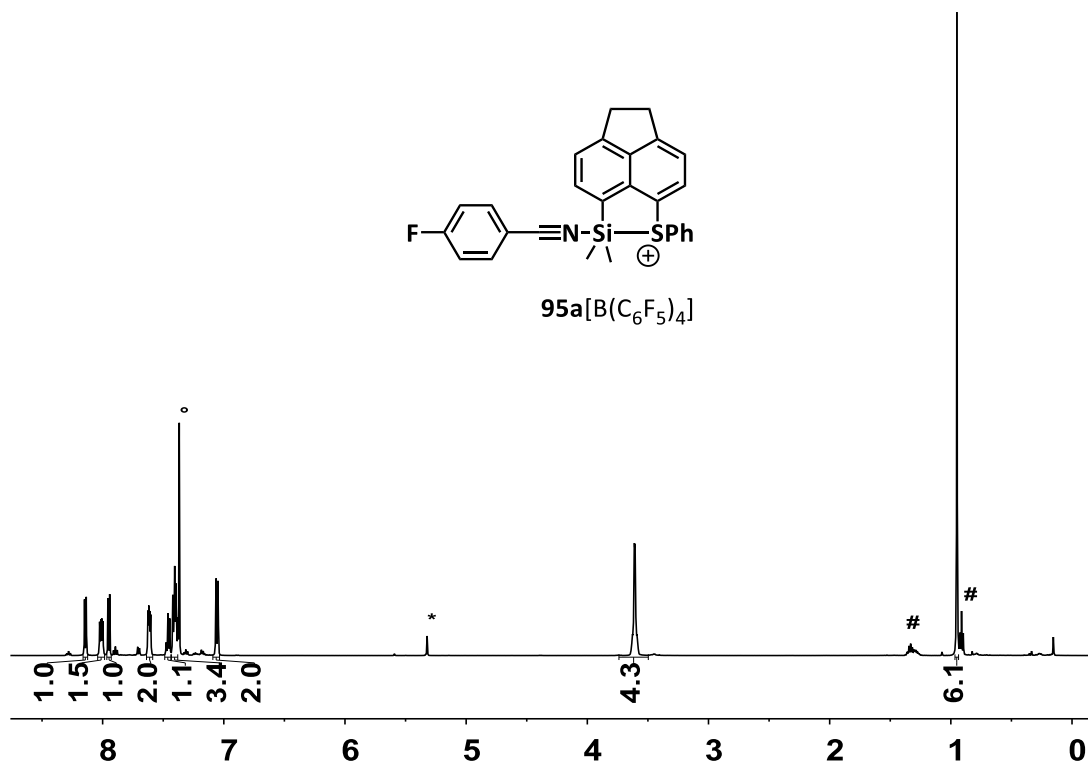


Figure 52 – ^1H NMR spectrum (500 MHz, 305 K, CD_2Cl_2) of dimethylsilylnitrilium borate **95a** $[\text{B}(\text{C}_6\text{F}_5)_4]$ (* CDHCl_2 , ° residual C_6H_6 , # residual *n*-pentane).

Next, the ^{19}F NMR resonance of nitrilium ions **94-97** will be discussed. To permit a direct comparison of the ^{19}F NMR chemical shifts, the ^{19}F NMR spectra have to be referenced to an internal standard. An obvious species for this purpose is tetrakis(pentafluorophenyl)borate. All samples were referenced via the ^{19}F NMR chemical shift of the *para*-fluorine atom of the borate ($\delta^{19}\text{F} = -163.44$, for details see Experimental Part). For comparison, the ^{19}F NMR chemical shift of FBN was measured in a mixture with trityl borate. No change in the NMR parameters was observed and, consequently, no interaction between the trityl cation and the nitrile takes place. This shows, that the interaction between FBN and Lewis acids is weak and a stable complex is only formed with strong Lewis acids.

Upon comparison of the ^{19}F NMR chemical shifts of nitrilium ions **94-97**, it was observed that they are all low-field shifted compared to free FBN ($\delta^{19}\text{F} = -87.8 - (-99.6)$ vs $\delta^{19}\text{F} = -103.4$). Even the *tert*-butyl-substituted derivative **95c** shows a slight low-field shift ($\delta^{19}\text{F} = -101.3$). Another important parameter directly related to the ^{19}F NMR resonance is the $^1J_{\text{C,F}}$ coupling constant of *para*-fluorobenzonitrilium ions **94-97**. Compared to the non-bonded FBN, this value increases ($^1J_{\text{C,F}} = 258-269$ Hz vs $^1J_{\text{C,F}} = 256$ Hz). A direct correlation between the ^{19}F NMR resonance and the $^1J_{\text{C,F}}$ coupling constant is expected. To evaluate this, the $^1J_{\text{C,F}}$ constant was plotted against the ^{19}F NMR chemical shift (Figure 53). The graph shows a linear correlation between these two parameters ($R^2 = 0.95$). FBN and the nitrilium ion **99** without an intramolecular donor form the lower and upper extremes of the series. The donor-stabilized silylnitrilium borates **94-97**[$\text{B}(\text{C}_6\text{F}_5)_4$] are located in between these extremes. However, the values of the hydridosilyl derivative **95d** (red) appears anomalous compared to the other derivatives and phenoxy-stabilized silyl cation **36**, here represented by derivative **96** (turquoise) was expected to exhibit a greater Lewis acidity compared to that of thiophenyl derivative **35a**, here represented by derivative **95a**. On the basis of the ^{19}F NMR chemical shift and the $^1J_{\text{C,F}}$ coupling constant of nitrilium ions **96** and **95a**, silyl cations **36** and **35a** seem to have the same Lewis acidity (Figure 53).

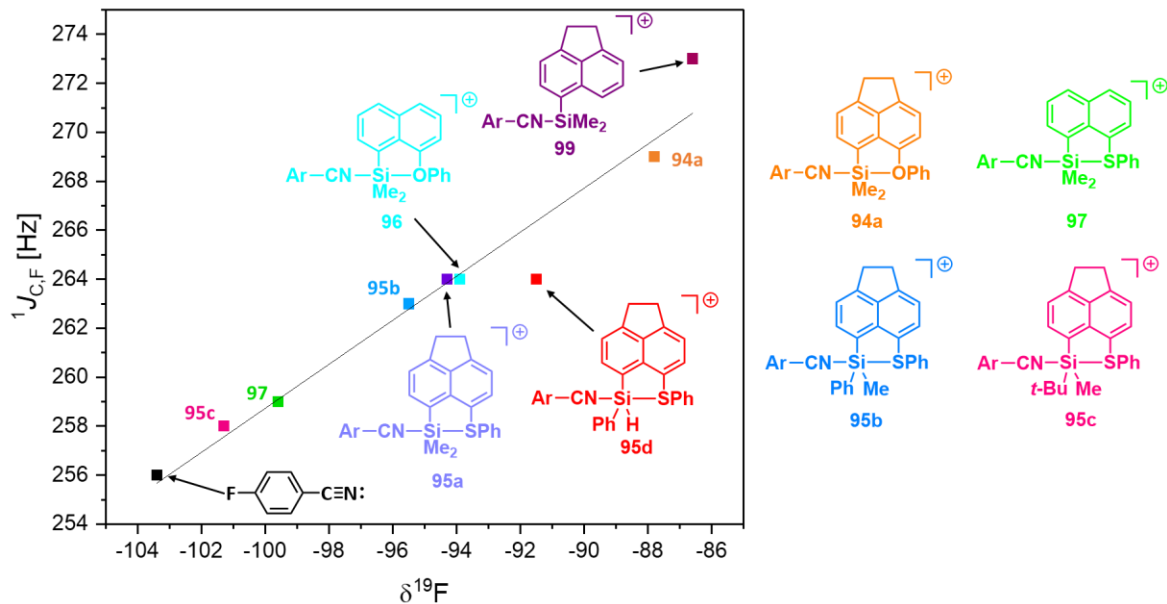


Figure 53 – Correlation of the ^{19}F NMR chemical shift and the $^1J_{\text{C,F}}$ coupling constant of nitrilium ions **94-97** ($R^2 = 0.95$).

A closer examination of the ^{19}F NMR spectrum of the naphthyl derivative **96** shows a broad signal for the *para*-fluoro substituent ($\delta^{19}\text{F} = -93.9$, $w(1/2) = 1343$ Hz). VT NMR spectra of species **96** reveal, that the signal splits into two sharp signals with $\delta^{19}\text{F} = -90.2$ ($w(1/2) = 23$ Hz) and -102.6 ($w(1/2) = 45$

Hz) (Figure 54, reference at 233 K $\delta^{19}\text{F} = 162.87$, for details see Experimental Part). The latter chemical shift was assigned to free FBN indicating that the nitrile is in excess.

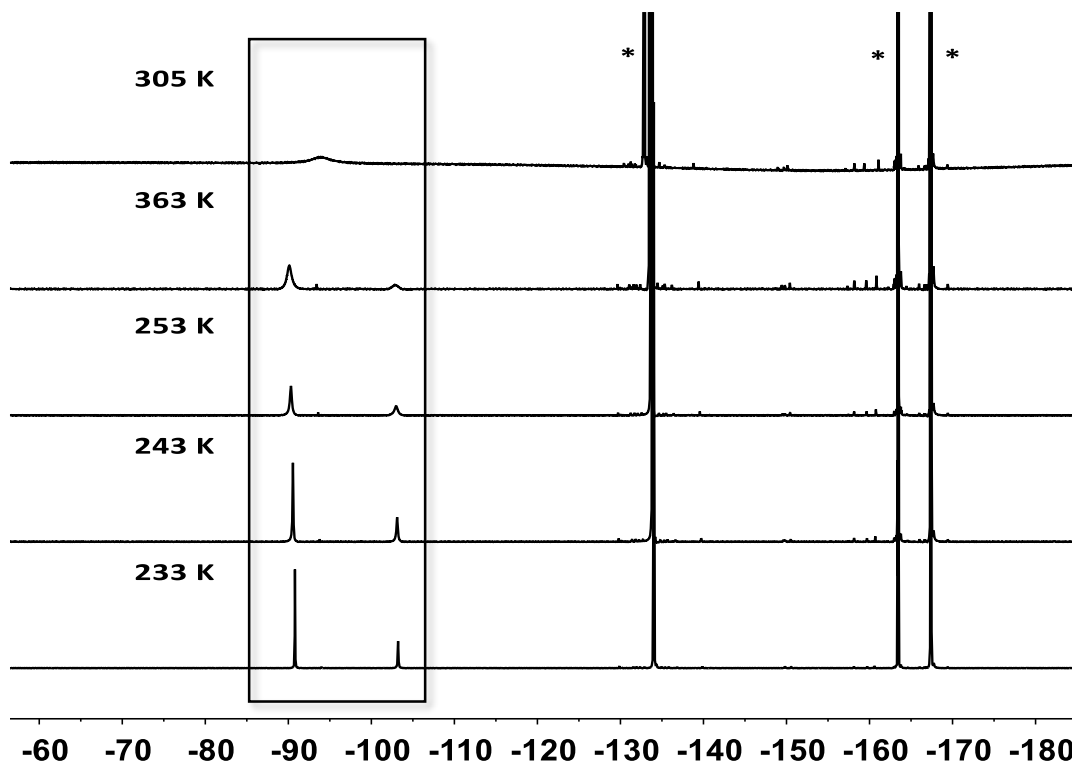


Figure 54 – VT ^{19}F NMR spectra (500 MHz, CD_2Cl_2) of phenoxy-stabilized silylnitrilium borate **96** $[\text{B}(\text{C}_6\text{F}_5)_4]^+[\text{B}(\text{C}_6\text{F}_5)_4]^-$.

The ^{19}F NMR resonance at $\delta^{19}\text{F} = -90.2$ corresponds to nitrilium ion **96**. The $^1J_{\text{C,F}}$ coupling constant of the phenoxy derivative **96** was extracted from the ^{19}F NMR spectrum at 233 K (Figure 55). The value increases from $^1J_{\text{C,F}} = 264$ Hz at r.t. to $^1J_{\text{C,F}} = 268$ Hz at 233 K. A reason for this observation is probably an exchange process including FBN attached to the silicon atom and free FBN. This exchange is fast on the NMR time scale at room temperature and leads to an average value for the $^1J_{\text{C,F}}$ coupling constant, line broadening as well as a high-field shift of the ^{19}F NMR resonance compared to the corresponding values for the nitrilium ion **96** in absence of FBN. Further experiments with the acenaphthene-substituted dimethylsilyl derivative **95a** with an excess of FBN confirm that the presence of excess FBN results in a decrease of the $^1J_{\text{C,F}}$ coupling constant compared to the value obtained with an equimolar amount of FBN and the silyl cation. For example, the ^{19}F NMR chemical shift of the thiophenyl derivative **95a** with 1 equiv. excess of FBN is $\delta^{19}\text{F} = -98.3$ compared to -94.3 without excess FBN and the $^1J_{\text{C,F}}$ coupling constant is 259 Hz compared to 264 Hz without excess FBN. This may explain why the hydridosilyl derivative **95d** does not fit into the correlation. The imbalance

in the stoichiometry for these two examples, **95d** and **96**, is probably caused by loss of the corresponding silyl borate during purification. The amount of FBN used is calculated in relation to the amount of the precursor silane used. If the formation of the silyl borate does not occur quantitatively or some amount of the cation gets lost during the purification, the nitrile is, consequently, in excess.

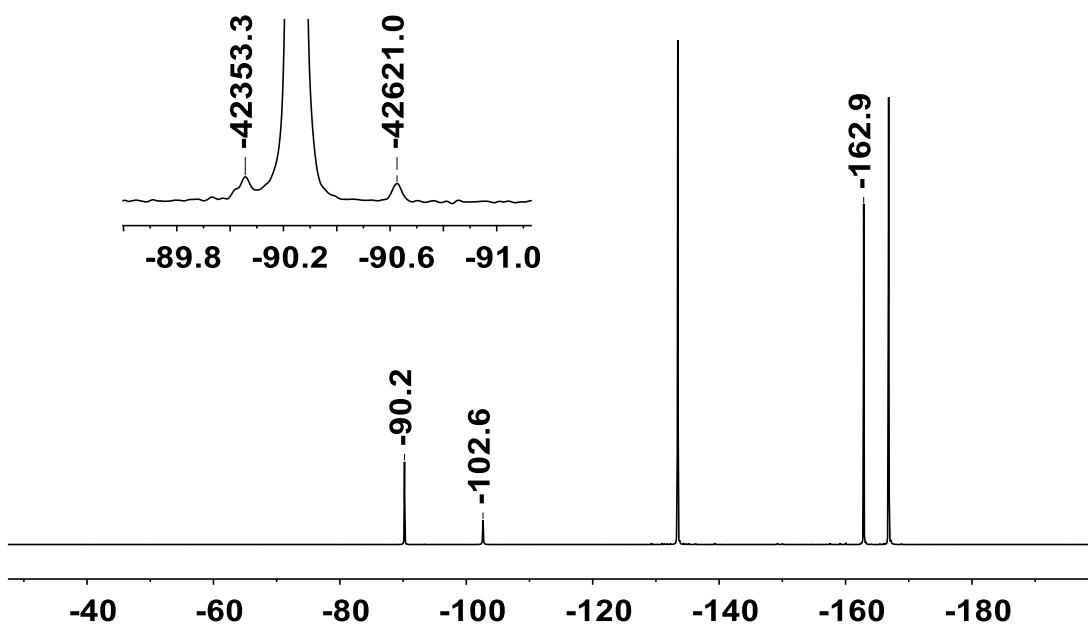


Figure 55 – $^{19}\text{F}\{^1\text{H}\}$ NMR spectrum (470 MHz, 233 K, CD_2Cl_2) of naphthyl substituted silylnitrilium borate **96** $[\text{B}(\text{C}_6\text{F}_5)_4]$.

The data were replotted using the $^1J_{\text{C,F}}$ coupling constant and the ^{19}F NMR resonance measured at 233 K for nitrilium ion **96** (Figure 56). As expected, the relative position of silyl cation **36** changes significantly.

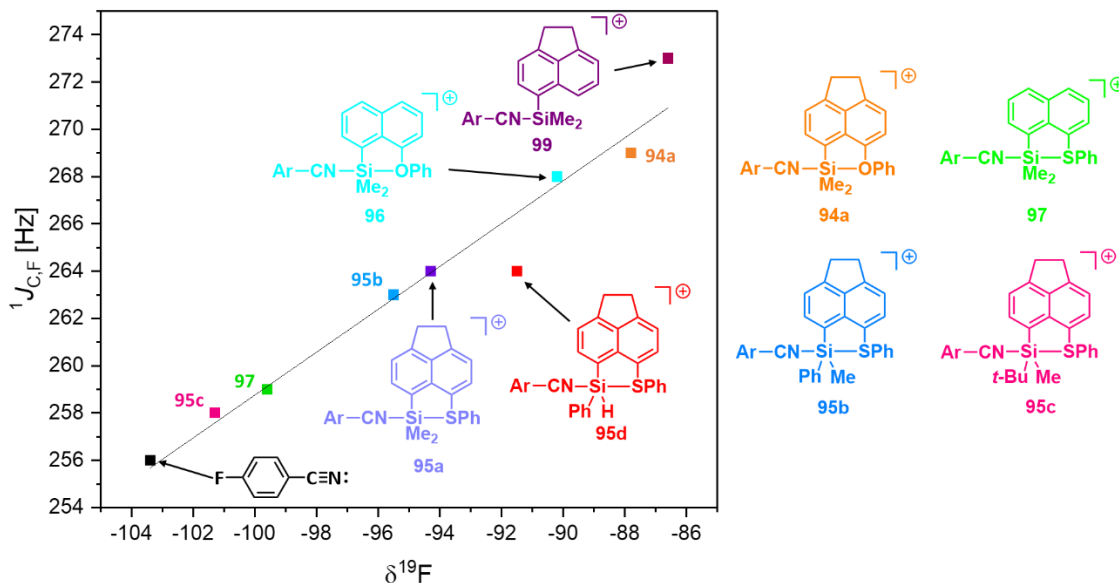


Figure 56 – Correlation of the ^{19}F NMR chemical shift and the $^1J_{\text{C,F}}$ coupling constant of nitrilium ions **94-97** with the corrected values for naphthyl-substituted phenoxy-stabilized derivative **96** ($R^2 = 0.95$).

The comparison of the dimethylsilyl and the phenylmethylsilyl thiophenyl-stabilized derivatives **95a** and **95b** shows a low-field shift of the ^{19}F NMR chemical shifts compared to the free nitrile of $\Delta\delta^{19}\text{F} = 9.1$ and 7.9 , respectively (Table 21), whereas for the *tert*-butylmethylsilyl derivative **95c** the value is $\Delta\delta^{19}\text{F} = 2.1$ (Table 21). The difference in the backbone can be compared using the dimethylsilyl derivatives **94/96** and **95a/97**. For the phenoxy-stabilized acenaphthyl and naphthyl derivatives **94/96**, the difference compared to free FBN is $\Delta\delta^{19}\text{F} = 15.6$ (**94**, ace) and 13.2 (**96**, naph), while for the thiophenyl-derivatives **95a/97** it is $\Delta\delta^{19}\text{F} = 9.1$ (**95a**, ace) and 3.8 (**97**, naph).

Table 21 – Difference of the ^{19}F NMR chemical shift and $^1J_{\text{C,F}}$ coupling constant of nitrilium ions **94-97** and **99** to free FBN (**94**: Ch = O, R¹ = R² = Me (ace), **95a**: Ch = S, R¹ = R² = Me (ace), **96**: Ch = O, R¹ = R² = Me (naph), **97**: Ch = S, R¹ = R² = Me (naph), **95b**: Ch = S, R¹ = Me, R² = Ph (ace), **95c**: Ch = S, R¹ = Me, R² = *t*-Bu (ace), **95d** Ch = S, R¹ = Ph, R² = H (ace)).

Silylnitrilium ion	Donor	$\delta^{19}\text{F}$	$\Delta\delta^{19}\text{F}$	$^1J_{\text{C,F}}$ [Hz]	$\Delta^1J_{\text{C,F}}$ [Hz]
99	-	-86.6	16.8	273	17
94	OPh	-87.8	15.6	269	13
96	OPh	-90.2 (233 K)	13.2	268 (233 K)	12
95d	SPh	-91.5	11.9	264	8
95a	SPh	-94.3	9.1	264	8
95b	SPh	-95.5	7.9	263	7
97	SPh	-99.6	3.8	259	3
95c	SPh	-101.3	2.1	258	2

Comparison of the phenoxy with the thiophenyl dimethylsilyl derivatives **94/95a** and **96/97** reveals that the low-field shift compared to free FBN is higher for the phenoxy-stabilized dimethylsilyl derivatives **94/96** ($\Delta\delta^{19}\text{F} = 15.6$ (**94**), 13.2 (**96**)) compared to its sulfur congeners **95a/97** which show a less pronounced low field shift ($\Delta\delta^{19}\text{F} = 9.1$ (**95a**), 3.8 (**97**)). The trend is the same for the acenaphthyl derivatives **94/95a** and the naphthyl derivatives **96/97**. This is also apparent by a direct comparison of the ^{19}F NMR chemical shifts ($\delta^{19}\text{F}(\mathbf{94}) - \delta^{19}\text{F}(\mathbf{95a}) = 9.5$ and $\delta^{19}\text{F}(\mathbf{96}) - \delta^{19}\text{F}(\mathbf{97}) = 9.4$). In conclusion, not only do the substituents at the silicon center affect the nitrile silicon interaction but also a difference is observed between phenoxy- and thiophenyl-stabilized derivatives **94/96** and **95a/97**. These data strongly suggest that the silicon-chalcogen interaction is retained upon coordination of FBN to the silicon center. To further support the retention of a Si – D binding interaction upon coordination of a nitrile is provided by the selenium derivatives **40** and **41** of K. R ger and S. Rathjen which show a pronounced Si-Se coupling in the NMR spectra (Figure 57).^[35, 78, 87b]

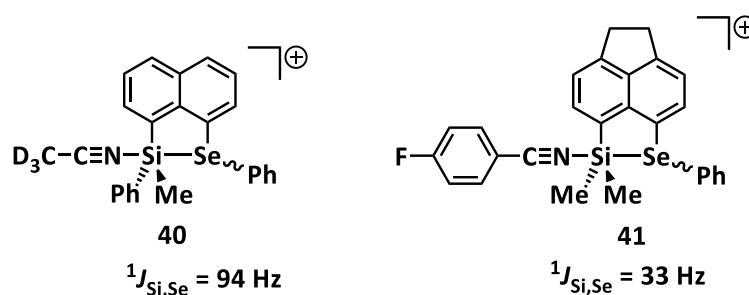


Figure 57 – Selenyl-stabilized silylnitrilium ions **40** and **41**.

Further support for a binding interaction between the silicon and the chalcogen atoms is provided by low temperature NMR experiments of the dimethylsilyl- and phenylmethylsilylsulfonium derivatives **95a** and **95b**. In analogy to the silylsulfonium ions **35**, a dynamic process was observed with coalescence of the signals assigned to the methyl groups in the ^1H NMR spectrum at 183 K for **95a** and 203 K for **95b**. For example, the VT NMR spectra of derivative **95b** are shown in Figure 58. The estimated free Gibbs energy for derivative **95a** is $\Delta G^{\text{exp}} = 34 \text{ kJmol}^{-1}$ and for derivative **95b** is $\Delta G^{\text{exp}} = 39 \text{ kJmol}^{-1}$.

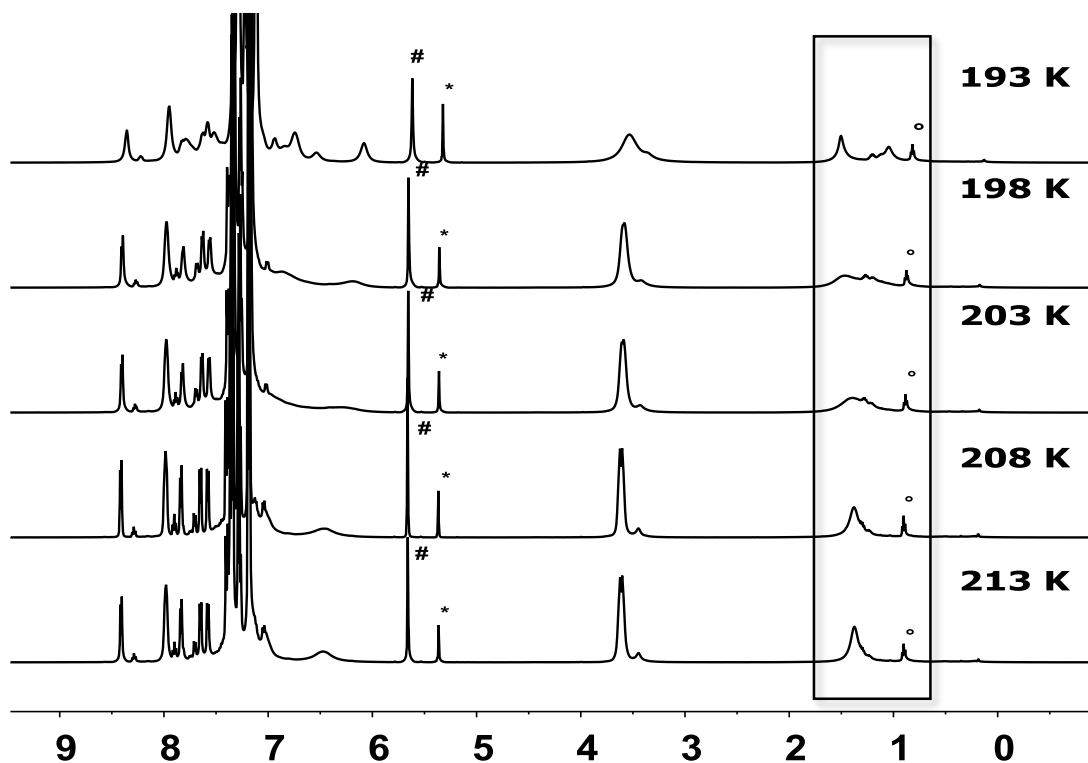


Figure 58 – VT ^1H NMR spectra (500 MHz, CD_2Cl_2) of phenylmethylsilyl nitrilium borate **95b** $[\text{B}(\text{C}_6\text{F}_5)_4]$ (* CDHCl_2 , # Ph_3CH , ° impurities).

The energy barriers for inversion at the sulfur atom in nitrilium ions **95a** and **95b** were calculated using DFT methods (M06-2X/Def2-TZVP). The values were determined to $\Delta G^{\text{calc}} = 35 \text{ kJmol}^{-1}$ and 37 kJmol^{-1} , respectively, and are consistent with the values obtained in the VT NMR experiments (Table 22).

Table 22 – Comparison of the calculated and experimental determined free Gibbs energy barrier of nitrilium ions **95a** and **95b** (M06-2X/Def2-TZVP).

R	$\Delta G^{\text{exp}} [\text{kJmol}^{-1}]$	$\Delta G^{\text{calc}} [\text{kJmol}^{-1}]$
Me (95a)	34 ± 1	35
Ph (95b)	39 ± 1	37

The inversion barriers obtained for nitrilium ions **95a** and **95b** are significantly lower than those for the corresponding silyl cations **35a** and **35b** ($\Delta G^{\text{exp}} = 74 \text{ kJmol}^{-1}$). This lowering of the inversion barrier is consistent with the expected weakening of the Si-Ch linkage in nitrilium ions **95a** and **95b** compared to silyl cations **35a** and **35b** due to the complexation of the nitrile.

Hydridosilyl derivative **95d** is unique due to the hydrogen substituent directly attached to the pentavalent silicon atom. The $^1J_{\text{Si,H}}$ coupling constant was extracted from the ^{29}Si - ^1H coupled INEPT NMR spectrum and is $^1J_{\text{Si,H}} = 298 \text{ Hz}$ (Figure 59). The magnitude of the $^1J_{\text{Si,H}}$ coupling constant increases from silane **43d** ($^1J_{\text{Si,H}} = 204 \text{ Hz}$) to silyl cation **35d** ($^1J_{\text{Si,H}} = 260 \text{ Hz}, 263 \text{ Hz}$) to the nitrilium ion **95d** ($^1J_{\text{Si,H}} = 298 \text{ Hz}$) which is consistent with an increase in the s-orbital contribution to the Si – H bond.^[53a]

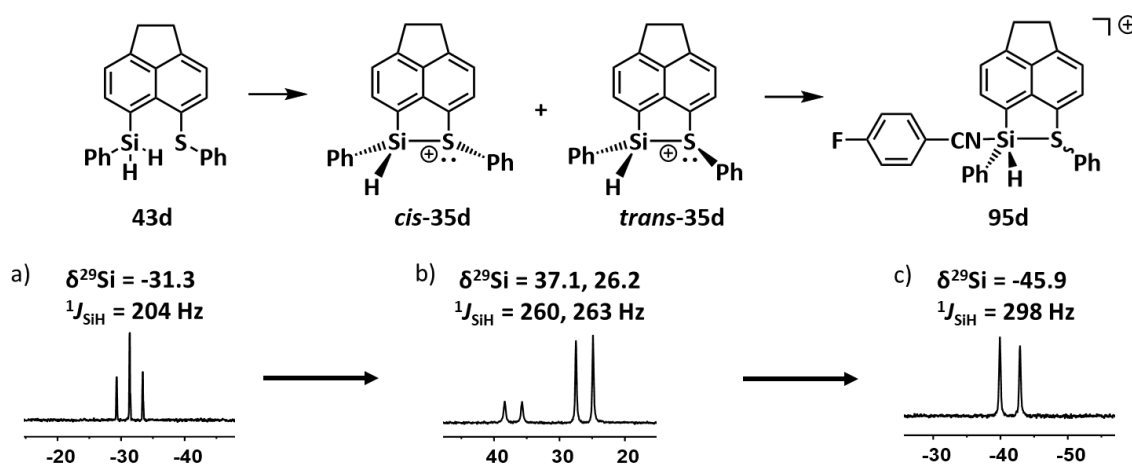


Figure 59 – ^{29}Si INEPT NMR spectra (99 MHz, 305 K, D3 = D4 = 0.001) of a) silane **43d** (C_6D_6), b) silyl borate **35d** $[\text{B}(\text{C}_6\text{F}_5)_4]$ (C_6D_6) and c) silylnitrilium borate **95d** $[\text{B}(\text{C}_6\text{F}_5)_4]$ (CD_2Cl_2).

In conclusion, the synthesis and purification of silylnitrilium borates **94-97** $[\text{B}(\text{C}_6\text{F}_5)_4]$ was described. All silylnitrilium borates **94-97** $[\text{B}(\text{C}_6\text{F}_5)_4]$ show a high-field shift of the ^{29}Si NMR resonance compared to the corresponding silyl borates **34-37** $[\text{B}(\text{C}_6\text{F}_5)_4]$ indicating an interaction between the positively charged silicon center and the nitrile. An exception is the *tert*-butylmethylsilyl derivative **95c** where, no difference between the ^{29}Si NMR resonances was observed. The ^{19}F NMR chemical shift of the *para*-fluoro substituent and the $^1J_{\text{C,F}}$ coupling constant are also influenced by the interaction. These values are even more sensitive as the ^{29}Si NMR chemical shift what is manifested with the *tert*-butyl-substituted derivative **95c**. Here, the ^{19}F NMR chemical shift and the $^1J_{\text{C,F}}$ coupling constant show a slight change indicating a slight interaction between the silicon center and FBN. Direct comparison of the dimethylsilyl derivatives **34/96** and **95a/97** show, that there is a significant difference between the phenoxy- and thiophenyl-stabilized derivatives, indicating, that the silicon-chalcogen linkage is

retained upon coordination of FBN. As a consequence, the silicon atom in silylnitrilium ions **94-97** is pentacoordinated. Further support for the pentacoordination is given by VT NMR experiments of derivatives **95a** and **95b** which reveal an inversion process at the sulfur atom which is in close analogy to silylsulfonium ions **35** and **37** (see Chapter 3.5). Moreover, the increase of the magnitude of the $^1J_{\text{Si,H}}$ coupling constant of the nitrilium ion **95d** ($^1J_{\text{Si,H}} = 298$ Hz) compared to the corresponding silyl cation **35d** ($^1J_{\text{Si,H}} = 260$ Hz, 263 Hz) reveals an increase in the s-orbital contribution to the Si – H bond and indicates that the silicon atom is pentacoordinated.

The coordination of FBN has revealed a distinct difference between the Lewis acidity of the donor-stabilized silyl cations which can be taken advantage of in the application of FBN as a probe for intramolecularly stabilized Lewis acids. This will be discussed in detail in the following chapter.

3.8 Applications and Reactivity

3.8.1 Assessment of the Lewis Acidity

Silyl cations are interesting compounds for the use as catalysts in various reactions such as Diels-Alder, Mukaiyama Aldol or hydrodefluorination reactions as well as in late-stage chemoselective functional-group manipulations of natural products.^[4, 9, 29a, 29c, 29d, 48, 86] Different silyl cations demonstrate different reactivities due to their substituents or stabilizing environment which influence their Lewis acidity. In this manner, their Lewis acidity often correlates with their efficiency. For that reason, it is of interest to find tools for the comparison and quantification of their Lewis acidity. Over the last decades different methods and scales for the comparison of Lewis acids have been developed and established.^[30] The most common experimental approaches are the Gutmann-Beckett and the Childs method. The Gutmann-Beckett method uses the ³¹P NMR chemical shift of Et₃PO which changes upon coordination to the Lewis acid of interest,^[31] whereas the Childs method relies on the change in the ¹H NMR chemical shift of the γ -H atom of crotonaldehyde upon coordination to a Lewis acid.^[33] Another method was developed by Hilt and co-workers. They use the ²H NMR chemical shift change of the γ -deuterium of perdeuterated pyridine upon coordination to quantify the Lewis acidity.^[34] While the Childs method cannot be applied to strong silyl Lewis acids, the Hilt and the Gutmann-Beckett methods reveal the high Lewis acidity of silylium ions.^[32, 34c] However, these methods have limitations due to the high Lewis basicity of the molecular probes. When either Et₃PO^[35] or C₆D₅N^[34c] was used to probe the Lewis acidity of intramolecularly stabilized silyl cations, the silicon donor interaction was broken by the strong silicon/probe interaction. A comparison of the Lewis acidity of the trimesitylsilylium ion **1** and dimethylsilylselenium ion **38**^[78] as determined using the Gutmann-Beckett method reveals a nearly identical Lewis acidity for both cations **1** and **38** despite their very distinct electronic properties as revealed by ²⁹Si NMR spectroscopy (see Figure 60).^[35]

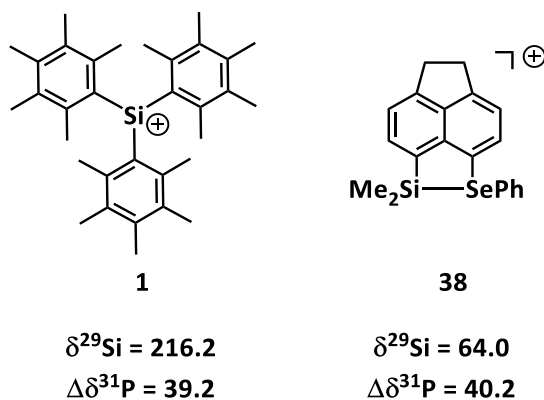


Figure 60 – Comparison of the ^{29}Si NMR resonances of trimesitylsilylium ion **1** and silylselenium ion **38** and their $\Delta\delta^{31}\text{P}$ value on the Gutmann-Beckett scale.^[35]

This demonstrates that there is a need for the development of a Lewis acidity scale which is applicable to intramolecularly stabilized silyl cations **34-38**.

In Chapter 3.7, the reaction of silyl cations **34-37** with nitriles, especially with 4-fluorobenzonitrile (FBN) was discussed. One essential observation made, was that the ^{19}F NMR resonance of the fluoro substituent in *para*-position at the nitrile moiety shows a distinct difference between silyloxonium ion **34** in comparison to silylsulfonium ion **35a**. Despite the coordination of the nitrile to the silicon center, the silicon chalcogen bond is not broken. Consequently, FBN was a promising candidate for the use as a probe for the comparison of the Lewis acidities of chalcogenyl-stabilized silyl cations **34-37**.

The well-known Lewis acid, tris(pentafluorophenyl)borane (BCF), was also included into this studies. A stable complex, **101**, between BCF and FBN was formed upon mixing both compounds in dichloromethane- d_2 . The ^{11}B NMR spectrum shows a relatively sharp resonance at $\delta^{11}\text{B} = -10.0$ ($w(1/2) = 275$ Hz) indicating tetra-coordination for the boron atom. Tetra-coordination at the boron atom in compound **101** is also supported by the small separation of the ^{19}F NMR resonances for the *p*- and *m*-fluoro substituents of the C_6F_5 -groups^[99] which is $\Delta\delta^{19}\text{F}^{m/p} = 7.2$. For comparison, the separation for $[\text{B}(\text{C}_6\text{F}_5)_4]^-$ is $\Delta\delta^{19}\text{F}^{m/p} = 3.9$ and for BCF is $\Delta\delta^{19}\text{F}^{m/p} = 20.1$. The molecular structure of borate **101** was confirmed unambiguously via X-ray diffraction analysis (Figure 61). The molecular structure confirms the conclusion, that the boron atom is tetra-coordinated as indicated by the sum of the bond angles around the boron atom $\Sigma\alpha(\text{BC}_3) = 340.0^\circ$. The length of the N – B bond is $d(\text{N} - \text{B}) = 158.8$ pm and is similar to the sum of the covalent radii for a N – B single bond ($\Sigma\text{cr}(\text{N}/\text{B}) = 156$ pm).^[79] The B-N-C bond angle is linear (179.7°) as expected. The N – C bond is with $d(\text{N} - \text{C}) = 114.6$ pm comparable to a regular N – C triple bond ($\Sigma\text{cr}(\text{N}/\text{C}) = 114$ pm).^[79]

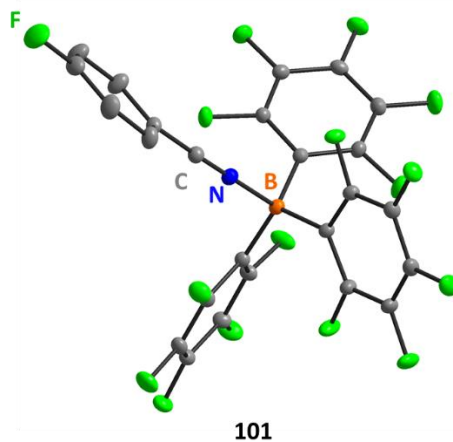


Figure 61 – Molecular structure of the complex **101** of BCF with FBN (thermal ellipsoids at 50 % probability, H atoms omitted for clarity). Pertinent bond length [pm] and angles [°]: B – N 158.77(11), C – N 114.56(10), C – C^{ipso} 142.47(10), B – N – C 179.732(77).

The ^{19}F NMR chemical shift of the *p*-fluoro substituent of FBN in complex **101** is $\delta^{19}\text{F} = -92.5$ and falls between the ^{19}F NMR chemical shift of dimethylsilyloxonium ion **96** and dimethylsilylsulfonium ion **95a** (Table 23). BCF adduct **101** has a $^1J_{\text{C,F}}$ coupling constant of 268.0 Hz, close to the value of silyloxonium ion **96**. The relative position of BCF differs in both scales, $\delta^{19}\text{F}$ and $^1J_{\text{C,F}}$ (Figure 62).

Table 23 – Calculated bond dissociation energy of the Si – N bond in nitrilium ions 94-97 and 99 in comparison with the BDE of the Si – C bond in the corresponding silyl cations 34-37 (M06-2X/Def2-TZVP) and in relation to the ^{19}F NMR resonance (CD_2Cl_2 , * measured at 233 K).

Compound	Donor	$\delta^{19}\text{F}$	$^1J_{\text{C,F}}$ [Hz]	BDE Si – N [kJmol ⁻¹]	FIA [kJmol ⁻¹]	FIA (SCIPCM) [kJmol ⁻¹]
99	-	-86.6	272.8	183	626	302
94	OPh	-87.8	269.1	96	516	215
96	OPh	-90.2*	267.7*	90	508	201
BCF	-	-92.5	268.0	80	185	123
95a	SPh	-94.3	264.1	70	480	182
95b	SPh	-95.5	262.6	72	473	186
97	SPh	-99.6	259	67	476	172
95c	SPh	-101.3	257.6	54	461	170

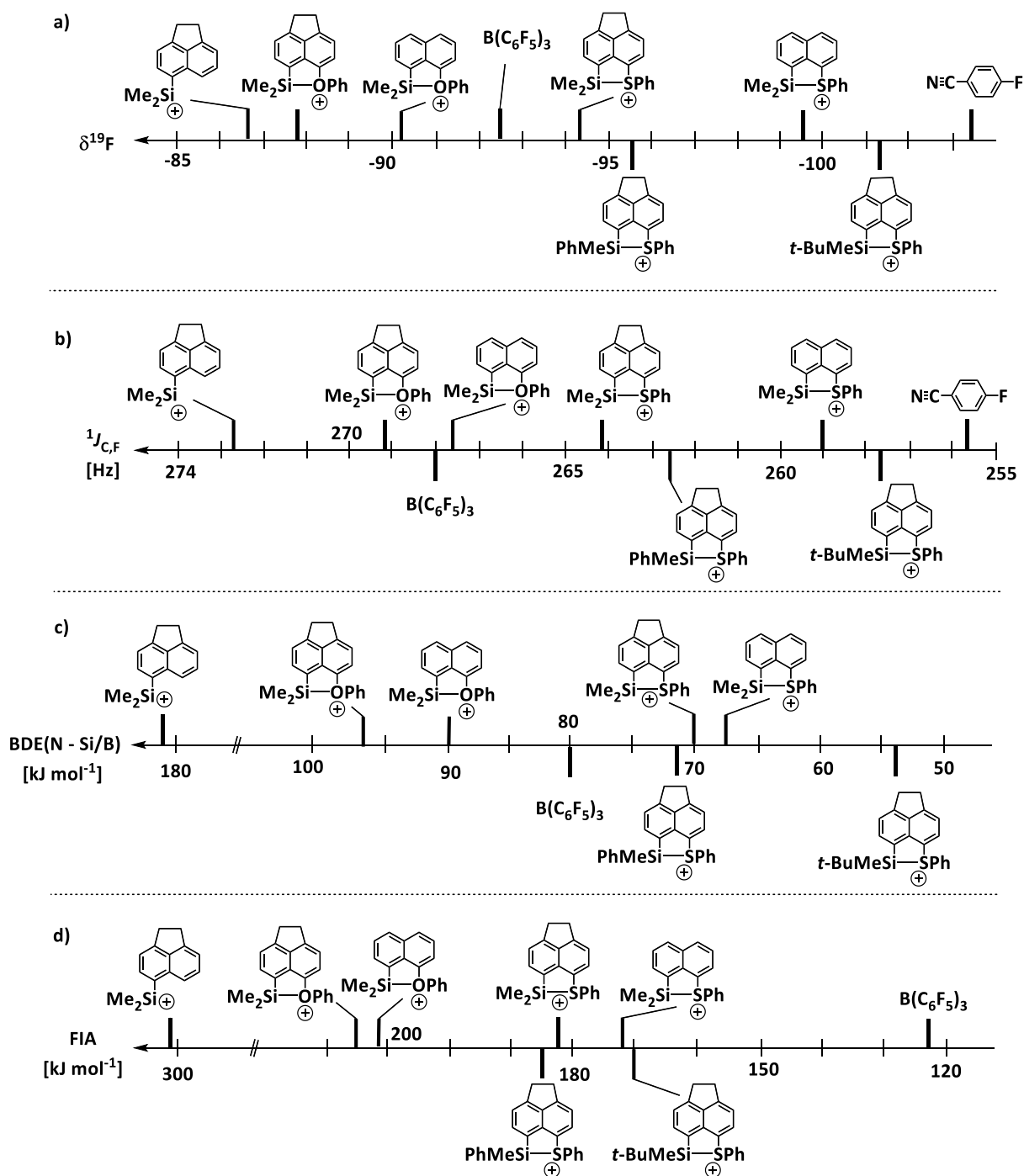
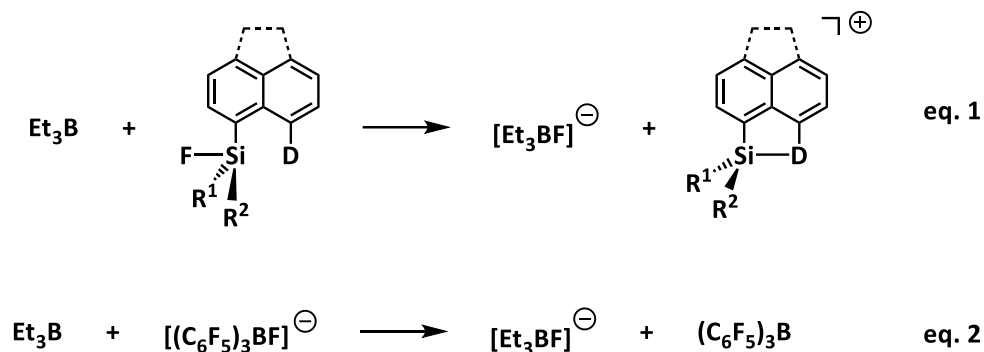


Figure 62 – Comparison of the different Lewis acidity scales for acenaphthyl and naphthyl silyl cations **34-37** and BCF. a) LA scale based on the $\delta^{19}\text{F}$ NMR resonance of the corresponding FBN complex (solvent CD_2Cl_2), b) LA scale based on the $^1J_{\text{C},\text{F}}$ coupling constant of the corresponding BCF complex, c) Scale based on the calculated complexation energy at M06-2X/Def2-TZVP, d) Scale based on the calculated fluorine ion affinity (FIA) at SCIPCM/M06-2X/Def2-TZVP for dichloromethane solution.

DFT calculations at M06-2X/Def2-TZVP level of theory were used to gain further insights into the bonding in nitrilium ions **94-97** and the Lewis acidity of silyl cations **34-37**. The complexation energy of FBN to the Lewis acid provides a first indication of the Lewis acidity. This energy is obtained, by calculation of the bond dissociation energy (BDE) of the Si – N bond and is also given in Table 23. For derivative **99** without a donor, the complexation energy is highest with $\text{BDE}(\text{Si} - \text{N}) = 183 \text{ kJmol}^{-1}$ and lowest for the *tert*-butylmethylsilyl derivative **95c** ($\text{BDE}(\text{Si} - \text{N}) = 54 \text{ kJmol}^{-1}$).

In general, the $\text{BDE}(\text{Si} - \text{N})$ scale reflects the order derived from the ^{19}F NMR chemical shift (Figure 62), and thus, the ^{19}F NMR chemical shift can be considered an indirect measure of the strength of the N – Si bond. One exception is the ordering of the dimethylsilyl- and phenylmethylsilylsulfonium ions **95a/95b**. The Si – N bond of dimethylsilyl derivative **95a** is 2 kJmol^{-1} weaker than that in phenylmethylsilyl derivative **95b**; however, the ^{19}F NMR chemical shift is at lower field indicating a higher Lewis acidity in **95a** compared to **95b**.

A well-established method for the comparison of the strength of Lewis acids is the fluorine ion affinity (FIA). The FIA is defined as the binding enthalpy of a Lewis acid with a fluoride ion in the gas phase. The binding enthalpy can be determined experimentally by ion cyclotron resonance spectroscopy or by Born-Fajans-Haber cycles.^[30] These methods were used to evaluate FIA's calculated using DFT methods, whereby the calculations were found to be suitable for the estimation of the FIA of Lewis acids. The FIA of silyl cations **34-37** was calculated according to equation 1 in Scheme 65 and are listed in Table 23 (M06-2X/Def2-TZVP). Here again, the strongest Lewis acid is silyl cation **98** without a donor and the weakest is the *tert*-butylmethylsilyl derivative **35c**. The order of the Lewis acidities of silyl cations **34-37** resulting from the FIA reflects the scale determined by the ^{19}F NMR chemical shift except for the phenylmethyl- and dimethylacenaphthyl silylsulfonium ions **35a/35b** (Figure 62). For these two, the scale given by the FIA predict an inverted order compared to the ^{19}F NMR chemical shift scale and reflects the result determined by the $\text{BDE}(\text{Si} - \text{N})$ method. One significant exception is the FIA calculated for BCF. The value is in a completely different range ($\text{FIA}(\text{BCF}) = 185 \text{ kJmol}^{-1}$ vs $\text{FIA} = 626\text{-}461 \text{ kJmol}^{-1}$ for silyl cations **34-37**).

Scheme 65 – Equation for the calculation of the FIA of silyl cations **34-37**.

Considering the equations used for the calculations of the FIA (Scheme 65), it is noticeable that in eq. 1 the reaction starts with two neutral compounds and two ionic compounds are the resulting products and in eq. 2 the reaction starts with the same charge as it ends. Computed FIA of cationic species in the gas-phase are strongly affected by charge neutralization and electrostatic attraction.^[30] To level these effects, a solvent was included in the calculation of the FIA resulting in much lower values for silyl cations **34-37** (FIA(SCIPCM) = 302-170 kJmol⁻¹, SCIPCM with dichloromethane as solvent, M06-2X/Def2-TZVP). However, the value for BCF is still distinctly lower (FIA(SCIPCM) = 123 kJmol⁻¹) and can, therefore, not be directly compared to the values of silyl cations **34-37**. Here, the limitations of the scales of calculated values become apparent. Using the FIA scale, charges of molecules are problematic and do not allow a direct comparison of compounds with different charges. Another limitation is manifested in the switched order of dimethylsilyl and phenylmethylsilyl derivative **35a/35b**. Here, the scales of the calculated values predict a higher Lewis acidity for the phenylmethylsilyl cation **35b** but the experimental scales show unambiguously that the dimethylsilyl cation **35a** exhibits a higher Lewis acidity. Considering the stabilizing effect of the phenyl group to the electron deficient silicon center, a reduced Lewis acidity of compound **35b** consequences. Therefore, the experimental scales reflect the expected difference of the Lewis acidity of these two examples **35a** and **35b** better than the scales based on calculated values. Furthermore, considering the distribution of the compounds on the scales, it becomes apparent, that in addition to the dimethylsilyl and phenylmethylsilyl derivatives **35a/35b**, the naphthyl silylsulfonium ion **37** and the *tert*-butylmethylsilyl derivative **35c** (in particular on the FIA scale) have similar values (Figure 62). In view of an estimated error of about ±1 kJmol⁻¹ of the calculated values, this proximity does not allow a distinction between the Lewis acidities of the pairs **35a/35b** and **37/35c**. With these limitations of the calculated scales in mind, the experimental scales based on NMR parameters, namely δ¹⁹F and ¹J_{C,F}, are considered more suitable for the evaluation of the Lewis acidity of intramolecularly stabilized

silyl Lewis acids compared to the scales based on calculated values. A limitation of the experimental scales might be the direct comparison of intramolecularly stabilized Lewis acids with non-stabilized Lewis acids. This becomes apparent through the comparison of silyl cations **34-37** with BCF. The relative ordering of BCF in both the $\delta^{19}\text{F}$ and $^1J_{\text{C,F}}$ scales is different. Further investigations with other non-stabilized Lewis acids have to be performed. Initial experiments with non-stabilized silyl Lewis acids were done by A. Merk. She prepared the FBN adducts of the trimesitylsilylium ion **1** and the triethylsilylium ion.^[100] These examples fit nicely into the experimental scales. Including other donor stabilized silyl cations such as halonium ions **103/104**, selenyl- and telluryl-stabilized derivatives **38**, **39** and **106**, investigations have revealed that the general order of the Lewis acidity of acenaphthyl- and naphthyl-based donor-stabilized silyl cations is $\text{Br} > \text{O} > \text{I} > \text{S} > \text{Se} > \text{Te}$ on all scales ($\delta^{19}\text{F}$, $^1J_{\text{C,F}}$, FIA, $\text{BDE}(\text{Si}-\text{N})$, Figure 63).

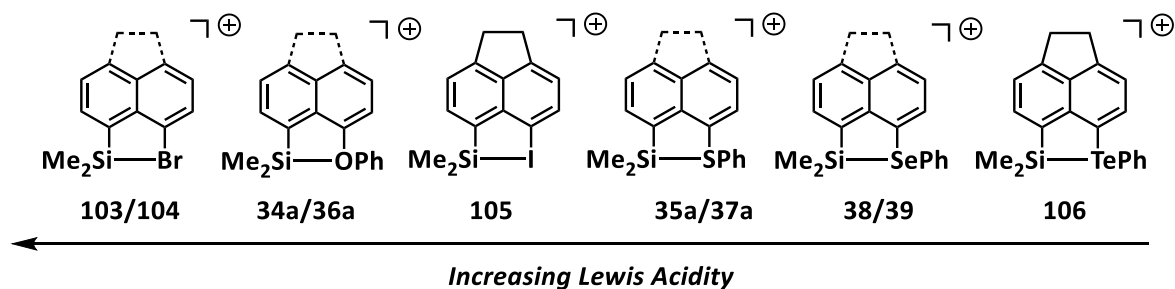
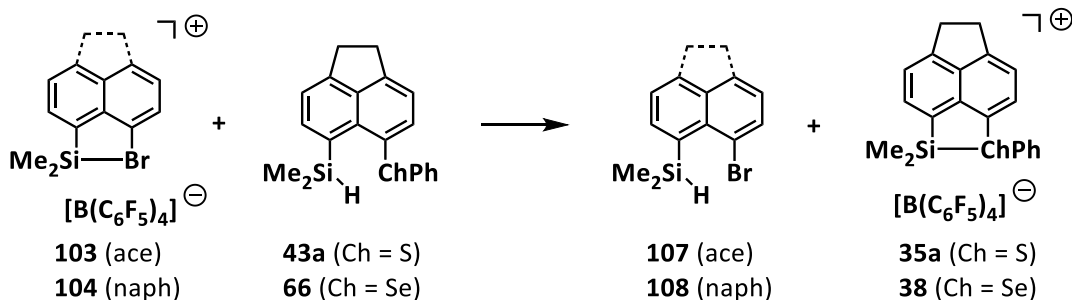


Figure 63 – Order of donor-stabilized silyl cations by their Lewis acidity.

Moreover, it becomes apparent that both experimental scales show a larger dispersion of the data for weak Lewis acids and a smaller separation for stronger Lewis acids. As a consequence, for strong Lewis acids, a certain degree of uncertainty has to be taken to account. Furthermore, acenaphthyl-based silyl Lewis acids are always stronger compared to their naphthyl-based analogs in accordance with the generally weaker Si/D interaction in acenaphthene derivatives.^[6a] Small irregularities between the FIA and the experimental scales can be rationalized considering the calculated structures of the molecules. In the thionyl-stabilized silyl cation **35a**, the bay angle is $\Sigma\beta = 353^\circ$, in the corresponding nitrilium ion **95a** it is $\Sigma\beta = 362^\circ$ and in silyl fluoride **102a**, it is $\Sigma\beta = 378^\circ$ ($\Sigma\beta = 368^\circ$ in unstrained acenaphthene). The trend shows, that the Si/D interaction in silyl cation **35a** and nitrilium ion **95a** is rather attractive while in silyl fluoride **102a** it becomes repulsive. The intramolecular interactions influence the calculated FIA values, resulting in a relatively high uncertainty. The order of Lewis acidity in the intramolecularly stabilized silyl cations was confirmed experimentally by A. Merk using the hydride transfer reaction of selenide **66** with bromonium borate

103[B(C₆F₅)₄] to give the less Lewis acidic selenyl-stabilized silyl borate **38**[B(C₆F₅)₄] and the bromo-substituted silane **107**. A similar reaction of bromonium borate **104**[B(C₆F₅)₄] with the thiophenyl-substituted silane **43a** shows the same result (Scheme 66).^[35,100]

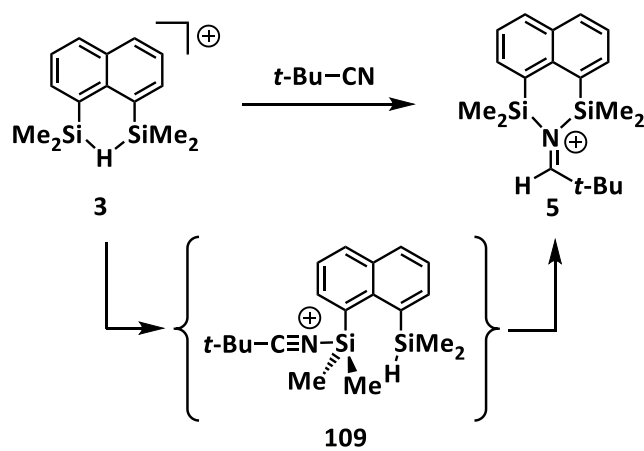


Scheme 66 – Hydride transfer reaction of bromonium borates **103**[B(C₆F₅)₄] and **104**[B(C₆F₅)₄] with silanes **43a** and **66**.^[35,100]

In conclusion, FBN is a valuable NMR probe to assess the inherent Lewis acidity of intramolecularly donor-stabilized acenaphthyl and naphthyl silyl cations **34-37**. This method enables the discrimination between the Lewis acidity of donor-stabilized silyl cations **34-37** even when the donor ability does not vary significantly. The FBN method is a useful tool for the design and fine-tuning of silyl Lewis acids.

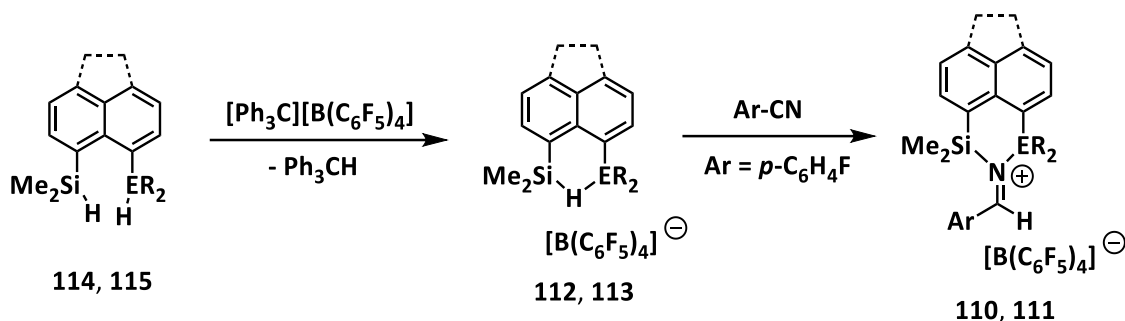
3.8.2 Reaction of Nitrilium Ions with a Si – H Source

R. Panisch showed in the studies on hydrogen-bridged silyl Lewis acids that the reaction of naphthyl-based silyl cation **3** with pivalonitrile did not give the corresponding nitrilium ion **109** but iminium ion **5** was formed (Scheme 67).^[101] Considering the reaction of silyl Lewis acids with nitriles,^[98] one can assume that pivalonitrile attacks the electron deficient silicon center to form nitrilium ion **109** as an intermediate and then an intramolecular hydrosilylation reaction takes place to form the final product, iminium ion **5**.



Scheme 67 – Reaction of naphthyl substituted hydrogen-bridged silyl cation **3** with pivalonitrile to give iminium ion **5**.

The results of R. Panisch were reproduced with the synthesis of iminium borates **110** $[\text{B}(\text{C}_6\text{F}_5)_4]$ and **111** $[\text{B}(\text{C}_6\text{F}_5)_4]$ by the reaction of the corresponding silyl borates **112** $[\text{B}(\text{C}_6\text{F}_5)_4]$ and **113** $[\text{B}(\text{C}_6\text{F}_5)_4]$ with 4-fluorobenzonitrile (FBN) (Scheme 68). To synthesize the silylgermyliminium borate **111** $[\text{B}(\text{C}_6\text{F}_5)_4]$, a Schlenk tube was charged with the corresponding silane **115** and a solution of trityl borate and FBN in 0.7 mL dichloromethane- d_2 was added at room temperature. The mixture was stirred for 5 min and transferred to an NMR tube for analysis. To generate bisilyliminium borate **110** $[\text{B}(\text{C}_6\text{F}_5)_4]$, the corresponding bis-dimethylsilyl borate **112** $[\text{B}(\text{C}_6\text{F}_5)_4]$ was prepared in benzene, purified by washing the unpolar phase, dried under high-vacuum and dissolved in chlorobenzene- d_5 . The formation of silyl borate **112** $[\text{B}(\text{C}_6\text{F}_5)_4]$ was confirmed using NMR spectroscopy ($\delta^{29}\text{Si} = 60.4$).^[87a] The NMR sample containing silyl borate **112** $[\text{B}(\text{C}_6\text{F}_5)_4]$ was transferred to a Schlenk tube charged with FBN. The mixture was stirred for 45 min and subsequently analysed via NMR spectroscopy. To compare, iminium ions **110** and **111** with Panisch's *tert*-butyl-substituted naphthyl iminium ion **5**, the NMR data are listed in Table 24.



Scheme 68 – Formation of iminium borates **110**[B(C₆F₅)₄] and **111**[B(C₆F₅)₄] via a reaction sequence including the Corey reaction of silanes **114** and **115** with trityl borate and subsequent reaction with FBN (**110**, **112**, **114**: ace, ER₂ = SiMe₂; **111**, **113**, **115**: naph, ER₂ = Ge(*n*-Bu)₂).

For instance, iminium ions **110** and **111** exhibit ²⁹Si NMR chemical shifts in the region of δ²⁹Si = 11.8–23.3. Hereby, two ²⁹Si NMR chemical shifts are detected for each compound, respectively. The reason is a *syn/anti* relation of the aryl substituent at the imine moiety relative to the silyl group for iminium ion **110** and the formation of *cis/trans*-isomers of iminium ion **111** (Figure 64).

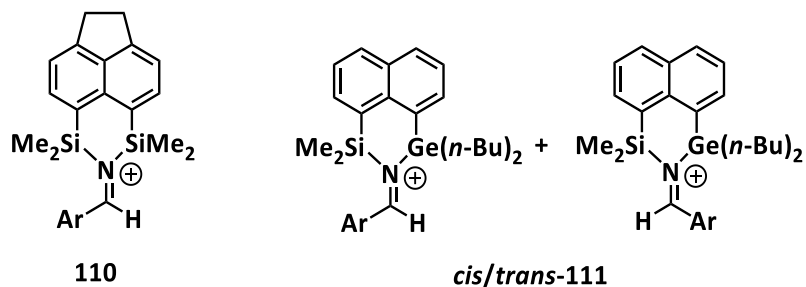


Figure 64 – *Syn/anti* relation of the aryl substituent relative to the silyl groups in **110** and *cis/trans*-isomers of **111** (Ar = *p*-C₆H₄F).

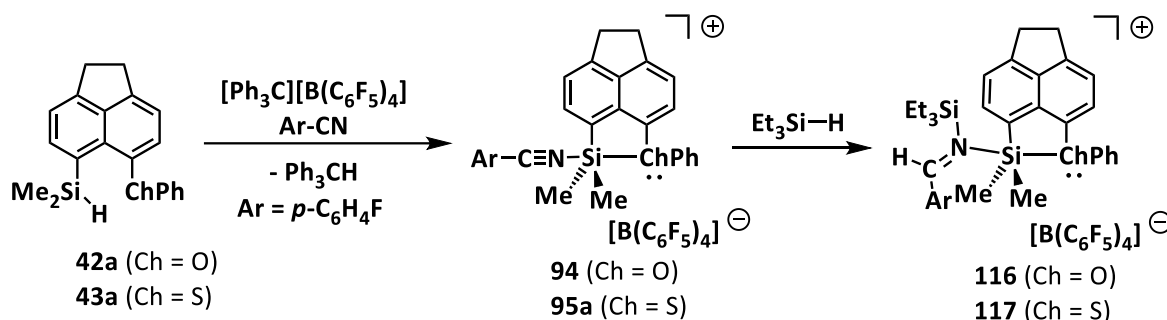
For germysilyliminium ion **111**, one isomer is in excess with a ratio of 80:20. The ²⁹Si NMR resonances show a correlation to hydrogen atoms which are distinctively low-field shifted with δ¹H = 9.12–9.53. These ¹H NMR resonances show a correlation to ¹³C NMR signals in the region of δ¹³C = 185.7–187.4 which is expected for the N=C group in iminium ions (for comparison: **5** δ¹³C = 206.5,^[101] [Me₂CNMe₂]⁺ δ¹³C = 189.5 or [H₂CNMe₂]⁺ δ¹³C = 201.6).^[102] Additionally, the ¹H/¹⁵N HMBC NMR spectrum of iminium borate **110**[B(C₆F₅)₄] reveals the correlation of the nitrogen atom with a ¹⁵N NMR chemical shift of δ¹⁵N = 229.5 to the ¹H NMR resonance at δ¹H = 9.12 (1 H), as well as to the two singlet signals at δ¹H = 0.48 and 0.63 (6 H, respectively) which were assigned to the SiMe₂ groups. These NMR data strongly indicate the formation of iminium ions **110** and **111**.

Table 24 – Selected NMR data of iminium ions **5**, **110** and **111**.

Compound	$\delta^{29}\text{Si}$	$\delta^1\text{H}$ (NCH)	$\delta^{15}\text{N}$	$\delta^{13}\text{C}$ (NC)
5 ^{a)}	11.3, 24.1 ^[101]	8.32 ^[101]	-	206.5 ^[101]
110 ^{c)}	15.7, 23.3	9.12	229.5	187.4
111 ^{b)}	11.8, 19.7*	9.32, 9.53*	-	185.7*, 186.5

a) In C_6D_6 , b) in CD_2Cl_2 , c) in $\text{C}_6\text{D}_5\text{Cl}$, * main compound.

Inspired by the reaction of hydrogen-bridged silyl cations with nitriles, the reaction of phenoxy- and thiophenyl-stabilized nitrilium borates **94** $[\text{B}(\text{C}_6\text{F}_5)_4]$ and **95a** $[\text{B}(\text{C}_6\text{F}_5)_4]$ with an external Si – H source to give the corresponding iminium borates **116** $[\text{B}(\text{C}_6\text{F}_5)_4]$ and **117** $[\text{B}(\text{C}_6\text{F}_5)_4]$ was investigated, whereby triethylsilane was chosen as an external Si – H source (Scheme 69).



Scheme 69 – Formation of nitrilium ions **94** and **95a** and the reaction with triethylsilane to give iminium ions **116** and **117**.

The reactions were carried out in benzene- d_6 at room temperature. The formation of nitrilium ions **94** and **95a** was confirmed via NMR spectroscopy, respectively, before triethylsilane was added. Both reactions, of phenoxy- and thiophenyl-stabilized nitrilium borates **94** $[\text{B}(\text{C}_6\text{F}_5)_4]$ and **95a** $[\text{B}(\text{C}_6\text{F}_5)_4]$, resulted in relative complex reaction mixtures. The ^{29}Si NMR spectrum of the reaction mixture of thiophenyl-stabilized derivative **117** shows seven signals ($\delta^{29}\text{Si} = -8.1, 12.4, 13.5, 34.0, 40.6, 41.0, 65.8$), whereby none was assigned to nitrilium ion **95a** ($\delta^{29}\text{Si} = 29.5$). The ^{29}Si NMR signals at $\delta^{29}\text{Si} = -8.1, 12.4, 13.5$ and 41.0 result from compounds which are in a relative low concentration compared to the main signal and seem to be side products of the reaction (integrals are 0.2-0.3 when main signal is set to an integral of 1). The main ^{29}Si NMR resonance is at $\delta^{29}\text{Si} = 65.8$ and was assigned to the corresponding silyl cation **35a**. The two remaining signals at $\delta^{29}\text{Si} = 34.0$ and 40.6 show a correlation in the $^1\text{H}/^{29}\text{Si}$ HMBC spectrum to the ^1H NMR resonance at $\delta^1\text{H} = 8.71$ (Figure 65). This ^1H NMR signal is in the same region compared to the signals which were assigned the NCH group of iminium ions **110** and **111** ($\delta^1\text{H} = 8.32$ - 9.53 , see above). In the $^1\text{H}/^{13}\text{C}$ HMQC spectrum, the ^1H NMR

resonance at $\delta^1\text{H} = 8.71$ shows a correlation to a ^{13}C NMR resonance at $\delta^{13}\text{C} = 191.3$ which is in the expected region for the $\text{N} = \text{C}$ group of iminium ions (see above).

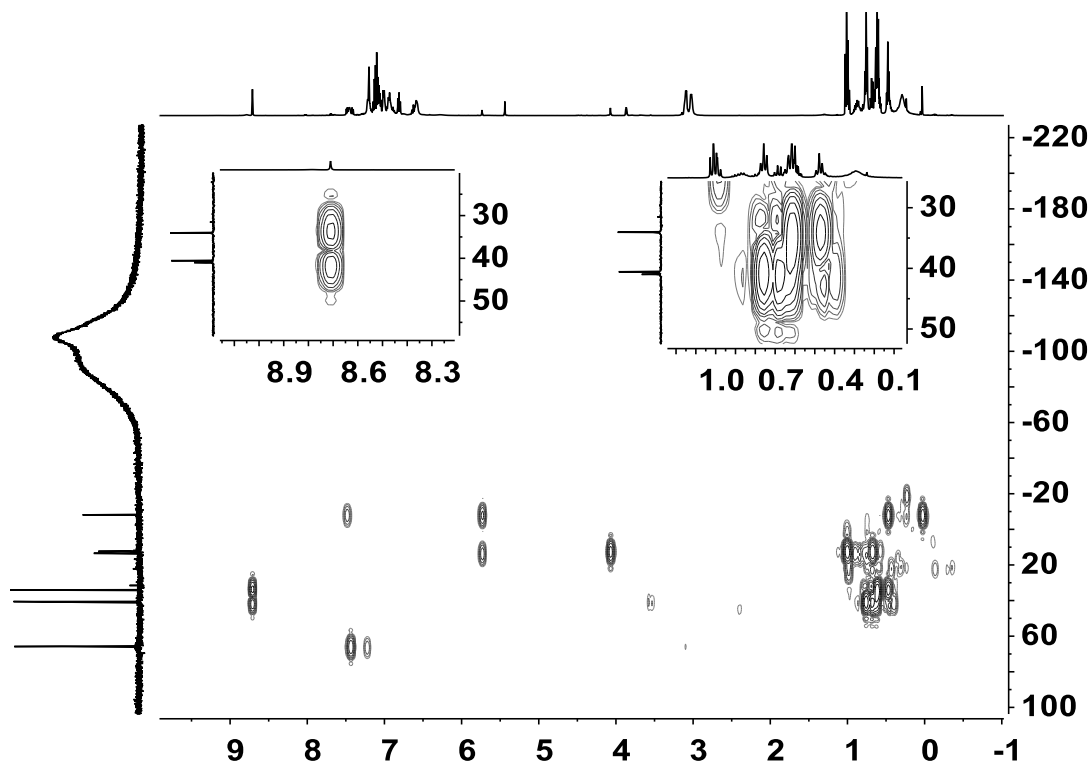


Figure 65 – $^1\text{H}/^{29}\text{Si}$ HMBC NMR spectrum (500 MHz, 305 K, C_6D_6) of the reaction mixture of thiophenyl stabilized nitrilium borate **95a** $[\text{B}(\text{C}_6\text{F}_5)_4]$ with triethylsilane.

The ^1H NMR signal at $\delta^1\text{H} = 8.71$ shows as well a correlation in the $^1\text{H}/^{15}\text{N}$ HMBC spectrum to the ^{15}N NMR chemical shift at $\delta^{15}\text{N} = 230.2$ (Figure 66). This ^{15}N NMR chemical shift is similar to that of the bis-dimethylsilyliminium ion **110** ($\delta^{15}\text{N} = 229.5$). The ^{15}N NMR resonance at $\delta^{15}\text{N} = 230.2$ shows correlations to the same signals in the high-field region of the ^1H NMR spectrum as the ^{29}Si NMR signal at $\delta^{29}\text{Si} = 34.0$ ($\delta^1\text{H} = 0.44\text{-}0.50$ and $0.57\text{-}0.66$). The differentiation between the dimethylsilyl and the triethylsilyl group cannot be made due to the overlap of the signals. Nevertheless, the NMR chemical shifts and their correlations strongly indicate the formation of the target compound, iminium ion **117**.

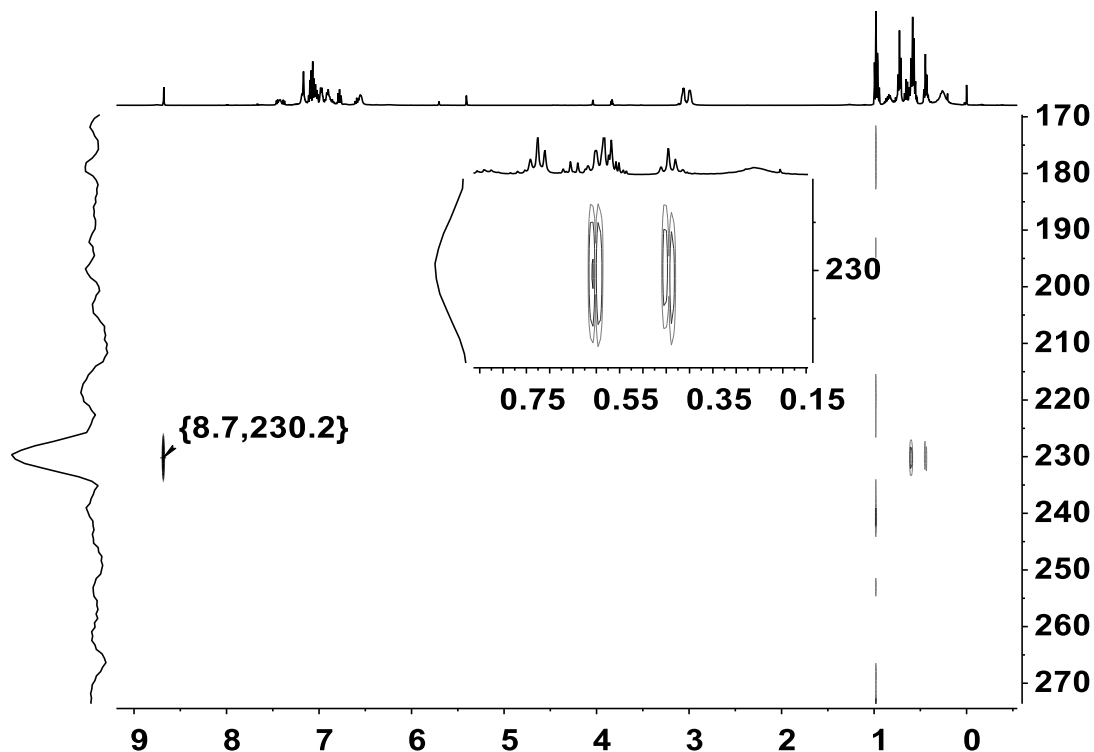


Figure 66 – $^1\text{H}/^{15}\text{N}$ HMBC NMR spectrum (500 MHz, 305 K, C_6D_6) of the reaction mixture of thiophenyl stabilized silylnitrilium borate **95a** $[\text{B}(\text{C}_6\text{F}_5)_4]$ with triethylsilane.

In the reaction mixture of phenoxy-stabilized derivative **116** four silicon species with two silicon centers, respectively, were detected. The main species shows the same correlations with similar NMR resonances compared to thiophenyl-stabilized derivative **117**. Selected NMR data are summarized in Table 25. In the ^{29}Si NMR spectrum of the reaction mixture of phenoxy-stabilized derivative **116**, the main signals are at $\delta^{29}\text{Si} = 17.9$ and 40.0 , whereby the first signal is similar to the ^{29}Si NMR resonance of nitrilium ion **94** ($\delta^{29}\text{Si} = 16.3$). The signal at $\delta^{29}\text{Si} = 17.9$ correlates in the $^1\text{H}/^{29}\text{Si}$ HMBC spectrum to a singlet signal at $\delta^1\text{H} = 0.57$, which was assigned to the SiMe_2 group. The second ^{29}Si NMR resonance at $\delta^{29}\text{Si} = 40.0$ correlates to two multiplets which were assigned to the SiEt_3 group (Figure 67). The ^1H NMR resonance which was assigned to the NCH group is at $\delta^1\text{H} = 8.98$ and the ^{15}N NMR resonance of silyliminium ion **116** is at $\delta^{15}\text{N} = 233.7$, and is in the same region compared to thiophenyl-stabilized derivative **117** (Table 25). Unlike the thiophenyl-stabilized derivative **117**, the corresponding silyl cation **34a** was not observed in the reaction mixture of phenoxy-stabilized silyliminium ion **116**. However, in addition to the main species **116**, three other silicon species with two different silicon centers, respectively, which correlate to a ^1H NMR resonance in the region of $\delta^1\text{H} = 8.5$ - 9.0 were detected ($\delta^{29}\text{Si} = 17.5$ and 27.3 , 27.7 and 34.0 , 32.0 and 40.6 , Figure 67).

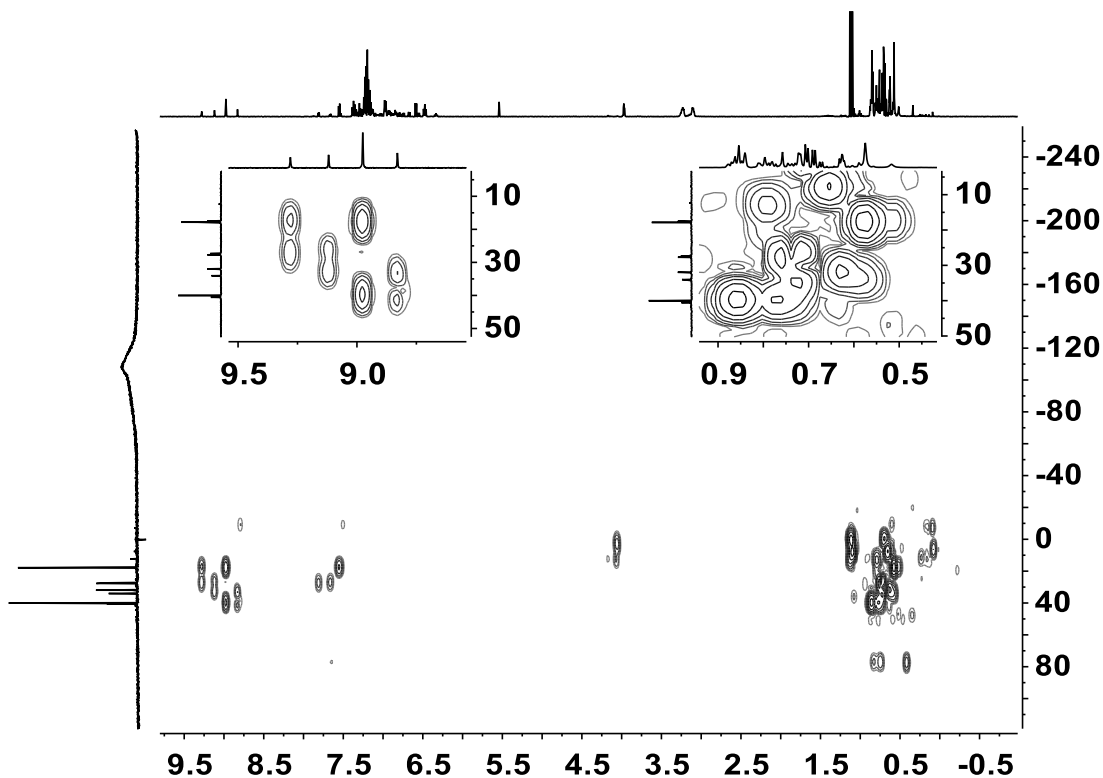


Figure 67 – $^1\text{H}/^{29}\text{Si}$ HMBC NMR spectrum (500 MHz, 305 K, C_6D_6) of the reaction mixture of phenoxy stabilized nitrilium borate **94** $[\text{B}(\text{C}_6\text{F}_5)_4]$ with triethylsilane.

An identification of the side products was not possible due to the complexity of the mixture. Furthermore, the decomposition of the products was fast and therefore the ^{13}C NMR spectrum could not be included in the discussion.

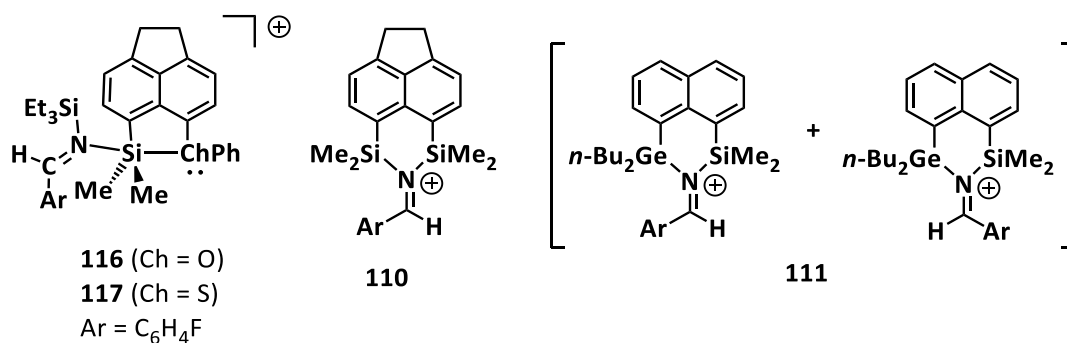
Table 25 – Selected NMR data of iminium ions **110**, **111**, **116** and **117**.

Compound	$\delta^{29}\text{Si}$	$\delta^1\text{H}$ (NCH)	$\delta^{15}\text{N}$	$\delta^{13}\text{C}$ (NC)
117 ^{a)}	34.0, 40.5	8.71	230.2	191.2
116 ^{a)}	17.9, 40.0	8.98	233.7	-
111 ^{b)}	11.8, 19.7*	9.32, 9.53*	-	185.7*, 186.5
110 ^{c)}	15.7, 23.3	9.12	229.5	187.4

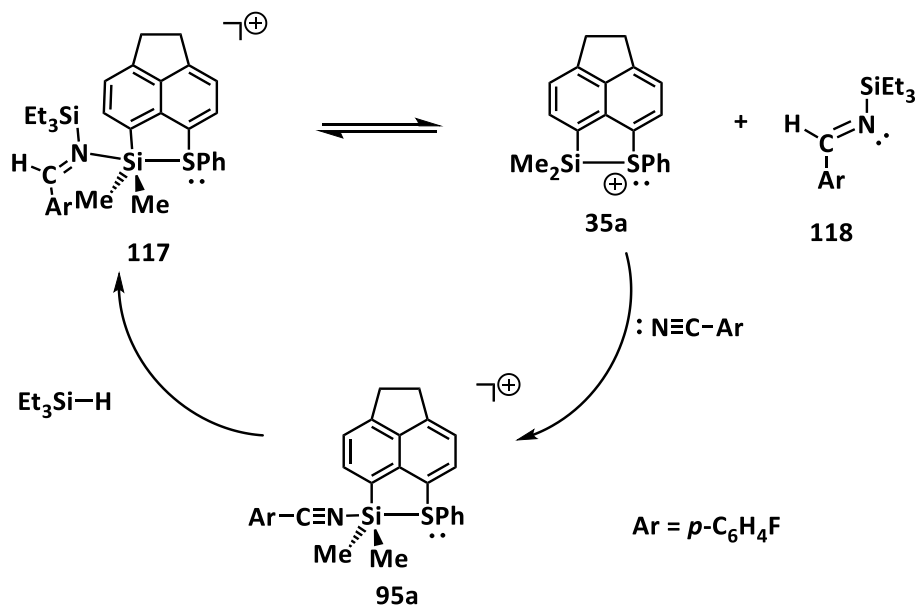
a) in C_6D_6 , b) in CD_2Cl_2 , c) in $\text{C}_6\text{D}_5\text{Cl}$, *main compound.

In conclusion, iminium borates **110** $[\text{B}(\text{C}_6\text{F}_5)_4]$, **111** $[\text{B}(\text{C}_6\text{F}_5)_4]$, **116** $[\text{B}(\text{C}_6\text{F}_5)_4]$ and **117** $[\text{B}(\text{C}_6\text{F}_5)_4]$ were obtained in relative complex reaction mixtures. Nevertheless, their identification was achieved using 2D NMR spectroscopy. Characteristic for iminium ions **110**, **111**, **116** and **117** is the correlation in the $^1\text{H}/^{29}\text{Si}$ HMBC NMR spectrum of the ^{29}Si NMR resonances of the SiMe_2 and SiEt_3 groups to the imine hydrogen atom as well as the correlation in the ^{15}N HMBC NMR spectrum of the ^{15}N NMR resonance

($\delta^{15}\text{N} = 230\text{-}234$) to the alkyl moieties attached to the silicon atoms. Even though, a complete structural elucidation was not possible to date, these experiments show, that nitrilium ions **94** and **95a** indeed react with an external Si – H source to give the corresponding iminium ions **116** and **117**. However, side products or products of following reactions were not identified. The reformation of silylsulfonium ion **35a** together with the complete consumption of triethylsilane and FBN gives rise to the question whether silylchalconium ions **34-35** can act as catalysts in hydrosilylation reactions of nitriles. This hypothesis is discussed in the following chapter.

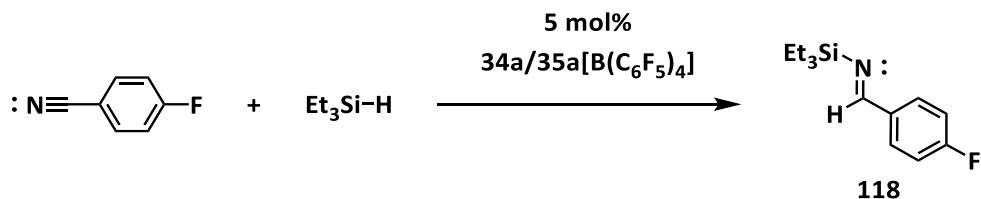


another nitrile to give nitrilium ion **95a**, which then reacts again with another silane to form iminium ion **117**. In this way the equilibrium product, silyl cation **35a**, would be removed from the equilibrium and the equilibrium educt, iminium ion **117**, is formed. In this manner, a catalytic cycle would be generated (Scheme 71).



Scheme 71 – Proposed mechanism for the catalytic hydrosilylation reaction of nitriles catalyzed by silyl cation **35a**.

To investigate this assumption, the catalytic activity of silyl cations **34a** and **35a** in the hydrosilylation reaction of nitriles was tested. Therefore, 4-fluorobenzonitrile (FBN) and triethylsilane were chosen as substrates (Scheme 72). FBN provides the possibility to monitor the reaction via ¹⁹F NMR spectroscopy.



Scheme 72 – Hydrosilylation reaction of FBN with triethylsilane and 5 mol% of silyl borate **34a**[B(C₆F₅)₄] and **35a**[B(C₆F₅)₄] as catalyst.

To begin, thiophenyl-stabilized silyl borate **35a**[B(C₆F₅)₄] was used as a catalyst. A Schlenk tube was charged with 0.06 equiv. of silane **43a** and 0.05 equiv. of trityl borate [Ph₃C][B(C₆F₅)₄]. Silane **43a** was used in excess to ensure complete consumption of trityl borate, since it could act as pre-catalyst (vide

infra). Benzene was added, the mixture was stirred for five minutes and silyl borate **35a**[B(C₆F₅)₄] was separated from the by-product, triphenylmethane, by washing the unpolar phase with benzene. After removal of the solvent under high-vacuum, 0.8 mL dichloromethane was added and the formation of silyl borate **35a**[B(C₆F₅)₄] was confirmed via NMR spectroscopy. Then, a Schlenk tube was charged with 1 equiv. FBN and the NMR sample containing silyl borate **35a**[B(C₆F₅)₄] was added and the mixture was stirred for five minutes. Subsequently, the mixture was cooled with an ice bath and 2 equiv. triethylsilane was added. After stirring for 45 minutes, the reaction mixture was transferred to an NMR tube for analysis. The ¹H NMR spectrum of the reaction mixture is shown in Figure 68 and reveals the signal at $\delta^1\text{H} = 9.07$ with an integral of 1 H atom, which is characteristic for the NCH group of imines (cf. $\delta^1\text{H} = 8.18\text{-}9.42$).^[50b, 104] The aryl hydrogen atoms of the C₆H₄F moiety can be observed in the low field region which shows two multiplets with an integral of 2 H atoms, respectively. The aliphatic region shows one multiplet with an integral of 6 H atoms which was assigned to the CH₂ group of the SiEt₃ moiety and another multiplet assigned to the corresponding CH₃ group. The latter multiplet has a too high integral for imine **118** (13 H instead of 9 H) probably due to overlap with residual catalyst or side products. The formation of side products can also be observed in the ¹⁹F NMR spectrum (Figure 69, a)). The main signal exhibits a ¹⁹F NMR chemical shift of $\delta^{19}\text{F} = -109.4$, which is high field shifted compared to FBN ($\delta^{19}\text{F} = -103.0$). With the main signal set to an integral of 1, the four side products exhibit integrals of 0.06-0.16 and the ¹⁹F NMR resonances are at $\delta^{19}\text{F} = -117.0, -113.6, -106.4$ and -100.6 . The ¹⁹F NMR chemical shift of FBN cannot be observed, hence, FBN was completely consumed. More importantly, the ¹H/²⁹Si HMBC NMR spectrum reveals cross peaks of a ²⁹Si NMR signal at $\delta^{29}\text{Si} = 8.1$ with the multiplet assigned to the CH₂ groups of the silyl moiety and the signal for the NCH moiety at $\delta^1\text{H} = 9.02$. The ²⁹Si NMR resonance ($\delta^{29}\text{Si} = 8.1$) is similar to other reported silylated imines (cf. $\delta^{29}\text{Si} = 7.7\text{-}9.3$).^[50b, 104a] A ¹⁵N NMR resonance at $\delta^{15}\text{N} = 344.8$ shows a correlation to the same signals in the ¹H/¹⁵N HMBC NMR spectrum as the ²⁹Si NMR resonance ($\delta^{29}\text{Si} = 8.1$) in the ¹H/²⁹Si HMBC NMR spectrum. All these NMR data strongly indicate the formation of hydrosilylation product **118**.

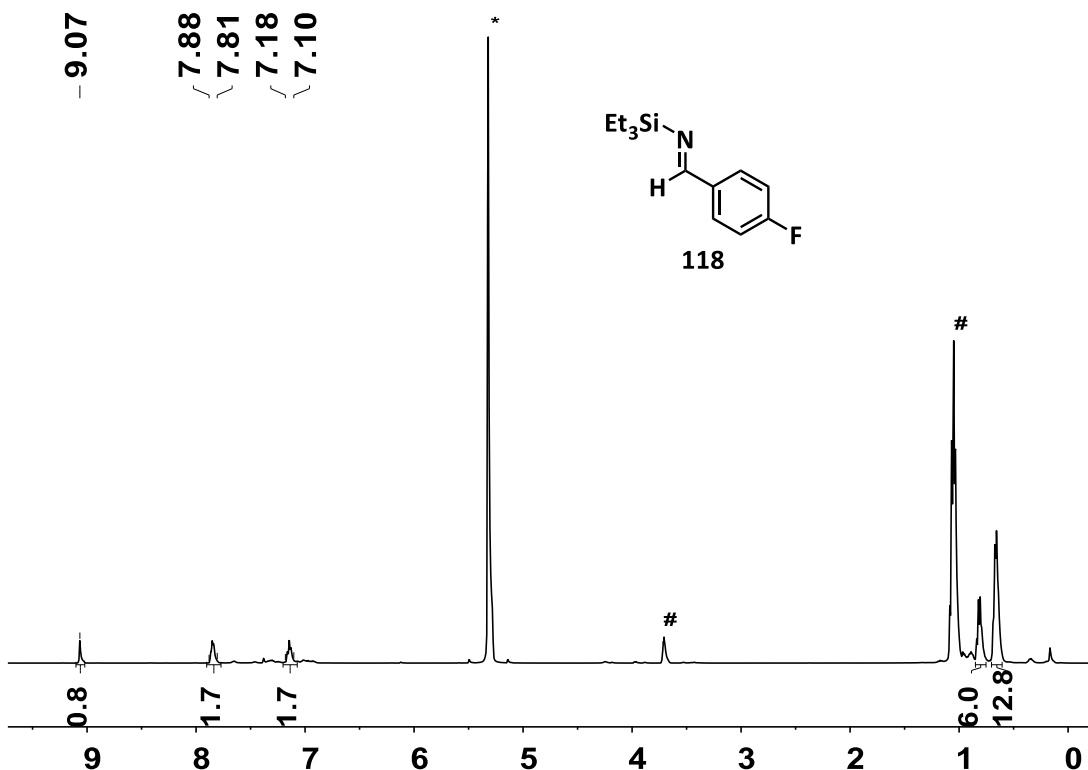


Figure 68 – ^1H NMR spectrum (500 MHz, 305 K, CH_2Cl_2 , without lock and shim, * CH_2Cl_2 : $\delta^1\text{H} = 5.32$, # Et_3SiH) of the reaction mixture of the hydrosilylation of FBN with Et_3SiH using thiophenyl-stabilized silyl borate **35a** $[\text{B}(\text{C}_6\text{F}_5)_4]$ as catalyst.

Encouraged by this result, the reaction was repeated with silylsulfonium and silyloxonium borate **34a** $[\text{B}(\text{C}_6\text{F}_5)_4]$ and **35a** $[\text{B}(\text{C}_6\text{F}_5)_4]$ as catalysts. In these experiments, the catalyst was prepared in situ, without any purification. All attempts resulted in complex reaction mixtures in which the main compounds identified were the substrates, FBN and Et_3SiH , and small amounts of the hydrosilylation product **118** together with several unidentified products, as illustrated by the ^{19}F NMR spectrum of one reaction mixture derived from using silylsulfonium borate **35a** $[\text{B}(\text{C}_6\text{F}_5)_4]$ as a catalyst (Figure 69, c)). In the experiments using silyloxonium borate **34a** $[\text{B}(\text{C}_6\text{F}_5)_4]$ as a catalyst not even traces of the product **118** were observed. Furthermore, a clear statement about what happened to the catalyst cannot be made, since only 5 mol% was used and the concentration was too low to be detected by NMR spectroscopy.

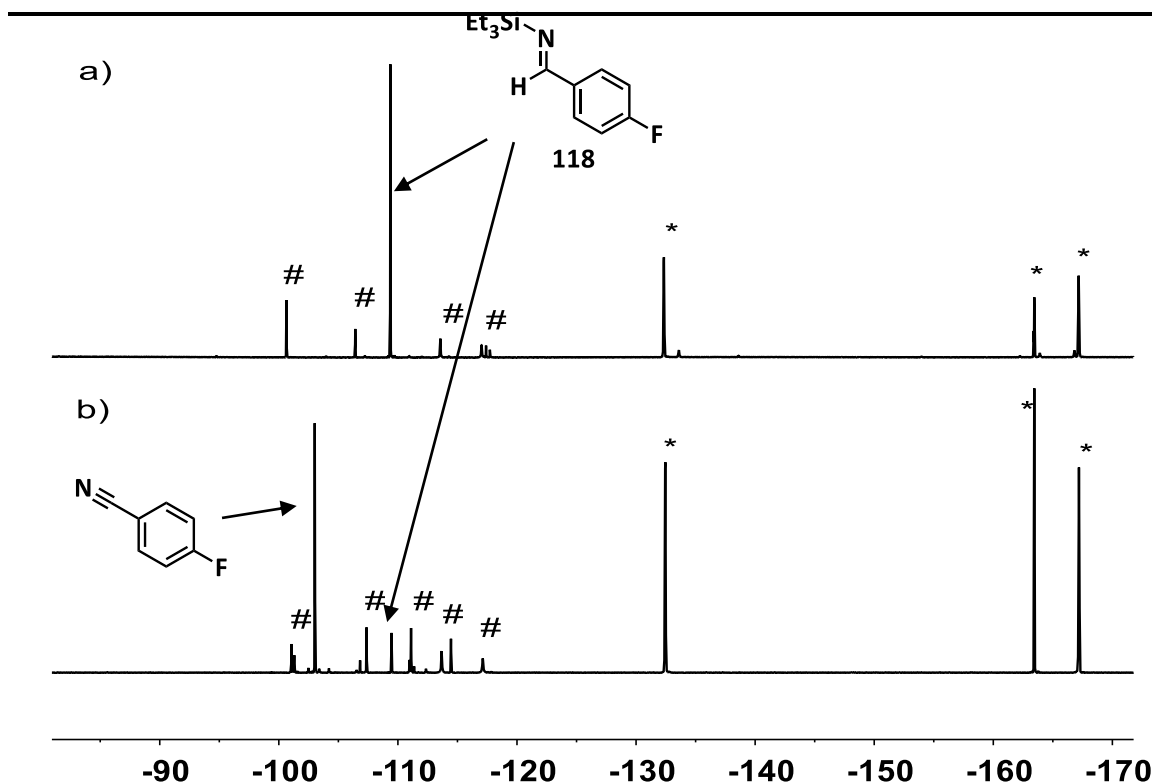


Figure 69 – ^{19}F NMR spectra (470 MHz, 300 K, CH_2Cl_2) of a) the reaction mixture of the first hydrosilylation experiment, catalyst **35a** $[\text{B}(\text{C}_6\text{F}_5)_4]$ prepared and purified prior to use; and b) the reaction mixture of a hydrosilylation experiment in which the catalyst **35a** $[\text{B}(\text{C}_6\text{F}_5)_4]$ was generated in situ (# unidentified side products, * $[\text{B}(\text{C}_6\text{F}_5)_4]$).

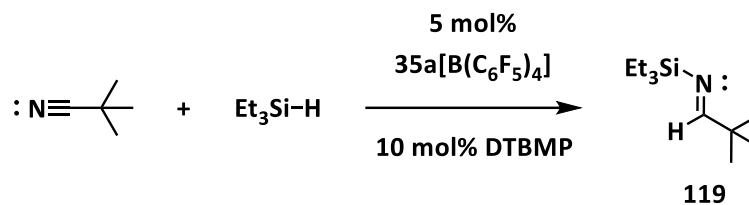
The assumption arises, that not silylsulfonium borate **35a** $[\text{B}(\text{C}_6\text{F}_5)_4]$ was the catalyst in the first experiment in which hydrosilylation product **118** was obtained almost quantitatively. A known competition reaction using strong Lewis acids as catalysts is the catalysis via *hidden protons*.^[105] Therefore, the experiment was repeated using silylsulfonium borate **35a** $[\text{B}(\text{C}_6\text{F}_5)_4]$ as a catalyst, whereby the catalyst mixture was directly prepared in CH_2Cl_2 . The formation of silylsulfonium borate **35a** $[\text{B}(\text{C}_6\text{F}_5)_4]$ was confirmed via NMR spectroscopy and the catalyst was stored for a week. After one week of storage, the ^{19}F NMR spectrum of silylsulfonium borate **35a** $[\text{B}(\text{C}_6\text{F}_5)_4]$ reveals the decomposition of the borate $[\text{B}(\text{C}_6\text{F}_5)_4]$ (similar to that observed in the experiments on the synthesis of hydrosilyloxonium ion **34d**, see Chapter 3.4), indicating the formation of protons in the reaction mixture.^[96] Using this mixture in the hydrosilylation reaction of FBN and Et_3SiH led to complete conversion of FBN and formation of hydrosilylation product **118**. In consequence, it is presumed that the catalysis took place via protons which might result from the decomposition of silyl borate **35a** $[\text{B}(\text{C}_6\text{F}_5)_4]$. Therefore, 2,6-di-*tert*-butyl-4-methylpyridine (DTBMP) was added as proton sponge to the following test reactions. The results are summarized in Table 26. The reaction of FBN and Et_3SiH was repeated in chlorobenzene to enable heating of the reaction mixture. The catalyst, **34a** $[\text{B}(\text{C}_6\text{F}_5)_4]$

or **35a**[B(C₆F₅)₄], was prepared in situ, in the presence of DTBMP. First FBN and then Et₃SiH were added at r.t. and the mixture was heated to 80 °C for 3-6 h; however, no conversion was observed (Table 26, Entry 3, 4). A substrate which is used extensively in the literature for hydrosilylation reactions is benzonitrile. Therefore, the hydrosilylation reaction of benzonitrile with silylsulfonium borate **35a**[B(C₆F₅)₄] as a catalyst was tested as well. However, no reaction was observed with either triethylsilane or with the more reactive phenyldimethylsilane.^[104a] Not even heating to 80 °C for 4 h lead to an observable reaction (Table 26, Entry 5, 6).

Table 26 – Summary of attempts for the hydrosilylation reaction of nitriles using silyl chalconium borates **34a**[B(C₆F₅)₄] and **35a**[B(C₆F₅)₄] as catalyst.

$ \begin{array}{c} \text{5 mol\%} \\ \text{34a,35a[B(C}_6\text{F}_5\text{)}_4\text{]} \\ \text{:N}\equiv\text{R}^1 + \text{R}^2_3\text{Si-H} \longrightarrow \text{R}^2_3\text{Si-N:} \\ \text{H} \quad \text{R}^1 \end{array} $									
Entry	Catalyst	T	t [h]	solvent	additives	R ¹	R ²	equiv. Silane	Conversion
1	35a	r.t.	16	CH ₂ Cl ₂	-	C ₆ H ₄ F	Et	2.5	traces
2	34a	r.t.	3	C ₆ H ₆	-	C ₆ H ₄ F	Et	1	0
3	35a	80 °C	6	C ₆ H ₅ Cl	DTBMP	C ₆ H ₄ F	Et	2	0
4	34a	80 °C	3	C ₆ H ₅ Cl	DTBMP	C ₆ H ₄ F	Et	2	0
5	35a	80 °C	5	C ₆ H ₅ Cl	DTBMP	Ph	Et	2	0
6	35a	80 °C	4	C ₆ H ₅ Cl	DTBMP	Ph	PhMe ₂	2	0

Seeing that the catalytic hydrosilylation of aryl-substituted nitriles did not work, alkyl-substituted nitriles were tested. Initially, pivalonitrile was used because of its relatively high boiling point (bp = 105 °C) and because it is easy to monitor using ¹H NMR spectroscopy. For the hydrosilylation reaction of pivalonitrile with triethylsilane, silylsulfonium borate **35a**[B(C₆F₅)₄] was freshly prepared in chlorobenzene with 10 mol% DTBMP as an additive (Scheme 73). First 1.0 equiv. pivalonitrile and subsequently 1.5 equiv. triethylsilane were added at r.t. to thiophenyl-stabilized silyl borate **35a**[B(C₆F₅)₄]. The mixture was stirred for one hour, then transferred to an NMR tube charged with a D₂O capillary for the lock signal and then analysed via NMR spectroscopy.



Scheme 73 – Hydrosilylation reaction of pivalonitrile with triethylsilane and silyl borate **35a**[B(C₆F₅)₄] as catalyst.

The ¹H NMR spectrum of the reaction mixture is shown in Figure 70. At δ¹H = 8.42, a resonance typical for the NCH group of imines (δ¹H = 8.18-9.42)^[50b, 104] was detected. In the aliphatic region, a singlet signal for 9 hydrogen atoms was found at δ¹H = 1.03 and was assigned to the *tert*-butyl group. The ¹H NMR chemical shift is high-field shifted compared to pivalonitrile (δ¹H = 1.13). Furthermore, a quartet at δ¹H = 0.65 (6 H) was observed and assigned to the CH₂ groups and the multiplet at δ¹H = 0.92-1.02 was assigned to the CH₃ groups of the ethyl moieties. The latter signal has a higher integral than expected for imine **119** due to overlap with a side product (14 H instead of 9 H, *vide infra*). The ¹H/¹⁵N HMBC NMR spectrum reveals correlations of the signal at δ¹⁵N = 331.2 to the ¹H NMR resonances assigned to the NCH group and the CH₂ group of the SiEt₃ moiety (cf. Et₃SiNC(C₆H₅F): δ¹⁵N = 344.8, see above).

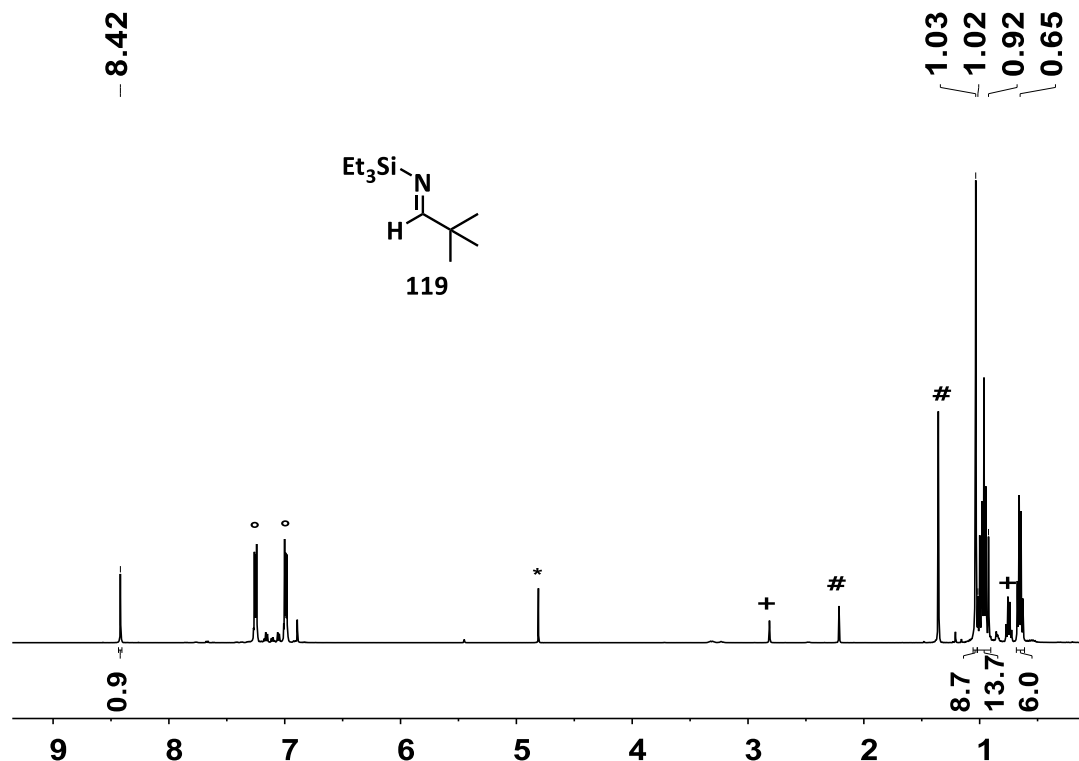


Figure 70 – ^1H NMR spectrum (500 MHz, 305 K, $\text{C}_6\text{H}_4\text{Cl}_2$, D_2O capillary for the lock signal) of the hydrosilylation reaction of pivalonitrile with triethylsilane and 5 mol% of silyl borate **35a** $[\text{B}(\text{C}_6\text{F}_5)_4]$ as catalyst (*DHO, #DTBMP, $^\circ\text{C}_6\text{H}_4\text{Cl}_2$, +side product, vide infra).

In the $^1\text{H}/^{29}\text{Si}$ HMBC NMR spectrum of the reaction mixture, two silicon species were observed (Figure 71). Imine **119** exhibits a ^{29}Si NMR chemical shift of $\delta^{29}\text{Si} = 5.8$ (cf. $\delta^{29}\text{Si} = 7.7\text{-}9.3$)^[50b, 104a], and shows a correlation to the signals assigned to the NCH and the SiEt_3 group. The other ^{29}Si NMR resonance is $\delta^{29}\text{Si} = 11.4$. This signal shows three correlations in the $^1\text{H}/^{29}\text{Si}$ HMBC spectrum to $\delta^1\text{H} = 0.75$, 0.92-1.02, 2.81. Consequently, the multiplet for the CH_3 groups ($\delta^1\text{H} = 0.92\text{-}1.02$) overlaps with the second species, what explains the higher than expected integral of this signal. Integration of the singlet signal at $\delta^1\text{H} = 2.81$ and the smaller multiplet at $\delta^1\text{H} = 0.75$ (Figure 72) reveals, that this signal might be assignable to amine **120** which is the product of a double hydrosilylation reaction of pivalonitrile (cf. $(\text{Et}_3\text{Si})_2\text{NCH}_2\text{Bu}$: $\delta^1\text{H} = 1.17$ (NCH₂), $\delta^{29}\text{Si} = 10.4$ in $\text{C}_6\text{D}_5\text{Br}$).^[50b] This is possible, since triethylsilane was used in excess (1.5 equiv.).

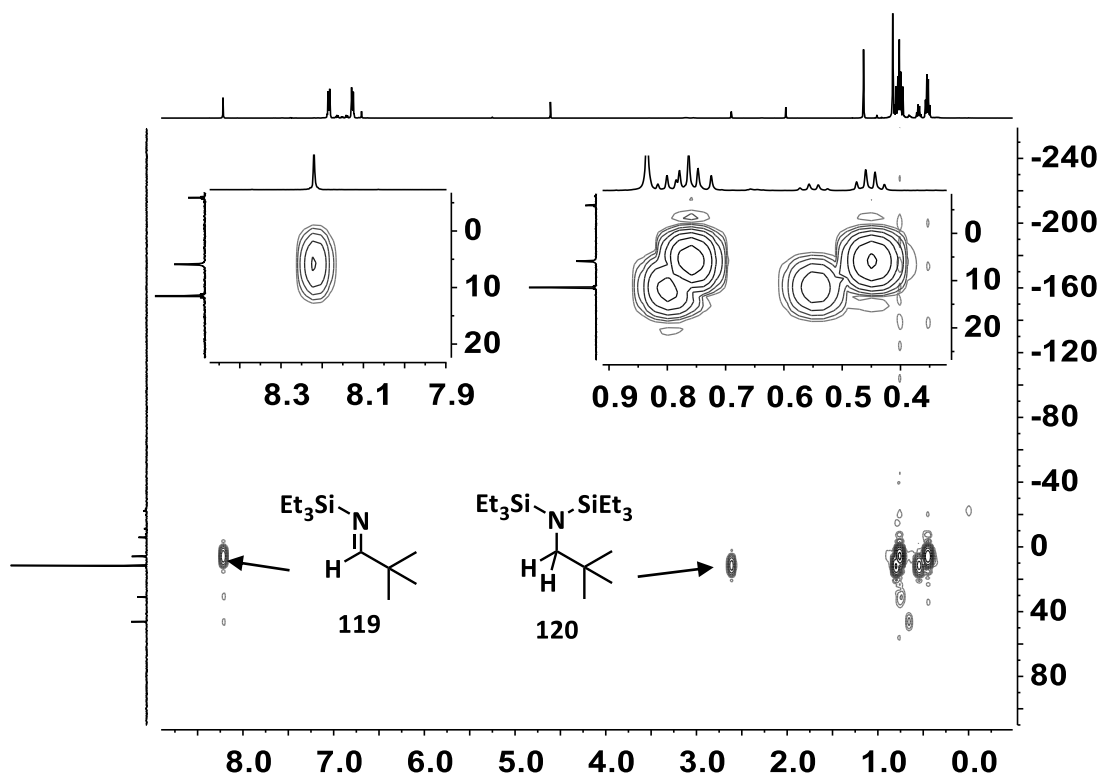


Figure 71 – $^1\text{H}/^{29}\text{Si}$ HMBC NMR spectrum (500 MHz, 305 K, $\text{C}_6\text{H}_4\text{Cl}_2$) of the hydrosilylation reaction of pivalonitrile with triethylsilane and 5 mol% of silyl borate **35a** [$\text{B}(\text{C}_6\text{F}_5)_4$] as catalyst.

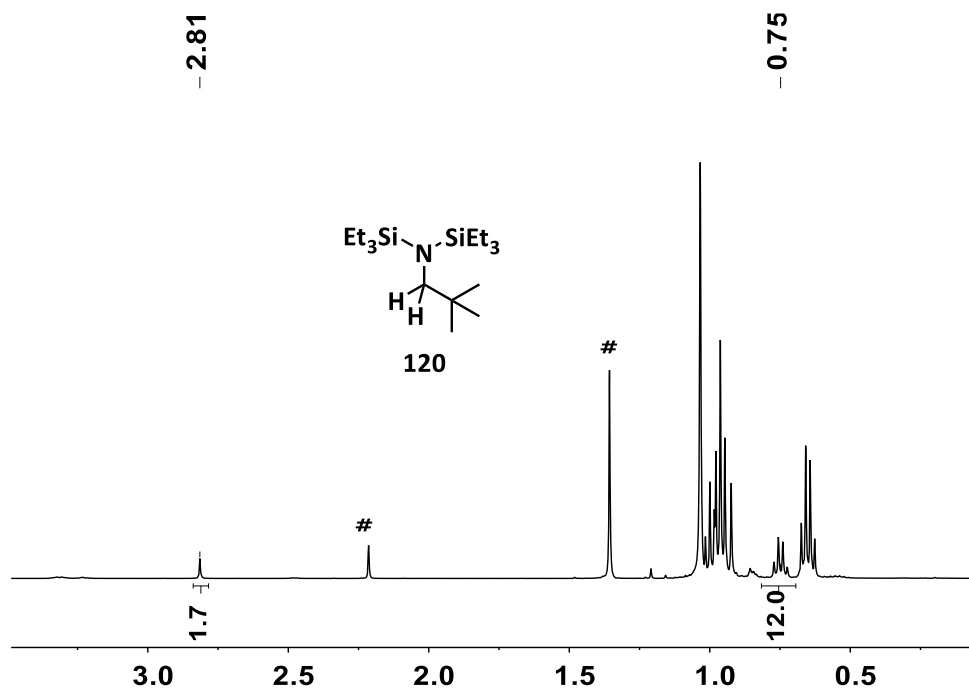


Figure 72 – Aliphatic region of the ^1H NMR spectrum (500 MHz, 305 K, $\text{C}_6\text{H}_4\text{Cl}_2$, D_2O capillary for the lock signal) of the hydrosilylation reaction of pivalonitrile with Et_3SiH and 5 mol% of silyl borate **35a** [$\text{B}(\text{C}_6\text{F}_5)_4$] as catalyst (#DTBMP).

Based on this result, a preliminary screening of the hydrosilylation reaction of alkyl nitriles using silylchalconium borates **34a**[B(C₆F₅)₄] and **35a**[B(C₆F₅)₄] as catalysts was performed. The results of this screening are summarized in Table 27. First, the reaction of pivalonitrile was repeated using 2 equiv. triethylsilane (Entry 2). After stirring for 120 min at r.t., the mixture was transferred to an NMR tube equipped with a D₂O capillary. The ¹H NMR spectrum shows two products, imine **119** and amine **120**, in a ratio of 83:17. This is the same ratio which was observed in the first attempt (Table 27, Entry 1). The second hydrosilylation reaction seems to be slow at r.t. and therefore, the NMR tube was heated to 80 °C for 160 min and analyzed again. The ratio of imine **119**/amine **120** was now found to be 54:46 (Entry 3). After further heating to 80 °C for 490 min the ratio of imine **119**/amine **120** is 34:66 (Entry 4). To push the equilibrium in favor of the amine **120**, the NMR sample was transferred to a Schlenk tube and an additional equiv. triethylsilane was added. After heating the mixture for a further 340 min, complete conversion to amine **120** was achieved (Entry 5).

To ensure the reaction is indeed catalyzed by silylsulfonium borate **35a**[B(C₆F₅)₄], an equimolar mixture of the substrates, pivalonitrile and triethylsilane, in 0.5 mL chlorobenzene was stirred for 195 min at 80 °C. No conversion was observed (Entry 6). Then 5 mol% trityl borate [Ph₃C][B(C₆F₅)₄] was added as pre-catalyst for the formation of [Et₃Si(Cl-benzene)]⁺ or rather [Et₃Si-NC(*t*-Bu)]⁺ (vide infra) and the mixture was stirred at 80 °C for 160 min. This resulted in the formation of 10 % imine **119** (Entry 7). The sample was stored for 2 weeks (20160 min) at r.t. and analysed again, whereafter a conversion of 30 % imine **120** was measured (Entry 8). Entries 7 and 8 demonstrate that the hydrosilylation reaction is slower with [Et₃Si(Cl-benzene)]⁺ or rather [Et₃Si-NC(*t*-Bu)]⁺ as a catalyst in comparison to using silylsulfonium borate **35a**[B(C₆F₅)₄] as a catalyst (Entry 1, 2). As a consequence, it is assumed that silylsulfonium ion **35a** is the actual catalyst in this reaction.

Other substrate combinations were tested. Changing the silane to dimethylphenylsilane, the conversion of pivalonitrile to amine **120a** is achieved at r.t. within 1080 min (Entry 9). Using triphenylsilane, the reaction is slower. After preparation of the sample, it was stirred over the weekend (3 days, 4320 min) at r.t. and the conversion achieved was only 22 % of imine **119b** (Entry 10). After heating to 80 °C for 340 min, complete conversion of pivalonitrile to the corresponding imine **119b** was obtained; the formation of the corresponding amine **120b** was not observed (Entry 11). This shows, that the selectivity of the reaction depends on the silane used. Other alkyl nitriles were tested, starting with acetonitrile. Here, the reaction was heated to 60 °C only because of the lower boiling point of acetonitrile. Surprisingly, no conversion to the corresponding hydrosilylation products was observed, neither with triethylsilane nor with the more reactive dimethylphenylsilane

(Entry 12, 13). The last substrate tested was cyclohexanecarbonitrile; here again, no conversion to the corresponding hydrosilylation products was observed (Entry 14).

Table 27 – Results of the screening of the hydrosilylation reaction of nitriles using silyloxonium and silylsulfonium borates **34a**[B(C₆F₅)₄] and **35a**[B(C₆F₅)₄] as catalysts and 10 mol% DTBMP as additive/proton sponge. The yield was determined via ¹H NMR spectroscopy using the methyl signal of DTBMP as internal standard (for details see Experimental Part). (**119**, **120**: SiR₂₃ = SiEt₃, **119a**, **120a**: SiR₂₃ = SiMe₂Ph, **119b**, **120b**: SiR₂₃ = SiPh₃).

Entry	Catalyst	T	t [min]	R ¹	Silane	equiv.	Yield of 119	Yield of 120
1	35a	r.t.	60	<i>t</i> -Bu	Et ₃ SiH	1.5	83	17
2	35a	r.t.	120	<i>t</i> -Bu	Et ₃ SiH	2	83	17
3	35a	80 °C	160	<i>t</i> -Bu	Et ₃ SiH	2	54	46
4	35a	80 °C	490	<i>t</i> -Bu	Et ₃ SiH	2	34	66
5	35a	80 °C	340	<i>t</i> -Bu	Et ₃ SiH	3	0	100
6	-	80 °C	195	<i>t</i> -Bu	Et ₃ SiH	1	0	0
7	[Ph ₃ C] ⁺	80 °C	160	<i>t</i> -Bu	Et ₃ SiH	1	10	0
8	[Ph ₃ C] ⁺	r.t.	20160	<i>t</i> -Bu	Et ₃ SiH	1	30	0
9	35a	r.t.	1080	<i>t</i> -Bu	PhMe ₂ SiH	2	0	95
10	35a	r.t.	4320	<i>t</i> -Bu	Ph ₃ SiH	2	22	0
11	35a	80 °C	330	<i>t</i> -Bu	Ph ₃ SiH	2	100	0
12	35a	60 °C	300	Me	Et ₃ SiH	2	0	0
13	35a	60 °C	315	Me	PhMe ₂ SiH	2	0	0
14	35a	80 °C	240	C ₆ H ₁₁	Et ₃ SiH	2	0	0
15	34a	r.t.	1020	<i>t</i> -Bu	Et ₃ SiH	1	traces	0
16	34a	80 °C	100	<i>t</i> -Bu	Et ₃ SiH	1	57	0
17	34a	80 °C	160	<i>t</i> -Bu	Et ₃ SiH	2	27	73
18	34a	80 °C	490	<i>t</i> -Bu	Et ₃ SiH	2	2	98
19	34a	r.t.	1440	<i>t</i> -Bu	PhMe ₂ SiH	2	20	0
20	34a	80 °C	260	<i>t</i> -Bu	PhMe ₂ SiH	2	0	100

Phenoxy-stabilized silyl cation **34a** appears to be less reactive in the hydrosilylation reaction of pivalonitrile. At room temperature, only traces of the hydrosilylation product **119** were observed (Table 27, Entry 15). Heating to 80 °C for 100 min leads to the formation of 57 % of the corresponding imine **119** (Entry 16). The conversion of pivalonitrile using 2 equiv. of triethylsilane leads to an imine **119**/amine **120** ratio of 27:73 after heating to 80 °C for 160 min (Entry 17). Nearly complete conversion to amine **120** was achieved after approximately 8 h at 80 °C (Entry 18). Using the more reactive dimethylphenylsilane, a conversion of 20 % to imine **119a** was achieved at r.t. after 24 h

(1440 min, Entry 19). This reaction mixture was then heated to 80 °C for 260 min, whereby complete conversion to amine **120** was obtained (Entry 20).

In conclusion, silyl borates **34a**[B(C₆F₅)₄] and **35a**[B(C₆F₅)₄] show catalytic activity in the hydrosilylation reaction of pivalonitrile. Other substrates, such as 4-fluorobenzonitrile, benzonitrile, cyclohexyl nitrile and acetonitrile do not undergo the hydrosilylation reaction with silyl borates **34a**[B(C₆F₅)₄] and **35a**[B(C₆F₅)₄] as catalysts. This is a rather surprising result, since other Lewis acids show a good catalytic activity with all these substrates.^[50b, 106] Entries 1 and 15 (Table 27) reveal that the phenoxy-stabilized silyl borate **34a**[B(C₆F₅)₄] shows a lower reactivity in the hydrosilylation reaction of pivalonitrile in comparison to the thiophenyl-stabilized derivative **35a** despite its higher Lewis acidity (Chapter 3.8.1). However, the second hydrosilylation reaction to amine **120** seems to be more efficient with silyloxonium borate **34a**[B(C₆F₅)₄] compared to silylsulfonium borate **35a**[B(C₆F₅)₄] as a catalyst. This is apparent via comparison of Entries 4 and 18 (Table 27). In these attempts, 2 equiv. Et₃SiH were used and the mixture was stirred at 80 °C for approximately 8 h. With silylsulfonium borate **35a**[B(C₆F₅)₄] an imine **119**/amine **120** ratio of 34:66 was obtained whereas silyloxonium borate **34a**[B(C₆F₅)₄] leads to a ratio of 2:98. Despite the limited scope of silylchalconium borates **34a**[B(C₆F₅)₄] and **35a**[B(C₆F₅)₄] regarding nitriles, the selectivity obtained using different silanes reveals the order expected: dimethylphenylsilane is more reactive than triethylsilane which is more reactive than triphenylsilane.

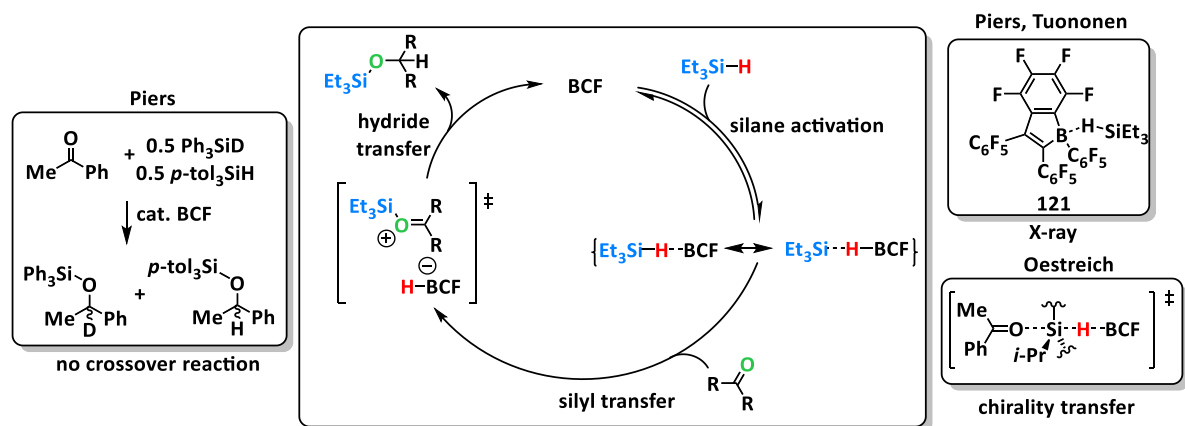
Due to the limited scope of substrates regarding the catalytic activity in the hydrosilylation reaction of nitriles of silylchalconium borates, **34a**[B(C₆F₅)₄] and **35a**[B(C₆F₅)₄], DFT calculations were performed to gain further insights to the mechanism and the limiting factor of this reaction. The results are discussed in the following chapter.

3.8.3.2 DFT Studies on the Mechanism of the Hydrosilylation Reaction of Nitriles

As shown in Chapter 3.8.3.1, silylchalconium borates **34a**[B(C₆F₅)₄] and **35a**[B(C₆F₅)₄] exhibit an unexpected limited scope in the catalytic hydrosilylation reactions of nitriles. Therefore, an investigation of the mechanism was performed to get insights into the limiting factors of this reaction. In this section, three possible pathways of the hydrosilylation reaction of nitriles using silylchalconium ions **34a** and **35a** as a catalyst will be discussed.

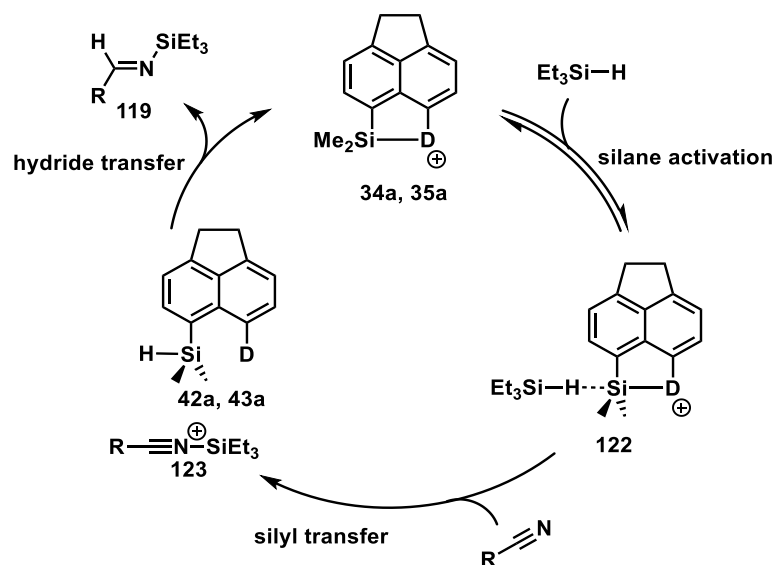
The mechanism of the hydrosilylation reaction of ketones with tris(pentafluorophenyl)borane (BCF) as Lewis acidic catalyst has been elucidated experimentally by the groups of Piers and Oestreich.^{[40a,}

^{107]} They suggest a three-step mechanism, which seems counterintuitive (Scheme 74). In the first step, BCF does not form a Lewis acid/base adduct with the ketone, instead it activates the Si–H bond by formation of a Si–H–B two-electron three-center bond. Piers and Tuononen were able to verify the existence of this kind of species via the synthesis and X-ray analysis of borane-silane complex **121**.^[108] In the subsequent step of the mechanism, a silyl transfer from the borane-silane complex to the carbonyl oxygen of the substrate takes place. Here, Oestreich and co-workers have shown, that this occurs in a S_N2-Si mechanism by using chiral silanes as probes.^[40a] The final step is the hydride transfer from the borate to the carbonyl carbon atom and liberation of the catalyst, BCF, and the product. This last step was investigated by Piers and co-workers. They found, that using mass-labeled silanes, no crossover reaction takes place, which indicates that the ion pair is not separated and the hydride transfer is fast.^[107]



Scheme 74 – Mechanism of the hydrosilylation reaction of carbonyl substrates using BCF as catalyst and its experimental elucidations.^[40a, 107-108]

This mechanism is transferable to silylchalconium ions **34a** and **35a** as shown in Scheme 75 and was, therefore, initially considered in the present DFT studies.



Scheme 75 – Possible mechanism for the hydrosilylation reaction of nitriles using silyl chalconium ions as a catalyst (D = OPh (**34a**), SPh (**35a**)).

All calculations were performed at the M06-2X/Def2-TZVP level of theory and included the solvent chlorobenzene using the SCRF model. Furthermore, the calculated free Gibbs energies were corrected with a factor obtained via the freqchk utility program by applying the solvent pressure ($p = 24.419$ MPa for chlorobenzene). The resulting free Gibbs energies for the Si – H activation mechanism are illustrated in Figure 73. The overall reaction is exothermic by 46 kJmol^{-1} for both silyloxonium and silylsulfonium ion **34a** and **35a**. However, the first step, the formation of the Si – H – Si adduct **122** is endothermic by 24 kJmol^{-1} for silylsulfonium ion **35a** and by 21 kJmol^{-1} for silyloxonium ion **34a**. The subsequent transfer of the triethylsilyl group to the nitrile is again exothermic ($\Delta G = -26 \text{ kJmol}^{-1}$ for **35a**; $\Delta G = -57 \text{ kJmol}^{-1}$ for **34a**). The final step, the hydride transfers from silanes **42a** and **43a** to silylated nitrile **123** with the formation of product **119** and regeneration of catalyst **34a** or **35a** is also an exothermic reaction ($\Delta G = -43 \text{ kJmol}^{-1}$ for **35a**; $\Delta G = -9 \text{ kJmol}^{-1}$ for **34a**). Consequently, the formation of the Si – H – Si complex **122** is, according to the calculations, the rate-limiting step in this reaction.

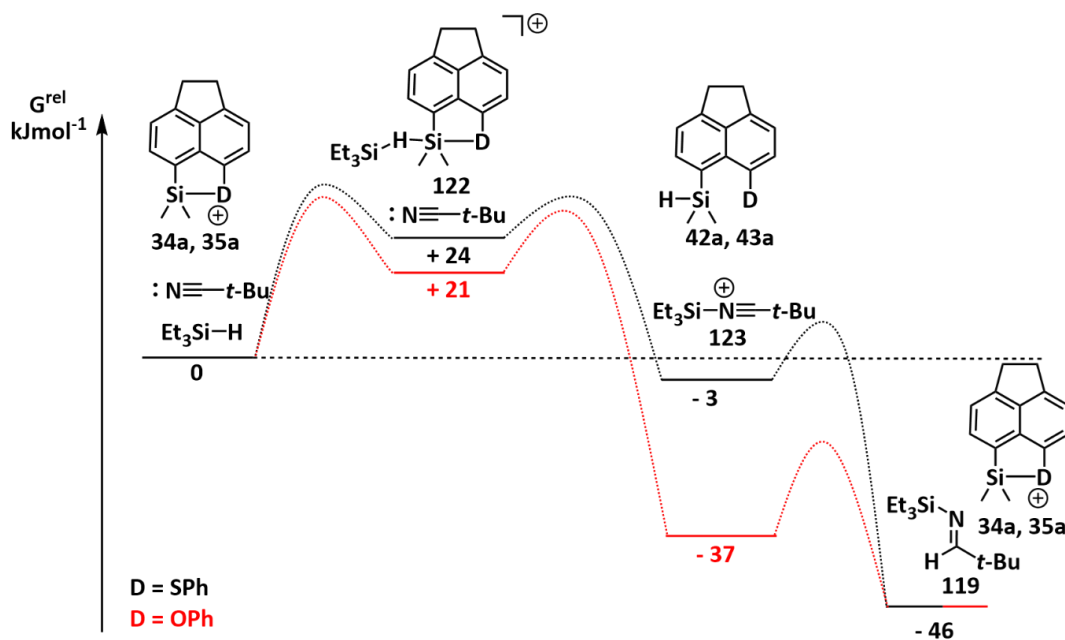
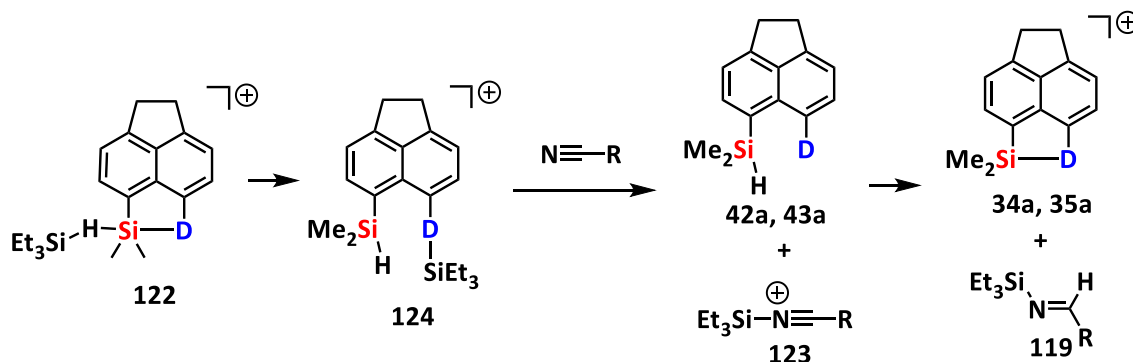


Figure 73 – Calculated relative free Gibbs energies of the hydrosilylation of nitriles with silyl chalconium ions **34a** and **35a** as catalyst: Si – H – Si route (M06-2X/Def2-TZVP, SCRF(solvent=chlorobenzene), $p = 24.419$ MPa).

An alternative pathway for the Si – H activation was also considered (Scheme 76). After activation of the Si – H bond by the formation of the Si – H – Si bridge in **122**, the heterolytic cleavage of the Si – H bond of triethylsilane is the next step as shown in Scheme 76. The triethylsilyl group is transferred to the donor substituent and silyl chalconium ion **124** is formed. In the reaction sequence for the hydrosilylation reaction of nitriles, the triethylsilyl group is then transferred from the donor substituent to the nitrile and the last step, the hydride transfers from silane **42a** or **43a** to silylated nitrilium ion **123**, is the same as in the previously discussed route.



Scheme 76 – Reaction of species **122** to form silylchalconium ion **124** and subsequent sequence of hydrosilylation of a nitrile.

The calculated free Gibbs energies of the second reaction pathway are illustrated in Figure 74. The first step, namely the Si – H – Si adduct **122** formation, remains the same as shown in the first mechanism. The subsequent heterolytic cleavage of the Et₃Si – H bond is endothermic for both silyl chalconium ions **34a** and **35a** ($\Delta G = +17$ kJmol⁻¹ for **35a**; $\Delta G = +15$ kJmol⁻¹ for **34a**). The silyl transfer from the chalcogen atom of **124** to pivalonitrile is exothermic ($\Delta G = -44$ kJmol⁻¹ for **124-S**; $\Delta G = -73$ kJmol⁻¹ for **124-O**). Consequently, the heterolytic cleavage of the Si – H bond with formation of **124** would be the rate-limiting step in this reaction pathway.

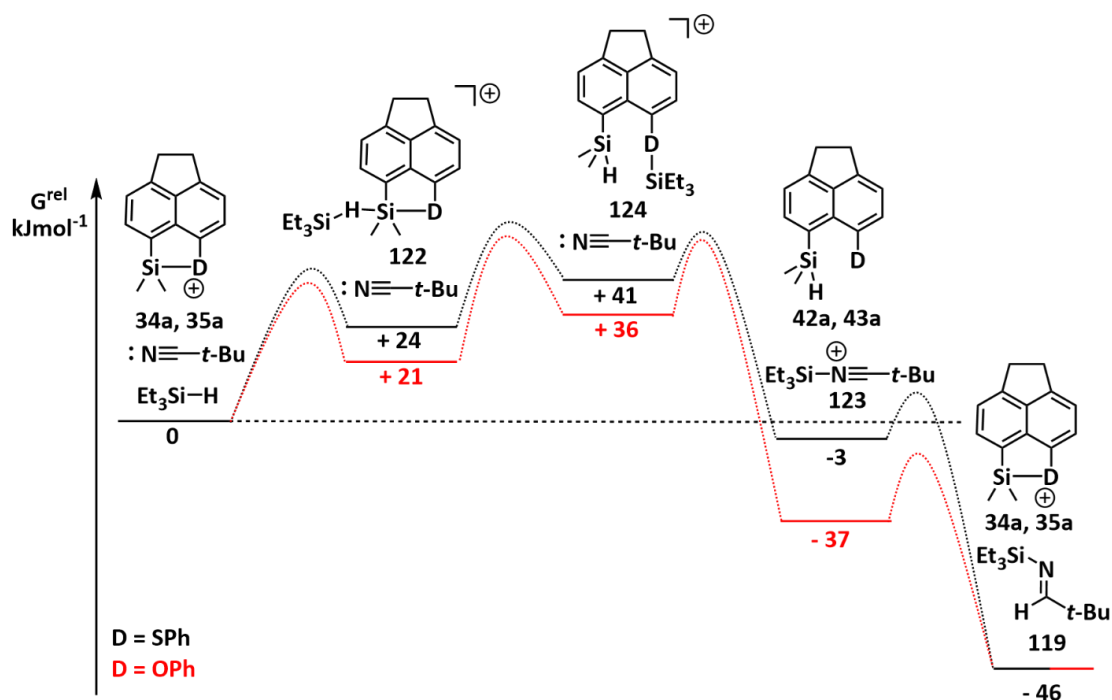
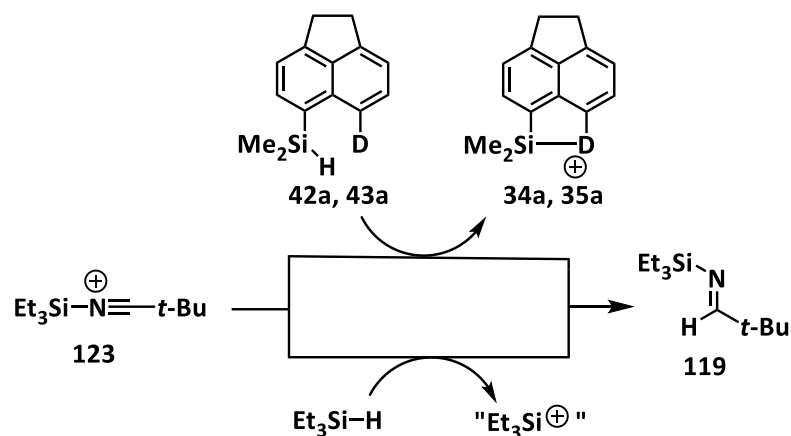


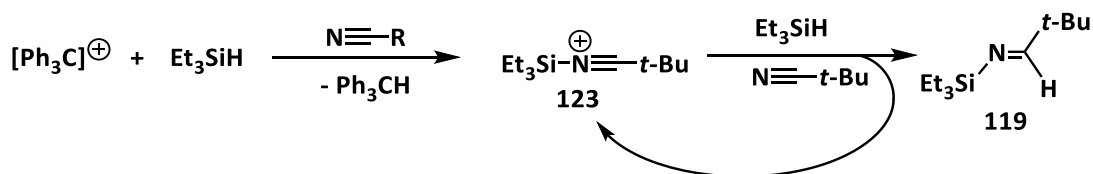
Figure 74 – Calculated relative free Gibbs energies of the hydrosilylation of nitriles with silyl chalconium ions **34a** and **35a** as catalyst: heterolytic cleavage of the Si – H bond (M06-2X/Def2-TZVP, SCRF(solvent=chlorobenzene), $p = 24.419$ MPa).

At this point, one should consider that there is also triethylsilane present in the reaction mixture which can transfer the hydride to silylnitrilium ion **123** instead of silanes **42a** or **43a** (Scheme 77).



Scheme 77 – Hydride transfer of silanes **42a**, **43a** or triethylsilane to silylnitrilium ion **123** to form hydrosilylation product **119**.

There are two reasons why triethylsilane is not believed to be the species which transfers a hydride to the silylated substrate **123**. The first reason is the result of a control reaction using a catalytic amount of trityl borate. In this reaction, the triethylsilyl cation is formed initially which would directly react with the nitrile to form silylated nitrilium ion **123** (Scheme 78). Then, the hydride is transferred to nitrilium ion **123** forming the hydrosilylation product **119** and nitrilium ion **123**, and thus, the silylated nitrilium ion **123** would be considered the catalyst of this reaction. However, the hydrosilylation reaction of pivalonitrile using trityl cation as a pre-catalyst was significantly slower compared to the reaction using silylsulfonium borate **35a**[B(C₆F₅)₄] as a catalyst (see Chapter 3.8.3.1).



Scheme 78 – Possible mechanism of the hydrosilylation reaction of nitriles using trityl cation as pre-catalyst.

The second reason is that, based on the Lewis acidity scale using 4-fluorobenzonitrile as a probe, triethylsilyl cation is a stronger Lewis acid compared to silyl cations **34a** and **35a** (see Chapter 3.8.1).^[35] Therefore, the formation of silyl cations **34a** and **35a** is preferred compared to the formation of triethylsilylcation and the hydride transfer of silane **42a** or **43a** to silylnitrilium ion **123** is more likely than of triethylsilane.

Recapitulating, the Si – H activation by silylchalconium ions **34a** and **35a** to give the Si – H – Si adduct **122** and subsequent heterolytic cleavage of the Si – H bond to give silylchalconium ion **124** are endothermic steps. In relation to the chalcogen atom used the calculated free Gibbs energies do not

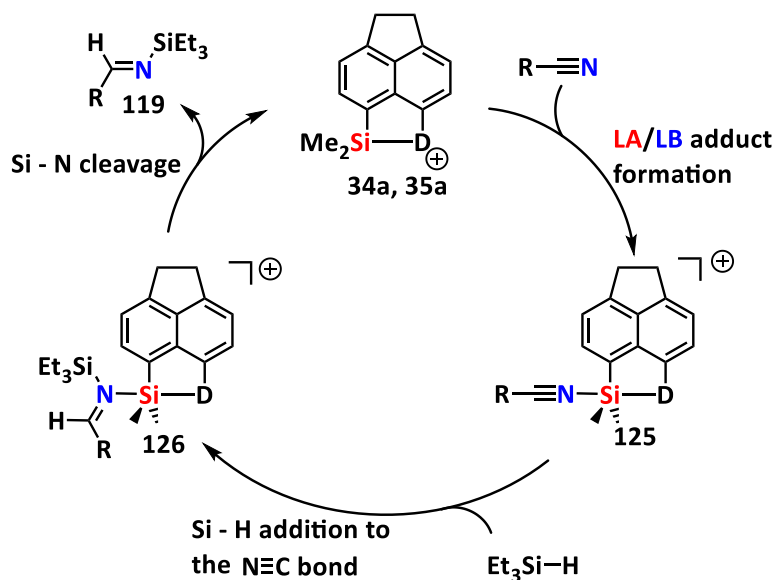
differ much (Si – H – Si formation: $\Delta G = +24 \text{ kJmol}^{-1}$ for SPh vs $\Delta G = +21 \text{ kJmol}^{-1}$ for OPh; subsequent Si – H cleavage: $\Delta G = +17 \text{ kJmol}^{-1}$ for SPh vs $\Delta G = +15 \text{ kJmol}^{-1}$ for OPh). The subsequent silyl and hydrogen transfer reactions are exothermic reactions. Therefore, the Si – H activation is most likely the rate-limiting step in these reaction pathways. As a consequence, according to the calculations, silyl cations **34a** and **35a** should both show a similar activity in the hydrosilylation reaction of pivalonitrile. Further calculations with benzonitrile as a substrate showed similar results compared to the calculations discussed with pivalonitrile as a substrate. The results are shown in Table 28.

Table 28 – Calculated free Gibbs energies for the hydrosilylation reaction of benzonitrile and pivalonitrile: Si – H activation mechanism (M06-2X/Def2-TZVP, SCRF(solvent=chlorobenzene), $p = 24.419 \text{ MPa}$).

Et ₃ Si source	Silyl transfer $\Delta G \text{ [kJmol}^{-1}\text{]}$		Hydride source	Hydride transfer $\Delta G \text{ [kJmol}^{-1}\text{]}$	
	<i>t</i> -Bu	Ph		<i>t</i> -Bu	Ph
122-S	-26	-24	43a	-43	-61
124-S	-43	-41			
122-O	-57	-55	42a	-9	-27
124-O	-73	-70			

The experimental results revealed, that with both catalysts **34a** and **35a**, only the hydrosilylation reaction of pivalonitrile is possible, whereas benzonitrile does not react. If the Si – H activation is the first step in the underlying mechanism of the hydrosilylation reaction, the cations **34a** and **35a** should have the same activity with both substrates, pivalonitrile and benzonitrile. Since this is not the case, the Si – H activation pathway does not seem to be the likely underlying mechanism. Another possible mechanism for the hydrosilylation reaction of nitriles using silylchalconium ions **34a** and **35a** as catalysts starts with the formation of a Lewis acid/base adduct and a subsequent Si – H addition to the unsaturated bond of the substrate as shown in Scheme 79.^[107] Silylchalconium ion **34a** or **35a** reacts with the nitrile to form nitrilium ion **125**. Nitrilium ion **125** reacts with triethylsilane to form

iminium ion **126** which is subsequently cleaved into product **119** regenerating silylchalconium ion **34a** or **35a**.



Scheme 79 – Possible mechanism for the hydrosilylation reaction of nitriles using silyl chalconium ions **34a** and **35a** as a catalyst.

The results of the calculation of the free Gibbs energies of this reaction pathway for the hydrosilylation reaction of pivalonitrile are shown in Figure 75. The formation of silylated nitrilium ions **125** is exothermic for both silyl chalconium ions **34a** and **35a** ($\Delta G = -18 \text{ kJmol}^{-1}$ for **35a** and $\Delta G = -42 \text{ kJmol}^{-1}$ for **34a**). The subsequent Si-H addition to the N-C triple bond with formation of iminium ions **126** is also exothermic for both nitrilium ions **125** ($\Delta G = -27 \text{ kJmol}^{-1}$ for **125-S** and $\Delta G = -43 \text{ kJmol}^{-1}$ for **125-O**). However, the heterolytic cleavage of the Si-N bond to release product **119** and reform the catalysts, silyl cations **34a** and **35a**, is, according to the calculations, an equilibrium with $\Delta G = 0 \text{ kJmol}^{-1}$ for iminium ion **126-S** and endothermic by 39 kJmol^{-1} for silyliminium ion **126-O**. This could explain why the reaction using silylsulfonium ion **35a** as a catalyst proceeds at r.t. while with silyloxonium ion **34a** the reaction has to be heated to $80 \text{ }^\circ\text{C}$ (see Chapter 3.8.3.1, Table 27).

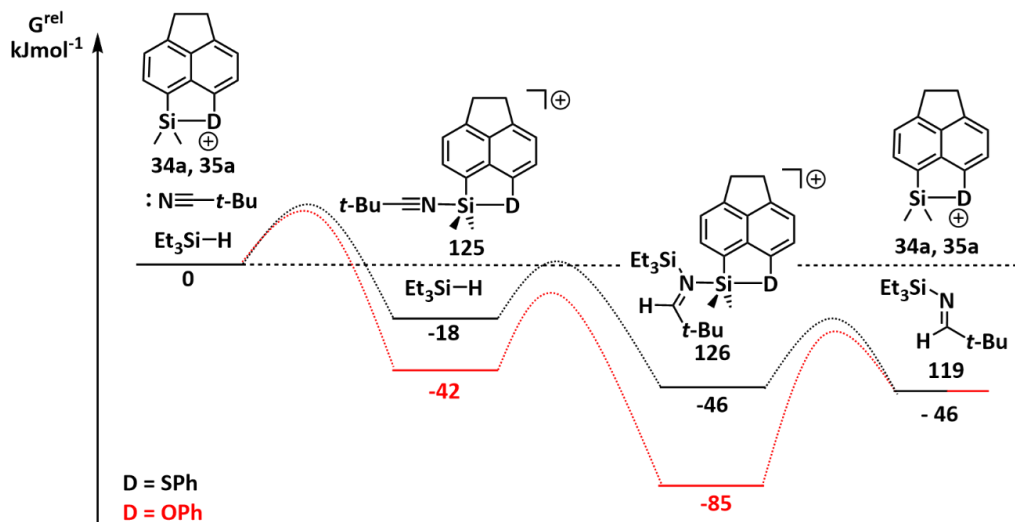


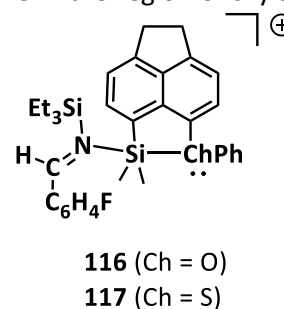
Figure 75 – Calculated relative free Gibbs energies of the hydrosilylation of nitriles with silyl chalconium ions **34a** and **35a** as catalyst via the formation of nitrilium ion (M06-2X/Def2-TZVP, SCRF(solvent=chlorobenzene), $p = 24.419$ MPa).

The free Gibbs energies of this reaction pathway were calculated for benzonitrile, acetonitrile and cyclohexanecarbonitrile as well. The results are summarized in Table 29. It becomes apparent, that the formation of nitrilium ions **125** and iminium ions **126** is an exothermic reaction in all cases (Table 29, a), b): $\Delta G = -11(-79) \text{ kJmol}^{-1}$). However, the heterolytic cleavage of the Si – N bond of iminium ions **126** is endothermic by 28-84 kJmol^{-1} . The only exception is the thionyl-stabilized *tert*-butyl-substituted iminium ion **125-S**. Here, the free Gibbs energy for the heterolytic cleavage of the Si – N bond is $\Delta G = 0 \text{ kJmol}^{-1}$, suggesting that reaction c) is an equilibrium for this substitution pattern.

Table 29 – Calculated free Gibbs energies for the hydrosilylation reaction of nitriles with silyl chalconium ions **34a** and **35a** as catalyst: LA/LB adduct mechanism (M06-2X/Def2-TZVP, SCRF(solvent=chlorobenzene), $p = 24.419$ MPa).

R	D	a) ΔG [kJmol ⁻¹]	b) ΔG [kJmol ⁻¹]	c) ΔG [kJmol ⁻¹]
<i>t</i> -Bu	SPh	-18	-27	0
<i>t</i> -Bu	OPh	-42	-43	+39
Ph	SPh	-11	-78	+28
Ph	OPh	-43	-78	+60
Me	SPh	-20	-76	+56
Me	OPh	-44	-79	+84
Cy	SPh	-13	-78	+51

Experimental indications for the formation of the intermediate phenoxy-stabilized silyliminium ion **125-O** and thiophenyl-stabilized silyliminium ion **126-S** were found. The ²⁹Si INEPT NMR spectrum of a reaction mixture of the hydrosilylation reaction of pivalonitrile with Et₃SiH using silylsulfonium borate **35a**[B(C₆F₅)₄] as a catalyst shows in addition to imine **119** and amine **120**, two additional ²⁹Si NMR chemical shifts at $\delta^{29}\text{Si} = 30.9$ and 46.2 (Figure 76). These signals are in the region of silylated iminium ions **116**, **117** (see Chapter 3.8.2). If the assumption of the equilibrium between iminium ion **126-S** and silyl cation **35a** plus hydrosilylation product **119** is correct, it is expected that iminium ion **126-S**, instead of the catalyst, silyl cation **35a**, would be present at the end of the reaction, since imine **119** is in excess present in the mixture and the equilibrium would shift in favor of iminium ion **126-S**.



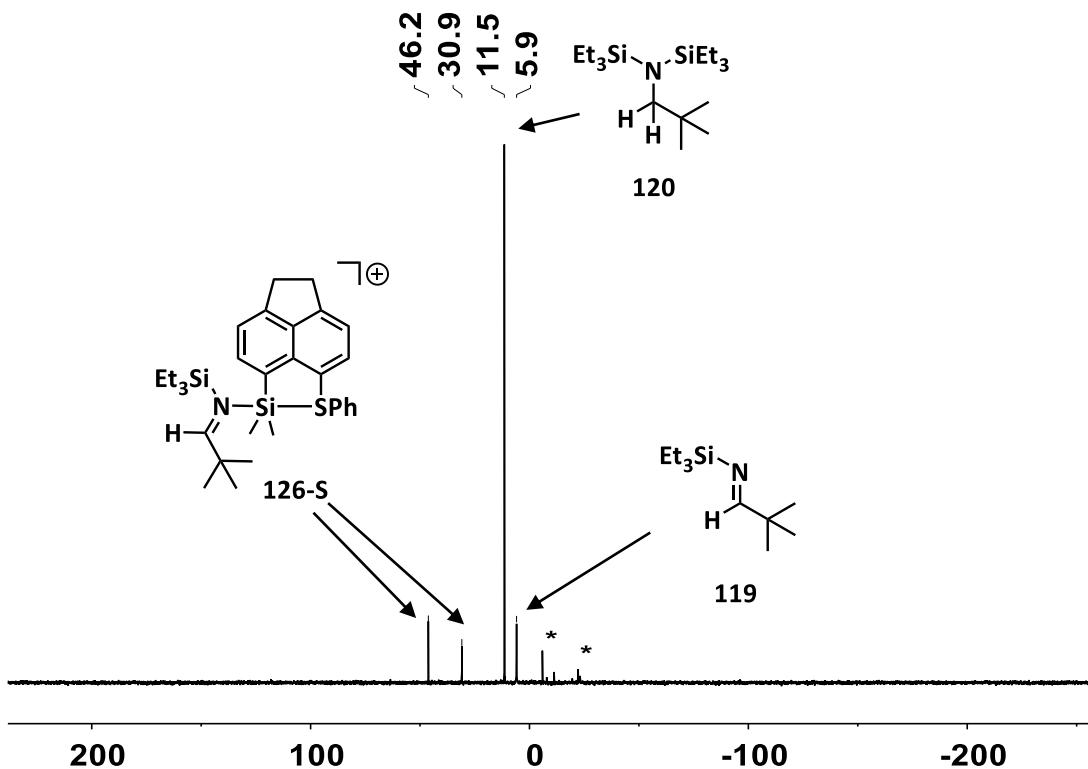


Figure 76 – ^{29}Si INEPT NMR spectrum (99 MHz, 305 K, $\text{C}_6\text{H}_4\text{Cl}_2$, $D1 = 0.0084$, $D4 = 0.0313$, *impurities) of the reaction mixture of the hydrosilylation reaction of pivalonitrile with triethylsilane using thiophenyl stabilized silyl borate **35a** $[\text{B}(\text{C}_6\text{F}_5)_4]$ as catalyst.

Evidence for the formation of nitrilium ion **125-O** was obtained via X-ray diffraction analysis. Even though the quality of the crystals was not good because of their small size and impurities within the crystal, the topology of the molecule could be secured (Figure 77). Pivalonitrile coordinates to the silicon atom and is *anti* relative to the oxygen atom and the oxygen atom exhibits a trigonal planar coordination sphere.

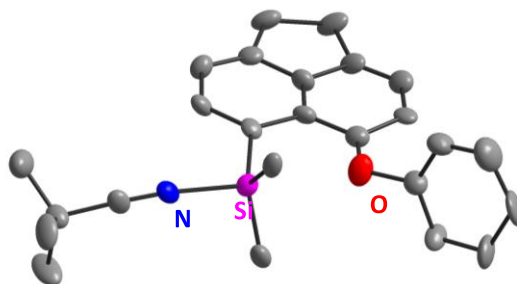
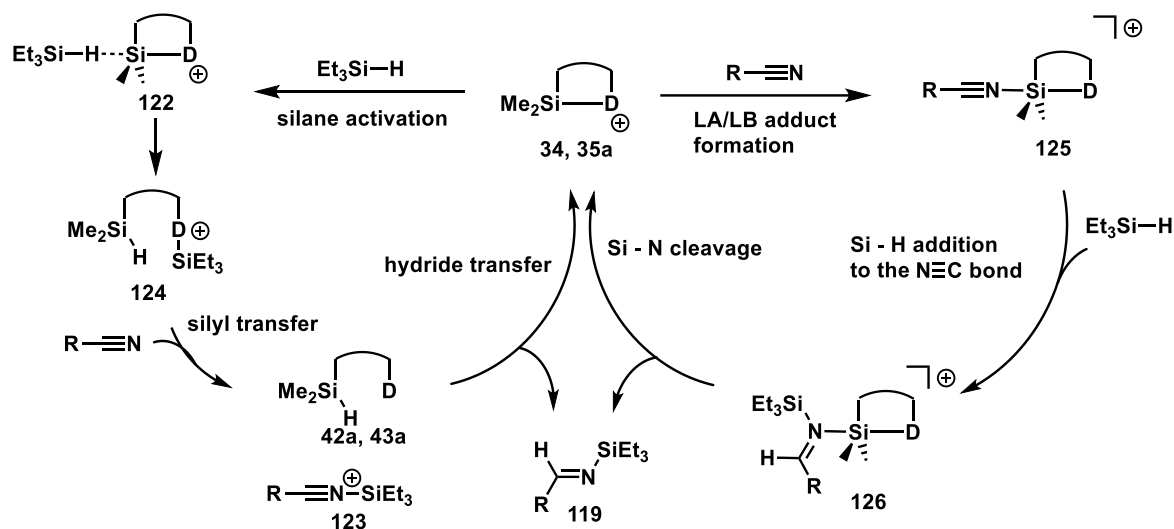


Figure 77 – Molecular structure of silyl nitrilium ion **125-O** in the crystal of **125-OCu** $[\text{B}_{12}\text{Br}_{12}]$ (thermal ellipsoids at 25 % probability, H atoms and counter ion are omitted for clarity).

In summary, three different pathways for the hydrosilylation reaction of nitriles using silylchalconium ions **34a** and **35a** as catalysts were investigated. The first mechanism includes the Si – H activation of triethylsilane via the formation of the Si – H – Si three-center two-electron bond between silyl cations **34a** and **35a** and triethylsilane (compound **122**) and in the second pathway the subsequent formation of silyl chalconium ion **124** from complex **122** was considered. The third mechanism starts with the formation of a LA/LB adduct between silyl cation **34a** or **35a** and the nitrile (species **125**) (Scheme 80).



Scheme 80 – Proposed mechanisms for the hydrosilylation reaction of nitriles using silyl chalconium ions **34a** and **35a** as catalyst.

According to the calculations, the Si – H activation is predicted to be an endothermic reaction for both silyl cations **34a** and **35a** while the formation of nitrilium ion **125** is exothermic (Figure 78).

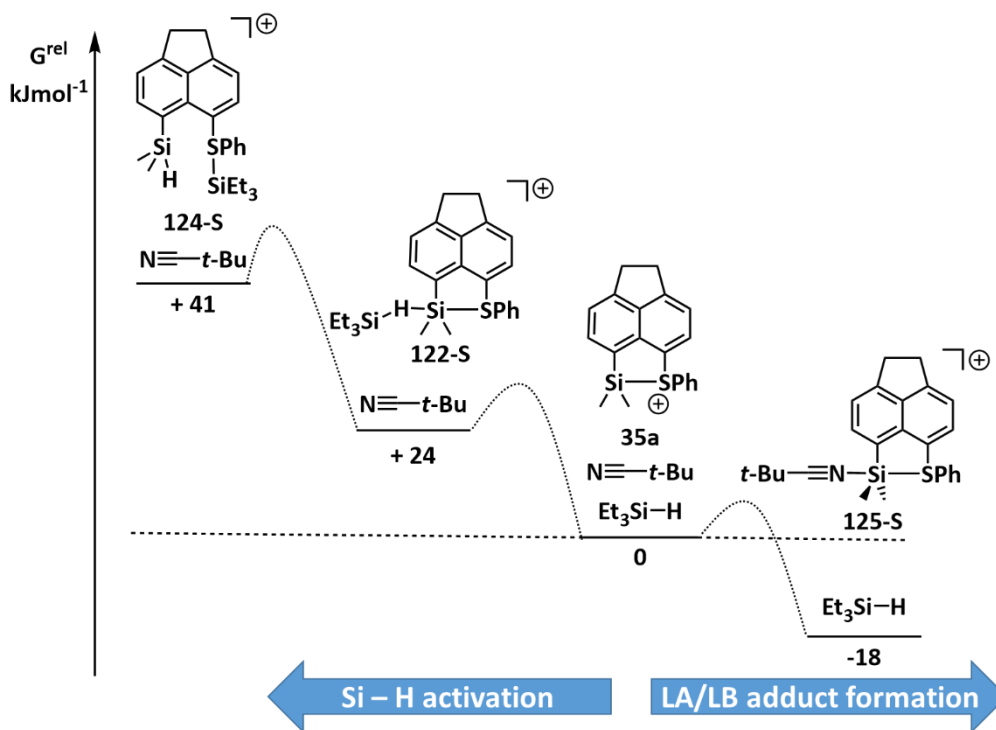
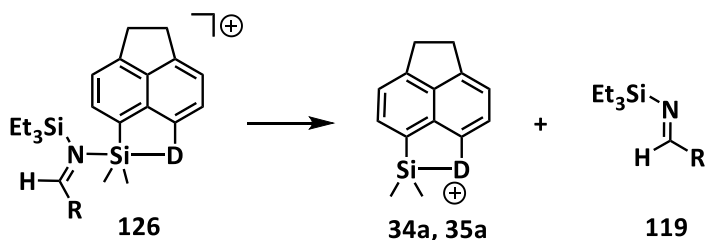


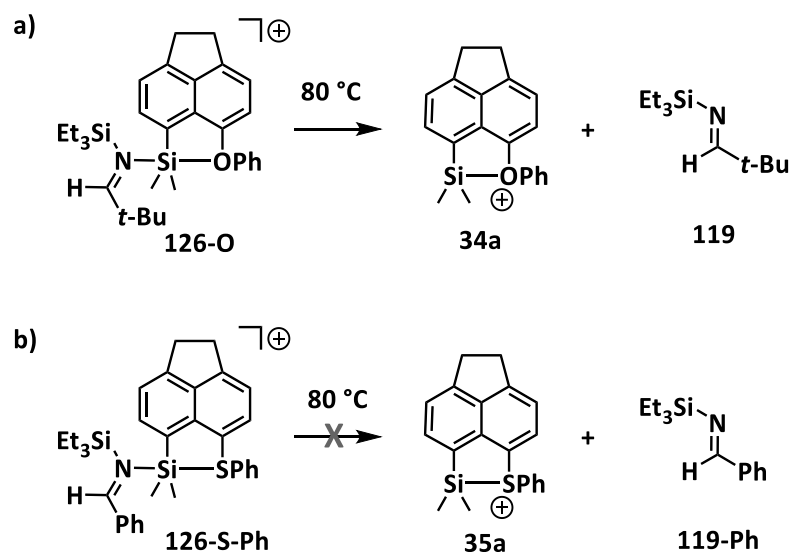
Figure 78 – Comparison of the calculated free Gibbs energies of the initial steps of both mechanisms, Si – H activation and LA/LB adduct formation for silyl sulfonium ion **35a** (M06-2X/Def2-TZVP, SCRF(solvent=chlorobenzene, $p = 24.419$ MPa)).

Considering the experimental results that reveal that silyl cations **34a** and **35a** are selective for pivalonitrile, the calculation results are reasonable. If one of the first two pathways is the underlying reaction pathway, the reaction should take place with benzonitrile as well as pivalonitrile; however, this is not the case. In the third mechanism, the last step, namely the cleavage of the Si – N bond of iminium ions **126** to release the hydrosilylation product **119** and silyl cation **34a** or **35a** is the rate-limiting step (Scheme 81). The following applies: the stronger the Si – N bond, the less likely is the bond dissociation. As a consequence, this explains, why the more Lewis acidic silyloxonium ion **34a** is less reactive in the hydrosilylation reaction of pivalonitrile.



Scheme 81 – Last step of the third mechanism (LA/LB pathway) of the hydrosilylation reaction of nitriles using silyl cations **34a** or **35a** as catalysts.

However, there is still an inconsistency. According to the calculations, the cleavage of phenoxy-stabilized silyliminium ion **126-O** into silyl cation **34a** and hydrosilylation product **119** is an endothermic reaction by 39 kJmol^{-1} . In the experiment, this reaction takes place via heating to $80 \text{ }^\circ\text{C}$ (Scheme 82, a)). However, the cleavage of thiophenyl-stabilized silyliminium ion **126-S-Ph** into the corresponding products **35a** and **119-Ph** is endothermic by 28 kJmol^{-1} . In contrast to the reaction of **126-O** into **34a** and **119** ($\Delta G = 39 \text{ kJmol}^{-1}$), the reaction with benzonitrile does not proceed via heating, despite the lower free Gibbs energy (Scheme 82, b)).



Scheme 82 – Cleavage of the Si – N bond of silyliminium ions **126-O** and **126-S-Ph** to release the catalyst **34a** and **35a** and the products **119** and **119-Ph**.

Moreover, it seems unreasonable that only pivalonitrile reacts and other alkyl-substituted nitriles do not. The calculations predict that, with acetonitrile and cyclohexanecarbonitrile, the last step of the reaction is endothermic by $51\text{-}84 \text{ kJmol}^{-1}$ (Table 29). The only reasonable explanation might be the different steric demand of the substituents. The steric demand of organic moieties can be compared via the *A value*. This value is based on the conformational analysis of mono-substituted cyclohexenes and is the energy difference between the axial and the equatorial conformers.^[66, 109] In Table 30, the *A value* for the substituents of the nitriles tested are listed in comparison to the calculated free Gibbs energy of the heterolytic cleavage of the Si – N bond in thiophenyl-substituted iminium ions **126-S**. Notably, the free Gibbs energy for the Si – N cleavage decreases when the steric demand increases. Hereby, the order of the steric demand reflects the order given by the free Gibbs energies.

Table 30 – Comparison of the steric demand of organic substituents (*A value*)^[66, 109] and the calculated free Gibbs energy for the heterolytic cleavage of the Si – N bond in thiophenyl substituted iminium ions **126-S** (M06-2X/Def2-TZVP, SCRF(solvent=chlorobenzene, *p* = 24.419 MPa).

Substituent	<i>A value</i> [kJmol ⁻¹]	ΔG [kJmol ⁻¹]
Me	7	+56
Cy	9	+51
Ph	12	+28
<i>t</i> -Bu	20	0

In conclusion, the DFT studies on the mechanism of the hydrosilylation reaction of nitriles using silylchalconium ions **34a** and **35a** as catalysts suggest that the reaction proceeds via the formation of the LA/LB adduct, nitrilium ions **125**, and not as described for the related reaction with BCF as Lewis acid via the Si – H activation. This conclusion is supported by the experimental results that show the limited scope of silyl cations **34a** and **35a**. Only the hydrosilylation reaction of pivalonitrile was catalyzed by silyl cations **34a** and **35a**. If the reaction would proceed via the Si – H activation, the hydrosilylation reaction of other nitriles using silyl cations **34a** and **35a** should also be possible, but this is not the case. The DFT calculations show that the crucial step of the reaction is the release of the catalyst **34a** or **35a** and the formation of the product **119**. The Si – N cleavage depends on the steric demand of the substituent, and thus, only the tert-butyl group of pivalonitrile is bulky enough.

3.8.3.3 Diels Alder Reaction

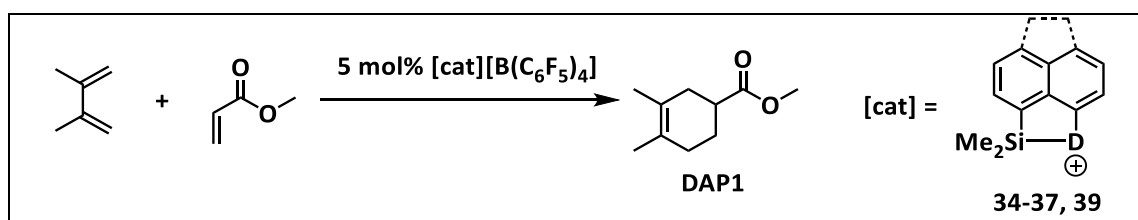
Another standard reaction catalyzed by Lewis acids is the Diels-Alder cyclization. Therefore, the presented silyl borates were tested as catalyst in various Diels-Alder test reactions. The first reaction chosen was the Diels-Alder cyclization of 2,3-dimethylbuta-1,3-diene with methyl acrylate as dienophile. The catalysts tested were dimethylsilyl borates **34a**[B(C₆F₅)₄], **35a**[B(C₆F₅)₄], **36a**[B(C₆F₅)₄], **37a**[B(C₆F₅)₄] and **39**[B(C₆F₅)₄]. The reaction was carried out either in dichloromethane at -80 °C or in chlorobenzene at r.t. with a catalyst charge of 5 mol% (Table 31). Entries 1-4 reveal the different catalytic activities of chalcogenyl-stabilized silyl borates **34a**[B(C₆F₅)₄], **36a**[B(C₆F₅)₄], **37a**[B(C₆F₅)₄] and **39**[B(C₆F₅)₄]. The isolated yield of Diels-Alder product **DAP1** is highest using acenaphthyl-substituted silyloxonium borate **34a**[B(C₆F₅)₄] as catalyst (yield = 75 %). In contrast, naphthyl-substituted thiophenyl-stabilized derivative **37a**[B(C₆F₅)₄] gave 24 % and selenyl-stabilized derivative **39**[B(C₆F₅)₄] gave 9 %.

To rule out the possibility of proton catalysis in this reaction out, it was repeated with acenaphthyl-substituted thiophenyl-stabilized derivative **35a** in the presence of the proton sponge 2,6-di-tert-butyl-4-methyl pyridine (DTBMP) (Entry 5). This time the reaction was carried out at r.t. and the GC measurement revealed, that the reaction was not complete, but the significant conversion (33 %) shows unambiguously that silyl cation **35a** catalyzes this reaction.

Table 31 – Results of the Diels Alder cyclization of 2,3-dimethylbuta-1,3-diene and methyl acrylate using silyl borates **34a**[B(C₆F₅)₄], **35a**[B(C₆F₅)₄], **36a**[B(C₆F₅)₄], **37a**[B(C₆F₅)₄] and **39**[B(C₆F₅)₄] as catalysts.

Entry	Catalyst	Catalyst charge	Reaction conditions	t [h]	Yield
1	36 (Naph, D = OPh)	5 mol%	DCM, -80 °C	1	65 % ^{a)}
2	37a (Naph, D = SPh)	5 mol%	DCM, -80 °C	1	24 % ^{a)}
3	39 (Naph, D = SePh)	5 mol%	DCM, -80 °C	1	9 % ^{a)}
4	34a (Ace, D = OPh)	5 mol%	DCM, -80 °C	1.5	75 % ^{a)}
5 ^{c)}	35a (Ace, D = SPh)	5 mol%	C ₆ H ₅ Cl, r.t.	1.5	33 % ^{b)}
6	-	-	DCM or C ₆ H ₅ Cl, r.t.	24	0 % ^{b)}

a) Isolated yield, b) GC yield, c) DTBMP added



The difference in the catalytic activity of chalcogenyl-stabilized silyl cations reflect nicely the order given by the Lewis acidity scale of the ^{19}F NMR resonance of the corresponding nitrilium ions as discussed in Chapter 3.8.1 (Figure 79).

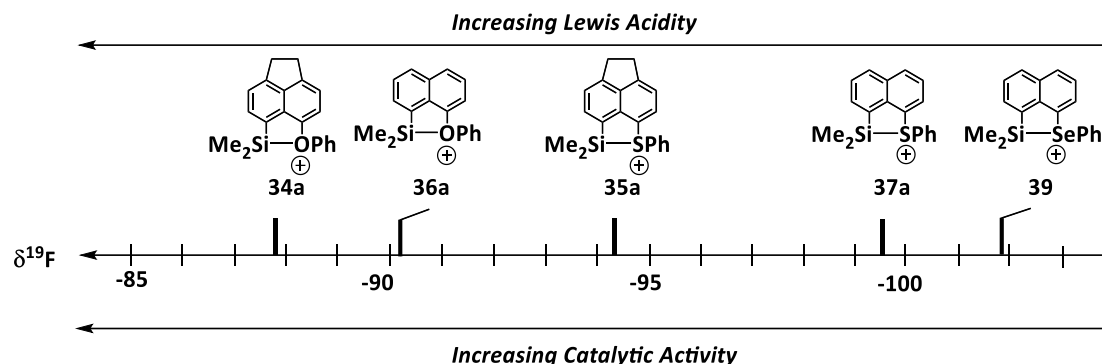


Figure 79 – Lewis acidity scale of intramolecularly stabilized silyl cations **34-37**, **39** based on the ^{19}F NMR chemical shift of the corresponding FBN nitrilium ions.

In the next step, enantioenriched chiral silyl borates **34b**[B(C₆F₅)₄], **35b**[B(C₆F₅)₄] and **37b**[B(C₆F₅)₄] should be used as catalysts to investigate if the stereo information is transferred from the cation to the Diels-Alder product. Unfortunately, the reaction of 2,3-dimethylbuta-1,3-diene with methyl acrylate as dienophile was not suitable for this purpose, since **DAP1** did not show a separation of the enantiomers at the chiral GC. The analysis via chiral GC is important to calculate the enantiomeric excess of the formed product. Therefore, other Diels-Alder test reactions were performed in order to find a reaction product, which is easy to analyze with locally available methods. The first test reaction was the cyclization of cyclopentadiene and acryl acetate to give **DAP2**. The reaction was carried out in C₆H₅Cl at -30 °C and in the presence of the proton sponge DTBMP. The results are summarized in Table 32. All experiments yielded in complete conversion of the substrates within one hour (determined via GC). Even the less reactive sulfonium borates **35**[B(C₆F₅)₄] show complete conversion. The substitution pattern at the silicon does not affect this as shown with derivative **35c** which exhibits the bulky *tert*-butyl moiety (Entry 4). To test whether the reaction takes place without catalyst, a sample with the two substrates and the proton sponge in chlorobenzene was stored at room temperature. The GC analysis shows 82 % of conversion after one hour at r.t. (Table 32, Entry 5). Consequently, no catalyst is needed to obtain **DAP2**. However, if the reaction is done without catalyst, a bad endo/exo ratio of 76:24 is obtained and the reaction is relatively slow compared to the reactions with catalysts **34a** and **35**. Here, with catalysts **34a** and **35a**, complete conversions are

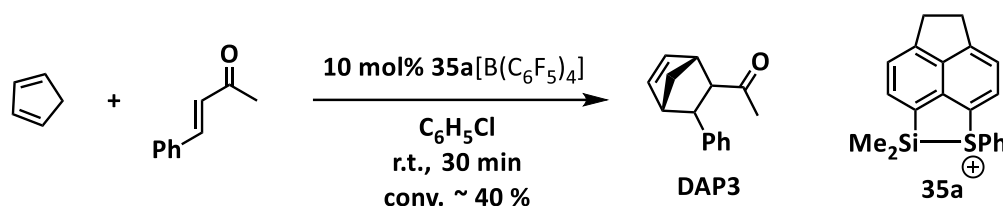
obtained within one hour at -30 °C and the endo/exo ratio is improved compared to the control sample.

Table 32 – Results of the Diels Alder cyclization of cyclopentadiene with acryl acetate catalyzed by silyl borates **34a**[B(C₆F₅)₄], **35a**[B(C₆F₅)₄], **35b**[B(C₆F₅)₄] and **35c**[B(C₆F₅)₄] (the yield and the endo/exo ratio were determined via GC).

Entry	Catalyst	Catalyst charge	Reaction conditions	time	Conversion	Endo:Exo
1	34a (R = Me, D = OPh)	5 mol%	C ₆ H ₅ Cl, -30 °C	1 h	100 %	94:6
2	35a (R = Me, D = SPh)	5 mol%	C ₆ H ₅ Cl, -30 °C	1 h	100 %	93:7
3	35b (R = Ph, D = SPh)	5 mol%	C ₆ H ₅ Cl, -30 °C	1 h	99 %	92:8
4	35c (R = <i>t</i> -Bu, D = SPh)	5 mol%	C ₆ H ₅ Cl, -30 °C	1 h	100 %	89:11
5	-	-	C ₆ H ₅ Cl, r.t.	1 h	82 %	76:24

DAP2 was separated at the chiral GC. Nonetheless, this Diels-Alder reaction was not suitable for the use as standard test reaction. The fact, that the cyclization takes place without catalyst is problematic. Even if the cyclization is slow, the endo/exo and the enantiomeric ratio can be falsified due to this. Furthermore, the substrates cannot be stored together and the substrate mixture has always to be prepared freshly, which makes this test reaction impractical.

The next consideration was the reaction of cyclopentadiene with 4-phenylbut-3-en-2-one as dienophile. For an initially test, the reaction was carried out using thiophenyl-stabilized dimethylsilyl borate **35a**[B(C₆F₅)₄] with a catalyst charge of 10 mol% in chlorobenzene at r.t. (Scheme 83). The reaction is slow under these conditions and the enantiomers of **DAP3** could not be separated at the chiral GC.



Scheme 83 – Diels Alder cyclization of cyclopentadiene with 4-phenyl-3-en-2-one catalyzed by thiophenyl stabilized silyl borate **35a**[B(C₆F₅)₄].

In the end, the Diels-Alder reaction of cyclohexadiene with acryl acetate was tested (Table 33). This substrate combination has the advantage, that the cyclization does not occur without catalyst at ambient conditions and the substrates can be stored as a mixture for several days. Initially, the reaction was carried out with the dimethylsilyl derivatives **34a** and **35a** as catalysts (Table 33, Entry 1, 2). The substrates were added to the catalyst at 0 °C and the mixture was stirred for 0.5 to 1 h while warming slowly to room temperature. Complete conversion and a good endo/exo ratio of 99:1 were obtained. Phenylmethylsilyl-substituted oxonium borate **34b**[B(C₆F₅)₄] shows as well a good catalytic activity under these conditions (100% conv., endo/exo = 99:1, Entry 3). However, with phenylmethylsilyl-substituted sulfonium borate **35b**[B(C₆F₅)₄] the reaction is slower and stops after 50 % conversion. Nevertheless, the enantiomerically enriched (+)-silane **43b** was used as precursor in the next attempt. The substrates were added at 0 °C and the reaction was stirred for 1.5 h under warming to room temperature. The GC analysis shows only 34 % conversion and the chiral GC reveals the racemic mixture of **DAP4**. In a next attempt, naphthyl derivative, sulfonium ion **37b** was used under the same conditions with (+)-silane **44** as precursor. Surprisingly, with catalyst **37b** complete conversion was obtained, while with the corresponding acenaphthyl derivative **35b** only 34 % conversion was observed. A reason might be a higher stability of naphthyl derivative **37b**. The decomposition of acenaphthyl derivative **35** would explain, why the reaction stopped after max. 50 % conversion. Unfortunately, despite the good catalytic activity of naphthyl derivative **37b**, no enantiomeric enrichment of **DAP4** was found as well. Since the experiments regarding the chiral memory of silyl cations **34b**, **35b** and **37b** showed, that they undergo fast racemization at room temperature, the Diels-Alder reaction was tested at -40 °C. This time oxonium borate **34b**[B(C₆F₅)₄] was used, since it shows a higher Lewis acidity and catalytic activity even at lower temperatures as thiophenyl-stabilized derivatives **35**. However, under these conditions, the catalytic activity of oxonium borate **34b**[B(C₆F₅)₄] is not good as well. Moreover, the small amount of **DAP4** which was obtained, does not have a measurable enantiomeric excess.

Table 33 – Results of the Diels Alder cyclization of cyclohexadiene with acryl acetate catalyzed by silyl borates **34a,b**[B(C₆F₅)₄], **35a,b**[B(C₆F₅)₄] and **37b**[B(C₆F₅)₄] (the yield and the endo/exo ratio were determined via GC, DTBMP was added in all attempts except Entry 7).

Entry	Catalyst	Cat. charge	T [°C]	t [h]	Conv.	Endo:Exo	ee [%]
1	34a (Ace, D = OPh, R = Me)	5 mol%	0 → r.t.	1	100 %	99:1	-
2	35a (Ace, D = SPh, R = Me)	5 mol%	0 → r.t.	0.5	100 %	99:1	-
3	34b (Ace, D = OPh, R = Ph)	5 mol%	0 → r.t.	0.5	100 %	99:1	-
4	35b (Ace, D = SPh, R = Ph)	3 mol%	r.t.	1.5	50 %	98:2	-
5*	35b (Ace, D = SPh, R = Ph)	3 mol%	0 → r.t.	1.5	34 %	-	0
6*	37b (Naph, D = SPh, R = Ph)	5 mol%	0 → r.t.	0.5	100 %	98:2	0
7*	34b (Ace, D = OPh, R = Ph)	5 mol%	-40	0.5	25 %	-	0

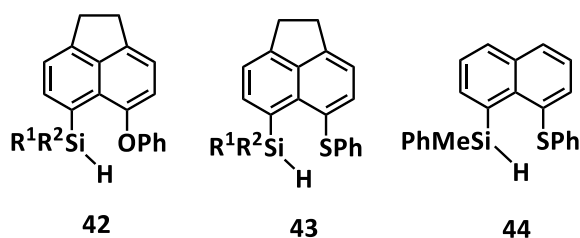
* Enantioenriched silane as precursor.

In conclusion, in the asymmetric Diels-Alder reactions the stereo information of chiral silyl cations **34b**, **35b** and **37b** was not transferred to the Diels-Alder product **DAP4**. Reasons for the loss of the stereo information is probably the reaction temperature. In Chapter 3.3.3, the experiments regarding the chiral integrity of silyl cations **34b**, **35b** and **37b** revealed that only at lower temperatures (-40 °C) no racemization takes place. However, the here tested asymmetric Diels-Alder reaction proceeds only at room temperature. Nevertheless, the tested silyl borates **34a,b**[B(C₆F₅)₄], **35a,b**[B(C₆F₅)₄], **36a**[B(C₆F₅)₄], **37a,b**[B(C₆F₅)₄] and **39**[B(C₆F₅)₄] show a good to moderate activities as catalysts in Diels-Alder reactions. In particular, the comparison of the dimethylsilyl borates **34a**[B(C₆F₅)₄], **35a**[B(C₆F₅)₄], **36a**[B(C₆F₅)₄], **37a**[B(C₆F₅)₄] and **39**[B(C₆F₅)₄] reveals a distinct activity of silylchalconium ions in relation to the donor substituent. Hereby, the order of the catalytic activity is OPh>SPh>SePh (Figure 79). This order reflects the order of the Lewis acidity scale using FBN as a probe and supports the prediction made regarding the reactivity of silylchalconium ions.

4 Summary and Future Perspectives

The focus of this work was the synthesis and characterization of intramolecularly phenoxy- and thiophenyl-stabilized silyl borates **34**[B(C₆F₅)₄], **35**[B(C₆F₅)₄] and **37**[B(C₆F₅)₄] with the naphthyl or acenaphthyl scaffold as backbone and the investigation of their reactivity and catalytic activity in hydrosilylation and Diels-Alder reactions. In this context, the analysis of the interaction between the silyl group and the stabilizing moiety, OPh or SPh, was of interest.

A variety of precursor silanes **42**, **43** and **44** with different substitution pattern was synthesized and fully characterized by multinuclear NMR and IR spectroscopy as well as X-ray diffraction (XRD) analysis. Hereby, the synthesis of thiophenyl-substituted derivatives **43** was performed by modification of the previous synthesis introduced by N. Kordts.^[6a, 87a] Instead of starting with installing the silyl group, the thiophenyl group was installed first. In this way, the introduction of different substitution patterns at the silyl substituent is more efficient (Chapter 3.1.1).



a: R¹ = R² = Me

b: R¹ = Me, R² = Ph

c: R¹ = Me, R² = *t*-Bu

d: R¹ = H, R² = Ph

Furthermore, the interactions of the *peri*-atoms in acenaphthyl silanes **42** and **43** were discussed. Structural parameters such as *peri*-distances, sum of the bay angles and out-of-plane distances in the crystal structures were disclosed. An interaction either between the hydrogen and the chalcogen atom (*syn*-conformers) or between the silicon and the chalcogen atom (*anti*-conformers, Figure 80) were indicated by QTAIM analysis.^[75] These indications are supported for the *anti*-structures by the geometrical goodness (($\Delta\Sigma(\Theta)$)) suggesting a beginning S_N2 reaction at the silicon center with the chalcogen atom as nucleophile and the hydride as leaving group. This suggestion is supported experimentally by the IR absorption band of the Si – H stretching vibration, which reflects the relative strength of the Si – H bond. The *anti*-structures show a bathochromic shift compared to the *syn*-structures, indicating the weakening of the Si – H bond in *anti*-structures (Chapter 3.1.4).

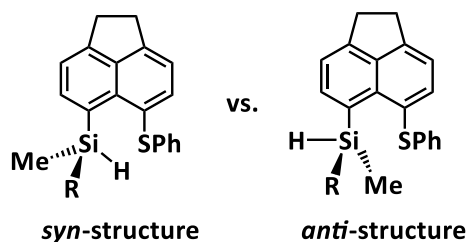
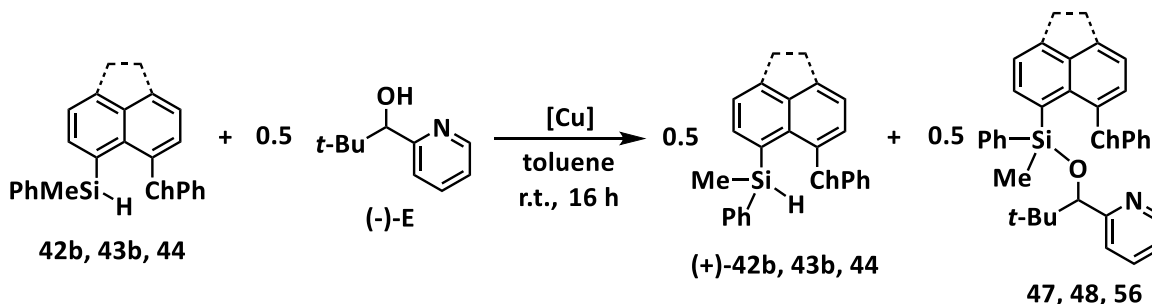


Figure 80 – *syn*- and *anti*-structures of silanes **43a,b,c** (R = Me (a), Ph (b), t-Bu (c)).

With regard to asymmetric catalysis, the chiral resolution of asymmetric-substituted silanes **42b**, **43b** and **44** was performed. Three different routes were tested, whereby the kinetic resolution by dehydrogenative, copper-catalyzed Si – O coupling turned out to be the method of choice for this system (Scheme 84). In the process, the biggest challenge was caused by a too close relation in properties of the resulting diastereomers or inertness of silanes against chiral auxiliaries. Nevertheless, enantiomeric enrichment of silanes **42b**, **43b** and **44** was obtained with good to moderate enantiomeric excesses (ee = 54-84 %) (Chapter 3.1.3).



Scheme 84 – Kinetic resolution of silanes **42b**, **43b** and **44** by the dehydrogenative Si – O coupling with an enantiomerically enriched alcohol (-)-E (**42b**, **47**: ace, Ch = O; **43b**, **48**: ace, Ch = S; **44**, **56**: naph, Ch = S).

Precursor silanes **42**, **43** and **44** were treated with trityl borate $[\text{Ph}_3\text{C}][\text{B}(\text{C}_6\text{F}_5)_4]$ to obtain the corresponding silyl borates **34** $[\text{B}(\text{C}_6\text{F}_5)_4]$, **35** $[\text{B}(\text{C}_6\text{F}_5)_4]$ and **37** $[\text{B}(\text{C}_6\text{F}_5)_4]$, which were fully characterized by multinuclear NMR spectroscopy. The results of the NMR spectroscopy, XRD analysis and DFT calculations reveal remarkable structural differences between silyloxonium and silylsulfonium ions **34** and **35/37**. While the oxygen atom in species **34** shows a trigonal planar coordination sphere, the sulfur atom in species **35/37** is trigonal pyramidal coordinated (Figure 81) (Chapters 3.2, 3.3).

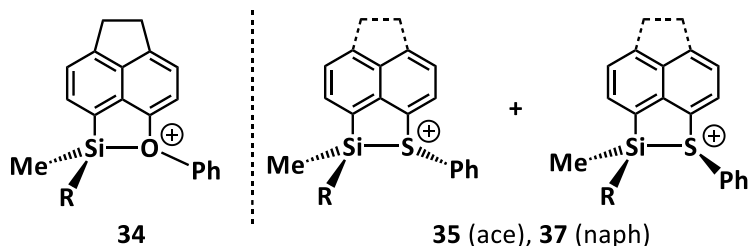


Figure 81 – Comparison of the coordination environment of the oxygen and sulfur atom in silyl chalconium ions **34** and **35/37** ($R^1 = R^2 = \text{Me}$ (a); $R^1 = \text{Me}$, $R^2 = \text{Ph}$ (b); $R^1 = \text{Me}$, $R^2 = t\text{-Bu}$ (c); $R^1 = \text{H}$, $R^2 = \text{Ph}$ (d)).

The trigonal planar coordination sphere of oxonium ions **34** contrasts the results of Ducos et al.. Silyl cation **28a** exhibits an oxygen atom with a certain trigonal pyramidalization ($\Sigma\alpha(\text{O}) = 344^\circ$). Therefore, the coordination environment of silyloxonium ions **34**, **36**, **72** and **73** was investigated by low temperature NMR experiments and DFT studies. Furthermore, the structures of model compounds **76**, **77** and **78** were calculated for comparison. The results demonstrate, that the substitution pattern at the silicon and the oxygen atom does not influence the coordination environment of the oxygen atom. Instead, the backbone and the intramolecular stabilization are an important factor for the coordination sphere of the oxygen atom. Especially the binaphthyl backbone forces the oxygen atom into a trigonal pyramidal coordination sphere (Figure 82) (Chapter 3.2.1).

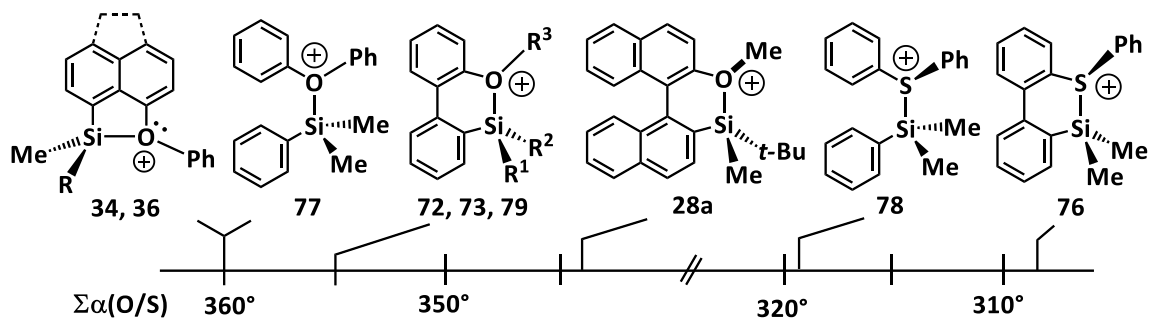
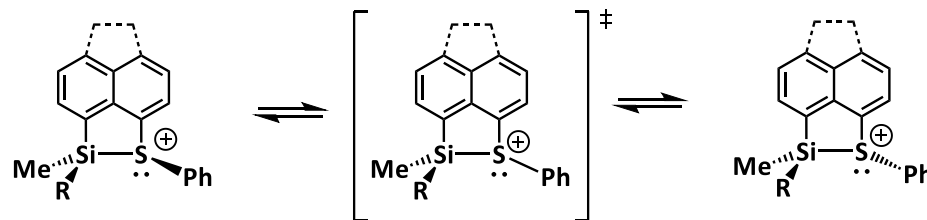


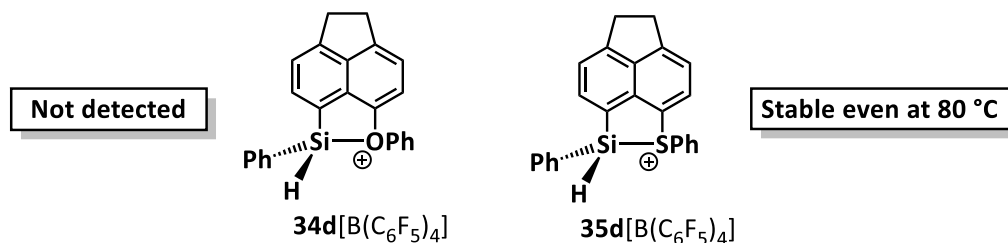
Figure 82 – Comparison of the sum of the bond angles around the oxygen or sulfur atom in silyloxonium and -sulfonium ions (silyloxonium ions **36**, **79**: XRD; silyloxonium ion **34**, **72**, **73**: DFT; model compounds **76**, **77**, **78**: DFT (model compounds were not synthesized and served only for theoretical comparison)).

High temperature NMR experiments of silylsulfonium ions **35** and **37** show a dynamic process within the molecule, visible by a significant line broadening and coalescence of the signals of the methyl groups at the silicon atom. As possible underlying processes the Si – S bond dissociation and the inversion process of the sulfur atom were discussed. Experimentally determined and by DFT methods calculated energy barriers strongly suggest the inversion process of the sulfur atom as underlying dynamic process (Scheme 85) (Chapter 3.5).



Scheme 85 – Inversion of the configuration of the sulfur atom in silylsulfonium ions **35** (ace) and **37** (naph, R = Me (a), Ph (b), t-Bu (c)).

This process was also observed in hydrogen-substituted silylsulfonium borate **35d**[B(C₆F₅)₄]. Species **35d** was characterized by multinuclear NMR spectroscopy, is stable for several days in benzene and does not decompose even under heating to 80 °C in toluene. Its stability is quite remarkable regarding the high lability of secondary silyl cations described in the literature.^[53a, 92] In the progress of this investigations, it was shown, that the thiophenyl group exhibits a better stabilizing effect than the phenoxy group. While silylsulfonium ion **35d** shows a high stability, silyloxonium ion **34d** could not be isolated or detected despite complete consumption of the precursor silane **42d**. Not even addition of a nitrile for further stabilization allowed to draw conclusions regarding the existence of silyloxonium ion **34d** (Chapter 3.4).



Chiral silyl cations **34b**, **35b** and **37b** were examined regarding their chiral integrity by treating the enantiomeric enriched silanes **42b**, **43b** and **44** with trityl borate to generate chiral silyl borates **34b**[B(C₆F₅)₄], **35b**[B(C₆F₅)₄] and **37b**[B(C₆F₅)₄] and subsequent treatment with triethyl borohydride to regenerate the starting silane **42b**, **43b** and **44** (Scheme 86). Regenerated silanes **42b**, **43b** and **44** were examined regarding their enantiomeric excess by chiral HPLC. The results show that chiral silyl chalconium ions **34b**, **35b** and **37b** undergo racemization during this experiment. Racemization was slowed down and even prevented by a low reaction temperature (-40 °C). For the use of chiral silyl chalconium borates **34b**[B(C₆F₅)₄], **35b**[B(C₆F₅)₄] and **37b**[B(C₆F₅)₄] as catalysts that means that the asymmetrical catalytic reactions have to be carried out at low reaction temperatures to conserve the chiral information of the catalysts (Chapter 3.3.3).

product was observed. Reasons for the loss of the stereo information is probably the racemization of chiral silyl cations **34b**, **35b** and **37b** at room temperature (Chapter 3.8.3.3).

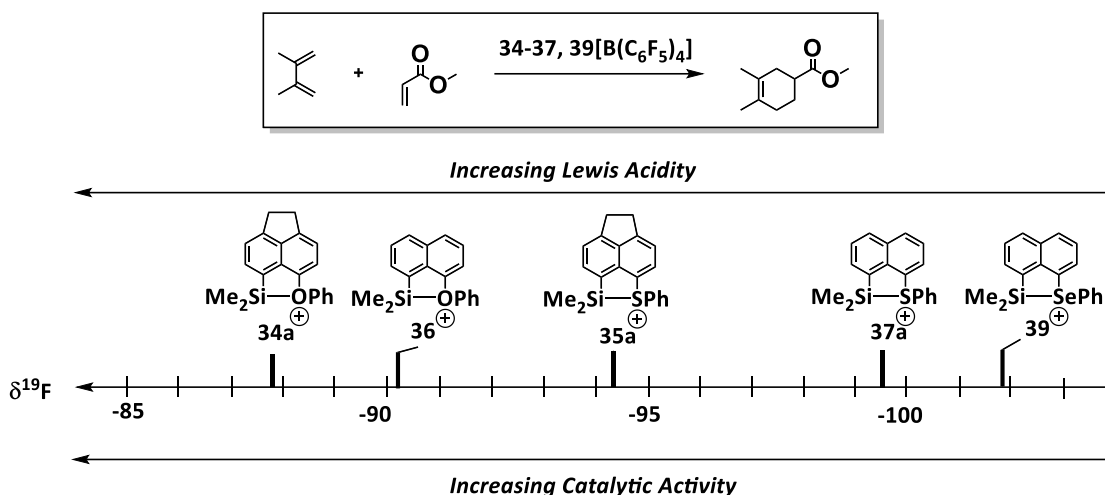
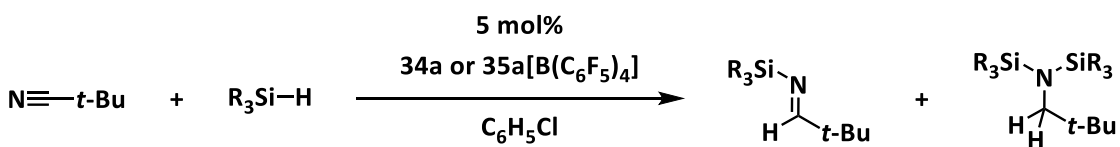


Figure 84 – Example for one Diels-Alder reaction tested and Lewis acidity scale of silylchalconium ions in relation to their catalytic activity.

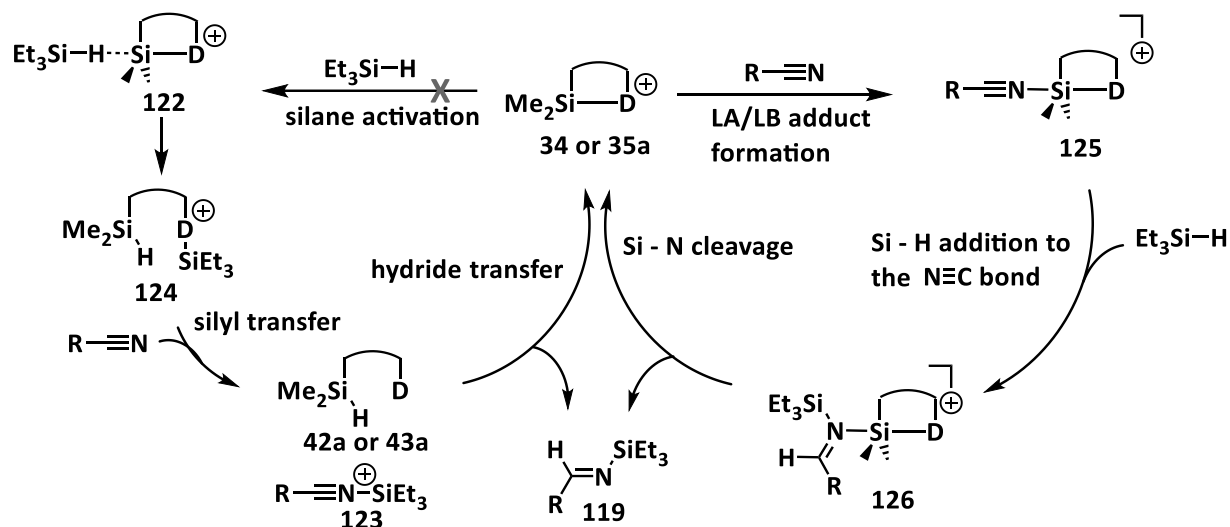
Regarding the hydrosilylation reaction of nitriles, silyl borates **34a** $[\text{B}(\text{C}_6\text{F}_5)_4]$ and **35a** $[\text{B}(\text{C}_6\text{F}_5)_4]$ show a catalytic activity against pivalonitrile (Scheme 89). Other substrates, such as 4-fluorobenzonitrile, benzonitrile, cyclohexanecarbonitrile and acetonitrile do not undergo the hydrosilylation reaction with silyl borates **34a** $[\text{B}(\text{C}_6\text{F}_5)_4]$ and **35a** $[\text{B}(\text{C}_6\text{F}_5)_4]$ as catalysts. This was a rather surprising result, since other Lewis acids show a good catalytic activity with all these substrates.^[50b, 106] Furthermore, phenoxy-stabilized silyl borate **34a** $[\text{B}(\text{C}_6\text{F}_5)_4]$ shows a lower catalytic activity in the hydrosilylation reaction of pivalonitrile in comparison to thiophenyl-stabilized derivative **35a** $[\text{B}(\text{C}_6\text{F}_5)_4]$ despite the higher Lewis acidity of silyl cation **34a** (Chapter 3.8.3.1).



Scheme 89 – Hydrosilylation reaction of pivalonitrile catalyzed by silyl borates **34a** $[\text{B}(\text{C}_6\text{F}_5)_4]$ and **35a** $[\text{B}(\text{C}_6\text{F}_5)_4]$.

The mechanism of the hydrosilylation reaction using silylchalconium ions **34a** and **35a** as catalysts was investigated by DFT calculations. Two different mechanisms were considered (Scheme 90). The first mechanism resembles the mechanism discussed in the literature for BCF catalyzed hydrosilylation reactions of ketones^[40a, 107] via the formation of a Si–H–Si three-center two-electron

bond between silyl cations and triethylsilane. The second mechanism was the classical LA/LB mechanism between silyl cation as the LA and the nitrile as the LB.

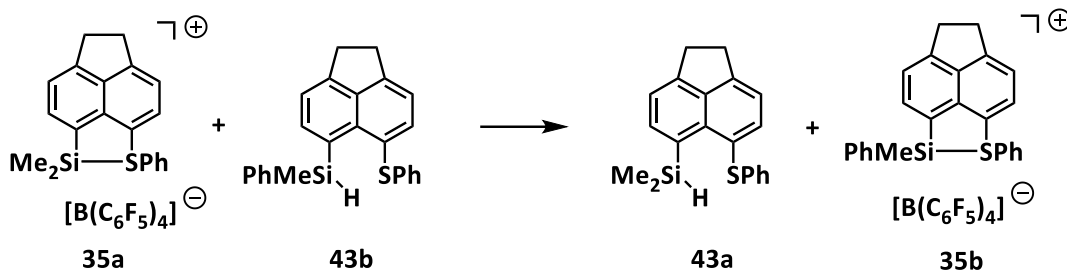


Scheme 90 – Proposed mechanisms for the hydrosilylation reaction using silyl cations **34a** and **35a** as catalysts.

According to the calculations, the Si – H activation is predicted to be an endothermic reaction for both silyl cations **34a** and **35a** and is therefore the rate-limiting step of this reaction pathway. In contrast, in the second mechanism, the rate-limiting step is the last step, namely the release of the hydrosilylation product and the regeneration of the catalyst **34a** or **35a**. In the experiments, the limited substrate scope of the catalysts **34a** and **35b** was revealed; in other words, only the hydrosilylation reaction of pivalonitrile was successful. If the rate-limiting step of the underlying mechanism would be the Si – H activation, the reaction should take place independent of the nitrile used as a substrate. However, if the rate-limiting step of the underlying mechanism is the release of the hydrosilylation product with the regeneration of the catalyst **34a** or **35a**, the effect of the substituent of the nitrile becomes an important factor. In consequence, this reaction pathway depends on the nitrile used as a substrate what gives rise to the conclusion, that the LA/LB pathway is the underlying mechanism.

In future investigations, the experimental proof of the Lewis acidity scale derived from the ^{19}F NMR chemical shift of FBN upon coordination to the silyl cation should be performed for the cases, in which the values of the ^{19}F NMR chemical shift and the $^1J_{\text{C,F}}$ coupling constant are close or the calculated scales (e.g. FIA) predict a different order compared to the NMR parameters. For example, for the dimethylsilyl and phenylmethylsilyl thiophenyl-stabilized derivatives **35a** and **35b** (Scheme

91) the calculations predict an inverse order compared to the experimental scales, $\delta^{19}\text{F}$ and $^1J_{\text{C,F}}$. Another example is the relative position of BCF, which shows distinct positions at both scales, $\delta^{19}\text{F}$ and $^1J_{\text{C,F}}$.



Scheme 91 – Hydride transfer reaction of silane **43b** with silyl cation **35a** to experimentally prove the order at the FBN Lewis acidity scale.

To date, the comparison of Lewis acids with different charges using calculated FIAs is problematic. In this context, it will be interesting to investigate, if the experimental scale using FBN as a probe gives better results. In general, the expansion of the Lewis acidity scale with other (intramolecularly or intermolecularly) stabilized and non-stabilized Lewis acids should be the focus of future investigations.

In terms of the catalytic activity of silylchalconium ions in hydrosilylation reactions, it is of interest to test other substrates such as ketones or aldehydes to further screen the scope of silyl cations **34a** and **35a**. In addition, it appears promising to also test selenyl-stabilized silyl cation **38** as a catalyst in the hydrosilylation reactions of nitriles. This work has shown, that the thiophenyl-stabilized silyl cation **35a** exhibits a higher catalytic activity in comparison to phenoxy-stabilized silyl cation **34a**, despite the silyl cation **34a** exhibits a higher Lewis acidity (Figure 85). The following applies: the higher the Lewis acidity of the catalyst is, the stronger is the bond of the catalyst with the hydrosilylation product and the less likely is the release of the product with regeneration of the catalyst. If the conclusion about the underlying mechanism is correct, the less Lewis acidic selenyl-stabilized silyl cation **38** should show a better catalytic activity than thiophenyl-stabilized silyl cation **35a** in the hydrosilylation reaction of nitriles.

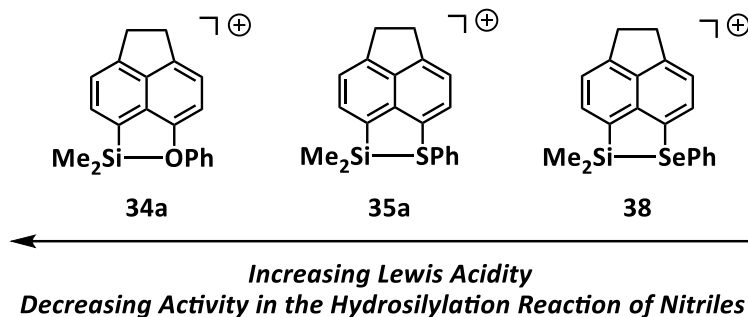
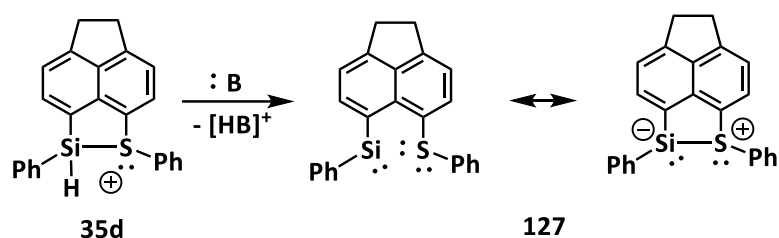


Figure 85 – Proposed order for the catalytic activity of silylchalconium ions **34a**, **35a** and **38** in the hydrosilylation reaction of nitriles.

Another topic for future investigations is the reactivity and catalytic activity of hydridosilyl cation **35d**. Furthermore, silyl cation **35d** is a promising precursor for the synthesis of the silylene **127**,^[92-93] which might be capable to activate small molecules such as H₂ and CO₂ and, therefore, provides new perspectives for this compound class.^[15e, 110]



Scheme 92 – Reaction of silyl cation **35d** with a base to generate silylene **127**.

5 Experimental Part

5.1 General Remarks

All experiments were carried out under argon or nitrogen atmosphere using Schlenk techniques. The glass equipment was stored in an oven at 120°C, evacuated and flushed with argon or nitrogen prior to use. The solvents *n*-pentane, *n*-hexane, benzene, tetrahydrofuran and diethyl ether were dried over sodium-potassium alloy and distilled under nitrogen atmosphere. Dichloromethane was dried over sodium hydride, and diglyme was dried over sodium. The deuterated solvents were first dried over NaK alloy and then either freshly condensed before use or stored over molecular sieve (4 Å).

Commercially available solid materials were stored and weighted in a glove box or dried under high-vacuum prior use. *n*-Butyllithium was used as a 1.6 M solution in *n*-hexane and *tert*-butyllithium as a 1.9 M solution in *n*-pentane. 1,8-Dibromonaphthalene, 5,6-dibromoacenaphthene, 1-bromo-8-dimethylsilylnaphthalene, 5-dimethylsilylacenaphthene and trityl borate [Ph₃C][B(C₆F₅)₄] were synthesized according to literature procedures.^[111] Sodium phenolate was prepared by the reaction of 1.1 equiv. sodium with 1.0 equiv. phenol in THF. The reaction mixture was heated to the boiling temperature for three hours, the excess of sodium was filtered off and the solvent was removed under low pressure.

Triethylsilane, dimethylphenylsilane, triphenylsilane, pivalonitrile, cyclohexanecarbonitrile, benzonitrile, methyl acrylate, cyclohexa-1,3-diene and 2,3-dimethylbuta-1,3-diene were dried and stored over molecular sieve (4 Å). Cyclopenta-1,3-diene was cracked and freshly distilled prior to use. Thin-layer chromatography was performed using commercial available aluminum foil (Fluka) coated with silica gel 60 and fluorescent indicator F254. For the column chromatography silica gel of the mesh size 60 from Merck was used. For preparative TLC, the pre-coated TLC plates *SIL G-200* from MACHEREY-NAGEL were used.

GC/MS spectra were performed on a Thermo Focus DSQ (stationary phase: DB5 column, length 25 m, diameter 0.2 mm, film thickness 0.33 µm; temperature program: T_{initial} = 60°C for 5 min, then heating with 10°C/min to T_{end} = 280°C, staying at this temp. for 10 min; detector: EI with 70 eV) or on a Shimadzu GCMS-QP2020 equipped with a Macherey-Nagel Optima 5 HT column (30 m, 0.25 mm ID, 0.25 µm film thickness) and a Shimadzu *GC/MS-QP2020 mass selective* detector. High resolution mass spectra were measured on a Finnigan-LCQ or a Finnigan-MAT95 spectrometer using ESI, CI or EI.

GC spectra were performed on a Shimadzu *GC-2010 Plus* equipped with a Macherey-Nagel Optima 5 MS column (15 m, 0.25 mm ID, 0.25 μm film thickness) and a flame ionization detector.

Chiral GC spectra were measured on a GC-2010 Plus from Shimadzu. The column used, is a FS-Lipodex E [Octakis-(2,3-di-O-pentyl-3-butyryl)- γ -cyclodextrin, 25 m, 0.25 mm, constant flow, carrier gas hydrogen: 1.5 $\text{cm}^3\text{min}^{-1}$] from Macherey-Nagel.

Chiral HPLC was performed on a Thermo Scientific Dionex Ultimate 3000 with a Lux 5 μm Cellulose-3, 250 x 4.6 mm column and a flow rate of the eluent of 1 mL/min at 25°C.

The determination of the optical rotation was performed using the Polartronic M from Schmidt+Haensch with Na-D-line (589 nm) at 20°C (cell lengths: 1 dm).

Infrared spectra were performed on a Bruker Tensor 27 spectrometer with a MKII Reflection Golden Gate Single Diamond ATR system.

NMR spectra were recorded on a Bruker Avance 500, a Bruker Avance III 500 spectrometer. ^1H NMR spectra were referenced to the residual solvent resonance as internal standard (benzene- d_6 : $\delta^1\text{H}(\text{C}_6\text{D}_5\text{H}) = 7.20$, toluene- d_8 : $\delta^1\text{H}(\text{C}_6\text{D}_5\text{CD}_2\text{H}) = 2.08$, chloroform- d_1 : $\delta^1\text{H}(\text{CHCl}_3) = 7.24$, chlorobenzene- d_5 : $\delta^1\text{H}(\text{C}_6\text{D}_4\text{HCl}) = 7.14$) and ^{13}C NMR spectra by using the central line of the solvent signal (benzene- d_6 : $\delta^{13}\text{C}(\text{C}_6\text{D}_6) = 128.0$, toluene- d_8 : $\delta^{13}\text{C}(\text{C}_6\text{D}_5\text{CD}_3) = 20.4$, chloroform- d_1 : $\delta^{13}\text{C}(\text{CDCl}_3) = 77.0$, chlorobenzene- d_5 : $\delta^{13}\text{C}(\text{C}_6\text{D}_5\text{Cl}) = 134.2$). ^{29}Si NMR spectra were referenced to an external standard ($^{29}\text{Si}(\text{Me}_2\text{SiHCl}) = 11.1$ versus tetramethylsilane (TMS)), ^{19}F NMR spectra against external CFCl_3 ($\delta^{19}\text{F}(\text{CFCl}_3) = 0.0$), and ^{11}B NMR spectra against $\text{BF}_3\cdot\text{OEt}_2$ ($\delta^{11}\text{B}(\text{BF}_3\cdot\text{OEt}_2) = 0.0$). The ^{29}Si NMR inverse gated spectra were recorded with a relaxation delay $D1 = 10$ s. The ^{29}Si INEPT spectra were recorded with delays $D3 = 0.0084$ and $D4 = 0.0313$ for SiMe_2 , $D3 = 0.0122$ and $D4 = 0.0313$ for SiMe or $D3 = 0.0013$ and $D4 = 0.0013$ for $\text{Si} - \text{H}$, if not given otherwise.

Single crystal X-ray analyses were performed on a Bruker Apex 2 with Mo $\text{K}\alpha$ -radiation. For solving and refining the molecular structures, SHELXL-97 was used and for the visualization Crystal Impact Diamond 4.2.

Combustion analyses (C, H, N, S) were obtained on a Euro EA Element Analyzer with EuroVector equipment. For silanes, combustion analysis values for carbon show often too low values, what may be attributed to the formation and incomplete combustion of silicon carbide, although vanadium pentoxide as combustion aid was used. Satisfactory combustion analyses could not be obtained from all silyl borates due to their high reactivity.

5.2 Syntheses of Starting Materials

5.2.1 Diaryl ethers

5-Bromo-6-phenoxyacenaphthene **45**^[6a]

In a three-necked flask with a reflux cooler and gas supply, 1.0 equiv. (2.00 g, 6.41 mmol) 5,6-dibromoacenaphthene, 0.5 equiv. (0.46 g, 3.21 mmol) copper(I) oxide and 1.0 equiv. (0.74 g, 6.41 mmol) sodium phenolate was suspended in diglyme. The reaction mixture was heated to 160-170°C for six hours. After termination of the reaction, the copper salts were removed by filtration of the reaction mixture through silica gel. After removing the solvent under low pressure, the product was purified by column chromatography using petroleum ether/dichloromethane (9:1, $R_F = 0.2$) as eluent. 5-Bromo-6-phenoxyacenaphthene **45** was obtained as a colorless solid. Yield: 1.56 g (4.80 mmol, 75 %).

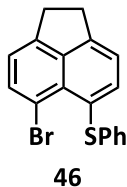


¹H NMR (500.13 MHz, 299.1 K, CD₂Cl₂) δ = 3.39 (s, 4 H, CH₂), 6.86-6.89 (m, 2 H, CH), 7.01-7.04 (m, 1 H, CH), 7.12-7.15 (m, 2 H, CH), 7.27-7.31 (m, 3 H, CH), 7.66 (d, $^3J = 7.3$ Hz, 1 H, CH). **¹³C{¹H} NMR** (125.77 MHz, 299.0 K, CD₂Cl₂) δ = 30.6 (CH₂), 111.2 (C), 117.5 (CH), 120.9 (CH), 121.4 (CH), 121.7 (CH), 122.4 (CH), 124.8 (C), 130.0 (CH), 134.4 (CH), 143.0 (C), 143.9 (C), 146.9 (C), 148.5 (C), 160.2 (C). **GC/MS** t_R = 25.7 min, m/z (%) = 51 (60), 63 (23), 77 (76), 94 (18), 122 (23), 139 (100), 152 (52), 168 (24), 218 (18), 145 (79), 324 (11) [M^+]. **EA** C₁₈H₁₃BrO, calculated: C 66.48, H 4.03; found: C 66.15, H 4.05.

5-Bromo-6-thiophenylacenaphthene **46**^[72a]

5,6-Dibromoacenaphthene (1.0 equiv., 15.42 mmol, 4.81 g) was dissolved in ca. 100 mL THF and cooled to -80 °C. Then, a 1.6 M solution of 1.0 equiv. (15.42 mmol, 9.64 mL) *n*-BuLi in *n*-hexane was added dropwise within 30 min. The reaction mixture was stirred for 110 min at -(70-80)°C. Subsequently, a solution of 1.0 equiv. (15.42 mmol, 3.37 g) diphenyl disulfide in ca. 20 mL THF was added within 30 min. The reaction mixture was stirred for further 90 min at -80 °C and was then allowed to warm up to r.t. over night. The reaction mixture was treated with 40 mL H₂O and the

product was extracted with diethyl ether (4 x 20 mL). The solvent was removed under reduced pressure and the residual solid was washed with hexanes (150 mL). After drying in HV the product **46** was obtained as light yellow solid. Yield 4.40 g (12.89 mmol; 80%).



¹H NMR (500.13 MHz, 297.9 K, C₆D₆) δ = 2.71-2.80 (m, 4 H, CH₂), 6.63 (d, ³J_{H,H} = 7.4 Hz, 1 H, CH), 6.78 (d, ³J_{H,H} = 7.2 Hz, 1 H, CH), 6.90-6.94 (m, 1 H, CH), 6.98-7.03 (m, 1 H, CH), 7.26-7.30 (m, 1 H, CH), 7.66-7.70 (m, 1 H, CH). **¹³C{¹H} NMR** (125.77 MHz, 297.9 K, C₆D₆) δ = 29.9 (CH₂), 30.1 (CH₂), 109.9 (C), 115.1 (C), 120.7 (CH), 121.0 (CH), 126.0 (CH), 127.4 (C), 129.4 (CH), 130.8 (C), 135.9 (CH), 138.4 (CH), 140.1 (C), 142.2 (C), 146.9 (C). **GC/MS** t_R = 30.2 min, m/z (%) = 130 (34), 152 (32), 184 (12), 242 (15), 260 (100), 340 (39) [M⁺].

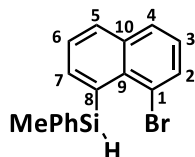
5.2.2 Bromo-Substituted Silyl Naphthalenes and Acenaphthenes

General Procedure A^[6a]: The starting material was dissolved in THF and cooled to -80 °C. Then *n*-butyl lithium was added dropwise. The reaction mixture was stirred for 60 min at that temperature. After the dropwise addition of the corresponding chlorosilane, the mixture was stirred for another 60 min at -80 °C and was then allowed to warm to room temperature over night. Thereafter, an aqueous NH₄Cl solution (ca. 20 mL) was added to the reaction mixture and the product was extracted with Et₂O (3 x 20 mL). The combined organic layer was dried over Na₂SO₄ and the solvent was removed under reduced pressure. The product was purified by column chromatography or crystallization.

8-Phenylmethylsilyl-1-bromonaphthalene^[87b]

The title silane was synthesized according to General Procedure **A** using 1.0 equiv. of 1,8-dibromonaphthalene (10.00 mmol, 2.86 g), 1.0 equiv. of *n*-butyllithium (10.00 mmol, 6.25 mL) and 1.0 equiv. of phenylmethylchlorosilane (10.00 mmol, 1.57 g). The product was purified by column

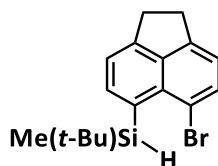
chromatography using petroleum ether as eluent. 8-Phenylmethylsilyl-1-bromonaphthalene was obtained as a yellow oil. Yield 1.62 g (4.93 mmol; 49 %).



$^1\text{H NMR}$ (500.13 MHz, 297.4 K, C_6D_6) δ = 0.86 (d, $^3J_{\text{H,H}} = 3.6$ Hz, 3 H, SiCH_3), 6.00 (q, $^3J_{\text{H,H}} = 3.6$ Hz, $^1J_{\text{Si,H}} = 203.5$ Hz, 1 H, SiH), 6.81 (t, $^3J_{\text{H,H}} = 7.8$ Hz, 1 H, 3-H), 7.07 (t, $^3J_{\text{H,H}} = 7.6$ Hz, 1 H, 6-H), 7.17-7.22 (m, 3 H, *o*-Ph-H, 2-H), 7.41 (dd, $^3J_{\text{H,H}} = 8.1$ Hz, $^4J_{\text{H,H}} = 1.0$ Hz, 1 H, 4-H), 7.50 (dd, $^3J_{\text{H,H}} = 8.2$ Hz, $^4J_{\text{H,H}} = 1.0$ Hz, 1 H, 5-H), 7.55-7.61 (m, 3 H, *m*-Ph-H, *p*-Ph-H), 8.00 (dd, $^3J_{\text{H,H}} = 7.0$ Hz, $^4J_{\text{H,H}} = 1.2$ Hz, 1 H, 7-H). $^{13}\text{C}\{^1\text{H}\}$ NMR (125.77 MHz, 297.6 K, C_6D_6) δ = -0.1 (SiCH_3), 123.8 (C-1), 125.7 (C-6), 126.1 (C-3), 128.2 (*m*-PhCH), 129.2 (*p*-PhCH), 129.6 (C-4), 131.9 (C-5), 132.6 (C-2), 134.7 (C-8), 135.0 (*o*-PhCH), 136.5 (C-9), 137.3 (C-10), 139.3 ($\text{SiC}(\text{CH}_3)_3$), 141.0 (C-7). $^{29}\text{Si}\{^1\text{H}\}$ INEPT NMR (99.31 MHz, 673.2 K, C_6D_6 , $D_3 = 0.0013$, $D_4 = 0.0013$) δ = -13.9.

5-Bromo-6-methyl-*tert*-butylsilylacenaphthene

The title silane was synthesized according to General Procedure **A** using 1.0 equiv. of 5-bromo-6-phenoxyacenaphthene (3.48 mmol, 1.09 g), 1.0 equiv. of *tert*-butyl lithium (3.48 mmol, 1.83 mL) and 1.0 equiv. of chloromethyl-*tert*-butylsilane (3.48 mmol, 0.48 g). The product was purified by column chromatography using *n*-pentane as eluent ($R_f = 0.50$). Silane **8a** was obtained as an orange solid. Yield: 0.87 g (2.62 mmol, 75 %).

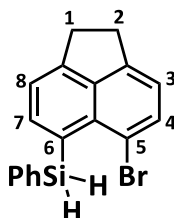


$^1\text{H NMR}$ (499.87 MHz, T = 305.1 K, C_6D_6) δ = 0.63 (d, $^3J = 3.8$ Hz, 3 H, SiCH_3), 1.15 (s, 9 H, $\text{SiC}(\text{CH}_3)_3$), 2.77-2.80 (m, 2 H, CH_2), 2.88-2.90 (m, 2 H, CH_2), 5.71 (q, $^3J = 3.6$ Hz, $^1J_{\text{Si,H}} = 199.7$ Hz, 1 H, SiH), 6.72 (dm, $^3J = 7.4$ Hz, 1 H, CH), 7.05 (dm, $^3J = 7.1$ Hz, 1 H, CH), 7.70 (d, $^3J = 7.4$ Hz, 1 H, CH), 7.73 (d, $^3J = 7.1$ Hz, 1 H, CH). $^{13}\text{C}\{^1\text{H}\}$ NMR (125.71 MHz, T = 305.0 K, C_6D_6) δ = -3.2 ($\text{Si}(\text{CH}_3)_2$), 17.9 (C, *t*-Bu),

28.7 (CH₃, *t*-Bu), 29.5 (CH₂), 30.2 (CH₂), 118.3 (C), 119.6 (CH), 120.5 (CH), 129.7 (C), 134.3 (CH), 136.1 (C), 140.2 (CH), 141.5 (C), 147.0 (C), 149.2 (C). ²⁹Si{¹H} NMR (99.31 MHz, T = 305.0 K, C₆D₆) δ = -3.0. HR/MS (EI): [C₁₇H₂₁BrSi], calculated: 332.0596; found: 332.0585.

5-Bromo-6-phenylsilylacenaphthene

The title silane was synthesized according to General Procedure **A** using 1.0 equiv. of 5-bromo-6-phenoxyacenaphthene (1.60 mmol, 500 mg), 1.0 equiv. of *n*-butyl lithium (1.60 mmol, 1.00 mL) and 1.0 equiv. of chlorophenylsilane (1.60 mmol, 0.21 mL). The product was purified by crystallization from hexanes. 5-Bromo-6-phenylsilylacenaphthene was obtained as a white solid. Yield: 377 mg (1.11 mmol, 69 %).



¹H NMR (500.13 MHz, 305.0 K, C₆D₆): δ = 2.79-2.82 (m, 2 H, CH₂, H-1), 2.87-2.90 (m, 2 H, CH₂, H-2), 5.94 (s, 2 H, ¹J_{H,Si} = 203.9 Hz, SiH₂), 6.71 (dm, ³J = 7.4 Hz, 1 H, H-3), 6.97 (dm, ³J = 7.0 Hz, 1 H, H-8), 7.21-7.23 (m, 4 H, Ph, overlap with C₆D₅H), 7.57 (d, ³J = 7.4 Hz, 1H, H-4), 7.69-7.71 (m, 2 H, *o*-Ph), 8.03 (d, ³J = 7.0 Hz, H-7). ¹³C{¹H} NMR (125.71 MHz, 305.0 K, C₆D₆) δ = 29.7 (CH₂, C-1), 30.4 (CH₂, C-2), 118.8 (C), 120.2 (CH, C-8), 120.7 (CH, C-3), 125.6 (C), 128.3 (CH, Ph), 129.5 (CH), 133.2 (CH, C-4), 135.4 (C), 135.7 (CH, *o*-Ph), 136.0 (C), 141.4 (C), 143.4 (CH, C-7), 146.8 (C), 150.3 (C). ²⁹Si{¹H} NMR (99.31 MHz, 305.0 K, C₆D₆) δ = -29.6. GC/MS t_R = 27.3 min, m/z (%) = 105 (14), 128 (14), 153 (74), 181 (76), 260 (100), 340 (7) [M⁺].

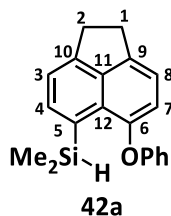
5.3 Syntheses of Naphthyl and Acenaphthyl Silanes

General Procedure B: The starting material was dissolved in THF and cooled to -80°C . Then *n*-butyl lithium was added dropwise and the reaction mixture was stirred for 70 minutes. During this time, the reaction mixture was allowed to warm to -30°C . Subsequently, the reaction mixture was cooled to -70°C and chlorodimethylsilane was added. The mixture was stirred for additional 30 minutes at -70°C and then warmed to r.t. over night. After completion of the reaction, NH_4Cl solution (10 mL) was added to the reaction mixture and the product was extracted with Et_2O (3 x 10 mL). The organic layer was dried over Na_2SO_4 and the solvent was removed under low pressure. The product was purified by column chromatography or crystallization.

General Procedure C: The starting material was dissolved in THF and cooled to -80°C . Then *n*-butyl lithium was added dropwise. The reaction mixture was stirred for 60 min at that temperature. A solution of diphenyl disulfide in THF was added dropwise and the mixture was stirred for another 60 min at -80°C . Then the mixture was allowed to warm to room temperature over night. An aqueous NH_4Cl solution (ca. 20 mL) was added to the reaction mixture and the product was extracted with Et_2O (3 x 20 mL). The combined organic layer was dried over Na_2SO_4 and the solvent was removed under reduced pressure. The product was purified by column chromatography or crystallization.

5-Dimethylsilyl-6-phenoxyacenaphthene **42a**^[6a]

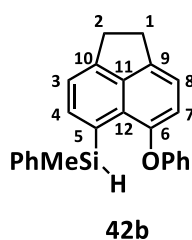
The title compound was synthesised according to general procedure **A** using 1.0 equiv. 5-bromo-6-phenoxyacenaphthene **45** (6.15 mmol, 2.00 g), 1.1 equiv. *n*-butyl lithium (6.77 mmol, 4.23 mL) and 1.0 equiv. chlorodimethylsilane (6.15 mmol, 0.68 mL). The product **42a** was purified by column chromatography using petroleum ether as eluent ($R_f = 0.44$). Silane **42a** was obtained as a colorless solid after crystallization from *n*-pentane at -25°C . Yield: 1.45 g (4.80 mmol, 78 %).



¹H NMR (499.87 MHz, 305.0 K, CD₂Cl₂) δ = 0.40 (d, ³J = 3.6 Hz, 6 H, Si(CH₃)₂), 3.34-3.37 (m, 2 H, CH₂, 1-H), 3.41-3.45 (m, 2 H, CH₂, 2-H), 4.62 (sept, ³J = 3.6 Hz, ¹J_{Si,H} = 190.9 Hz, 1 H, SiH), 6.82 (d, ³J = 7.5 Hz, 1 H, CH, 7-H), 7.10-7.11 (m, 2 H, CH, Ph), 7.14-7.18 (m, 2 H, CH, 8-H, *p*-Ph), 7.33 (dm, ³J = 6.9 Hz, 1 H, CH, 3-H), 7.37-7.42 (m, 2 H, CH, Ph), 7.79 (d, ³J = 6.8 Hz, 1 H, CH, 4-H). **¹³C{¹H} NMR** (125.71 MHz, 305.0 K, CD₂Cl₂) δ = -1.5 (Si(CH₃)₂), 30.1 (CH₂, C-1), 31.4 (CH₂, C-2), 114.7 (CH, C-7), 119.5 (CH, C-8), 120.4 (CH, C-3), 120.5 (CH, Ph), 124.2 (CH, Ph), 128.1 (C, C-5), 129.1 (C), 130.4 (CH, Ph), 137.6 (CH, C-4), 141.3 (C), 141.6 (C), 148.8 (C, C-10/12), 152.9 (C, C-6), 157.6 (C, *ipso*-C-Ph). **²⁹Si{¹H} NMR** (99.31 MHz, 305.0 K, CD₂Cl₂) δ = -14.0. **²⁹Si INEPT NMR** (99.31 MHz, T = 305.0 K, CD₂Cl₂) δ = -14.0. **GC/MS** t_R = 24.3 min, m/z (%) = 51 (32), 59 (18), 135 (36), 152 (74), 165 (31), 211 (100), 226 (54), 271 (17), 287 (27), 304 (38) [M⁺]. **IR** (ATR, liquid): $\tilde{\nu}$ (Si-H) [cm⁻¹] = 2097, 2142. **EA** C₂₀H₂₀OSi, calculated: C 78.90, H 6.62; found: C 78.83, H 6.96. **HR/MS** (EI): [C₂₀H₂₀OSi], calc: 304.1283; found: 304.1270

5-Methylphenylsilyl-6-phenoxyacenaphthene **42b**^[112]

The title compound **42b** was synthesized according to general procedure **B** using 1.0 equiv. (2.00 mmol, 0.65 g) 5-Bromo-6-phenoxyacenaphthene **45**, 1.0 equiv. (2.00 mmol, 1.26 mL) *n*-butyl lithium and 1.2 equiv. (2.40 mmol, 376 mg) chloro(methyl)phenylsilane. In addition, 1.1 equiv. (2.20 mmol, 256 mg) TMEDA was added to the starting material before adding *n*-butyl lithium. The product **42b** was purified by column chromatography using *n*-pentane as eluent (R_F = 0.20). The product **42b** was obtained as a colorless oil. Yield 0.40 mg (1.11 mmol; 55 %).

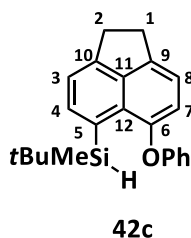


¹H NMR (499.9 MHz, 298.1 K, C₆D₆) δ = 0.84 (d, ³J_{H,H} = 3.7 Hz, 3 H, SiCH₃), 2.98-3.02 (m, 2 H, 1-H), 3.05-3.08 (m, 2 H, 2-H), 5.63 (q, ³J_{H,H} = 3.7 Hz, ¹J_{H,Si} = 196.2 Hz, 1 H, Si-H), 6.75 (d, ³J_{H,H} = 6.6 Hz, 1 H, 7-H), 6.81-6.83 (m, 2 H, O-*o*-Ph), 6.87-6.92 (m, 2 H, 8-H, O-*p*-Ph), 7.04-7.09 (m, 2 H, O-*m*-Ph), 7.13-7.19 (m, 4 H, Si-*m/p*-Ph, 3-H), 7.58-7.61 (m, 2 H, Si-*o*-Ph), 7.99 (d, ³J_{H,H} = 6.9 Hz, 1 H, 4-H) ppm. **¹³C{¹H} NMR** (125.7 MHz, 297.8 K, C₆D₆) δ = -2.9 (SiCH₃), 29.7 (CH₂, C-2), 31.0 (CH₂, C-1), 113.8 (C-7), 119.4 (C-8), 120.2 (C-3), 120.7 (CH, OPh), 123.8 (CH, OPh), 125.7 (C, C-5), 127.9 (CH), 128.9 (CH), 129.2 (C), 129.9 (CH), 135.0 (CH, SiPh), 138.2 (C, Si-*ipso*-Ph), 139.3 (CH, C-4), 140.5 (C), 141.4 (C), 148.6 (C), 153.3 (C,

C-6), 156.8 (C, O-*ipso*-Ph). $^{29}\text{Si}\{^1\text{H}\}$ INEPT NMR (99.3 MHz, 297.9 K, C_6D_6) $\delta = -14.7$. IR (ATR, fest): $\tilde{\nu}(\text{Si-H}) [\text{cm}^{-1}] = 2096, 2136$. GC-MS $t_{\text{R}} = 32.8$ min, $m/z (M^+) = 366$. HR/MS calculated: $m/z = 366.1440$; found (EI): $m/z = 366.1442$.

5-Methyl-*tert*-butylsilyl-6-phenoxyacenaphthene **42c**^[112]

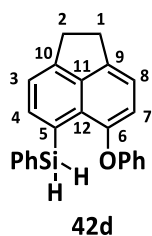
The title compound **42c** was synthesized according to general procedure **B** using 1.0 equiv. (1.00 mmol, 325 mg) 5-bromo-6-phenoxyacenaphthene **45**, 1.1 equiv. (1.10 mmol, 0.70 mL) *n*-butyl lithium and 1.5 equiv. (1.50 mmol, 205 mg) chloro(*tert*-butyl)methylsilane. The chlorosilane was added at -50 °C and the reaction mixture was stirred for further 60 min at this temperature. The product **42c** was purified by column chromatography using *n*-pentane as eluent ($R_{\text{f}} = 0.26$). The product **42c** was obtained as a colorless oil. Yield 134 mg (0.39 mmol; 39 %).



^1H NMR (499.9 MHz, 298.1 K, C_6D_6) $\delta = 0.56$ (d, $^3J_{\text{H,H}} = 3.8$ Hz, 3 H, SiMe), 1.19 (s, 9 H, Sit-Bu), 2.98-3.02 (m, 2 H, 1-H), 3.05-3.09 (m, 2 H, 2-H), 4.95 (q, $^3J_{\text{H,H}} = 3.8$ Hz, $^1J_{\text{H,Si}} = 192.9$ Hz, 1 H, Si-H), 6.85 (d, $^3J_{\text{H,H}} = 7.5$ Hz, 1 H, 7-H), 6.91-6.96 (m, 2 H, 3-H, *p*-Ph), 7.07-7.10 (m, 2 H, *o*-Ph), 7.12-7.16 (m, 2 H, *m*-Ph), 7.21-7.22 (m, 1 H, 3-H), 7.98 (d, $^3J_{\text{H,H}} = 6.9$ Hz, 1 H, 4-H). $^{13}\text{C}\{^1\text{H}\}$ NMR (125.7 MHz, 297.8 K, C_6D_6) $\delta = -4.8$ (SiCH₃), 18.1 (C, *t*-Bu), 28.5 (CH₃, *t*-Bu), 29.6 (CH₂, C-2), 30.9 (CH₂, C-1), 114.9 (CH, C-7), 119.3 (CH, C-8), 119.9 (CH, C-3), 120.8 (CH, Ph), 123.7 (CH, Ph), 125.9 (C, C-5), 129.5 (C), 130.1 (CH, Ph), 139.0 (CH, C-4), 141.0 (C), 141.4 (C), 148.2 (C), 153.2 (C, C-6), 157.6 (C, *i*-Ph). $^{29}\text{Si}\{^1\text{H}\}$ INEPT NMR (99.3 MHz, 297.9 K, C_6D_6) $\delta = -21.9$. GC-MS $t_{\text{R}} = 26.5$ min, $m/z (M^+) = 346$. HR/MS calculated: $m/z = 346.1747$; found (EI): $m/z = 346.1757$. IR (ATR, solid): $\tilde{\nu}(\text{Si-H}) [\text{cm}^{-1}] = 2090, 2151$. EA $\text{C}_{23}\text{H}_{26}\text{SiO}$, calculated: C 79.72, H 7.56, solid: C 80.00, H 7.66

6-Phenoxy-5-phenylsilylacenaphthene 42d^[113]

The title compound **42d** was synthesized according to general procedure **A** using 1.0 equiv. (1.00 mmol, 325 mg) 5-bromo-6-phenoxyacenaphthene **45**, 1.2 equiv. *n*-BuLi (1.20 mmol, 0.75 ml) and 1.0 equiv. (1.00 mmol, 0.13 ml) phenylchlorosilane. The product **42d** was purified by crystallization from *n*-pentane and obtained as a white solid. Yield 271 mg (0.77 mmol, 77 %).



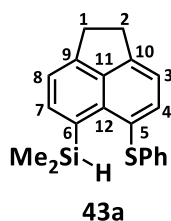
¹H NMR (300.14 MHz, 295.0 K, C₆D₆): δ = 2.95-3.06 (m, 4 H, CH₂), 5.61 (s, ¹J_{H,Si} = 201.8 Hz, 2 H, SiH₂), 6.79 (d, ³J_{H,H} = 7.6 Hz, 1 H, H-7), 6.86-6.91 (m, 4 H, H-6, OPh), 7.04-7.08 (m, 2 H, OPh), 7.12-7.19 (m, 4 H, H-3, Si-*m/p*-Ph), 7.64-7.67 (m, 2 H, Si-*o*-Ph), 7.96 (d, ³J_{H,H} = 6.8 Hz, 1 H, H-4). **¹³C{¹H} NMR** (75.48 MHz, 295.0 K, C₆D₆): δ = 29.7 (CH₂), 31.1 (CH₂), 114.6 (CH), 119.5 (CH), 120.2 (CH), 120.4 (CH), 121.9 (C), 123.7 (CH), 128.1 (CH), 129.3 (CH, C-3), 129.4 (C), 129.9 (CH), 134.6 (C), 135.7 (CH, Si-*o*-Ph), 140.3 (CH, C-4), 140.9 (C), 141.2 (C), 149.1 (C), 152.7 (C), 157.3 (C). **²⁹Si{¹H} NMR** (99.31 MHz, 305.0 K, C₆D₆): δ = -30.7. **²⁹Si INEPT NMR** (99.31 MHz, 305.0 K, C₆D₆, D3 = D4 = 0.001 s): δ = -30.6 (tm, ¹J_{H,Si} = 201.8 Hz). **GC-MS** R_t 32.3 min, *m/z* (%) = 77 (25) C₆H₅, 152 (46) C₁₂H₈, 197 C₁₂H₉OSi (19), 271 (21) C₁₈H₁₁OSi, 273 (100) C₁₈H₁₃OSi, 274 (62) C₁₈H₁₄OSi, 352 (58) [M+]. **IR** (ATR, fest): $\tilde{\nu}$ (Si-H) [cm⁻¹] = 2117. **HR-MS** calc: *m/z* = 352.1283; found (EI): *m/z* = 351.9593 **EA** C₂₄H₂₀OSi, calc: C 81.78, H 5.72, found: C 81.64, H 5.98.

5-Thiophenyl-6-dimethylsilylacenaphthene 43a^[6a]

A Schlenk flask was charged with 1 equiv. 5-bromo-6-dimethylsilylacenaphthene (1.70 mmol, 500 mg) and the solid was dissolved in ca. 50 mL THF and cooled to -40° C. Then 1 equiv. *n*-butyl lithium (1.70 mmol, 1.1 mL) was added dropwise and the reaction mixture was stirred for 70 minutes. During this time, the reaction mixture was allowed to warm to -10° C. Subsequently, the reaction mixture was cooled to -35° C and a solution of 1 equiv. of diphenyl disulfide in 3 mL THF was added. The mixture was stirred for additional 30 minutes at -35° C and then warmed to r.t. over night. After

completion of the reaction, NH_4Cl solution (10 mL) was added to the reaction mixture and the product was extracted with Et_2O (3 x 10 mL). The organic layer was dried over Na_2SO_4 and the solvent was removed under low pressure. The product **43a** was obtained as a colorless solid after crystallization from *n*-pentane at 6°C. Yield 250 mg (0.77 mmol, 45%).

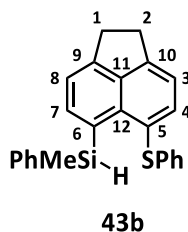
Alternatively, the title compound **43a** was synthesized according to general procedure **A** via lithiation of 5-bromo-6-thiophenylacenaphthene **46** and subsequent addition of dimethylchlorosilane using 1.0 equiv. (2.99 mmol, 1.02 g) 5-bromo-6-thiophenylacenaphthene, 1.1 equiv. *n*-butyl lithium (3.29 mmol, 2.05 mL) and 1.1 equiv. (3.29 mmol, 0.37 mL) dimethylchlorosilane. The product **43a** was obtained as a colorless solid after crystallization from *n*-pentane at 6°C. Yield 676 mg (2.12 mmol, 71%).



$^1\text{H NMR}$ (499.87 MHz, 305.0 K C_6D_6) δ = 0.63 (d, 3J = 3.5 Hz, 6 H, $\text{Si}(\text{CH}_3)_2$), 2.91-2.94 (m, 2 H, CH_2 , 1-H), 2.97-3.00 (m, 2 H, CH_2 , 2-H), 5.39 (sept, $^3J_{\text{H,H}}$ = 3.5 Hz, $^1J_{\text{Si-H}}$ = 198.4 Hz, 1 H, SiH), 6.82 (t, 3J = 7.3 Hz, 1 H, CH, *p*-Ph), 6.90-6.93 (m, 2 H, CH, *m*-Ph), 6.98 (dm, 3J = 7.2 Hz, 1 H, CH, 3-H), 7.03-7.05 (m, 2 H, CH, *o*-Ph), 7.15 (dm, 3J = 7.0 Hz, 1 H, CH, 8-H), 7.88 (d, 3J = 7.2 Hz, 1 H, CH, 4-H), 8.02 (d, 3J = 7.0 Hz, 1 H, CH, 7-H). $^{13}\text{C}\{^1\text{H}\}$ NMR (125.77 MHz, 300.1 K, C_6D_6) δ = 0.2 ($\text{Si}(\text{CH}_3)_2$), 30.0 (CH_2 , C-2), 30.2 (CH_2 , C-1), 120.1 (CH, C-8), 120.5 (CH, C-2), 125.2 (CH, *p*-Ph), 126.4 (C, C-5), 126.9 (CH, *o*-Ph), 129.1 (CH, *m*-Ph), 131.3 (C, C-6), 139.3 (C, C-5), 139.81 (CH), 139.84 (CH), 140.9 (C), 141.6 (C, *ipso*-Ph), 149.2 (C), 149.6 (C). $^{29}\text{Si}\{^1\text{H}\}$ NMR (125.71 MHz, 305.0 K, C_6D_6) δ = -17.7. IR (ATR, liquid): $\tilde{\nu}(\text{Si-H})$ [cm^{-1}] = 2106 cm^{-1} . GC/MS t_{R} = 26.5 min, m/z (%) = 51 (31), 59 (17), 75 (19), 77 (44), 152 (70), 165 (24), 213 (20), 227 (100), 305 (64), 319 (29) [M^+]. HR/MS (CI, isobutane): [$\text{C}_{20}\text{H}_{20}\text{SSi}$], calculated: 320.1049; found: 320.1039. EA $\text{C}_{20}\text{H}_{20}\text{SSi}$, calculated: C 74.95, H 6.29, S 10.00; found: C 74.36, H 6.38, S 9.84.

5-Thiophenyl-6-phenylmethylsilylacenaphthene 43b

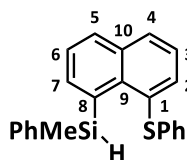
The title compound **43b** was synthesized according to general procedure **A** using 1.0 equiv. (4.31 mmol, 1.47 g) 5-bromo-6-thiophenylacenaphthene **46**, 1.0 equiv. (4.31 mmol, 2.69 mL) *n*-butyl lithium and 1.0 equiv. (4.31 mmol, 0.65 mL) chloro(methyl)phenylsilane. The product **43b** was purified by crystallization from *n*-pentane and obtained as a colorless solid. Yield 1.07 g (2.80 mmol; 65 %).



¹H NMR (499.87 MHz, 305.1 K, C₆D₆) δ = 0.88 (d, ³J = 3.6 Hz, 3 H, SiCH₃), 2.91-3.95 (m, 2 H, CH₂), 2.96-3.00 (m, 2H, CH₂), 5.89 (q, ³J = 3.4 Hz, ¹J_{H,Si} = 202.8 Hz, 1 H, SiH), 6.80-6.83 (m, 1 H, CH, *S-p*-Ph), 6.87-6.92 (m, 4 H, CH, *S-m/o*-Ph), 6.96 (d, ³J = 7.3 Hz, 1 H, CH, 3-H), 7.10 (d, ³J = 7.0 Hz, 1 H, CH, 8-H), 7.14-7.17 (m, 3 H, CH, *Si-m/p*-Ph), 7.60-7.64 (m, 2 H, CH, *Si-o*-Ph), 7.79 (d, ³J = 7.1 Hz, 1 H, CH, 4-H), 8.05 (d, ³J = 7.0 Hz, 1 H, CH, 7-H). **¹³C{¹H} NMR** (125.71 MHz, 305.0 K, C₆D₆) δ = -1.0 (SiCH₃), 30.1 (CH₂, C-2), 30.3 (CH₂, C-1), 120.2 (CH, C-8), 120.7 (CH, C-3), 125.1 (CH, *S-p*-Ph), 126.7 (C, C-5), 126.9 (CH, *S-m*-Ph), 128.1 (CH, *Si-m*-Ph), 128.8 (CH, *S-p*-Ph), 128.9 (C, C-6), 129.0 (CH, *S-o*-Ph), 134.9 (CH, *Si-o*-Ph), 139.3 (C, *Si-ipso*-Ph), 139.5 (C, C-12), 139.7 (CH, C-4), 140.9 (C, C-11), 141.5 (C, *S-ipso*-Ph), 141.9 (CH, C-7), 149.5 (C, C-10), 149.7 (C, C-9). **²⁹Si{¹H} NMR** (99.31 MHz, 305.0 K, C₆D₆) δ = -17.2. **GC/MS** t_R = 30.8 min, m/z (%) = 51 (16), 77 (38), 152 (71), 227 (64), 289 (100), 305 (24), 367 (41), 382 (23) [M⁺]. **HR/MS** calculated: m/z = 382.1206; found (EI): m/z = 382.1196. **IR** (ATR, solid): $\tilde{\nu}$ (Si-H) [cm⁻¹] = 2091. **EA** C₂₅H₂₂SSi, calculated: C 78.48, H 5.80, S 8.38; found: C 78.57, H 6.63, S 8.08.

1-Thiophenyl-8-phenylmethylsilylnaphthalene 44^[114]

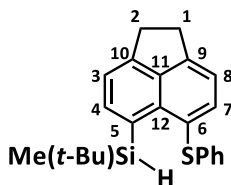
The title compound **44** was synthesized according to general procedure **C** using 1.0 equiv. (3.06 mmol, 1.00 g) 8-phenylmethylsilyl-1-bromonaphthalene, 1.0 equiv. (3.06 mmol, 1.91 mL) *n*-butyl lithium and 1.0 equiv. (3.06 mmol, 0.67 g) diphenyl disulfide. The product **44** was purified by column chromatography using petroleum ether/ethyl acetate (99:1) as eluent (R_F = 0.26) and was obtained as a colorless solid after crystallization from *n*-pentane at -18 °C. Yield 0.96 g (2.70 mmol; 88 %).

**44**

^1H NMR (500.13 MHz, 298.4 K, C_6D_6) δ = 0.85 (d, $^3J_{\text{H,H}} = 3.5$ Hz, 3 H, SiCH_3), 5.87 (q, $^3J_{\text{H,H}} = 3.5$ Hz, $^1J_{\text{H,Si}} = 203.0$ Hz, 1 H, SiH), 6.75-6.85 (m, 5 H, SPh), 7.07 (t, $^3J_{\text{H,H}} = 7.6$ Hz, 1 H, 3-H), 7.12-7.16 (m, 3 H, Si-*m*-Ph, Si-*p*-Ph), 7.21-7.24 (m, 1 H, 6-H), 7.51-7.56 (m, 2 H, Si-*o*-Ph), 7.59 (dd, $^3J_{\text{H,H}} = 8.1$ Hz, $^4J_{\text{H,H}} = 1.2$ Hz, 1 H, 4-H), 7.66 (dd, $^3J_{\text{H,H}} = 8.1$ Hz, $^4J_{\text{H,H}} = 1.1$ Hz, 1 H, 5-H), 7.75 (dd, $^3J_{\text{H,H}} = 7.2$ Hz, $^4J_{\text{H,H}} = 1.3$ Hz, 1 H, 2-H), 8.08 (dd, $^3J_{\text{H,H}} = 6.9$ Hz, $^4J_{\text{H,H}} = 1.0$ Hz, 1 H, 7-H). **$^{13}\text{C}\{^1\text{H}\}$ NMR** (125.77 MHz, 298.3 K, C_6D_6) δ = -0.5 (SiCH_3), 125.4 (CH), 126.0 (CH), 126.2 (CH), 127.2 (C), 128.5 (CH), 128.7 (CH), 129.0 (CH), 131.5 (CH), 131.9 (C), 132.1 (CH), 134.2 (CH), 134.7 (CH), 135.6 (C), 137.6 (C), 139.6 (C), 140.6 (CH), 140.6 (C), 140.9 (CH). **$^{29}\text{Si}\{^1\text{H}\}$ NMR** (99.31 MHz, 673.2 K, C_6D_6) δ = -16.9. **IR** (ATR, solid): $\tilde{\nu}(\text{Si-H})$ [cm^{-1}] = 2144. **HR/MS** calculated: $m/z = 356.1055$; found (ESI): $m/z = 355.0595$. **EA** $\text{C}_{23}\text{H}_{20}\text{SSi}$, calculated.: C 77.48, H 5.65; S 8.99, found: C 76.41, H 5.98, S 8.60.

5-Thiophenyl-6-methyl-*tert*-butylsilylacenaphthene **43c**

The title compound **43c** was synthesized according to general procedure **B** using 1.0 equiv. (990.43 μmol , 338 mg) 5-bromo-6-thiophenylacenaphthene **46**, 1.0 equiv. (990.43 μmol , 0.63 mL) *n*-butyl lithium and 1.0 equiv. (990.43 μmol , 94 mg) chloro(*tert*-butyl)methyl silane. The product **43c** was purified by crystallization from *n*-pentane and obtained as an orange solid. Yield 107 mg (297.13 μmol , 30 %).

**43c**

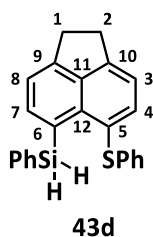
^1H NMR (500.13 MHz, 298.9 K, C_6D_6) δ = 0.54 (d, $^3J_{\text{H,H}} = 3.4$ Hz, 3 H, SiCH_3), 1.19 (s, 9 H, Si(*t*-Bu)), 2.91-2.95 (m, 2 H, CH_2), 2.98-3.02 (m, 2 H, CH_2), 5.41 (q, $^3J_{\text{H,H}} = 3.3$ Hz, $^1J_{\text{H,Si}} = 199.8$ Hz, 1 H, SiH), 6.82-6.85 (m, 1 H, *p*-Ph), 6.92-6.95 (m, 2 H, *m*-Ph), 6.98 (d, $^3J_{\text{H,H}} = 7.1$ Hz, 1 H, 3-H), 7.05-7.06 (m, 2 H, *o*-Ph), 7.16

(d, $^3J_{\text{H,H}} = 7.0$ Hz, 1 H, 8-H), 7.88 (d, $^3J_{\text{H,H}} = 7.1$ Hz, 1 H, 4-H), 8.01 (d, $^3J_{\text{H,H}} = 7.0$ Hz, 1 H, 7-H). $^{13}\text{C}\{^1\text{H}\}$ NMR (125.71 MHz, 305.0 K, C_6D_6) $\delta = -3.2$ (SiCH_3), 18.5 (C, *t*Bu), 30.0 (CH_2 , C-2), 30.3 (CH_2 , C-1), 119.8 (CH, C-8), 120.5 (CH, C-3), 125.2 (CH, *p*-Ph), 126.9 (C, *ipso*-Ph), 127.2 (CH, *o*-Ph), 129.1 (CH, *m*-Ph), 129.6 (C, C-6), 139.4 (C, C-12), 139.8 (CH, C-4), 140.2 (CH, C-7), 141.0 (C, C-5), 141.3 (C, C-11), 149.2 (C, C-9), 149.5 (C, C-10). $^{29}\text{Si}\{^1\text{H}\}$ NMR (99.36 MHz, 299.1 K, C_6D_6) $\delta = -3.3$. HR/MS calculated: $m/z = 362.1519$; found (EI): $m/z = 362.1508$. IR (ATR, solid): $\tilde{\nu}(\text{Si-H}) [\text{cm}^{-1}] = 2175$. EA $\text{C}_{23}\text{H}_{26}\text{SSi}$, calculated: C 72.19, H 7.23, S 8.84; found: C 75.14, H 8.15, S 7.70.

6-Phenylsilyl-5-thiophenylacenaphthene **43d**

The title silane **43d** was synthesized according to general procedure **C** using 1.0 equiv. (757.43 μmol , 257 mg) of 6-phenylsilyl-5-bromoacenaphthene, 1.0 equiv. (757.43 μmol , 0.47 mL) *n*-butyl lithium and 1.0 equiv. (757.43 μmol , 166 mg) diphenyl disulfide in 5 mL THF. After aqueous work up and crystallization from hexanes, the product **43d** was obtained as a white solid. Yield 21 mg (60.59 μmol , 8%).

Alternatively, the title compound **43d** was synthesized according to general procedure **A** using 1.0 equiv. (3.00 mmol, 1.02 g) 5-bromo-6-thiophenylacenaphthene **46**, 1.0 equiv. (3.00 mmol, 1.88 mL) *n*-BuLi and 1.0 equiv. (3.00 mmol, 0.39 mL) chlorophenylsilane. After aqueous work up and crystallization from hexanes, the product was obtained as a white solid. Yield 0.98 g (2.88 mmol, 96%).



^1H NMR (500.13 MHz, 298.9 K, C_6D_6) $\delta = 2.87$ -2.96 (m, 4 H, CH_2), 5.80 (s, $^1J_{\text{H,Si}} = 203.8$ Hz, 2 H, SiH_2), 6.80-6.84 (m, 1 H, *S-p*-Ph), 6.87-6.90 (m, 2 H, *S-m*-Ph), 6.92-6.95 (m, 3 H, *S-o*-Ph, 3/4-H), 7.06 (dm, $^3J_{\text{H,H}} = 6.9$ Hz, 1 H, 8-H), 7.13-7.16 (m, 3 H, SiPh), 7.63-7.67 (m, 2 H, SiPh), 7.78 (d, $^3J_{\text{H,H}} = 7.2$ Hz, 1 H, 3/4-H), 8.08 (d, $^3J_{\text{H,H}} = 6.9$ Hz, 1 H, 7-H). $^{13}\text{C}\{^1\text{H}\}$ NMR (125.71 MHz, 305.0 K, C_6D_6) $\delta = 30.1$ (CH_2), 30.4 (CH_2), 120.4 (CH, C-3/4), 120.7 (CH), 125.2 (C), 125.6 (C), 126.3 (C), 126.9 (CH, *S-m*-Ph), 129.1 (CH, SPh), 129.1 (CH, SPh), 135.5 (CH, SiPh), 135.9 (C), 139.5 (C), 139.7 (CH), 140.9 (C), 141.3 (C), 143.4

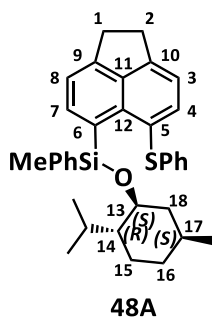
(CH, C-7), 149.8 (C), 150.3 (C). $^{29}\text{Si}\{^1\text{H}\}$ NMR (99.36 MHz, 299.1 K, C_6D_6) $\delta = -31.3$. IR (ATR, solid): $\tilde{\nu}(\text{Si-H}) [\text{cm}^{-1}] = 2151, 2088$. EA $\text{C}_{24}\text{H}_{20}\text{SSi}$, calculated: C 78.21, H 5.47, S 8.70; found: C 77.29, H 5.44, S 8.16.

5.4 Chiral Resolution of Acenaphthyl Silanes

5.4.1 Pd-NP Catalyzed Dehydrogenative Si-O Coupling

Siloxanes 48A

A reaction tube was charged with 1.0 equiv. (259.02 μmol , 99.1 mg) 6-methylphenylsilyl-5-thiophenylacenaphthene **43b**, 2.5 equiv. (652.08 μmol , 101.9 mg) (-)-menthol **A** and 10.1 mg Pd nanoparticles. The solids were suspended in 1.0 mL *n*-Bu₂O. The reaction mixture was degassed and heated to 64 – 67°C for 20 h. The reaction mixture was cooled to r.t. and filtered through silica gel. After removal of the solvent, the crude product was purified by preparative TLC (petroleum ether/ethyl acetate (99:1)) and a mixture of both siloxanes **48A** was obtained. Yield: 16 mg (28.49 μmol , 11%).

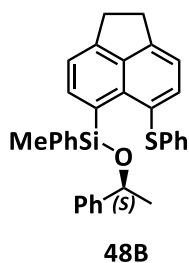


^1H NMR (499.87 MHz, 296.1 K, CDCl_3) $\delta = 0.29$ (d, $^3J_{\text{H,H}} = 6.9$ Hz, 3 H, CH_3 -*i*-Pr), 0.63 (d, $^3J_{\text{H,H}} = 6.9$ Hz, 3 H, CH_3 -*i*-Pr), 0.70 (d, $^3J_{\text{H,H}} = 6.1$ Hz, 3H, CH_3 -*i*-Pr), 0.76 (s, 3 H, SiCH_3), 0.77-0.79 (m, 2 H), 0.79 (s, 3 H, SiCH_3), 0.80-0.83 (m, 8 H), 0.88 (d, $^3J_{\text{H,H}} = 7.1$ Hz, 3H, CH_3 -*i*-Pr), 0.91-0.94 (m, 2 H), 0.97-1.08 (m, 4 H), 1.16-1.28 (m, 5 H), 1.48-1.58 (m, 6 H), 3.20-3.26 (m, 1 H, 13-H), 3.32-3.37 (m, 1 H, 13-H), 3.42-3.50 (m, 8 H, ace- CH_2), 6.46-6.68 (m, 4 H), 6.91-6.93 (m, 6 H), 7.02-7.13 (m, 8 H), 7.30-7.35 (m, 5 H), 7.45-7.47 (m, 2 H), 7.61-7.63 (m, 2 H), 8.55 (d, $^3J_{\text{H,H}} = 7.1$ Hz, 2 H, 7-H) (the overall integral is by 4 H too high due to overlap with impurities). $^{13}\text{C}\{^1\text{H}\}$ NMR (125.77 MHz, 298.7 K, C_6D_6) $\delta = 0.4$ (CH_3 , SiCH_3), 1.0 (CH_3 , SiCH_3), 13.3, 14.4, 14.8, 15.6, 15.9, 21.6, 22.4, 22.4, 22.8, 22.8, 25.3, 25.3, 30.2 (CH_2 , ace), 30.4 (CH_2 , ace), 34.7 (CH_2), 34.7 (CH_2), 45.2 (CH_2), 45.6 (CH_2), 50.4 (CH, C-14), 50.4 (CH, C-14), 72.9

(CH, C-13), 73.5 (CH, C-13), 119.9 (CH), 120.3 (CH), 124.1 (C), 124.6 (CH), 125.7 (C), 126.4 (CH), 127.5 (CH), 127.8 (CH), 128.0 (CH), 128.2 (CH), 128.4 (CH), 129.4 (C), 129.6 (C), 133.1 (CH), 139.0 (CH), 139.1 (CH), 141.1 (CH), 141.3 (CH), 141.4 (CH), 149.3 (C). $^{29}\text{Si}\{^1\text{H}\}$ NMR (99.31 MHz, 296.1 K, CDCl_3) $\delta = -8.4, -9.6$.

Siloxanes 48B

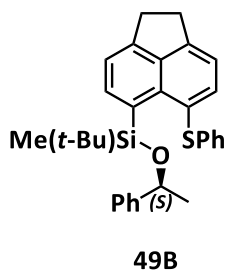
A reaction tube was charged with 1.0 equiv. (262.42 μmol , 100.4 mg) 6-methylphenylsilyl-5-thiophenylacenaphthene **43b** and 15.0 mg Pd nanoparticles. The solids were suspended in 1.0 mL *n*- Bu_2O and 2.5 equiv. (625.00 μmol , 0.75 mL) (*S*)-(-)-phenylethanol **B** were added. The reaction mixture was degassed and heated to 100°C for 16 h. The reaction mixture was cooled to r.t. and filtered through silica gel. After removal of the solvent, the crude product was purified by preparative TLC (petroleum ether/ethyl acetate (99:1)) and a mixture of both siloxanes **48B** was obtained. Yield: 16 mg (31.49 μmol ; 12%).



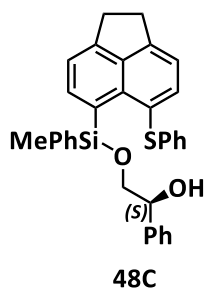
^1H NMR (300.23 MHz, 298.2 K, CDCl_3) $\delta = 0.62$ (s, 3 H, SiCH_3), 0.78 (s, 3 H, SiCH_3), 1.29-1.32 (m, 6 H, CH_3), 3.39-3.53 (m, 8 H, CH_2), 4.70-4.78 (m, 2 H, OCHMePh), 6.44-6.51 (m, 4 H), 6.90-6.94 (m, 6 H), 7.02-7.33 (m, 25 H, overlap with CHCl_3), 7.48-7.50 (m, 1 H), 7.61-7.65 (m, 2 H), 8.35 (d, $^3J_{\text{H,H}} = 7.1$ Hz, 1 H), 8.72 (d, $^3J_{\text{H,H}} = 7.1$ Hz, 1 H). $^{13}\text{C}\{^1\text{H}\}$ NMR (125.77 MHz, 298.7 K, CDCl_3) $\delta = 0.0$ (CH_3 , SiCH_3), 0.5 (CH_3 , SiCH_3), 26.9 (CH_3), 30.2 (CH_2), 30.4 (CH_2), 71.1 (CH), 71.5 (CH), 109.7 (C), 119.9 (CH, ace), 120.0 (CH), 120.4, 124.7, 124.9 (C), 125.7 (CH, ace), 125.8 (CH, Ph), 126.5 (CH), 126.6, 126.7 (CH), 127.5 (CH), 127.5 (CH), 128.1, 128.2, 128.4 (CH, ace), 128.5 (CH, ace), 133.2 (CH), 133.3, 138.9 (CH), 141.0 (CH, C-7), 139.3 (C, ace), 140.3 (C, ace), 148.3 (C, ace), 146.8 (C, *ipso*-Ph), 149.2 (C, ace). $^{29}\text{Si}\{^1\text{H}\}$ INEPT NMR (59.65 MHz, 298.2 K, CDCl_3) $\delta = -7.7, -6.5$.

Siloxanes 49B

A reaction tube was charged with 1.0 equiv. (269.16 μmol , 97.6 mg) 6-methyl-*tert*-butylsilyl-5-thiophenylacenaphthene **43c** and 9.7 mg Pd nanoparticles. The solids were suspended in 1.0 mL *n*-Bu₂O and 2.5 equiv. (672.90 μmol , 0.80 mL) (*S*)-(-)-phenylethanol **B** were added. The reaction mixture was degassed and heated to 100°C for 4 days. The reaction mixture was cooled to r.t. and filtered through silica gel. 91 mg (253.01 μmol , 94 %) of the starting silane **43c** were recovered. No product could be observed.

**Siloxanes 48C**

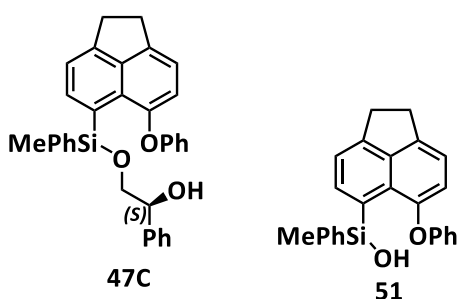
A reaction tube was charged with 1.0 equiv. (250.00 μmol , 95.7 mg) 6-methylphenylsilyl-5-thiophenylacenaphthene **43b**, 1.0 equiv. (250.00 μmol , 34.5 mg) (*S*)-(+)-1-phenyl-1,2-ethandiol **C** and 6.5 mg Pd nanoparticles. The solids were suspended in 1.0 mL *n*-Bu₂O. The reaction mixture was degassed and heated to 70°C for 4 h. No reaction was observed. Therefore, the temperature was changed to 100°C for further 16 h. The reaction was cooled to r.t. and filtrated through silica gel. After removal of the solvent, the crude product was purified by preparative TLC (petroleum ether/ethyl acetate (9:1)). One main fraction was recovered. Due to its complexity, no clear assignment of the signals was made. The product **48C** was not identified unambiguously.



²⁹Si{¹H} INEPT NMR (99.31 MHz, 296.0 K, CDCl₃) δ = -6.2, -4.9, -4.6, -4.5, -4.4.

Siloxanes 47C

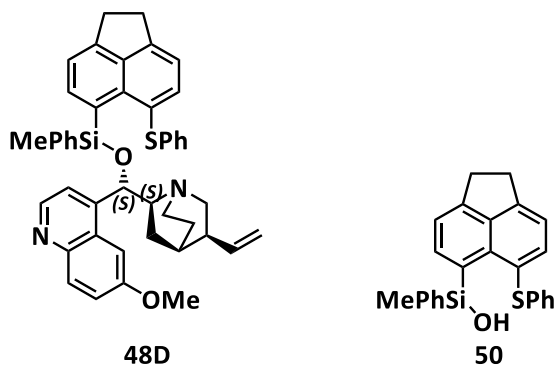
A reaction tube was charged with 0.9 equiv. (133.96 μmol , 49.1 mg) 6-phenoxy-5-methylphenylsilylacenaphthene **42b**, 1.0 equiv. (149.82 μmol , 20.7 mg) (*S*)-(+)-1-phenyl-1,2-ethandiol **C** and 5.3 mg Pd nanoparticles. The solids were suspended in 0.7 mL *n*-Bu₂O. The reaction mixture was degassed and heated to 70°C for 16 h. The reaction was cooled to r.t. and filtrated through silica gel. After removal of the solvent, the crude product was purified by preparative TLC (cyclohexane/ethyl acetate (9:1)). A mixture of the products **47C** and most likely the silanol **51** was obtained.



²⁹Si{¹H} INEPT NMR (99.31 MHz, 296.0 K, CDCl₃) δ = -2.0 (tentatively assigned to **51**), -1.7, -1.4.

Siloxanes 48D

A reaction tube was charged with 1.0 equiv. (250.00 μmol , 95.7 mg) 6-methylphenylsilyl-5-thiophenylacenaphthene **43b**, 1.0 equiv. (250.00 μmol , 81.1 mg) (+)-quinidine **D** and 9.0 mg Pd nanoparticles. The solids were suspended in 1.0 mL *n*-Bu₂O. The reaction mixture was degassed and heated to 100°C for 16 h. Colorless crystals formed at the glass wall of the tube. Therefore, further 1.0 mL *n*-Bu₂O was added. The mixture was heated for further 2 days at 100 °C. A reaction control via NMR spectroscopy showed the formation of silanol **50**. After additional 16 h of stirring at 100 °C, the reaction was stopped by cooling to r.t. and filtration through silica gel. After removal of the solvent, the crude product was purified by preparative TLC (pentane/ethyl acetate (99:1)). Two main fractions were collected: the first fraction was the starting silane **43b** (25 mg, 65.00 μmol , 26 %) and the second fraction was the silanol **50** (15 mg, 37.50 μmol , 15 %). The NMR data of silanol **50** is given below. The products **48D** were not obtained.



$^1\text{H NMR}$ (300.23 MHz, 298.2 K, CDCl_3) δ = 0.77 (s, 3 H, SiCH_3), 3.40-3.52 (m, 4 H, CH_2), 6.66-6.72 (m, 2 H), 6.99-7.06 (m, 3 H), 7.13-7.23 (m, 3 H), 7.30-7.34 (m, 1 H), 7.38-7.43 (m, 3 H), 7.69 (d, $^3J_{\text{H,H}} = 7.1$ Hz, 1 H), 8.21 (d, $^3J_{\text{H,H}} = 7.0$ Hz, 1 H). $^{29}\text{Si}\{^1\text{H}\}$ INEPT NMR (59.65 MHz, 298.2 K, CDCl_3) δ = -4.5.

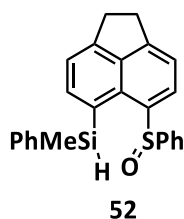
Single crystals suitable for X-ray diffraction analysis of silanol **50** were obtained from this batch.

5.4.2 Kinetic Resolution – Oxidation of Thiophenyl Group

Experiment 1: A Schlenk flask was charged with 1.0 equiv. (250.00 μmol , 95.7 mg) 6-methylphenylsilyl-5-thiophenylacene **43b** in 2 mL DCM. Then 4.0 equiv. (1.00 mmol, 172 μL) (+)-diethyl L-tartrate and 2.0 equiv. (500.00 μmol , 148 μL) titanium tetrakispropoxide were added at r.t.. The mixture was then cooled to -40 $^\circ\text{C}$ before adding 1.0 equiv. (250.00 μmol , 25 μL) *tert*-butyl hydroperoxide. The progress of the reaction was monitored by TLC. After 17 h stirring at -40 $^\circ\text{C}$ no reaction was observed. The mixture was warmed to -20 $^\circ\text{C}$ and stirred for further 3 h, but still no reaction could be observed. The mixture was warmed to r.t. and stirred for 3 days. Then the reaction was stopped by filtration through a thin layer of silica gel. After removal of the solvent and subsequent purification by column chromatography (petroleum ether/ethyl acetate 8:2) 80 mg (209.10 μmol , 84 %) of the starting silane were recovered. The product **52** was not observed.

Experiment 2: A flask was charged with 0.04 equiv. (20.00 μmol , 5.3 mg) vanadyl acetylacetonate and 0.06 equiv. (30.00 μmol , 9.8 mg) (*R,R*)-*N,N'*-bissalicyl-*N,N'*-dimethyl-1,1-diaminocyclohexane^[67] in 4 mL chloroform. The mixture was stirred for 45 min at r.t. until a color change was observed. Then 1.0 equiv. (500.00 μmol , 191.3 mg) 6-methylphenylsilyl-5-thiophenylacene **43b** was dissolved in 1 mL chloroform and added to the reaction mixture at r.t.. The mixture was stirred for 10 min and then cooled to 0 $^\circ\text{C}$. When the temperature was reached, 1.5 equiv. (750.00 μmol , 0.77 mL, 30%(ww) in H_2O) H_2O_2 were added to the mixture and it was stirred at 0 $^\circ\text{C}$ for 16 h. The reaction progress was

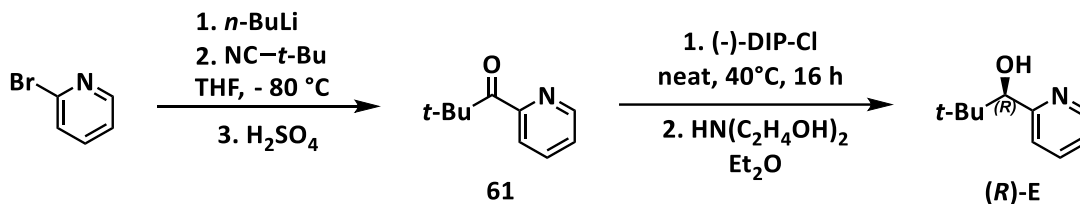
monitored via TLC. After 16 h at 0 °C no reaction was observed. The mixture was warmed to 10 °C and stirred for further 20 h. No significant conversion was observed. Further 0.5 equiv. (250.00 μmol, 0.25 mL) H₂O₂ was added and the mixture was stirred at 10 °C for further 23 h. The reaction was stopped by adding 15 mL H₂O and the organic compounds were extracted with DCM (3 x 15 mL). After drying the organic layer over Na₂SO₄ and removal of the solvent, the crude product was purified via column chromatography (petroleum ether/ethyl acetate 9:1). 140 mg (365.92 μmol, 73%) of the starting silane **43b** were recovered. The second fraction (25 mg) was a mixture of at least five silicon species.



²⁹Si{¹H} INEPT NMR (99.31 MHz, 296.0 K, CDCl₃) δ = -4.0, -5.3, -6.2, -11.3, -17.2 (**43b**).

5.4.3 Kinetic Resolution - Dehydrogenative Si-O Coupling

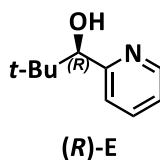
(*R*)-2,2-Dimethyl-1-(pyridin-3-yl)propan-1-ol (*R*)-E



The first step is the synthesis of 2-pivaloylpyridine **61**. Therefore, a round-bottom Schlenk flask was charged with 1.0 equiv. (30.00 mmol, 2.86 mL) 2-bromopyridine and ca. 100 mL THF. The mixture was cooled to -80 °C and 1.0 equiv. (30.00 mmol, 18.75 mL) *n*-BuLi was added slowly (within 30 min). The color of the reaction mixture changed from light yellow to red. After stirring for 2 h at this temperature, 1.0 equiv. (30.00 mmol, 3.32 mL) pivalonitrile was added. The reaction mixture was stirred for 1 h at -80 °C and was then warmed slowly to -50 °C (within 1h). Then the cooling bath was removed and the mixture was stirred for further 1.5 h. A solid precipitated. The reaction mixture was then transferred to a flask which was cooled with an ice bath and charged with ca. 60 mL 1 M H₂SO₄

and a big stirring bar (Circulus). This mixture was stirred for 1.5 h. Subsequently, the phases were separated and the product **61** was extracted from the aqueous layer with Et₂O (3 x 20 mL). The combined organic layers were dried over Na₂SO₄ and the solvent was removed. If everything works fine, there is no need for further purification. If not: purification via distillation (so far, that was not necessary for me). 2-Pivaloylpyridine **61** was obtained as a light yellow liquid with a yield of 4.61 g (28.24 mmol, 94 %).

The second step is the reduction of 2-pivaloylpyridine **61**. Therefore, a round-bottom Schlenk flask was charged with 1.0 equiv. (15.38 mmol, 2.51 g) (-)-B-chlorodiisopinocampheylborane ((-)-DIP-Cl). Then 1.0 equiv. (15.38 mmol, 4.93 g) 2-pivaloylpyridine **61** were added and the mixture was stirred at 40 °C for 6 h. After cooling the reaction mixture to r.t., the mixture was dissolved in ca. 50 mL Et₂O. In a separated flask with stirring bar, 3.0 equiv. (46.14 mmol, 4.45 mL) diethanolamine was dissolved in ca. 20 mL Et₂O. The reaction mixture was transferred to the diethanolamine at r.t. and the mixture was stirred for 3 h. A white solid precipitated. The precipitate was filtered off and the solvent was removed. The crude product (**R**)-**E** was purified via column chromatography with petroleum ether/ethyl acetate (8:2 → 7:3) as eluent. The product (**R**)-**E** was obtained as a colorless oily liquid with a yield of 1.39 g (8.41 mmol, 55 %) and an optical rotation of $[\alpha] = 11.41^\circ$ ($c = 1 \text{ molL}^{-1}$, CHCl₃) and an enantiomeric excess of ee = 96 % (chiral GC).



¹H NMR (300.14 MHz, 295.1 K, CDCl₃) $\delta = 0.92$ (s, 9 H, t-Bu), 4.38 (s, 1 H), 4.68 (brs, 1 H, OH), 7.13-7.18 (m, 1 H), 7.22-7.27 (m, 1 H), 7.58-7.65 (m, 1 H), 8.47-8.51 (m, 1 H). ¹³C{¹H} NMR (75.48 MHz, 295.4 K, CDCl₃) $\delta = 25.9$ (CH₃, t-Bu), 36.3 (C, t-Bu), 80.4 (CH, OC), 122.3 (CH), 122.9 (CH), 135.6 (CH), 147.8 (CH), 160.1 (C). ¹H/¹⁵N HMBC NMR (500.45 MHz, 300.0 K, CDCl₃) $\delta = 300.5$. Chiral GC $t_R = 56.6$ (88.6 %), 57.3 (11.4 %).

General Procedure for the Kinetic Resolution of Silanes

A Schlenk flask was charged with copper(I)chloride and triphenylphosphane in a ratio of 1:2. Toluene was added and the mixture was stirred until triphenylphosphane was dissolved. Subsequently sodium *tert*-butoxide (equimolar to CuCl) was added at r.t. and the mixture was stirred until the color turned yellow (5 – 10 min). The pyridyl alcohol (**R**)-**E** was dissolved in toluene and added at r.t. to the catalyst mixture. The mixture turned orange. Subsequently the silane was added either as a solid in one portion or dissolved in toluene whereupon the mixture turned brown-red. After stirring for approximately 16 h, the reaction mixture was filtrated through a thin layer of silica gel to remove the Cu(I) species, the solvent was removed and the crude product was purified by a two-step column chromatography if not mentioned otherwise in the details. The first column chromatography (eluent petroleum ether/ethyl acetate 100:0 → 50:50) with a short column resulted in two fraction: 1. (+)-Silane + Ph₃P, 2. Siloxanes + impurities. Both fractions needed further purification which is specified for each compound in detail below.

6-Phenoxy-5-methylphenylsilylacenaphthene **42b**

The kinetic resolution of the title compound **42b** was performed four times with slightly altered conditions and outcomes which are listed in Table 34. **Entry 1**: Silane **42b** added as solid in one portion. In all other entries the silane **42b** was dissolved in toluene prior to the addition. **Entry 3**: The alcohol/toluene solution was added at r.t., the silane **42b**/toluene mixture at -40 °C, the mixture was warmed slowly to -13°C as a color change was observable, the mixture was cooled again to -35°C and stirred at this temperature for 1 h, afterwards the mixture was slowly warmed to r.t. over night. **Entry 4**: The catalyst was prepared as usual at r.t., then the mixture was cooled with an ice bath, first the alcohol/toluene and subsequently the silane **42b**/toluene mixture was added dropwise, the mixture was warmed slowly to r.t. over night.

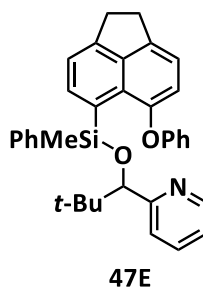
Table 34 – Reaction conditions and yields of the attempts for the kinetic resolution of 6-phenoxy-5-methylphenylsilylacenaphthene **42b** ($[\alpha]_D$ measured in Et₂O).

Entry	Catalyst CuCl	Silane 42b	Alcohol (<i>R</i>)-E	T	Yield Silane 42b	ee/ $[\alpha]_D$ Silane 42b	Yield Siloxane 47E	dr Siloxane 47E
1	0.2 equiv. 144.6 μmol	1.0 equiv. 723.0 μmol	0.55 equiv. 397.6 μmol	r.t.	82 % ^{a)}	-	21 % ^{b)}	89:11
2	0.2 equiv. 259.7 μmol	1.0 equiv. 1.3 mmol	0.5 equiv. 649.3 μmol	r.t. (31°C)	85 %	ee = 2 % $[\alpha] = +0.4^\circ$ (0.04 molL ⁻¹)	12 %	68:32
3	0.2 equiv. 151.5 μmol	1.0 equiv. 783.0 μmol	0.5 equiv. 391.5 μmol	-40°C	62 %	ee = 44 % $[\alpha] = +5^\circ$ (0.006 molL ⁻¹)	10 %	86:14
4	0.2 equiv. 305.6 μmol	1.0 equiv. 3.06 mmol	0.53 equiv. 1.61 mmol	0°C	52 %	ee = 56 % $[\alpha] = +12^\circ$ (0.01 molL ⁻¹)	61 % ^{b),c)}	85:15

a) mixture with Ph₃P, yield calculated from ¹H NMR and GC/MS, b) used for reduction from siloxane to (-)-silane, c) not pure.

Purification

Entry 1: column chromatography (eluent petroleum ether/ethyl acetate 100:0 → 70:30). **Entry 2:** First column chromatography (eluent petroleum ether/ethyl acetate 99:1 → 90:10). Fraction 1 ((+)-silane **42b** + Ph₃P) was further purified by oxidation of the phosphane with H₂O₂. Therefore, the solid were dissolved in petroleum ether and 1.0 mL H₂O₂ (30w% in H₂O) was added at r.t. after stirring the mixture for 16 h the solid which precipitated was filtered off and the phases were separated. The solvent of the organic layer was removed and the residue was purified via recrystallization from hexanes. The second fraction (siloxanes **47E**) was purified via preparative TLC (eluent petroleum ether/ethyl acetate 90:10). **Entry 3:** First short column chromatography (eluent petroleum ether/ethyl acetate 100:0 → 0:100) resulting in two fractions. Fraction 1 ((+)-silane **42b** + Ph₃P) was further purified by oxidation (see Entry 2) of the Ph₃P (0.7 mL H₂O₂ 30w% in H₂O) subsequent filtration and recrystallization from hexanes. Fraction 2 (siloxanes **47E**) was purified via preparative TLC (eluent petroleum ether/ethyl acetate 90:10). **Entry 4:** First short column chromatography (eluent petroleum ether/ethyl acetate 100:0 → 0:100) resulting in two fractions. Fraction 1 ((+)-silane **42b** + Ph₃P) was further purified by oxidation (see Entry 2) of the Ph₃P (0.7 mL H₂O₂ 30w% in H₂O) subsequent filtration and recrystallization from hexanes. Fraction 2 (siloxanes **47E**) was not further purified. The crude fraction 2 was used for the reduction of siloxane to obtain (-)-silane **42b**.

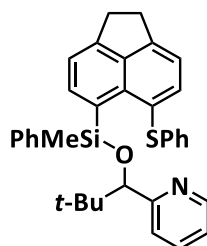


¹H NMR (499.87 MHz, 305.0 K, C₆D₆) δ = 0.99 (s, 3 H, SiCH₃), 1.21 (s, 9 H, *t*-Bu), 2.99-3.04 (m, 2 H, CH₂), 3.12-3.17 (m, 2 H, CH₂), 5.02 (s, 1 H, OCH), 6.47 (dm, ³J_{H,H} = 7.7 Hz, 2 H, OPh), 6.50-6.53 (m, 1 H, Py), 6.56 (d, ³J_{H,H} = 7.5 Hz, 1 H, 7-H), 6.78-6.81 (m, 2 H, Si-*m*-Ph), 6.82-6.85 (m, 2H, 8-H, *O*-*ipso*-Ph), 6.89-6.97 (m, 4 H, Py, OPh, Si-*p*-Ph), 7.16-7.18 (m, 2 H, Si-*o*-Ph), 7.26 (dm, ³J_{H,H} = 7.9 Hz, 1 H, Py), 7.46 (dm, ³J_{H,H} = 6.9 Hz, 1 H, 3-H), 8.27-8.31 (m, 1 H, Py), 8.96 (d, ³J_{H,H} = 6.9 Hz, 4-H). Additional signals for second diastereomer: 0.57 (s, SiCH₃), 1.06 (s, *t*-Bu), 4.94 (s, OCH), 7.51 (d, ³J_{H,H} = 7.0 Hz, 3-H), 8.47-8.49 (m, Py), 8.96 (d, ³J_{H,H} = 7.0 Hz, 4-H). **¹³C{¹H} NMR** (125.71 MHz, 305.0 K, C₆D₆) δ = -2.0 (SiCH₃), 26.8 (CH₃, *t*-Bu), 29.6 (CH₂), 31.0 (CH₂), 36.8 (C, *t*-Bu), 84.5 (CH, OC), 112.0 (CH, C-7), 120.3 (CH, C-3), 121.3 (CH), 121.3 (CH, Py), 123.1 (CH, Py), 124.0 (CH), 126.1 (C), 127.1 (CH), 128.2 (CH, Py), 128.7 (C), 129.6 (CH), 133.6 (CH), 134.5 (CH, Py), 138.5 (CH, C-4), 139.0 (C), 140.0 (C, ace), 141.4 (C, ace), 147.5 (CH, Py), 148.5 (C, ace), 153.4 (C, C-6), 155.4 (C, *O*-*ipso*-Ph), 162.3 (C, Py). **²⁹Si{¹H} NMR** (99.31 MHz, 305.0 K, C₆D₆) δ = -5.0 (main), -4.6. **¹H/¹⁵N HMBC NMR** (499.87 MHz, 305.0 K, C₆D₆) δ = 316.5 (main), 317.5. **EA** C₃₅H₃₅NO₂Si, calc: C 79.35, H 6.66, N 2.64, found: C 61.48, H 6.15, N 2.11.

6-Methylphenylsilyl-5-thiophenylacenaphthene **43b**

For the chiral resolution of 1.0 equiv. (1.05 mmol, 401.0 mg) of the title compound **43b** 0.2 equiv. (213.14 μmol, 21.1 mg) copper(I)chloride, 0.4 equiv. (242.34 μmol, 111.3 mg) triphenylphosphane, 0.2 equiv. (208.11 μmol, 20.0 mg) sodium *tert*-butoxide and 0.55 equiv. (576.75 μmol, 95.3 mg in 3.5 mL toluene) of the pyridyl alcohol (**R**)-**E** were used. The catalyst was prepared in 2.0 mL toluene and the silane **43b** was added as a solid in one portion. The crude product was an oil which was adsorbed on silica for a solid deposition at the column. Eluent for column chromatography petroleum ether/ethyl acetate 98:2 → 90:10. Two fractions collected: the first fraction was the (+)-silane **43b** and Ph₃P, which was further purified via preparative TLC (eluent petroleum ether/ethyl acetate 99:1, TLC was three times eluted). The yield of (+)-silane **43b** ([α]_D = 11, c = 0.06 molL⁻¹, in Et₂O; ee = 66 %)

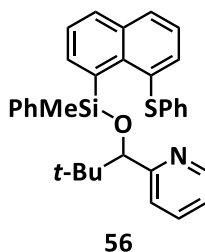
was 113.0 mg (295.35 μmol , 56 %). The second fraction contained the siloxanes **48E** and impurities. Siloxanes **48E** were obtained purely by adding a pentane/ethyl acetate 9:1 mixture to the oil. Siloxanes **48E** were dissolved and the impurities precipitated. After removal of the solvent, siloxanes **48E** were obtained as a colorless viscous oil. The yield of siloxanes **48E** was 171.0 mg (313.29 μmol , 60 %).



^1H NMR (499.87 MHz, 305.0 K, C_6D_6) δ = 1.09 (s, 3 H, SiCH_3), 1.19 (s, 9 H, *t*-Bu), 2.94-2.98 (m, 2 H, CH_2), 3.05-3.09 (m, 2 H, CH_2), 5.00 (s, 1 H, OCH), 6.49-6.53 (m, 1 H, Py), 6.56-6.59 (m, 2 H), 6.70-6.74 (m, 3 H), 6.77-6.81 (m, 2 H, SiPh), 6.84-6.91 (m, 2 H, Py), 6.93 (dm, $^3J_{\text{H,H}} = 7.2$, 1 H, 3-H), 7.18-7.21 (m, 2 H, Py), 7.22-7.25 (m, 2 H, SiPh), 7.43 (dm, $^3J_{\text{H,H}} = 7.1$, 1 H, 8-H), 7.66 (d, $^3J_{\text{H,H}} = 7.1$ Hz, 1 H, 4-H), 8.28-8.30 (m, 1 H, Py), 9.19 (d, $^3J_{\text{H,H}} = 7.1$ Hz, 7-H). Additional signals for second diastereomer: 0.66 (s, SiCH_3), 1.03 (s, *t*-Bu), 4.96 (s, OCH), 6.64-6.68 (m), 7.03-7.07 (m), 7.10-7.14 (m), 7.49 (dm, $^3J_{\text{H,H}} = 7.0$ Hz), 7.53-7.56 (m), 7.59 (dm, $^3J_{\text{H,H}} = 7.9$ Hz), 7.69 (d, $^3J_{\text{H,H}} = 7.2$ Hz), 8.46-8.49 (m), 8.62 (d, $^3J_{\text{H,H}} = 7.0$), 9.32 (d, $^3J_{\text{H,H}} = 7.1$ Hz). **$^{13}\text{C}\{^1\text{H}\}$ NMR** (125.71 MHz, 305.0 K, C_6D_6) δ = -0.6 (SiCH_3), 26.8 (CH_3 , *t*-Bu), 30.0 (CH_2), 30.3 (CH_2), 36.8 (C, *t*-Bu), 84.5 (CH, OC), 120.2 (CH, C-8), 120.6 (CH, C-3), 121.2 (CH, Py), 123.2 (CH, Py), 124.8 (CH), 126.3 (C), 126.8 (CH), 127.3 (CH), 127.9 (CH), 128.6 (CH), 129.0 (C, C-6), 133.1 (CH, SiPh), 134.4 (CH), 139.4 (CH, C-4), 139.4 (C), 140.0 (C), 140.9 (C, ace), 141.3 (CH, C-7), 141.4 (C), 147.5 (CH, Py), 149.3 (C, ace), 149.6 (C, ace), 162.2 (C, Py). Additional signals for the second diastereomer: -0.2 (SiCH_3), 26.7 (CH_3 , *t*-Bu), 36.7 (C, *t*-Bu), 83.9 (CH, OC), 120.3 (CH), 120.6 (CH), 121.7 (CH), 122.9 (CH), 124.7 (CH), 126.2 (C), 126.5 (CH), 127.1, (CH), 127.9 (CH), 128.3 (CH), 129.0 (C), 135.1 (CH), 139.5 (CH), 139.6 (C), 140.1 (CH), 141.2 (C), 141.3 (CH), 141.7 (C), 148.0 (CH), 163.7 (C). **$^{29}\text{Si}\{^1\text{H}\}$ NMR** (99.31 MHz, 305.0 K, C_6D_6) δ = -8.1 (main), -7.6. **$^1\text{H}/^{15}\text{N}$ HMBC NMR** (499.87 MHz, 305.0 K, C_6D_6) δ = 310.6, 307.8 (main).

8-Methylphenylsilyl-1-thiophenylnaphthalene 44

For the chiral resolution of 1.0 equiv. (818.94 μmol , 292.0 mg) of the title compound **44** 0.1 equiv. (163.78 μmol , 16.0 mg) copper(I)chloride, 0.2 equiv. (327.58 μmol , 86.0 mg) triphenylphosphane, 0.1 equiv. (163.78 μmol , 16.0 mg) sodium *tert*-butoxide and 0.6 equiv. (491.36 μmol , 81.0 mg in 2 mL toluene) of pyridyl alcohol (**R**)-**E** were used. The catalyst was prepared in 2 mL toluene and the silane was added as a solid. The first column chromatography resulted in two fractions: 1. (+)-silane **44** + Ph_3P (209 mg), 2. siloxanes **56** + impurities (217 mg). Preparative TLC of the first fraction (eluent petroleum ether, eluted three times) gave 86.0 mg (241.19 μmol , 59 %) of (+)-silane **44** ($[\alpha]_{\text{D}} = 17$, $c = 0.04 \text{ molL}^{-1}$, in Et_2O ; ee = 84 %). Preparative TLC of the second fraction (eluent petroleum ether/ethyl acetate 9:1) gave 159.0 mg (305.90 μmol , 75 %) of siloxanes **56**.



^1H NMR (499.87 MHz, 305.1 K, C_6D_6) $\delta = 1.07$ (s, 3 H, SiCH_3), 1.15 (s, 9 H, *t*-Bu), 4.91 (s, 1 H, OCH), 6.40-6.43 (m, 2 H, SPh), 6.48-6.52 (m, 1 H, Py), 6.65-6.71 (m, 3 H, SPh), 6.74-6.78 (m, 2 H), 6.83-6.88 (m, 2H, Py), 7.04-7.10 (m, 3 H, naph, Py), 7.13-7.17 (m, 2 H, SiPh), 7.56-7.61 (m, 1 H, 6-H), 7.62-7.67 (m, 2 H, SiPh), 7.76-7.79 (m, 1 H), 8.26-8.29 (m, 1 H, Py), 9.24-9.28 (m, 7-H), the sum of the integrals in the aromatic region is by 1 H too high, most likely due to overlap with the second diastereomer. Additional signals for second diastereomer: 0.63 (s, SiCH_3), 0.99 (s, *t*-Bu), 4.90 (s, OCH), 6.36-6.39 (m), 6.57-6.59 (m), 7.43-7.48 (m), 7.49-7.52 (m), 8.44-8.47 (m, Py), 9.33-9.36 (m, 7-H). **$^{13}\text{C}\{^1\text{H}\}$ NMR** (125.71 MHz, 305.0 K, C_6D_6) $\delta = -0.6$ (SiCH_3), 26.7 (CH_3 , *t*-Bu), 36.6 (C, *t*-Bu), 84.4 (CH, OC), 120.9 (CH, Py), 122.9 (CH, Py), 125.0 (CH), 125.8 (CH, naph), 125.8 (CH), 126.7 (CH, SPh), 127.1 (CH), 127.6 (CH), 128.5 (CH), 131.2 (C), 131.3 (CH), 131.5 (CH), 132.6 (CH), 134.1 (C, C-8/Si-*ipso*-Ph), 134.2 (CH), 135.4 (C), 137.1 (CH), 139.2 (C, C-8/Si-*ipso*-Ph), 140.1 (CH, C-7), 140.1 (C), 140.9 (C), 147.3 (CH, Py), 161.9 (C, Py). Additional signals for the second diastereomer: -0.1 (SiCH_3), 26.6 (CH_3 , *t*-Bu), 36.5 (C, *t*-Bu), 83.3 (CH, OC), 121.5 (CH), 122.7 (CH), 124.9 (CH), 135.6 (C), 140.6 (C), 141.7 (C), 147.9 (CH), 163.4 (C). **$^{29}\text{Si}\{^1\text{H}\}$ NMR** (99.31 MHz, 305.0 K, C_6D_6) $\delta = -11.2$ (main), -10.9. **$^1\text{H}/^{15}\text{N}$ HMBC NMR** (499.87 MHz,

305.0 K, C₆D₆) δ = 316.6. **HRMS** protonated at N atom C₃₃H₃₄NOSSi, found: 520.2128, calculated 520.2130.

5.4.4 Reduction of Siloxanes

The siloxanes were dissolved in 2-20 mL diethylether and di-*iso*-butylaluminiumhydride (1 M in *n*-hexane) was added at r.t.. The mixture was stirred for 16 h and afterwards quenched by addition of 1-20 mL 1 M HCl. The two phasic mixture was stirred for 20-60 min, the phases were separated and the product was extracted from the aqueous layer (3 x 5-20 mL Et₂O). After removal of the solvent, the product was purified via column chromatography or preparative TLC (eluent PE). Details see Table 35. **Entry 1:** Reaction in 20 mL Et₂O, work up with 20 mL 1 M HCl. **Entry 2:** Reaction in 4 mL Et₂O, work up with 3 mL 1 M HCl. **Entry 3:** Reaction in 2 mL Et₂O, work up with 1 mL 1 M HCl.

Table 35 – Batches of the reduction of siloxanes **47E**, **48E** and **56** to the corresponding (-)-silanes **42b**, **43b** and **44** ($[\alpha]_D$ measured in Et₂O).

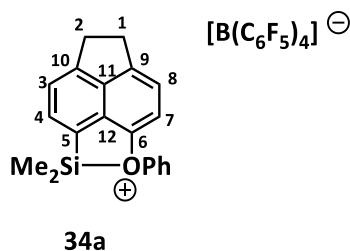
Entry	Compound	1.0 equiv. siloxane	2.0-2.5 equiv. DIBAL-H	Yield	$[\alpha]_D$ (-)-silane	ee (-)-silane
1	47E	993 mg (1.87 mmol)	4.70 ml (4.69 mmol)	561 mg (82 %)	-11° (0.02 molL ⁻¹)	64 %
2	48E	174 mg (318.79 μ mol)	0.64 mL (637.58 μ mol)	97 mg (80 %)	-11° (0.05 molL ⁻¹)	64 %
3	56	158 mg (303.98 μ mol)	0.76 mL (759.94 μ mol)	75 mg (69 %)	-15° (0.04 molL ⁻¹)	54 %

5.5 Synthesis of Silyl Borates

General Procedure D: The silane and trityl borate $[\text{Ph}_3\text{C}][\text{B}(\text{C}_6\text{F}_5)_4]$ were dissolved in benzene. Then the solution of the trityl borate was added to the silane at r.t. and the biphasic reaction mixture was stirred for 30 min. Subsequently, the phases were separated, the upper, nonpolar phase was removed and the polar phase was washed with benzene three times. After removing the solvent under low pressure, the residue was dissolved in a deuterated solvent and analyzed by NMR spectroscopy.

Phenoxy-Stabilized Silyl Borate **34a** $[\text{B}(\text{C}_6\text{F}_5)_4]^{[6a]}$

Silyl borate **34a** $[\text{B}(\text{C}_6\text{F}_5)_4]$ was synthesized according to general procedure **D** using 1.1 equiv. of silane **42a** (460 μmol , 140 mg) and 1.0 equiv. of trityl borate (438 μmol , 404 mg).

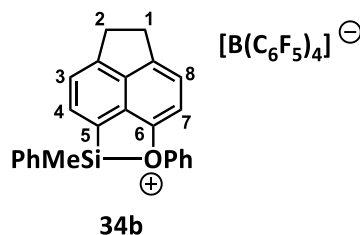


^1H NMR (499.87 MHz, 297.8 K, C_7D_8) δ = 0.31 (s, 6 H, $\text{Si}(\text{CH}_3)$), 3.02-3.06 (m, 2 H, CH_2 , 2-H), 3.10-3.14 (m, 2 H, CH_2 , 1-H), 6.13 (d, 3J = 7.8 Hz, 1 H, CH, 7-H), 6.60-6.63 (m, 2 H, CH, Ph), 6.79 (dm, 3J = 7.9 Hz, 1 H, CH, 8-H), 7.16-7.24 (m, 3 H, CH, Ph), 7.27 (dm, 3J = 7.0 Hz, 1 H, CH, 3-H), 7.55 (d, 3J = 7.0 Hz, 1 H, CH, 4-H). **^1H NMR** (499.87 MHz, 305.1 K, C_6D_6) δ = 0.41 (s, 6 H, $\text{Si}(\text{CH}_3)_2$), 3.13-3.15 (m, 2 H, CH_2 , 2-H), 3.24-3.26 (m, 2 H, CH_2 , 1-H), 6.25 (d, 3J = 7.8 Hz, 1 H, CH, 7-H), 6.72-6.73 (m, 2 H, CH, Ph), 6.91 (d, 3J = 7.8 Hz, 1 H, CH, 8-H), 7.27-7.30 (m, 2 H, CH, Ph), 7.33-7.34 (m, 1 H, CH, *p*-Ph), 7.41 (d, 3J = 7.0 Hz, 1 H, CH, 3-H), 7.67 (d, 3J = 7.0 Hz, 1 H, CH, 4-H). **$^{13}\text{C}\{^1\text{H}\}$ NMR** (75.48 MHz, 297.8 K, C_7D_8) δ = -0.5 ($\text{Si}(\text{CH}_3)_2$), 30.7 (CH_2 , C-2), 32.5 (CH_2 , C-1), 108.6 (CH, C-7), 115.2 (C, C-5), 119.6 (CH, C-8), 121.6 (CH, Ph), 124.2 (CH, C-3), 124.8 (C), 131.8 (CH, Ph), 132.4 (CH, Ph), 134.7 (CH, C-4), 137.1 (dm, 1J = 235.4 Hz, $[\text{B}(\text{C}_6\text{F}_5)_4]$), 139.1 (dm, 1J = 233.6 Hz, $[\text{B}(\text{C}_6\text{F}_5)_4]$), 139.1 (C), 146.1 (C), 148.3 (C, *ipso*-Ph), 149.2 (dm, 1J = 248.9 Hz, $[\text{B}(\text{C}_6\text{F}_5)_4]$), 151.6 (C), 152.4 (C, C-6). The broad signal of the *ipso*-C atom of the borate anion is hidden by a triplet signal of the solvent toluene- d_8 . **$^{13}\text{C}\{^1\text{H}\}$ NMR** (125.71 MHz, 305.0 K, C_6D_6) δ = -0.6 ($\text{Si}(\text{CH}_3)_2$), 30.5 (CH_2 , C-2), 32.3 (CH_2 , C-1), 108.5 (CH, C-7), 115.0 (C, C-5), 119.4 (CH, C-8), 121.4 (CH, Ph), 124.0 (CH, C-3), 124.2-125.7 (C, $[\text{B}(\text{C}_6\text{F}_5)_4]$), 124.5 (C), 131.6 (CH, Ph), 132.2

(CH, Ph), 134.5 (CH, C-4), 137.0 (dm, $^1J = 233.5$ Hz, $[B(C_6F_5)_4]$, CF), 128.9 (dm, $^1J = 233.0$ Hz, $[B(C_6F_5)_4]$, CF), 138.9 (C), 145.9 (C), 147.9 (C, *p*-Ph), 149.1 (dm, $^1J = 241.9$ Hz, $[B(C_6F_5)_4]$, CF), 151.3 (C), 152.1 (C, C-6). $^{29}Si\{^1H\}$ NMR (99.36 MHz, 299.6 K, C_6D_6) $\delta = 77.4$. $^{19}F\{^1H\}$ NMR (470.30 MHz, 305.0 K, C_6D_6) $\delta = -166.7$ -(-166.4) (m, 8 F, $[B(C_6F_5)_4]$), -162.6 (t, $^3J_{F,F} = 20.6$ Hz, 4 F, $[B(C_6F_5)_4]$), -132.1-(-131.8) (m, 8 F, $[B(C_6F_5)_4]$). $^{11}B\{^1H\}$ NMR (160.46 MHz, 298.5 K, C_7D_8) $\delta = -16.7$.

Phenoxy-Stabilized Methylphenylsilyl borate **34b** $[B(C_6F_5)_4]^{[112]}$

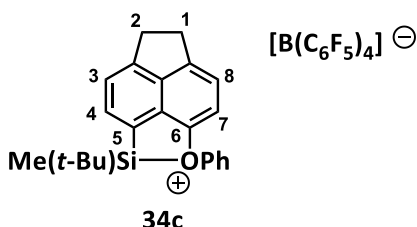
The title compound **34b** $[B(C_6F_5)_4]$ was synthesized according to general procedure **D** using 1.1 equiv. (410 μ mol, 151 mg) of 5-methylphenylsilyl-6-phenoxyacenaphthene **42b** and 1.0 equiv. (380 μ mol, 346 mg) of trityl borate.



1H NMR (499.9 MHz, 305.0 K, C_6D_6) $\delta = 0.63$ (s, 3 H, SiCH₃), 3.07-3.12 (m, 2 H, CH₂), 3.19-3.24 (m, 2 H, CH₂), 6.15 (d, $^3J_{H,H} = 7.8$ Hz, 1 H, 7-H), 6.82-6.84 (m, 1 H, 8-H), 6.98-7.02 (m, 2 H, SiPh), 7.08-7.13 (m, 3 H, SiPh), 7.28-7.33 (m, 1 H, OPh), 7.35-7.38 (m, 1 H, 3-H), 7.61 (d, $^3J_{H,H} = 7.0$ Hz, 1 H, 4-H), the signals of *m*- and *o*-OPh were not found. $^{13}C\{^1H\}$ NMR (125.7 MHz, 305.0 K, C_6D_6) $\delta = -3.9$ (SiCH₃), 30.6 (CH₂), 32.4 (CH₂), 108.7 (CH, C-7), 112.1 (C, C-5), 119.7 (CH, C-8), 121.6 (CH, SiPh), 124.2 (CH, C-3), 125.0 (C, *ipso*-SiPh), 125.5 (C, C-12), 129.4 (CH, SiPh), 131.3 (CH, SiPh), 135.2 (CH), 135.5 (CH, SiPh), 135.9 (CH, C-4), 138.9 (C, C-11), 149.8 (C), 147.9 (C), 151.5 (C), 151.9 (C, C-6). $^{29}Si\{^1H\}$ NMR (99.3 MHz, 305.0 K, C_6D_6) $\delta = 60.8$ ppm. $^{11}B\{^1H\}$ NMR (160.46 MHz, 305.0 K, C_6D_6) $\delta = -16.0$. $^{19}F\{^1H\}$ NMR (470.30 MHz, 305.0 K, C_6D_6) $\delta = -166.7$ -(-166.4) (m, 8 F, $[B(C_6F_5)_4]$), -162.6 (t, $^3J_{F,F} = 20.6$ Hz, 4 F, $[B(C_6F_5)_4]$), -132.1-(-131.8) (m, 8 F, $[B(C_6F_5)_4]$).

Phenoxy-Stabilized *tert*-Butylmethylsilyl Borate 34c[B(C₆F₅)₄]^[112]

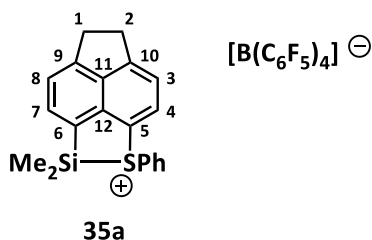
The title compound **34c[B(C₆F₅)₄]** was synthesized according to general procedure **D** using 1.0 equiv. (380 μmol, 130 mg) of 5-methylphenylsilyl-6-phenoxyacenaphthene **42c** and 1.0 equiv. (380 μmol, 346 mg) of trityl borate.



¹H NMR (499.9 MHz, 305.1 K, C₆D₆) δ = 0.37 (s, 3 H, CH₃), 0.69 (s, 9 H, *t*-Bu), 2.99-3.03 (m, 2 H, CH₂), 3.11-3.15 (m, 2 H, CH₂), 6.18 (d, *J*_{H,H} = 7.8 Hz, 1 H, 7-H), 6.78-6.81 (m, 1 H, 8-H), 7.13-7.24 (m, 4 H, overlap with C₆D₅H), 7.28-7.31 (m, 1 H, 3-H), 7.50 (d, *J*_{H,H} = 7.1 Hz, 1 H, 4-H), OPh signals broad and not listed. ¹³C{¹H} NMR (125.7 MHz, 305.1 K, C₆D₆) δ = -4.9 (SiCH₃), 20.8 (C, *t*-Bu), 23.8 (CH₃, *t*-Bu), 30.5 (CH₂), 32.3 (CH₂), 108.7 (CH, C-7), 113.3 (C, C-5), 119.5 (CH, C-8), 121.4 (CH, OPh), 124.0 (CH, C-3), 125.0 (C, C-12), 131.6 (CH, OPh), 132.1 (CH, OPh), 135.1 (CH, C-4), 138.8 (C, C-11), 146.0 (C, C-9), 149.5 (C, *ipso*-OPh), 151.3 (C, C-10), 153.0 (C, C-6). ²⁹Si{¹H} NMR (99.3 MHz, 305.1 K, C₆D₆) δ = 72.2. ¹⁹F{¹H} NMR (470.30 MHz, 305.0 K, C₆D₆) δ = -166.7-(-166.4) (m, 8 F, [B(C₆F₅)₄]), -162.6 (t, ³*J*_{F,F} = 20.6 Hz, 4 F, [B(C₆F₅)₄]), -132.1-(-131.8) (m, 8 F, [B(C₆F₅)₄]).

Thiophenyl-Stabilized Silyl Borate 35a[B(C₆F₅)₄]^[6a]

Silyl borate **35a[B(C₆F₅)₄]** was synthesized according to general procedure **D** using 1.0 equiv. of silane **43a** (380 μmol, 122 mg) and 1.0 equiv. of trityl borate (380 μmol, 350 mg). The reaction was carried out directly in benzene-*d*₆.

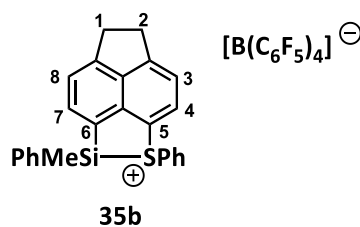


¹H NMR (499.87 MHz, 298.3 K, C₆D₆) δ = -0.01 (s, 3 H, *syn*-Si(CH₃)), 0.47 (s, 3 H, *anti*-Si(CH₃)), 3.02-3.05 (m, 2 H, CH₂), 3.09-3.12 (m, 2 H, CH₂), 6.54 (d, ³*J* = 7.7 Hz, 2 H, CH, *o*-Ph), 6.91-6.94 (m, 2 H, CH,

m-Ph), 7.01-7.05 (m, 2 H, CH, *p*-Ph, 3-H), 7.13 (d, $^3J = 7.5$ Hz, 1 H, CH, 4-H), 7.23 (d, $^3J = 7.0$ Hz, 1 H, CH, 8-H), 7.43 (d, $^3J = 7.0$ Hz, 1 H, CH, 7-H). $^{13}\text{C}\{^1\text{H}\}$ NMR (125.70 MHz, 298.4 K, C_6D_6) $\delta = -3.0$ (*syn*-Si(CH₃)₂), -0.3 (*anti*-Si(CH₃)₂), 30.9 (CH₂, C-2), 31.2 (CH₂, C-1), 117.0 (C), 121.4 (C, C-6), 122.5 (CH), 123.1 (CH, C-8), 124.6 (CH), 124.2-126.0 (C, [B(C₆F₅)₄]), 128.4 (CH, *o*-Ph), 131.3 (CH, *m*-Ph), 132.6 (CH), 133.4 (CH, C-4), 136.9 (CH, C-7), 137.0 (dm, $^1J_{\text{C,F}} = 246.6$ Hz, CF, [B(C₆F₅)₄]), 138.5 (C), 138.9 (dm, $^1J_{\text{C,F}} = 232.8$ Hz, CF, [B(C₆F₅)₄]), 139.3 (C), 149.1 (d, $^1J_{\text{C,F}} = 241.4$ Hz, CF, [B(C₆F₅)₄]), 152.2 (C), 154.2 (C). $^{29}\text{Si}\{^1\text{H}\}$ NMR (99.36 MHz, 298.3 K, C_6D_6) $\delta = 65.8$. $^{11}\text{B}\{^1\text{H}\}$ NMR (160.46 MHz, 298.9 K, C_6D_6) $\delta = -16.6$. $^{19}\text{F}\{^1\text{H}\}$ NMR (470.30 MHz, 305.0 K, C_6D_6) $\delta = -166.7$ -(-166.4) (m, 8 F, [B(C₆F₅)₄]), -162.6 (t, $^3J_{\text{F,F}} = 20.6$ Hz, 4 F, [B(C₆F₅)₄]), -132.1 -(-131.8) (m, 8 F, [B(C₆F₅)₄]).

Thiophenyl-Stabilized Methylphenylsilyl Borate **35b**[B(C₆F₅)₄]

The title compound **35b**[B(C₆F₅)₄] was synthesized according to general procedure **D** using 1.0 equiv. (347 μmol , 133 mg) of 6-methylphenylsilyl-5-thiophenylacenaphthene **43b** and 1.0 equiv. (347 μmol , 312 mg) of trityl borate.

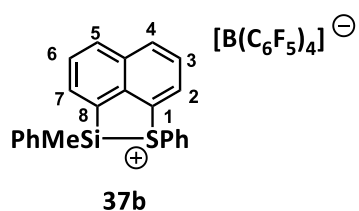


^1H NMR (499.9 MHz, 305.1 K, C_7D_8) $\delta = 0.33$ (s, 2 H, SiCH₃, *trans*-**35b**), 0.79 (s, 3 H), SiCH₃, *cis*-**35b**), 3.03-3.17 (m, 7 H, CH₂), 6.15 (dm, $^3J_{\text{H,H}} = 7.9$ Hz, 2 H, *S*-*o*-Ph, *cis*-**35b**), 6.54-6.59 (m, 3 H, SPh), 6.70-6.75 (m, 1 H, *S*-*p*-Ph, *cis*-**35b**), 6.79-6.87 (m, 4 H), 6.92-6.99 (m, 3 H, SPh), 7.02-7.20 (m, 9 H), 7.22-7.27 (m, 2 H), 7.40 (d, $^3J_{\text{H,H}} = 7.0$ Hz, 1 H, 7-H, *cis*-**35b**), 7.43 (d, $^3J_{\text{H,H}} = 7.0$ Hz, 0.6 H, 7-H, *trans*-**35b**). $^{13}\text{C}\{^1\text{H}\}$ NMR (125.7 MHz, 305.1 K, C_7D_8) $\delta = -4.4$ (SiCH₃, *trans*-**35b**), -2.8 (SiCH₃, *cis*-**35b**), 31.0 (CH₂), 31.4 (CH₂), 116.1 (C), 117.3 (C), 119.0 (C-6), 122.7 (CH), 122.8 (CH), 123.4 (CH), 123.5 (CH), 123.6 (C), 125.5 (CH), 126.5 (C), 127.8 (CH, SPh), 128.3 (CH), 128.6 (CH), 129.0 (CH), 129.3 (CH), 129.7 (CH), 130.5 (CH), 131.5 (CH, SPh), 131.6 (CH), 132.8 (CH, SPh), 133.9 (CH), 134.2 (CH), 134.4 (CH), 134.9 (CH), 135.8 (CH), 137.0 (dm, $^1J_{\text{C,F}} = 246.3$ Hz, [B(C₆F₅)₄]⁻), 138.3 (CH, C-7), 138.4 (CH, C-7), 138.9 (dm, $^1J_{\text{C,F}} = 244.1$ Hz, [B(C₆F₅)₄]⁻), 139.4 (C), 139.6 (C), 139.7 (C), 139.9 (C), 149.2 (dm, $^1J_{\text{C,F}} = 240.0$ Hz, [B(C₆F₅)₄]⁻), 153.0 (C), 154.4 (C), 154.5 (C). $^{29}\text{Si}\{^1\text{H}\}$ NMR (99.3 MHz, 305.1 K, C_7D_8) $\delta = 53.9$ (*cis*-**35b**),

51.2 (*trans*-**35b**). $^{11}\text{B}\{^1\text{H}\}$ NMR (160.38 MHz, 305.1 K, C_7D_8) $\delta = -16.0$. $^{19}\text{F}\{^1\text{H}\}$ NMR (470.30 MHz, 305.1 K, C_7D_8) $\delta = -166.6$ -(-166.4) (m, 8 F, $[\text{B}(\text{C}_6\text{F}_5)_4]$), -162.7 (t, $^3J_{\text{F,F}} = 20.6$ Hz, 4 F, $[\text{B}(\text{C}_6\text{F}_5)_4]$), -131.8-(-131.6) (m, 8 F, $[\text{B}(\text{C}_6\text{F}_5)_4]$).

Naphthyl-Substituted Thiophenyl-Stabilized Methylphenylsilyl Borate **37b** $[\text{B}(\text{C}_6\text{F}_5)_4]^{[114]}$

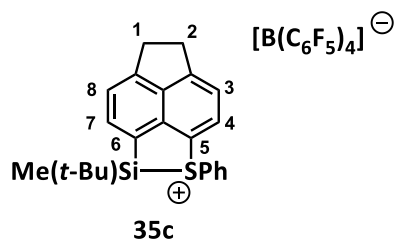
The title compound **37b** $[\text{B}(\text{C}_6\text{F}_5)_4]$ was synthesized according to general procedure **D** using 1.0 equiv. (433 μmol , 154 mg) of 8-methylphenylsilyl-1-thiophenyl-naphthalene **44** and 1.0 equiv. (433 μmol , 400 mg) of trityl borate.



^1H NMR (499.87 MHz, 263.0 K, $\text{C}_6\text{D}_5\text{CD}_3$) $\delta = 0.22$ (s, 2 H, SiCH_3 , *trans*-**37b**), 0.64 (s, 3 H, SiCH_3 , *cis*-**37b**), 5.98 (d, $^3J_{\text{H-H}} = 8.0$ Hz, 2 H, S-o-Ph, *cis*-**37b**), 6.36 (d, $^3J_{\text{H-H}} = 7.8$ Hz, 1 H, S-o-Ph, *trans*-**37b**), 6.49 (t, $^3J_{\text{H-H}} = 7.7$ Hz, 2 H), 6.64-6.70 (m, 3 H), 6.70-6.75 (m, 1 H), 6.76-6.82 (m, 2 H), 6.82-6.90 (m, 2 H), 6.93-7.06 (m, 4.5 H), 7.06-7.12 (m, 2.5 H), 7.16-7.21 (m, 2 H), 7.21-7.25 (m, 1 H), 7.35-7.41 (m, 1.7 H), 7.42-7.48 (m, 0.5 H), 7.69-7.74 (m, 1 H), 7.74-7.78 (m, 2 H). $^{13}\text{C}\{^1\text{H}\}$ NMR (125.71 MHz, 296.4 K, C_7D_8) $\delta = -6.1$ (SiCH_3 , *trans*-**37b**), -3.4 (CH_3 , *cis*-**37b**), 122.3 (C), 122.7 (C), 124.5 (C), 126.6 (C), 128.3 (C), 128.6 (C), 129.3 (C), 129.9 (C), 130.3 (C), 130.7 (C), 132.9 (CH), 133.3 (CH), 134.2 (CH), 134.4 (CH), 136.1 ($[\text{B}(\text{C}_6\text{F}_5)_4]^-$), 136.8 (CH), 138.0 ($[\text{B}(\text{C}_6\text{F}_5)_4]^-$), 139.7 (C), 139.9 ($[\text{B}(\text{C}_6\text{F}_5)_4]^-$), 142.3 (CH), 144.5 (CH), 149.2 (d, $J = 241.3$ Hz, $[\text{B}(\text{C}_6\text{F}_5)_4]^-$). $^{29}\text{Si}\{^1\text{H}\}$ NMR (99.31 MHz, 295.8 K, C_6D_6) $\delta = 42.7$ (*trans*-**37b**), 45.2 (*cis*-**37b**). $^{11}\text{B}\{^1\text{H}\}$ NMR (160.38 MHz, 296.0 K, C_6D_6) $\delta = -16.0$. $^{19}\text{F}\{^1\text{H}\}$ NMR (470.30 MHz, 296.0 K, C_6D_6) $\delta = -166.6$ -(-166.4) (m, 8 F, $[\text{B}(\text{C}_6\text{F}_5)_4]$), -162.4 (t, $^3J_{\text{F,F}} = 20.8$ Hz, 4 F, $[\text{B}(\text{C}_6\text{F}_5)_4]$), -131.8-(-131.6) (m, 8 F, $[\text{B}(\text{C}_6\text{F}_5)_4]$).

Thiophenyl-Stabilized *tert*-Butylmethylsilyl Borate 35c[B(C₆F₅)₄]

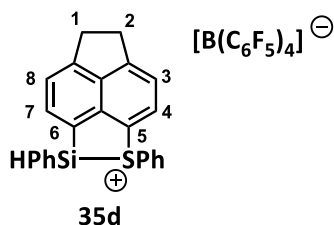
The title compound **35c**[B(C₆F₅)₄] was synthesized according to general procedure **D** using 1.0 equiv. (389 μmol, 141 mg) of 6-*tert*-butylmethylsilyl-6-thiophenylacenaphthene **43c** and 1.0 equiv. (389 μmol, 359 mg) of trityl borate.



¹H NMR (499.9 MHz, 298.1 K, C₆D₆) δ = 0.12 (s, 3H, CH₃), 0.89 (s, 9 H, *t*-Bu), 3.05-3.25 (m, 4 H, CH₂), 6.67 (dm, *J*_{H,H} = 7.9 Hz, 2 H, *o*-Ph), 7.03-7.08 (m, 2 H, *m*-Ph), 7.11-7.12 (m, 1 H, 3-H), 7.13-7.16 (m, 1 H, *p*-Ph), 7.27-7.30 (m, 1 H, 8-H), 7.34 (dm, *J*_{H,H} = 7.0 Hz, 1 H, 8-H), 7.56 (d, *J*_{H,H} = 7.0 Hz, 1 H, 7-H). **¹³C{¹H} NMR** (125.7 MHz, 297.8 K, C₆D₆) δ = -7.3 (SiCH₃), 20.7 (C, *t*-Bu), 24.3 (CH₃, *t*-Bu), 30.9 (CH₂), 31.3 (CH₂), 116.7 (C), 119.6 (C-6), 122.6 (CH, C-3), 123.1 (CH, C-8), 124.4 (C), 124.4-126.1 (brm, [B(C₆F₅)₄]⁻), 128.4 (CH, *o*-Ph), 131.4 (CH, *m*-Ph), 132.6 (CH, *p*-Ph), 133.5 (CH, C-4), 137.0 (dm, ¹*J*_{C,F} = 240.1 Hz, [B(C₆F₅)₄]⁻), 137.4 (CH, C-7), 138.9 (dm, ¹*J*_{C,F} = 238.5 Hz, [B(C₆F₅)₄]⁻), 139.3 (C), 139.3 (C), 149.1 (dm, ¹*J*_{C,F} = 244.1 Hz, [B(C₆F₅)₄]⁻), 152.5 (C), 154.4 (C). **²⁹Si{¹H} NMR** (99.3 MHz, 297.9 K, C₆D₆) δ = 70.0. **²⁹Si{¹H} NMR** (99.3 MHz, 297.9 K, CD₂Cl₂) δ = 70.5. **¹¹B{¹H} NMR** (160.38 MHz, 305.0 K, C₆D₆) δ = -16.0. **¹⁹F{¹H} NMR** (470.30 MHz, 305.1 K, C₆D₆) δ = -166.6-(-166.4) (m, 8 F, [B(C₆F₅)₄]⁻), -162.7 (t, ³*J*_{F,F} = 20.7 Hz, 4 F, [B(C₆F₅)₄]⁻), -132.0-(-131.7) (m, 8 F, [B(C₆F₅)₄]⁻).

Thiophenyl-Stabilized Hydridophenylsilyl Borate 35d[B(C₆F₅)₄]

The title compound **35d**[B(C₆F₅)₄] was synthesized according to general procedure **D** using 1.0 equiv. (380 μmol, 140 mg) of 6-phenylsilyl-5-thiophenylacenaphthene **43d** and 1.0 equiv. (380 μmol, 350 mg) of trityl borate.



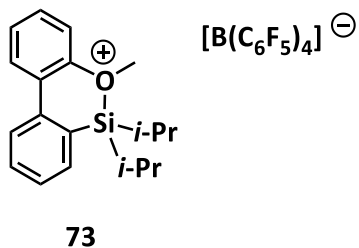
For the integration in the ^1H NMR spectrum the multiplet of the CH_2 groups was set to 4, the signals for the SiH are broadened and overlap and were therefore integrated as 1 signal. The signals in the ^{13}C spectrum show significant line broadening as well.

^1H NMR (499.9 MHz, 298.1 K, C_6D_6) δ = 3.03-3.17 (m, 4 H, CH_2), 5.62, 5.74 (2 brs, 1 H, SiH_2), 6.12-6.20 (brm, 1 H, SPh), 6.54-6.64 (brm, 2 H, SPh), 6.68-6.79 (brm, 1 H, SPh), 6.83-6.93 (brm, 3 H), 6.95-6.18 (brm, 5 H), 7.22-7.26 (brm, 1 H, 8-H), 7.38-7.46 (brm, 1 H, 7-H). $^{13}\text{C}\{^1\text{H}\}$ NMR (125.7 MHz, 297.8 K, C_6D_6) δ = 30.9 (CH_2), 31.4 (CH_2), 115.0 (C), 116.6 (C), 120.9 (C), 122.5 (CH), 123.4 (CH, C-8), 123.7 (C), 124.2-126.0 (brm, $[\text{B}(\text{C}_6\text{F}_5)_4]^-$), 127.9 (CH, SPh), 129.1 (CH), 130.6 (CH, SPh), 131.5 (C), 131.7 (CH), 134.0 (CH), 134.6 (CH), 136.4 (CH), 137.0 (dm, $^1J_{\text{C,F}} = 241.5$ Hz, $[\text{B}(\text{C}_6\text{F}_5)_4]^-$), 138.9 (dm, $^1J_{\text{C,F}} = 241.8$ Hz, $[\text{B}(\text{C}_6\text{F}_5)_4]^-$), 139.4 (CH, C-7), 139.6 (C), 149.1 (dm, $^1J_{\text{C,F}} = 243.2$ Hz, $[\text{B}(\text{C}_6\text{F}_5)_4]^-$), 153.5 (C), 154.4 (C). $^{29}\text{Si}\{^1\text{H}\}$ NMR (99.3 MHz, 297.9 K, C_6D_6) δ = 26.0 (*trans*-**35d**), 37.0 (*cis*-**35d**). ^{29}Si INEPT NMR (99.3 MHz, 297.9 K, C_6D_6) δ = 26.0 (d, $^1J_{\text{Si,H}} = 259.7$ Hz), 37.0 (d, $^1J_{\text{Si,H}} = 263.3$ Hz). $^{11}\text{B}\{^1\text{H}\}$ NMR (160.38 MHz, 305.0 K, C_6D_6) δ = -16.0. $^{19}\text{F}\{^1\text{H}\}$ NMR (470.30 MHz, 305.1 K, C_6D_6) δ = -166.6-(-166.2) (m, 8 F, $[\text{B}(\text{C}_6\text{F}_5)_4]^-$), -162.5 (t, $^3J_{\text{F,F}} = 20.7$ Hz, 4 F, $[\text{B}(\text{C}_6\text{F}_5)_4]^-$), -132.0-(-131.8) (m, 8 F, $[\text{B}(\text{C}_6\text{F}_5)_4]^-$).

Biphenyl-Substituted Silyloxonium Borates

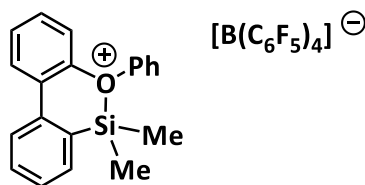
To generate biphenyl-substituted silyloxonium borates **72**, **73** $[\text{B}(\text{C}_6\text{F}_5)_4]$, 1 equiv. of the corresponding silane **74** or **75** was dissolved in 0.3 mL dichloromethane- D_2 as well as 1 equiv. of trityl borate. The solution with the trityl borate was transferred to an NMR tube and cooled to -80 °C. Then, the solution of the silane **74** or **75** was added slowly to the trityl borate. The NMR tube was closed and the mixture was mixed while keeping it as cold as possible. The subsequent NMR analysis was carried out at -70 - (-90) °C.

Di-*iso*-propylsilyloxonium borate **73** $[\text{B}(\text{C}_6\text{F}_5)_4]$ was obtained using 1.0 equiv. (77.05 μmol , 23 mg) of biphenyl-di-*iso*-propyl silane **75** and 1.0 equiv. (77.05 μmol , 56 mg) of trityl borate. The NMR analysis revealed that the reaction was not complete at -70 °C. Therefore, the sample was warmed to r.t. for 2 min and then cooled to -80 °C for the NMR measurement.



$^1\text{H NMR}$ (499.9 MHz, 183.0 K, CD_2Cl_2) δ = 1.01 (d, J = 7.4 Hz, 6H, $\text{SiCH}(\text{CH}_3)_2$), 1.20 (d, J = 7.3 Hz, 6H, $\text{SiCH}(\text{CH}_3)_2$), 1.66 – 1.52 (m, 2H, $\text{SiCH}(\text{CH}_3)_2$), 4.53 (s, 3H, OCH_3), 7.61 – 7.52 (m, 3H, HAr), 7.64 (t, J = 7.5 Hz, 1H, HAr), 7.73 (d, J = 7.3 Hz, 1H, HAr), 7.77 (t, J = 7.7 Hz, 1H, HAr), 7.89 (t, J = 9.8 Hz, 2H, HAr). $^{13}\text{C}\{^1\text{H}\}$ NMR (125.7 MHz, 183.0 K, CD_2Cl_2) δ = 11.9 ($\text{SiCH}(\text{CH}_3)_2$), 16.0 ($\text{SiCH}(\text{CH}_3)_2$), 16.5 ($\text{SiCH}(\text{CH}_3)_2$), 74.1 (OCH_3), 119.5, 123.1 (brs, $\text{C}^{\text{ipso}}\text{-B}(\text{C}_6\text{F}_5)_4$), 123.8, 127.2, 128.9, 129.4, 130.2, 131.4, 131.6, 133.9, 134.1, 135.9 (d, J = 240.2 Hz, $\text{-B}(\text{C}_6\text{F}_5)_4$), 136.9, 137.8 (d, J = 242.0 Hz, $\text{-B}(\text{C}_6\text{F}_5)_4$), 147.6 (d, J = 241.4 Hz, $\text{-B}(\text{C}_6\text{F}_5)_4$), 150.3. ^{29}Si INEPT NMR (99.3 MHz, 183 K, CD_2Cl_2): δ = 49.3.

Dimethylsilyloxonium borate **72** $[\text{B}(\text{C}_6\text{F}_5)_4]$ was obtained using 1.0 equiv. (101.82 μmol , 31 mg) of biphenyl-dimethyl silane **74** and 1.0 equiv. (101.82 μmol , 74 mg) of trityl borate.

**72**

$^1\text{H NMR}$ (499.9 MHz, 183.0 K, CD_2Cl_2) δ = 0.77 (s, 6 H, SiMe_2), 6.94-7.02 (m, 1 H), 7.06-7.13 (m, 7 H, Ph_3CH), 7.14-7.22 (m, 5 H, Ph_3CH), 7.26-7.37 (m, 10 H, Ph_3CH), 7.44-7.53 (m, 4 H), 7.57-7.67 (m, 3 H), 7.80-7.86 (m, 1 H), 7.99-8.07 (m, 2 H). The overall integral is too high due to overlap with Ph_3CH and other impurities. $^{29}\text{Si}\{^1\text{H}\}$ INEPT NMR (99.3 MHz, 183.0 K, CD_2Cl_2) : δ = 59.5.

5.5.1 Chiral Memory Experiments

A Schlenk tube was charged with 1.0 equiv. of silane (-)-**42b**, (-)-**43b** or (+)-**44** and a second Schlenk tube was charged 1.0 equiv. of trityl borate $[\text{Ph}_3\text{C}][\text{B}(\text{C}_6\text{F}_5)_4]$. The solids were dissolved in DCM or chlorobenzene, respectively. The silane was cooled to the temperature indicated in Table 36 and trityl borate was added. The mixture was stirred for the time indicated in Table 36. Then, sodium triethyl borohydride in toluene was added and the mixture was stirred overnight. The solvent was removed and the residue was suspended in petroleum ether. The mixture was filtrated through a thin layer of silica, the solvent was removed and the crude product was purified via preparative TLC (eluent petroleum ether). After the purification, the formation of silanes was confirmed by NMR spectroscopy and then their optical rotation was measured and their ee was determined via chiral HPLC (Table 37).

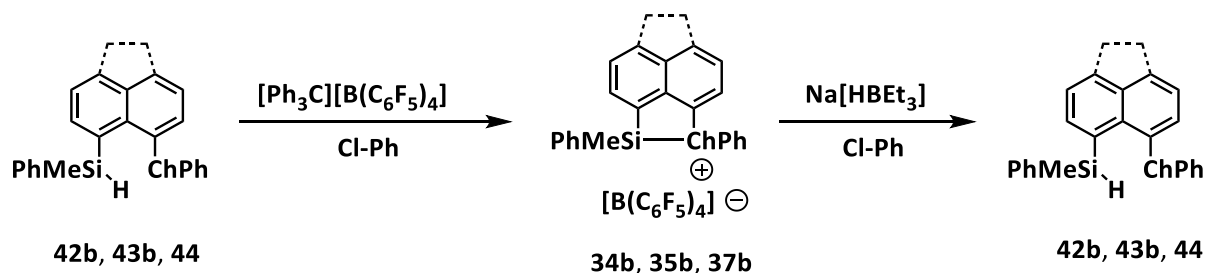


Table 36 – Batches, reaction conditions and yields of the chiral memory experiments.

Compound	Silane	Trityl borate	$\text{Et}_3\text{B-H}$ (1 M in toluene)	Conditions	Yield
(+)-44	106.6 μmol , 38 mg	106.6 μmol , 98 mg	159.9 μmol , 0.15 mL	Cl-Ph, r.t., 30 min	24 %
(-)-42b	177.3 μmol , 65 mg	173.5 μmol , 160 mg	266.0 μmol , 0.27 mL	Cl-Ph, -40 °C, 30 min	14 %
(-)-42b	180.1 μmol , 66 mg	180.1 μmol , 166 mg	270.1 μmol , 0.27 mL	DCM, -80 °C, 20 min	0 %
(-)-43b	252.5 μmol , 97 mg	252.5 μmol , 233 mg	328.2 μmol , 0.33 mL	Cl-Ph, -40 °C, 15 min	14 %

Table 37 – Results of the optical rotation and the chiral HPLC analysis of the chiral memory experiments-

Silane	$[\alpha]_D$ start	ee start	$[\alpha]_D$ end	ee end
(+)-44	+17° (0.04 molL ⁻¹ , Et ₂ O)	84 %	0° (0.004 molL ⁻¹ , Et ₂ O)	-
(-)-42b	-11° (0.02 molL ⁻¹ , Et ₂ O)	54 %	-4° (0.005 molL ⁻¹ , Et ₂ O)	32 %
(-)-42b	-11° (0.02 molL ⁻¹ , Et ₂ O)	54 %	decomposition	decomposition
(-)-43b	-10° (0.05 molL ⁻¹ , Et ₂ O)	64 %	-9° (0.006 molL ⁻¹ , Et ₂ O)	64 %

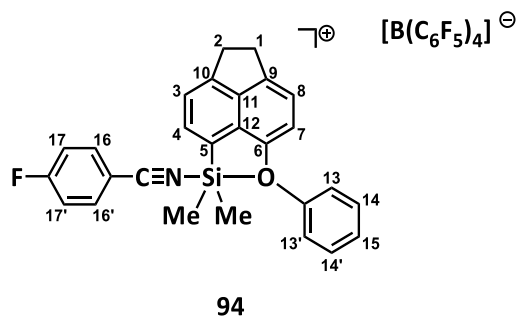
5.6 Syntheses of Silylnitrilium Borates

General Procedure E: A Schlenk tube was charged with the corresponding silane and trityl borate $[\text{Ph}_3\text{C}][\text{B}(\text{C}_6\text{F}_5)_4]$ and the solids were dissolved in benzene. The reaction mixture was stirred at r.t. for 20 min. Then, the phases were separated, the upper, nonpolar phase was removed and the polar phase was washed twice with benzene. After removing the solvent under reduced pressure, 4-fluorobenzonitrile was dissolved in 0.6 mL deuterated methylene chloride or deuterated benzene and added to the residue. Afterwards, the reaction mixture was stirred for further 15 min and subsequently transferred to a NMR tube for analysis.

General procedure F: Trityl borate $[\text{Ph}_3\text{C}][\text{B}(\text{C}_6\text{F}_5)_4]$ and 4-fluorobenzonitrile were dissolved in CD_2Cl_2 . This solution was added to a solution of the corresponding silane in CD_2Cl_2 . The reaction mixture was stirred for 5 min and subsequently transferred to a NMR tube for analysis.

Dimethylsilylnitrilium Borate **94** $[\text{B}(\text{C}_6\text{F}_5)_4]$

Nitrilium borate **94** $[\text{B}(\text{C}_6\text{F}_5)_4]$ was synthesized according to general procedure **E** using 1.0 equiv. of 6-phenoxy-5-dimethylsilylacenaphthene **42a** (379.46 μmol , 116 mg), 1.0 equiv. of trityl borate (379.46 μmol , 349 mg) and 1.0 equiv. of 4-fluorobenzonitrile (379.46 μmol , 46 mg) (NMR spectroscopy in benzene- d_6) or general procedure **F** using 1.0 equiv. of 5-dimethylsilyl-6-phenoxyacenaphthene **42a** (132.36 μmol , 40 mg), 1.0 equiv. of trityl borate (132.36 μmol , 122 mg) and 1.0 equiv. of 4-fluorobenzonitrile (132.36 μmol , 16 mg). Nitrilium ion **94** decomposes in dichloromethane- d_2 within one day.



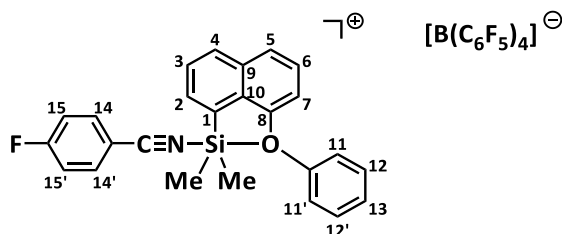
$^1\text{H NMR}$ (499.87 MHz, 305.1 K, C_6D_6): δ = 0.74 (s, 6 H, $\text{Si}(\text{CH}_3)_2$), 3.03-3.05 (m, 2 H, CH_2 , H-1), 3.16-3.18 (m, 2H, CH_2 , H-2), 6.58-6.64 (m, 3 H, H-17, H-17', H-7), 6.89-6.91 (m, 2 H, H-13, H-13'), 6.92-6.96 (m, 3 H, H-16, H-16', H-8), 7.00-7.05 (m, 1 H, H-15), 7.14-7.19 (m, 2 H, H-14, H-14'), 7.31 (d, $^3J_{\text{H,H}} = 7.2$ Hz,

1 H, H-3), 7.72 (d, $^3J_{H,H} = 7.1$ Hz, 1 H, H-4). $^{13}\text{C}\{^1\text{H}\}$ NMR (125.71 MHz, 305.0 K, C_6D_6): $\delta = 0.8$ ($\text{Si}(\text{CH}_3)_2$), 29.7 (CH_2), 31.3 (CH_2), 98.4 (C-CN), 113.0 (C-7), 115.5 (C-5), 118.3 (d, $^2J_{C,F} = 23.5$ Hz, C-17, C-17'), 120.5, 120.6 (C-3, C-8), 121.0 (C-13, C-13'), 122.0 (CN), 123.9-126.0 (C, $[\text{B}(\text{C}_6\text{F}_5)_4]^-$), 126.3 (C-15), 126.9 (C-12), 131.0 (C-14, C-14'), 136.4 (C-4), 137.0 (dm, $^1J_{C,F} = 233.2$ Hz, CF, $[\text{B}(\text{C}_6\text{F}_5)_4]^-$), 137.7 (d, $^3J_{C,F} = 11.2$ Hz, C-16, C-16'), 138.9 (dm, $^1J_{C,F} = 232.6$ Hz, CF, $[\text{B}(\text{C}_6\text{F}_5)_4]^-$), 140.8 (C-11), 142.0 (C-9), 149.0 (d, $^1J_{C,F} = 239.0$ Hz, CF, $[\text{B}(\text{C}_6\text{F}_5)_4]^-$), 151.2 (C-6), 152.9 (C-10), 154.2 (C, C-Ph), 168.7 (d, $^1J_{C,F} = 264.6$ Hz, CF). $^{19}\text{F}\{^1\text{H}\}$ NMR (470.30 MHz, 305.0 K, C_6D_6): -167.5-(-167.3) (m, 8 F, *m*-F, $[\text{B}(\text{C}_6\text{F}_5)_4]^-$), -163.44 (t, $^3J_{F,F} = 20.5$ Hz, 4 F, *p*-F, $[\text{B}(\text{C}_6\text{F}_5)_4]^-$), -133.0-(-132.8) (m, 8 F, *o*-F, $[\text{B}(\text{C}_6\text{F}_5)_4]^-$), -89.8 (s, 1 F, CF). $^{29}\text{Si}\{^1\text{H}\}$ NMR (99.31 MHz, 305.0 K, C_6D_6): $\delta = 15.4$. $^{11}\text{B}\{^1\text{H}\}$ NMR (160.38 MHz, 305.1 K, C_6D_6): $\delta = -16.1$.

^1H NMR (499.87 MHz, 305.1 K, CD_2Cl_2): $\delta = 1.08$ (s, 6 H, $\text{Si}(\text{CH}_3)_2$), 3.44-3.46 (m, 2 H, CH_2 , H-1), 3.54-3.56 (m, 2H, CH_2 , H-2), 6.84 (d, $^3J_{H,H} = 7.7$ Hz, 1 H, H-7), 7.18-7.20, 7.24-7.29, 7.31-7.37 (3 m, 19 H, H-8, CH-Ph, Ph_3CH), 7.42-7.46 (m, 2H, H-17, H-17'), 7.49-7.53 (m, 3 H, H-3, CH-Ph), 7.94 (d, $^3J_{H,H} = 7.0$ Hz, 1 H, H-4), 8.00-8.03 (m, 2 H, H-16). $^{19}\text{F}\{^1\text{H}\}$ NMR (470.28 MHz, 305.1 K, CD_2Cl_2): $\delta = -167.4$ -(-167.2) (m, 8 F, *m*-F, $[\text{B}(\text{C}_6\text{F}_5)_4]^-$), -163.44 (t, $^3J_{F,F} = 20.5$ Hz, 4 F, *p*-F, $[\text{B}(\text{C}_6\text{F}_5)_4]^-$), -133.0-(-132.9) (m, 8 F, *o*-F, $[\text{B}(\text{C}_6\text{F}_5)_4]^-$), -87.9 (s, 1 F, CF). $^{29}\text{Si}\{^1\text{H}\}$ NMR (99.31 MHz, 305.0 K, CD_2Cl_2): $\delta = 16.3$.

Naphthyl-Substituted Dimethylsilylnitrilium Borate **96** $[\text{B}(\text{C}_6\text{F}_5)_4]$

Nitrilium borate **96** $[\text{B}(\text{C}_6\text{F}_5)_4]$ was synthesized according to general procedure **E** using 1.0 equiv. of 8-phenoxy-1-dimethylsilylnaphthalene (251.41 μmol , 70 mg), 1.0 equiv. of trityl borate (251.41 μmol , 230 mg) and 1.0 equiv. of 4-fluorobenzonitrile (251.41 μmol , 30 mg).



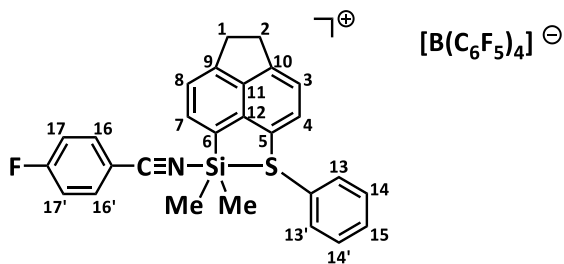
96

^1H NMR (499.87 MHz, 305.0 K, CD_2Cl_2) $\delta = 1.07$ (s, 6 H, $\text{Si}(\text{CH}_3)_2$), 6.70 (d, $^3J_{H,H} = 7.8$ Hz, 1 H, H-7), 7.35-7.37 (m, 2 H, H-11, H-11'), 7.39-7.43 (m, 3 H, H-15, H-15'), 7.47 (t, $^3J_{H,H} = 8.0$ Hz, 1 H, H-6), 7.52 (t, $^3J_{H,H} = 7.5$ Hz, 1 H, H-13), 7.65 (t, $^3J_{H,H} = 7.9$ Hz, 2 H, H-12, H-12'), 7.70-7.76 (m, 2 H, H-4, H-5), 8.04-

8.06 (m, 3 H, H-14, H-14'), 8.12 (d, $^3J_{H,H} = 7.0$ Hz, 1 H, H-3), 8.18 (d, $^3J_{H,H} = 8.3$ Hz, 1 H, H-2). $^{13}\text{C}\{^1\text{H}\}$ NMR (125.71 MHz, 305.0 K, CD_2Cl_2) $\delta = 2.6$ ($\text{Si}(\text{CH}_3)_2$), 103.1 ($\underline{\text{C}}\text{-CN}$), 109.5 (C-7), 118.8 (d, $^2J_{\text{C,F}} = 23.3$ Hz, C-15, C-15'), 120.9 (CN), 121.9 (C-1), 123.2 (C-11, C-11'), 123.7 – 125.7 (brm, $[\text{B}(\text{C}_6\text{F}_5)_4]$, C), 124.3 (C-4/C-5), 127.4, 127.6, 128.4 (C-6, C-4/C-5, C-13), 128.9 (C-9/C-10), 131.8 (C-12, C-12'), 132.7 (C-2), 134.8 (C-3), 134.9 (C-9/C-10), 136.9 (d, $^1J_{\text{C,F}} = 243.5$ Hz, $[\text{B}(\text{C}_6\text{F}_5)_4]$, CF), 137.6 (d, $^3J_{\text{C,F}} = 10.2$ Hz, C-14, C-14'), 138.9 (d, $^1J_{\text{C,F}} = 244.1$ Hz, $[\text{B}(\text{C}_6\text{F}_5)_4]$, CF), 148.8 (d, $^1J_{\text{C,F}} = 241.0$ Hz, $[\text{B}(\text{C}_6\text{F}_5)_4]$, CF), 152.3 ($\underline{\text{C}}\text{-Ph}$), 154.4 (C-8), 168.3 (d, $^1J_{\text{C,F}} = 264.4$ Hz, CF). $^{29}\text{Si}\{^1\text{H}\}$ NMR (99.31 MHz, 305.0 K, CD_2Cl_2) $\delta = 1.6$. $^{19}\text{F}\{^1\text{H}\}$ NMR (470.30 MHz, 233.1 K, CD_2Cl_2) $\delta = -166.9$ –(-166.7) (m, 8 F, $[\text{B}(\text{C}_6\text{F}_5)_4]$), -162.87 (t, $^3J_{\text{F,F}} = 21.0$ Hz, 4 F, $[\text{B}(\text{C}_6\text{F}_5)_4]$), -133.6–(-133.3) (m, 9 F, $[\text{B}(\text{C}_6\text{F}_5)_4]$), -102.6 (s, 0.5 F), -90.2 (s, 1 F). $^{11}\text{B}\{^1\text{H}\}$ NMR (160.38 MHz, 305.1 K, CD_2Cl_2) $\delta = -16.6$.

Dimethylsilylnitrilium Borate **95a** $[\text{B}(\text{C}_6\text{F}_5)_4]$

The nitrilium borate **95a** $[\text{B}(\text{C}_6\text{F}_5)_4]$ was synthesized according to general procedure **E** using 1.0 equiv. of 6-dimethylsilyl-5-thiophenylacenaphthene **43a** (233.99 μmol , 75 mg), 1.0 equiv. of trityl borate (233.99 μmol , 215 mg) and 1.0 equiv. of 4-fluorobenzonitrile (233.99 μmol , 28 mg).



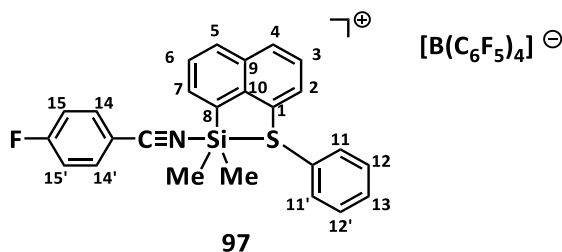
95a

^1H NMR (499.87 MHz, 298.7 K, CD_2Cl_2): $\delta = 0.95$ (s, 6 H, $\text{Si}(\text{CH}_3)_2$), 3.58-3.64 (m, 4 H, $2 \times \text{CH}_2$), 7.04-7.07 (m, 2 H, H-13, H13'), 7.38-7.43 (m, 4 H, H-14, H-14', H-17, H-17'), 7.44-7.48 (m, 1 H, H-15), 7.60-7.64 (m, 2 H, H-3, H-8), 7.95 (d, $^3J_{H,H} = 7.4$ Hz, 1 H, H-4), 8.00-8.02 (m, 2 H, H-16, H-16'), 8.14 (d, $^3J_{H,H} = 7.1$ Hz, 1 H, H-7). $^{13}\text{C}\{^1\text{H}\}$ NMR (125.71 MHz, 298.7 K, CD_2Cl_2): $\delta = 2.7$ ($\text{Si}(\text{CH}_3)_2$), 31.5 (CH_2), 31.7 (CH_2), 103.0 ($\underline{\text{C}}\text{-CN}$), 118.8 (d, $^2J_{\text{C,F}} = 23.4$ Hz, C-17, C-17'), 120.0, 120.1 (C, CN), 122.1 (C-6), 122.6, 122.9 (C-3, C-8), 128.8 (C-13, C-13'), 130.6 (C, C-Ph), 131.2 (C-14, C-14'), 135.8 (C-4), 136.9 (dm, $^1J_{\text{C,F}} = 243.0$ Hz, CF, $[\text{B}(\text{C}_6\text{F}_5)_4]^-$), 137.6 (d, $^3J_{\text{C,F}} = 10.4$ Hz, C-16, C-16'), 138.8 (C-7), 138.9 (dm, $^1J_{\text{C,F}} = 245.1$ Hz, CF, $[\text{B}(\text{C}_6\text{F}_5)_4]$), 139.6 (C), 140.4 (C), 148.8 (dm, $^1J_{\text{C,F}} = 242.0$ Hz, CF, $[\text{B}(\text{C}_6\text{F}_5)_4]$), 153.2

(C), 153.6 (C), 168.3 (d, $^1J_{C,F} = 264.0$ Hz, CF). $^{19}\text{F}(^1\text{H})$ NMR (470.28 MHz, 298.7 K, CD_2Cl_2): $\delta = -167.4$ -(-167.2) (m, 8 F, *m*-F, $[\text{B}(\text{C}_6\text{F}_5)_4]^-$), -163.44 (t, $^3J_{F,F} = 20.5$ Hz, 4 F, *p*-F, $[\text{B}(\text{C}_6\text{F}_5)_4]^-$), -132.9-(-132.7) (m, 8 F, *o*-F, $[\text{B}(\text{C}_6\text{F}_5)_4]^-$), -94.3 (s, 1 F, CF). $^{29}\text{Si}(^1\text{H})$ NMR (99.31 MHz, 298.7 K, CD_2Cl_2): $\delta = 29.5$. $^{11}\text{B}(^1\text{H})$ NMR (160.38 MHz, 305.0 K, CD_2Cl_2): $\delta = -16.6$.

Naphthyl-Substituted Dimethylsilylnitrilium Borate **97** $[\text{B}(\text{C}_6\text{F}_5)_4]$

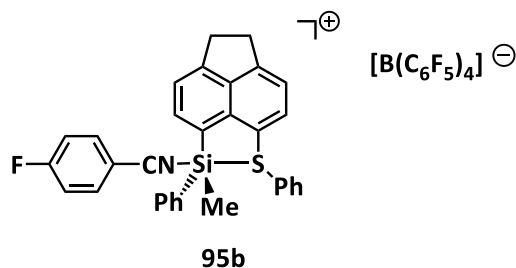
Nitrilium borate **97** $[\text{B}(\text{C}_6\text{F}_5)_4]$ was synthesized according to general procedure **E** using 1.0 equiv. of 8-dimethylsilyl-1-thiophenylnaphthalene (244.49 μmol , 72 mg), 1.0 equiv. of trityl borate (244.49 μmol , 226 mg) and 1.0 equiv. of 4-fluorobenzonitrile (244.49 μmol , 30 mg). The nitrilium borate **97** $[\text{B}(\text{C}_6\text{F}_5)_4]$ was only obtained in a mixture with trityl borate. Impurities or residual solvent in the starting silane might be the reason for this imbalance in the batch.



^1H NMR (499.87 MHz, 305.0 K, CD_2Cl_2): $\delta = 0.95$ (s, 6 H, $\text{Si}(\text{CH}_3)_2$), 7.04-7.07 (m, 2 H, SPh), 7.22-7.32 (m, 5 H, NC-Ar), 7.40-7.46 (m, 2 H, SPh), 7.48-7.55 (m, 2 H), 7.77-7.91 (m, 7 H, 6-H, NC-Ar, $[\text{CPh}_3]^+$), 8.05-8.09 (m, 1 H), 8.24-8.33 (m, 3 H, 7-H, $[\text{CPh}_3]^+$), the overall integral is by 6 H too high, due to residual $[\text{CPh}_3]^+$ and excess 4-fluorobenzonitrile. $^{13}\text{C}(^1\text{H})$ NMR (125.71 MHz, 305.0 K, CD_2Cl_2): $\delta = 1.8$ ($\text{Si}(\text{CH}_3)_2$), 106.5 (C), 117.9 (d, $J_{C,F} = 22.9$ Hz, NC-Ar), 119.2 (C), 125.6 (C), 126.5 (CH), 128.5 (CH), 128.5 (C-8), 128.8 (CH, SPh), 128.8 (C), 129.3 (CH), 129.8 (CH), 131.2 (CH), 137.0 (dm, $^1J_{C,F} = 240.9$ Hz, CF, $[\text{B}(\text{C}_6\text{F}_5)_4]^-$), 131.6 (CH), 133.6 (CH), 134.2 (d, $J_{C,F} = 15.7$ Hz, NC-Ar), 134.8 (C), 136.3 (d, $^3J_{C,F} = 10.6$ Hz, NC-Ar), 137.4 (CH), 138.9 (dm, $^1J_{C,F} = 238.7$ Hz, CF, $[\text{B}(\text{C}_6\text{F}_5)_4]^-$), 140.2 (C), 148.8 (dm, $^1J_{C,F} = 242.0$ Hz, CF, $[\text{B}(\text{C}_6\text{F}_5)_4]^-$), 166.9 (d, $^1J_{C,F} = 259.9$ Hz, CF). $^{19}\text{F}(^1\text{H})$ NMR (470.28 MHz, 305.0 K, CD_2Cl_2): $\delta = -167.4$ -(-167.0) (m, 8 F, $[\text{B}(\text{C}_6\text{F}_5)_4]^-$), -163.44 (t, $^3J_{F,F} = 19.4$ Hz, 4 F, *p*-F, $[\text{B}(\text{C}_6\text{F}_5)_4]^-$), -132.8 (brs, 8 F, $[\text{B}(\text{C}_6\text{F}_5)_4]^-$), -99.5 (s, 1.7 F, CF). $^{29}\text{Si}(^1\text{H})$ NMR (99.31 MHz, 305.0 K, CD_2Cl_2): $\delta = 26.1$. $^{11}\text{B}(^1\text{H})$ NMR (160.38 MHz, 305.0 K, CD_2Cl_2): $\delta = -16.5$.

Phenylmethylsilylnitrilium Borate 95b[B(C₆F₅)₄]

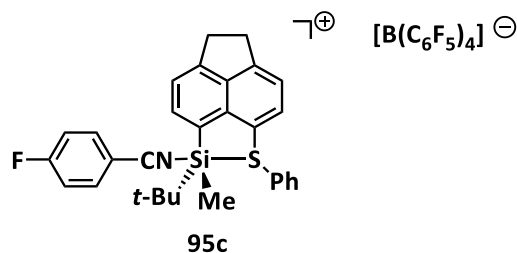
Nitrilium borate **95b**[B(C₆F₅)₄] was synthesized according to general procedure **F** using 1.0 equiv. (135.91 μmol, 52 mg) of 6-methylphenylsilyl-5-thiophenylacenaphthene **43b**, 1.0 equiv. (135.91 μmol, 125 mg) of trityl borate and 1.0 equiv. (135.91 μmol, 16 mg) of 4-fluorobenzonitrile.



¹H NMR (499.87 MHz, 305.0 K, CD₂Cl₂): δ = 1.32 (s, 3 H, SiCH₃), 3.61-3.69 (m, 4 H, CH₂), 5.61 (s, 1 H, Ph₃CH), 6.68-6.71 (m, 2 H, S-o-Ph), 7.11-7.16 (m, 2 H, S-m-Ph), 7.17-7.21 (m, 6 H, Ph₃CH), 7.23-7.29 (m, 6 H, Si-m-Ph, S-p-Ph, Ph₃CH), 7.30-7.35 (m, 8 H, NC-Ar, Ph₃CH), 7.38-7.43 (m, 3 H, Si-o/p-Ph), 7.62 (dm, ³J_{H,H} = 7.3 Hz, 3-H), 7.70 (dm, ³J_{H,H} = 7.2 Hz, 8-H), 7.82-7.86 (m, 2 H, NC-Ar), 7.88 (d, ³J_{H,H} = 7.4 Hz, 4-H), 8.33 (d, ³J_{H,H} = 7.1 Hz, 7-H). **¹³C{¹H} NMR** (125.71 MHz, 305.0 K, CD₂Cl₂): δ = 1.2 (CH₃), 31.5 (CH₂), 31.7 (CH₂), 57.6 (Ph₃CH), 104.0 (CN), 118.5 (d, ²J_{C,F} = 23.2 Hz, NC-Ar), 119.2 (C, C-6), 120.4 (C), 120.6 (C, C-CN), 122.6 (CH, C-8), 122.9 (CH, C-3), 123.8-125.6 (brs, C, [B(C₆F₅)₄]⁻), 126.9 (CH), 128.1 (CH, S-o-Ph), 128.8 (CH, Ph₃CH), 129.6 (CH), 129.9 (CH), 130.0 (CH, Ph₃CH), 130.4 (C, Si-i-Ph), 130.5 (CH, S-m-Ph), 132.1 (C), 132.6 (CH), 133.7 (CH, Si-Ph), 136.4 (CH, C-4), 137.0 (dm, ¹J_{C,F} = 243.6 Hz, CF, [B(C₆F₅)₄]⁻), 137.1 (d, J_{C,F} = 10.3 Hz, CH, NC-Ar), 138.9 (dm, ¹J_{C,F} = 244.3 Hz, CF, [B(C₆F₅)₄]⁻), 140.4 (C, C-9/12), 140.5 (CH, C-7), 144.7 (CH, Ph₃CH), 148.8 (dm, ¹J_{C,F} = 241.4 Hz, CF, [B(C₆F₅)₄]⁻), 153.3 (C), 154.0 (C-9/12), 167.9 (d, ¹J_{C,F} = 262.6 Hz, NC-Ar, CF). **¹¹B{¹H} NMR** (160.38 MHz, 305.0 K, CD₂Cl₂): δ = -16.5 ([B(C₆F₅)₄]⁻). **¹⁹F{¹H} NMR** (470.28 MHz, 305.0 K, CD₂Cl₂): δ = -167.4-(-167.2) (m, *m*-F, [B(C₆F₅)₄]⁻), -163.44 (t, ³J_{F,F} = 20.4 Hz, *o*-F, [B(C₆F₅)₄]⁻), -132.9-(-132.7) (m, *o*-F, [B(C₆F₅)₄]⁻), -95.5 (s, 1 F, CF). **²⁹Si{¹H} NMR** (99.31 MHz, 305.0 K, CD₂Cl₂): δ = 6.4.

***tert*-Butylmethylsilylnitrilium Borate 95c[B(C₆F₅)₄]**

Nitrilium borate **95c**[B(C₆F₅)₄] was synthesized according to general procedure **F** using 1.0 equiv. (123.85 μmol, 44.9 mg) of 6-*tert*-butylphenylsilyl-5-thiophenylacenaphthene **43c**, 1.0 equiv. (123.85 μmol, 114.2 mg) of trityl borate and 1.0 equiv. (123.85 μmol, 15.0 mg) of 4-fluorobenzonitrile.



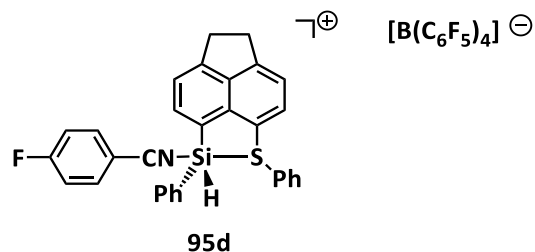
¹H NMR (499.87 MHz, 296.0 K, CD₂Cl₂): δ = 0.57 (s, 3 H, CH₃), 1.20 (s, 9 H, *t*-Bu), 3.60-3.68 (m, 4 H, CH₂), 7.11-7.14 (m, 2 H, *S*-*o*-Ph), 7.22-7.26 (m, 6 H, HCPH₃, NC-Ar), 7.49-7.53 (m, 2 H, *m*-Ph), 7.59-7.63 (m, 1 H, *p*-Ph), 7.66 (dm, ³*J*_{H,H} = 7.5 Hz, 1 H, 3/4-H), 7.71-7.78 (m, 4 H, NC-Ar, 8-H), 8.00 (d, ³*J*_{H,H} = 7.5 Hz, 1 H, 3/4-H), 8.05 (d, ³*J*_{H,H} = 7.0 Hz, 1 H, 7-H). **¹³C{¹H} NMR** (125.71 MHz, 296.0 K, CD₂Cl₂): δ = -6.0 (CH₃), 21.7 (CH₃, *t*-Bu), 25.3 (C, *t*-Bu), 31.7 (CH₂), 32.0 (CH₂), 107.6 (CN), 117.8 (d, ²*J*_{C,F} = 23.8 Hz, NC-Ar), 119.0 (C, C-5), 120.3 (C, C-6), 123.2 (CH, C-3), 123.7 (CH, C-8), 123.8-125.5 (brs, C, [B(C₆F₅)₄]⁻), 125.1 (C), 128.40 (C), 129.3 (CH, *o*-Ph), 132.1 (CH, *m*-Ph), 133.3 (CH, *p*-Ph), 134.3 (CH, C-4), 135.7 (d, *J*_{C,F} = 9.7 Hz, CH, NC-Ar), 136.8 (dm, ¹*J*_{C,F} = 252.2 Hz, CF, [B(C₆F₅)₄]⁻), 138.2 (CH, C-7), 138.8 (dm, ¹*J*_{C,F} = 248.8 Hz, CF, [B(C₆F₅)₄]⁻), 140.0 (C, C-12), 140.1 (C), 148.7 (dm, ¹*J*_{C,F} = 242.5 Hz, CF, [B(C₆F₅)₄]⁻), 153.1 (C, C-9), 155.1 (C-10), 166.2 (d, ¹*J*_{C,F} = 257.6 Hz, NC-Ar, CF). **¹¹B{¹H} NMR** (160.38 MHz, 296.0 K, CD₂Cl₂): δ = -16.6 ([B(C₆F₅)₄]⁻). **¹⁹F{¹H} NMR** (470.29 MHz, 296.0 K, CD₂Cl₂): δ = -167.4-(-167.1) (m, *m*-F, [B(C₆F₅)₄]⁻), -163.44 (t, ³*J*_{F,F} = 20.4 Hz, *o*-F, [B(C₆F₅)₄]⁻), -133.1-(-132.8) (m, *o*-F, [B(C₆F₅)₄]⁻), -101.3 (s, 1 F, CF). **²⁹Si{¹H} NMR** (99.31 MHz, 296.0 K, CD₂Cl₂): δ = 70.2.

Phenylhydrosilylnitrilium Borate 95d[B(C₆F₅)₄]

An NMR tube was charged with 1.0 equiv. (56.98 μmol, 21 mg) of 6-phenylsilyl-5-thiophenylacenaphthene **43d** and 1.0 equiv. (56.98 mmol, 53 mg) of trityl borate. The tube was evacuated, flushed with Ar and cooled to -40°C. Then 0.7 mL chlorobenzene-d₅ were added slowly. The NMR tube was sealed and shaken while keeping the temperature as low as possible. The silane **43d** did not dissolve well at this temperature, therefore the mixture was slowly warmed to r.t.. The

sample was analysed via NMR spectroscopy. After 3 weeks storage, 1.0 equiv. (56.98 μmol , 7 mg) of 4-fluorobenzonitrile were added to the sample at r.t.. The NMR analysis revealed the formation of the title compound **95d**[B(C₆F₅)₄].

In a second batch the title compound **95d**[B(C₆F₅)₄] was prepared according to the slightly altered general procedure **E** using 1.0 equiv. (175.00 μmol , 65 mg) of silane **43d**, 1.0 equiv. (175.00 μmol , 161 mg) of trityl borate and 1.0 equiv. (175.00 μmol , 21 mg) of 4-fluorobenzonitrile. For this batch the nitrile was added prior to washing the reaction mixture. It was possible to dry the nitrilium borate **95d**[B(C₆F₅)₄] under high-vacuum without significant decomposition. The NMR spectra were measured in dichloromethane-d₂.



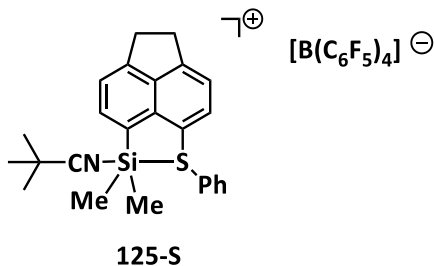
¹H NMR (499.87 MHz, 305.0 K, C₆D₅Cl): δ = 3.16-3.21 (m, 2 H, CH₂), 3.23-3.28 (m, 2 H, CH₂), 5.45 (s, 1 H, Ph₃CH), 6.13 (s, 1 H, SiH), 6.70-6.74 (m, 4 H, S-*o*-Ph, NC-Ar), 6.98-7.03 (m, 3 H, SPh), 7.05-7.09 (m, 9 H, Ph₃CH), 7.14-7.17 (m, 8 H, Ph₃CH), 7.20-7.28 (m, 5 H, NC-Ar, SiPh), 7.46-7.50 (m, 3 H, SiPh, 8-H), 8.24 (d, ³J_{H,H} = 7.1 Hz, 1 H, 7-H). **¹³C{¹H} NMR** (125.71 MHz, 305.0 K, C₆D₅Cl): δ = 30.8 (CH₂), 31.0 (CH₂), 57.3 (Ph₃CH), 105.5 (CN), 116.0 (C, C-6), 117.6 (d, ²J_{C,F} = 23.1 Hz, NC-Ar), 119.9 (C), 121.1 (C, C-CN), 121.9 (CH, C-8), 122.2 (CH, C-3), 122.4 (C), 125.6 (C), 126.5 (CH, Ph₃CH), 127.1 (CH), 128.5 (CH), 128.7 (CH), 129.4 (CH), 130.0 (CH), 130.9 (CH, SiPh), 131.8 (C), 133.0 (CH), 136.2 (d, J_{C,F} = 10.2 Hz, CH, NC-Ar), 136.4 (CH), 136.8 (dm, ¹J_{C,F} = 240.6 Hz, CF, [B(C₆F₅)₄]⁻), 138.7 (dm, ¹J_{C,F} = 244.2 Hz, CF, [B(C₆F₅)₄]⁻), 139.7 (C, C-9/12), 140.2 (C), 140.7 (CH, C-7), 144.2 (CH, Ph₃CH), 148.8 (dm, ¹J_{C,F} = 240.5 Hz, CF, [B(C₆F₅)₄]⁻), 152.0 (C), 153.8 (C-9/12), 167.1 (d, ¹J_{C,F} = 263.9 Hz, NC-Ar, CF). **¹¹B{¹H} NMR** (160.38 MHz, 305.0 K, C₆D₅Cl): δ = -16.3 ([B(C₆F₅)₄]⁻). **¹⁹F{¹H} NMR** (470.28 MHz, 305.0 K, C₆D₅Cl): δ = -166.4-(-166.1) (m, *m*-F, [B(C₆F₅)₄]⁻), -162.4 (t, ³J_{F,F} = 21.4 Hz, *o*-F, [B(C₆F₅)₄]⁻), -131.9-(-131.7) (m, *o*-F, [B(C₆F₅)₄]⁻), -93.8 (s, 1 F, CF). **²⁹Si{¹H} NMR** (99.31 MHz, 305.0 K, C₆D₅Cl): δ = -46.0 (¹J_{Si,H} = 297.6 Hz).

¹H NMR (499.87 MHz, 305.0 K, CD₂Cl₂): δ = 3.45-3.51 (m, 4 H, CH₂), 6.03 (s, 1 H, SiH), 6.73-6.74 (m, 2 H, SPh), 7.01-7.03 (m, 1 H), 7.09-7.18 (m, 4 H), 7.23-7.26 (m, 2 H), 7.32-7.35 (m, 1 H), 7.37-7.39 (m, 2

H), 7.45 (dm, $^3J_{\text{H,H}} = 7.3$ Hz, 1 H, 3/4-H), 7.53 (dm, $^3J_{\text{H,H}} = 7.2$ Hz, 1 H, 8-H), 7.75 (dm, $^3J_{\text{H,H}} = 7.3$ Hz, 1 H, 3/4-H), 7.81-7.83 (m, 2 H, NC-Ar), 8.18 (dm, $^3J_{\text{H,H}} = 7.1$ Hz, 1 H, 7-H). $^{19}\text{F}\{^1\text{H}\}$ NMR (470.28 MHz, 305.0 K, CD_2Cl_2): $\delta = -167.5$ -(-167.1) (m, *m*-F, $[\text{B}(\text{C}_6\text{F}_5)_4]^-$), -162.4 (m, *o*-F, $[\text{B}(\text{C}_6\text{F}_5)_4]^-$), -132.8 (brs, *o*-F, $[\text{B}(\text{C}_6\text{F}_5)_4]^-$), -91.5 (s, 1 F, CF). ^{29}Si NMR (99.31 MHz, 305.0 K, CD_2Cl_2): $\delta = -41.4$ ($^1J_{\text{Si,H}} = 295.2$ Hz).

Pivalonitrilium Borate **125-S**^[115]

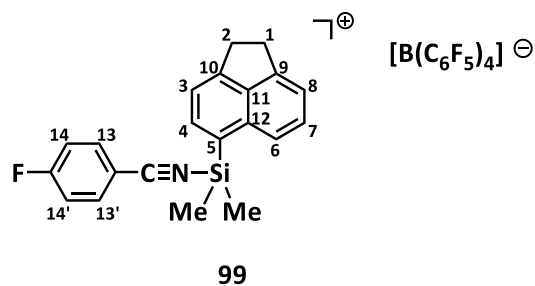
Nitrilium borate **125-S** $[\text{B}(\text{C}_6\text{F}_5)_4]$ was synthesized according to general procedure E using 1.0 equiv. (200.00 μmol , 64 mg) of 5-dimethylsilyl-6-thiophenylacenaphthene **43a** and 1.0 equiv. (200.00 μmol , 184.5 mg) of trityl borate and 0.9 equiv. (180.00 μmol , 15.0 mg) of pivalonitrile. The NMR was measured in $\text{C}_6\text{H}_5\text{Cl}$ with a D_2O -capillary for the lock signal.



^1H NMR (4998.9 MHz, 305.0 K, $\text{C}_6\text{H}_5\text{Cl}/\text{D}_2\text{O}$ -capillary): $\delta = 0.70$ (s, 6 H, $\text{Si}(\text{CH}_3)_2$), 1.20 (s, 9 H, $\text{C}(\text{CH}_3)_3$), 3.15-3.17 (m, 2 H, CH_2), 3.21-3.22 (m, 2 H, CH_2), 6.75-6.77 (m, 2 H, Ar-H), 7.29-7.30 (m, 1 H, H-12), 7.37 (t, $^3J = 7.90$ Hz, 1 H, Ar-H), 7.51 (d, $^3J = 7.28$ Hz, 1 H, Ar-H), 7.84 (d, $^3J = 7.13$ Hz, 1 H, H-11). The ^1H NMR chemical shifts of three aromatic hydrogen atoms could not be assigned due to overlap with the solvent chlorobenzene. $^{13}\text{C}\{^1\text{H}\}$ NMR (125.71 MHz, 305.0 K, $\text{C}_6\text{H}_5\text{Cl}/\text{D}_2\text{O}$ -capillary): $\delta = 3.9$ (CH_3 , $\text{Si}(\text{CH}_3)_2$), 26.3 (CH_3 , $\text{C}(\text{CH}_3)_3$), 29.0 (C, $\text{C}(\text{CH}_3)_3$), 30.5 (CH_2), 30.6 (CH_2), 110.4 (C, CN), 120.6 (CH), 120.9 (CH), 121.1 (CH, C-12), 121.9 (CH), 123.9-125.7 (C, $[\text{B}(\text{C}_6\text{F}_5)_4]^-$), 126.7 (C), 127.4 (CH), 128.5 (CH), 135.4-135.9 (brm, C, $[\text{B}(\text{C}_6\text{F}_5)_4]^-$), 136.1 (CH), 138.5 (dm, $^1J_{\text{C,F}} = 245.2$ Hz, CF, $[\text{B}(\text{C}_6\text{F}_5)_4]^-$), 138.6 (CH, C-11), 139.1 (C), 142.1 (CH), 143.1 (CH), 148.7 (dm, $^1J_{\text{C,F}} = 242.1$ Hz, CF, $[\text{B}(\text{C}_6\text{F}_5)_4]^-$), 151.6 (C), 152.7 (C). $^{29}\text{Si}\{^1\text{H}\}$ NMR (99.3 MHz, 305.0 K, $\text{C}_6\text{H}_5\text{Cl}/\text{D}_2\text{O}$ -capillary): $\delta = -3.30$. $^{11}\text{B}\{^1\text{H}\}$ NMR (160.40 MHz, 305.1 K, $\text{C}_6\text{H}_5\text{Cl}/\text{D}_2\text{O}$ -capillary): $\delta = 16.4$. $^{19}\text{F}\{^1\text{H}\}$ NMR (470.30 MHz, 305.1 K, $\text{C}_6\text{H}_5\text{Cl}/\text{D}_2\text{O}$ -capillary): $\delta = -166.6$ (t, $^3J_{\text{F,F}} = 17.9$ Hz, 8 F, *m*-F, $[\text{B}(\text{C}_6\text{F}_5)_4]^-$), -162.7 (t, $^3J_{\text{F,F}} = 20.7$ Hz, 4 F, *p*-F, $[\text{B}(\text{C}_6\text{F}_5)_4]^-$), -132.0 (brs, 8 F, *o*-F, $[\text{B}(\text{C}_6\text{F}_5)_4]^-$).

Silylnitrilium Borate 99[B(C₆F₅)₄] without a Donor

Nitrilium borate **99**[B(C₆F₅)₄] was synthesized according to general procedure **F** using 1.0 equiv. of 5-dimethylsilylacenaphthene **100** (250.00 μmol, 53 mg), 1.0 equiv. of trityl borate (250.00 μmol, 230 mg) and 1.0 equiv. of 4-fluorobenzonitrile (250.00 μmol, 30 mg). Nitrilium ion **99** is not stable and decomposes within one day.



¹H NMR (499.87 MHz, 305.1 K, CD₂Cl₂): δ = 1.26 (s, 6 H, Si(CH₃)₂), 3.53 (brs, 4 H, 2 × CH₂), 7.40-7.44 (m, 2 H, H-14, H-14'), 7.50 (d, ³J_{H,H} = 6.9 Hz, 1 H, H-3), 7.54 (d, ³J_{H,H} = 7.0 Hz, 1 H, H-8), 7.71-7.74 (m, 1 H, H-7), 7.84 (d, ³J_{H,H} = 8.3 Hz, 1 H, H-6), 7.93 (d, ³J_{H,H} = 6.9 Hz, 1 H, H-4), 8.01-8.06 (m, 2 H, H-13, H-13'). **¹³C{¹H} NMR** (125.71 MHz, 305.0 K, CD₂Cl₂): δ = -0.9 (Si(CH₃)₂), 30.9 (CH₂), 97.8 (C-CN), 118.9 (C, C-5), 119.8, 120.1 (CH, C-3, C-14, C-14', overlapping with CN), 121.0 (CH, C-6), 121.6 (CH, C-8), 132.8-125.7 (brs, C, [B(C₆F₅)₄]⁻), 130.8 (CH, C-7), 134.7 (C, C-12), 137.0 (dm, ¹J_{C,F} = 242.2 Hz, CF, [B(C₆F₅)₄]⁻), 138.8 (CH, C-4), 139.0 (dm, ¹J_{C,F} = 233.2 Hz, CF, [B(C₆F₅)₄]⁻), 139.9 (d, ³J_{C,F} = 10.3 Hz, C-13, C-13'), 146.8 (C, C-11), 148.9 (dm, ¹J_{C,F} = 241.0 Hz, CF, [B(C₆F₅)₄]⁻), 149.4 (C, C-9), 154.9 (C, C-10), 170.4 (d, ¹J_{C,F} = 277.5 Hz, CF). **¹⁹F{¹H} NMR** (470.28 MHz, 305.0 K, CD₂Cl₂): δ = -167.5-(-167.2) (m, 8 F, *m*-F, [B(C₆F₅)₄]⁻), -163.44 (t, ³J_{F,F} = 20.4 Hz, 4 F, *o*-F, [B(C₆F₅)₄]⁻), -133.0-(-132.8) (m, 8 F, *o*-F, [B(C₆F₅)₄]⁻), -86.6 (s, 1 F, CF). **²⁹Si{¹H} NMR** (99.31 MHz, 305.0 K, CD₂Cl₂): δ = 23.0. **¹¹B{¹H} NMR** (160.38 MHz, 305.1 K, CD₂Cl₂): δ = -16.4.

FBN-BCF Complex 101

A Schlenk tube was charged with 94 mg (183.60 μmol) of tris(pentafluorophenyl)borane, 22 mg (183.60 μmol) of 4-fluorobenzonitrile and 52 mg (56.38 μmol) of trityl borate. The solids were dissolved in 0.7 mL CD₂Cl₂ and the mixture was stirred for 20 min at r.t.. Then the mixture was

transferred to a NMR tube for analysis. Trityl borate was added as internal reference for the ^{19}F NMR spectroscopy.

^1H NMR (499.87 MHz, 305.0 K, CD_2Cl_2): δ = 7.35-7.43 (brm, 2 H, CN-Ar, *m*-CH), 7.69 (d, $^3J_{\text{H,H}} = 7.5$ Hz, $[\text{CPh}_3]^+$, *o*-CH), 7.89 (t, $^3J_{\text{H,H}} = 7.8$ Hz, $[\text{CPh}_3]^+$, *m*-CH), 7.94-7.05 (brm, 2 H, CN-Ar, *o*-CH), 8.28 (t, $^3J_{\text{H,H}} = 7.5$ Hz, $[\text{CPh}_3]^+$, *p*-CH). $^{13}\text{C}\{^1\text{H}\}$ NMR (125.71 MHz, 305.0 K, CD_2Cl_2): δ = 102.0 (NC-Ar), 114.5 (NC-Ar), 115.7 (NC-Ar), 119.0 (d, $^2J_{\text{C,F}} = 13.5$ Hz, NC-Ar), 123.4-125.5 (brs, C, $[\text{B}(\text{C}_6\text{F}_5)_4]^-$), 131.2 ($[\text{CPh}_3]^+$, CH), 136.8 (dm, $^1J_{\text{C,F}} = 241.4$ Hz, CF, $[\text{B}(\text{C}_6\text{F}_5)_4]^-$), 138.0 (dm, $^1J_{\text{C,F}} = 249.0$ Hz, C_6F_5 , *m*-CF), 138.8 (dm, $^1J_{\text{C,F}} = 247.6$ Hz, CF, $[\text{B}(\text{C}_6\text{F}_5)_4]^-$), 140.6 ($[\text{CPh}_3]^+$, CH), 141.1 (dm, $^1J_{\text{C,F}} = 251.0$ Hz, C_6F_5 , *p*-CF), 143.3 ($[\text{CPh}_3]^+$, CH), 144.2 ($[\text{CPh}_3]^+$, CH), 148.8 (d, $^1J_{\text{C,F}} = 240.8$ Hz, CF, $[\text{B}(\text{C}_6\text{F}_5)_4]^-$, C_6F_5 , *o*-CF), 168.7 (d, $^1J_{\text{C,F}} = 269.9$ Hz, NC-Ar, CF), 211.5 ($[\text{CPh}_3]^+$). $^{11}\text{B}\{^1\text{H}\}$ NMR (160.38 MHz, 305.0 K, CD_2Cl_2): δ = -10.0 (N-B), -16.6 ($[\text{B}(\text{C}_6\text{F}_5)_4]^-$). $^{19}\text{F}\{^1\text{H}\}$ NMR (470.28 MHz, 305.0 K, CD_2Cl_2): δ = -167.4-(-167.2) (m, *m*-F, $[\text{B}(\text{C}_6\text{F}_5)_4]^-$), -164.0-(-163.9) (m, 6 F, *m*- C_6F_5), -163.44 (t, $^3J_{\text{F,F}} = 20.3$ Hz, *o*-F, $[\text{B}(\text{C}_6\text{F}_5)_4]^-$), -156.8 (t, $^3J_{\text{F,F}} = 20.2$ Hz, 3 F, *p*- C_6F_5), -134.5-(-134.3) (m, 6 H, *o*- C_6F_5), -132.9-(-132.5) (m, *o*-F, $[\text{B}(\text{C}_6\text{F}_5)_4]^-$), -92.5 (s, 1 F, CF).

4-Fluorobenzonitrile + Tritylborate in CD_2Cl_2

^1H NMR (499.87 MHz, 305.0 K, CD_2Cl_2): δ = 7.19-7.25 (m, 2 H, CN-Ar, *m*-CH), 7.69-7.72 (m, 8 H, $[\text{CPh}_3]^+$, *o*-CH, CN-Ar, *o*-CH), 7.89 (t, $^3J_{\text{H,H}} = 7.8$ Hz, 6 H, $[\text{CPh}_3]^+$, *m*-CH), 8.28 (t, $^3J_{\text{H,H}} = 7.5$ Hz, 3 H, $[\text{CPh}_3]^+$, *p*-CH). $^{13}\text{C}\{^1\text{H}\}$ NMR (125.71 MHz, 305.0 K, CD_2Cl_2): δ = 109.3 ($\underline{\text{C}}$ -CN), 117.4 (d, $^2J_{\text{C,F}} = 22.8$ Hz, CN-Ar, *m*-CH), 118.7 (CN), 123.7-125.7 (brs, C, $[\text{B}(\text{C}_6\text{F}_5)_4]^-$), 131.2 ($[\text{CPh}_3]^+$, *m*-CH), 135.3 (d, $^3J_{\text{C,F}} = 9.4$ Hz, CN-Ar, *o*-CH), 136.9 (dm, $^1J_{\text{C,F}} = 243.4$ Hz, CF, $[\text{B}(\text{C}_6\text{F}_5)_4]^-$), 138.9 (dm, $^1J_{\text{C,F}} = 244.0$ Hz, CF, $[\text{B}(\text{C}_6\text{F}_5)_4]^-$), 140.6 ($[\text{CPh}_3]^+$, *ipso*-C), 143.2 ($[\text{CPh}_3]^+$, *o*-CH), 144.1 ($[\text{CPh}_3]^+$, *p*-CH), 148.8 (d, $^1J_{\text{C,F}} = 239.7$ Hz, CF, $[\text{B}(\text{C}_6\text{F}_5)_4]^-$), 165.7 (d, $^1J_{\text{C,F}} = 255.7$ Hz, CF), 211.6 ($[\text{CPh}_3]^+$). $^{19}\text{F}\{^1\text{H}\}$ NMR (470.28 MHz, 305.0 K, CD_2Cl_2): δ = -167.4-(-167.2) (m, 8 F, *m*-F, $[\text{B}(\text{C}_6\text{F}_5)_4]^-$), -163.44 (t, $^3J_{\text{F,F}} = 20.4$ Hz, 4 F, *o*-F, $[\text{B}(\text{C}_6\text{F}_5)_4]^-$), -132.9-(-132.7) (m, 8 F, *o*-F, $[\text{B}(\text{C}_6\text{F}_5)_4]^-$), -103.4 (s, 1 F, CF). $^{11}\text{B}\{^1\text{H}\}$ NMR (160.38 MHz, 305.1 K, CD_2Cl_2): δ = -16.6.

5.6.1 Assessment of the Lewis Acidity

The samples of the silylnitrilium borates **94-97** were prepared according to the procedures in Chapter 5.6.

For the reference an NMR sample was prepared using fluorobenzene (302 μmol , 28 μL), trityl borate (302 μmol , 278 mg) and 4-fluorobenzonitrile (302 μmol , 37 mg) in 0.55 mL dichloromethane- d_2 .

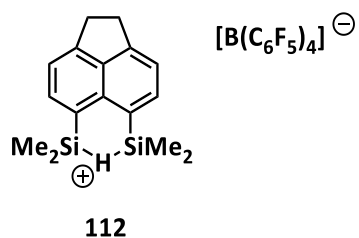
Table 38 – ^{19}F NMR chemical shifts of the *p*-fluorine of $[\text{B}(\text{C}_6\text{F}_5)_4]^-$ and free 4-fluorobenzonitrile (FBN) referenced against fluorobenzene $\delta^{19}\text{F} = -113.78$ at different temperatures

T [K]	$\delta^{19}\text{F}$ $[\text{B}(\text{C}_6\text{F}_5)_4]^-$	$\delta^{19}\text{F}$ FBN
305	-163.44	-103.43
293	-163.37	-
283	-163.29	-103.38
273	-163.20	-
263	-163.12	-103.33
253	-163.04	-
243	-162.96	-103.30
233	-162.87	-103.29
223	-162.79	-103.30
213	-162.73	-
203	-162.63	-103.30
193	-162.57	-103.31

5.7 Synthesis of Silyliminium Borates

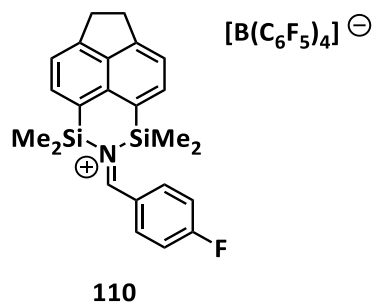
Bis-dimethylsilyliminium Borate **110**[B(C₆F₅)₄]

To synthesize iminium borate **110**[B(C₆F₅)₄], first the corresponding silyl borate **112**[B(C₆F₅)₄] was prepared. A Schlenk tube was charged with 1.0 equiv. (314.21 μmol, 85 mg) of 5,6-bis-dimethylsilylacenaphthene **114** and 1.0 equiv. (314.21 μmol, 289 mg) of trityl borate. Then 1.5 mL benzene was added and the mixture was stirred for 1 h. Thereby, first the formation of two phases was observed, then a yellow solid precipitated. The solvent was removed via syringe and the remaining solid was washed (1 x 1.5 mL benzene, 2 x 3.0 mL benzene and *n*-pentane (1:1)) and subsequently dried under high-vacuum. The resulting silyl borate **112**[B(C₆F₅)₄] was dissolved in 0.7 mL chlorobenzene-*d*₅ for NMR spectroscopic analysis. The ¹H NMR spectrum shows broadened signals. The NMR data is in accordance with the literature.^[87a]



¹H NMR (499.87 MHz, 305.0 K, C₆D₅Cl): δ = 0.50 (s, 12 H, w(1/2) = 14.1 Hz), 2.92 (s, 4 H, w(1/2) = 14.2 Hz), 3.29 (s, 1 H, w(1/2) = 17.4 Hz), 7.01 (s, 5 H, overlap with the solvent, w(1/2) = 18.5 Hz), 7.23 (s, 2 H, w(1/2) = 12.7 Hz). ³C{¹H} NMR (125.71 MHz, 305.0 K, C₆D₅Cl): δ = -1.4, 30.5, 120.2, 121.0, 123.8-125.8 (brm, [B(C₆F₅)₄]), 135.4, 136.9 (dm, ¹J_{C,F} = 236.8 Hz, [B(C₆F₅)₄]), 137.0, 138.3, 138.8 (dm, ¹J_{C,F} = 235.9 Hz, [B(C₆F₅)₄]), 149.0 (dm, ¹J_{C,F} = 240.9 Hz, [B(C₆F₅)₄]), 153.7. ²⁹Si{¹H} INEP NMR (D3 = 0.0084, D4 = 0.0313, 99.31 MHz, 305.0 K, C₆D₅Cl): δ = 60.4.

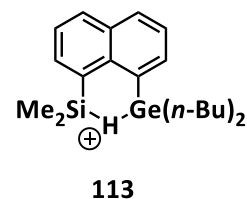
A Schlenk tube was charged with 1.0 equiv. (314.21 μmol, 38 mg) of 4-fluorobenzonitrile and the NMR sample with the bis-dimethylsilyl borate **112**[B(C₆F₅)₄] was added. The solution was stirred for 45 min at r.t. and then analysed by NMR spectroscopy. The title compound **110**[B(C₆F₅)₄] was not obtained purely, therefore only those chemical shifts, which were assigned unambiguously to iminium borate **110**[B(C₆F₅)₄] are listed. A complete characterization was not possible.

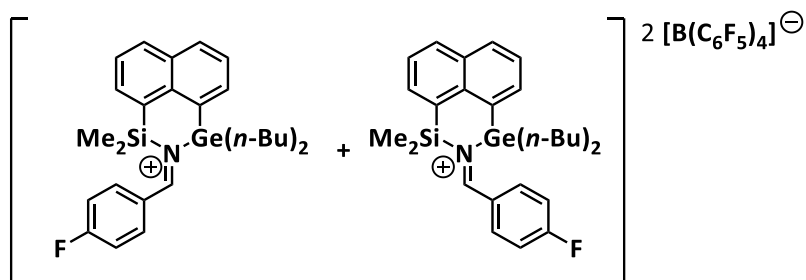


^1H NMR (499.87 MHz, 305.0 K, $\text{C}_6\text{D}_5\text{Cl}$): δ = 0.48 (s, 6 H, CH_3), 0.63 (s, 6 H, CH_3), 3.12-3.18 (m, 6 H, CH_2), 7.02-7.07 (m, 4 H, NC-Ar, overlap with impurities), 7.23-7.26 (m, 2 H, 3/8-H), 7.46-7.48 (m, 1 H, 4/7-H), 7.49-7.55 (m, 3 H, NC.Ar, 4/7-H), 9.12 (s, 1 H, 13-H). **$^{13}\text{C}\{^1\text{H}\}$ NMR** (125.71 MHz, 305.0 K, $\text{C}_6\text{D}_5\text{Cl}$): δ = -1.5 (CH_3), 1.9 (CH_3), 117.3 (d, $^2J_{\text{C,F}} = 22.9$ Hz, NC-Ar), 122.6, 124.4 (C, C-5/6), 123.5-125.4 (brm, C, $[\text{B}(\text{C}_6\text{F}_5)_4]$), 135.0 (d, $J_{\text{C,F}} = 10.7$ Hz, CH, NC-Ar), 136.5 (dm, $^1J_{\text{C,F}} = 232.7$ Hz, CF, $[\text{B}(\text{C}_6\text{F}_5)_4]$), 138.4 (dm, $^1J_{\text{C,F}} = 232.9$ Hz, CF, $[\text{B}(\text{C}_6\text{F}_5)_4]$), 148.5 (dm, $^1J_{\text{C,F}} = 241.6$ Hz, CF, $[\text{B}(\text{C}_6\text{F}_5)_4]$), 135.0 (d, $^1J_{\text{C,F}} = 10.7$ Hz, NC-Ar), 168.2 (d, $^1J_{\text{C,F}} = 267.4$ Hz, NC-Ar, CF), 187.4 (CH, C-13). **$^{11}\text{B}\{^1\text{H}\}$ NMR** (160.38 MHz, 305.0 K, $\text{C}_6\text{D}_5\text{Cl}$): δ = -16.2 ($[\text{B}(\text{C}_6\text{F}_5)_4]$). **$^{19}\text{F}\{^1\text{H}\}$ NMR** (470.29 MHz, 305.0 K, $\text{C}_6\text{D}_5\text{Cl}$): δ = -167.4-(-167.2) (m, 8 F, *m*-F, $[\text{B}(\text{C}_6\text{F}_5)_4]$), -163.4 (t, $^3J_{\text{F,F}} = 20.6$ Hz, 4 F, *o*-F, $[\text{B}(\text{C}_6\text{F}_5)_4]$), -133.0-(-132.7) (m, 8 F, *o*-F, $[\text{B}(\text{C}_6\text{F}_5)_4]$), -101.3 (s, 1 F, CF), -93.3 (s, 0.5 F), -92.6 (brs, 0.2 F). **$^{29}\text{Si}\{^1\text{H}\}$ NMR** (99.31 MHz, 305.0 K, $\text{C}_6\text{D}_5\text{Cl}$): δ = 15.7, 23.3. **$^1\text{H}/^{15}\text{N}$ HMBC NMR** (499.87 MHz, 305.0 K, $\text{C}_6\text{D}_5\text{Cl}$): δ = 229.5.

(Dimethylsilyl)(di-*n*-butylgermyl)iminium Borate **111** $[\text{B}(\text{C}_6\text{F}_5)_4]$

A Schlenk tube was charged with 1.1 equiv. (184.89 μmol , 69 mg) of 1-di-*n*-butylgermyl-8-dimethylsilylnaphthalene **115**. A solution of 1.0 equiv. (166.40 μmol , 154 mg) of trityl borate and 1.0 equiv. (166.40 μmol , 20 mg) of 4-fluorobenzonitrile in 0.7 mL dichloromethane- d_2 was added to the precursor **115** at r.t. and the solution was stirred for five minutes before transferring it to an NMR tube for analysis. The title compound **111** $[\text{B}(\text{C}_6\text{F}_5)_4]$ was not obtained purely, besides impurities, the corresponding silylgermyl cation **113** was detected. Furthermore, two stereoisomers in the ratio of 80:20 of the title ion **111** were formed. A complete characterization was not possible.



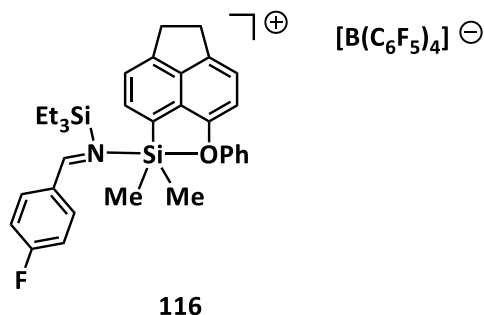


111

$^1\text{H NMR}$ (499.87 MHz, 305.0 K, CD_2Cl_2): δ = 0.43 (s, 0.8 H), 0.60 (s, 0.8 H), 0.74 (t, $^3J_{\text{H,H}} = 7.0$ Hz, 6.0 H, CH_3 (*n*-Bu)), 0.78-0.82 (m, 3.5 H), 0.85-0.89 (m, 2.3 H), 0.92 (s, 6.5 H, $\text{Si}(\text{CH}_3)_2$), 0.93-0.97 (m, 3.0 H), 0.99-0.14 (m, 1.4 H), 1.09-1.11 (m, 1.0 H), 1.12-1.56 (m, 19.7 H), 1.59-1.74 (m, 4.2 H), 1.99-2.12 (m, 0.6 H), 4.36 (s, 0.3 H), 5.62 (s, 1.5 H, Ph_3CH), 7.05 (t, $^3J_{\text{H,H}} = 7.4$ Hz), 7.19-7.22 (m, 9.3 H, Ph_3CH), 7.24-7.28 (m, 4.3 H, Ph_3CH), 7.31-7.36 (m, 9.2 H, Ph_3CH), 7.46-7.55 (m, 3.5 H), 7.66-7.81 (m, 5.2 H), 7.87-7.98 (m, 4.8 H), 8.10-8.22 (m, 2.8 H), 9.32 (s, 0.2 H), 9.53 (s, 0.9 H). $^{13}\text{C}\{^1\text{H}\}$ NMR (125.71 MHz, 305.0 K, CD_2Cl_2): δ = -0.9, 1.1, 1.5, 13.4, 13.6, 20.7, 25.9, 26.2, 26.5, 26.7, 57.6 (Ph_3CH), 118.6 (d, $J = 22.6$ Hz), 123.8-125.5 (brm, C, $[\text{B}(\text{C}_6\text{F}_5)_4]$), 126.8 (d, $J = 5.4$ Hz), 127.0 (Ph_3CH), 129.0 (Ph_3CH), 130.0 (Ph_3CH), 133.0, 133.1, 133.8, 134.2, 134.4, 134.9 (d, $J = 9.4$ Hz), 135.7, 137.0 (dm, $J = 241.3$ Hz, CF, $[\text{B}(\text{C}_6\text{F}_5)_4]$), 138.9 (dm, $J = 244.9$ Hz, CF, $[\text{B}(\text{C}_6\text{F}_5)_4]$), 139.8, 144.7, 148.9 (dm, $J = 241.0$ Hz, CF, $[\text{B}(\text{C}_6\text{F}_5)_4]$), 168.8 (d, $J = 265.6$ Hz), 185.7, 186.5. $^{11}\text{B}\{^1\text{H}\}$ NMR (160.38 MHz, 305.0 K, CD_2Cl_2): δ = -16.5 ($[\text{B}(\text{C}_6\text{F}_5)_4]$). $^{19}\text{F}\{^1\text{H}\}$ NMR (470.30 MHz, 305.1 K, CD_2Cl_2): δ = -167.4-(-167.2) (m, 8 F, *m*-F, $[\text{B}(\text{C}_6\text{F}_5)_4]$), -163.4 (t, $^3J_{\text{F,F}} = 21.0$ Hz, 4 F, *o*-F, $[\text{B}(\text{C}_6\text{F}_5)_4]$), -133.0-(-132.7) (m, 8 F, *o*-F, $[\text{B}(\text{C}_6\text{F}_5)_4]$), -94.7 (s, 0.6 F, CF), -94.4 (s, 0.2 F). $^{29}\text{Si}\{^1\text{H}\}$ INEPT NMR (D3 = 0.0083, D4 = 0.0313, 99.31 MHz, 305.0 K, CD_2Cl_2): δ = 11.8 (**111**), 19.7 (**111**, main), 41.1 (**113**).

Phenoxyl-Substituted Dimethylsilyliminium Borate **116** $[\text{B}(\text{C}_6\text{F}_5)_4]$

A Schlenk tube was charged with 1.0 equiv. (358.01 μmol , 109 mg) of silane **42a**, 1.0 equiv. (358.01 μmol , 330 mg) of trityl borate and 1.0 equiv. (358.01 μmol , 43 mg) of 4-fluorobenzonitrile. The solids were dissolved in 0.8 mL benzene- D_6 and the mixture was stirred for 30 min. 1.0 equiv. (358.01 μmol , 0.06 mL) of triethylsilane was added at r.t. and the mixture was stirred for 5 min prior to transferring it to an NMR tube for analysis. The mixture contains the title compound **116** $[\text{B}(\text{C}_6\text{F}_5)_4]$ and at least three further species, whereby a complete characterization was not possible. Due to fast decomposition, the ^{13}C NMR data was not included.

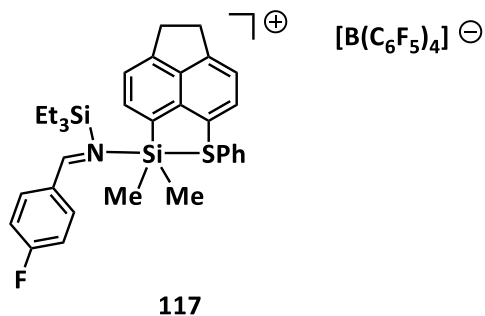


^1H NMR (499.87 MHz, 305.0 K, C_6D_6): δ = 0.52 (brs, 1.4 H), 0.57 (s, 6 H, SiMe_2 , title compound), 0.59 (brs, 1 H), 0.62-0.64 (m, 4.4 H, side product 2), 0.67 (d, $^3J_{\text{H,H}} = 3.1$ Hz, 1.2 H), 0.69 (d, $^3J_{\text{H,H}} = 3.1$ Hz, 3.6 H), 0.70-0.71 (m, 5 H), 0.71-0.73 (m, 4.9 H, side product 1), 0.73-0.75 (m, 1.5 H), 0.76 (s, 2.6 H), 0.77-0.82 (m, 6.3 H, SiEt_3 , title compound), 0.83-0.89 (m, 11.9 H, SiEt_3 , title compound), 3.07-3.18 (m, 4 H, CH_2), 3.20-3.28 (m, 4 H, CH_2), 5.54 (s, 0.9 H, Ph_3CH), 6.32-6.36 (m, 0.5 H), 6.47 (t, $^3J_{\text{H,H}} = 8.3$ Hz, 1.8 H), 6.55 (d, $^3J_{\text{H,H}} = 7.7$ Hz, 0.3 H), 6.59 (d, $^3J_{\text{H,H}} = 7.7$ Hz, 0.9 H), 6.67 (d, $^3J_{\text{H,H}} = 7.7$ Hz, 0.3 H), 6.74 (d, $^3J_{\text{H,H}} = 7.7$ Hz, 0.3 H), 6.77-6.81 (m, 0.6 H), 6.83-6.90 (m, 2 H), 6.91-6.95 (m, 1.7 H), 6.95-7.00 (m, 3.4 H), 7.01-7.11 (m, 1.7 H), 7.12-7.26 (m, 18.6 H, Ph_3CH), 7.28 (d, $^3J_{\text{H,H}} = 7.1$ Hz, 0.9 H), 7.31-7.34 (m, 0.8 H), 7.37 (t, $^3J_{\text{H,H}} = 7.8$ Hz, 2.4 H), 7.52-7.57 (m, 1.1 H, title compound), 7.66 (d, $^3J_{\text{H,H}} = 7.0$ Hz, 0.2 H), 7.81 (d, $^3J_{\text{H,H}} = 7.1$ Hz, 0.2 H), 8.83 (s, 0.3 H, NCH, side product 3), 8.98 (s, 1 H, NCH, title compound), 9.12 (s, 0.3 H, NCH, side product 2), 9.28 (s, 0.2 H, NCH, side product 1). **$^{19}\text{F}\{^1\text{H}\}$ NMR** (470.30 MHz, 305.1 K, C_6D_6): δ = -167.4-(-167.2) (m, 8 F, *m*-F, $[\text{B}(\text{C}_6\text{F}_5)_4]^-$), -163.4 (t, $^3J_{\text{F,F}} = 21.0$ Hz, 4 F, *o*-F, $[\text{B}(\text{C}_6\text{F}_5)_4]^-$), -132.7-(-132.4) (m, 8 F, *o*-F, $[\text{B}(\text{C}_6\text{F}_5)_4]^-$), -96.9 (brs, 0.1 F), -95.5 (s, 0.4 F), -95.1 (s, 0.1 F), -94.1 (s, 0.1 F). **$^{29}\text{Si}\{^1\text{H}\}$ INEPT NMR** (D3 = 0.0083, D4 = 0.0313, 99.31 MHz, 305.0 K, C_6D_6): δ = 17.5 (side product 1), 17.9 (title compound), 27.3 (side product 1), 27.7 (side product 2), 32.0 (side product 2), 34.0 (side product 3), 40.0 (title compound), 40.6 (side product 3). **$^1\text{H}/^{15}\text{N}$ HMBC NMR** (499.87 MHz, 305.0 K, C_6D_6): δ = 233.7.

Thiophenyl-Substituted Dimethylsilyliminium Borate 117 $[\text{B}(\text{C}_6\text{F}_5)_4]$

A Schlenk tube was charged with 1.0 equiv. (368.15 μmol , 218 mg) of silane **43a** and 1.0 equiv. (368.15 μmol , 339 mg) of trityl borate. The solids were dissolved in ca. 1 mL benzene- D_6 and the mixture was stirred for 20 min at r.t.. Then 1.0 equiv. (368.15 μmol , 44 mg) of 4-fluorobenzonitrile was added and the mixture was stirred for 5 h at r.t.. Subsequently, 1.0 equiv. (368.15 μmol , 0.06 mL) of triethylsilane was added at r.t. and the mixture was stirred for 15 min prior to transferring it

to an NMR tube for analysis. The title compound **117**[B(C₆F₅)₄] was obtained in a mixture with at least two side products. A complete characterization was not possible.



¹H NMR (499.87 MHz, 305.0 K, C₆D₆): δ = 0.30 (brs, 6H, SiMe₂, silyl cation), 0.44-0.49 (m, 4.7 H, title compound), 0.57-0.66 (m, 10.7 H, title compound), 0.67-0.70 (m, 2.1 H), 0.74-0.77 (m, 6.8 H, title compound), 0.84-0.92 (m, 2.6 H), 0.98-1.03 (m, 6.2 H), 3.02-3.11 (m, 5.6 H, CH₂), 6.54-6.65 (m, 2.5 H), 6.79-6.84 (m, 1.3 H), 6.88-6.97 (m, 3.4 H), 6.97-7.02 (m, 2.8 H), 7.05-7.15 (m, 6.8 H), 7.39-7.50 (m, 1.4 H), 8.71 (s, 0.5 H, NCH, title compound). **¹³C{¹H} NMR (125.71 MHz, 305.0 K, C₆D₆)** δ = 4.1 (CH₂), 5.1, 5.9 (CH₃), 5.9 (CH₃), 6.1 (CH₃), 6.2 (CH₃), 6.4 (CH₂), 6.6 (CH₂), 7.7 (CH₂), 7.9 (CH₂), 30.1 (CH₂), 30.9 (CH₂), 31.0 (CH₂), 31.2 (CH₂), 114.4 (d, $J_{C,F}$ = 21.0 Hz, CH), 114.8 (d, $J_{C,F}$ = 21.2 Hz, CH), 117.1 (C), 117.4 (d, $J_{C,F}$ = 22.2 Hz, CH), 117.5 (d, $J_{C,F}$ = 22.8 Hz, CH), 118.8 (CH), 119.8 (CH), 121.5 (CH), 122.5 (CH), 123.1 (CH), 124.0-125.8 (brm, [B(C₆F₅)₄]⁻), 124.7 (C), 126.7 (CH), 127.5 (CH), 128.4 (CH), 129.4 (CH), 130.3 (CH), 130.3 (CH), 131.3 (CH), 132.7 (CH), 133.4 (CH), 133.8 (C), 134.0 (d, $J_{C,F}$ = 10.4 Hz, CH), 135.4 (C), 135.5 (C), 136.9 (CH), 137.0 (d, $J_{C,F}$ = 233.5 Hz, [B(C₆F₅)₄]⁻), 138.5 (C), 138.9 (d, $J_{C,F}$ = 233.0 Hz, [B(C₆F₅)₄]⁻), 139.3 (C), 139.5 (C), 140.6 (d, $J_{C,F}$ = 2.6 Hz, C), 143.5 (d, $J_{C,F}$ = 3.0 Hz, C), 145.7 (C), 147.9 (C), 149.1 (d, $J_{C,F}$ = 241.4 Hz, [B(C₆F₅)₄]⁻), 152.3 (C), 154.2 (C), 168.2 (d, $J_{C,F}$ = 266.5 Hz, C), 191.3 (CH). **²⁹Si{¹H} NMR (99.31 MHz, 305.0 K, C₆D₆):** δ = 12.4 (side product 1), 13.5 (side product 2), 34.0 (title compound), 40.6 (title compound), 65.8 (silyl cation). **¹H/¹⁵N HMBC NMR (499.87 MHz, 305.0 K, C₆D₆):** δ = 230.2.

5.8 Catalytic Reactions with Silyl Borates as Catalysts

5.8.1 Hydrosilylation Reaction

General Procedure G: A Schlenk tube was charged with 75.00 μmol of silane **42a** or **43a**, 75.00 μmol (69.0 mg) of trityl borate $[\text{Ph}_3\text{C}][\text{B}(\text{C}_6\text{F}_5)_4]$ and 150.00 μmol (30.8 mg) of DTBMP and the solids were dissolved in 0.5 mL chlorobenzene. The mixture was stirred for 10 min at r.t.. Subsequently, 1.50 mmol (0.17 mL) of pivalonitrile and 1.50-4.50 mmol of the corresponding silane (Et_3SiH , Me_2PhSiH or Ph_3SiH) was added. The mixture was stirred for the time and at the temperature given below and then transferred to an NMR tube equipped with a D_2O capillary for analysis. The yield of the product was determined via ^1H NMR spectroscopy. Therefore, the integral of the *para*-methyl group of DTBMP was used as internal standard. Here, it is important to mention, that the integration contains an error which is induced by the different relaxation times of the CH moiety of the imine and the CH_2 group of the amine (Figure 86). The ^1H NMR spectra of all catalytic hydrosilylation reactions were measured with a relaxation time of $\text{D1} = 1$ s.

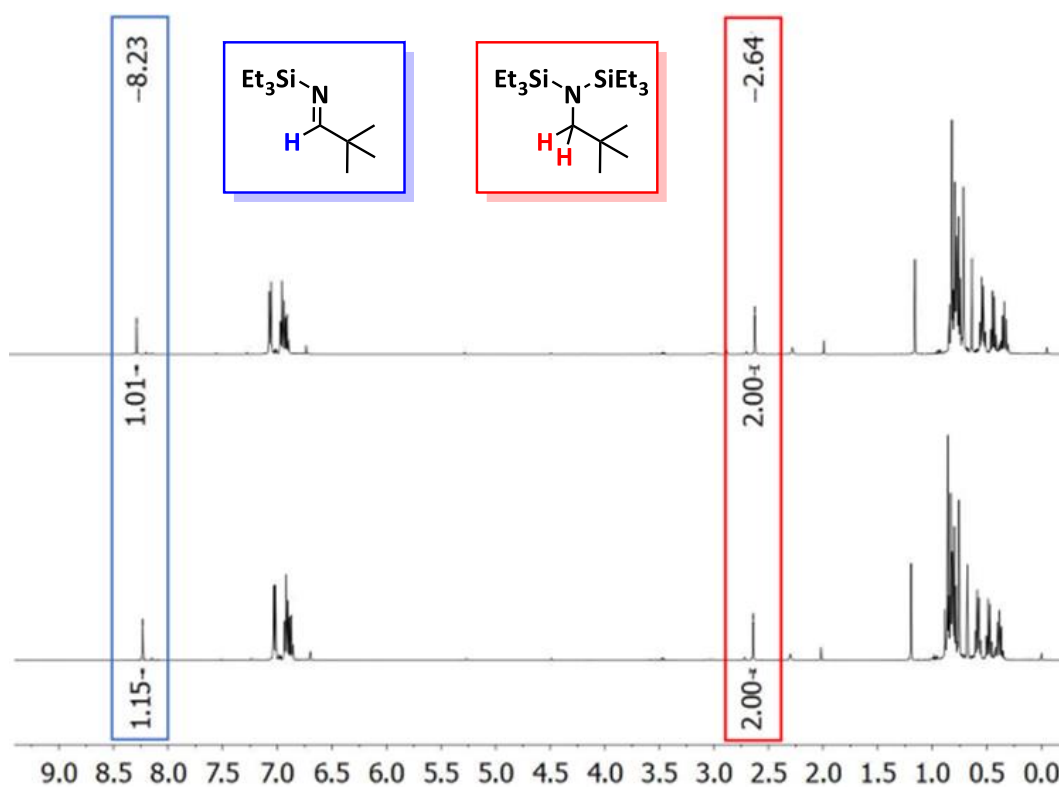
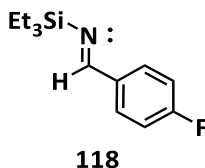


Figure 86 – ^1H NMR spectra (500 MHz, 305 K, $\text{C}_6\text{H}_5\text{Cl}/\text{D}_2\text{O}$ -capillary) of the reaction mixture of the hydrosilylation reaction of pivalonitrile with triethylsilane. Above $\text{D1} = 1$ s, below $\text{D1} = 20$ s.

Silylimine 118

A Schlenk tube was charged with 0.06 equiv. (62.40 μmol , 20.0 mg) of 5-dimethylsilyl-6-thiophenylacenaphthene **43b** and 0.06 equiv. (61.80 μmol , 57.0 mg) of trityl borate. The solids were dissolved in 1 mL benzene and the mixture was stirred for 15 min at r.t.. The polar layer was washed with benzene (3 x 1 mL) and the solvent was removed under low pressure. The residual was dissolved in 0.8 mL dichloromethane- d_2 and transferred to an NMR tube for analysis.

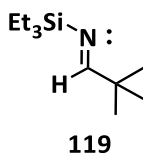
The next day, a Schlenk tube was charged with 1.0 equiv. (990.80 μmol , 120.0 mg) 4-fluorobenzonitrile. The NMR sample containing silyl borate **35a**[$\text{B}(\text{C}_6\text{F}_5)_4$] was added to FBN and the mixture was stirred for 5 min at r.t.. Then the mixture was cooled with an ice bath and 2.0 equiv. (1.98 mmol, 0.32 mL) of triethylsilane was added slowly to the mixture. The mixture was stirred for 45 min while warming slowly to r.t.. The mixture was transferred to an NMR tube for analysis. Complete consumption of FBN and the quantitative formation of silylimine **118** was observed.



^1H NMR (499.87 MHz, 305.0 K, CH_2Cl_2): δ = 0.61-0.68 (m, 6H, CH_2), 0.82-0.93 (m, 29 H, CH_3 , overlap with residual Et_3SiH), 6.93-7.01 (m, 2 H, CH), 7.65-7.71 (m, 2 H, CH), 8.90 (s, 1H, NCH). $^{19}\text{F}\{^1\text{H}\}$ NMR (470.29 MHz, 305.0 K, CH_2Cl_2): δ = -109.4. $^{29}\text{Si}\{^1\text{H}\}$ NMR (99.31 MHz, 305.0 K, CH_2Cl_2): δ = 8.1. $^1\text{H}/^{15}\text{N}$ HMBC NMR (499.87 MHz, 305.0 K, CH_2Cl_2): δ = 344.8.

Silylimine 119

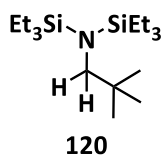
Imine **119** was obtained according to general procedure **G** using 5-dimethylsilyl-6-thiophenylacenaphthene **43a** (24.0 mg, 75.00 μmol) and 2.0 equiv. of triethylsilane (0.48 mL, 3.00 mmol). Stirring the mixture for 120 min at r.t. resulted in a yield of 83 %. Using 5-dimethylsilyl-6-phenoxyacenaphthene **42a** (22.8 mg, 75.00 μmol) as precursor and 1.0 equiv. of triethylsilane (0.24 mL, 1.50 mmol) after 100 min stirring at 80 $^\circ\text{C}$, a yield of 50 % was obtained.



^1H NMR (499.90 MHz, 305.0 K, $\text{C}_6\text{H}_5\text{Cl}/\text{D}_2\text{O}$ -capillary): δ = 0.49 (q, 3J = 6.98 Hz, 6 H, $\text{Si}(\text{CH}_2\text{CH}_3)_3$), 0.80 (t, 3J = 7.92 Hz, 9 H, $\text{Si}(\text{CH}_2\text{CH}_3)_3$), 0.86 (m, 9 H, $\text{C}(\text{CH}_3)_3$), 8.24 (s, 1 H, N-CH). **$^{29}\text{Si}\{^1\text{H}\}$ NMR** (99.30 MHz, T = 305.0 K, $\text{C}_6\text{H}_5\text{Cl}/\text{D}_2\text{O}$ -capillary): δ = 6.0. **$^1\text{H}/^{15}\text{N}$ HMBC NMR** (499.90 MHz, 305.0 K, $\text{C}_6\text{H}_5\text{Cl}/\text{D}_2\text{O}$ -capillary): δ = 331.2.

Disilylamin 120

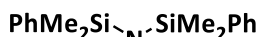
Amine **120** was obtained according to general procedure **G** using 5-dimethylsilyl-6-thiophenylacenaphthene **43a** (24.0 mg, 75.00 μmol) and 3.0 equiv. of triethylsilane (0.72 mL, 4.50 mmol). After stirring the mixture for 340 min at 80 °C, quantitative formation of amine **120** was obtained. Using 5-dimethylsilyl-6-phenoxyacenaphthene **42a** (22.8 mg, 75.00 μmol) as precursor and 2.0 equiv. of triethylsilane (0.48 mL, 3.00 mmol), stirring for 470 min at 80 °C, a yield of 95 % was obtained.



^1H NMR (499.90 MHz, 305.0 K, $\text{C}_6\text{H}_5\text{Cl}/\text{D}_2\text{O}$ -capillary): δ = 0.55 (q, 3J = 7.91 Hz, 12 H, $\text{Si}(\text{CH}_2\text{CH}_3)_3$), 0.74 (s, 9 H, $\text{C}(\text{CH}_3)_3$), 0.81 (t, 3J = 7.95 Hz, 18 H, $\text{Si}(\text{CH}_2\text{CH}_3)_3$), 2.62 (s, 2 H, N- CH_2). **$^{13}\text{C}\{^1\text{H}\}$ NMR** (125.70 MHz, 305.0 K, $\text{C}_6\text{H}_5\text{Cl}/\text{D}_2\text{O}$ -capillary): δ = 4.6 (CH_2 , $\text{Si}(\text{CH}_2\text{CH}_3)_3$), 5.3 (CH_3 , $\text{Si}(\text{CH}_2\text{CH}_3)_3$), 26.7 (CH_3 , $\text{C}(\text{CH}_3)_3$), 30.4 (C , $\text{C}(\text{CH}_3)_3$), 54.1 (CH_2 , N- CH_2). **$^{29}\text{Si}\{^1\text{H}\}$ NMR** (99.30 MHz, 305.0 K, $\text{C}_6\text{H}_5\text{Cl}/\text{D}_2\text{O}$ -capillary): δ = 11.6.

Disilylamin 120a^[115]

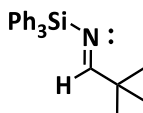
Amine **120a** was obtained according to general procedure **G** using 5-dimethylsilyl-6-thiophenylacenaphthene **43a** (24.0 mg, 75.00 μmol) and 2.0 equiv. of dimethylphenylsilane (0.47 mL, 3.00 mmol). Stirring the mixture for 18 h at r.t. resulted in a yield of 92 %. Using 5-dimethylsilyl-6-phenoxyacenaphthene **42a** (22.8 mg, 75.00 μmol) as precursor and 2.0 equiv. of dimethylphenylsilane (0.47 mL, 3.00 mmol), after stirring for 22 h at r.t. a yield of 20 % was obtained. Stirring for further 260 min at 80 °C led to quantitative formation of amine **120a**.

**120a**

^1H NMR (499.90 MHz, 305.0 K, $\text{C}_6\text{H}_5\text{Cl}/\text{D}_2\text{O}$ -capillary): δ = 0.26 (s, 12 H, $\text{Si}(\underline{\text{C}}\text{H}_3)_2$), 0.67 (s, 9 H, $\text{C}(\underline{\text{C}}\text{H}_3)_3$), 2.89 (s, 2 H, $\text{N}-\underline{\text{C}}\text{H}_2$), 7.07-7.12 (m, 6 H, *m*-Ph, *p*-Ph), 7.41-7.43 (m, 4 H, *o*-Ph). **$^{13}\text{C}\{^1\text{H}\}$ NMR** (125.70 MHz, 305.0 K, $\text{C}_6\text{H}_5\text{Cl}/\text{D}_2\text{O}$ -capillary): δ = 0.0 (CH_3 , $\text{Si}(\underline{\text{C}}\text{H}_3)_2$), 26.4 (CH_3 , $\text{C}(\underline{\text{C}}\text{H}_3)_3$), 30.4 (C, $\underline{\text{C}}(\text{CH}_3)_3$), 54.7 (CH_2 , $\text{N}-\underline{\text{C}}\text{H}_2$), 124.9 (CH, Ph), 125.3 (CH, Ph) 131.4 (CH, *ortho*-Ph), 131.6 (C, C_{ipso}). **$^{29}\text{Si}\{^1\text{H}\}$ NMR** (99.30 MHz, 305.0 K, $\text{C}_6\text{H}_5\text{Cl}/\text{D}_2\text{O}$ -capillary): δ = 0.5.

Silylimine 119b^[115]

Imine **119b** was obtained according to general procedure **G** using 5-dimethylsilyl-6-thiophenylacenaphthene **43a** (24.0 mg, 75.00 μmol) and 2.0 equiv. of triphenylsilane (781.2 mg, 3.00 mmol). Stirring the mixture for 3 days at r.t. resulted in a yield of 22 %. Stirring for further 330 min at 80 $^\circ\text{C}$ led to quantitative formation of amine **119b**.

**119b**

^1H NMR (499.90 MHz, 305.0 K, $\text{C}_6\text{H}_5\text{Cl}/\text{D}_2\text{O}$ -capillary): δ = 0.92 (s, 9 H, $\text{C}(\underline{\text{C}}\text{H}_3)_3$), 7.11-7.13 (m, 9 H, *m*-Ph, *p*-Ph), 7.57-7.59 (m, 6 H, *o*-Ph), 8.32 (s, 1 H, $\text{N}-\underline{\text{C}}\text{H}$). **$^{13}\text{C}\{^1\text{H}\}$ NMR** (125.70 MHz, 305.0 K, $\text{C}_6\text{H}_5\text{Cl}/\text{D}_2\text{O}$ -capillary): δ = 25.6 (CH_3 , $\text{C}(\underline{\text{C}}\text{H}_3)_3$), 39.7 (C, $\underline{\text{C}}(\text{CH}_3)_3$), 128.2 (CH, *m/p*-Ph), 133.9 (C, C_{ipso}) 135.5 (CH, *o*-Ph), 185.4 (CH, $\text{N}-\underline{\text{C}}\text{H}$). **$^{29}\text{Si}\{^1\text{H}\}$ NMR** (99.30 MHz, 305.0 K, $\text{C}_6\text{H}_5\text{Cl}/\text{D}_2\text{O}$ -capillary): δ = -18.4.

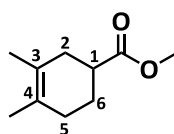
5.8.2 Diels-Alder Reaction (DAR)

DAR 1: The catalyst was prepared freshly by the reaction of 0.06 equiv. (150 μmol) of the corresponding naphthyl or acenaphthyl silane and 0.05 equiv. (135 μmol , 125 mg) of trityl borate in 0.5 mL dichloromethane either at r.t. or at $-80\text{ }^\circ\text{C}$. After stirring for 10-30 min, the catalyst mixture was cooled to $-80\text{ }^\circ\text{C}$ and a mixture of 1.0 equiv. (2.73 mmol, 0.25 mL) of methyl acrylate and 2.0 equiv. (5.46 mmol, 0.60 mL) of 2,3-dimethylbuta-1,3-diene in 0.5 mL dichloromethane was added slowly. (Batch for the reaction with silyl borate **35a**[$\text{B}(\text{C}_6\text{F}_5)_4$]: silane **43a** (81 μmol , 26 mg), trityl borate (75 μmol , 69 mg), methylacrylate (1.5 mmol, 0.11 mL), 2,3-dimethylbuta-1,3-diene (3.0 mmol, 0.34 mL), DTBMP (150 μmol , 31 mg), the reaction was carried out at r.t. in $\text{C}_6\text{H}_5\text{Cl}$.) The mixture was stirred for 60-90 min. Then the reaction was quenched with 0.5 mL saturated NaHCO_3 solution and the product was extracted with dichloromethane (3 x 5 mL). The organic layer was dried over Na_2SO_4 and the solvent was removed under reduced pressure. The Diels-Alder product **DAP1** was purified by column chromatography using petroleum ether/ethyl acetate (95:5) as eluent. Details see Table 39.

Table 39 – Details and yield of Diels Alder test reaction 1 using different catalysts.

Entry	Catalyst	Amount silane [mg]	Reaction conditions	t [min]	Yield
1	36 (Naph, D = OPh)	42	DCM, $-80\text{ }^\circ\text{C}$	60	65 % ^{a)}
2	37a (Naph, D = SPh)	44	DCM, r.t. $\rightarrow -80\text{ }^\circ\text{C}$	60	24 % ^{a)}
3	39 (Naph, D = SePh)	51	DCM, r.t. $\rightarrow -80\text{ }^\circ\text{C}$	60	9 % ^{a)}
4	34a (Ace, D = OPh)	46	DCM, $-80\text{ }^\circ\text{C}$	90	75 % ^{a)}
5 ^{c)}	35a (Ace, D = SPh)	26	$\text{C}_6\text{H}_5\text{Cl}$, r.t.	90	33 % ^{b)}
6 ^{c)}	-	-	$\text{C}_6\text{H}_5\text{Cl}$, r.t.	1 d	0 % ^{b)}

a) Isolated yield, b) GC yield, c) addition of DTBMP.



DAP1

¹H NMR (500.13 MHz, 299.2 K, C_6D_6) δ = 1.51 (s, 3 H, CH_3), 1.53 (s, 3 H, CH_3), 1.66-1.74 (m, 3 H), 1.92-1.95 (m, 1 H), 2.01-2.07 (m, 1 H), 2.22-2.24 (m, 1 H), 2.43-2.48 (m, 1 H, 1-H), 3.42 (s, 3 H, OCH_3).

$^{13}\text{C}\{^1\text{H}\}$ NMR (125.77 MHz, 299.3 K, C_6D_6) δ = 18.9 (CH_3), 19.0 (CH_3), 26.2 (CH_2 , C-6), 31.2 (CH_2 , C-5), 34.1 (CH_2 , C-2), 40.3 (CH , C-1), 51.1 (OCH_3), 124.0 (C, C-4), 125.2 (C, C-3), 175.6 (CO). GC t_{R} = 1.3 (methyl acrylate), 10.0 (DTBMP), 10.1 (**DAP1**), 13.1 (Ph_3CH), 15.6 (5-thiophenylacenaphthene) min.

DAR 2: The catalyst was prepared freshly by the reaction of 0.06 equiv. (83 μmol) of the corresponding silane and 0.05 equiv. (75 μmol , 69 mg) of trityl borate in 0.3 mL chlorobenzene at r.t.. Additionally, 0.06 equiv. (90 μmol , 18 mg) DTBMP was added. After stirring for 10-30 min, the catalyst mixture was cooled to $-30\text{ }^\circ\text{C}$ and a mixture of 1.0 equiv. (1.5 mmol, 0.11 mL) of methyl acrylate and 2.0 equiv. (3.0 mmol, 0.34 mL) of 2,3-dimethylbuta-1,3-diene in 0.1 mL chlorobenzene was added slowly. (Batch for the reaction with silyl borate **34a**[$\text{B}(\text{C}_6\text{F}_5)_4$]: silane **42a** (99 μmol , 30 mg), trityl borate (99 μmol , 90 mg), methylacrylate (1.5 mmol, 0.11 mL), 2,3-dimethylbuta-1,3-diene (3.0 mmol, 0.34 mL), DTBMP (99 μmol , 20 mg.) The mixture was stirred for 60 min. A sample (0.2 mL) of the reaction mixture was filtrated through a short column of silica (2-3 cm in a Pasteur pipette) and diluted in ca. 1 mL dichloromethane. This solution was used for the GC analysis. Details see Table 40.

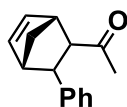
Table 40 – Details and yield of Diels Alder test reaction 2 using different catalysts.

Entry	Catalyst	Amount silane [mg]	Reaction conditions	Time [min]	Conversion	Endo:Exo
1	34a (R = Me, D = OPh)	30	$\text{C}_6\text{H}_5\text{Cl}$, $-30\text{ }^\circ\text{C}$	60	100 %	94:6
2	35a (R = Me, D = SPh)	26	$\text{C}_6\text{H}_5\text{Cl}$, $-30\text{ }^\circ\text{C}$	60	100 %	93:7
3	35b (R = Ph, D = SPh)	32	$\text{C}_6\text{H}_5\text{Cl}$, $-30\text{ }^\circ\text{C}$	60	99 %	92:8
4	35c (R = <i>t</i> -Bu, D = SPh)	30	$\text{C}_6\text{H}_5\text{Cl}$, $-30\text{ }^\circ\text{C}$	60	100 %	89:11
5	-	-	$\text{C}_6\text{H}_5\text{Cl}$, r.t.	7 d	98 %	76:24

GC t_{R} = 1.3 (methyl acrylate), 8.4 (cyclopentadiene-dimer), 9.0 (exo-**DAP2**), 9.1 (endo-**DAP2**), 10.1 (DTBMP), 13.1 (Ph_3CH), 14.2 (5-phenoxyacenaphthene), 15.6 (5-thiophenylacenaphthene) min.

DAR 3: A Schlenk tube was charged with 0.1 equiv. (79 μmol , 25 mg) of 6-dimethylsilyl-5-thiophenylacenaphthene **43a**, (0.1 equiv. (72 μmol , 66 mg) of trityl borate and 0.2 equiv. (145 μmol , 30 mg) of DTBMP and 0.3 mL chlorobenzene was added at r.t.. The mixture was stirred for 10 min and cooled

with an ice bath. A solution of 1.0 equiv. (0.8 mmol, 105 mg) (*E*)-4-phenylbut-3-en-2-one and 4.2 equiv. (3.0 mmol, 0.25 mL) cyclopentadiene in 0.5 mL chlorobenzene was added slowly. The mixture was stirred for 30 min. A sample (0.2 mL) of the reaction mixture was filtrated through a short column of silica (2-3 cm in a Pasteur pipette) and diluted in ca. 1 mL dichloromethane. This solution was used for the GC analysis.



DAP3

Conversion 40 %. **GC** t_R = 8.4 (*E*-4-phenylbut-3-en-2-one), 10.1 (DTBMP), 11.9 (exo-**DAP3**), 12.1 (endo-**DAP3**), 13.1 (Ph_3CH), 15.6 (5-thiophenylacenaphthene) min.

DAR 4: The catalyst was prepared freshly by the reaction of 0.06 equiv. (83 μmol) or 0.03 equiv. (52 μmol) of the corresponding silane and 0.05 equiv. (75 μmol , 69 mg) or 0.03 equiv. (45 μmol , 41 mg) of trityl borate in 0.3 mL chlorobenzene at r.t.. Additionally, 0.06 equiv. (150 μmol , 31 mg) or 0.06 equiv. (90 μmol , 18 mg) of DTBMP was added. After stirring for 10-30 min, the catalyst mixture was cooled to the temperature indicated in Table 41 and a mixture of 1.0 equiv. (1.5 mmol, 0.14 mL) of methyl acrylate and 1.5-2.0 equiv. (2.25-3.0 mmol, 0.21-0.29 mL) of cyclohexadiene in 0.1 mL chlorobenzene was added slowly. The mixture was stirred for 30-90 min. A sample (0.2 mL) of the reaction mixture was filtrated through a short column of silica (2-3 cm in a Pasteur pipette) and diluted in ca. 1 mL dichloromethane. This solution was used for the GC analysis. Details see Table 41.

Table 41 – Details and GC yield of Diels Alder test reaction 4 using different catalysts.

Entry	Catalyst	Cat. charge	Amount silane [mg]	T [°C]	t [min]	Conv.	Endo:Exo	ee [%]
1	34a (Ace, D = OPh, R = Me)	5 mol%	25	0 → r.t.	60	100 %	99:1	-
2	35a (Ace, D = SPh, R = Me)	5 mol%	26	0 → r.t.	30	100 %	99:1	-
3	34b (Ace, D = OPh, R = Ph)	5 mol%	30	0 → r.t.	30	100 %	99:1	-
4	35b (Ace, D = SPh, R = Ph)	3 mol%	20	r.t.	90	50 %	98:2	-
5*	35b (Ace, D = SPh, R = Ph)	3 mol%	20	0 → r.t.	90	34 %	-	0
6*	37b (Naph, D = SPh, R = Ph)	5 mol%	29	0 → r.t.	30	100 %	98:2	0
7*	34b (Ace, D = OPh, R = Ph)	5 mol%	42	-40	30	25 %	-	0

*precursor enantiomerically enriched.

GC t_R = 1.3 (methyl acrylate), 1.6 (cyclohexadiene), 9.8 (exo-DAP4), 10.0 (endo-DAP4), 10.1 (DTBMP), 13.1 (Ph₃CH), 14.2 (5-phenoxyacenaphthene), 15.6 (5-thiophenylacenaphthene) min.

5.9 Calculation of the Free Gibbs Energy Barrier from VT NMR Data

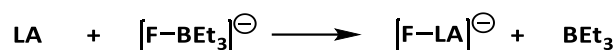
The free Gibbs energy barrier of the inversion process of the silylsulfonium ions **35a,b,d** and **37b** were calculated from the coalescence temperature (T_{coal}) and the difference of the separate signals ν_A and ν_B ($\Delta\nu$) using equation 1:

$$\Delta G^{\text{exp}} = RT_{\text{coal}}(22.96 + \ln(T_{\text{coal}}/\Delta\nu)) \text{ (eq. 1).}^{[60]}$$

6 Computational Details

All quantum chemical calculations were carried out using the Gaussian09 package.^[116] The molecular structure optimizations were performed using the M06-2X functional along with the Def2-TZVP basis set for the elements F, S, O, Si, C, B, H.^[117] Every stationary point was identified by a subsequent frequency calculation either as a minimum (Number of imaginary frequencies (NIMAG): 0) or as a transition state (NIMAG: 1). All obtained SCF energies (E(SCF)) and the absolute computed Gibbs free energies at T = 298.15 K and p = 0.101 MPa (1 atm) in the gas phase (G298) are given in the additional file (SKD-Computed_Energies.docx).

The fluorine ion affinity (FIA) for cations **xx** and BCF was calculated according the reaction in Scheme 93. The SCF energies (E(SCF)) for the FIA were calculated at the M06-2X/Def2-TZVP level of theory with inclusion of solvent effects using the SCIPM model with dichloromethane as a solvent. The SCF energies (E(SCF)) are given in the additional file (SKD-Computed_Energies.docx).



Scheme 93 – Reaction used to calculate the fluorine ion affinity (FIA) of cations and BCF (LA = silyl cation **xx**, BCF).

For the calculations of the mechanism of the hydrosilylation reaction of nitriles, the absolute computed Gibbs free energies were calculated at the M06-2X/Def2-TZVP level of theory including the solvent chlorobenzene using the SCRF model. The obtained free Gibbs energies were corrected with a factor obtained via the freqchk utility program by applying the solvent pressure ($p = 24.419$ MPa (241 atm) for chlorobenzene). These data can also be found in the additional file (SKD-Computed_Energies.docx).

The optimized molecular structures of all calculated compounds are given as Cartesian coordinates in the structure file (SKD-Computed_Molecular_Structures.xyz).

For the assignment of the IR bands of the *syn*- and *anti*-structures of silanes **x-x** (SPh, R = Me, *t*-Bu, Ph), their molecular structures were calculated at the M06-2X/Def2-TZVP level of theory at T = 298.15 K and p = 0.101 MPa (1 atm) in the gas phase with a subsequent frequency analysis. To account for anharmonicity effects, a scaling factor for the Si – H vibration was determined from the correlation of the computed data and the experimental results for silanes **x-x** and triethylsilane (Figure 87). The scaling factor is given by the slope of the line of best fit which is 0.9619 ± 0.00295 .

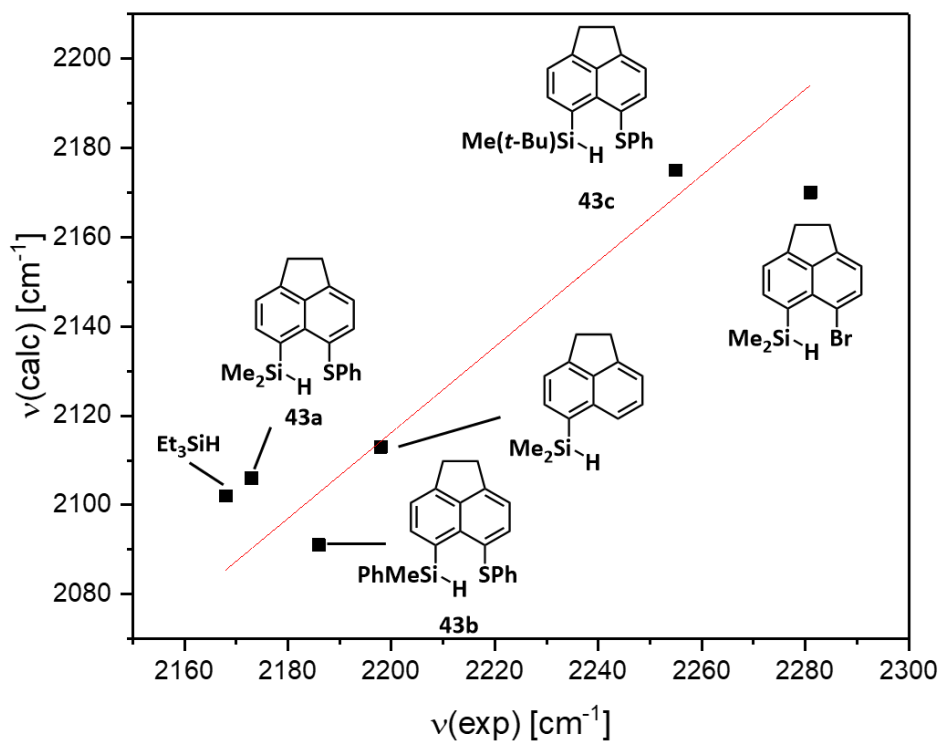


Figure 87 – Correlation of the calculated wavenumber obtained at M06-2X/Def2-TZVP of the $\nu(\text{Si} - \text{H})$ vibration and the experimental value for silanes **43a,b,c**, 5-bromo-6-dimethylsilyl acenaphthene, 5-dimethylsilyl acenaphthene and triethylsilane.

The figures of the calculated molecular structures were generated using the software GaussView 5.0.

7 Literature

- [1] W. Zulehner, B. Neuer, G. Rau, in *Silicon - Ullmann's Encyclopedia of Industrial Chemistry*, **2000**.
- [2] a) M. G. Voronkov, *Russ. J. Appl. Chem.* **2007**, *80*, 2190-2196; b) P. G. Neudeck, *Journal of Electronic Materials* **1995**, *24*, 283-288; c) M. A. Green, *Journal of Materials Science: Materials in Electronics* **2007**, *18*, 15-19; d) S. D. Wolf, A. Descoedres, Z. C. Holman, *Green* **2012**, *2*, 7-24.
- [3] L. Rösch, P. John, R. Reitmeier, in *Silicon Compounds - Ullmann's Encyclopedia of Industrial Chemistry*, **2000**.
- [4] a) Y. Seo, M. R. Gagné, *ACS Catal.* **2018**, *8*, 6993-6999; b) B. Rubial, A. Ballesteros, J. M. González, *Eur. J. Org. Chem.* **2018**, *2018*, 6194-6198; c) M. A. Radtke, T. H. Lambert, *Chem. Sci.* **2018**, *9*, 6406-6410; d) S. Popov, B. Shao, A. L. Bagdasarian, T. R. Benton, L. Zou, Z. Yang, K. N. Houk, H. M. Nelson, *Science* **2018**, *361*, 381-387; e) T. Gatzemeier, P. S. J. Kaib, J. B. Lingnau, R. Goddard, B. List, *Angew. Chem. Int. Ed.* **2018**, *57*, 2464-2468; f) B. Shao, A. L. Bagdasarian, S. Popov, H. M. Nelson, *Science* **2017**, *355*, 1403-1407; g) B. S. Moyer, M. R. Gagné, *Synlett* **2017**, *28*, 2429-2434; h) H. F. T. Klare, *ACS Catal.* **2017**, 6999-7002; i) A. Gudz, P. R. Payne, M. R. Gagné, *Organomet.* **2017**, *36*, 4047-4053; j) M. Devillard, B. de Bruin, M. A. Siegler, J. I. van der Vlugt, *Chem. Eur. J.* **2017**, *23*, 13628-13632; k) T. A. Bender, P. R. Payne, M. R. Gagné, *Nat. Chem.* **2017**, *10*, 85; l) S. M. Banik, A. Levina, A. M. Hyde, E. N. Jacobsen, *Science* **2017**, *358*, 761-764; m) T. Gatzemeier, M. van Gemmeren, Y. Xie, D. Höfler, M. Leutzsch, B. List, *Science* **2016**, *351*, 949-952; n) Q.-A. Chen, H. F. T. Klare, M. Oestreich, *J. Am. Chem. Soc.* **2016**, *138*, 7868-7871; o) T. Stahl, H. F. T. Klare, M. Oestreich, *ACS Catal.* **2013**, *3*, 1578-1587; p) H. F. T. Klare, M. Oestreich, *Dalton Trans.* **2010**, *39*, 9176-9184.
- [5] T. Müller, in *Advances in Organometallic Chemistry, Vol. 53* (Eds.: R. West, A. F. Hill, F. G. A. Stone), Academic Press, **2005**, pp. 155-215.
- [6] a) N. Kordts, S. Künzler, S. Rathjen, T. Sieling, H. Großekappenberg, M. Schmidtman, T. Müller, *Chem. Eur. J.* **2017**, *23*, 10068-10079; b) T. Müller, in *Organosilicon Chemistry V, Vol. 116*, 34 ed. (Eds.: N. Auner, J. Weis), VCH, Weinheim, **2003**.
- [7] V. Y. Lee, *Russ. Chem. Rev.* **2019**, *88*, 351-369.
- [8] a) J. B. Lambert, Y. Zhao, *Angew. Chem.* **1997**, *109*, 389-391; b) T. Müller, Y. Zhao, J. B. Lambert, *Organomet.* **1998**, *17*, 278-280.
- [9] T. Müller, in *Functional Molecular Silicon Compounds I: Regular Oxidation States* (Ed.: D. Scheschkewitz), Springer International Publishing, Cham, **2014**, pp. 107-162.
- [10] a) C. A. Reed, *Acc. Chem. Res.* **1998**, *31*, 133-139; b) I. Krossing, I. Raabe, *Angew. Chem. Int. Ed.* **2004**, *43*, 2066-2090; c) T. Küppers, E. Bernhardt, R. Eujen, H. Willner, C. W. Lehmann, *Angew. Chem. Int. Ed.* **2007**, *46*, 6346-6349; d) A. Avelar, F. S. Tham, C. A. Reed, *Angew. Chem. Int. Ed.* **2009**, *48*, 3491-3493; e) M. Kessler, C. Knapp, V. Sagawe, H. Scherer, R. Uzun, *Inorg. Chem.* **2010**, *49*, 5223-5230.
- [11] a) C. A. Reed, Z. Xie, R. Bau, A. Benesi, *Science* **1993**, *262*, 402-404; b) J. B. Lambert, S. Zhang, C. L. Stern, J. C. Huffman, *Science* **1993**, *260*, 1917-1918.

- [12] K.-C. Kim, C. A. Reed, D. W. Elliott, L. J. Mueller, F. Tham, L. Lin, J. B. Lambert, *Science* **2002**, *297*, 825-827.
- [13] a) T. Müller, *Angew. Chem. Int. Ed.* **2001**, *40*, 3033-3036; b) R. Panisch, M. Bolte, T. Müller, *J. Am. Chem. Soc.* **2006**, *128*, 9676-9682.
- [14] a) D. Pla, O. Sadek, S. Cadet, B. Mestre-Voegtli, E. Gras, *Dalton Trans.* **2015**, *44*, 18340-18346; b) Y.-F. Li, Y. Kang, S.-B. Ko, Y. Rao, F. Sauriol, S. Wang, *Organomet.* **2013**, *32*, 3063-3068; c) S. Bontemps, M. Devillard, S. Mallet-Ladeira, G. Bouhadir, K. Miqueu, D. Bourissou, *Inorg. Chem.* **2013**, *52*, 4714-4720; d) J. Beckmann, E. Hupf, E. Lork, S. Mebs, *Inorg. Chem.* **2013**, *52*, 11881-11888; e) B. A. Surgenor, M. Bühl, A. M. Z. Slawin, J. D. Woollins, P. Kilian, *Angew. Chem. Int. Ed.* **2012**, *51*, 10150-10153; f) P. Wawrzyniak, A. L. Fuller, A. M. Z. Slawin, P. Kilian, *Inorg. Chem.* **2009**, *48*, 2500-2506; g) C. Breliere, F. Carre, R. J. P. Corriu, W. E. Douglas, M. Poirier, G. Royo, M. Wong Chi Man, *Organomet.* **1992**, *11*, 1586-1593.
- [15] a) G. Erker, D. W. Stephan, in *Frustrated Lewis Pairs I: Uncovering and Understanding in Top. Curr. Chem.*, **2013**; b) G. Erker, D. W. Stephan, in *Frustrated Lewis Pairs II: Expanding the Scope in Top. Curr. Chem.*, **2013**; c) D. W. Stephan, G. Erker, *Angew. Chem. Int. Ed.* **2010**, *49*, 46-76; d) D. W. Stephan, G. Erker, *Angew. Chem. Int. Ed.* **2015**, *54*, 6400-6441; e) P. P. Power, *Nature* **2010**, *463*, 171-177.
- [16] M. Reißmann, A. Schäfer, S. Jung, T. Müller, *Organomet.* **2013**, *32*, 6736-6744.
- [17] a) S. Duttwyler, Q.-Q. Do, A. Linden, K. K. Baldrige, J. S. Siegel, *Angew. Chem. Int. Ed.* **2008**, *47*, 1719-1722; b) P. Romanato, S. Duttwyler, A. Linden, K. K. Baldrige, J. S. Siegel, *J. Am. Chem. Soc.* **2010**, *132*, 7828-7829; c) P. Romanato, S. Duttwyler, A. Linden, K. K. Baldrige, J. S. Siegel, *J. Am. Chem. Soc.* **2011**, *133*, 11844-11846.
- [18] J. Y. Corey, *J. Am. Chem. Soc.* **1975**, *97*, 3237-3238.
- [19] J. B. Lambert, Y. Zhao, H. Wu, *J. Org. Chem.* **1999**, *64*, 2729-2736.
- [20] a) A. Schäfer, M. Reißmann, A. Schäfer, W. Saak, D. Haase, T. Müller, *Angew. Chem. Int. Ed.* **2011**, *50*, 12636-12638; b) A. Schäfer, M. Reißmann, S. Jung, A. Schäfer, W. Saak, E. Brendler, T. Müller, *Organomet.* **2013**, *32*, 4713-4722.
- [21] Q. Wu, Z.-W. Qu, L. Omann, E. Irran, H. F. T. Klare, M. Oestreich, *Angew. Chem. Int. Ed.* **2018**, *57*, 9176-9179.
- [22] I. Mallov, A. J. Ruddy, H. Zhu, S. Grimme, D. W. Stephan, *Chem. Eur. J.* **2017**, *23*, 17692-17696.
- [23] D. G. Gusev, O. V. Ozerov, *Chem. Eur. J.* **2011**, *17*, 634-640.
- [24] a) V. J. Scott, R. Çelenligil-Çetin, O. V. Ozerov, *J. Am. Chem. Soc.* **2005**, *127*, 2852-2853; b) C. Douvris, O. V. Ozerov, *Science* **2008**, *321*, 1188-1190; c) C. Douvris, C. M. Nagaraja, C.-H. Chen, B. M. Foxman, O. V. Ozerov, *J. Am. Chem. Soc.* **2010**, *132*, 4946-4953.
- [25] N. Kordts, C. Borner, R. Panisch, W. Saak, T. Müller, *Organomet.* **2014**, *33*, 1492-1498.
- [26] A. Merk, H. Großekappenberg, M. Schmidtman, M.-P. Luecke, C. Lorent, M. Driess, M. Oestreich, H. F. T. Klare, T. Müller, *Angew. Chem. Int. Ed.* **2018**, *57*, 15267-15271.
- [27] N. von Wolff, G. Lefèvre, J. C. Berthet, P. Thuéry, T. Cantat, *ACS Catal.* **2016**, *6*, 4526-4535.
- [28] K. Hara, R. Akiyama, M. Sawamura, *Org. Lett.* **2005**, *7*, 5621-5623.

- [29] a) H. F. T. Klare, K. Bergander, M. Oestreich, *Angew. Chem. Int. Ed.* **2009**, *48*, 9077-9079; b) V. H. G. Rohde, P. Pommerening, H. F. T. Klare, M. Oestreich, *Organomet.* **2014**, *33*, 3618-3628; c) V. H. G. Rohde, M. F. Müller, M. Oestreich, *Organomet.* **2015**, *34*, 3358-3373; d) P. Shaykhutdinova, M. Oestreich, *Organomet.* **2016**, *35*, 2768-2771; e) P. Shaykhutdinova, S. Kemper, M. Oestreich, *Eur. J. Org. Chem.* **2018**, *2018*, 2896-2901; f) P. Shaykhutdinova, M. Oestreich, *Org. Lett.* **2018**, *20*, 7029-7033; g) P. Shaykhutdinova, M. Oestreich, *Synthesis* **2019**, *51*, 2221-2229.
- [30] L. Greb, *Chem. Eur. J.* **2018**, *24*, 17881-17896.
- [31] a) U. Mayer, V. Gutmann, W. Gerger, *Monatsh. Chem.* **1975**, *106*, 1235-1257; b) M. A. Beckett, D. S. Brassington, S. J. Coles, M. B. Hursthouse, *Inorg. Chem. Commun.* **2000**, *3*, 530-533.
- [32] H. Großekappenberg, M. Reißmann, M. Schmidtman, T. Müller, *Organomet.* **2015**, *34*, 4952-4958.
- [33] R. F. Childs, D. L. Mulholland, A. Nixon, *Can. J. Chem.* **1982**, *60*, 801-808.
- [34] a) G. Hilt, A. Nödling, *Eur. J. Org. Chem.* **2011**, *2011*, 7071-7075; b) G. Hilt, F. Pünner, J. Möbus, V. Naseri, M. A. Bohn, *Eur. J. Org. Chem.* **2011**, *2011*, 5962-5966; c) A. R. Nödling, K. Mütter, V. H. G. Rohde, G. Hilt, M. Oestreich, *Organomet.* **2014**, *33*, 302-308.
- [35] S. Künzler, S. Rathjen, A. Merk, M. Schmidtman, T. Müller, *Chem. Eur. J.* **2019**, *25*, 15123-15130.
- [36] a) R. Murugavel, M. Bhattacharjee, H. W. Roesky, *Appl. Organomet. Chem.* **1999**, *13*, 227-243; b) D. B. Cordes, P. D. Lickiss, F. Rataboul, *Chem. Rev.* **2010**, *110*, 2081-2173.
- [37] a) J. Morell, S. Chatterjee, P. J. Klar, D. Mauder, I. Shenderovich, F. Hoffmann, M. Fröba, *Chem. Eur. J.* **2008**, *14*, 5935-5940; b) F. Hoffmann, M. Fröba, *Chem. Soc. Rev.* **2011**, *40*, 608-620.
- [38] a) J. Heppekausen, R. Stade, R. Goddard, A. Fürstner, *J. Am. Chem. Soc.* **2010**, *132*, 11045-11057; b) J. Heppekausen, R. Stade, A. Kondoh, G. Seidel, R. Goddard, A. Fürstner, *Chem. Eur. J.* **2012**, *18*, 10281-10299.
- [39] a) M. A. Brook, *Silicon in Organic, Organometallic, and Polymer Chemistry, Vol. 1*, John Wiley and Sons, Inc., **2010**; b) W. Malisch, B. Klüpfel, D. Schumacher, M. Nieger, *J. Organomet. Chem.* **2002**, *661*, 95-110.
- [40] a) S. Rendler, M. Oestreich, *Angew. Chem. Int. Ed.* **2008**, *47*, 5997-6000; b) T. Fallon, M. Oestreich, *Angew. Chem. Int. Ed.* **2015**, *54*, 12488-12491.
- [41] C. Strohmman, M. Bindl, V. C. Fraaß, J. Hörnig, *Angew. Chem. Int. Ed.* **2004**, *43*, 1011-1014.
- [42] a) R. J. P. Corriu, A. Kpoton, M. Poirier, G. Royo, J. Y. Corey, *J. Organomet. Chem.* **1984**, *277*, C25-C30; b) L. J. P. van der Boon, S.-i. Fuku-en, J. C. Slootweg, K. Lammertsma, A. W. Ehlers, *Top. Catal.* **2018**, *61*, 674-684; c) R. S. Berry, *J. Chem. Phys.* **1960**, *32*, 933-938.
- [43] S. G. Koller, J. O. Bauer, C. Strohmman, *Angew. Chem. Int. Ed.* **2017**, *56*, 7991-7994.
- [44] M. Oestreich, U. K. Schmid, G. Auer, M. Keller, *Synthesis* **2003**, *17*, 2725-2739.
- [45] a) A. Kawachi, H. Maeda, K. Mitsudo, K. Tamao, *Organomet.* **1999**, *18*, 4530-4533; b) J. O. Bauer, C. Strohmman, *Angew. Chem. Int. Ed.* **2014**, *53*, 720-724; c) J. O. Bauer, C. Strohmman,

- J. Am. Chem. Soc.* **2015**, *137*, 4304-4307; d) P. Ducos, V. Liautard, F. Robert, Y. Landais, *Chem. Eur. J.* **2015**, *21*, 11573-11578.
- [46] a) M. Johannsen, K. A. Jørgensen, G. Helmchen, *J. Am. Chem. Soc.* **1998**, *120*, 7637-7638; b) G. A. Olah, G. Rasul, G. K. S. Prakash, *J. Am. Chem. Soc.* **1999**, *121*, 9615-9617.
- [47] a) A. Fernandes, C. Laye, S. Pramanik, D. Palmeira, Ö. Ö. Pekel, S. Massi, M. Schmidtman, T. Müller, F. Robert, Y. Landais, *accepted*; b) A. Fernandes, *Dissertation, Université de Bordeaux 2018*; c) C. Laye, *ongoing Dissertation, Université de Bordeaux*.
- [48] H. Yamamoto, *Lewis acids in organic synthesis, Vol. 16*, **2002**.
- [49] M. Oestreich, *Chem. Eur. J.* **2006**, *12*, 30-37.
- [50] a) D. V. Gutsulyak, G. I. Nikonov, *Angew. Chem. Int. Ed.* **2010**, *49*, 7553-7556; b) M. Pérez, Z.-W. Qu, C. B. Caputo, V. Podgorny, L. J. Hounjet, A. Hansen, R. Dobrovetsky, S. Grimme, D. W. Stephan, *Chem. Eur. J.* **2015**, *21*, 6491-6500.
- [51] a) M. Panunzio, P. Zarantonello, *Org. Process Res. Dev.* **1998**, *2*, 49-59; b) A. H. Mermerian, G. C. Fu, *Angew. Chem. Int. Ed.* **2005**, *44*, 949-952.
- [52] G. L. Larson, E. Torres, *J. Organomet. Chem.* **1985**, *293*, 19-27.
- [53] a) H. Großekappenberg, *Dissertation, Carl von Ossietzky Universität Oldenburg 2016*; b) D. Cory, A. Wong, W. M. Ritchey, *J. Organomet. Chem.* **1982**, *235*, 277-285.
- [54] J. B. G. Lambert, S. Gronert, H. F. Shurvell, D. A. Lightner, *Spektroskopie - Strukturaufklärung in der Organischen Chemie*, Pearson Deutschland, **2012**.
- [55] S. Rendler, G. Auer, M. Keller, M. Oestreich, *Adv. Synth. Catal.* **2006**, *348*, 1171-1182.
- [56] V. T. Trepohl, R. Fröhlich, M. Oestreich, *Tetrahedron* **2009**, *65*, 6510-6518.
- [57] D. E. J. E. Robinson, S. D. Bull, *Tetrahedron: Asymm.* **2003**, *14*, 1407-1446.
- [58] S. Pramanik, A. Fernandes, V. Liautard, M. Pucheault, F. Robert, Y. Landais, *Chem. Eur. J.* **2019**, *25*, 728-732.
- [59] M. Oestreich, G. Auer, M. Keller, *Eur. J. Org. Chem.* **2005**, *2005*, 184-195.
- [60] H. Günther, *NMR Spectroscopy - Basic Principles, Concepts and Applications in Chemistry, Vol. 3*, WILEY-VCH, **2013**.
- [61] a) K.-i. Shimizu, T. Kubo, A. Satsuma, *Chem. Eur. J.* **2012**, *18*, 2226-2229; b) M. Jeon, J. Han, J. Park, *ChemCatChem* **2012**, *4*, 521-524.
- [62] a) Y. Cao, Z.-X. Chen, *Phys. Chem. Chem. Phys.* **2007**, *9*, 739-746; b) X. Y. Zhu, J. M. White, M. Wolf, E. Hasselbrink, G. Ertl, *J. Phys. Chem.* **1991**, *95*, 8393-8402; c) M. Bowker, L. Gilbert, J. Counsell, C. Morgan, *J. Phys. Chem. C* **2010**, *114*, 17142-17147; d) A. Shavorskiy, M. J. Gladys, G. Held, *Phys. Chem. Chem. Phys.* **2008**, *10*, 6150-6159.
- [63] E. Hupf, E. Lork, S. Mebs, J. Beckmann, *Organomet.* **2015**, *34*, 3873-3887.
- [64] S. Rendler, O. Plefka, B. Karatas, G. Auer, R. Fröhlich, C. Mück-Lichtenfeld, S. Grimme, M. Oestreich, *Chem. Eur. J.* **2008**, *14*, 11512-11528.
- [65] a) W. Adam, C. M. Mitchell, C. R. Saha-Möller, T. Selvam, O. Weichold, *J. Mol. Cat. A - Chem.* **2000**, *154*, 251-255; b) E. Cecchet, F. Di Furia, G. Licini, G. Modena, *Tetrahedron: Asymm.* **1996**, *7*, 369-372.

- [66] J. Clayden, N. Greeves, S. G. Warren, *Organic chemistry*, Oxford University Press, Oxford; New York, **2012**.
- [67] J. Sun, C. Zhu, Z. Dai, M. Yang, Y. Pan, H. Hu, *J. Org. Chem.* **2004**, *69*, 8500-8503.
- [68] a) G. Chelucci, F. Soccolini, *Tetrahedron: Asymm.* **1992**, *3*, 1235-1238; b) M. Zaidlewicz, A. Tafelska-Kaczmarek, A. Prewysz-Kwinto, *Tetrahedron: Asymm.* **2005**, *16*, 3205-3210.
- [69] R. K. Dhar, P. D. Gagare, P. V. Ramachandran, in *Encyclopedia of Reagents for Organic Synthesis*, John Wiley & Sons, Ltd, **2001**.
- [70] M. B. Díaz-Valenzuela, S. D. Phillips, M. B. France, M. E. Gunn, M. L. Clarke, *Chem. Eur. J.* **2009**, *15*, 1227-1232.
- [71] M. Mantina, A. C. Chamberlin, R. Valero, C. J. Cramer, D. G. Truhlar, *J. Phys. Chem. A* **2009**, *113*, 5806-5812.
- [72] a) L. K. Aschenbach, F. R. Knight, R. A. M. Randall, D. B. Cordes, A. Baggott, M. Bühl, A. M. Z. Slawin, J. D. Woollins, *Dalton Trans.* **2012**, *41*, 3141-3153; b) E. Hupf, *Dissertation, Universität Bremen* **2015**.
- [73] **!!! INVALID CITATION !!!** .
- [74] R. M. Badger, *J. Chem. Phys.* **1934**, *2*, 128-131.
- [75] The analysis of the electron density in the framework of Bader's theory of atoms in molecules (QTAIM) and the corresponding 2D Laplacian contour plots were contributed by T. Müller, Carl von Ossietzky Universität Oldenburg.
- [76] a) E. Hupf, M. Olaru, C. I. Raț, M. Fugel, C. B. Hübschle, E. Lork, S. Grabowsky, S. Mebs, J. Beckmann, *Chem. Eur. J.* **2017**, *23*, 10568-10579; b) U. Kolb, M. Beuter, M. Draeger, *Inorg. Chem.* **1994**, *33*, 4522-4530.
- [77] A. P. Bento, F. M. Bickelhaupt, *J. Org. Chem.* **2007**, *72*, 2201-2207.
- [78] S. Rathjen, *ongoing Dissertation, Carl von Ossietzky Universität Oldenburg*.
- [79] P. Pyykkö, M. Atsumi, *Chem. Eur. J.* **2009**, *15*, 12770-12779.
- [80] F. Weinhold, R. West, *Organomet.* **2011**, *30*, 5815-5824.
- [81] a) A. Schäfer, M. Reißmann, A. Schäfer, M. Schmidtman, T. Müller, *Chem. Eur. J.* **2014**, *20*, 9381-9386; b) Z. Xie, R. Bau, C. A. Reed, *J. Chem. Soc.; Chem. Commun.* **1994**, 2519-2520; c) M. Driess, R. Barmeyer, C. Monsé, K. Merz, *Angew. Chem. Int. Ed.* **2001**, *40*, 2308-2310.
- [82] M. Kira, T. Hino, H. Sakurai, *J. Am. Chem. Soc.* **1992**, *114*, 6697-6700.
- [83] a) S. Shambayati, S. L. Schreiber, J. F. Blake, S. G. Wierschke, W. L. Jorgensen, *J. Am. Chem. Soc.* **1990**, *112*, 697-703; b) S. Grabowsky, M. F. Hesse, C. Paulmann, P. Luger, J. Beckmann, *Inorg. Chem.* **2009**, *48*, 4384-4393.
- [84] a) E. S. Stoyanov, G. Gunbas, N. Hafezi, M. Mascal, I. V. Stoyanova, F. S. Tham, C. A. Reed, *J. Am. Chem. Soc.* **2012**, *134*, 707-714; b) Y. Sarazin, J. A. Wright, M. Bochmann, *J. Organomet. Chem.* **2006**, *691*, 5680-5687.
- [85] Y. Mo, Y. Zhang, J. Gao, *J. Am. Chem. Soc.* **1999**, *121*, 5737-5742.
- [86] A. D. Dilman, S. L. Ioffe, *Chem. Rev.* **2003**, *103*, 733-772.

- [87] a) N. Kordts, *Dissertation, Carl von Ossietzky Universität Oldenburg* **2015**; b) K. Rüger, *Master Thesis, Carl von Ossietzky Universität Oldenburg* **2015**.
- [88] P. Tholen, *Internship Report, Carl von Ossietzky Universität Oldenburg* **2016**.
- [89] R. Corriu, C. Guerin, *J. Organomet. Chem.* **1980**, *195*, 261-274.
- [90] L. J. P. van der Boon, L. van Gelderen, T. R. de Groot, M. Lutz, J. C. Slootweg, A. W. Ehlers, K. Lammertsma, *Inorg. Chem.* **2018**, *57*, 12697-12708.
- [91] a) I. Ugi, D. Marquarding, H. Klusacek, P. Gillespie, F. Ramirez, *Acc. Chem. Res.* **1971**, *4*, 288-296; b) E. P. A. Couzijn, J. C. Slootweg, A. W. Ehlers, K. Lammertsma, *J. Am. Chem. Soc.* **2010**, *132*, 18127-18140; c) V. V. Negrebetsky, E. P. Kramarova, A. G. Shipov, Y. I. Baukov, A. A. Korlyukov, D. E. Arkhipov, A. R. Bassindale, P. G. Taylor, S. Y. Bylikin, *J. Organomet. Chem.* **2018**, *872*, 31-39.
- [92] C. Gerdes, W. Saak, D. Haase, T. Müller, *J. Am. Chem. Soc.* **2013**, *135*, 10353-10361.
- [93] L. Albers, J. Baumgartner, C. Marschner, T. Müller, *Chem. Eur. J.* **2016**, *22*, 7970-7977.
- [94] a) P. Jutzi, E.-A. Bunte, *Angew. Chem.* **1992**, *104*, 1636-1638; b) T. Müller, P. Jutzi, T. Kühler, *Organomet.* **2001**, *20*, 5619-5628.
- [95] Q. Wu, E. Irran, R. Müller, M. Kaupp, H. F. T. Klare, M. Oestreich, *Science* **2019**, *365*, 168-172.
- [96] C. A. Reed, K.-C. Kim, E. S. Stoyanov, D. Stasko, F. S. Tham, L. J. Mueller, P. D. W. Boyd, *J. Am. Chem. Soc.* **2003**, *125*, 1796-1804.
- [97] a) B. E. Dial, P. J. Pellechia, M. D. Smith, K. D. Shimizu, *J. Am. Chem. Soc.* **2012**, *134*, 3675-3678; b) K. Nikitin, R. O'Gara, *Chem. Eur. J.* **2019**, *25*, 4551-4589.
- [98] a) C. Gerdes, *Dissertation, Carl von Ossietzky Universität Oldenburg* **2012**; b) Z. Xie, D. J. Liston, T. Jelínek, V. Mitro, R. Bau, C. A. Reed, *J. Chem. Soc., Chem. Commun.* **1993**, 384-386.
- [99] T. Beringhelli, D. Donghi, D. Maggioni, G. D'Alfonso, *Coord. Chem. Rev.* **2008**, *252*, 2292-2313.
- [100] A. Merk, *ongoing Dissertation, Carl von Ossietzky Universität Oldenburg*.
- [101] R. Panisch, *Dissertation, Carl von Ossietzky Universität Oldenburg* **2008**.
- [102] C. Rabiller, J. P. Renou, G. J. Martin, *J. Chem. Soc., Perkin Trans. 2* **1977**, 536-541.
- [103] O. Riant, N. Mostefai, J. Courmarcel, *Synthesis* **2004**, *2004*, 2943-2958.
- [104] a) S. Wübbolt, M. Oestreich, *Synlett* **2017**, *28*, 2411-2414; b) L. Paquin, J. Hamelin, F. Texier-Boullet, *Synthesis* **2006**, *2006*, 1652-1656.
- [105] a) R. K. Schmidt, K. Müther, C. Mück-Lichtenfeld, S. Grimme, M. Oestreich, *J. Am. Chem. Soc.* **2012**, *134*, 4421-4428; b) P. N. Liu, Z. Y. Zhou, C. P. Lau, *Chem. Eur. J.* **2007**, *13*, 8610-8619.
- [106] a) N. Gandhamsetty, J. Jeong, J. Park, S. Park, S. Chang, *J. Org. Chem.* **2015**, *80*, 7281-7287; b) T. Hackel, N. A. McGrath, *Molecules* **2019**, *24*, 432.
- [107] D. J. Parks, J. M. Blackwell, W. E. Piers, *J. Org. Chem.* **2000**, *65*, 3090-3098.
- [108] A. Y. Houghton, J. Hurmalainen, A. Mansikkamäki, W. E. Piers, H. M. Tuononen, *Nat. Chem.* **2014**, *6*, 983.
- [109] E. Ruch, I. Ugi, *Topics in Stereochemistry, Vol. 4*, John Wiley and Sons, Inc., **1969**.

-
- [110] K. Tamao, K. Nagata, M. Asahara, A. Kawachi, Y. Ito, M. Shiro, *J. Am. Chem. Soc.* **1995**, *117*, 11592-11593.
- [111] a) B. Su, J. F. Hartwig, *Angew. Chem. Int. Ed.* **2018**, *57*, 10163-10167; b) N. Lühmann, H. Hirao, S. Shaik, T. Müller, *Organomet.* **2011**, *30*, 4087-4096; c) J. C. W. Chien, W. M. Tsai, M. D. Rausch, *J. Am. Chem. Soc.* **1991**, *113*, 8570-8571; d) J. Beckmann, T. G. Do, S. Grabowsky, E. Hupf, E. Lork, S. Mebs, *Z. anorg. allg. Chem.* **2013**, *639*, 2233-2249; e) N. Lühmann, *Dissertation, Carl von Ossietzky Universität Oldenburg* **2011**.
- [112] M. S. Würdemann, *Bachelor Thesis, Carl von Ossietzky Universität Oldenburg* **2017**.
- [113] J. Becker, *Internship Report, Carl von Ossietzky Universität Oldenburg* **2017**.
- [114] M. Wernke, *Internship Report, Carl von Ossietzky Universität Oldenburg* **2016**.
- [115] S. Brand, *Internship Report, Carl von Ossietzky Universität Oldenburg* **2019**.
- [116] M. J. Frisch, G. W. Trucks, H. B. Schlegel, G. E. Scuseria, M. A. Robb, J. R. Cheeseman, G. Scalmani, V. Barone, B. Mennucci, G. A. Petersson, H. Nakatsuji, M. Caricato, X. Li, H. P. Hratchian, A. F. Izmaylov, J. Bloino, G. Zheng, J. L. Sonnenberg, M. Hada, M. Ehara, K. Toyota, R. Fukuda, J. Hasegawa, M. Ishida, T. Nakajima, Y. Honda, O. Kitao, H. Nakai, T. Vreven, J. J. A. Montgomery, J. E. Peralta, F. Ogliaro, M. Bearpark, J. J. Heyd, E. Brothers, K. N. Kudin, V. N. Staroverov, T. Keith, R. Kobayashi, J. Normand, K. Raghavachari, A. Rendell, J. C. Burant, S. S. Iyengar, J. Tomasi, M. Cossi, N. Rega, J. M. Millam, M. Klene, J. E. Knox, J. B. Cross, V. Bakken, C. Adamo, J. Jaramillo, R. Gomperts, R. E. Stratmann, O. Yazyev, A. J. Austin, R. Cammi, C. Pomelli, J. W. Ochterski, R. L. Martin, K. Morokuma, V. G. Zakrzewski, G. A. Voth, P. Salvador, J. J. Dannenberg, S. Dapprich, A. D. Daniels, O. Farkas, J. B. Foresman, J. V. Ortiz, J. Cioslowski, D. J. Fox, *Gaussian 09, Revision D.01, Gaussian, Inc., Wallingford CT, 2013*.
- [117] a) D. Rappoport, F. Furche, *J. Chem. Phys.* **2010**, *133*, 134105; b) A. J. Cohen, P. Mori-Sánchez, W. Yang, *Chem. Rev.* **2012**, *112*, 289-320; c) Y. Zhao, D. G. Truhlar, *J. Chem. Phys.* **2006**, *125*, 194101.